DANMARKS OG GRØNLANDS GEOLOGISKE UNDERSØGELSE **RAPPORT 2022/31**

Upper seal characterising and capacity evaluation based on cuttings analysis of the Nini-4 well

Project Greensand Phase 2 W3.7 report

Niels H. Schovsbo, Henrik I. Petersen, Rikke Weibel & Niels Springer

GEOLOGICAL SURVEY OF DENMARK AND GREENLAND
DANISH MINISTRY OF CLIMATE, ENERGY AND UTILITIES

G E U S

Upper seal characterising and capacity evaluation based on cuttings analysis of the Nini-4 well

Project Greensand Phase 2 WP 3.7 report

Niels H. Schovsbo, Henrik I. Petersen, Rikke Weibel & Niels Springer

Confidential report

Copy No.

Released 31.12.2023

EUDP

Funded by the European Union
NextGenerationEU

GEOLOGICAL SURVEY OF DENMARK AND GREENLAND
DANISH MINISTRY OF CLIMATE, ENERGY AND UTILITIES

GEUS

Table of Contents

SUMMARY CAPROCK

The Nini West depleted oil field is sealed by a 340 m thick primary caprock succession that belongs to the Horda to mid Lark Fm and a 550 m thick secondary caprock succession that belong to the mid to upper Lark Fm (Figure 1A). The combined Nini West Seal Complex is thus almost 900 m thick (c.f. Petersen et al., 2022). The above lying strata i.e. the remaining c. 800 m belongs to the Nolde Sand and the Nordland Group and is here considered as overburden.

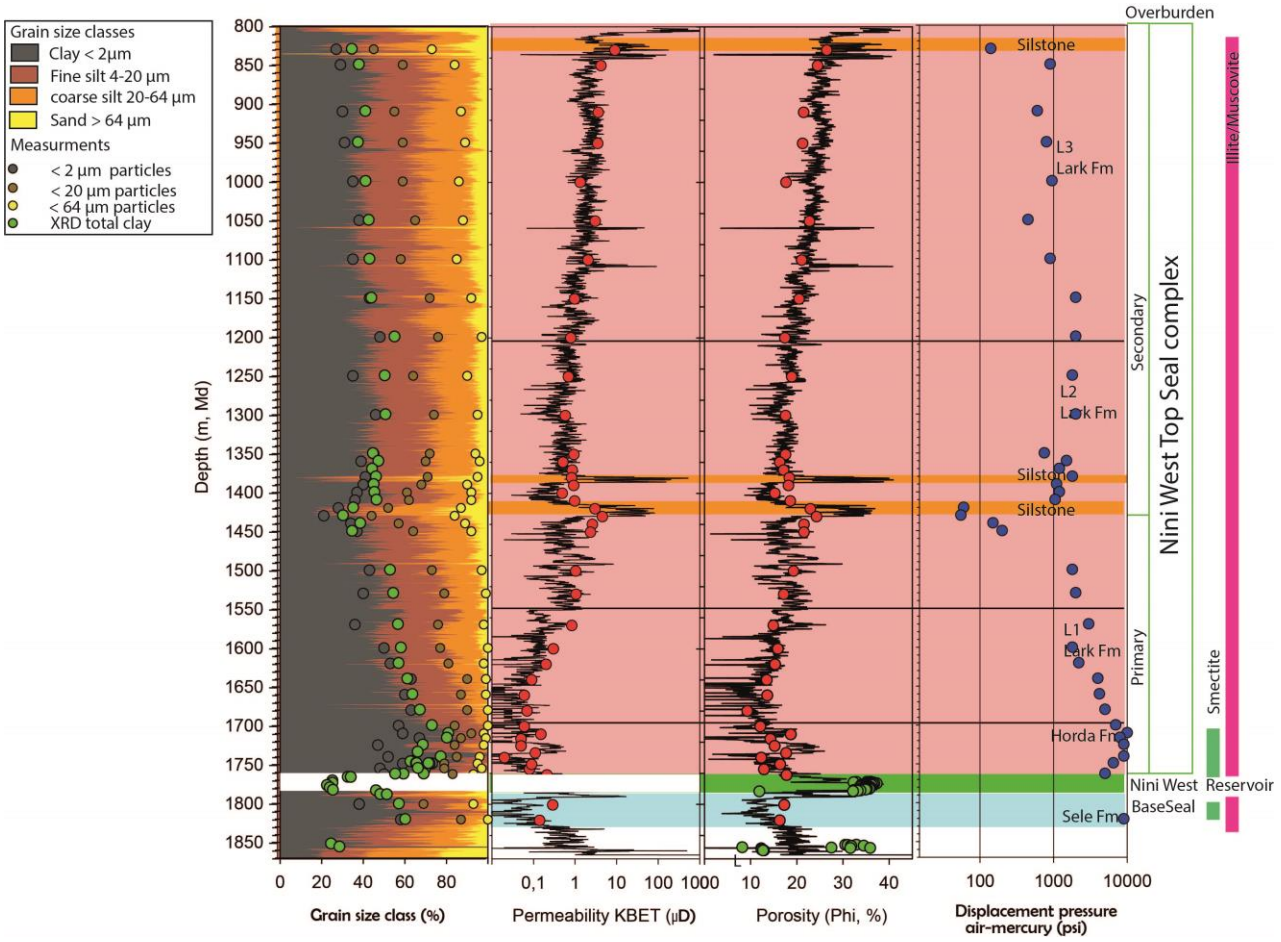

Figure 1A Summary of the petrophysical evaluation of the Nini West Seal Complex in the Nini-4 well.

The Nini West primary top seal, base and lateral seals were examined in Project Greensand Phase 1 (Schovsbo, 2020; Schovsbo et al., 2021; Petersen et al., 2022 – reprinted in Appendix G). The present study deals with the secondary seal based on 38 cuttings samples from the Nini-4, Nini-1, and Nini-2 wells. From the Nini-4 well 30 cuttings samples underwent an extensive analytical program that included determination of the elemental composition, mineralogy, grain size distribution, porosity, permeability, surface area, pore size structure distribution and Hg injection capillary pressure data (MICP). In addition, grain size distributions were studied in eight samples from the Nini-1 and Nini-2 wells. Digital rocks analysis were performed on selected cuttings representing coarse beds in all three wells.

Based on the analytical results, the petrophysical model for the Nini West Seal Complex (c.f. Petersen et al., 2022) has been updated and extended. A petrophysical workflow is described that includes algorithms for calculating Volume of clay (Vclay), Volume of fine silt, Volume of coarse silt, Volume of sand, Total Porosity (PHI), grain density, specific surface area (S_S), permeability following the Kozeny equation (K_{BET}) based on wire-line logs.

Mineralogical studies based on X-ray diffraction (XRD) and supplemented with thin section petrography shows that the secondary seal is quartz rich with illite and kaolinite as the dominating clay minerals. Minor amounts of K-feldspar and plagioclase, pyrite, siderite and calcite also occur. Three sandy siltstones beds occur between 1375–1425 m and 830–850 m. These have a high content of quartz, K-feldspar and plagioclase. The clay content has been evaluated from well logs calibrated with grain size data and XRD measurements. In the primary seal (lower Lark (L1) and part of mid Lark (L2), or 1400 – 1750 m), the volume of clay is generally above 60% and occasionally up to 80% (Figure 1A). In the Lark Fm, the volume of clay range between 20–40%. A relative high volume of clay (average clay content of 38%) has been measured in the secondary seal (part of L2 and upper Lark (L3)) between 1150–1400 m, which is higher than the over- and underlying Lark Fm that has an average of 24–27% clay. The high clay content is also reflected in the sand fraction where the 1150–1400 m interval on average has the lowest content (7%) compared to the overlying and underlying Lark Fm that has on average 14–16% sand.

The total porosity (PHI) increases from rather stable values around 20% in the basal part of the secondary seal to around 30% in the topmost parts of the secondary seal. This stratigraphical upward increase in porosity is very systematic and likely compaction driven reflecting the rather shallow burial of the topmost part of the secondary seal. Higher total porosities than in the mudstone are measured and modelled in the sandy siltstone beds than in the shale section (Figure 1A). The modelled total porosities range up to over 30%. This is higher than the measured cuttings, however, cuttings tend to be biased towards more cemented parts of the formation than uncemented parts that may tend to disintegrate and thus the measurements are expected to underestimate the real porosity.

Table 1 Summary of the petrophysical interpretation of the permeability and total porosity within the Nini West Seal Complex. K_{BET} is modelled from the surface area, total porosity, and grain density. P10, P50, P90 reflect different percentiles of the data assuming a log-normal distribution. Secondary seal includes porous beds.

Seal	K_{BET} Mean (arithmetic)	K_{BET} P10	K_{BET} P50	K_{BET} P90	Total Porosity Mean	Total Porosity P10	Total Porosity P50	Total Porosity P90
	µD	µD	µD	µD	%	%	%	%
Secondary	2.71	0.30	1.34	6.12	21.8	15.6	21.2	28.8
Primary	0.46	0.04	0.20	1.05	16.7	11.2	16.0	23.0
Base/lateral	0.43	0.03	0.18	0.97	15.8	11.9	15.5	20.1

Most of the mudstones in the secondary seal have broad unimodal pore throat size distributions and

most have pore throat sorting (PTS) index between 1.5–2.0 that characterises a medium sorted sediment. Compared to the primary seal then no samples in the secondary seal have mean hydraulic radius (MHR) less than 6–8 nm, that characterises a very fine grained and tight sediment. Four samples in the secondary seal have pore throats >100 nm. These are all sandy siltstones and have bimodal pore size distributions.

Average modelled permeabilities in the secondary seal is 2.7 µD with values ranging up to 6.1 µD (P90). This is higher than in the primary seal where average permeabilities are 0.46 µD with values ranging up to 1.05 µD (P90, Table 1, Figure 1A). Highest permeabilities are measured in sandy siltstone beds (Figure 1A). The higher permeabilities in the secondary seal is also reflected in the air-mercury displacement pressure that lies between 1000–9000 psi in the lower seal whereas it typical range around 1000 psi and as low as 100 psi in the upper seal (Figure 1A).

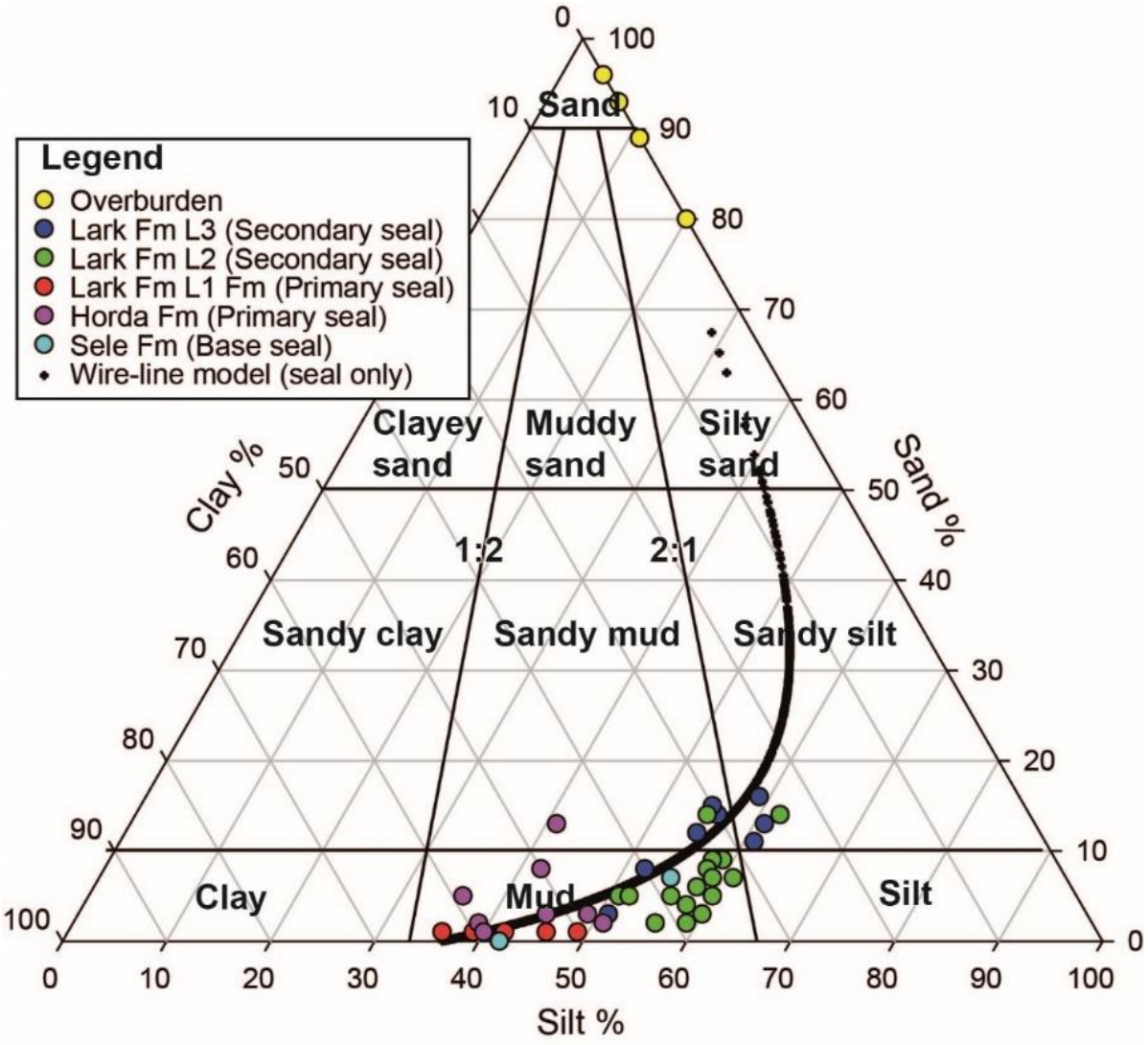

Figure 2B Summary of the rock type classification of cuttings samples in the Nini-4/4a, Nini-1 and Nini-2 wells. Rock type classification is after Folk et al. (1970). The wireline model trajectory is from the Nini-4 well.

The sealing capacity of the secondary seal is evaluated based on two different estimates for the dense CO_2 displacement pressure (P_{cd}) calculated assuming a depth of 1400 m and of 1200 m. These depths reflect hypothetical scenarios where supercritical CO_2 has accumulated at the base of the secondary seal or within the secondary seal. The capacity estimates are expressed as the maximum vertical column (H_{max}) of dense CO_2 that the caprock can withhold before displacement of the wetting brine phase in the caprock assuming that the caprock surface properties are affected by CO_2. For both depth scenarios we find that the secondary seal has a seal capacity of a CO_2 max column of more than 100 m (117–144 m). This should be seen in comparison with the possible maximum column heights in the secondary storage sites that presumably would be the sandy siltstone beds that has a maximum thickness of 10 m (Figure 1A), which leaves a reasonable caprock safety column overhead for CO_2 sequestration in the reservoir even for the most pessimistic scenario. The evaluation of the column heights should however be viewed here only tentative and should be evaluated in a full 3D model.

SUMMARY POROUS BEDS IN CAPROCK

Porous beds occur in the Lark Fm (Figure 1A). These were identified during drilling and described in the final well report (see Schovsbo, 2020 for a summary) and a target analytical program was carried out to describe them and to investigate if other porous beds occur in the seal section.

The occurrence of porous beds above the Nini West Frigg reservoir has been made with reference to the Nini-4 well and in selected samples in Nini-1 and Nini-2 based on well log correlations to Nini-4. In Nini-4, three sandy siltstones beds occur between 1375–1425 m and 830–850 m. The petrophysical model and cuttings samples show that the three beds consist of coarse grain particles and that the beds are porous (Figure 1A). Cuttings samples across the beds are classified as sandy siltstones (Figure 1B) and porosity can be seen in Micro CT scanning images and in thin sections. The log derived total porosity in these zones are estimated to exceed 30%, which is supported that are supported by measurements of up to 25% porosity from mercury injection on picked cuttings.

A vertical fining trend of the sandy siltstone beds from Nini-4 and towards Nini-1 and Nini-2 could be established based on eight samples analysed in Nini-1 and Nini-2. This grain size trend supports the log correlations that show that the beds are thinner towards Nini-1 and Nini-2.

Thin sections and SEM studied in Nini-4 show that the sandy siltstone intervals (cutting base depth 1420, 1430 and 1440 m – note that these are slightly offset to deeper levels according to log readings - contain grains that range from coarse silt to sand (30–140 µm) with average of approximately 80 µm, i.e. within the very fine sand fraction. Detrital grains in the sandy siltstone beds consist of mainly quartz and small amounts of K-feldspar, plagioclase, glauconitic clasts, mica, bioclasts, leucoxene, titanite and tourmaline. Common authigenic phases comprise siderite rhombs between cleavage planes of mica and in open pores, pyrite framboids and pore-filling calcite cement.

Digital rock analysis of the cuttings has provided estimates of texture, porosity, grain size distribution, capillary entry pressures and absolute permeabilities (See Appendix E for further details). CT-imaging show preserved mm-scaled primary structures. Permeabilities from digital rock analysis have an arithmetic mean of 193 mD and harmonic mean of 44 mD. It varies from a maximum of 675 mD to minimum of 4.8 mD, although lower values could be obtained near the extremities of the sandy siltstone laminations, where open intergranular pores become increasingly sparse. Average porosity of 23% lies below the true total porosity in the sandy siltstone laminations (see Table E1 in Appendix E). The in-plane permeability of the sandy siltstone laminations is 4-5 orders of magnitude greater than the range of 2.4–4.6 µD over 1410–1450 m estimated from the Kozeny equation using the measured BET surface area of the cuttings batches (see section on Specific surface and permeability models).

Permeability inferred from lab mercury intrusion via the Swanson equation lie in the range 26–231 μD over 1410–1450 m (see section on Mercury injection capillary pressure). This is still 3 orders of magnitude less than the average permeability and 1-2 orders above the minimum value there.

For upscaling of in-plane permeability of the sandy siltstone laminations to permeability of the sandy-bed/mudstone composite parallel to bedding, the above-mentioned arithmetic and harmonic means could be taken as local upper and lower bounds albeit with reductions for by cross-sectional area to account for tortuosity (See Appendix E for proposed workflows). Assuming such reductions the range in overall permeability parallel is roughly estimated to range between 10–50 mD.

SUMMARY OVERBURDEN

The overburden consists of the sequence from seabed and down to the top of the Lark Fm that in the Nini-4 is composed of the Nordland Group, including Nolde Sand. This section has only been logged with logging while drilling tools and as the section gave poor returns to surface not all cuttings intervals where available for sampling.

In total, five cuttings samples were analysed (200 m, 280 m, 380 m, 700 m and 740 m, measured depth below RT). All samples were composed of unconsolidated fine sand (see sieve analysis in Appendix A). The rock types in the overburden thus range according to Folk et al. (1970) between sand to silty sand (Figure 1B). Mineralogically the samples are composed of quartz (50–67%) with common K-feldspar (10–28%) and plagioclase (6–16%). Full mineralogical analysis is presented in Appendix F.

The analysis of this section indicate that no sealing beds occur and that the overburden should be considered porous and permeable.

INTRODUCTION

The purpose of the EUDP (Energy Technology Development and Demonstration Program) funded Project Greensand is to examine if Paleocene sands in the Siri Canyon can be utilized for safe long-term storage of CO_2. Here we report on the Phase 2 of the project that specifically tests the Nini West depleted oil reservoir as a potential CO_2 storage site. The report included data and interpretations made within the Work Package 3 termed Work Task 3.7 that characterised and test cuttings samples from the secondary seal in the laboratory at various conditions and thus contributes to the overall evaluation of the storage site feasibility.

The analytical workflow follows the work stream outlined during Project Greensand Phase 1. Samples are from the uppermost primary seal with main focus on the secondary seal whereas the focus on Greensand Phase 1 was only on the primary seal as reported by Schovsbo (2020), Holmslykke et al. (2021), Schovsbo et al. (2021) and Petersen et al. (2022). The work stream for both studies aims at examining the geological related seal parameters in as broad and multidisciplinary a framework as possible, however, evaluation of the seal is a multifaceted exercise since many parameters impact on seal capacity including also Wells and Operational Design and Practices (c.f. Bruno et al., 2014). These other aspects of the seal evaluation are dealt with in other parts of Project Greensand.

STRATIGRAPHY AND SAMPLING

A description of the geological setting, the lithostratigraphic units, and well correlations within the Nini West Seal Complex was prepared in Greensand Phase 1 (c.f. Schovsbo, 2020) and is briefly outlined here. The lithostratigraphy established for the Nini-4 well is based on the log stratigraphy for the North Sea outlined by Schiøler et al. (2007) (Figures 2–3). The seal in the Nini West area was divided into a primary and a secondary seal by Schovsbo (2020). The primary seal in the Nini West Field is in the Nini-4 well 340 m thick and composed of shales that belong to the Eocene to Miocene Horda Fm and the lower to mid Lark Fm (Figure 4). The Horda Fm is characterised by greenish grey to greyish green fissile mudstones. Subordinate limestone beds and thin layers of black mudstones occur at some levels in the formation. The lower Lark Fm is dominated by dark, greenish grey, non-fissile mudstones with subordinate intervals of brownish grey mudstones. The secondary seal in the Nini-4 well is 550 m thick and belongs to the mid to upper Lark Fm. This shale succession is composed of pale to dark brownish grey mudstones with subordinate intervals of greenish grey mudstones. The combined seal sequence is thus almost 900 m thick in the Nini West area. The above lying strata, i.e. the remaining c. 800 m, belongs to the Nolde Sand and the Nordland Group is considered as overburden (Figure 4).

In Project Greensand Phase 2, 30 samples were picked from the Nini-4 well to complement the sampling from the primary seal, the base seal, and the lateral seal (Sele Fm) in the Nini-4 and Nini 4a wells made as part of the Greensand phase 1 study (Figure 4, Table 2). The samples were all picked from the wet cuttings fraction within the depth interval from the seabed and to 1570 m i.e. to the top of the sampled intervals from the Greensand phase 1 sample suite. In addition, eight samples were picked from the Nini-1 and Nini-2 wells within the depth interval 1360–1410 m (Figure 5). Only grain size distributions were analysed in these samples to investigate if trends in grain size between Nini-4, Nini-1 and Nini-2 could be established for the sandy siltstone beds.

Cuttings samples have an inborn uncertainty with respect to representation of the actual depth interval either due to caving or from miscalculated depths. One way to evaluate the depth relationship is by comparing calculated API for the cuttings based on elemental determinations with wireline log measured API. By doing this we find a good match (see Figure 4) that indicates that most cuttings safely can be interpreted to represent the true depth interval. Exceptions are seen for some samples from the sandy siltstone beds. The bed with low API at 1375 m is not reflected in the API calculated on cuttings. For the low GR bed at around 1425 m then cuttings with similar lower API values is measured albeit towards a slightly deeper than expected from the GR log. This suggest that the low API content from the upper bed is not sampled and that the low API content from the lower bed have been sampled but in a broader depth range. For the other samples then the overburden sample at 400 m have a significant lower API to represent the actual depth level.

Concluding remarks

The Greensand phase 2 sampling complement the sampling made in phase 1 and together they represent a full characterisation of the Nini West Seal Complex (primary and secondary seal). In

addition, available samples from the overburden were investigated. The good match between calculated cuttings API and wireline log API values indicates that the cuttings generally represent the true depth interval. For the low API beds between 1375-1425 m then only the lower bed appears to have been sampled in the cuttings and this in a broader depth range than compared to the subsurface. One overburden sample have an API value that are all too low than compared to the wireline GR curve.

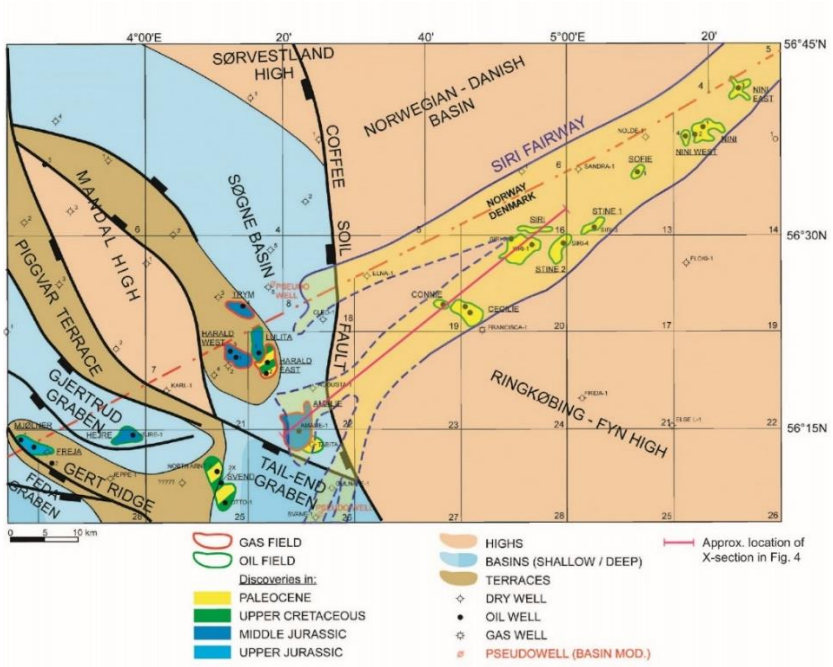

Figure 2 Siri Canyon with location of the Nini West Field and the Nini-4 well. From Ohm et al. (2006).

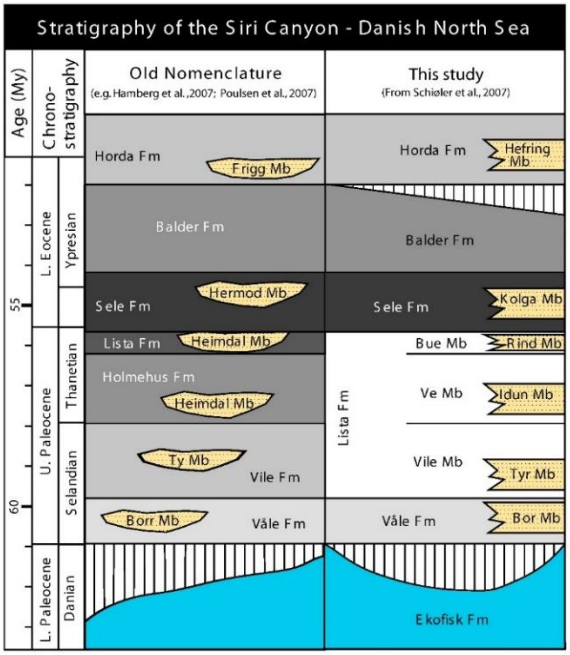

Figure 3 Stratigraphy of the reservoir and lowermost seal. The Nini West reservoir is the Frigg Sand Member that here is partly remobilised with the Hermod Sand Member.

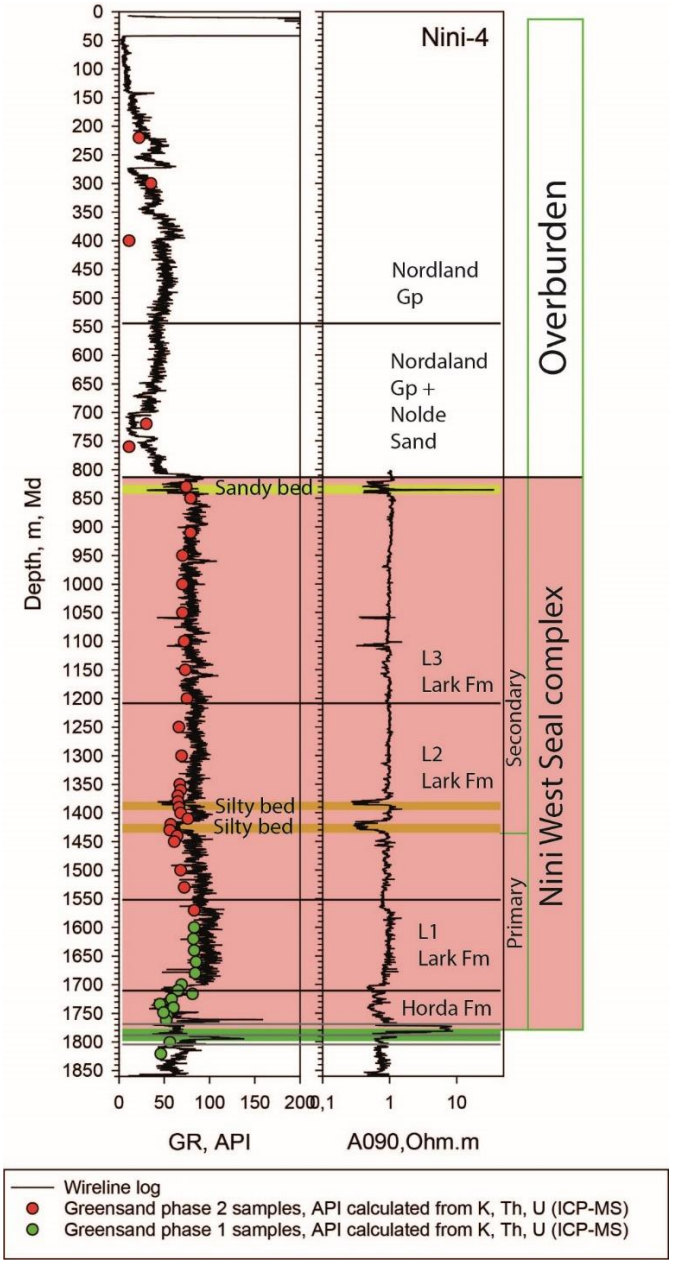

Figure 4 Seal and overburden units in the Nini-4 well. Stratigraphy is after Schiøler et al. (2007). The base seal below the Nini West reservoir (below Frigg sand marked with green box) is the Sele and Lista Fms (c.f. Figure 3). Sample position (base cuttings sample interval) of samples picked in the Nini-4 well are plotted with API calculated from K, Th, and U content. Note that the sample API calculation is not porosity corrected and thus not directly comparable to the GR curve, however, the good match between sample API and wireline log API values indicates that the cuttings represent the true depth interval.

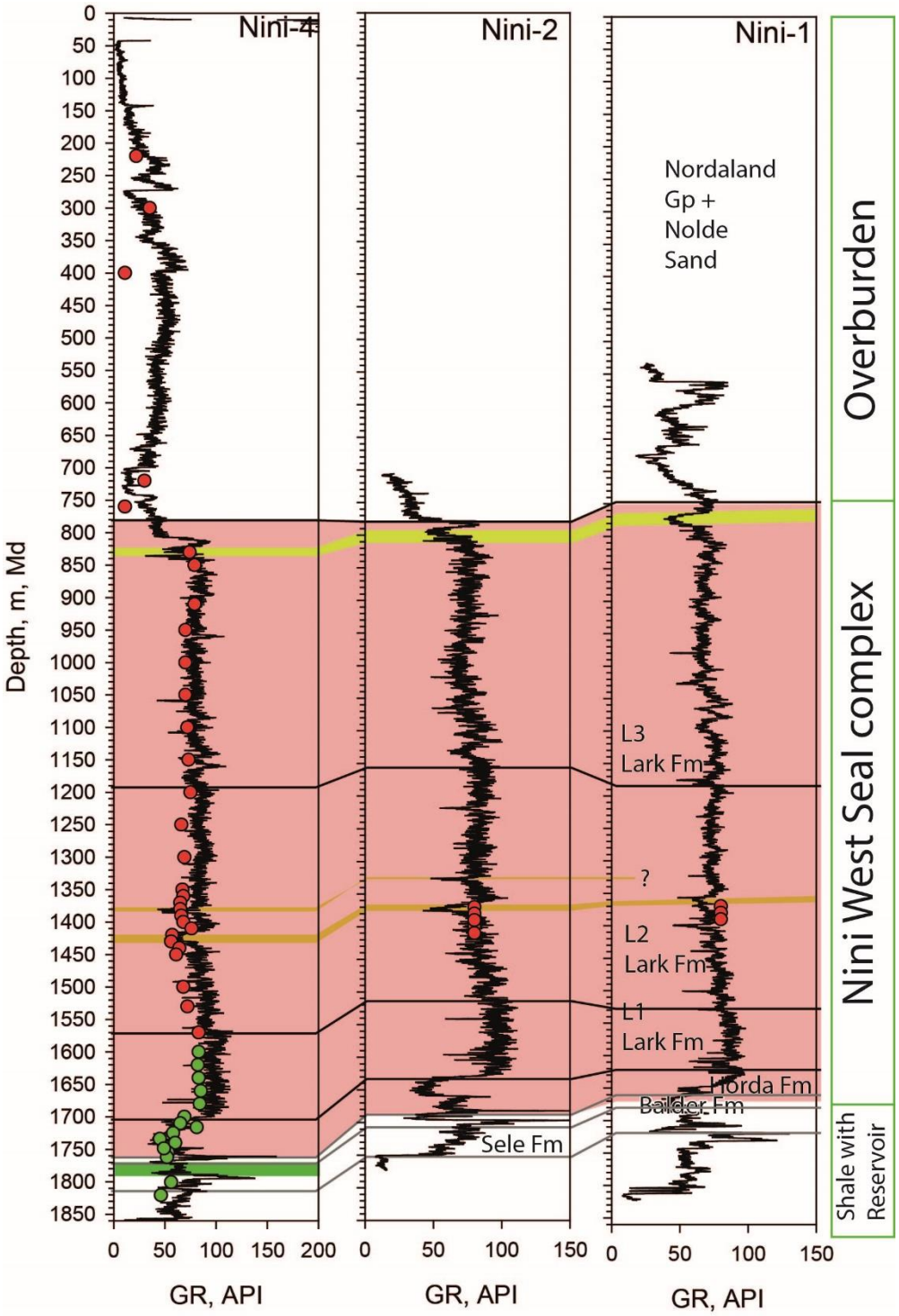

Figure 5 Sample depth plotted as the base of the cuttings sample interval in the Nini-4, Nini-2 and Nini-1 wells (red = Greensand phase 2 study (this study); green = Greensand phase 1 study (Schovsbo et al., 2021). The Nini-4 sample positions are shown with API calculated from K, Th, and U content. Sine determinations for K, Th, and U were not made for the Nini-2 and Nini-1 samples then these are shown with a fixed value of 80 API.

Table 2 Samples and lithostratigraphy for the Greensand phase 2 samples.

Laboratory number	Well	Depth top (m, md)	Depth base (m, md)	Formation	Material	Seal
46482	Nini-4	200	220	n.d.	wet cuttings	overburden -loose sand
46483	Nini-4	280	300	n.d.	wet cuttings	overburden -loose sand
46484	Nini-4	380	400	n.d.	wet cuttings	overburden -loose sand
46485	Nini-4	700	720	Nolde sand	wet cuttings	overburden -loose sand
46486	Nini-4	740	760	Nolde sand	wet cuttings	overburden -loose sand
46487	Nini-4	820	830	Lark	wet cuttings	Secondary
46488	Nini-4	840	850	Lark	wet cuttings	Secondary
46489	Nini-4	900	910	Lark	wet cuttings	Secondary
46490	Nini-4	940	950	Lark	wet cuttings	Secondary
46491	Nini-4	990	1000	Lark	wet cuttings	Secondary
46492	Nini-4	1040	1050	Lark	wet cuttings	Secondary
46493	Nini-4	1090	1100	Lark	wet cuttings	Secondary
46494	Nini-4	1140	1150	Lark	wet cuttings	Secondary
46495	Nini-4	1190	1200	Lark	wet cuttings	Secondary
46496	Nini-4	1240	1250	Lark	wet cuttings	Secondary
46497	Nini-4	1290	1300	Lark	wet cuttings	Secondary
46498	Nini-4	1340	1350	Lark	wet cuttings	Secondary
46499	Nini-4	1350	1360	Lark	wet cuttings	Secondary
46500	Nini-4	1360	1370	Lark	wet cuttings	Secondary
46501	Nini-4	1370	1380	Lark	wet cuttings	Secondary
46502	Nini-4	1380	1390	Lark	wet cuttings	Secondary
46503	Nini-4	1390	1400	Lark	wet cuttings	Secondary
46504	Nini-4	1400	1410	Lark	wet cuttings	Secondary
46505	Nini-4	1410	1420	Lark	wet cuttings	Secondary
46506	Nini-4	1420	1430	Lark	wet cuttings	Secondary
46507	Nini-4	1430	1440	Lark	wet cuttings	Secondary
46508	Nini-4	1440	1450	Lark	wet cuttings	Secondary
46509	Nini-4	1490	1500	Lark	wet cuttings	Secondary
46510	Nini-4	1520	1530	Lark	wet cuttings	Secondary
46511	Nini-4	1560	1570	Lark	wet cuttings	Secondary
46717	Nini-1	1360	1370	Lark	wet cuttings	Secondary
46718	Nini-1	1370	1380	Lark	wet cuttings	Secondary
46719	Nini-1	1380	1390	Lark	wet cuttings	Secondary
46720	Nini-1	1390	1400	Lark	wet cuttings	Secondary
46721	Nini-2	1360	1370	Lark	wet cuttings	Secondary
46722	Nini-2	1370	1380	Lark	wet cuttings	Secondary
46723	Nini-2	1380	1390	Lark	wet cuttings	Secondary
46724	Nini-2	1400	1410	Lark	wet cuttings	Secondary

CLEANING AND PREPARATION PROCEDURES

30 samples were picked from the wet cuttings fraction from the Nini-4 well and eight from the Nini-1 and Nini-2 wells. Each sample represent approximately 60-gram material and was cleaned with dichloromethane to remove oil-based drilling-mud contamination and then extracted in a soxhlet apparatus with dichloromethane and methanol solution (Table 2). The size fraction 1–4 mm was selected after sieving. For the overburden, the fraction larger than 0.250 mm was used. After cleaning, the sample was split into several aliquots and 20 grams was crushed to rock power.

Concluding remarks

The samples are all reactive towards demineralised water, tap water and water tuned to a composition alike reservoir formation brine (c.f. Olsen et al., 2020) and thus traditional washing of the cuttings was not possible. The cleaning procedure followed here only clean the cuttings in dichloromethane and methanol that effectively removed oil mud system and salt from the brine ensuring a near complete cleaning of the cuttings. We tested if washing of the cuttings after the first dichloromethane treatment with formation brine was possible to cleaning the cuttings more efficient, however, the results were mixed, and the procedure was not implemented. We recommend to further test the cleaning procedures in future sampling.

BATCH EXPERIMENTS

Batch experiments were not conducted to examine the reactivity of the secondary seal towards CO_2 as this was done on the lower seal during Project Greensand Phase 1 (Holmslykke et al., 2021). The reactivity of the primary seal after exposure of samples to CO_2 saturated brine for more than 4 months was limited and therefore the seal rock was judged to be chemically stable. Limited reactions were observed with heulandite-filled diatom frustules and siderite. These minerals occur much less abundant in the secondary seal and thus this section is regarded to be even less reactive towards reactions with CO_2 saturated brines than the primary seal.

PARTICLE SIZE DISTRIBUTION

Particle size distributions were determined at the Chemical department at GEUS following the ISO 17892-4:2016 standard (l).

Approximately 30 gram of uncrushed sample materiel was disintegrated in water. For clay size and fine silt determinations the hydrometer sedimentation method was used. Coarser size fractions were determined by sieving. For fine grain sizes the procedure is aligned with the sedimentation process of particles settling through a liquid, where the difference in settling rate allow the particle size classes to be determined by applying Stokes law. For the sand dominated overburden samples the grain sizes were only determined by sieving and confirmed by grain size measurements in thin sections.

Results

The full grain size analysis including determination of clay and fine silt was successfully completed for 33 samples as five samples were dominated by sand sized material and were only sieved (Table 3). Averages of the grain size distributions are presented in Table 4. More detailed results of the sieved samples are presented in Appendix A. All results are presented in Appendix F.

According to Folk et al. (1970) clay-, mud- and siltstones are characterised by <10% sand particles; claystones have >2:1 clay:silt ratio; mudstones between 2:1 and 1:2 clay:silt ratio and siltstones have higher than 1:2 clay:silt ratio. Following this classification, then the primary seal can be classified as composed of mudstones and the secondary seal as composed of mudstones to sandy mudstones with a few sandy siltstone beds (Table 3). Cuttings sample from the interval 1420–1430 m contains 16% sand particles and only 17% clay particles and is thus a sandy siltstone according to Folk et al. (1970). Likewise, a relative high sand content characterises the top 300 m of the secondary seal from 800–1100 m where the rock types are sandy mudstone to sandy siltstone as the sand content range between 11–28% and the clay content range between 20–30%.

The grain size in the Nini-2 and Nini-1 wells within the interval 1370–1410 m i.e. the correlatable interval of the zone where the porous sandy siltstone beds occur in the Nini-4 well (c.f. Figure 5) all but one classify as mudstones and thus have less coarse material than observed in the Nini-4 well (Table 3). Based on this we cannot confirm a coarsening trend towards the Nini-1 and Nini-2 wells from Nini-4 well. Instead, it appears that there exists a fining trend. This in corroborated from the well log correlation (Figure 5) where the GR log motif of the sandy siltstone beds identified in Nini-4 well appear tinner and less pronounced in Nini-1 and Nini-2 wells. However, we cannot exclude the possibility that the cuttings samples did not adequately represent the subsurface and thus that coarse beds exist in the wells.

Table 3 Results of particle size distribution analysis. For the overburden samples (220–760 m) the grain sizes were determined with sieves and no determinations below coarse silt were made. See Appendix A for all results.

Material	Well	Depth base (m, md)	Formation	Sand > 63 µm (%)	Coarse Silt 63-20 µm (%)	Fine Silt 20-2 µm (%)	Clay (< 2 µm) (%)	SUM	< 63 µm (%)	Clay+ Silt (<20 µm) (%)	Dry weight sample (g)	Weight of fraction > 63 µm (g)	Classification Folk et al.
cuttings	Nini-4	220	n.d.	89	11			100	11		30,20		Silty sand
cuttings	Nini-4	300	n.d.	80	20			100	20		31,14		Silty sand
cuttings	Nini-4	400	n.d.	96	4			100	4		30,47		Sandstone
cuttings	Nini-4	720	Nolde sand	89	11			100	11		31,16		Silty sand
cuttings	Nini-4	760	Nolde sand	93	7			100	7		31,12		Sandstone
cuttings	Nini-4	830	Lark Fm L3	28	35	18	20	100	72	37	30,44	8,39	Sandy siltstone
cuttings	Nini-4	850	Lark Fm L3	16	29	30	25	100	84	55	31,50	4,93	Sandy mudstone
cuttings	Nini-4	910	Lark Fm L3	13	36	25	26	100	87	51	31,54	4,16	Sandy siltstone
cuttings	Nini-4	950	Lark Fm L3	11	33	28	28	100	89	56	31,92	3,52	Sandy mudstone
cuttings	Nini-4	1000	Lark Fm L3	14	32	24	30	100	86	54	31,14	4,32	Sandy mudstone
cuttings	Nini-4	1050	Lark Fm L3	12	28	27	33	100	88	60	30,88	3,82	Sandy mudstone
cuttings	Nini-4	1100	Lark Fm L3	15	32	23	30	100	85	53	31,05	4,71	Sandy mudstone
cuttings	Nini-4	1150	Lark Fm L3	8	23	29	40	100	92	69	31,58	2,51	Mudstone
cuttings	Nini-4	1200	Lark Fm L3	3	22	28	46	100	97	75	30,72	0,91	Mudstone
cuttings	Nini-4	1250	Lark Fm L2	9	30	29	32	100	91	61	32,28	3,02	Mudstone
cuttings	Nini-4	1300	Lark Fm L2	5	23	28	44	100	95	72	31,48	1,51	Mudstone
cuttings	Nini-4	1350	Lark Fm L2	5	25	27	43	100	95	70	30,81	1,62	Mudstone
cuttings	Nini-4	1360	Lark Fm L2	4	27	31	38	100	96	69	31,43	1,18	Mudstone
cuttings	Nini-4	1370	Lark Fm L2	8	30	24	37	100	92	62	32,77	2,70	Mudstone
cuttings	Nini-4	1380	Lark Fm L2	5	26	30	39	100	95	69	32,50	1,64	Mudstone
cuttings	Nini-4	1390	Lark Fm L2	9	26	28	36	100	91	65	31,57	2,98	Mudstone
cuttings	Nini-4	1400	Lark Fm L2	9	34	24	33	100	91	57	33,16	3,00	Mudstone
cuttings	Nini-4	1410	Lark Fm L2	9	33	26	33	100	91	59	31,18	2,70	Mudstone
cuttings	Nini-4	1420	Lark Fm L2	14	38	24	24	100	86	48	33,00	4,59	Sandy siltstone
cuttings	Nini-4	1430	Lark Fm L2	16	43	23	17	100	84	40	31,78	5,15	Sandy siltstone
cuttings	Nini-4	1440	Lark Fm L2	11	35	23	30	100	89	54	30,61	3,37	Sandy mudstone
cuttings	Nini-4	1450	Lark Fm L2	8	31	27	34	100	92	61	32,58	2,68	Mudstone
cuttings	Nini-4	1500	Lark Fm L2	2	25	30	42	100	98	73	29,89	0,62	Mudstone
cuttings	Nini-4	1530	Lark Fm L2	2	21	39	39	100	98	78	31,23	0,52	Mudstone
cuttings	Nini-4	1570	Lark Fm L1	2	22	40	35	100	98	75	30,49	0,72	Mudstone
cuttings	Nini-4	1600	Lark Fm L1	1	23	27	50	100	99	76	30,09	0,25	Mudstone
cuttings	Nini-4	1620	Lark Fm L1	1	17	28	53	100	99	82	28,15	0,28	Mudstone
cuttings	Nini-4	1640	Lark Fm L1	1	9	27	63	100	99	90	30,00	0,23	Mudstone
cuttings	Nini-4	1660	Lark Fm L1	1	12	27	60	100	99	87	30,01	0,34	Mudstone
cuttings	Nini-4	1680	Lark Fm L1	1	10	27	63	100	99	90	30,02	0,16	Mudstone
cuttings	Nini-4	1700	Lark Fm L1 -Horda	1	16	27	57	100	99	83	29,98	0,32	Mudstone
cuttings	Nini-4	1710	Horda	2	6	33	59	100	98	92	27,2	0,5	Mudstone
cuttings	Nini-4	1716	Horda	2	12	20	67	100	98	87	30,02	0,54	Mudstone
cuttings	Nini-4	1725	Horda	2	14	37	47	100	98	83	29,98	0,65	Mudstone
cuttings	Nini-4	1734	Horda	n.d.									
cuttings	Nini-4	1740	Horda	3	11	33	52	100	97	86	26,87	0,82	Mudstone
cuttings	Nini-4	1755	Horda	3	18	31	48	100	97	79	29,95	0,80	Mudstone
core	Nini-4	1762,27	Horda	8	10	33	50	100	92	83	30,23	2,32	Mudstone
core	Nini-4	1748,65	Horda	5	16	20	59	100	95	79	30,35	1,40	Mudstone
core	Nini-4a	1910,37	Horda	13	17	24	46	100	87	70	24,12	3,06	Sandy mudstone
core	Nini-4a	1915,46	Horda	4	17	26	53	100	96	79	29,58	1,23	Mudstone
core	Nini-4a	1902,72	Horda	1	15	25	59	100	99	84	30,23	0,42	Mudstone
core	Nini-4a	1955,56	Horda	85	n.d.				15		30,54	25,88	
core	Nini-4	1800,76	Sele	7	24	31	38	100	93	69	30,11	2,14	Mudstone
core	Nini-4	1820,79	Sele	0	13	29	58	100	100	87	28,51	0,01	Mudstone
cuttings	Nini-1	1370	Lark	14	36	19	31	100	86	58	30,35	4,20	Sandy mudstone
cuttings	Nini-1	1380	Lark	6	39	19	36	100	94	59	30,07	1,86	Mudstone
cuttings	Nini-1	1390	Lark	7	39	20	34	100	93	59	29,95	2,05	Mudstone
cuttings	Nini-1	1400	Lark	3	37	23	37	100	97	62	30,06	0,94	Mudstone
cuttings	Nini-2	1370	Lark	5	36	27	32	100	95	62	30,15	1,62	Mudstone
cuttings	Nini-2	1380	Lark	7	36	24	32	100	93	61	30,25	2,16	Mudstone
cuttings	Nini-2	1390	Lark	5	36	25	34	100	95	62	29,82	1,40	Mudstone
cuttings	Nini-2	1410	Lark	5	34	26	35	100	95	64	30,17	1,54	Mudstone

Table 4 Average grain sizes for overburden, secondary and primary seal.

	Sand > 63 µm (%)	Coarse Silt 63-20 µm (%)	Fine Silt 20–2 µm (%)	Clay (< 2 µm) (%)
Overburden 200–800 m	90	10	0	0
Secondary seal 830–1100 m	16	32	25	27
Secondary seal 1150–1400 m	7	27	28	38
Secondary seal 1400–1450 m	14	39	23	24
Primary seal 1450–1850 m	3	16	29	52

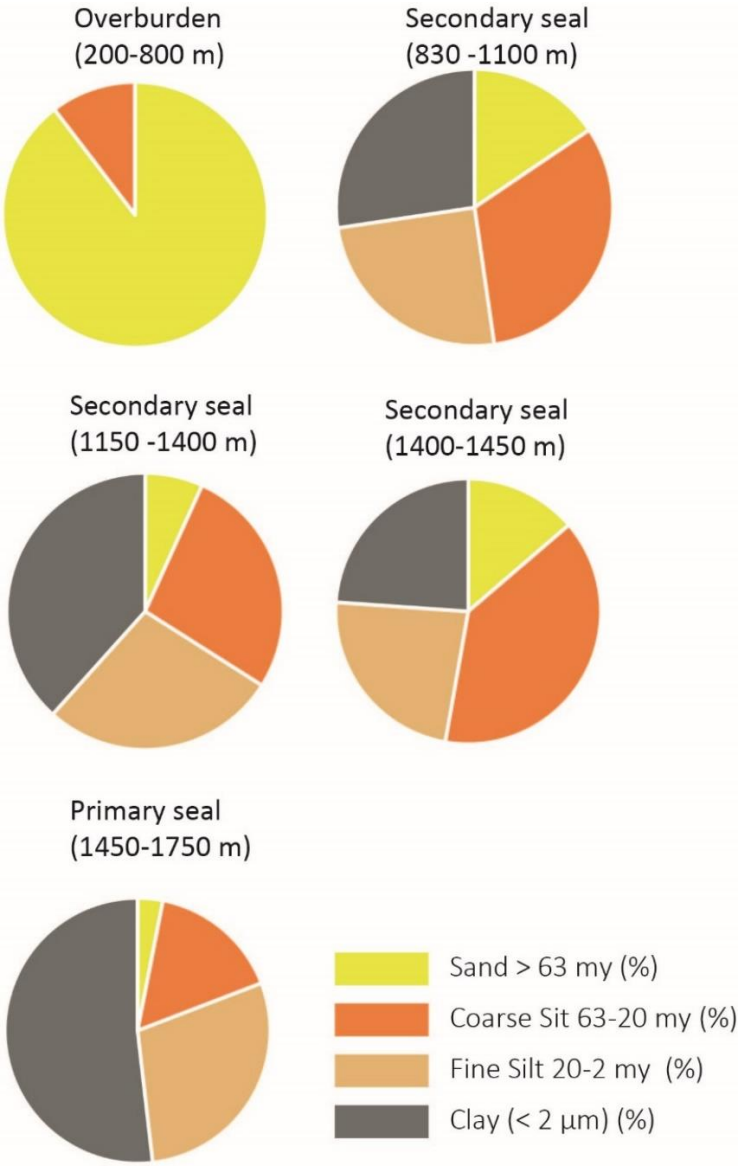

Figure 6 Grain size distribution of the primary seal (Horda Fm and lower to mid Lark Fm) and the secondary seal (mid to upper Lark Fm). Results are presented in Table 4.

Coarse particles

Coarse-grained fractions separated during grain size analyse were examined under microscope (Figure 11). The coarse-grained fraction consists dominantly of single grains with a minor component of cemented grain aggregates (Figure 11). The aggregates both reflect cemented parts with a muddy matrix and cemented parts with a coarser matrix. Based on this it is likely that the grain size fractions represent true single grain size distribution albeit with a tendency to overestimate the coarser grain sizes.

The coarser particles separated from the particle size determinations in the secondary seal are clearly detrital grains. This is contrary to what was observed in the Horda Fm were the coarse-grained particles mostly were diagenetic formed minerals such as heulandite that precipitated in the sand size as replacements of bioclasts or as silt size crystals within the matrix (Schovsbo et al., 2021).

The distribution of coarser grains in the secondary seal varies. Within the interval 1420–1440 m the cuttings classify as sandy siltstones to sandy mudstones and have visible porosity (Table 3, Figure 11). Such rock type can also be seen in the top part of the secondary seal i.e. at 830 m. Trends and heterogeneities in the grain packing can also be seen in some cuttings samples (c.f. 1450 m, Figure 11) that appear composed of alternating silt and fine sand laminae.

The cuttings sample depths are given as base of cuttings interval and compared to the wireline log response there is an offset in a low GR log response and the presence of coarser grains in the cuttings. Coarser grains thus appear in the cuttings at deeper level and in a broader interval. This suggest that the rock response is smeared out as compared to the subsurface. However, the good comparison between cuttings API and GR log API (c.f. Figure 4) suggested that cuttings generally are on par with the actual depth.

The secondary seal in the interval 1150–1400 m - largely the upper L2 unit - has on average the highest clay content 38% compared to the overlying and underlying Lark Fm that has 24–27% clay. This difference in clay content is also reflected in the less abundant sand fraction where the 1150–1400 m interval on average has 7% sand and the overlying and underlying Lark Fm has 14–16% sand (Figure 6, Table 4). For a sealing perspective both the relative proportion of notable clay size particles and the texture matters. Both in the top part of the primary seal (1530–1570 m) and within parts of the secondary seal rocks, coarse grains are seen to lie isolated within a clay matrix. The effect here will have neglectable effect on the permeability since the pore space between coarse grains are limited and/or is not connected. In the topmost part of the secondary seal the rock type change to sandy mudstones to sandy siltstones with fine lamination (Table 3, Figure 11). Such changes are likely cause permeability to increase and thus to lower the sealing capacity as grain supported rock types typical have very limited seal capacity.

See also the XRD and Petrology Section for analysis of thin sections and the section on MICP experiments**.**

Grain size relationships

The relationships between grain size classes are presented in Figure 7. For fine and coarse silt fractions there appear to be a good relation to clay size given with the two equations for fine silt and for coarse silt (shown in Figure 7):

$$\text{Less than 20 µm (\%)} = 193 \cdot \text{Vclay (\%)} / (16.4 + \text{Vclay (\%)}) \quad (1)$$

$$\text{Less than 63 µm (\%)} = 111 \cdot \text{Vclay (\%)} / (2.25 + \text{Vclay(\%)}) \quad (2)$$

For these equations to be valid then the samples should belong to the same overall depositional environment and all particles should be detrital. In Nini West the depositional system is deep marine with distal turbidites delivering coarser particles. We know that not all particles are detrital- especially at high clay content were diagenetic grains are present such as in the Horda Fm. Also, some grains are cemented, which will lead to over estimation of the sizes.

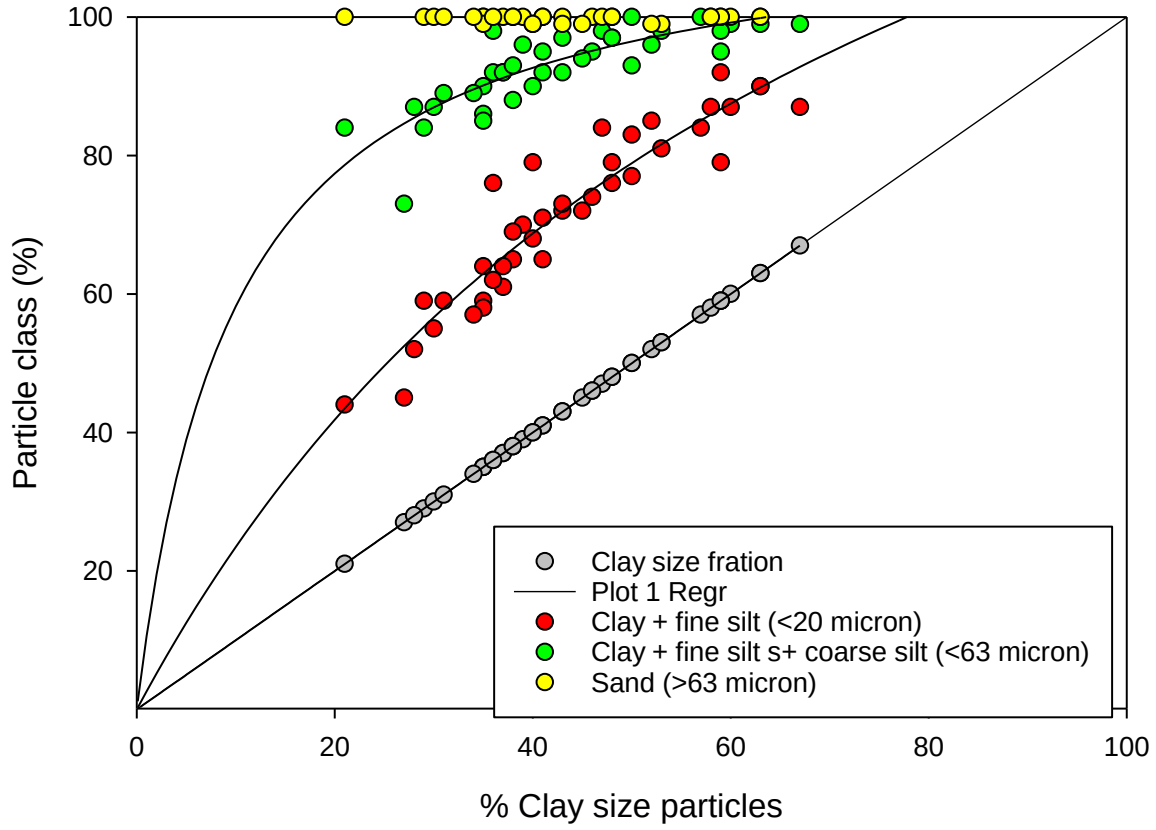

Figure 7 Relationship between clay size particles and fine and coarse silt. Regression lines represent the hyperbolic formula f (x) = ax/(b + x).

Concluding remarks

The primary seal can be classified as composed of mudstones (>33% clay) and the secondary seal as composed of a mixture of mudstones, sandy mudstones and sandy siltstones. Cuttings sample from the interval 1420–1430 m contains 16% sand particles and only 17% clay particles and classify as sandy siltstone. Correlatable intervals in Nini-1 and -2 wells all classify as mudstones and thus have less coarse material than observed in the Nini-4 well. This in corroborated from the well log correlation (Figure 5) where the low GR motif of the sandy siltstone beds identified in the Nini-4 well are less pronounced in Nini-1 and Nini-2 wells. The secondary seal interval 1150–1400 m - largely the upper L2 unit - has on average highest clay content 38% compared to the overlying and underlying Lark Fm that contain 24–27% clay. This difference in clay content is also reflected in the sand fraction where the 1150–1400 m interval on average has 7% sand and the overlying and underlying Lark has 14–16% sand. This mid interval is thus suspected to have the highest sealing capacity within the secondary seal.

DIGITAL ROCK ANALYSIS

Four samples from the Nini-4 and two samples from Nini-2 and Nini-1 wells were sent to Wintershall Dea (WD) for digital rock analysis. All samples contain cuttings that were selected under microscope to represent the coarsest pieces from the interval were the sandy siltstone beds occur. The Nini-4 samples were the only well that had cuttings that could be imaged as samples from the Nini-2 and Nini-1 wells did not contain grains that were coarse enough (Figures 8 and 9). Full reporting is presented in Appendix E.

The cuttings samples from the Nini-4 well were: 1410–1420 m; 1420–1430 m; 1430–1440 m; 1440–1450 m. At WD, the cuttings were sieved to >1 mm. All particles in each depth interval were then poured into a glass tube holder with a 7.5 mm inner diameter for quick low-resolution micro-CT scanning. The central vertical slices of the 3D images of the cuttings stacks. From these scans, particles identified as likely having sandy/silty internal structure of interest were selected and combined across the 4 depths and presented in Figure 8. Barite was removed from these selected particles by razor blade, to improve image quality. Selected particles were stacked in glass tube holder of 5.6 mm inner diameter for quick higher-resolution micro-CT scanning.

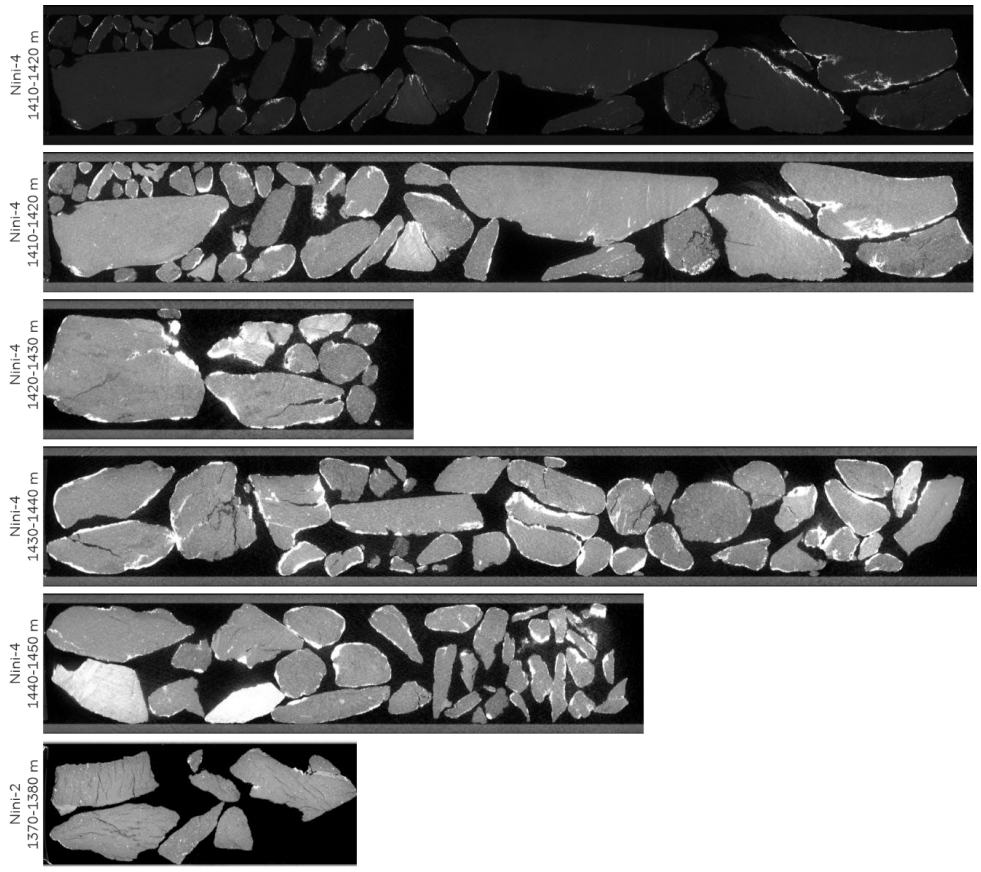

Figure 8 Micro CT-images of cuttings from interval 1370–1450 m. Picture curtsey Andrew Fogden, WD. See Appendix E for details.

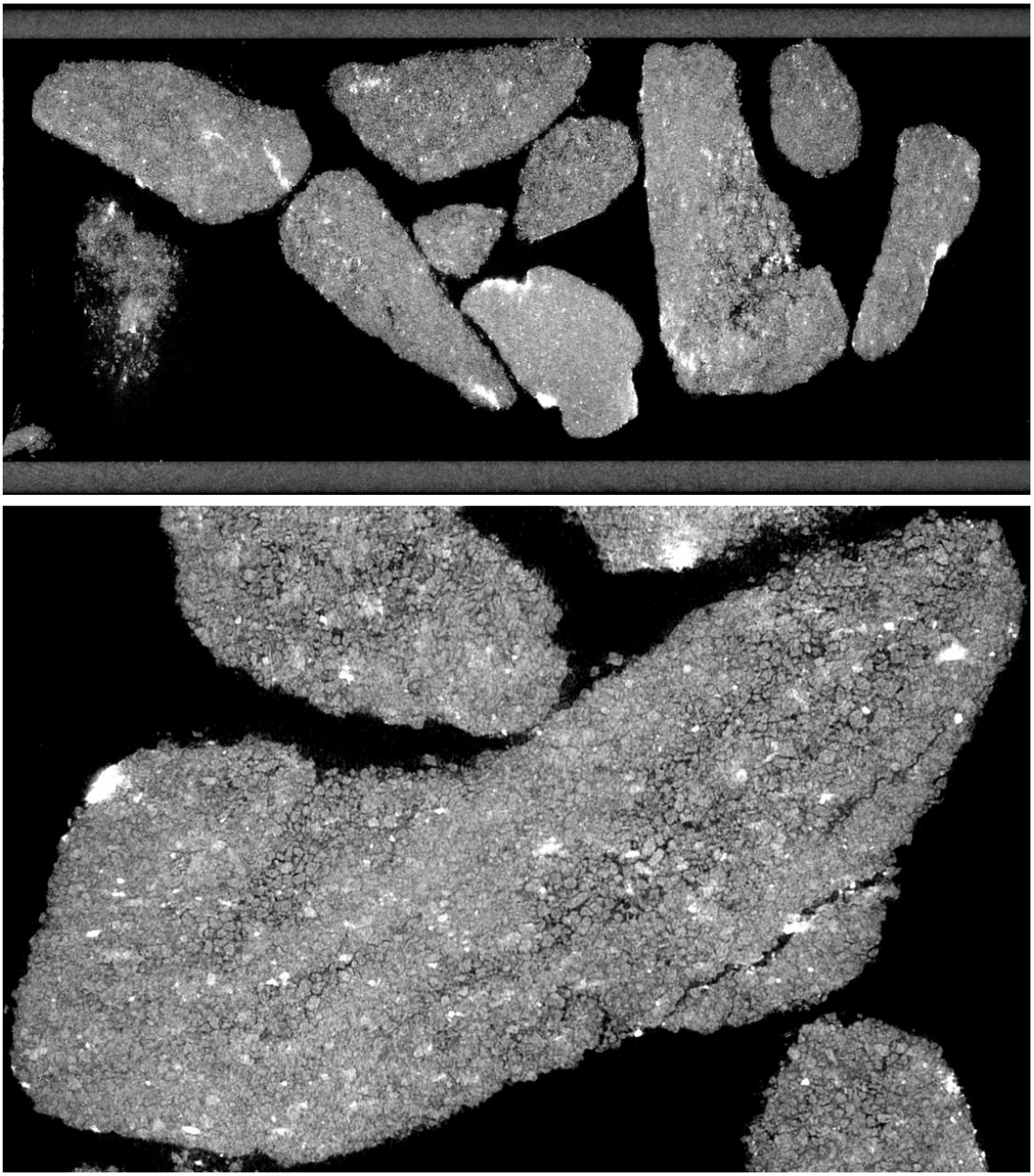

Figure 9 Close-up of cuttings presented in Figure 8. Picture curtsey Andrew Fogden, WD. See Appendix E for details.

From the CT-images it is clear that the clayey siltstone/sandstone structures are preserved, at least on the mm scale. There were also many larger weighting particles (mainly barite) from the drilling mud that form a cake on the cuttings piece exteriors, but most of this was quite easily removed. Some infiltration of finer particles from the drilling mud into the rock structures is suspected to have occurred, but this will be almost negligible since the rock is too tight to allow these finer particles to penetrate beyond the outermost pore.

Concluding remarks

CT-images of selected coarse cuttings from the sandy siltstone beds show preserved mm-scaled primary structures. Digital rock analysis of the cuttings has provided estimates of texture, porosity, grain size distribution, capillary entry pressures and absolute permeabilities (See Appendix E for further details).

Permeabilities from digital rock analysis have an arithmetic mean of 193 mD and harmonic mean of 44 mD. It varies from a maximum of 675 mD to minimum of 4.8 mD, although lower values could be obtained near the extremities of the sandy siltstone laminations, where open intergranular pores become increasingly sparse. Average porosity of 23% lies below the true total porosity in the sandy siltstone laminations (see Table E1 in Appendix E). The in-plane permeability of the sandy siltstone laminations is 4–5 orders of magnitude greater than the range of 2.4–4.6 μD over 1410–1450 m estimated from the Kozeny equation using the measured BET surface area of the cuttings batches (see section on Specific surface and permeability models).

Permeability inferred from lab mercury intrusion via the Swanson equation lie in the range 26–231 μD over 1410–1450 m (see section on Mercury injection capillary pressure). This is still 3 orders of magnitude less than the average permeability and 1–2 orders above the minimum value there.

For upscaling of in-plane permeability of the sandy siltstone laminations to permeability of the sandy-bed/mudstone composite parallel to bedding, the above-mentioned arithmetic and harmonic means could be taken as local upper and lower bounds albeit with reductions for by cross-sectional area to account for tortuosity (See Appendix E for proposed workflows). Assuming such reductions the range in overall permeability parallel is roughly estimated to range between 10–50 mD.

BULK AND CLAY MINERALOGY AND PETROGRAPHY

Bulk rock and clay mineralogy of the samples were obtained from X-ray diffraction (XRD) performed by a Panalytical-X-Pert Pro at DTU. Bulk rock samples were crushed in steel mortar and mounted in disks with random orientation. Orientated samples were prepared by suspending 0.03 g of the clay fraction into 1.5 ml distilled water and evenly spread on a glass plate. The orientated samples were analysed untreated, ethylene glycol saturated for two days at 60 °C and heated for two hours at 350 °C and 550 °C. Semi-quantification was performed by multiplying peak height with correction factors similar to the method by Hillier (2003).

Results

Composition of the seal and overburden, based on XRD, is presented in Figure 10. The Sele Fm has relatively high contents of illite (≈40%) and quartz (34–37%) besides minor amounts (< 4%) of K-feldspar, plagioclase, pyrite, kaolinite, smectite and occasionally zeolites (heulandite). The Horda Fm is characterized by a relatively high content of smectite (typically > 30%) besides common illite (9–40%). The lower part of the Horda Fm has common zeolites (heulandite), whereas the central part has more common cristobalite (Figure 10). Kaolinite, quartz, plagioclase, siderite and pyrite are present in minor amounts in most of the Horda Fm. The mineralogical composition of the Sele and Horda Fms have previously been reported (Schovsbo et al., 2021; Petersen et al., 2022).

The lowermost part of Lark Fm, L1, is characterized by abundant illite (33–40%), quartz (28–40%) and kaolinite (9–18%). Quartz generally increases upwards in L1, whereas kaolin decreases. Chlorite is commonly present in the L1 interval, although only in small amounts. Pyrite, siderite and calcite occur in small amounts in most samples. The middle part of Lark Fm, L2, is generally quartz rich and with relatively common illite and kaolinite. K-feldspar and plagioclase, pyrite, siderite and calcite are present in all samples. The sandy intervals mainly have a high content of quartz, K-feldspar and plagioclase. The combined clay (mainly illite and kaolinite) content gradually increases from 23% at 1450 m in Lark L2 to 47% at 1200 m in Lark L3 (Figure 10). The uppermost part of Lark Fm, L3, is also characterized by abundant quartz (upward increasing) and with relatively common illite and kaolinite. K-feldspar, plagioclase, pyrite and calcite are present in most samples, whereas siderite is relatively rare.

The remaining part of the Nordland Group, including Nolde Sand, is rich in quartz (50–67%) and with common K-feldspar (10–28%) and plagioclase (6–16%). An unknow mineral with a peak at 8.43Å, possibly wavellite or a zeolite, have been identified in the two uppermost samples. Further analysis by thin section is required to confirm the interpretation.

Assumed artefacts, such as barite (> 5%), gypsum (< 2%) and halite (< 6%), have been removed from the XRD plot presented in Figure 10. These minerals are likely to origin from drilling mud, fluids or precipitation of formation water in the cuttings samples. Although most barite origins from drilling mud surrounding the cuttings fragments, authigenic barite has been identified as a rare authigenic phase (see Petrography section). Barite rims were also identified from digital rock analysis.

Petrography of the cuttings and coarse-grained fraction separated from grain size analysis

Wet cuttings samples were washed and the 1–4 mm fraction was used for thin sections. Grain concentrates were prepared by washing wet cuttings samples on a 63 µm sieve. Ultra-thin (10 µm) polished thin sections were prepared from blue epoxy impregnated grain concentrates in addition to washed and dried cuttings samples. The thin sections were investigated by transmitted and reflected light microscope and supplemented by scanning electron microscopy (SEM) of carbon-coated thin sections using a Zeiss Sigma 300 VP operating at 10–15 kV equipped with double Bruker energy dispersive X-ray spectrometers (EDS) with 30 mm^2 active areas. Grain sizes were obtained for specific samples by measuring the long axis of minimum 50 grains in the grain concentrates.

An overview of cuttings samples and grain concentrates from the Lark Fm is presented in Figure 11. Mudstone (according to Folk et al., 1970) is the most common lithology of both the primary and secondary seal (Table 3). Sandy mudstone in the primary seal and sandy mudstone and sandy siltstone in the secondary seal occur also. Quartz makes up most of the sand and silt sized grains. Glauconitic clasts, feldspar grains and bioclasts, either pyritized or calcareous, are common components also.

The lowermost part of Lark Fm, L1, consists mainly of micaceous mudclasts, which can be glauconitic, rare carbonate-cemented siltstones, rare pyritized mudclasts and possibly diatomite (Figure 12). The composition of L1 is available only from one thin section of cuttings samples and one grain concentrate (NI4-1570cu, NI4-1570gr). Detrital grains consist of quartz, plagioclase, K-feldspar, glauconitic clasts, bioclasts, mica and rutile. Authigenic phases comprise siderite preferentially between cleavage planes of mica and pyrite as framboids or replacement/filling of bioclasts (Figure 12).

The uppermost part of Lark Fm, L2, varies in composition from mainly micaceous mudstones to glauconitic silt- to very fine sandy siltstones. Calcareous mudstones are occasional present. The sandy siltstone intervals (1420, 1430 and 1440 m) contain grains of the sizes ranging from coarse silt to sand 30–140 µm with average of approximately 80 µm, which is very fine sand. Detrital grains in sandy siltstones consist of mainly quartz and small amounts of K-feldspar, plagioclase, glauconitic clasts, mica, bioclasts, leucoxene, titanite and tourmaline. Common authigenic phases in the siltstones and very fine sandstones comprise siderite rhombs between cleavage planes of mica and in open pores, pyrite framboids and pore-filling calcite cement (Figure 13). Apatite cemented areas occasionally occurs in mudstones. Zeolite, possibly heulandite, occurs as pore-filling cement and in oversized pores, some of which clearly remnants after bioclasts (Figure 13). Rare authigenic phases include K-feldspar overgrowths, anatase, barite and kaolinite, the latter occurring both as replacement of muscovite and as very fine crystals forming a pore-filling cement. Barite is a rare authigenic phase enclosed in heulandite filling of bioclast, contrary to the much more common barite occurring in drilling mud encircling the cuttings fragments.

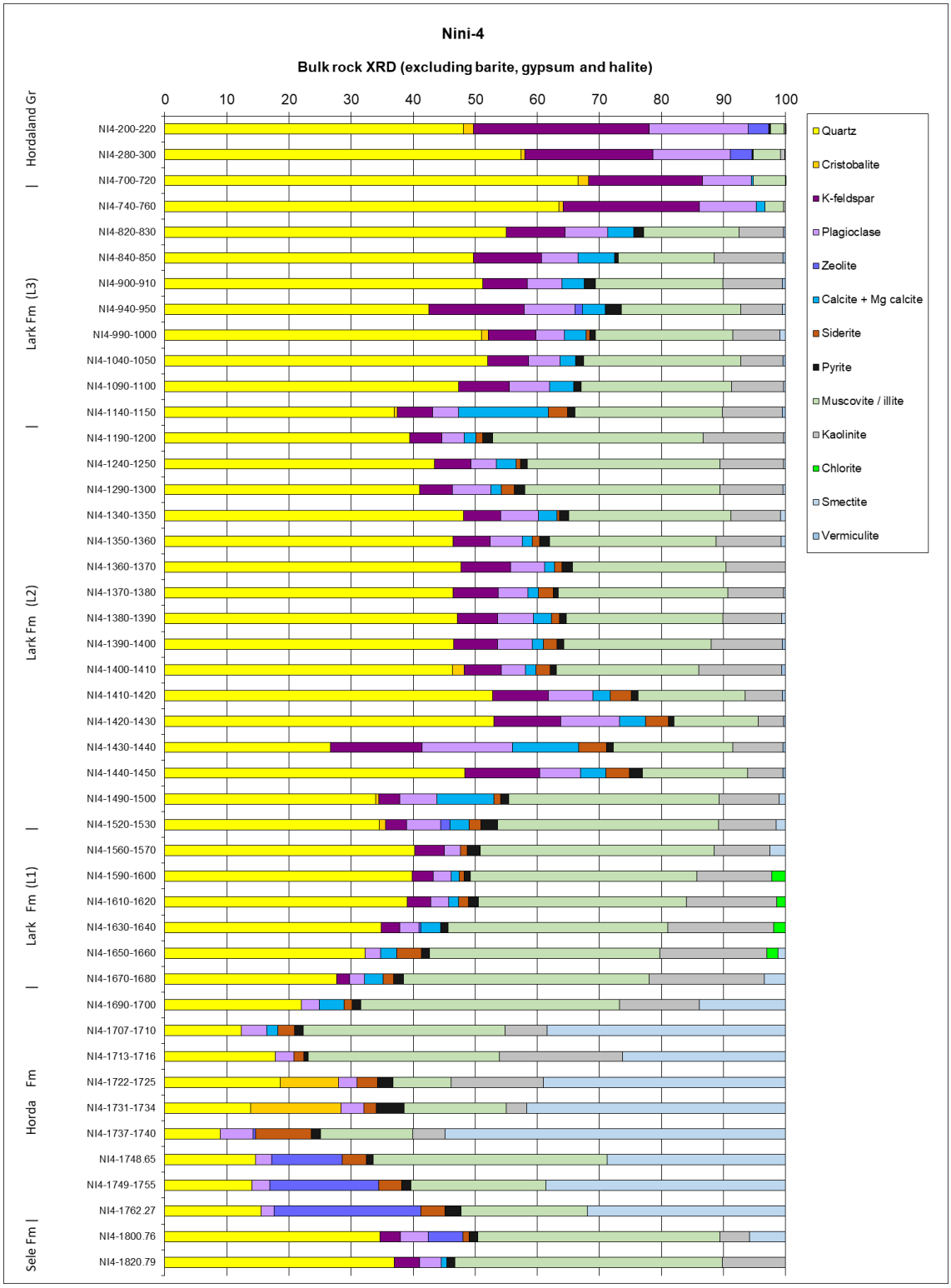

Figure 10 Bulk rock mineralogy based on XRD of bulk and clay fraction. Barite, gypsum and halite have been removed from the plot since they mainly origin from drilling mud/fluids. Depths are presented as intervals for cuttings samples, and with exact depths for core samples.

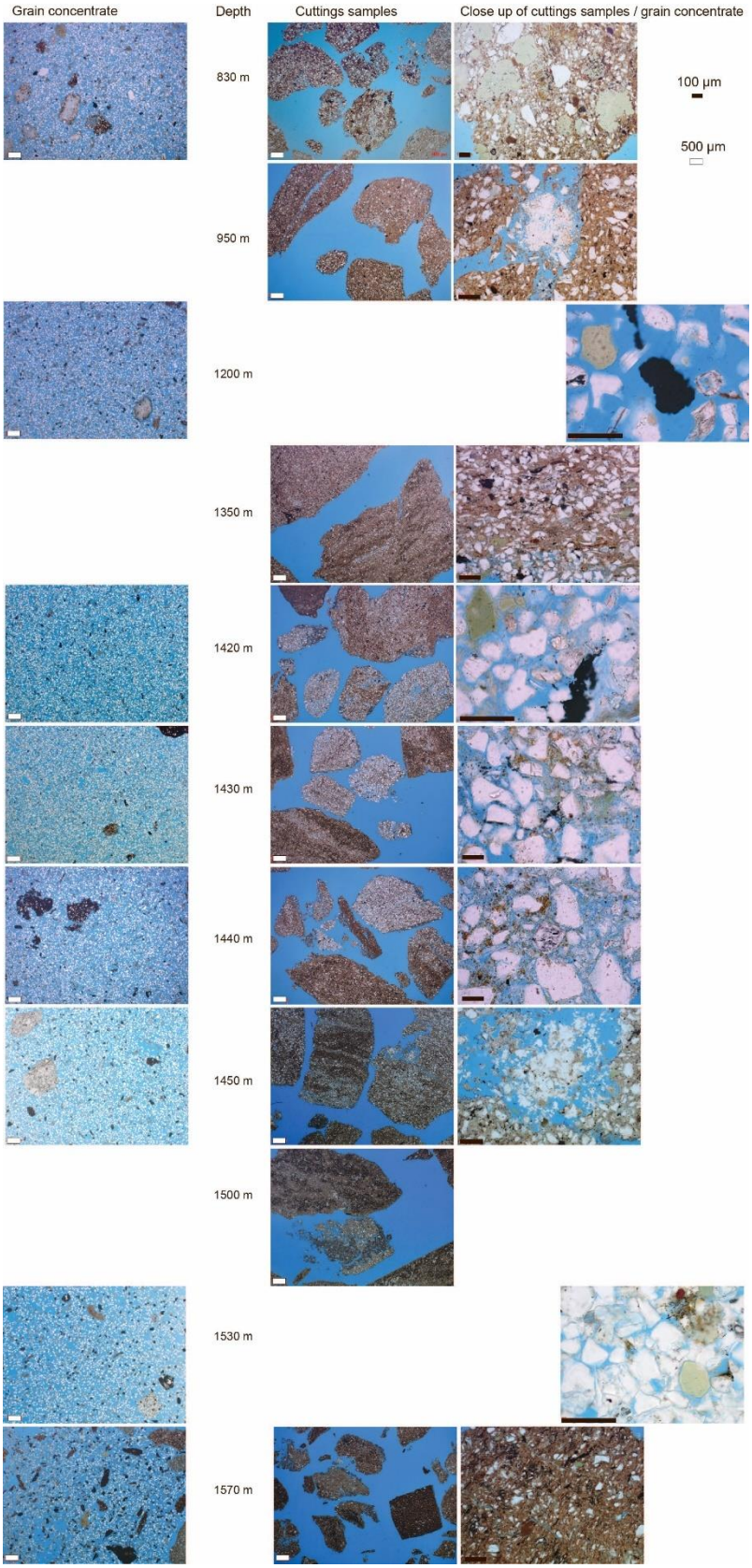

Figure 11 Overview photos of cuttings samples and grain concentrates. Bar scale in white is 500 µm and in black 100 µm.

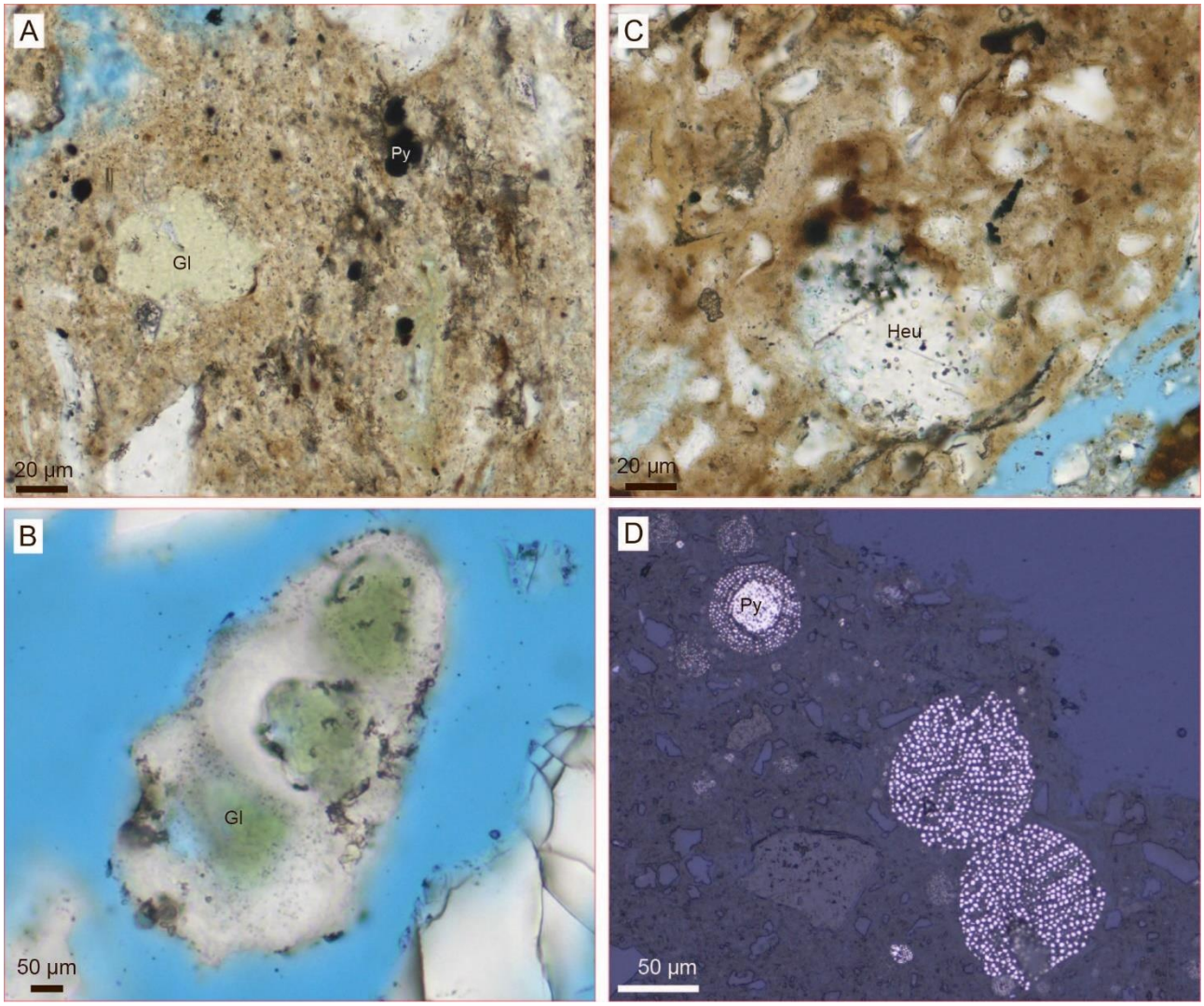

Figure 12 Lowermost part of Lark Fm, L1. **A.** Glauconitic clasts (Gl), glauconized mica, quartz and pyrite framboids (Py) in a clayey matrix. **B.** Zeolite, probably heulandite, (Heu) filling an oversized pore possibly after a bioclast. **C.** Glauconitic (Gl) filling of a bioclast. **D.** Pyrite framboids (Py) of various sizes. Reflected light.

The uppermost part of Lark Fm, L3, consists mainly of glauconitic sandy siltstones, although glauconitic mudstones, calcareous mudstones and very fine-grained sandstones may also be present. The detrital grains in the sandstones are mainly quartz, K-feldspar, plagioclase and glauconitic clasts. Authigenic cements are mainly calcite, siderite, pyrite and zeolites, probably heulandite. Siderite preferentially occurs as tiny crystals between cleavage planes in mica. A zeolite, probably, heulandite occurs as cement in oversized pores and as filling of bioclasts (Figure 14).

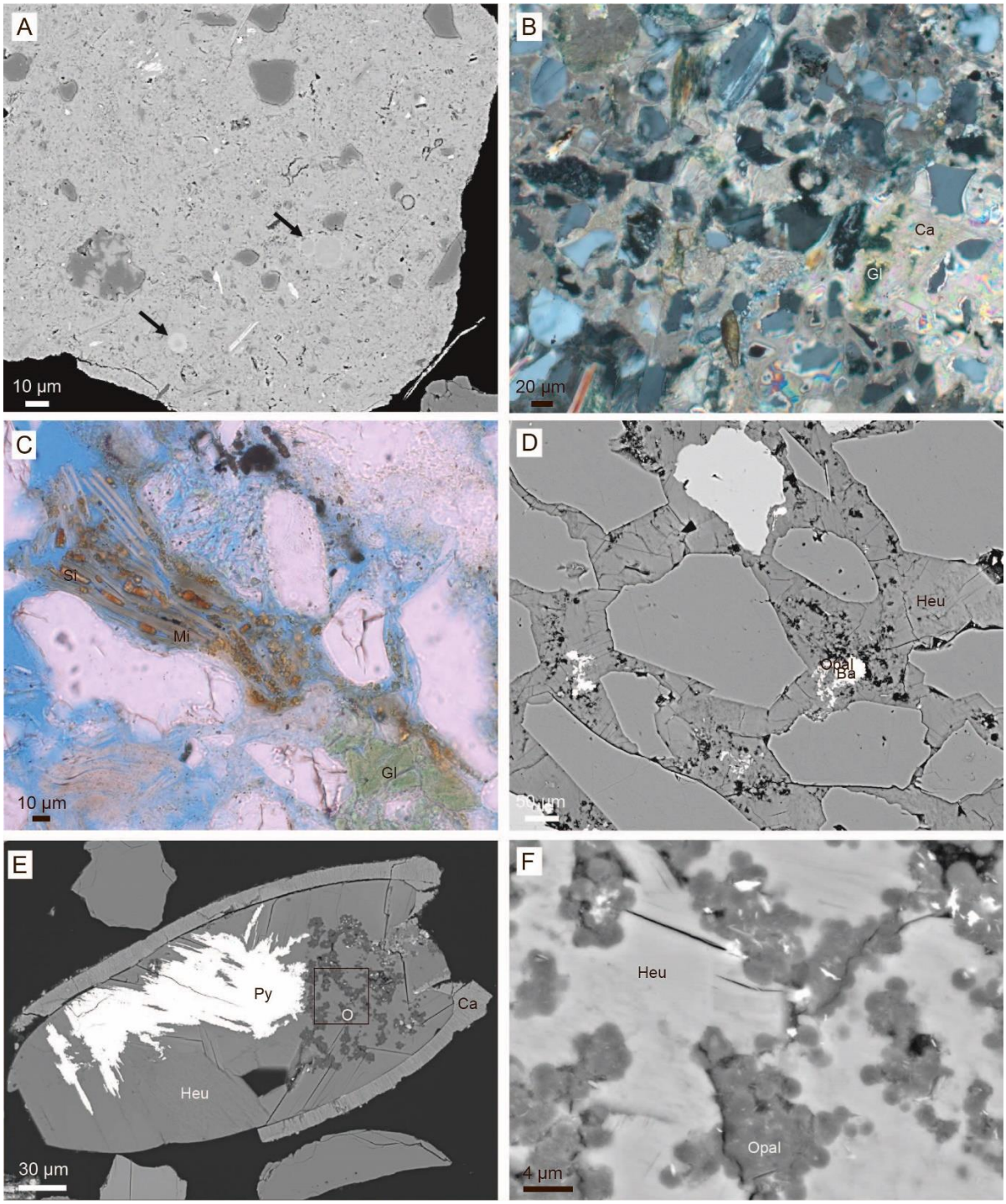

Figure 13 Middle part of Lark Fm, L2. **A.** Bioclasts (arrows), quartz and K-feldspar-quartz intergrown grains in a clayey matrix. **B.** Quartz, feldspar, mica, glauconitic clasts and bioclasts enclosed in calcite cement. Crossed nicols. **C.** Tiny siderite crystals preferentially growing between cleavage planes in muscovite (Mi) and adjacent to glauconitic clast Gl). **D.** Heulandite (Heu) as pore-filling cement enclosing authigenic barite (Ba). Backscatter electron micrograph. **E.** Lepidospheres (O, opal) and pyrite (Py) enclosed in heulandite (Heu) filling of calcareous bioclast (Ca). Backscatter electron micrograph. **F.** Close up of square in E.

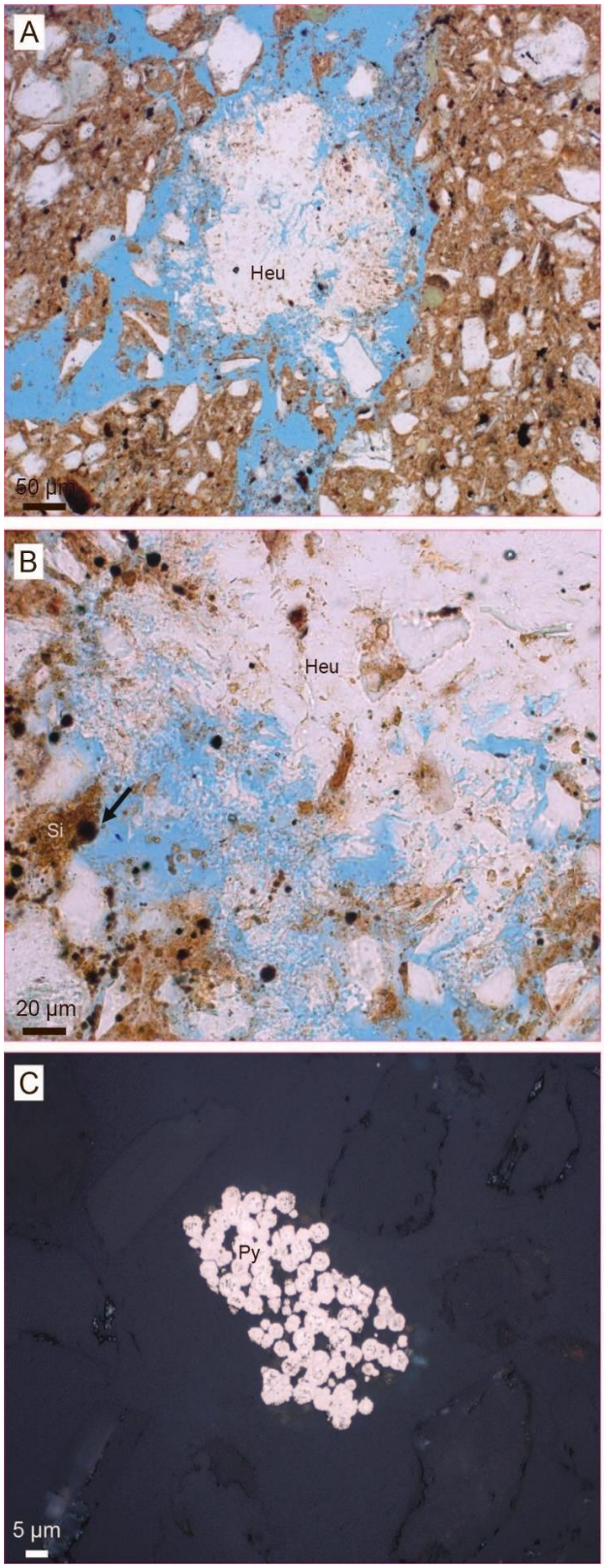

Figure 14 The uppermost part of the Lark Fm, L3. **A.** Heulandite (Heu) filling of oversized pore, possibly a former bioclast. **B.** Heulandite seem to enclose siderite (Si) and possibly pyrite (Py). **C.** Framboids of pyrite. Reflected light.

Grain size and total clay content

There is an overall good relationship between clay size determinations determined by particles settling rates (ISO 17892-4:2016) and total clay mineralogy content as determined from bulk XRD analysis (Figure 15). The ratio between the two determinations is slightly higher than 1:1 trend (Figure 15) suggesting that the clay mineral volume tend to overestimate the clay size volume. It is, however, not clear exactly how much the XRD determined clay mineral content overestimate the clay volume content since other clay sized particles could be present such as opal, quartz and heulandite . Likewise, clay particles may not have been totally dissociated and could have ended up in a coarser fraction than clay. The relationship, however, in Figure 15 largely confirms the semi-quantitative determination of clay minerals using peak height with corrections factors and can be used to further tune the corrections factors for especially smectite that is likely too high.

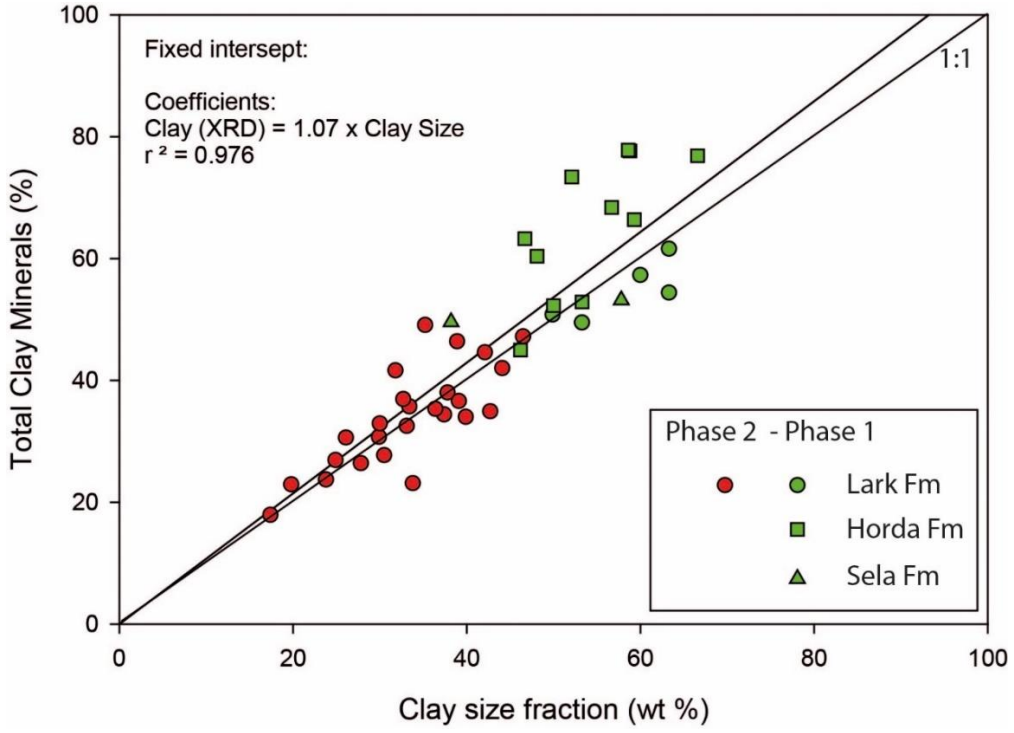

Figure 15 Comparison between volume of clay from grain size determinations (Table 3) and clay mineral content determined by XRD.

Concluding remarks

The lowermost part of Lark Fm, L1, is characterized by abundant illite (33–40%), quartz (28–40%) and kaolinite (9–18%). Quartz generally increases upwards in L1, whereas kaolin decreases. Chlorite is commonly present in the L1 interval, although only present in small amounts. Pyrite, siderite and calcite occur in small amounts in most samples. The middle part of Lark Fm, L2, is generally rich in quartz and with relatively common illite and kaolinite. K-feldspar and plagioclase, pyrite, siderite and

calcite are present in all samples. The sandy intervals mainly have a high content of quartz, K-feldspar and plagioclase. The combined clay (mainly illite and kaolinite) content gradually increases from 23% at 1450 m in L2 to 47% at 1200 m in L3. The uppermost part of Lark Fm, L3, is also characterized by abundant quartz (upward increasing) and with relatively common illite and kaolinite. K-feldspar, plagioclase, pyrite and calcite are present in most samples, whereas siderite is relatively rare. The Overburden consisting of the remaining part of the Nordland Gp, including Nolde Sand, is rich in quartz (50–67%) and with common K-feldspar (10–28%) and plagioclase (6–16%).

Mudstone is the most common lithology within the primary and secondary seal. Sandy mudstones occur in both seals and in addition sandy siltstones occur in the secondary seal. Quartz makes up most of the sand and silt sized grains with glauconitic clasts, feldspar grains and bioclasts, either pyritized or calcareous, as secondarily common components.

ORGANIC CARBON AND TOTAL SULPHUR CONTENTS

Total Carbon (TC, wt.%), Total Organic Carbon (TOC, wt.%) and Total Sulphur (TS, wt.%) content were determined by combustion in a LECO CS-200 induction furnace after elimination of carbonate-bonded carbon by prolonged HCl treatment. In-house and international standards were measured during analysis and the analytical reproducibility is 0.1 wt.% for all. In addition, Rock-Eval type pyrolysis was carried out using a HAWK instrument (Wildcat Instruments, USA). Calibration was done using the IFP-160000 standard with one blank and one in-house (Marl Slate) control standards being run for every 10 samples to ensure instrument stability. The S_2 peak represents the remaining generation potential in the sample that is liberated during pyrolysis. Based on the Rock-Eval pyrolysis the Hydrogen Index (HI) was calculated from the S_2 yield by normalising to the TOC content ((S_2/TOC) · 100). T_{max} represents the temperature at which the maximum rate of hydrocarbon generation (S_2) occurs. The S_1 peak, representing free hydrocarbons in the sample, was not considered here due to the samples were extracted before pyrolysis. For reference see e.g. Bordenave et al. (1993). The analyses were conducted at GEUS.

The TOC content in the samples from the secondary seal ranges between 0.7–2.3 wt.% with average of 1.3 wt.% (Table 5, Figure 16). The content is lowest between 1400–1440 m where the sandy siltstone beds occur suggesting that dilution of organic carbon by enhanced influx of detrital material occurred assuming a constant rate of organic carbon. A second low in TOC concentrations is seen in the top of the Lark Fm towards the sandy siltstone bed at 840 m (Figure 16). The Inorganic Carbon (TIC - difference between TOC and TC contents) range 0.3–1.3 wt.% (Figure 16) corresponding to 4–16 wt.% total carbonate content. Compared to the Horda Fm the Lark Fm is relative more carbonate rich, which is also observed from mineralogy analysis (Figure 10). Peaks in TIC are seen between 1400–1440 m where also the sandy siltstone occur. Here carbonate cemented coarse grain domains occur (Figure 11) suggesting that the high carbonate here might reflect carbonate cementation of the beds. We also observe a peak in TIC within the sandy siltstone bed at 840 m (Figure 16).

Sulphur content peak at the Lark L1 and L2 boundary where up to 3 wt.% have been measured. High values are also observed in the mid part of Lark L3 (Figure 16). XRD and Micro CT scanning data show that barite ($BaSO_4$) from the mud system is present in the cuttings samples despite cleaning efforts. This is also confirmed from elemental determination of Ba in the samples and thus the sulphur content cannot be interpreted only to represent depositional enriched sulphur. We do think that the long-term rise in S from Horda Fm and up through the Lark L1 reflect a real increase since it also parallels the rise in TOC content (Figure 16). However, some of the high values in the Lark L3 may reflect mud system additives.

The HI values reach a maximum of 168 mg HC/g TOC, but typically range between 80–110 mg HC/g TOC (Table 5), suggesting that the organic matter dominantly is terrigenous, perhaps mixed with minor amounts of algae-derived kerogen. Lowest HI are seen in the overburden signalling the presence of oxidised refractory organic matter here. The T_{max} ranges from 329–429 °C, reflecting the low thermal maturity of the primary seal. Values <400 °C are unreliable, likely caused by low TOC content.

Concluding remarks

The primary and secondary seal of the Nini West is organic-lean, and the organic matter in the rock matrix is mainly composed of less reactive kerogen i.e. with low HI values. This suggests that the low TOC content will not have an adverse effect on seal integrity. High carbonate content is associated with the sandy siltstone beds and the shales around. Here carbonate cement has been observed and suggests that the beds are at least partly cemented. Alternatively, the carbonate reflects high biogenic carbon i.e. shells and/or tests. These later have, however, not been observed in the coarse fractions separated by sieving and thus is not deemed likely.

Table 5 LECO and Rock Eval data.

Material	Well	Depth top (m, md)	Depth bund (m, md)	Formation	Internal number	TOC (wt%)	TC (wt%)	TIC (wt%)	TS (wt%)	Tmax (°C)	S1 (mg HC/g rock)	S2 (mg HC/ g rock)	HI (mg HC/g TOC
cuttings	Nini-4	200	220	n.d.		0,14	0,24	0,10	0,32	329	0,01	0,05	37
cuttings	Nini-4	280	300	n.d.		0,22	0,23	0,01	0,23	423	0,02	0,08	37
cuttings	Nini-4	380	400	n.d.		0,33	0,35	0,02	1,02	419	0,02	0,15	46
cuttings	Nini-4	700	720	Nolde sand		0,39	0,46	0,07	0,43	420	0,02	0,13	33
cuttings	Nini-4	740	760	Nolde sand		0,12	0,12	0,01	0,51	394	0,01	0,05	43
cuttings	Nini-4	820	830	Lark		1,33	1,57	0,24	1,78	403	0,11	0,52	39
cuttings	Nini-4	840	850	Lark		1,27	2,16	0,89	0,68	422	0,20	2,13	168
cuttings	Nini-4	900	910	Lark		1,63	2,10	0,47	1,57	425	0,17	1,98	121
cuttings	Nini-4	940	950	Lark		1,88	2,47	0,60	1,61	424	0,16	2,39	127
cuttings	Nini-4	990	1000	Lark		1,43	1,87	0,44	1,03	427	0,09	1,55	108
cuttings	Nini-4	1040	1050	Lark		1,59	1,85	0,26	1,17	426	0,08	1,63	102
cuttings	Nini-4	1090	1100	Lark		1,66	2,16	0,50	1,19	427	0,10	1,97	119
cuttings	Nini-4	1140	1150	Lark		1,37	2,68	1,31	1,04	424	0,08	1,43	104
cuttings	Nini-4	1190	1200	Lark		1,52	1,84	0,32	1,18	426	0,08	1,58	104
cuttings	Nini-4	1240	1250	Lark		1,30	1,55	0,26	0,80	426	0,07	1,41	109
cuttings	Nini-4	1290	1300	Lark		1,09	1,51	0,42	0,80	427	0,07	1,55	142
cuttings	Nini-4	1340	1350	Lark		1,00	1,15	0,15	0,77	427	0,07	1,32	132
cuttings	Nini-4	1350	1360	Lark		1,12	1,27	0,15	0,73	427	0,07	1,34	120
cuttings	Nini-4	1360	1370	Lark		1,24	1,38	0,13	1,09	426	0,08	1,46	117
cuttings	Nini-4	1370	1380	Lark		1,02	1,52	0,50	0,75	426	0,07	1,28	125
cuttings	Nini-4	1380	1390	Lark		0,72	1,16	0,44	1,15	424	0,25	0,96	132
cuttings	Nini-4	1390	1400	Lark		0,79	1,19	0,40	1,06	424	0,07	1,02	128
cuttings	Nini-4	1400	1410	Lark		0,92	1,39	0,46	0,76	427	0,07	1,12	121
cuttings	Nini-4	1410	1420	Lark		0,72	1,44	0,72	0,50	427	0,06	0,87	121
cuttings	Nini-4	1420	1430	Lark		0,72	1,66	0,94	0,57	426	0,06	0,89	124
cuttings	Nini-4	1430	1440	Lark		0,84	1,74	0,90	0,61	429	0,07	1,23	147
cuttings	Nini-4	1440	1450	Lark		0,91	1,78	0,87	0,79	428	0,06	1,18	130
cuttings	Nini-4	1490	1500	Lark		1,09	2,27	1,19	1,05	427	0,08	1,36	125
cuttings	Nini-4	1520	1530	Lark		1,67	2,26	0,59	1,47	428	0,12	2,02	121
cuttings	Nini-4	1560	1570	Lark		2,32	2,75	0,43	1,99	413	0,20	2,09	90

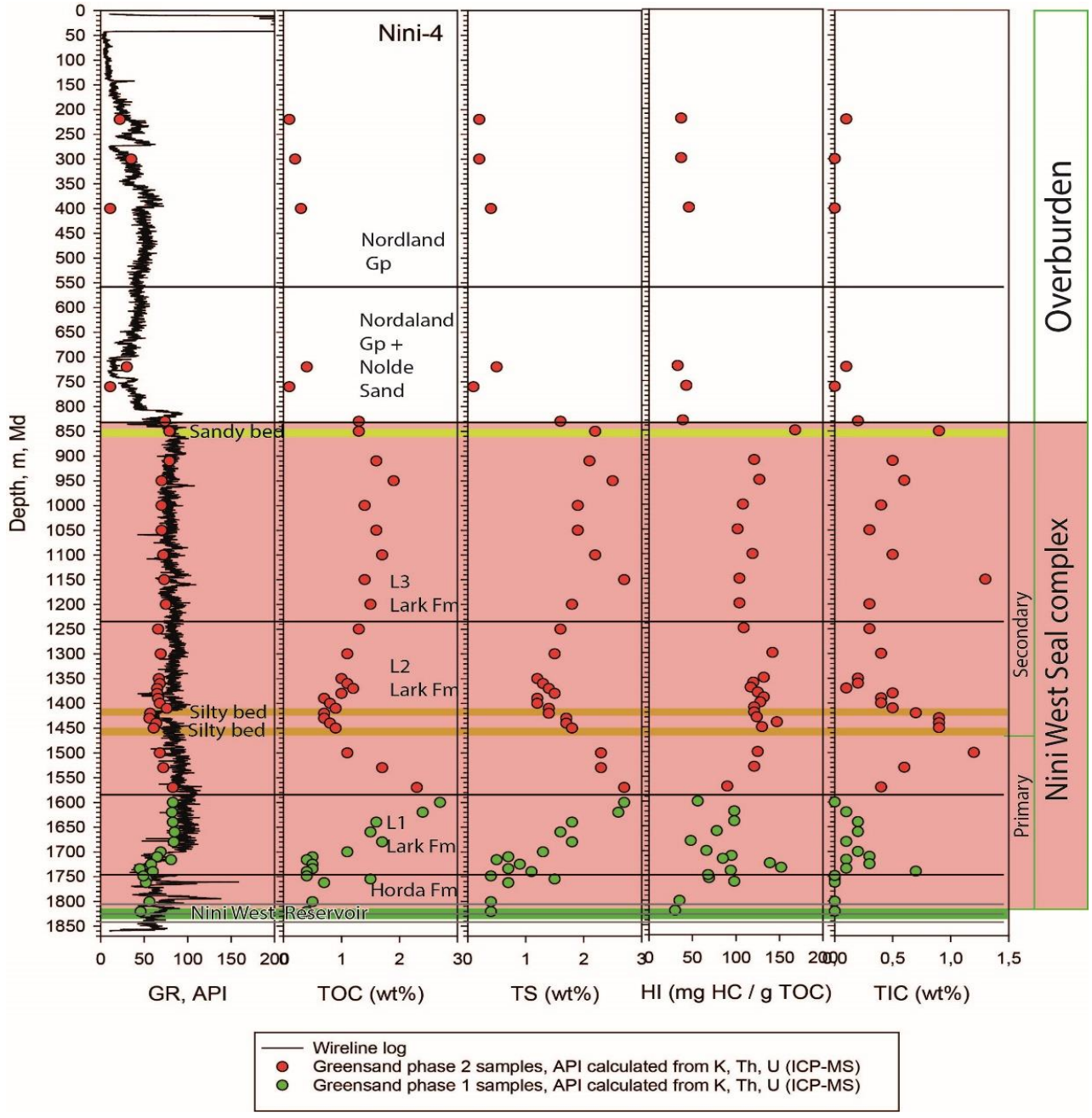

Figure 16 Organic Carbon (TOC), Sulphur (TS), Hydrogen Index (HI) and Inorganic Carbon (TIC) profiles in the Nini-4 well.

ELEMENTAL COMPOSITION

Trace element concentrations were measured on a Perkin Elmer NexION 1000 ICP Mass Spectrometer (ICP-MS) instrument and major elements using a Perkin Elmer Avio 200 ICP Optical Emission Spectrometer (ICP-OES) at GEUS (internal laboratory reference 22-007). Preparation for each analysis type was done by dissolving crushed material in HF and HNO_3 acid for two days at 130 °C. For determination of Si a special preparation method was used using borate melt before analysing in the ICP-OES apparatus. Calibration was made using the standards OU-6, OShBo, GONV-1, BVA-1, Disko-1, BHVO-2 and BCR-2. An overview of the elemental composition, average, median and minimum and maximum for the analysed samples is presented in Table 6. The full dataset is presented in Appendix F. Hand-held XRF (HH-XRF) determinations of element composition were not measured on the Greensand phase 2 samples since the quality of these measurements are not high enough compared to the determined elements by the ICP-MS and ICP-OES techniques that were conducted (Schovsbo et al., 2021). In addition, SiO_2 determinations are now measured as part of a new major element determination made by ICP-OES which was the main reason for using HH-XRF on Greensand Phase 1 samples.

Results

The analysis provides both major, minor and trace element concentrations (Table 6). The chemical difference between the muddy seal samples and the overburden sandy samples is clear. The clay dominated seal section has low SiO_2 and high Al_2O_3 content whereas the coarse-grained overburden section has high SiO_2 and low Al_2O_3 content (Figure 17). The Lark L3 and Lark L2 samples have a low content of redox elements such as U (average 3.2–2.7 ppm with peak U content in the top of Lark 1 Figure 17), Mo (average 1.4–1.9 ppm) and V (average 123–127 ppm) that are typically enriched under stagnant and reducing bottom waters. This lack of enrichment agrees with the lithology descriptions – greenish shales – and the refractive nature of organic carbon that suggests an oxic depositional environment. No statistically significant relationship between uranium and TOC could be established. This again agrees well with the terrestrial nature of the organic matter that has a less pronounced tendency to lead to a uranium enrichment.

To examine the relationship between clay size particles and natural radioactivity the API values for a “theoretical” gamma ray response were calculated based on the ICP-MS and ICP-OES measured K, Th and U content using the formulas from Ellis and Singer (2007):

$$\text{Sum Gamma ray (SGR) (API)} = 16 \cdot \text{K (\%)} + 8 \cdot \text{Th (ppm)} + 4 \cdot \text{U (ppm)}$$

$$\text{Clean Gamma ray (CGR) (API)} = 16 \cdot \text{K (\%)} + 8 \cdot \text{Th (ppm)}$$

The relationship between the clay size fraction, SGR and CGR is shown in Figure 18. Horda and Lark Fms show different relationships with Lark showing the best correlation between clay size particles and SGR and CGR of the two. This agrees with studies of the lower seal where Schovsbo et al. (2021) and Petersen et al. (2022) showed that the gamma ray curve was a poor proxy for the clay content within the smectite rich Horda Fm. In the Lark Fm, however, illite clays dominate (Figure 10), which

yields both a higher natural radiative response pr clay volume and a better relationship between clay volume and GR, as illite exhibit less variability with respect to the content of radioactive K and Th, whereas the K content in smectite depends on the illite interlays and can be quite variable.

In Figure 18 different SGR and CGR models for estimating the clay content in the Lark Fm are presented. The model between SGR and clay volume that applies 40 API for 0% clay and 140 for 100% clay is like the model used for estimating the Vclay from the GR curve presented in the "Petrophysical Evaluation and models" section. Here a value of 35 API @ 0% clay and 150 API @ 100% clay was used. However, it should be noted that the Gamma ray tool measures the radioactivity in a volume of rock around the well bore and thus also depends on porosity whereas the Ellis and Singer (2007) formula calculate the API on a weight basis and does not take porosity into considerations. Also, the presence of K containing mud and formation brine affect the gamma ray tool readings. Due to this we should not expect a full agreement between the theoretical API values and the readings from the borehole.

Concluding remarks

Calculated API values from ICP-MS and ICP-OES for samples show a good relationship to the API measured in the bore hole. This indicate that the cuttings depth represents true depth intervals. We also observed a good relationship between Al content and total clay content. The secondary seal has low content of redox sensitive metals (U, Mo and V) which reflect the rather oxygenated environment that the shale was deposited in.

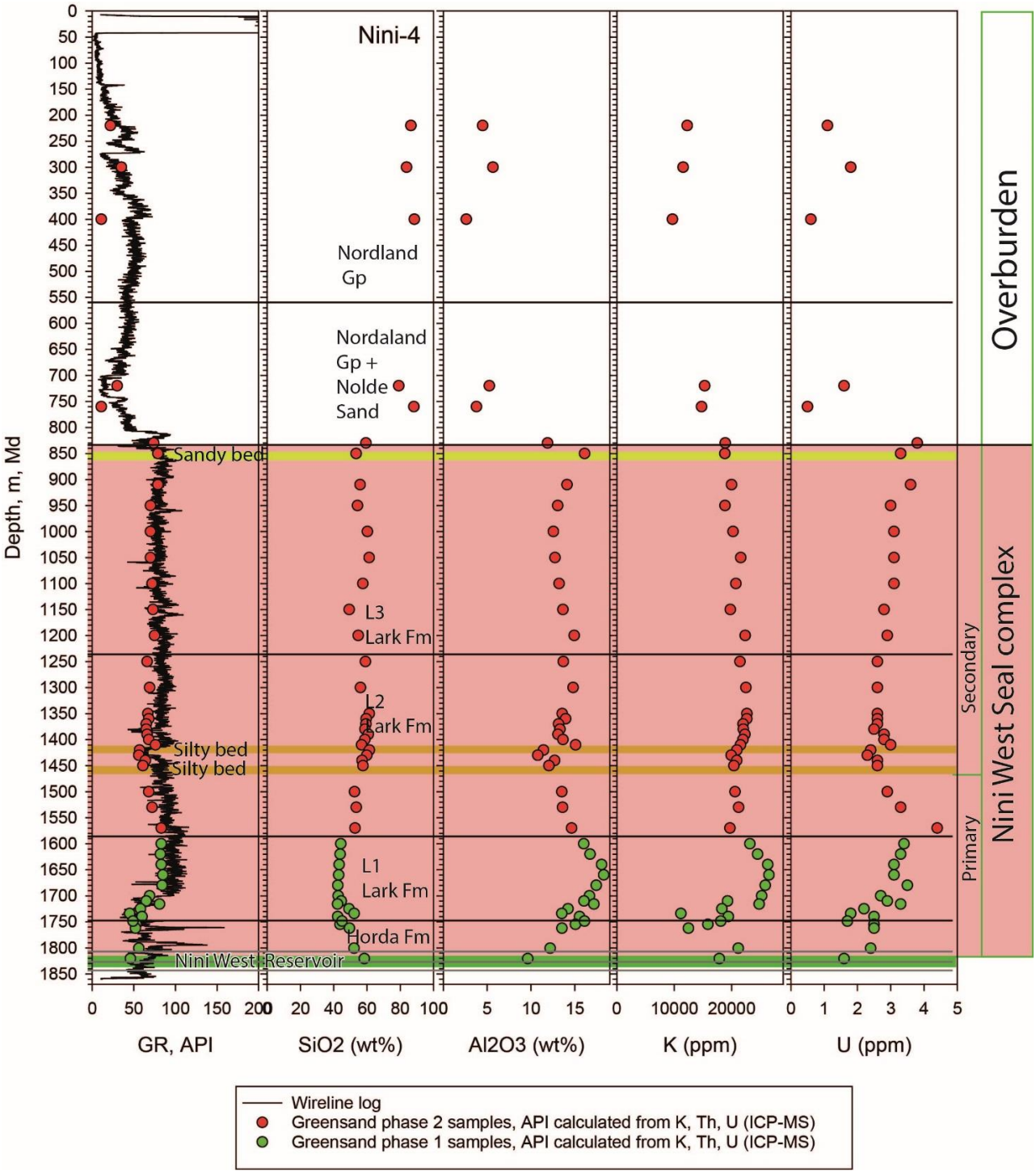

Figure 17 Calculated SGR (using the formula of Ellis and Singer, 2007) and wireline GR curve and selected major and trace elements from the Nini-4 well.

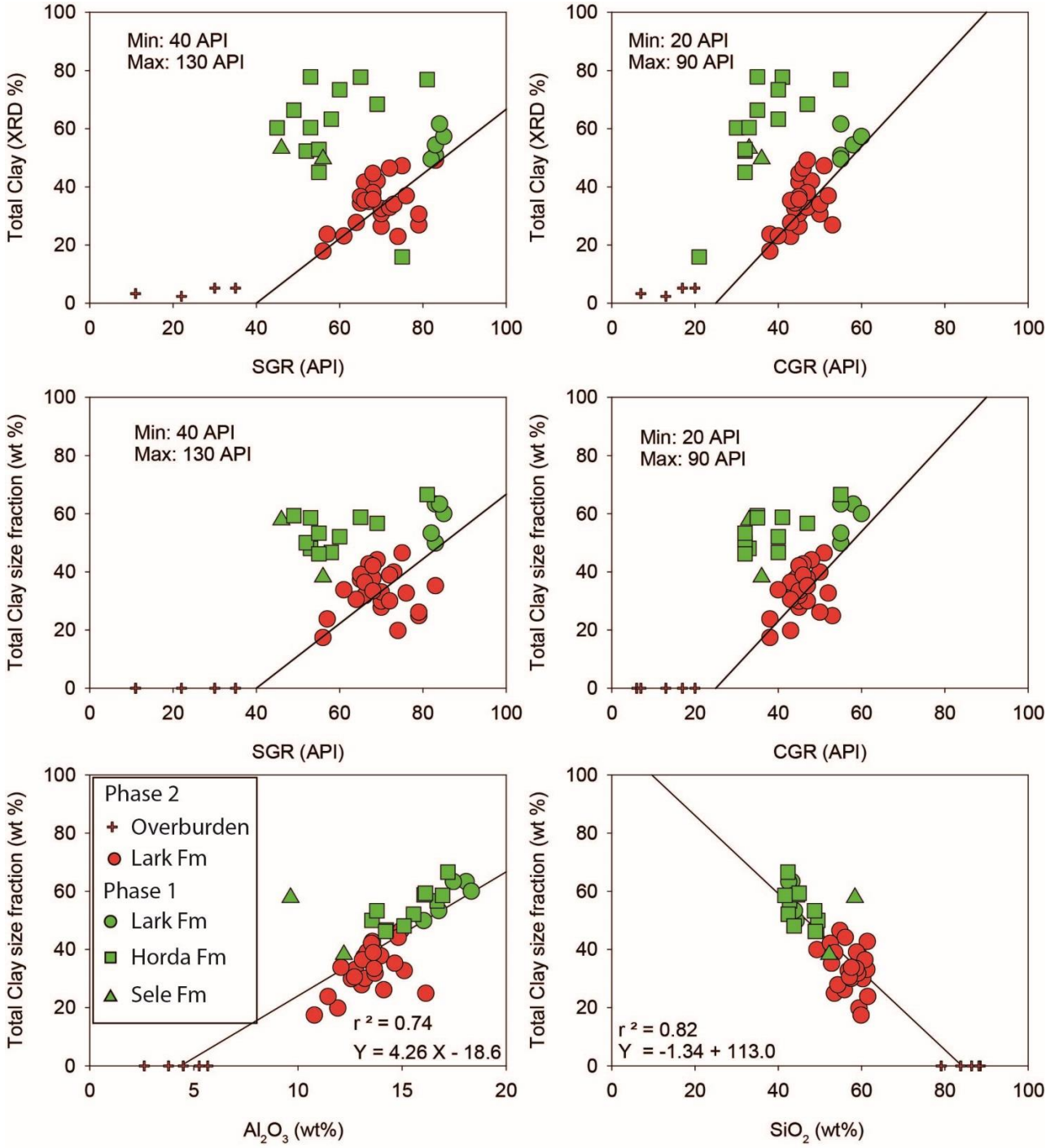

Figure 18 Relationship between clay size fraction and calculated API responses (SGR and CGR) and major elemental composition. API response is calculated from ICP-MS/OES determined elements. SGR include contribution from U, Th and K and CGR include contribution from Th and K only (c.f. Ellis and Singer, 2007). Minimum and maximum represent API at 0 and 100% clay respectively.

Table 6 Major and trace elements overburden and secondary seal (L3 and L2) in the Nini-4 well. Data is presented in Appendix F.

	Nordaland Gp and Nolde				Lark L3				Lark L2			
	Average	Std	Minimum	Maximum	Average	Std	Minimum	Maximum	Average	Std	Minimum	Maximum
SiO2(wt%)	85,2	3,9	79,1	88,5	56,3	3,8	49,3	61,3	58,2	2,6	52,5	61,5
TiO2(wt%)	0,34	0,19	0,09	0,59	0,82	0,03	0,76	0,87	0,79	0,03	0,73	0,85
Al2O3 (wt%)	4,4	1,2	2,6	5,7	13,6	1,3	11,9	16,1	13,2	1,1	10,8	15,1
Fe2O3 (wt%)	2,0	0,6	1,3	2,7	5,5	0,7	4,8	6,9	5,6	0,4	4,8	6,3
MnO(wt%)	0,02	0,01	0,01	0,03	0,04	0,01	0,03	0,05	0,06	0,01	0,03	0,07
MgO(wt%)	0,42	0,2	0,2	0,7	1,5	0,2	1,2	1,8	1,8	0,2	1,6	2,2
CaO(wt%)	0,87	0,1	0,7	0,9	2,7	1,3	1,7	6,1	2,1	0,8	1,1	4,1
Na2O(wt%)	0,84	0,4	0,3	1,5	1,1	0,1	1,0	1,3	1,2	0,1	1,2	1,4
K2O(wt%)	1,53	0,3	1,2	1,8	2,4	0,2	2,3	2,7	2,6	0,1	2,4	2,7
P2O5(wt%)	0,02	0,0	0,0	0,1	0,1	0,0	0,1	0,2	0,1	0,0	0,1	0,1
Li, ppm	8,9	4,1	4,9	14,7	74,4	9,1	62,0	87,7	74,1	7,7	63,6	92,5
Sc, ppm	3,5	1,9	1,6	5,6	12,7	1,2	11,1	14,7	13,6	1,0	11,5	15,4
V, ppm	34,9	19,5	14,3	65,2	126,4	8,9	114,3	142,4	122,5	8,7	105,5	138,2
Cr, ppm	29,6	16,2	16,2	54,0	97,8	6,4	86,3	110,7	112,5	6,6	102,3	125,6
Co, ppm	4,6	1,3	3,1	6,5	18,4	3,8	14,1	23,5	20,7	2,7	15,6	24,0
Ni, ppm	7,6	3,3	3,2	12,4	37,1	6,1	30,0	50,1	42,8	6,8	32,2	60,2
Cu, ppm	6,9	2,7	2,6	9,2	24,5	3,6	19,3	29,4	23,6	4,7	15,6	34,6
Zn, ppm	21,6	9,9	6,6	32,5	52,0	14,6	30,5	79,1	52,3	11,6	37,1	81,1
Ga, ppm	5,1	1,7	3,0	6,8	17,2	1,5	15,0	20,0	16,9	1,4	13,8	19,4
Rb, ppm	38,5	6,3	28,4	45,2	89,8	9,3	76,8	108,1	105,3	8,1	89,4	116,4
Sr, ppm	96,9	27,3	55,5	124,2	665,7	158,6	491,9	1001,1	691,2	125,9	512,7	970,5
Y,ppm	6,8	3,6	2,9	9,9	22,3	1,0	20,4	23,7	23,0	1,1	21,4	25,6
Zr, ppm	84,6	51,4	26,2	153,7	188,6	21,6	158,6	221,5	176,9	18,2	145,4	208,2
Nb, ppm	5,6	3,8	1,9	11,0	17,5	0,8	16,0	18,5	17,9	0,5	16,6	18,8
Mo, ppm	1,2	1,5	0,4	3,9	1,9	1,5	0,9	4,6	1,4	0,5	1,0	2,3
Cs, ppm	0,9	0,4	0,4	1,3	5,7	1,2	4,1	7,9	6,6	1,0	4,6	7,8
Ba, ppm	1135	1044	330	2694	13715	5398	8133	26098	15126	3581	9616	23111
La, ppm	9,3	4,8	4,8	15,0	33,8	2,1	30,0	37,1	32,4	2,4	27,4	35,6
Ce, ppm	21,4	12,1	11,1	38,4	76,5	6,5	68,5	87,6	74,1	6,4	61,0	82,2
Pr, ppm	2,15	1,22	1,07	3,78	7,69	0,61	6,75	8,75	8,27	0,60	7,28	9,33
Nd, ppm	8,02	4,62	3,95	14,19	28,19	2,29	24,51	32,16	30,28	1,99	27,15	33,43
Sm, ppm	1,53	0,89	0,72	2,75	5,28	0,47	4,53	6,06	5,68	0,38	5,07	6,30
Eu, ppm	0,31	0,17	0,17	0,56	1,14	0,10	1,00	1,26	1,06	0,09	0,93	1,20
Gd, ppm	1,37	0,77	0,59	2,30	4,83	0,33	4,29	5,40	4,97	0,29	4,53	5,46
Tb, ppm	0,21	0,11	0,09	0,35	0,75	0,05	0,67	0,82	0,77	0,04	0,71	0,86
Dy, ppm	1,24	0,64	0,53	1,88	4,24	0,28	3,72	4,64	4,31	0,22	3,96	4,78
Ho, ppm	0,26	0,13	0,11	0,38	0,86	0,04	0,76	0,90	0,87	0,04	0,81	0,94
Er, ppm	0,74	0,38	0,33	1,07	2,41	0,11	2,18	2,58	2,42	0,10	2,28	2,63
Tm, ppm	0,12	0,06	0,05	0,19	0,39	0,02	0,35	0,42	0,38	0,02	0,36	0,41
Yb, ppm	0,78	0,39	0,34	1,14	2,42	0,10	2,24	2,60	2,40	0,09	2,22	2,52
Lu, ppm	0,12	0,06	0,05	0,18	0,37	0,01	0,35	0,39	0,36	0,01	0,33	0,38
Hf, ppm	2,53	1,47	0,80	4,42	5,32	0,64	4,42	6,29	4,89	0,51	4,00	5,70
Ta, ppm	0,48	0,26	0,13	0,84	1,22	0,06	1,15	1,31	1,21	0,04	1,13	1,27
Pb, ppm	8,95	1,02	7,80	10,09	27,78	3,26	23,40	34,22	26,21	2,60	21,72	32,02
Th, ppm	2,87	1,53	1,24	4,83	11,41	0,83	10,32	12,68	10,54	0,93	8,90	12,54
U, ppm	1,12	0,57	0,51	1,81	3,19	0,31	2,84	3,75	2,67	0,25	2,30	3,30

SPECIFIC SURFACE AREA AND PERMEABILITY MODELS

The specific surface area was measured at DTU using the Brunauer–Emmett–Teller (BET) method. The surface area results are summarised in Table 7. Details for each sample is presented in Appendix B. The specific surface measurements range from 11.8–22.5 m^2/g with the general value around 18 m^2/g. The lowest surface area is measured in sample #820 m that also represents one of the most coarse-grained samples (c.f. Tables 3 and 7).

Received laboratory report:

The samples were analysed using a Quantachrome autosorb iQ at DTU.
To determine the internal surface area by the BET method, the quantity of nitrogen gas adsorbed into or desorbed from the sample at equilibrium vapour pressure was measured (Petrophysical laboratory at DTU). Data were obtained by adding or removing a known quantity of nitrogen gas into or out of a sample cell containing 0.5 to 1 g of degassed sample material maintained at a constant temperature.

The BET monolayer surface area calculation requires a so-called BET cross-plot 1/ [$W(P_0/P)$–1] vs. P/P_0, but restricted to the linear region of the adsorption isotherm. The standard BET procedure requires a minimum of three points in the relative pressure range. Determination of the monolayer surface area from the BET theory (Brunauer et al., 1938) use the BET equation:

$$\frac{1}{W((P_0 / P)-1)} = \frac{1}{W_m C} + \frac{C-1}{W_m C}\left(\frac{P}{P_0}\right)$$

where, W is the weight of the total nitrogen gas adsorbed at a relative pressure, P/P_0, and W_m is the weight of adsorbate constituting a monolayer of surface coverage. The BET C-term is related to the energy of adsorption in the first adsorbed layer. The weight of a monolayer of adsorbate W_m and C can be obtained from the slope (s) and intercept (i) in the linear 1/ [W (P_0/P)–1] vs. P/P_0 plot, where:

$$s = \frac{C-1}{W_m C}, \qquad i = \frac{1}{W_m C}, \qquad W_m = \frac{1}{s+i}$$

The slope (s) and intercept (i) are listed in the sample file (Appendix B). With knowledge of the molecular cross-sectional area A_{cs} of the adsorbate nitrogen molecule (for a hexagonal close-packed nitrogen monolayer at 77 K, the cross-sectional area (A_{cs}) for nitrogen is 16.2 Å). The total surface area S_t of the sample material can be expressed as:

$$S_t = \frac{W_m N A_{cs}}{M}$$

where, N is Avogadro's number and M is the molar mass (molecular weight) of the adsorbate (nitrogen). The surface area (S_t) is listed in Table 7 and for each sample in Appendix B.

In order to find the linear range of the BET plot for microporous materials in a way that reduces any subjectivity in assessment of the monolayer capacity, Rouquerol et al. (2007) suggested a formal

procedure based on the criteria that (1) the quantity of *C* must be positive (i.e. any negative value is an indication that data are outside the valid range of the BET equation) and (2) the application of the BET equation is limited to the relative pressure range where the term n(1– P/P_0) continuously increases with P/P_0 (n is the adsorbed amount). This procedure is suggested in the ISO 9277:2010 standard.

Table 7 Surface area (BET) results and modelled permeabilities (K_{BET}).

Laboratory number	Internal number	Material	Well	Depth top (m, md)	Depth base (m, md)	Surface Areal, m2/g	Permeability K_BET (µD)
46487		cuttings	Nini-4	820	830	11,8	9,15
46488		cuttings	Nini-4	840	850	14,4	4,21
46489		cuttings	Nini-4	900	910	13,6	3,64
46490		cuttings	Nini-4	940	950	14,1	3,53
46491		cuttings	Nini-4	990	1000	14,9	1,34
46492		cuttings	Nini-4	1040	1050	14,7	3,07
46493		cuttings	Nini-4	1090	1100	15,8	2,06
46494		cuttings	Nini-4	1140	1150	22,1	0,98
46495		cuttings	Nini-4	1190	1200	22,1	0,79
46496		cuttings	Nini-4	1240	1250	22,5	0,69
46497		cuttings	Nini-4	1290	1300	21,8	0,58
46498		cuttings	Nini-4	1340	1350	17,3	0,94
46499		cuttings	Nini-4	1350	1360	21,7	0,51
46500		cuttings	Nini-4	1360	1370	17,3	0,86
46501		cuttings	Nini-4	1370	1380	19,5	0,83
46502		cuttings	Nini-4	1380	1390	18,0	0,93
46503		cuttings	Nini-4	1390	1400	18,8	0,49
46504		cuttings	Nini-4	1400	1410	18,3	0,98
46505		cuttings	Nini-4	1410	1420	15,2	3,04
46506		cuttings	Nini-4	1420	1430	13,5	4,56
46507		cuttings	Nini-4	1430	1440	14,5	2,63
46508		cuttings	Nini-4	1440	1450	15,1	2,36
46509		cuttings	Nini-4	1490	1500	19,7	1,04
46510		cuttings	Nini-4	1520	1530	16,1	1,06
46511		cuttings	Nini-4	1560	1570	15,9	0,84

Permeability models from BET

Modelled permeability was estimated from capillary tube models, which use easily measured physical properties such as porosity and specific surface area data (Kozeny, 1927).

$$K_{BET} = c\frac{\varphi^3}{(1-\varphi)^2 S_s^{\,2}}$$

where K_{BET} is the permeability, φ is porosity, S_s is specific surface (grain-surface area per grain volume). The c factor is the Kozeny constant that will have a value between 0.22–0.24 depending on porosity (Mortensen et al., 1998).

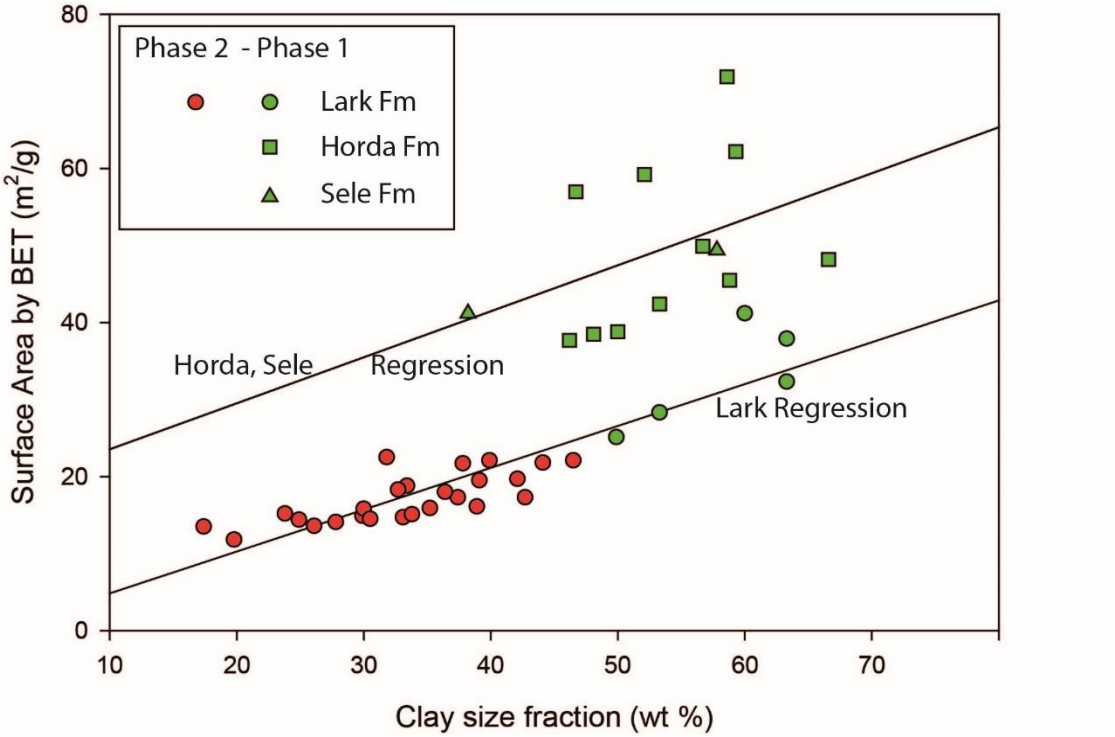

Figure 19 Relationship between Clay size fraction and surface area measurements by BET. The linear relationship BET (m^2/g) = 0.81 · clay (%) – 2.32 m^2/g (r^2 = 0.57) has been used in the petrophysical interpretation of the surface area for the primary seal (Petersen et al., 2022). For the secondary seal the relationship: BET (m^2/g) = 0.54 · clay (%) – 0.61 m^2/g (r^2 = 0.81) is used. The offset between the Horda and the Lark regression lines reflect the difference in mineralogy between the smectite rich Horda Fm and the illite rich Lark Fm.

There is a statistically significant linearly correlation between the surface area determined by BET and total clay content as reflected by the clay size fraction (Figure 19). Since the surface area - both internal and external - varies per clay type, then the correlation differs between the Horda Fm and the Lark Fm. In the smectite rich Horda and Sele Fms a higher surface area pr. clay volume can be seen compared to the illite dominated Lark Fm (Figure 19). For interpreting the surface area in the secondary seal, we applied the regression line defined by the Lark Fm samples.

We note that the BET measurements do not discriminate between internal or external surface of a mineral. Hence the relationship may estimate a too high external surface. In the secondary seal we use an estimate based on illite rick samples and thus the contribution from internal surface is expected to be minor.

Concluding remarks

The specific surface area of the seal samples is high which is in agreement with the clay mineral composition and fine-grained nature of the rock. The measurement of specific surface is used as a key input in modelling the permeabilities. The permeability is modelled based on the Kozeny equation for both samples and wireline logs. We use a separate surface area model for the secondary seal due to the different mineralogy compared to previous model for the primary seal (c.f. Petersen et al. 2022). The secondary seal has less surface pr. clay volume since this clay is dominated by illite rather than smectite/illite.

MERCURY INJECTION CAPILLARY PRESSURE

Mercury injection capillary pressure (MICP) studies were carried out at Core Technical Services (CTS), Aberdeen, on a Micromeritics Instrument Corporation AutoPore IV 9500 porosimeter. Air-mercury, drainage capillary pressure tests were run from vacuum to 60,000 psia (400 MPa) pressure. Cleaned and dried mm-sized cuttings samples of 4.7–6.8 g material were analysed and approximately 80 pressure steps recorded for each sample during an injection test; equilibrium was assumed after each pressure increment when the rate of mercury intrusion drop below 0.001 µL/g-sec. Besides a capillary pressure curve, mercury injection tests also offer information on the pore throat size distribution and sorting, entry/displacement pressures and theoretical permeability, and thereby important data for an evaluation of the caprock sealing capacity (Table 8). All samples from Nini-4 except the unconsolidated overburden samples were analysed and relevant diagrams of the 25 samples are included in Appendix C. An explanation to the results in Table 8 is given below:

Mercury injection porosity is determined from the following equation:

$$\text{Hg-porosity [\%]} = (\text{Hg pore volume}) / (\text{Hg bulk volume}) \cdot 100\%$$

The mercury porosity is often lower than the helium porosity, particularly for micro porous lithologies, because mercury, at maximum injection pressure of 60,000 psia, will not enter the pore volume concealed in pores with throat radius below ~2 nm.

Permeability. Also known as the theoretical or Swanson permeability K_w or $K_{Swanson}$ is a model brine permeability determined from the following equation:

$$K_w = 431\left(\frac{S_b}{P_c}\right)_A^{2.109} \qquad \text{[mD] @ 1000 psi effective stress (eq. 1)}$$

The expression $(S_b/P_c)_A$ is Swanson's parameter where S_b denotes the mercury saturation [% relative to bulk volume] and P_c is the injection (or capillary) pressure [psia]. The parameter is found as the maximum value of the relation (S_b/P_c) calculated for all pressure steps during a mercury injection run. In this study Swanson's K_w provide an independent to evaluate the performance of the calculated K_{BET} permeability that is based on the Kozeny equation (see previous chapter).

Hg P_{cd}. Air-mercury displacement pressure is determined from the intersection by the tangent to the capillary transition zone (plateau) with the "Drainage Cycle Injection Pressure" axis at the "Equivalent Saturation" = 1.0 in the "Entry Pressure" diagram included with the AutoPore raw data file. The pressure reading is reported in [psia] and normally identifies an injection pressure where 10–20% of the pore volumes have been saturated by invading mercury.

A/B P_{cd}. Air-brine displacement pressure is calculated from the above air-mercury displacement pressure by a conversion constant of 0.196 determined from the relation between the effective surface tension for the air-brine and for the air-mercury. The result is given in [MPa].

$scCO_2$ P_{cd}. Dense (super critical) CO_2-brine displacement pressure for the Nini West caprock system. The dense CO_2 displacement pressure is calculated from the air-mercury displacement pressure by conversions involving the relation between the effective surface tension $(IFT)_e$ at the specified depth for $scCO_2$-brine and air-mercury as given below in Table 9. The conversion constants are 0.098 for Lark L2 and 0.101 Lark L3, and the results are further recalculated to [MPa].

Column height H_{max}. The seal capacity H_{max}, expressed as the maximum height of a buoyant non-wetting fluid column of dense CO_2 the seal will resist, can be calculated from the following equation where P_{cd} is the $scCO_2$ displacement pressure:

$$H_{max} = P_{cd}/(g \cdot (\rho_w - \rho_{nw})) \text{ [m]}$$

g is the acceleration of gravity, and ρ is the density of brine (ρ_w) and $scCO_2$ (ρ_{nw}), all in SI units as presented in Tables 8 and 9.

Pore throat data. The median pore throat radius r_{50} identifies the radius where 50% of the pore volume have been invaded by mercury; the result is given in nano meter [nm]. The minimum pore throat radius r which can be invaded by mercury at a certain pressure is calculated from the Washburn equation (Washburn, 1921):

$$r = (2\sigma \cdot \cos\Theta)/P_c$$

where σ and Θ is the surface tension and contact angle between air and mercury, and P_c is the injection (or capillary) pressure. The quantity $(\sigma \times \cos\Theta)$ is also known as the effective surface tension $(IFT)_e$.

The pore throat sorting (PTS) index characterises the degree of ordering of the pore network from the following expression (Jennings, 1987):

$$PTS = \sqrt{\frac{(\text{Third-quartilepressure})}{(\text{First-quartilepressure})}}.$$

The first and third quartile pressures are read directly from the mercury injection capillary pressure curve at the 25% and 75% Hg-saturations. PTS ≈1 characterises the perfect homogeneous pore network (one pore size), PTS ≤1.5 is a unimodal very well sorted network.

MHR. The Mean Hydraulic Radius r_h is the average pore throat radius of the sample in [µm].

Table 8 Upper seal petrophysical data obtained from high pressure mercury injection measured at cuttings from the Nini-4 well. 'Labcon' and 'Rescon': laboratory and reservoir P, T conditions. * indicate samples with a bi-modal pore-throat size distribution (all classify as sandy siltstones). Abbreviations: $P_{cd:}$ Capillary displacement pressure; other as given in the text above.

Sample	Lark Fm	Porosity	Perm.	Hg P_{cd}	A/B P_{cd}	$scCO_2$ P_{cd}	H_{max}	Pore throat data		MHR
ID	Member	by Hg	k_w	Labcon	Labcon	Rescon	(waterwet)	radius r_{50}	PTS	radius r_h
		[%]	[µD]	[psia]	[MPa]	[MPa]	[m]	[nm]	Index	[µm]
46487	L3	26.50	96	140	0.2	0.1	34	110	2.6	0.299
46488		24.50	3.58	900	1.2	0.6	217	33	2.0	0.043
46489		21.51	5.10	600	0.8	0.4	145	39	2.2	0.067
46490		21.27	3.01	800	1.1	0.6	193	29	2.2	0.065
46491		17.68	1.45	950	1.3	0.7	229	31	1.8	0.036
46492		22.75	5.28	450	0.6	0.3	109	36	2.3	0.076
46493		21.07	2.32	900	1.2	0.6	217	27	2.1	0.061
46494		20.52	0.99	2000	2.7	1.4	483	22	1.6	0.020
46495		17.42	0.51	2000	2.7	1.4	483	19	1.8	0.030
46496	L2	18.91	0.68	1800	2.4	1.2	421	19	1.9	0.032
46497		17.56	0.48	2000	2.7	1.4	468	19	1.8	0.031
46498		17.55	1.97	750	1.0	0.5	175	28	2.2	0.063
46499		16.31	0.69	1500	2.0	1.0	351	21	2.0	0.041
46500		17.16	0.68	1200	1.6	0.8	281	20	2.0	0.036
46501		18.40	0.54	1800	2.4	1.2	421	18	2.0	0.034
46502		18.21	0.92	1100	1.5	0.7	257	23	2.0	0.047
46503		15.27	0.65	1200	1.6	0.8	281	24	1.8	0.039
46504		18.59	0.86	1050	1.4	0.7	245	23	2.0	0.039
46505		22.93	161	60	0.1	0.0	14	152/24 *	3.9 *	0.604
46506		24.28	231	55	0.1	0.0	13	152/23 *	4.2 *	0.541
46507		21.56	55	150	0.2	0.1	35	71	3.2 *	0.289
46508		21.57	26	200	0.3	0.1	47	49	3.1 *	0.218
46509		19.29	0.69	1800	2.4	1.2	421	19	1.8	0.029
46510		17.17	0.44	2000	2.7	1.4	468	18	1.8	0.033
46511		14.92	0.12	3000	4.1	2.0	701	11	1.8	0.012

The relationship between modelled permeabilities from specific surface areas using the Kozeny equation (K_{BET}) and the theoretical or Swanson permeability (K_w or $K_{Swanson}$) is shown in Figure 20. This comparison shows that there is a correlation between the two measurements, but this may be circumstantial as many low permeability samples fall into a disordered cloud around 1 uD, and five bi-modal or poorly sorted samples have been excluded because they fall way-off the model line in Figure 20.

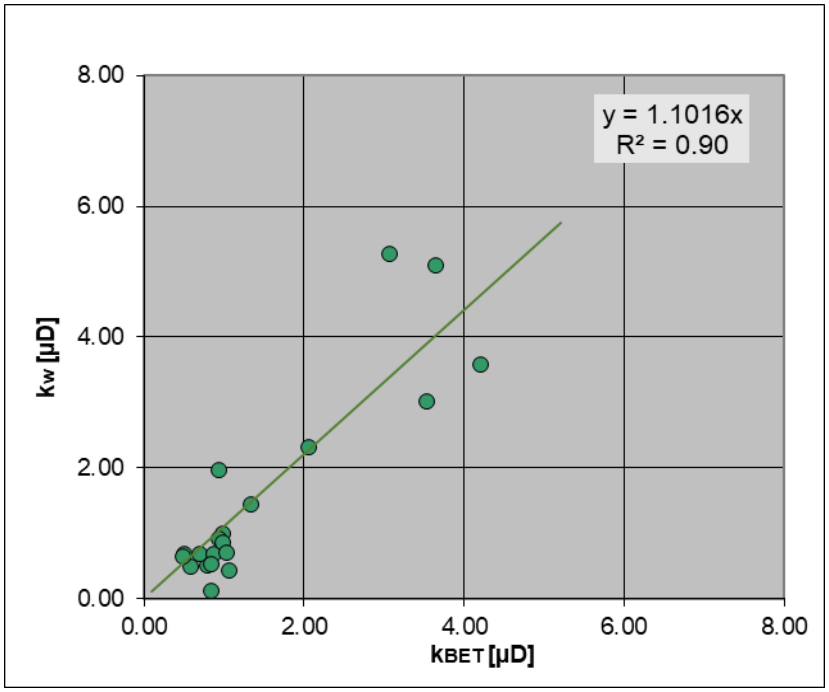

Figure 20 Relationship between permeability modelled from specific surface determinations (K_{BET}) using the Kozeny equation and the theoretical or Swanson permeability (K_w). Five sandy siltstone samples that have high permeability due to mainly bimodal pore structure or just poor sorting are not included.

From inspection of the MICP diagrams, most of the secondary seal mudstones have a broad unimodal pore throat size distributions (Figure 21) and most have PTS index between 1.5 and 2.0 (Table 8) that characterises a medium sorted sediment. Compared to the primary seal then no samples in the secondary seal have extremely small throat sizes, r_{50} and MHR of 6–8 nm, that characterises a very fine grained and tight sediment (Table 8). Four samples have pore throats > 100 nm. These are all classified as sandy siltstones and have bimodal pore size distributions.

As pore throat size is the major controlling property on permeability and capillary pressure and thereby the most important parameter for determining the displacement pressure in the CO_2 - brine - mudstone system, ie. the pressure where dense CO_2 is expected to invade the Nini West caprock, then some examples of the capillary pressure curves measured for the Nini mudstones are shown in Figure 21.

Hg-injection, representative sample for Lark Fm L3: 46490 / PTS Index = 2.2

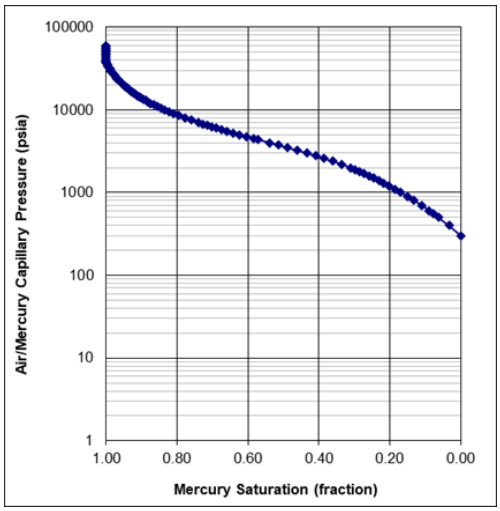

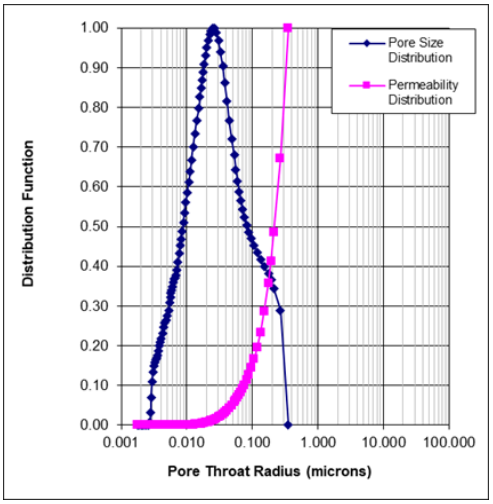

Hg-injection, representative sample for L ark Fm L2: 46504 / PTS Index = 2.0

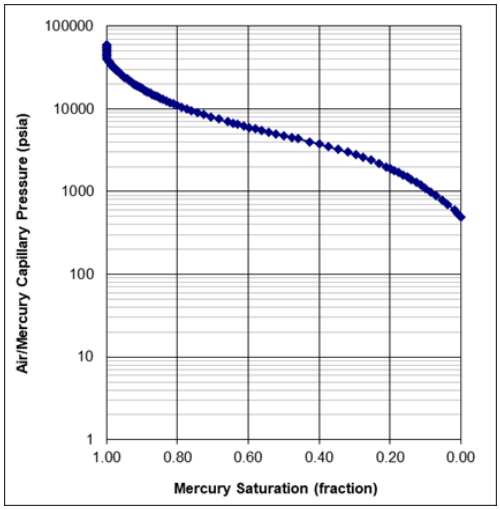

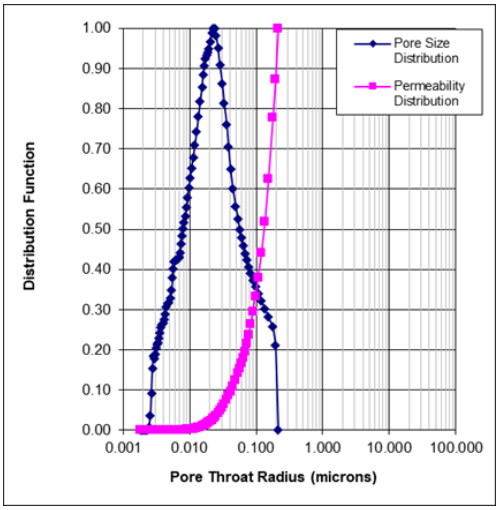

Hg-injection, representative sample for Lark Fm L2, bimodal: 46505 / PTS Index = 3.9

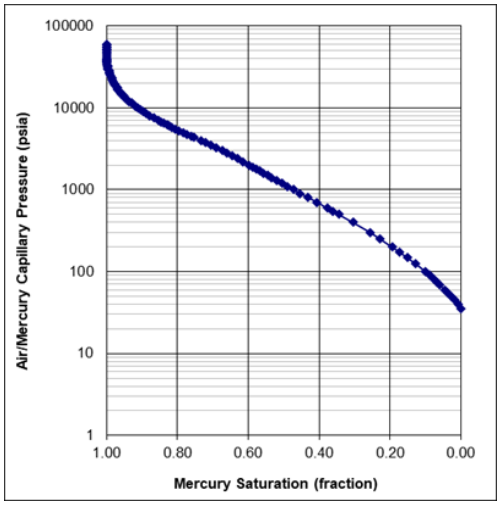

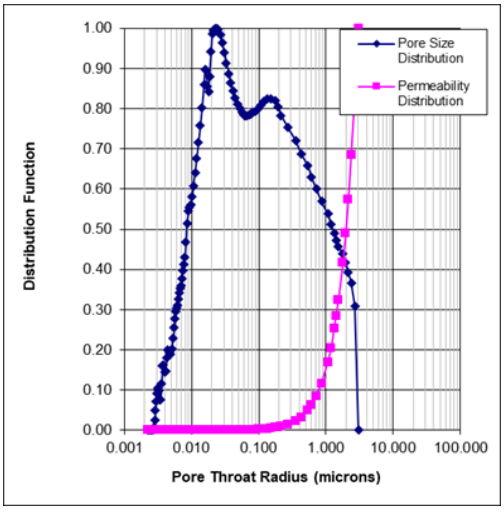

Figure 21 (previous page) High pressure mercury injection diagrams for the Nini West secondary seal; air-mercury capillary pressure curves (left), and pore throat radius distribution diagrams (right). The seal capacity is significantly below the results observed for the primary seal (Schovsbo et al., 2021; Petersen et al., 2022) with displacement pressures of 500–2000 psi. Pore size distributions peak around 20–30 nm throat radius with bi-modal samples exceeding 100 nm which serves to underpin the declining seal capacity.

In Figure 22 the depth profiles of the $K_{BET,}$ K_w or $K_{Swanson}$ and the air-mercury displacement pressures are presented. The two permeabilities in Figure 22 is compared with the K_{BET} wire-line log model (see Petrophysical Evaluation and Models). The K_{BET} and the $K_{Swanson}$ estimates track the K_{BET} wire-line log with $K_{Swanson}$ showing clear deviations towards higher permeabilities especially foe the sandy siltstone beds. This suggests that the modelled K_{BET} should be regarded as minimum permeability especially for sandy siltstone beds. For these beds wireline model for the K_{BET} is higher in the sandy siltstone beds than calculated from the samples by either K_{BET} or $K_{Swanson}$. The reason for this that the wireline model predicts the presence of less clayey and more porous lithologies and that the measurements tend to be made on mainly cemented cuttings that will survive the drilling process hence these are biased towards lower permeabilities and lower porosities.

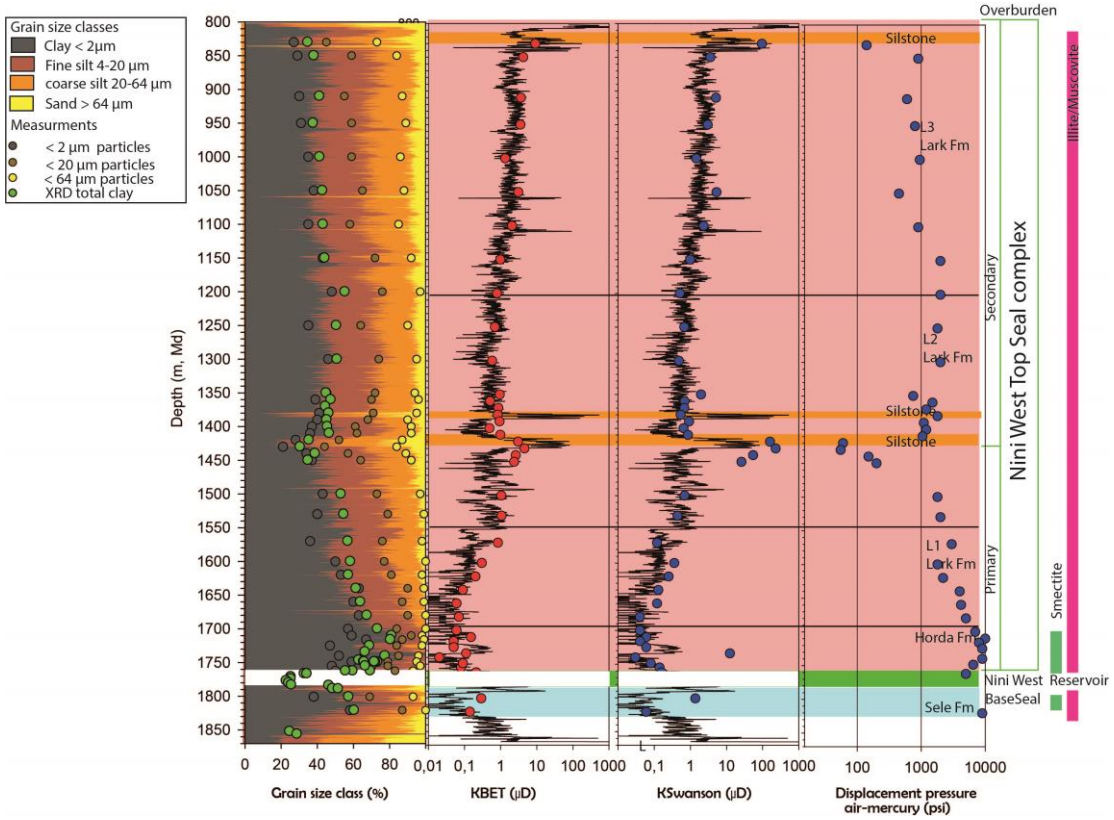

Figure 22 Grain size, permeabilities (K_{BET} and $K_{Swanson}$) and air-mercury displacement pressure. For porosity variation see Figure 24.

The air-mercury displacement pressure has a clear peak in the Horda Fm where values up to 10 000 psi is reached (Figure 22). In the secondary seal, low displacement pressures are seen in the lower part around the sandy siltstone beds. In the other Lark samples – both from the upper primary seal and from the mid secondary seal stable high values of around 1000–2000 psi is measured. From around 1050 m the entry pressures are below 1000 psi (Figure 22).

The variation in displacement pressures largely reflect the variation in proportion of clay size particles in the shales and are inverse proportional to the quartz content. Mudstones all have high displacement pressure (>1000 psi) with the smectite rich mudstones having significant higher up to 10 000 psi. Lowest displacement pressures are within the sandy siltstones that occur within the interval 1400–1440 m and in the top of Lark L3 where shales with low to no seal capacity occur.

Concluding remarks on sealing capacity

The petrophysical parameters at reservoir conditions used in the calculation of the seal capacity is shown in Table 9. The capacity is expressed as the maximum vertical column H_{max1} of dense CO_2 the caprock can withhold before displacement of the wetting brine phase in the caprock, on the condition that the caprock remains strongly water-wet (ie. contact angle $\Theta = 0°$, so $\cos \Theta = 1$ in the Washburn equation). However, the condition of wettability at reservoir conditions for shales has been questioned, and there are very conflicting results on the subject. A review can be found in Jafari and Jung (2016), and we will here use a conservative (pessimistic) estimate of 60° for the contact angle (ie. contact angle $\Theta = 60°$, so $\cos \Theta = 0.5$ in the Washburn equation), which means that the caprock in a less water-wet scenario will hold back only half the column height H_{max2} (Table 9). Besides the two wettability scenarios, the table gives two different estimates for the dense CO_2 displacement pressure P_{cd} calculated based on a depth at 1400 m and at 1200 m. These scenarios reflect situation where supercritical CO_2 has accumulated at the base of the Secondary seal or within the Secondary seal and thus a breach or by-pass of the primary seal and accumulation in a secondary storage site that will be composed of the sandy siltstone beds.

For both scenarios we find a max CO_2 column within the interval 110–140 m. This very conservative estimate should be seen in comparison with the possible maximum column heights in the secondary storage sites. These beds have a thickness of about 10 m and there is a comfortable caprock safety column overhead for CO_2 sequestration in the reservoir even for the most pessimistic scenario. The evaluation of the column heights should however be viewed here only tentative and should be evaluated in a full 3D model.

Table 9 Upper seal fluid and capacity data at reservoir conditions estimated for the Nini West storage site. P, T conditions from Olsen et al. (2020), density data at P, T conditions from NIST Webbook (2022), IFT data from Liu et al. (2016) and other data from the present study. Observe that average and peak data are given for both the lower and upper member of the Nini West Upper seal complex. Column height H_{max1} assumes the caprock is strongly water wet, H_{max2} is less water wet, i.e. corrected for a change in contact angle of 60° (Jafari and Jung, 2016).

Depth	Pore P	Temp.	TDS	ρ_w (brine)	ρ_{nw} ($scCO_2$)	IFT ($scCO_2$-brine)	P_{cd}	H_{max1} *	H_{max2} *	Comment
[m]	[MPa]	[°C]	[mg/L]	[kg/m^3]	[kg/m^3]	[mN/m]	[MPa]	[m]	[m]	
1200	13.5	40	75000	1046.5	753.64	37	0.67	235	117	Avg. L3
							1.39	483	241	Max. L3
1400	15.8	45	83000	1051	756.6	36	0.83	287	144	Avg. L2
							1.69	584	292	Max. L2

PETROPHYSICAL EVALUATIONS AND MODELS

The objectives of the petrophysical evaluation and modelling are to update and extend the petrophysical model of the primary seal to the secondary seal by means of calibration to measured properties such as total porosity, permeability, and clay content. Below is outlined the petrophysical workflow, the lower seal model and the modifications that has been made to adapt it to the secondary seal.

Petrophysical workflow

- Geological analysis i.e. structuring of the seal into primary seal, secondary seal and overburden and mapping of porous and permeable beds within the seal
- Sampling of representative rock types. Analysis of the elemental composition and mineralogy to study the relationship to the GR curve
- Volume of clay particles from experiments determined to calibrate wireline based Vclay model and to update the geological model
- Total porosity determinations to calibrate the wireline grain density and total porosity models
- Thin section to validate rock types and to examine mineralogy and porosity
- Surface area and Vclay combined with total porosity to model permeability and to calibrate wire-line models
- Measurement of the air-mercury displacement pressure by MICP and subsequent capacity estimation of the seal sections.
- Mudgas to examine upwards migration

The Nini-4 well is considered to have a good bore hole and few erroneous readings. Hence steps in the workflow to edit logs for removing artefacts from poor hole conditions or the like has not been included.

Summary of the petrophysical model for the primary seal – the Petersen et al. (2022) model

A petrophysical model for the primary seal was presented by Schovsbo et al. (2021) in the GEUS report series and by Petersen et al. (2022) in a peer-reviewed scientific paper. This model consists of wireline based calculations of total porosity, grain density, clay volume and permeability based on core and cuttings data calibrated to wireline logs.

In the primary seal the total clay content measured by XRD compared poor to the down-hole gamma ray log variation caused by the variable clay mineral assemblage and the “hot” organic rich zones. Relative low gamma ray responses were notably seen in the smectite rich intervals likely reflecting its low K content. Following this observation, the clay volume was modelled from the VP/VS ratio that also is known to be lithological sensitive using

$$\text{Total clay content (\%)} = (VP/VS - 1.8) / 0.013$$

The constants 1.8 and 0.013 was empirical determined from the Nini-4 VP/VS log representing high and low total clay content determined from XRD measurements on core and cuttings.

Total porosity (PHI) was evaluated from the formation density log combined with a grain density model as:

$$PHI\ (\%) = (\sigma_{grain} - \sigma_{bulk}) / (\sigma_{grain} - \sigma_{fluid})$$

and

$$\sigma_{grain} = (1 - V_{clay}) \cdot 2.7\ g/cm^3 + (V_{clay}) \cdot 2.3\ g/cm^3$$

where σ_{grain} is the grain density calculated from the volume of clay (V_{clay}) assuming a grain density of 2.7 g/cm^3 for clean reservoir and a grain density for pure clay of 2.3 g/cm^3, σ_{bulk} is the bulk formation density from the density log and σ_{fluid} is the fluid density assumed to be 1.05 g/cm^3 reflecting a medium saline brine in the Nini area.

Permeability was estimated from capillary tube models, which use easily measured physical properties such as porosity, grain density and specific surface area data (Kozeny, 1927).

$$K_{BET} = c\frac{\varphi^3}{(1-\varphi)^2\ {S_s}^2}$$

where K_{BET} is the permeability, φ is porosity, S_s is specific surface (grain-surface area per grain volume). The c factor is the Kozeny constant that will have a value between 0.22–0.24 depending on porosity (Mortensen et al., 1998).

The input to the wireline model consisted of porosity, grain density and the surface area determined from the V_{clay} and surface areas relationship. The linear relationship

$$S_s\ (m^2/g) = 0.81 \cdot \text{Clay (\%)} - 2.32\ m^2/g$$

was used in the petrophysical interpretation of the surface area for the primary seal based on empirical data from the primary seal in the Nini-4 well.

Petrophysical model for the secondary seal

The petrophysical model for the primary seal cannot be extended to also account for the upper seal mainly due to a shift in relationship between the Vp/Vs ratio and clay volume that occur around 1440 m and likely related to the pore pressure regime shift, which impact the sonic logs. However, since we observe a shift in clay mineral assemblages from a smectite rich Horda and to an illite rich rock in the Lark then the ability of the GR log to model the Vclay is restored.

The Petersen et al. model has been improved and modified to extend the petrophysical model to the secondary seal so that Vclay is calculated according to:

$$\text{Vclay} = (\text{GR reading} - GR_{min}) / (GR_{max} - GR_{min})$$

where GR_{min} represent 0 clay and GR_{max} represent 100% clay. The values are determined as 35 and 150 API respectively from cross-plotting GR and Vclay determined from grain size determinations.

The % clay and silt fractions are determined from:

$$\text{Smaller than 20 µm (\%)} = 193 \cdot \text{Vclay (\%)} / (16.4 + \text{Vclay (\%)})$$

$$\text{Smaller than 63 µm (\%)} = 111 \cdot \text{Vclay (\%)} / (2.25 + \text{Vclay(\%)})$$

The sand fraction is determined from:

$$\text{Larger than 63 µm (wt\%)} = 100 \text{ (\%)} - \text{Less than 63 µm (\%)}$$

Carbonate cemented beds:

Carbonate stringers occur notably in the Horda Fm. These can be identified as having low porosity (<< 10%). Currently these beds have not been flagged out and will be considered as sandy/silty beds due to their low GR response. In statistical summaries these beds are removed by removing low porosity log readings (<10%).

Additionally, the empirical relationship (from Figure 19) for calculating the specific surface in the secondary seal is:

$$S_s\ (m^2/g) = 0.54 \cdot \text{clay(\%)} - 0.61\ m^2/g$$

This new correlation is introduced to account for lower surface pr. volume of clay in the illite rich Lark than in the smectite rich Horda Fm. As the S_s measured by the BET method cannot distinguish between inner and outer surface area, which might lead to an overestimation of the outer surface areas in smectite rich layers.

Seal Rock types

Figure 23 presents a triangular rock type classification based on the sand, silt and clay content according to Folk et al. (1970). The seal samples mostly plot within the mudstone field and towards the sandy siltstone field. Overburden samples plot within the Sand to silty sand. A trajectory of the wireline grain seize model is included with the diagram in which the proportion of clay size particle has been calculated from the Vp/Vs ratio in the primary seal and the GR curve in the secondary seal, and used to calculate the silt and sand content. This model generally tracks the trend defined by the samples although it, at high clay contents, tends to plot with too low silt and too high sand content.

The wire-line model indicate that the seal section includes silty sand rock types and thus that the cuttings do not reflect the full range in rock types present in the seal.

From Figure 24 it can be seen that these silty sand beds are estimated to occur within the sandy siltstones and thus that they do not represent any new coarse beds, but rather an indication that the sandy siltstone beds may be coarser grained that the cuttings reflect. Within these intervals we have studied all cuttings sample intervals available, and thus no new samples can be provided to test this hypothesis. We know that the cuttings represent average compositions and thus that the grain size also represent averages. Hence the classification sandy siltstone is valid for the average interval and does not exclude that it is composed of discrete distributions of sand-silt-clay beds. We could in fact expect this since the Micro CT scanning show lamination on a mm-scale. However, for this to be solved and clarified we need core from the interval. Any such discrete sand-silt-clay beds are below the resolution of the logs, e.g approximately 15 cm.

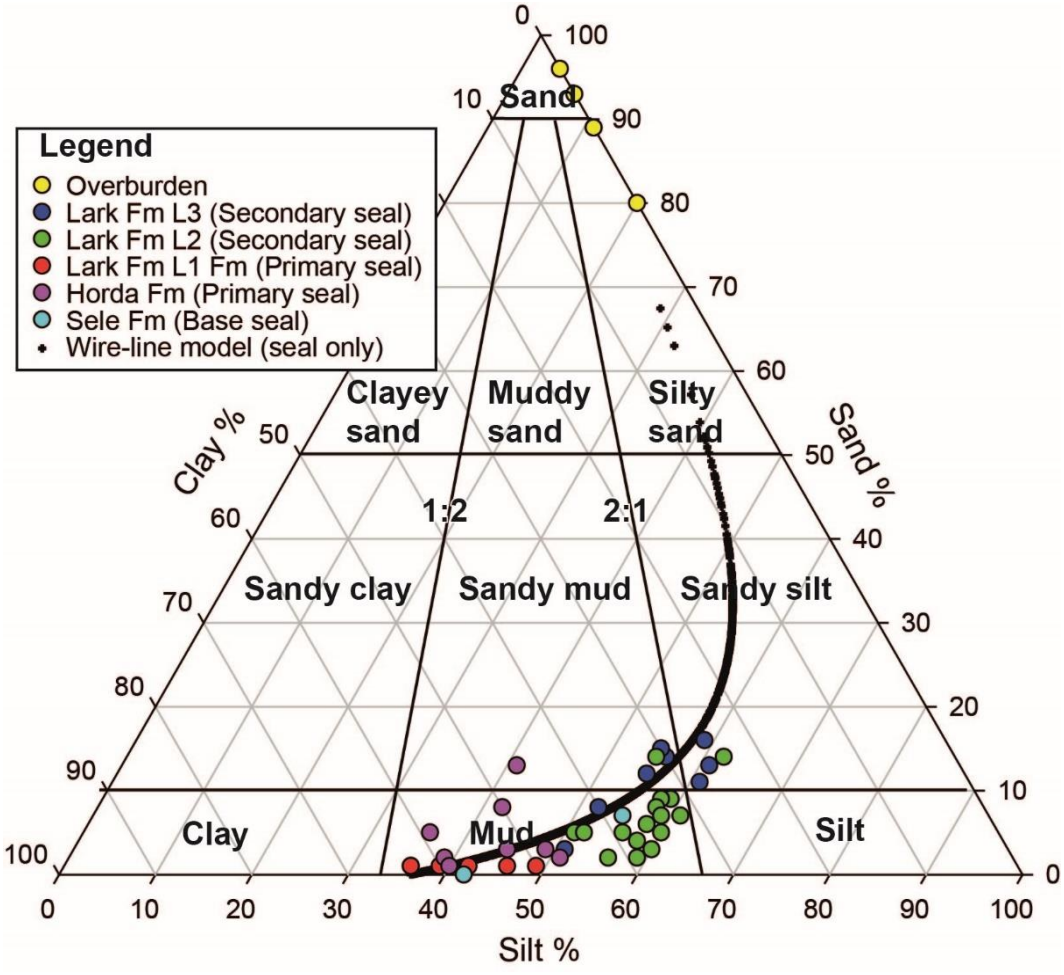

Figure 23 Rock type classification. In the wire-line model in Nini-4. Only seal samples with total porosity >10% is shown. Classification is after Folk et al. (1970).

Vclay, total porosity and permeability in the upper seal

Figure 23 presents the petrophysical model for the Nini-4 seal complex applying the Petersen et al. (2022) model for the base and primary seal and with the modified Petersen et al. model adapted (modifications mentioned above wrt. Vclay and S_s) for the secondary seal. For the grain size the Vclay has been used to estimate the silt and sand fractions according to Figure 7.

The Vclay model show that the clay content slightly fluctuates between 40–50% with the exception of the lower part where the sandy siltstone beds occur. Here Vclay less than 20% have been modelled. The modelling of the coarser fractions indicate that sand sized particles only occur in minor fractions typical is less than 10% apart for the interval 1375–1425 m where the sand content increase together with the silt size fraction.'

The total porosity increases from rather stable value around 20% in the basal part of the secondary seal to around 30–35% in the top of the secondary seal. This stratigraphical upward increase is almost linear and is likely to be compaction driven reflecting the rather shallow burial of the top of the secondary seal of 850 m.

High porosities are modelled in the sandy siltstone beds and in the upper most sandy beds in Lark (Figure 24). The log derived porosities are much higher than measured on cuttings. For the wireline model to be incorrect we would assume either erroneous log readings or change in rock types to one with a significant lighter grain type such a diatomite or the like. We do not have indication that the density reading is in error across the beds, and we do not have indications from XRD that minerals with low grain density such as opal is present (Figure 10). Instead, XRD suggest that quartz is present. Besides, it is more likely that the porosity measured on the cuttings are too low as the cuttings are likely to be biased towards more cemented parts of the formation that can retain its structure during drilling rather than uncemented grains that will disintegrate.

Modelled permeability exhibit lowest values in the Horda Fm and lowermost Lark Fm where values around 0.3 µD is typical (Figure 24). From the lower Lark – L1 – and throughout the Lark Fm the permeabilities increases to around typical values of 3–5 µD i.e. about a 10-fold increase. Peak values are associated in the sandy siltstone beds.

In Schovsbo et al. (2021) we estimated that the modelled averages permeabilities of the primary and secondary seal were also most equal i.e. having averages of about 0.3–0.4 µD. The reason for this discrepancy was that the petrophysical model in phase 1 was not able to pick-up the decreasing clay content that is seen upwards in the Lark Fm, and did not correct for shift in mineralogy that affect the surface area of the clays. This possibility was also commented on by Schovsbo et al. (2021) that stated: "If more analysis from the Lark Fm will be available, then it is likely that the petrophysical parameters will be selected for each formation due their different clay mineralogical composition".

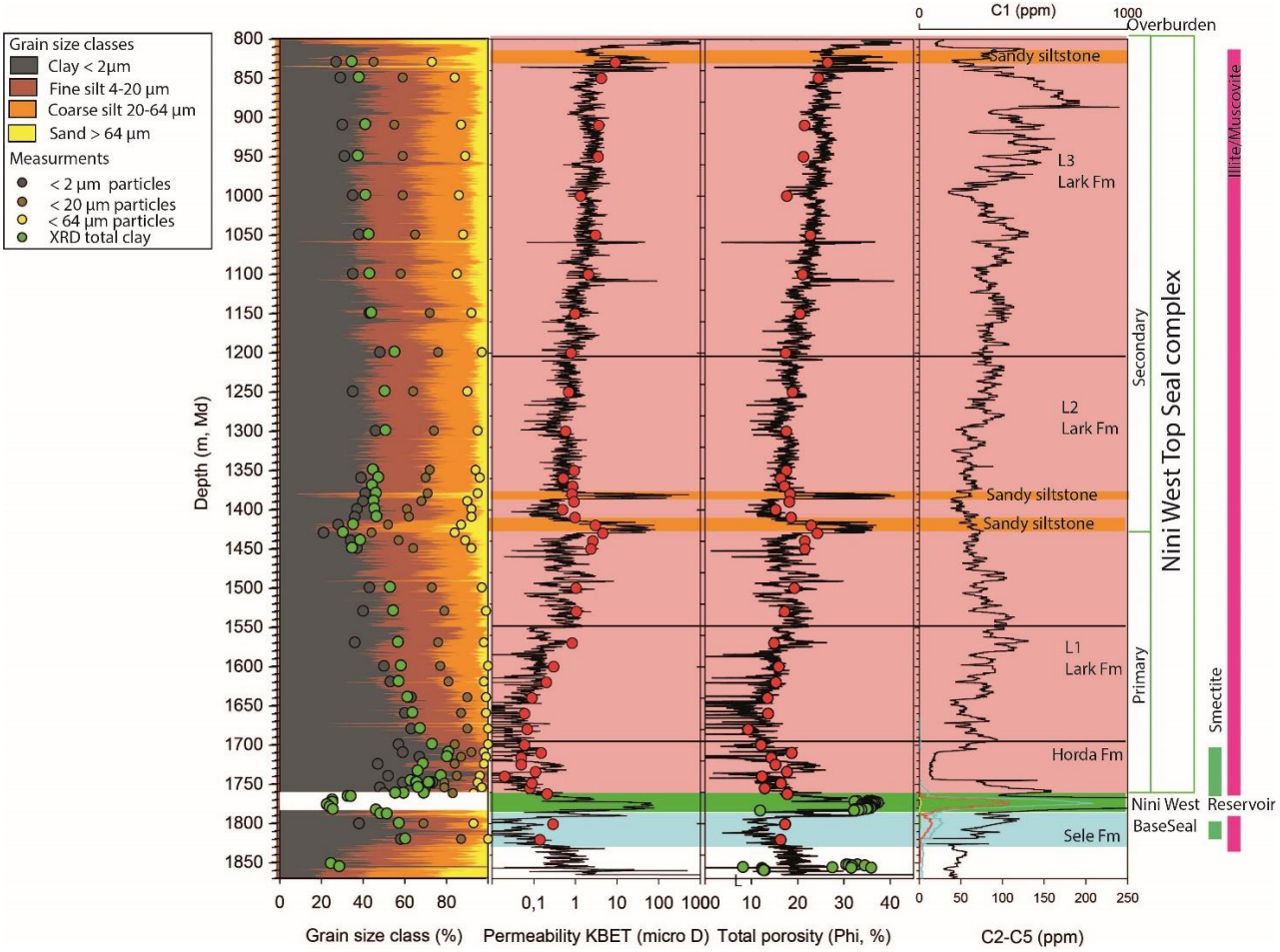

Figure 24 Grain size, permeability (K_{BET}), total porosity (PHI) and mudgas logs of the Nini-4 well. Mudgas legend: Black, methane (C1); green, ethane (C2); red, propane (C3).

Concluding remarks

The petrophysical model for the Nini West seal (the Petersen et al. model) has been updated to also account for the secondary seal based on 30 cuttings samples analysed for grain size distribution, elemental composition, total porosity and mercury injection.

The petrophysical workflow is described and algorithms for calculating Volume of clay (Vclay), Volume of fine silt, Volume of coarse silt, Volume of sand, Total Porosity (PHI), grain density, specific surface area (S_S), permeability following the Kozeny equation (K_{BET}) based on wireline logs are presented.

MUDGAS LOGS

No additional mudlogs were evaluated in the report compared to those reported in Schovsbo et al. (2021) and Petersen et al. (2022).

Of interest here is that the porous sandy siltstone beds in the 1400–1440 m interval of Nini-4 are not picked up by enhanced gas composition (Figure 24). This suggest that the beds not are in communication with the Frigg Reservoir and that no migration through the lower seal section has occurred. In terms of saturations, the beds are thus 100% water saturated.

Concluding remarks

The general very low gas concentrations and the gas composition in the seal complex demonstrate that the caprock has an efficient sealing capability that area-wise seems to extend beyond the Nini West Field. This is supported by: 1. Only very limited vertical migration of thermogenic gas into the lower part of the primary seal (Horda Fm and Lark L1); 2. No migration of thermogenic gas into the upper part of the primary seal and the secondary seal; 3. Many hundreds of meters of caprock is overlying the vertical thermogenic gas migration front; 4. The gas recorded in most of the seal complex and the overburden is very likely non-moveable *in situ* generated biogenic gas.

SALINITY ANALYSIS IN POROUS BEDS

The sandy siltstone beds in the Lark Fm have distinct lower resistivities than the shaly Lark (Figure 25). The decrease in resistivity likely indicate that saline brine is present in a porous rock within the beds. To investigate this a bit further we tried to guess estimate the salinity of the water using the Archie equation:

$$S_w^{\,n} = \frac{R_w}{(\Phi^m \times R_t)}$$

where:

S_w = water saturation, n = saturation exponent, R_w = formation water resistivity at formation temperature, Φ = porosity, m = cementation exponent; R_t = resistivity of the formation.

Assuming that $S_w = 1$ for the beds as indicated by the mudlog gas composition (c.f. Figure 24) then

$$R_w = R_t \times \Phi^{m/n}$$

To estimate R_w in the sandy siltstone beds we use the porosity from the density log and a temperature gradient of 35 ^oC pr. km. For the interval @ 1422 m. R_o from the deep resistivity log is 0.386 ohm.m and PHI is 30.7%. If the bed consists of loosely consolidated sandy siltstone then the normal assumptions that m is 2 and n is 1 might not be true. If we assume that m = 1.5 and n =0.6. Then R_w is 0.107 ohm @ 45 ^oC corresponding to about a 30 000 NaCl equivalent brine. If on the other hand n =1 then R_w is 0.064 ohm corresponding to an 80 000 NaCl equivalent brine.

The above calculations suggest that there is a large uncertainty of the salinity estimation. The estimates easily range between one third to near equal salinities as in the Frigg Reservoir where the salinity is 87 900 ppm NaCl equivalents (Holmslykke et al., 2021).

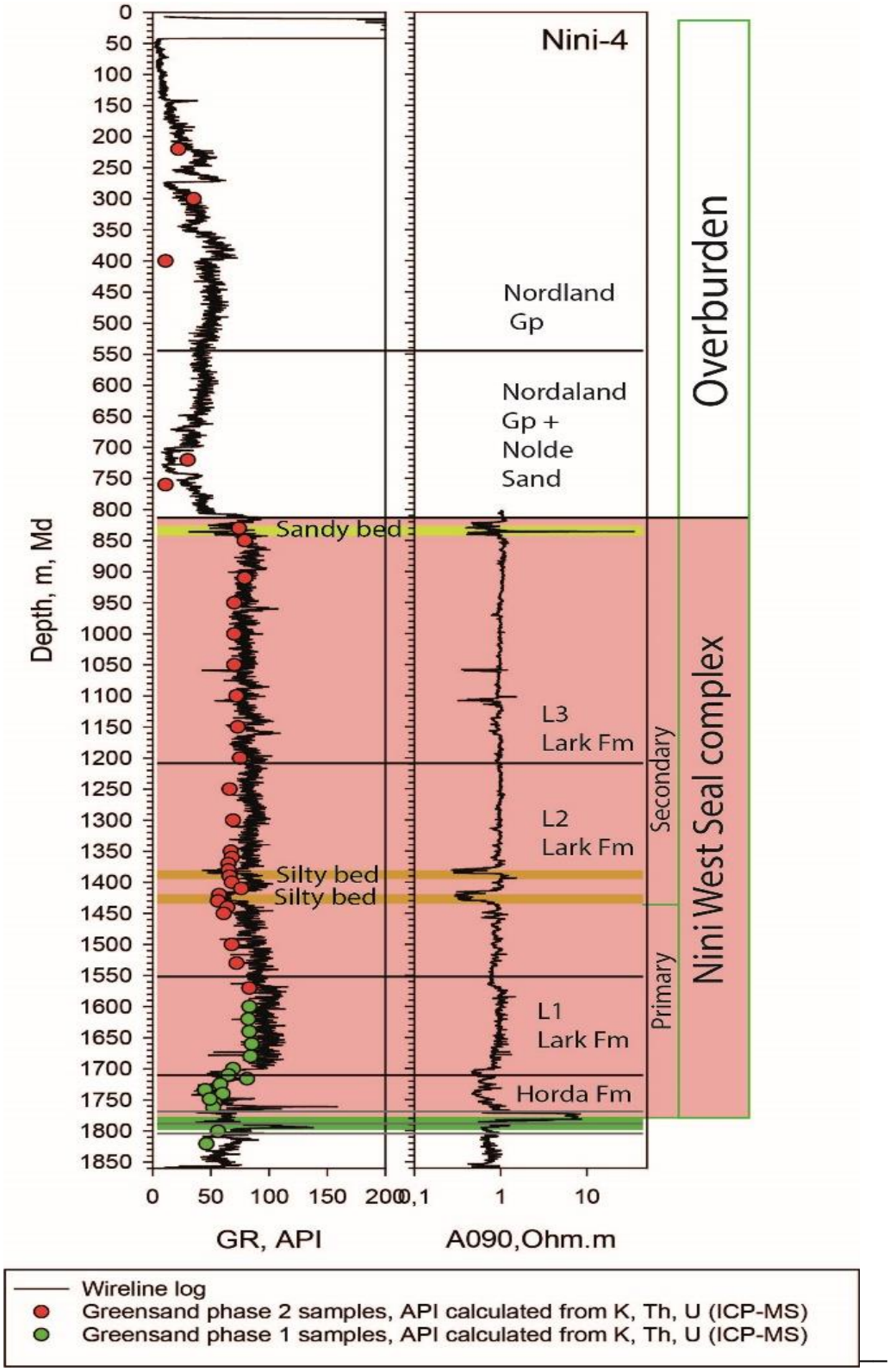

Figure 25 Nini-4 well profile showing GR and deep resistivity logs.

ACKNOWLEDGMENT

The EUDP funded “Project Greensand Phase 2” is acknowledge for financial support. The Project Greensand consists of a large consortium led by INEOS and Wintershall DEA and wherein GEUS is acting as research partner. The technical teams at GEUS and DTU are thanked for analytical assistance.

REFERENCES

Bordenave, M.L., Espitalié, J., Leplat, P., Oudin, J.L., Vandenbrouke, M., 1993. Chapter II.2. Screening techniques for source rock evaluation. In: Bordenave, M.L. (Ed), Applied petroleum geochemistry. Éditions Technip, Paris, 219–278.

Brunauer, S., Emmett, P. H., Teller, E., 1938. Adsorption of gases in multimolecular layers. Journal of the American Chemical Society 60, 309–319.

Bruno, M.S., Lao, K., Diessl, J., Childers, B., Xiang, J., White, N., van der Veer, E., 2014. Development of improved caprock integrity analysis and risk assessment techniques. Energy Procedia 63, 4708–4744.

Ellis, D.V., Singer, J.M., 2007. Well logging for earth scientists. 2nd edition. Springer, Dorderecht, the Netherlands, 687 pp.

Folk, R.L., Andrews, P.B., Lewis, D.W., 1970. Detrital sedimentary rock classification and nomenclature for use in New Zealand. New Zealand Journal of Geology and Geophysics, 13, 937–968.

Hillier, S., 2003. Quantitative analysis of clay and other minerals in sandstones by X-ray powder diffraction (XRPD). In: Worden, R.H. and Morad, S. (Eds), Clay mineral cements in sandstones. International Association of Sedimentologists Special Publication 34, 213–251.

Holmslykke, H.D., Weibel, R., Lorentzen, H.J., Schovsbo, N.H., 2020. Capatibility analysis of the Palecene sand reservoir of the Nini West Field to CO_2 – first results of batch experiments. Danmarks and Grønlands Geologiske Undersøgelse Rapport 2020/31, 15 pp.

ISO 17892-4, 2016. Geotechnical investigation and testing - Laboratory testing of soil - Part 4: Determination of particle size distribution, 31 pp.

ISO 9277, 2010. Determination of the specific surface area of solids by gas adsorption – BET method, 24 pp.

Jafari, M., Jung, J., 2016. The change in contact angle at unsaturated CO_2-water conditions: implication on geological carbon dioxide sequestration. Geochem. Geophys. Geosyst. 17, 3969–3982; https://doi.org/10.1002/2016GC006510

Jennings, J.B., 1987. Capillary pressure techniques: Application to exploration and development geology. AAPG Bulletin 71, 1196–1209.

Kozeny, J. 1927. Über kapillare Leitung des Wassers im Boden. Sitzungsberichte der Kaiserlichen Akademie der Wissenschaften, Wien, 136, 271–306.

Liu, Y., Li, H.A., Okuno, R., 2016. Measurements and modeling of interfacial tension for CO_2/CH_4/brine systems under reservoir conditions. Industrial & Engineering Chemistry Research 55, 12358−12375.

Mbia, E., Fabricious, I.L., Collins, O.O., 2013. Equivalent pore radius and velocity of elastic waves in shale. Skjold Flank-1 Well, Danish North Sea. Journal of Petroleum Science and Engineering 109, 280–290. https://doi.org/10.1016/j.petrol.2013.08.026

Mortensen, J., Engstrøm, F., Lind, I., 1998. The relation among porosity, permeability, and specific surface of chalk from the Gorm field, Danish North Sea. SPE Reservoir Evaluation and Engineering 1, 245–251.

NIST Chemistry Webbook, 2020. National Institute of Standards and Technology, US Department of Commerce. Thermophysical Properties of Fluid Systems (nist.gov).

Ohm, S.E., Karlsen, D.A., Roberts, A., Johannessen, E., Høiland, O., 2006. The Paleocene sandy Siri fairway: an efficient "pipeline" draining the prolific Central Graben? Journal of Petroleum Geology 29, 53–82.

Olsen, D., Mohammadkhani, S., Weibel, R., Schovsbo, N.H., 2020. Preliminary results of CO2-flooding experiment Exp-1. Greensand Project Phase 1 WP2. Danmarks and Grønlands Geologiske Undersøgelse Rapport 2020/54, 19 pp.

Petersen, H.I., Springer, N., Weibel, R., Schovsbo, N.H., 2022. Sealing capability of the Eocene–Miocene Horda and Lark formations of the Nini West depleted oil field – implications for safe CO2 storage in the North Sea. International Journal of Greenhouse Gas Control 118, 103675. https://doi.org/10.1016/j.ijggc.2022.103675

Riding, J.B., Rochelle, C.A., 2005. The IEA Weyburn CO_2 monitoring and storage project. Final report of the European Team. British Geological Survey Research Report RR/05/03. http://nora.nerc.ac.uk/id/eprint/3682/1/RR05003.pdf

Rouquerol, J., Llewellyn, P., Rouquerol, F., 2007. Is the BET equation applicable to microporous adsorbents? Characterization of Porous Solids VII. P.

Schiøler, P., Andsbjerg, J., Clausen, O.R., Dam, G., Dybkjær, K., Hamberg, L., Heilmann-Clausen, C., Johannesen, E.P., Kristensen, L.E., Prince, I., Rasmussen, J.A., 2007. Lithostratigraphy of the Palaeogene–Lower Neogene succession of the Danish North Sea. Geological Survey of Denmark and Greenland Bulletin 12, 77 pp.

Schovsbo, N.H., 2020. Evaluation and risking of the seal capacity for CO_2 storage in the Nini West Oil Field, Denmark. Project Greensand WP4 TRL3. Danmarks and Grønlands Geologiske Undersøgelse Rapport 2020/26, 61 pp.

Schovsbo, N.H., Petersen, H.I., Weibel, R., Holmslykke, H.D. and Springer, N., 2021. Characterising and evaluation of the seal capacity based on core and cutting analysis of the Nini-4 and Nini-4a wells. Project Greensand – WP4 final report. Danmarks og Grønlands Geologiske Undersøgelse Rapport 2021/38.

Swanson, B.F., 1981. A simple correlation between permeabilities and mercury capillary pressures. Journal of Petroleum Technology, 2498–2504.

Washburn, E.W., 1921. Note on a method of determining the distribution of pore sizes in a porous material. Proceedings of the National Academy of Science 7, 115–116.

APPENDIX A – GRAIN SIZE ANALYSIS

Grain Size Distribution
Geotechnical

Sample Id: Nini-4 200-220
Lab. Id: 46482
Projekt Niels Schovsbo
Subject: 0
Date: 08-03-2022
Executed: PS
Remarks:

GEUS

Total Weight 30,2 g

Size Fractions

Sieve Analysis

	Size	Size	Weight	Weight	Cumulated amount passing
	mm	Φ	g	%	%
Gravel	16,00	-4,00	0,00	0,00	100,00
	8,00	-3,00	0,00	0,00	100,00
	4,00	-2,00	0,00	0,00	100,00
	2,80	-1,49	0,06	0,20	99,80
	2,00	-1,00	0,59	1,95	97,85
Sand	1,40	-0,49	1,23	4,07	93,77
	1,00	0,00	1,48	4,90	88,87
	0,710	0,49	0,36	1,19	87,68
	0,500	1,00	0,63	2,09	85,60
	0,355	1,49	1,30	4,30	81,29
	0,250	2,00	2,21	7,32	73,97
	0,180	2,47	2,02	6,69	67,28
	0,125	3,00	4,96	16,42	50,86
	0,090	3,47	8,00	26,49	24,37
	0,075	3,74	2,53	8,38	15,99
	0,063	3,99	1,65	5,46	10,53
	< 0,063	> 3,99	3,18	10,53	0,00

Size Classes (DGF-Bulletin 1 1988)

		Weight %
Silt and clay	(< 0,063 mm):	10,53
Sand, fine	(0,063 mm - 0,200 mm):	58,67
Sand, medium	(0,2 mm - 0,6 mm):	17,39
Sand, coarse	(0,6 mm - 2 mm):	11,26
Gravel	(> 2 mm):	2,15
Sum:		100,00

Moments Measures (Folk and Wards)

Percentile Amount in sieve	Percentile Amount passing	d(mm)	Φ
5%	95%	1,58	-0,66
16%	84%	0,45	1,16
25%	75%	0,26	1,92
40%	60%	0,16	2,68
Median 50%	50%	0,12	3,01
75%	25%	0,09	3,46
84%	16%	0,08	3,74
90%	10%	-------	-------
95%	5%	-------	-------

Moments Statistics

Mean	2,64
Sorting	-------
Skewness	-------
Kurtosis	-------
Uniformity Coefficient	-------

The analysis is executed according to DS 405.9 extended by sieves to the ½ phi scale

Size Classes and Percentiles are found by linear interpolation

Formulas

Mean (ϕ16%+ϕ84%+ϕ50%) / 3 (Folk and Ward 1957)

Sorting (ϕ84%-ϕ16%) / 4 + (ϕ95%-ϕ5%) / 6,6 (Folk and Ward 1957)

Kurtosis (ϕ95% - ϕ5%) / (2,44 * (ϕ75% - ϕ25%)) (Folk and Ward 1957)

Skewness (ϕ16%+ϕ84% - 2*ϕ50%) / (2*(ϕ84%-ϕ16%)) + (ϕ5%+ϕ95% - 2*ϕ50%) / (2*(ϕ95%-ϕ5%)) (Folk and Ward 1957)

Uniformity Coefficient (d60% / d10%) (dgf-Bulletin 1988)

Mean, sorting, skewness and kurtosis are based on "Amount in sieve". Uniformity coefficient is based on "Amount passing".

Øster Voldgade 10 1350 København K
Tel.: +45 38 14 20 00 Telefax: +45 38 14 20 50
Email: GEUS@geus.dk
www.geus.dk

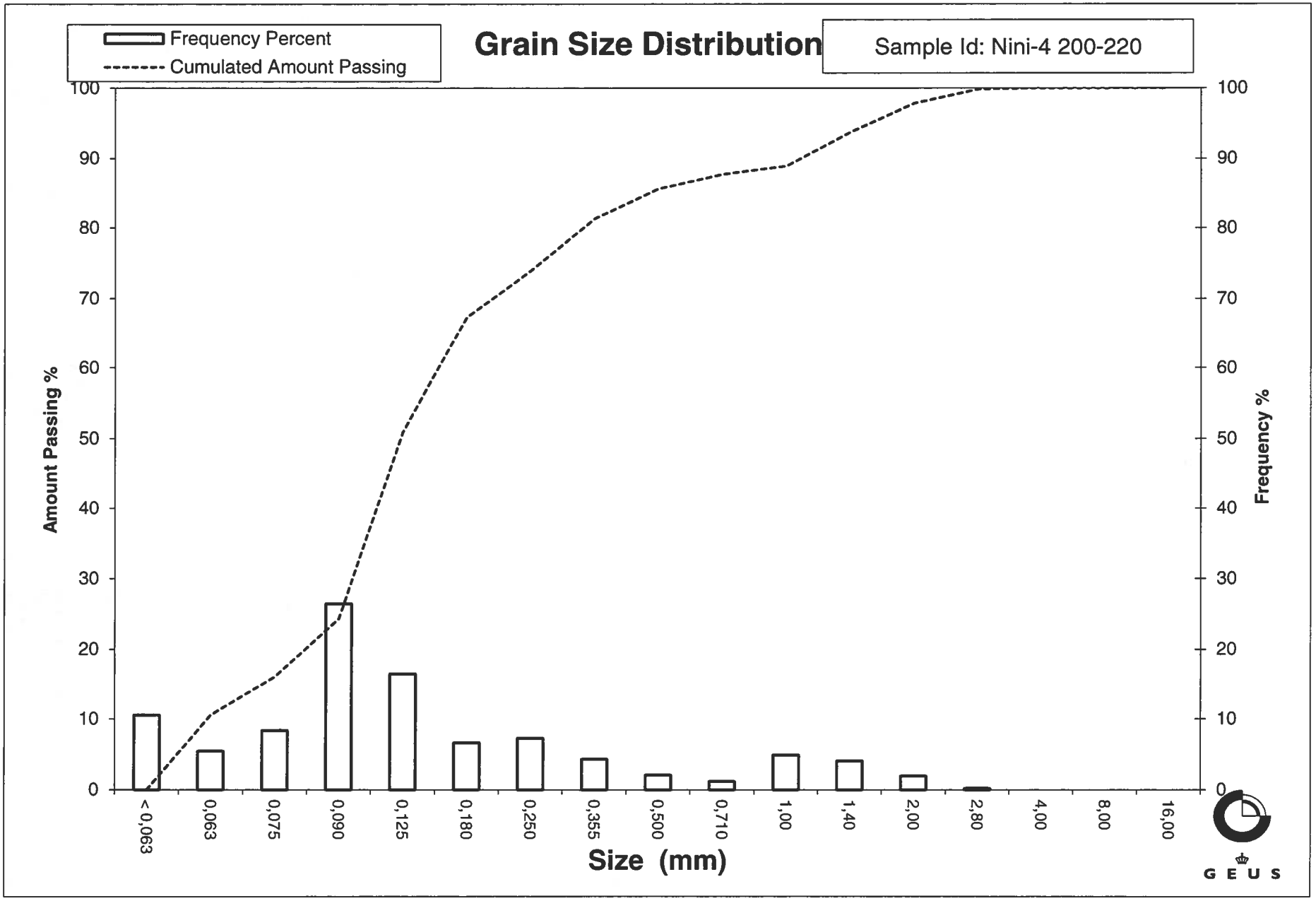
Frequency Percent
Cumulated Amount Passing
Grain Size Distribution
Sample Id: Nini-4 200-220
Amount Passing %
Frequency %
100
90
80
70
60
50
40
30
20
10
0
< 0,063
0,063
0,075
0,090
0,125
0,180
0,250
0,355
0,500
0,710
1,00
1,40
2,00
2,80
4,00
8,00
16,00
Size (mm)
GEUS

Grain Size Distribution
Geotechnical

Sample Id: Nini-4 280-300
Lab. Id: 46483
Projekt Niels Schovsbo
Subject: 0
Date: 08-03-2022
Executed: PS
Remarks:

Total Weight 31,14 g

Size Fractions

Sieve Analysis

	Size	Size	Weight	Weight	Cumulated amount passing
	mm	Φ	g	%	%
Gravel	16,00	-4,00	0,00	0,00	100,00
	8,00	-3,00	0,00	0,00	100,00
	4,00	-2,00	0,08	0,26	99,74
	2,80	-1,49	0,71	2,28	97,46
	2,00	-1,00	0,79	2,54	94,93
Sand	1,40	-0,49	0,73	2,34	92,58
	1,00	0,00	2,40	7,71	84,87
	0,710	0,49	1,24	3,98	80,89
	0,500	1,00	0,78	2,50	78,39
	0,355	1,49	1,24	3,98	74,41
	0,250	2,00	1,38	4,43	69,97
	0,180	2,47	1,44	4,62	65,35
	0,125	3,00	4,22	13,55	51,80
	0,090	3,47	5,96	19,14	32,66
	0,075	3,74	2,17	6,97	25,69
	0,063	3,99	1,82	5,84	19,85
	< 0,063	> 3,99	6,18	19,85	0,00

Size Classes (DGF-Bulletin 1 1988)

		Weight %
Silt and clay	(< 0,063 mm):	19,85
Sand, fine	(0,063 mm - 0,200 mm):	46,83
Sand, medium	(0,2 mm - 0,6 mm):	12,91
Sand, coarse	(0,6 mm - 2 mm):	15,35
Gravel	(> 2 mm):	5,07
Sum:		100,00

Moments Measures (Folk and Wards)

Percentile Amount in sieve	Percentile Amount passing	d(mm)	Φ
5%	95%	2,02	-1,02
16%	84%	0,94	0,09
25%	75%	0,38	1,41
40%	60%	0,16	2,66
Median 50%	50%	0,12	3,04
75%	25%	0,07	3,76
84%	16%	-------	-------
90%	10%	-------	-------
95%	5%	-------	-------

Moments Statistics

Mean	1,57
Sorting	-------
Skewness	-------
Kurtosis	-------
Uniformity Coefficient	-------

The analysis is executed according to DS 405.9 extended by sieves to the ½ phi scale

Size Classes and Percentiles are found by linear interpolation

Formulas

Mean (ϕ16%+ϕ84%+ϕ50%) / 3 (Folk and Ward 1957)

Sorting (ϕ84%-ϕ16%) / 4 + (ϕ95%-ϕ5%) / 6,6 (Folk and Ward 1957)

Kurtosis (ϕ95% - ϕ5%) / (2,44 * (ϕ75% - ϕ25%)) (Folk and Ward 1957)

Skewness (ϕ16%+ϕ84% - 2*ϕ50%) / (2*(ϕ84%-ϕ16%)) + (ϕ5%+ϕ95% - 2*ϕ50%) / (2*(ϕ95%-ϕ5%)) (Folk and Ward 1957)

Uniformity Coefficient (d60% / d10%) (dgf-Bulletin 1988)

Mean, sorting, skewness and kurtosis are based on "Amount in sieve". Uniformity coefficient is based on "Amount passing".

Øster Voldgade 10 1350 København K
Tel.: +45 38 14 20 00 Telefax: +45 38 14 20 50
Email: GEUS@geus.dk
www.geus.dk

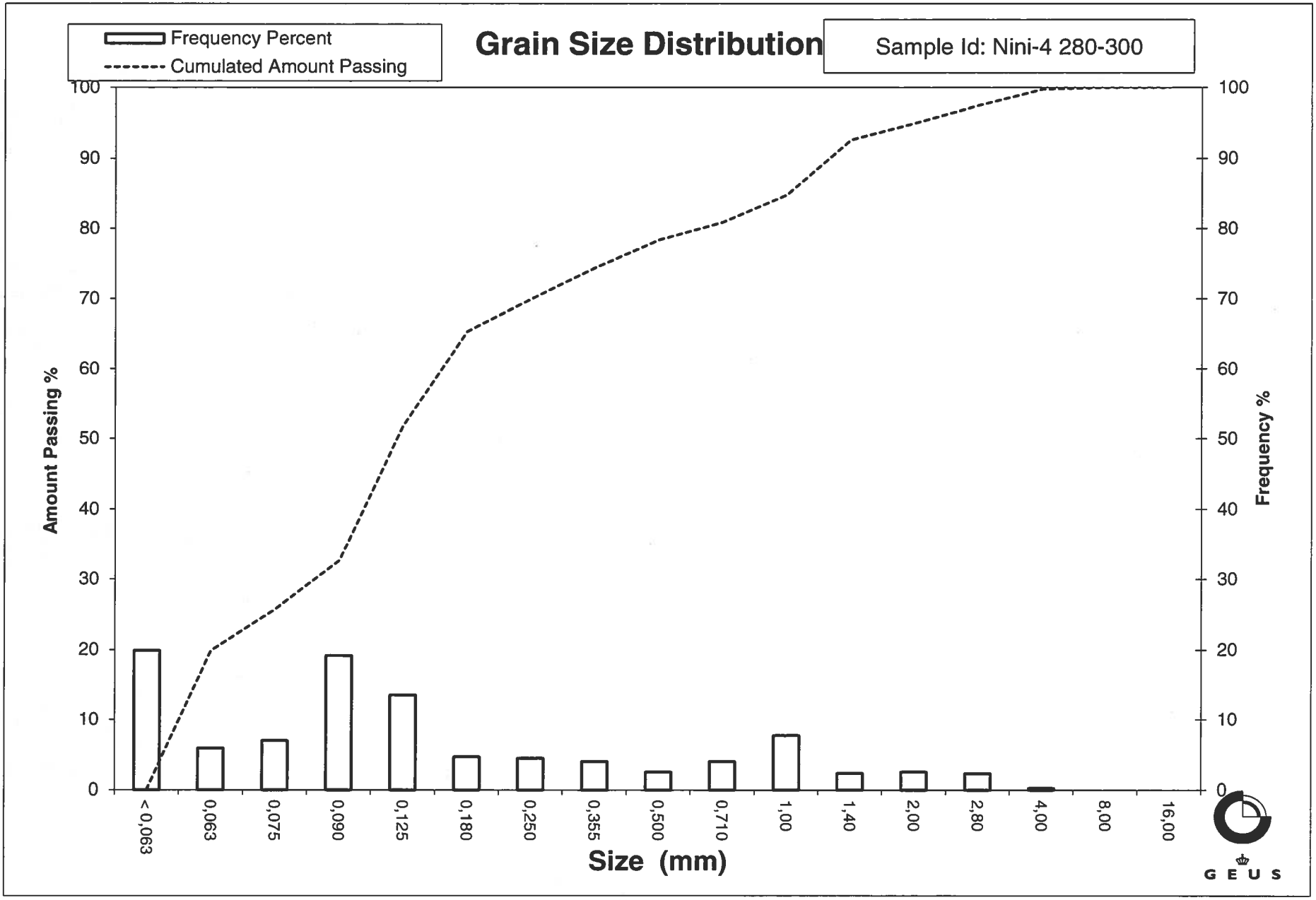
Frequency Percent
Cumulated Amount Passing
Grain Size Distribution
Sample Id: Nini-4 280-300
Amount Passing %
Frequency %
100
90
80
70
60
50
40
30
20
10
0
< 0,063
0,063
0,075
0,090
0,125
0,180
0,250
0,355
0,500
0,710
1,00
1,40
2,00
2,80
4,00
8,00
16,00
Size (mm)
GEUS

Grain Size Distribution
Geotechnical

Sample Id: Nini-4 380-400
Lab. Id: 46484
Projekt Niels Schovsbo
Subject: 0
Date: 08-03-2022
Executed: PS
Remarks:

G E U S

Total Weight 30,47 g

Size Fractions

Sieve Analysis

	Size	Size	Weight	Weight	Cumulated amount passing
	mm	Φ	g	%	%
Gravel	16,00	-4,00	0,00	0,00	100,00
	8,00	-3,00	0,00	0,00	100,00
	4,00	-2,00	0,08	0,26	99,74
	2,80	-1,49	0,79	2,59	97,14
	2,00	-1,00	2,71	8,89	88,25
Sand	1,40	-0,49	3,14	10,31	77,95
	1,00	0,00	5,12	16,80	61,14
	0,710	0,49	3,67	12,04	49,10
	0,500	1,00	3,25	10,67	38,43
	0,355	1,49	2,19	7,19	31,24
	0,250	2,00	2,02	6,63	24,61
	0,180	2,47	1,83	6,01	18,61
	0,125	3,00	3,21	10,53	8,07
	0,090	3,47	1,29	4,23	3,84
	0,075	3,74	0,06	0,20	3,64
	0,063	3,99	0,01	0,03	3,61
	< 0,063	> 3,99	1,10	3,61	0,00

Size Classes (DGF-Bulletin 1 1988)

		Weight %
Silt and clay	(< 0,063 mm):	3,61
Sand, fine	(0,063 mm - 0,200 mm):	16,71
Sand, medium	(0,2 mm - 0,6 mm):	23,19
Sand, coarse	(0,6 mm - 2 mm):	44,74
Gravel	(> 2 mm):	11,75
Sum:		100,00

Moments Measures (Folk and Wards)

Percentile	Percentile		
Amount in sieve	Amount passing	d(mm)	Φ
5%	95%	2,61	-1,38
16%	84%	1,75	-0,81
25%	75%	1,33	-0,41
40%	60%	0,97	0,04
Median 50%	50%	0,73	0,45
75%	25%	0,26	1,97
84%	16%	0,17	2,59
90%	10%	0,14	2,89
95%	5%	0,10	3,33

Moments Statistics

Mean	0,74
Sorting	1,56
Skewness	0,24
Kurtosis	0,81
Uniformity Coefficient	7,20

The analysis is executed according to DS 405.9 extended by sieves to the ½ phi scale

Size Classes and Percentiles are found by linear interpolation

Formulas

Mean (ϕ16%+ϕ84%+ϕ50%) / 3 (Folk and Ward 1957)

Sorting (ϕ84%-ϕ16%) / 4 + (ϕ95%-ϕ5%) / 6,6 (Folk and Ward 1957)

Kurtosis (ϕ95% - ϕ5%) / (2,44 * (ϕ75% - ϕ25%)) (Folk and Ward 1957)

Skewness (ϕ16%+ϕ84% - 2*ϕ50%) / (2*(ϕ84%-ϕ16%)) + (ϕ5%+ϕ95% - 2*ϕ50%) / (2*(ϕ95%-ϕ5%)) (Folk and Ward 1957)

Uniformity Coefficient (d60% / d10%) (dgf-Bulletin 1988)

Mean, sorting, skewness and kurtosis are based on "Amount in sieve". Uniformity coefficient is based on "Amount passing".

Øster Voldgade 10 1350 København K
Tel.: +45 38 14 20 00 Telefax: +45 38 14 20 50
Email: GEUS@geus.dk
www.geus.dk

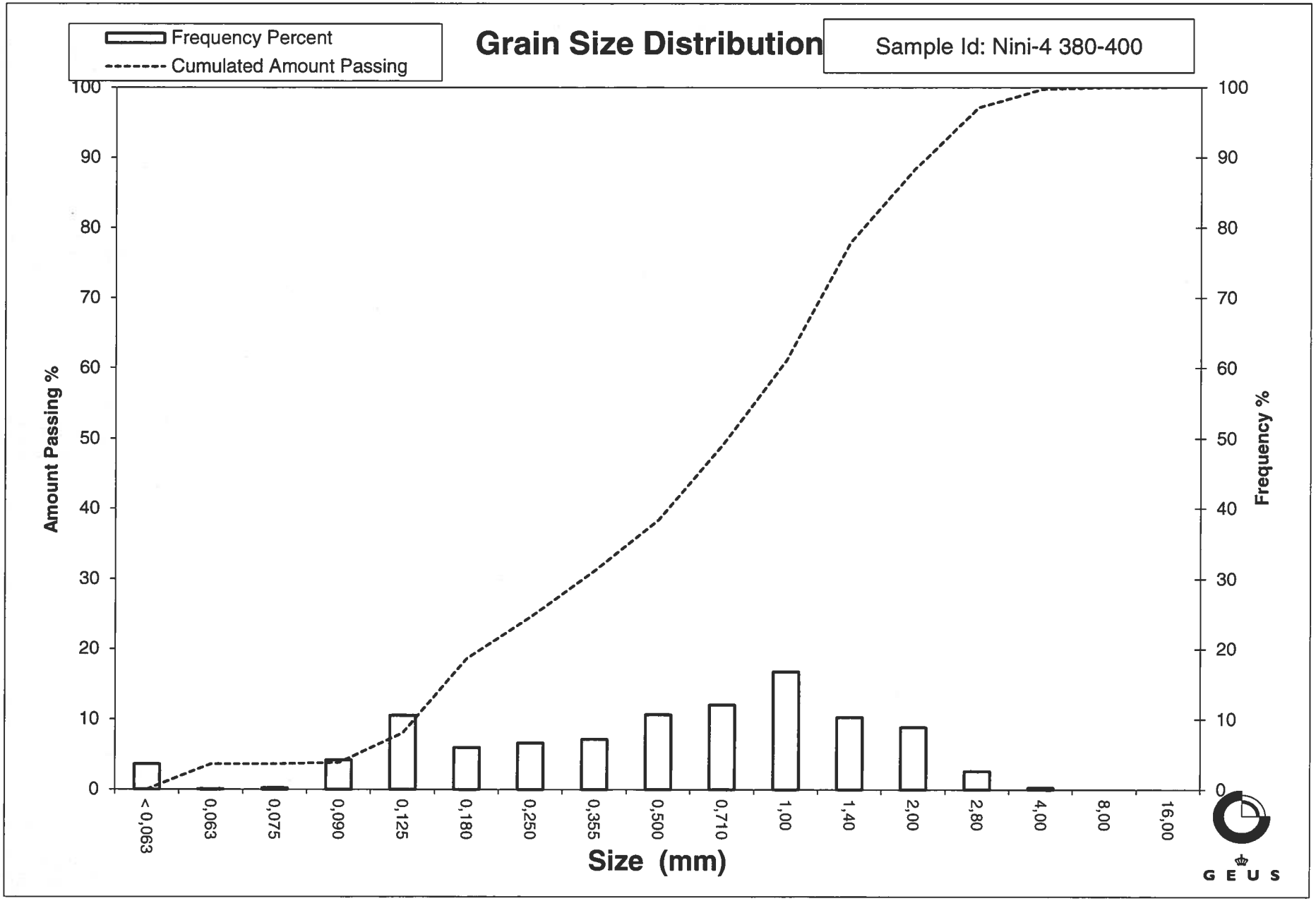
Frequency Percent
Cumulated Amount Passing
Grain Size Distribution
Sample Id: Nini-4 380-400
Amount Passing %
Frequency %
100
90
80
70
60
50
40
30
20
10
0
< 0,063
0,063
0,075
0,090
0,125
0,180
0,250
0,355
0,500
0,710
1,00
1,40
2,00
2,80
4,00
8,00
16,00
Size (mm)
GEUS

Grain Size Distribution
Geotechnical

Sample Id: Nini-4 700-720
Lab. Id: 46485
Projekt Niels Schovsbo
Subject: 0
Date: 08-03-2022
Executed: PS
Remarks:

GEUS

Total Weight 31,16 g

Size Fractions

Sieve Analysis

	Size	Size	Weight	Weight	Cumulated amount passing
	mm	Φ	g	%	%
Gravel	16,00	-4,00	0,00	0,00	100,00
	8,00	-3,00	0,00	0,00	100,00
	4,00	-2,00	0,00	0,00	100,00
	2,80	-1,49	0,00	0,00	100,00
	2,00	-1,00	0,00	0,00	100,00
Sand	1,40	-0,49	0,00	0,00	100,00
	1,00	0,00	0,17	0,55	99,45
	0,710	0,49	0,12	0,39	99,07
	0,500	1,00	0,20	0,64	98,43
	0,355	1,49	0,22	0,71	97,72
	0,250	2,00	0,69	2,21	95,51
	0,180	2,47	5,95	19,09	76,41
	0,125	3,00	10,72	34,40	42,01
	0,090	3,47	8,33	26,73	15,28
	0,075	3,74	0,83	2,66	12,61
	0,063	3,99	0,46	1,48	11,14
	< 0,063	> 3,99	3,47	11,14	0,00

Size Classes (DGF-Bulletin 1 1988)

		Weight %
Silt and clay	(< 0,063 mm):	11,14
Sand, fine	(0,063 mm - 0,200 mm):	70,73
Sand, medium	(0,2 mm - 0,6 mm):	16,87
Sand, coarse	(0,6 mm - 2 mm):	1,27
Gravel	(> 2 mm):	0,00
Sum:		100,00

Moments Measures (Folk and Wards)

Percentile Amount in sieve	Percentile Amount passing	d(mm)	Φ
5%	95%	0,25	2,01
16%	84%	0,21	2,27
25%	75%	0,18	2,49
40%	60%	0,15	2,70
Median 50%	50%	0,14	2,86
75%	25%	0,10	3,28
84%	16%	0,09	3,46
90%	10%	-------	-------
95%	5%	-------	-------

Moments Statistics

Mean	2,86
Sorting	-------
Skewness	-------
Kurtosis	-------
Uniformity Coefficient	-------

The analysis is executed according to DS 405.9 extended by sieves to the ½ phi scale

Size Classes and Percentiles are found by linear interpolation

Formulas

Mean (ϕ16%+ϕ84%+ϕ50%) / 3 (Folk and Ward 1957)

Sorting (ϕ84%-ϕ16%) / 4 + (ϕ95%-ϕ5%) / 6,6 (Folk and Ward 1957)

Kurtosis (ϕ95% - ϕ5%) / (2,44 * (ϕ75% - ϕ25%)) (Folk and Ward 1957)

Skewness (ϕ16%+ϕ84% - 2*ϕ50%) / (2*(ϕ84%-ϕ16%)) + (ϕ5%+ϕ95% - 2*ϕ50%) / (2*(ϕ95%-ϕ5%)) (Folk and Ward 1957)

Uniformity Coefficient (d60% / d10%) (dgf-Bulletin 1988)

Mean, sorting, skewness and kurtosis are based on "Amount in sieve". Uniformity coefficient is based on "Amount passing".

Øster Voldgade 10 1350 København K
Tel.: +45 38 14 20 00 Telefax: +45 38 14 20 50
Email: GEUS@geus.dk
www.geus.dk

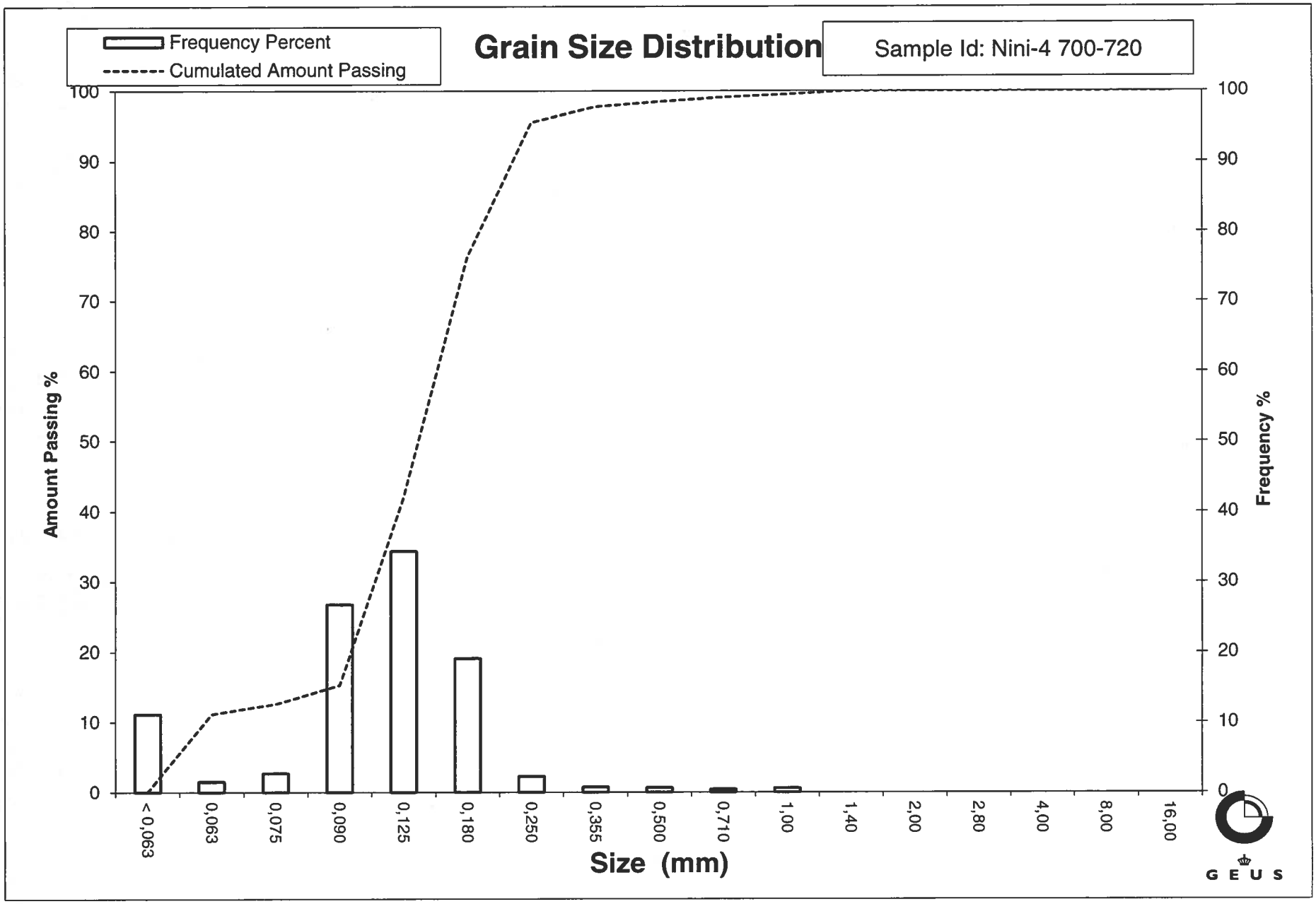
Frequency Percent
Cumulated Amount Passing
Grain Size Distribution
Sample Id: Nini-4 700-720
Amount Passing %
Frequency %
100
90
80
70
60
50
40
30
20
10
0
< 0,063
0,063
0,075
0,090
0,125
0,180
0,250
0,355
0,500
0,710
1,00
1,40
2,00
2,80
4,00
8,00
16,00
Size (mm)
GEUS

Grain Size Distribution
Geotechnical

Sample Id: Nini-4 740-760
Lab. Id: 46486
Projekt Niels Schovsbo
Subject: 0
Date: 08-03-2022
Executed: PS
Remarks:

Total Weight 31,12 g

Size Fractions

Sieve Analysis

	Size	Size	Weight	Weight	Cumulated amount passing
	mm	Φ	g	%	%
Gravel	16,00	-4,00	0,00	0,00	100,00
	8,00	-3,00	0,00	0,00	100,00
	4,00	-2,00	0,00	0,00	100,00
	2,80	-1,49	0,00	0,00	100,00
	2,00	-1,00	0,00	0,00	100,00
Sand	1,40	-0,49	0,00	0,00	100,00
	1,00	0,00	0,58	1,86	98,14
	0,710	0,49	0,07	0,22	97,91
	0,500	1,00	0,05	0,16	97,75
	0,355	1,49	0,11	0,35	97,40
	0,250	2,00	1,77	5,69	91,71
	0,180	2,47	14,39	46,24	45,47
	0,125	3,00	9,90	31,81	13,66
	0,090	3,47	1,63	5,24	8,42
	0,075	3,74	0,28	0,90	7,52
	0,063	3,99	0,21	0,67	6,84
	< 0,063	> 3,99	2,13	6,84	0,00

Size Classes (DGF-Bulletin 1 1988)

		Weight %
Silt and clay	(< 0,063 mm):	6,84
Sand, fine	(0,063 mm - 0,200 mm):	51,84
Sand, medium	(0,2 mm - 0,6 mm):	39,15
Sand, coarse	(0,6 mm - 2 mm):	2,17
Gravel	(> 2 mm):	0,00
Sum:		100,00

Moments Measures (Folk and Wards)

Percentile	Percentile		
Amount in sieve	Amount passing	d(mm)	Φ
5%	95%	0,31	1,69
16%	84%	0,24	2,07
25%	75%	0,22	2,15
40%	60%	0,20	2,31
Median 50%	50%	0,19	2,42
75%	25%	0,14	2,79
84%	16%	0,13	2,95
90%	10%	0,10	3,31
95%	5%	-------	-------

Moments Statistics

Mean	2,48
Sorting	-------
Skewness	-------
Kurtosis	-------
Uniformity Coefficient	2,01

The analysis is executed according to DS 405.9 extended by sieves to the ½ phi scale

Size Classes and Percentiles are found by linear interpolation

Formulas

Mean (ϕ16%+ϕ84%+ϕ50%) / 3 (Folk and Ward 1957)

Sorting (ϕ84%-ϕ16%) / 4 + (ϕ95%-ϕ5%) / 6,6 (Folk and Ward 1957)

Kurtosis (ϕ95% - ϕ5%) / (2,44 * (ϕ75% - ϕ25%)) (Folk and Ward 1957)

Skewness (ϕ16%+ϕ84% - 2*ϕ50%) / (2*(ϕ84%-ϕ16%)) + (ϕ5%+ϕ95% - 2*ϕ50%) / (2*(ϕ95%-ϕ5%)) (Folk and Ward 1957)

Uniformity Coefficient (d60% / d10%) (dgf-Bulletin 1988)

Mean, sorting, skewness and kurtosis are based on "Amount in sieve". Uniformity coefficient is based on "Amount passing".

Øster Voldgade 10 1350 København K
Tel.: +45 38 14 20 00 Telefax: +45 38 14 20 50
Email: GEUS@geus.dk
www.geus.dk

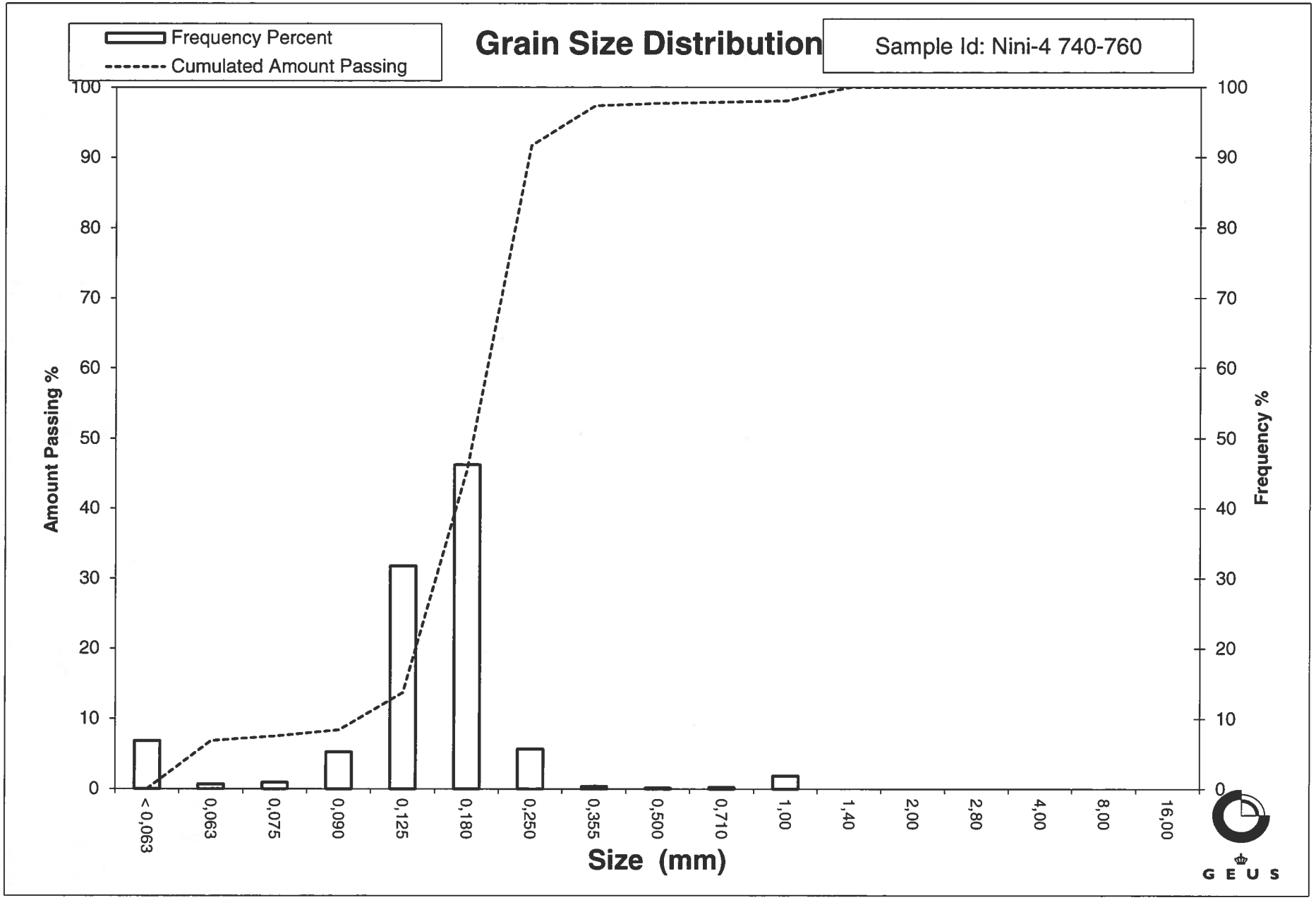
Frequency Percent
Cumulated Amount Passing
Grain Size Distribution
Sample Id: Nini-4 740-760
Amount Passing %
Frequency %
100
90
80
70
60
50
40
30
20
10
0
< 0,063
0,063
0,075
0,090
0,125
0,180
0,250
0,355
0,500
0,710
1,00
1,40
2,00
2,80
4,00
8,00
16,00
Size (mm)
GEUS

APPENDIX B - BET ANALYSIS

Quantachrome® ASiQwin™- Automated Gas Sorption Data
Acquisition and Reduction

version 5.21

Analysis Report
Operator: DIJUVA Date:2022/03/25 Operator: DIJUVA Date:2022/04/28
Sample ID: 46487 Nini-4 Filename: 220325-01.qps
Sample Desc: 820-830m Comment: _6 Point BET
Sample Weight: 1.264 g Instrument: Autosorb iQ Station 1
Approx. Outgas Time:3.1 hrs Final Outgas Temp.:60 °C Extended info: Available
Analysis gas: Nitrogen Non-ideality: 6.58e-05 1/Torr CellType: 9mm
Analysis Time: 0:20 hr:min Bath temp.: 77.35 K
Analysis Mode: Standard VoidVol Remeasure:off
VoidVol. Mode: He Measure Cold Zone V: 5.48268 cc Warm Zone V: 7.27636 cc
Data Reduction Parameters
Thermal Transpiration: onEff. mol. diameter (D): 3.54 ÅEff. cell stem diam. (d): 4.0000 mm

Adsorbate modelNitrogen Temperature 77.350K
Molec. Wt.: 28.013 Cross Section: 16.200 Å² Liquid Density: 0.806 g/cc

Relative Pressure P/Po	Volume @ STP cc/g	1 / [W((Po/P) - 1)] 1/g
5.03540e-02	2.3927	1.7731e+01
1.03517e-01	2.7454	3.3652e+01
1.47867e-01	2.9810	4.6576e+01
1.97416e-01	3.2310	6.0913e+01
2.47185e-01	3.4834	7.5419e+01
2.96817e-01	3.7480	9.0109e+01

BET summary
Slope = 292.815 1/g
Intercept = 3.158e+00 1/g
Correlation coefficient, r = 0.999987
C constant= 93.725

Surface Area = 11.766 m²/g

Quantachrome® ASiQwin™- Automated Gas Sorption Data
Acquisition and Reduction

version 5.21

Analysis Report
Operator: DIJUVA Date:2022/03/25 Operator: DIJUVA Date:2022/03/25
Sample ID: 46488 Nini-4 Filename: 220325-02.qps
Sample Desc: 840-850m Comment: _6 Point BET
Sample Weight: 1.5455 g Instrument: Autosorb iQ Station 1
Approx. Outgas Time:3.1 hrs Final Outgas Temp.:60 °C Extended info: Available
Analysis gas: Nitrogen Non-ideality: 6.58e-05 1/Torr CellType: 9mm
Analysis Time: 0:23 hr:min Bath temp.: 77.35 K
Analysis Mode: Standard VoidVol Remeasure:off
VoidVol. Mode: He Measure Cold Zone V: 5.48268 cc Warm Zone V: 7.22503 cc
Data Reduction Parameters
Thermal Transpiration: onEff. mol. diameter (D): 3.54 ÅEff. cell stem diam. (d): 4.0000 mm

Adsorbate modelNitrogen Temperature 77.350K
Molec. Wt.: 28.013 Cross Section: 16.200 Å² Liquid Density: 0.806 g/cc

Relative Pressure P/Po	Volume @ STP cc/g	1 / [W((Po/P) - 1)] 1/g
5.30221e-02	2.9100	1.5395e+01
1.01179e-01	3.3105	2.7206e+01
1.51679e-01	3.6500	3.9194e+01
2.02238e-01	3.9678	5.1120e+01
2.52344e-01	4.2830	6.3051e+01
3.01928e-01	4.6116	7.5042e+01

BET summary
Slope = 238.867 1/g
Intercept = 2.873e+00 1/g
Correlation coefficient, r = 0.999986
C constant= 84.144

Surface Area = 14.406 m²/g

Quantachrome® ASiQwin™- Automated Gas Sorption Data
Acquisition and Reduction

version 5.21

Analysis Report
Operator: DIJUVA Date:2022/03/28 Operator: DIJUVA Date:2022/03/28
Sample ID: 46489 Nini-4 Filename: 220328-01.qps
Sample Desc: 900-910m Comment: _6 Point BET
Sample Weight: 1.9325 g Instrument: Autosorb iQ Station 1
Approx. Outgas Time:3.1 hrs Final Outgas Temp.:60 °C Extended info: Available
Analysis gas: Nitrogen Non-ideality: 6.58e-05 1/Torr CellType: 9mm
Analysis Time: 0:25 hr:min Bath temp.: 77.35 K
Analysis Mode: Standard VoidVol Remeasure:off
VoidVol. Mode: He Measure Cold Zone V: 5.42613 cc Warm Zone V: 7.2461 cc
Data Reduction Parameters
Thermal Transpiration: onEff. mol. diameter (D): 3.54 ÅEff. cell stem diam. (d): 4.0000 mm

Adsorbate modelNitrogen Temperature 77.350K
Molec. Wt.: 28.013 Cross Section: 16.200 Å² Liquid Density: 0.806 g/cc

Relative Pressure P/Po	Volume @ STP cc/g	1 / [W((Po/P) - 1)] 1/g
4.76232e-02	2.7455	1.4573e+01
9.81025e-02	3.1403	2.7714e+01
1.50443e-01	3.4624	4.0922e+01
2.00937e-01	3.7535	5.3604e+01
2.50753e-01	4.0439	6.6216e+01
3.00227e-01	4.3468	7.8972e+01

BET summary
Slope = 254.129 1/g
Intercept = 2.609e+00 1/g
Correlation coefficient, r = 0.999986
C constant= 98.421

Surface Area = 13.564 m²/g

Quantachrome® ASiQwin™- Automated Gas Sorption Data
Acquisition and Reduction

version 5.21

Analysis Report

Operator: DIJUVA Date:2022/03/28 Operator: DIJUVA Date:2022/03/28
Sample ID: 46490 Nini-4 Filename: 220328-02.qps
Sample Desc: 940-950m Comment: _6 Point BET
Sample Weight: 1.4212 g Instrument: Autosorb iQ Station 1
Approx. Outgas Time:3.1 hrs Final Outgas Temp.:60 °C Extended info: Available
Analysis gas: Nitrogen Non-ideality: 6.58e-05 1/Torr CellType: 9mm
Analysis Time: 0:23 hr:min Bath temp.: 77.35 K
Analysis Mode: Standard VoidVol Remeasure:off
VoidVol. Mode: He Measure Cold Zone V: 5.51239 cc Warm Zone V: 7.23151 cc

Data Reduction Parameters

Thermal Transpiration: onEff. mol. diameter (D): 3.54 ÅEff. cell stem diam. (d): 4.0000 mm

Adsorbate modelNitrogen Temperature 77.350K
Molec. Wt.: 28.013 Cross Section: 16.200 Å² Liquid Density: 0.806 g/cc

Relative Pressure P/Po	Volume @ STP cc/g	1 / [W((Po/P) - 1)] 1/g
4.97836e-02	2.8402	1.4759e+01
1.01427e-01	3.2611	2.7694e+01
1.52706e-01	3.5950	4.0112e+01
1.96197e-01	3.8559	5.0648e+01
2.52384e-01	4.1942	6.4400e+01
3.02856e-01	4.5147	7.6990e+01

BET summary
Slope = 245.121 1/g
Intercept = 2.652e+00 1/g
Correlation coefficient, r = 0.999986
C constant= 93.417

Surface Area = 14.055 m²/g

Quantachrome® ASiQwin™- Automated Gas Sorption Data
Acquisition and Reduction

version 5.21

Analysis Report
Operator: DIJUVA Date:2022/04/05 Operator: DIJUVA Date:2022/04/06
Sample ID: 46491 Nini-4b Filename: 220405-01.qps
Sample Desc: 990-1000m Comment: _6 Point BET
Sample Weight: 1.5512 g Instrument: Autosorb iQ Station 1
Approx. Outgas Time:3.1 hrs Final Outgas Temp.:60 °C Extended info: Available
Analysis gas: Nitrogen Non-ideality: 6.58e-05 1/Torr CellType: 9mm
Analysis Time: 0:25 hr:min Bath temp.: 77.35 K
Analysis Mode: Standard VoidVol Remeasure:off
VoidVol. Mode: He Measure Cold Zone V: 5.45388 cc Warm Zone V: 7.26467 cc
Data Reduction Parameters
Thermal Transpiration: onEff. mol. diameter (D): 3.54 ÅEff. cell stem diam. (d): 4.0000 mm

Adsorbate modelNitrogen Temperature 77.350K
Molec. Wt.: 28.013 Cross Section: 16.200 Å² Liquid Density: 0.806 g/cc

Relative Pressure P/Po	Volume @ STP cc/g	1 / [W((Po/P) - 1)] 1/g
5.11981e-02	3.0523	1.4145e+01
1.01020e-01	3.4559	2.6016e+01
1.51852e-01	3.7925	3.7772e+01
2.02301e-01	4.1088	4.9384e+01
2.51841e-01	4.4331	6.0754e+01
3.01161e-01	4.7773	7.2176e+01

BET summary
Slope = 231.628 1/g
Intercept = 2.478e+00 1/g
Correlation coefficient, r = 0.999983
C constant= 94.479

Surface Area = 14.876 m²/g

Quantachrome® ASiQwin™- Automated Gas Sorption Data
Acquisition and Reduction

version 5.21

Analysis Report
Operator: DIJUVA Date:2022/04/06 Operator: DIJUVA Date:2022/04/06
Sample ID: 46492 Nini-4b Filename: 220406-01.qps
Sample Desc: 1040-1050m Comment: _6 Point BET
Sample Weight: 0.9761 g Instrument: Autosorb iQ Station 1
Approx. Outgas Time:3.1 hrs Final Outgas Temp.:60 °C Extended info: Available
Analysis gas: Nitrogen Non-ideality: 6.58e-05 1/Torr CellType: 9mm
Analysis Time: 0:20 hr:min Bath temp.: 77.35 K
Analysis Mode: Standard VoidVol Remeasure:off
VoidVol. Mode: He Measure Cold Zone V: 5.68507 cc Warm Zone V: 7.18716 cc
Data Reduction Parameters
Thermal Transpiration: onEff. mol. diameter (D): 3.54 ÅEff. cell stem diam. (d): 4.0000 mm

Adsorbate modelNitrogen Temperature 77.350K
Molec. Wt.: 28.013 Cross Section: 16.200 Å² Liquid Density: 0.806 g/cc

Relative Pressure P/Po	Volume @ STP cc/g	1 / [W((Po/P) - 1)] 1/g
5.01440e-02	3.0534	1.3833e+01
9.65262e-02	3.4290	2.4929e+01
1.47366e-01	3.7614	3.6765e+01
1.97784e-01	4.0694	4.8476e+01
2.47739e-01	4.3834	6.0112e+01
2.97285e-01	4.7143	7.1800e+01

BET summary
Slope = 233.982 1/g
Intercept = 2.219e+00 1/g
Correlation coefficient, r = 0.999992
C constant= 106.458

Surface Area = 14.744 m²/g

Quantachrome® ASiQwin™- Automated Gas Sorption Data
Acquisition and Reduction

version 5.21

Analysis Report
Operator: DIJUVA Date:2022/04/06 Operator: DIJUVA Date:2022/04/07
Sample ID: 46493 Nini-4 Filename: 220406-02.qps
Sample Desc: 1090-1100m Comment: _6 Point BET
Sample Weight: 1.2265 g Instrument: Autosorb iQ Station 1
Approx. Outgas Time:3.1 hrs Final Outgas Temp.:60 °C Extended info: Available
Analysis gas: Nitrogen Non-ideality: 6.58e-05 1/Torr CellType: 9mm
Analysis Time: 0:26 hr:min Bath temp.: 77.35 K
Analysis Mode: Standard VoidVol Remeasure:off
VoidVol. Mode: He Measure Cold Zone V: 5.6738 cc Warm Zone V: 7.14692 cc
Data Reduction Parameters
Thermal Transpiration: onEff. mol. diameter (D): 3.54 ÅEff. cell stem diam. (d): 4.0000 mm

Adsorbate modelNitrogen Temperature 77.350K
Molec. Wt.: 28.013 Cross Section: 16.200 Å² Liquid Density: 0.806 g/cc

Relative Pressure P/Po	Volume @ STP cc/g	1 / [W((Po/P) - 1)] 1/g
5.00553e-02	3.2297	1.3054e+01
1.01819e-01	3.6720	2.4701e+01
1.53176e-01	4.0389	3.5833e+01
1.96723e-01	4.3245	4.5311e+01
2.52780e-01	4.7068	5.7506e+01
3.02943e-01	5.0793	6.8460e+01

BET summary
Slope = 218.604 1/g
Intercept = 2.282e+00 1/g
Correlation coefficient, r = 0.999985
C constant= 96.789

Surface Area = 15.766 m²/g

Quantachrome® ASiQwin™- Automated Gas Sorption Data
Acquisition and Reduction

version 5.21

Analysis Report
Operator: DIJUVA Date:2022/04/07 Operator: DIJUVA Date:2022/04/07
Sample ID: 46494 Nini-4 Filename: 220407-01.qps
Sample Desc: 1140-1150m Comment: _6 Point BET
Sample Weight: 1.7752 g Instrument: Autosorb iQ Station 1
Approx. Outgas Time:3.1 hrs Final Outgas Temp.:60 °C Extended info: Available
Analysis gas: Nitrogen Non-ideality: 6.58e-05 1/Torr CellType: 9mm
Analysis Time: 0:33 hr:min Bath temp.: 77.35 K
Analysis Mode: Standard VoidVol Remeasure:off
VoidVol. Mode: He Measure Cold Zone V: 5.57294 cc Warm Zone V: 7.16183 cc
Data Reduction Parameters
Thermal Transpiration: onEff. mol. diameter (D): 3.54 ÅEff. cell stem diam. (d): 4.0000 mm

Adsorbate modelNitrogen Temperature 77.350K
Molec. Wt.: 28.013 Cross Section: 16.200 Å² Liquid Density: 0.806 g/cc

Relative Pressure P/Po	Volume @ STP cc/g	1 / [W((Po/P) - 1)] 1/g
5.21871e-02	4.5936	9.5905e+00
1.01631e-01	5.1849	1.7458e+01
1.48017e-01	5.6402	2.4646e+01
1.97954e-01	6.1065	3.2338e+01
2.47804e-01	6.5724	4.0105e+01
2.96927e-01	7.0623	4.7847e+01

BET summary
Slope = 155.897 1/g
Intercept = 1.525e+00 1/g
Correlation coefficient, r = 0.999990
C constant= 103.258

Surface Area = 22.122 m²/g

Quantachrome® ASiQwin™- Automated Gas Sorption Data
Acquisition and Reduction

version 5.21

Analysis Report
Operator: DIJUVA Date:2022/04/07 Operator: DIJUVA Date:2022/04/21
Sample ID: 46495 Nini-4 Filename: 220407-02.qps
Sample Desc: 1190-1200m Comment: _6 Point BET
Sample Weight: 1.8688 g Instrument: Autosorb iQ Station 1
Approx. Outgas Time:3.1 hrs Final Outgas Temp.:60 °C Extended info: Available
Analysis gas: Nitrogen Non-ideality: 6.58e-05 1/Torr CellType: 9mm
Analysis Time: 0:30 hr:min Bath temp.: 77.35 K
Analysis Mode: Standard VoidVol Remeasure:off
VoidVol. Mode: He Measure Cold Zone V: 7.56458 cc Warm Zone V: 7.22023 cc
Data Reduction Parameters
Thermal Transpiration: onEff. mol. diameter (D): 3.54 ÅEff. cell stem diam. (d): 4.0000 mm

Adsorbate modelNitrogen Temperature 77.350K
Molec. Wt.: 28.013 Cross Section: 16.200 Å² Liquid Density: 0.806 g/cc

Relative Pressure P/Po	Volume @ STP cc/g	1 / [W((Po/P) - 1)] 1/g
4.66254e-02	4.4842	8.7261e+00
9.95284e-02	5.1261	1.7252e+01
1.47163e-01	5.5928	2.4686e+01
1.97576e-01	6.0624	3.2497e+01
2.47265e-01	6.5407	4.0183e+01
2.96468e-01	7.0418	4.7880e+01

BET summary
Slope = 156.292 1/g
Intercept = 1.587e+00 1/g
Correlation coefficient, r = 0.999977
C constant= 99.493

Surface Area = 22.058 m²/g

Quantachrome® ASiQwin™- Automated Gas Sorption Data
Acquisition and Reduction

version 5.21

Analysis Report
Operator: JCT Date:2022/04/20 Operator: JCT Date:2022/04/21
Sample ID: 46496 Nini-4 Filename: 220420-01.qps
Sample Desc: 1240-1250m Comment: _6 Point BET
Sample Weight: 1.1249 g Instrument: Autosorb iQ Station 1
Approx. Outgas Time:3.1 hrs Final Outgas Temp.:60 °C Extended info: Available
Analysis gas: Nitrogen Non-ideality: 6.58e-05 1/Torr CellType: 9mm
Analysis Time: 0:28 hr:min Bath temp.: 77.35 K
Analysis Mode: Standard VoidVol Remeasure:off
VoidVol. Mode: He Measure Cold Zone V: 7.82205 cc Warm Zone V: 7.31879 cc
Data Reduction Parameters
Thermal Transpiration: onEff. mol. diameter (D): 3.54 ÅEff. cell stem diam. (d): 4.0000 mm

Adsorbate modelNitrogen Temperature 77.350K
Molec. Wt.: 28.013 Cross Section: 16.200 Å² Liquid Density: 0.806 g/cc

Relative Pressure P/Po	Volume @ STP cc/g	1 / [W((Po/P) - 1)] 1/g
5.06848e-02	4.2709	1.0002e+01
1.00478e-01	4.8185	1.8548e+01
1.51977e-01	5.2807	2.7154e+01
2.02374e-01	5.7160	3.5515e+01
2.52270e-01	6.1486	4.3903e+01
3.02106e-01	6.5996	5.2481e+01

BET summary
Slope = 168.368 1/g
Intercept = 1.525e+00 1/g
Correlation coefficient, r = 0.999984
C constant= 111.393

Surface Area = 20.498 m²/g

Quantachrome® ASiQwin™- Automated Gas Sorption Data
Acquisition and Reduction

version 5.21

Analysis Report
Operator: JCT Date:2022/04/21 Operator: DIJUVA Date:2022/04/21
Sample ID: 46497 Nini-4 Filename: 220421-01.qps
Sample Desc: 1290-1300m Comment: _6 Point BET
Sample Weight: 1.1778 g Instrument: Autosorb iQ Station 1
Approx. Outgas Time:3.1 hrs Final Outgas Temp.:60 °C Extended info: Available
Analysis gas: Nitrogen Non-ideality: 6.58e-05 1/Torr CellType: 9mm
Analysis Time: 0:25 hr:min Bath temp.: 77.35 K
Analysis Mode: Standard VoidVol Remeasure:off
VoidVol. Mode: He Measure Cold Zone V: 7.69522 cc Warm Zone V: 7.39912 cc
Data Reduction Parameters
Thermal Transpiration: onEff. mol. diameter (D): 3.54 ÅEff. cell stem diam. (d): 4.0000 mm

Adsorbate modelNitrogen Temperature 77.350K
Molec. Wt.: 28.013 Cross Section: 16.200 Å² Liquid Density: 0.806 g/cc

Relative Pressure P/Po	Volume @ STP cc/g	1 / [W((Po/P) - 1)] 1/g
4.82027e-02	4.5636	8.8791e+00
9.98172e-02	5.1699	1.7161e+01
1.51079e-01	5.6494	2.5205e+01
2.01542e-01	6.1001	3.3108e+01
2.51793e-01	6.5472	4.1126e+01
3.01139e-01	7.0117	4.9170e+01

BET summary
Slope = 158.799 1/g
Intercept = 1.224e+00 1/g
Correlation coefficient, r = 0.999980
C constant= 130.762

Surface Area = 21.763 m²/g

Quantachrome® ASiQwin™- Automated Gas Sorption Data
Acquisition and Reduction

version 5.21

Analysis Report
Operator: DIJUVA Date:2022/04/21 Operator: DIJUVA Date:2022/04/22
Sample ID: 46498 Nini-4 Filename: 220421-02.qps
Sample Desc: 1340-1350m Comment: _6 Point BET
Sample Weight: 1.7412 g Instrument: Autosorb iQ Station 1
Approx. Outgas Time:3.1 hrs Final Outgas Temp.:60 °C Extended info: Available
Analysis gas: Nitrogen Non-ideality: 6.58e-05 1/Torr CellType: 9mm
Analysis Time: 0:32 hr:min Bath temp.: 77.35 K
Analysis Mode: Standard VoidVol Remeasure:off
VoidVol. Mode: He Measure Cold Zone V: 5.35714 cc Warm Zone V: 7.29953 cc
Data Reduction Parameters
Thermal Transpiration: onEff. mol. diameter (D): 3.54 ÅEff. cell stem diam. (d): 4.0000 mm

Adsorbate modelNitrogen Temperature 77.350K
Molec. Wt.: 28.013 Cross Section: 16.200 Å² Liquid Density: 0.806 g/cc

Relative Pressure P/Po	Volume @ STP cc/g	1 / [W((Po/P) - 1)] 1/g
4.74463e-02	3.5339	1.1277e+01
9.87729e-02	4.0202	2.1812e+01
1.50089e-01	4.4116	3.2028e+01
2.00234e-01	4.7784	4.1922e+01
2.49780e-01	5.1500	5.1726e+01
2.99300e-01	5.5411	6.1677e+01

BET summary
Slope = 199.523 1/g
Intercept = 1.970e+00 1/g
Correlation coefficient, r = 0.999982
C constant= 102.297

Surface Area = 17.284 m²/g

Quantachrome® ASiQwin™- Automated Gas Sorption Data
Acquisition and Reduction

version 5.21

Analysis Report
Operator: DIJUVA Date:2022/04/22 Operator: DIJUVA Date:2022/04/22
Sample ID: 46499 Nini-4 Filename: 220422-01.qps
Sample Desc: 1350-1360m Comment: _6 Point BET
Sample Weight: 1.3112 g Instrument: Autosorb iQ Station 1
Approx. Outgas Time:3.1 hrs Final Outgas Temp.:60 °C Extended info: Available
Analysis gas: Nitrogen Non-ideality: 6.58e-05 1/Torr CellType: 9mm
Analysis Time: 0:27 hr:min Bath temp.: 77.35 K
Analysis Mode: Standard VoidVol Remeasure:off
VoidVol. Mode: He Measure Cold Zone V: 5.68853 cc Warm Zone V: 7.09843 cc
Data Reduction Parameters
Thermal Transpiration: onEff. mol. diameter (D): 3.54 ÅEff. cell stem diam. (d): 4.0000 mm

Adsorbate modelNitrogen Temperature 77.350K
Molec. Wt.: 28.013 Cross Section: 16.200 Å² Liquid Density: 0.806 g/cc

Relative Pressure P/Po	Volume @ STP cc/g	1 / [W((Po/P) - 1)] 1/g
4.86908e-02	4.4676	9.1665e+00
9.71794e-02	5.0526	1.7046e+01
1.49288e-01	5.5546	2.5278e+01
1.99741e-01	6.0145	3.3204e+01
2.50071e-01	6.4746	4.1208e+01
2.99147e-01	6.9502	4.9137e+01

BET summary
Slope = 159.109 1/g
Intercept = 1.485e+00 1/g
Correlation coefficient, r = 0.999988
C constant= 108.145

Surface Area = 21.685 m²/g

Quantachrome® ASiQwin™- Automated Gas Sorption Data
Acquisition and Reduction

version 5.21

Analysis Report
Operator: DIJUVA Date:2022/04/22 Operator: DIJUVA Date:2022/04/22
Sample ID: 46500 Nini-4 Filename: 220422-02.qps
Sample Desc: 1360-1370m Comment: _6 Point BET
Sample Weight: 2.2606 g Instrument: Autosorb iQ Station 1
Approx. Outgas Time:3.1 hrs Final Outgas Temp.:60 °C Extended info: Available
Analysis gas: Nitrogen Non-ideality: 6.58e-05 1/Torr CellType: 9mm
Analysis Time: 0:37 hr:min Bath temp.: 77.35 K
Analysis Mode: Standard VoidVol Remeasure:off
VoidVol. Mode: He Measure Cold Zone V: 5.32898 cc Warm Zone V: 7.048 cc
Data Reduction Parameters
Thermal Transpiration: onEff. mol. diameter (D): 3.54 ÅEff. cell stem diam. (d): 4.0000 mm

Adsorbate modelNitrogen Temperature 77.350K
Molec. Wt.: 28.013 Cross Section: 16.200 Å² Liquid Density: 0.806 g/cc

Relative Pressure P/Po	Volume @ STP cc/g	1 / [W((Po/P) - 1)] 1/g
4.96608e-02	3.5256	1.1859e+01
9.62472e-02	3.9804	2.1408e+01
1.47904e-01	4.3889	3.1644e+01
1.99040e-01	4.7671	4.1709e+01
2.48090e-01	5.1366	5.1395e+01
3.01232e-01	5.5603	6.2032e+01

BET summary
Slope = 198.849 1/g
Intercept = 2.135e+00 1/g
Correlation coefficient, r = 0.999984
C constant= 94.127

Surface Area = 17.327 m²/g

Quantachrome® ASiQwin™- Automated Gas Sorption Data
Acquisition and Reduction

version 5.21

Analysis Report
Operator: DIJUVA Date:2022/04/22 Operator: DIJUVA Date:2022/04/22
Sample ID: 46501 Nini-4 Filename: 220422-03.qps
Sample Desc: 1370-1380m Comment: _6 Point BET
Sample Weight: 1.6826 g Instrument: Autosorb iQ Station 1
Approx. Outgas Time:3.1 hrs Final Outgas Temp.:60 °C Extended info: Available
Analysis gas: Nitrogen Non-ideality: 6.58e-05 1/Torr CellType: 9mm
Analysis Time: 0:27 hr:min Bath temp.: 77.35 K
Analysis Mode: Standard VoidVol Remeasure:off
VoidVol. Mode: He Measure Cold Zone V: 7.7167 cc Warm Zone V: 7.1359 cc
Data Reduction Parameters
Thermal Transpiration: onEff. mol. diameter (D): 3.54 ÅEff. cell stem diam. (d): 4.0000 mm

Adsorbate modelNitrogen Temperature 77.350K
Molec. Wt.: 28.013 Cross Section: 16.200 Å² Liquid Density: 0.806 g/cc

Relative Pressure P/Po	Volume @ STP cc/g	1 / [W((Po/P) - 1)] 1/g
4.62603e-02	3.9893	9.7282e+00
1.01360e-01	4.5875	1.9672e+01
1.48889e-01	4.9966	2.8012e+01
1.99167e-01	5.4080	3.6795e+01
2.49059e-01	5.8203	4.5593e+01
2.98569e-01	6.2505	5.4487e+01

BET summary
Slope = 176.852 1/g
Intercept = 1.630e+00 1/g
Correlation coefficient, r = 0.999987
C constant= 109.509

Surface Area = 19.512 m²/g

Quantachrome® ASiQwin™- Automated Gas Sorption Data
Acquisition and Reduction

version 5.21

Analysis Report
Operator: DIJUVA Date:2022/04/22 Operator: DIJUVA Date:2022/04/25
Sample ID: 46502 Nini-4 Filename: 220422-04.qps
Sample Desc: 1380-1390m Comment: _6 Point BET
Sample Weight: 0.8805 g Instrument: Autosorb iQ Station 1
Approx. Outgas Time:3.1 hrs Final Outgas Temp.:60 °C Extended info: Available
Analysis gas: Nitrogen Non-ideality: 6.58e-05 1/Torr CellType: 9mm
Analysis Time: 0:24 hr:min Bath temp.: 77.35 K
Analysis Mode: Standard VoidVol Remeasure:off
VoidVol. Mode: He Measure Cold Zone V: 5.9725 cc Warm Zone V: 7.0997 cc
Data Reduction Parameters
Thermal Transpiration: onEff. mol. diameter (D): 3.54 ÅEff. cell stem diam. (d): 4.0000 mm

Adsorbate modelNitrogen Temperature 77.350K
Molec. Wt.: 28.013 Cross Section: 16.200 Å² Liquid Density: 0.806 g/cc

Relative Pressure P/Po	Volume @ STP cc/g	1 / [W((Po/P) - 1)] 1/g
5.21342e-02	3.7254	1.1813e+01
9.61505e-02	4.1541	2.0489e+01
1.47022e-01	4.5629	3.0224e+01
1.97155e-01	4.9454	3.9731e+01
2.47626e-01	5.3384	4.9329e+01
2.97795e-01	5.7616	5.8893e+01

BET summary
Slope = 191.238 1/g
Intercept = 1.999e+00 1/g
Correlation coefficient, r = 0.999984
C constant= 96.653

Surface Area = 18.022 m²/g

Quantachrome® ASiQwin™- Automated Gas Sorption Data
Acquisition and Reduction

version 5.21

Analysis Report
Operator: DIJUVA Date:2022/04/25 Operator: DIJUVA Date:2022/04/25
Sample ID: 46503 Nini-4 Filename: 220425-01.qps
Sample Desc: 1390-1400m Comment: _6 Point BET
Sample Weight: 1.591 g Instrument: Autosorb iQ Station 1
Approx. Outgas Time:3.1 hrs Final Outgas Temp.:60 °C Extended info: Available
Analysis gas: Nitrogen Non-ideality: 6.58e-05 1/Torr CellType: 9mm
Analysis Time: 0:25 hr:min Bath temp.: 77.35 K
Analysis Mode: Standard VoidVol Remeasure:off
VoidVol. Mode: He Measure Cold Zone V: 7.68415 cc Warm Zone V: 7.32994 cc
Data Reduction Parameters
Thermal Transpiration: onEff. mol. diameter (D): 3.54 ÅEff. cell stem diam. (d): 4.0000 mm

Adsorbate modelNitrogen Temperature 77.350K
Molec. Wt.: 28.013 Cross Section: 16.200 Å² Liquid Density: 0.806 g/cc

Relative Pressure P/Po	Volume @ STP cc/g	1 / [W((Po/P) - 1)] 1/g
4.85822e-02	3.8939	1.0492e+01
9.94897e-02	4.4132	2.0030e+01
1.50257e-01	4.8338	2.9269e+01
2.00309e-01	5.2259	3.8350e+01
2.49979e-01	5.6233	4.7423e+01
2.99542e-01	6.0391	5.6657e+01

BET summary
Slope = 183.387 1/g
Intercept = 1.667e+00 1/g
Correlation coefficient, r = 0.999988
C constant= 110.997

Surface Area = 18.819 m²/g

Quantachrome® ASiQwin™- Automated Gas Sorption Data
Acquisition and Reduction

version 5.21

Analysis Report
Operator: DIJUVA Date:2022/04/25 Operator: DIJUVA Date:2022/04/25
Sample ID: 46504 Nini-4 Filename: 220425-02.qps
Sample Desc: 1400-1410m Comment: _6 Point BET
Sample Weight: 1.0441 g Instrument: Autosorb iQ Station 1
Approx. Outgas Time:3.1 hrs Final Outgas Temp.:60 °C Extended info: Available
Analysis gas: Nitrogen Non-ideality: 6.58e-05 1/Torr CellType: 9mm
Analysis Time: 0:25 hr:min Bath temp.: 77.35 K
Analysis Mode: Standard VoidVol Remeasure:off
VoidVol. Mode: He Measure Cold Zone V: 7.34089 cc Warm Zone V: 7.3534 cc
Data Reduction Parameters
Thermal Transpiration: onEff. mol. diameter (D): 3.54 ÅEff. cell stem diam. (d): 4.0000 mm

Adsorbate modelNitrogen Temperature 77.350K
Molec. Wt.: 28.013 Cross Section: 16.200 Å² Liquid Density: 0.806 g/cc

Relative Pressure P/Po	Volume @ STP cc/g	1 / [W((Po/P) - 1)] 1/g
4.85751e-02	3.7443	1.0910e+01
1.01502e-01	4.2734	2.1151e+01
1.46711e-01	4.6400	2.9648e+01
1.96318e-01	5.0243	3.8900e+01
2.46241e-01	5.4188	4.8236e+01
3.02999e-01	5.9005	5.8948e+01

BET summary
Slope = 188.333 1/g
Intercept = 1.914e+00 1/g
Correlation coefficient, r = 0.999983
C constant= 99.386

Surface Area = 18.305 m²/g

Quantachrome® ASiQwin™- Automated Gas Sorption Data
Acquisition and Reduction

version 5.21

Analysis Report
Operator: DIJUVA Date:2022/04/25 Operator: DIJUVA Date:2022/04/25
Sample ID: 46505 Nini-4 Filename: 220425-03.qps
Sample Desc: 1410-1420m Comment: _6 Point BET
Sample Weight: 1.5547 g Instrument: Autosorb iQ Station 1
Approx. Outgas Time:3.1 hrs Final Outgas Temp.:60 °C Extended info: Available
Analysis gas: Nitrogen Non-ideality: 6.58e-05 1/Torr CellType: 9mm
Analysis Time: 0:22 hr:min Bath temp.: 77.35 K
Analysis Mode: Standard VoidVol Remeasure:off
VoidVol. Mode: He Measure Cold Zone V: 7.5701 cc Warm Zone V: 7.34432 cc
Data Reduction Parameters
Thermal Transpiration: onEff. mol. diameter (D): 3.54 ÅEff. cell stem diam. (d): 4.0000 mm

Adsorbate modelNitrogen Temperature 77.350K
Molec. Wt.: 28.013 Cross Section: 16.200 Å² Liquid Density: 0.806 g/cc

Relative Pressure P/Po	Volume @ STP cc/g	1 / [W((Po/P) - 1)] 1/g
5.13210e-02	3.1000	1.3962e+01
1.00911e-01	3.5230	2.5490e+01
1.51588e-01	3.8747	3.6895e+01
2.01974e-01	4.2032	4.8178e+01
2.51897e-01	4.5354	5.9401e+01
3.01482e-01	4.8784	7.0788e+01

BET summary
Slope = 226.399 1/g
Intercept = 2.487e+00 1/g
Correlation coefficient, r = 0.999985
C constant= 92.051

Surface Area = 15.215 m²/g

Quantachrome® ASiQwin™- Automated Gas Sorption Data
Acquisition and Reduction

version 5.21

Analysis Report
Operator: DIJUVA Date:2022/04/25 Operator: DIJUVA Date:2022/04/25
Sample ID: 46506 Nini-4 Filename: 220425-04.qps
Sample Desc: 1420-1430m Comment: _6 Point BET
Sample Weight: 1.1843 g Instrument: Autosorb iQ Station 1
Approx. Outgas Time:3.1 hrs Final Outgas Temp.:60 °C Extended info: Available
Analysis gas: Nitrogen Non-ideality: 6.58e-05 1/Torr CellType: 9mm
Analysis Time: 0:23 hr:min Bath temp.: 77.35 K
Analysis Mode: Standard VoidVol Remeasure:off
VoidVol. Mode: He Measure Cold Zone V: 7.74049 cc Warm Zone V: 7.37252 cc
Data Reduction Parameters
Thermal Transpiration: onEff. mol. diameter (D): 3.54 ÅEff. cell stem diam. (d): 4.0000 mm

Adsorbate modelNitrogen Temperature 77.350K
Molec. Wt.: 28.013 Cross Section: 16.200 Å² Liquid Density: 0.806 g/cc

Relative Pressure P/Po	Volume @ STP cc/g	1 / [W((Po/P) - 1)] 1/g
5.21438e-02	2.7475	1.6020e+01
9.63761e-02	3.0862	2.7651e+01
1.47346e-01	3.4037	4.0622e+01
1.97526e-01	3.7004	5.3223e+01
2.53793e-01	4.0288	6.7546e+01
2.97569e-01	4.3037	7.8757e+01

BET summary
Slope = 254.869 1/g
Intercept = 2.924e+00 1/g
Correlation coefficient, r = 0.999984
C constant= 88.167

Surface Area = 13.509 m²/g

Quantachrome® ASiQwin™- Automated Gas Sorption Data
Acquisition and Reduction

version 5.21

Analysis Report
Operator: DIJUVA Date:2022/04/27 Operator: DIJUVA Date:2022/04/27
Sample ID: 46507 Nini-4 Filename: 220427-01.qps
Sample Desc: 1430-1440m Comment: _6 Point BET
Sample Weight: 1.7097 g Instrument: Autosorb iQ Station 1
Approx. Outgas Time:3.1 hrs Final Outgas Temp.:60 °C Extended info: Available
Analysis gas: Nitrogen Non-ideality: 6.58e-05 1/Torr CellType: 9mm
Analysis Time: 0:23 hr:min Bath temp.: 77.35 K
Analysis Mode: Standard VoidVol Remeasure:off
VoidVol. Mode: He Measure Cold Zone V: 5.44297 cc Warm Zone V: 7.21911 cc
Data Reduction Parameters
Thermal Transpiration: onEff. mol. diameter (D): 3.54 ÅEff. cell stem diam. (d): 4.0000 mm

Adsorbate modelNitrogen Temperature 77.350K
Molec. Wt.: 28.013 Cross Section: 16.200 Å² Liquid Density: 0.806 g/cc

Relative Pressure P/Po	Volume @ STP cc/g	1 / [W((Po/P) - 1)] 1/g
4.90338e-02	2.9673	1.3903e+01
9.86560e-02	3.3724	2.5968e+01
1.50750e-01	3.7134	3.8247e+01
2.01449e-01	4.0284	5.0105e+01
2.51281e-01	4.3397	6.1878e+01
3.01100e-01	4.6698	7.3815e+01

BET summary
Slope = 236.948 1/g
Intercept = 2.430e+00 1/g
Correlation coefficient, r = 0.999986
C constant= 98.492

Surface Area = 14.548 m²/g

Quantachrome® ASiQwin™- Automated Gas Sorption Data
Acquisition and Reduction

version 5.21

Analysis Report
Operator: DIJUVA Date:2022/04/27 Operator: DIJUVA Date:2022/04/27
Sample ID: 46508 Nini-4 Filename: 220427-02.qps
Sample Desc: 1440-1450m Comment: _6 Point BET
Sample Weight: 1.4972 g Instrument: Autosorb iQ Station 1
Approx. Outgas Time:3.1 hrs Final Outgas Temp.:60 °C Extended info: Available
Analysis gas: Nitrogen Non-ideality: 6.58e-05 1/Torr CellType: 9mm
Analysis Time: 0:24 hr:min Bath temp.: 77.35 K
Analysis Mode: Standard VoidVol Remeasure:off
VoidVol. Mode: He Measure Cold Zone V: 5.50888 cc Warm Zone V: 7.22605 cc
Data Reduction Parameters
Thermal Transpiration: onEff. mol. diameter (D): 3.54 ÅEff. cell stem diam. (d): 4.0000 mm

Adsorbate modelNitrogen Temperature 77.350K
Molec. Wt.: 28.013 Cross Section: 16.200 Å² Liquid Density: 0.806 g/cc

Relative Pressure P/Po	Volume @ STP cc/g	1 / [W((Po/P) - 1)] 1/g
5.18558e-02	3.1025	1.4105e+01
1.01348e-01	3.5155	2.5668e+01
1.51863e-01	3.8595	3.7119e+01
2.02431e-01	4.1815	4.8565e+01
2.52238e-01	4.5043	5.9919e+01
3.02037e-01	4.8420	7.1507e+01

BET summary
Slope = 228.718 1/g
Intercept = 2.339e+00 1/g
Correlation coefficient, r = 0.999987
C constant= 98.767

Surface Area = 15.072 m²/g

Quantachrome® ASiQwin™- Automated Gas Sorption Data
Acquisition and Reduction

version 5.21

Analysis Report
Operator: DIJUVA Date:2022/04/27 Operator: DIJUVA Date:2022/04/28
Sample ID: 46509 Nini-4 Filename: 220427-03.qps
Sample Desc: 1490-1500m Comment: _6 Point BET
Sample Weight: 1.9237 g Instrument: Autosorb iQ Station 1
Approx. Outgas Time:3.1 hrs Final Outgas Temp.:60 °C Extended info: Available
Analysis gas: Nitrogen Non-ideality: 6.58e-05 1/Torr CellType: 9mm
Analysis Time: 0:30 hr:min Bath temp.: 77.35 K
Analysis Mode: Standard VoidVol Remeasure:off
VoidVol. Mode: He Measure Cold Zone V: 5.35819 cc Warm Zone V: 7.12665 cc
Data Reduction Parameters
Thermal Transpiration: onEff. mol. diameter (D): 3.54 ÅEff. cell stem diam. (d): 4.0000 mm

Adsorbate modelNitrogen Temperature 77.350K
Molec. Wt.: 28.013 Cross Section: 16.200 Å² Liquid Density: 0.806 g/cc

Relative Pressure P/Po	Volume @ STP cc/g	1 / [W((Po/P) - 1)] 1/g
4.69281e-02	4.1089	9.5882e+00
1.01344e-01	4.6805	1.9278e+01
1.48492e-01	5.0766	2.7485e+01
1.98544e-01	5.4773	3.6188e+01
2.48306e-01	5.8809	4.4942e+01
2.97607e-01	6.3093	5.3732e+01

BET summary
Slope = 175.669 1/g
Intercept = 1.384e+00 1/g
Correlation coefficient, r = 0.999991
C constant= 127.948

Surface Area = 19.669 m²/g

Quantachrome® ASiQwin™- Automated Gas Sorption Data
Acquisition and Reduction

version 5.21

Analysis Report
Operator: DIJUVA Date:2022/04/28 Operator: DIJUVA Date:2022/04/28
Sample ID: 46510 Nini-4 Filename: 220428-01.qps
Sample Desc: 1520-1530m Comment: _6 Point BET
Sample Weight: 1.6142 g Instrument: Autosorb iQ Station 1
Approx. Outgas Time:3.1 hrs Final Outgas Temp.:60 °C Extended info: Available
Analysis gas: Nitrogen Non-ideality: 6.58e-05 1/Torr CellType: 9mm
Analysis Time: 0:22 hr:min Bath temp.: 77.35 K
Analysis Mode: Standard VoidVol Remeasure:off
VoidVol. Mode: He Measure Cold Zone V: 7.41947 cc Warm Zone V: 7.43942 cc
Data Reduction Parameters
Thermal Transpiration: onEff. mol. diameter (D): 3.54 ÅEff. cell stem diam. (d): 4.0000 mm

Adsorbate modelNitrogen Temperature 77.350K
Molec. Wt.: 28.013 Cross Section: 16.200 Å² Liquid Density: 0.806 g/cc

Relative Pressure P/Po	Volume @ STP cc/g	1 / [W((Po/P) - 1)] 1/g
4.87788e-02	3.3728	1.2165e+01
1.00548e-01	3.8230	2.3396e+01
1.51571e-01	4.1744	3.4242e+01
2.01676e-01	4.5021	4.4896e+01
2.51434e-01	4.8346	5.5588e+01
3.00736e-01	5.1894	6.6310e+01

BET summary
Slope = 214.435 1/g
Intercept = 1.737e+00 1/g
Correlation coefficient, r = 0.999993
C constant= 124.444

Surface Area = 16.110 m²/g

Quantachrome® ASiQwin™- Automated Gas Sorption Data
Acquisition and Reduction

version 5.21

Analysis Report
Operator: DIJUVA Date:2022/04/28 Operator: DIJUVA Date:2022/04/28
Sample ID: 46511 Nini-4 Filename: 220428-02.qps
Sample Desc: 1560-1570m Comment: _6 Point BET
Sample Weight: 1.5747 g Instrument: Autosorb iQ Station 1
Approx. Outgas Time:3.1 hrs Final Outgas Temp.:60 °C Extended info: Available
Analysis gas: Nitrogen Non-ideality: 6.58e-05 1/Torr CellType: 9mm
Analysis Time: 0:24 hr:min Bath temp.: 77.35 K
Analysis Mode: Standard VoidVol Remeasure:off
VoidVol. Mode: He Measure Cold Zone V: 5.46609 cc Warm Zone V: 7.33594 cc
Data Reduction Parameters
Thermal Transpiration: onEff. mol. diameter (D): 3.54 ÅEff. cell stem diam. (d): 4.0000 mm

Adsorbate modelNitrogen Temperature 77.350K
Molec. Wt.: 28.013 Cross Section: 16.200 Å² Liquid Density: 0.806 g/cc

Relative Pressure P/Po	Volume @ STP cc/g	1 / [W((Po/P) - 1)] 1/g
5.06973e-02	3.3446	1.2776e+01
9.95955e-02	3.7670	2.3494e+01
1.51077e-01	4.1191	3.4568e+01
2.01656e-01	4.4491	4.5426e+01
2.51927e-01	4.7784	5.6390e+01
3.01328e-01	5.1265	6.7312e+01

BET summary
Slope = 217.080 1/g
Intercept = 1.778e+00 1/g
Correlation coefficient, r = 0.999989
C constant= 123.085

Surface Area = 15.912 m²/g

Quantachrome® ASiQwin™- Automated Gas Sorption Data
Acquisition and Reduction

version 5.21

Analysis Report
Operator: DIJUVA Date:2022/05/02 Operator: DIJUVA Date:2022/05/04
Sample ID: 46511b Nini-4 Filename: 220502-02.qps
Sample Desc: 1560 - 1570m Comment: _6 Point BET
Sample Weight: 1.737 g Instrument: Autosorb iQ Station 1
Approx. Outgas Time:3.1 hrs Final Outgas Temp.:60 °C Extended info: Available
Analysis gas: Nitrogen Non-ideality: 6.58e-05 1/Torr CellType: 9mm
Analysis Time: 0:23 hr:min Bath temp.: 77.35 K
Analysis Mode: Standard VoidVol Remeasure:off
VoidVol. Mode: He Measure Cold Zone V: 7.58068 cc Warm Zone V: 7.25311 cc
Data Reduction Parameters
Thermal Transpiration: onEff. mol. diameter (D): 3.54 ÅEff. cell stem diam. (d): 4.0000 mm

Adsorbate modelNitrogen Temperature 77.350K
Molec. Wt.: 28.013 Cross Section: 16.200 Å² Liquid Density: 0.806 g/cc

Relative Pressure P/Po	Volume @ STP cc/g	1 / [W((Po/P) - 1)] 1/g
4.86994e-02	3.1178	1.3137e+01
1.00407e-01	3.5431	2.5205e+01
1.51206e-01	3.8784	3.6751e+01
2.01407e-01	4.1902	4.8157e+01
2.51269e-01	4.5092	5.9548e+01
3.00461e-01	4.8482	7.0883e+01

BET summary
Slope = 228.866 1/g
Intercept = 2.097e+00 1/g
Correlation coefficient, r = 0.999993
C constant= 110.134

Surface Area = 15.078 m²/g

APPENDIX C – MICP ANALYSIS

The capillary pressure and pore network characteristics were measured by the automatic mercury injection technique for 25 cuttings samples. Sampling details, laboratory constants used during the data reduction and diagrams necessary for the seal capacity evaluation are shown in the data sheets below. A listing of selected MICP data for all samples is given in Table 9. The total set of raw data and diagrams were forwarded to GEUS in an Excel file from Core Technical Services, Aberdeen.

Mercury Injection Capillary Pressure Data	Well: Nini-4
Project: Greensand Phase 2	Cuttings Lark Fm

Sample Identification	46487	
Sample Depth	820,00	m
Plug Permeability (Air)	n/a	mD
Log Porosity	0,23	fraction

Injection Sample Porosity	0,265	fraction
Injection Sample Pore Vol	0,741	cc
Injection Sample Bulk Vol	2,802	cc
Injection Sample Weight	5,150	g

Mean Hydraulic Radius	0,299	microns
Swanson's Parameter	0,019	
FZI	-	

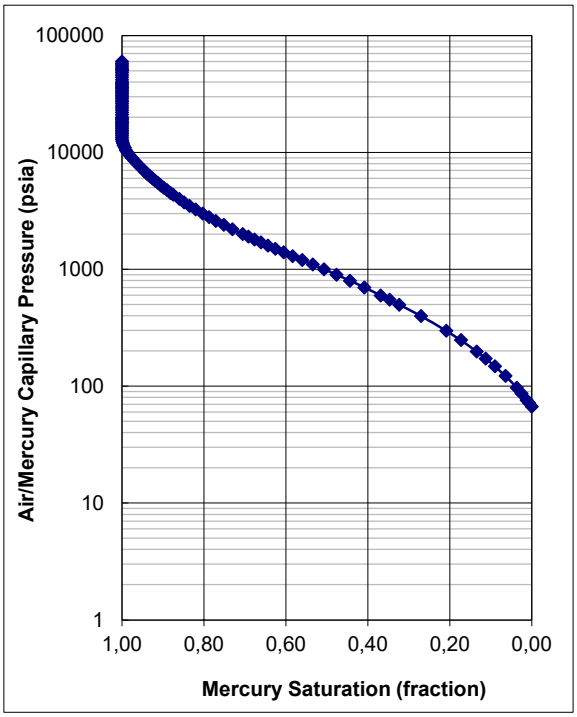

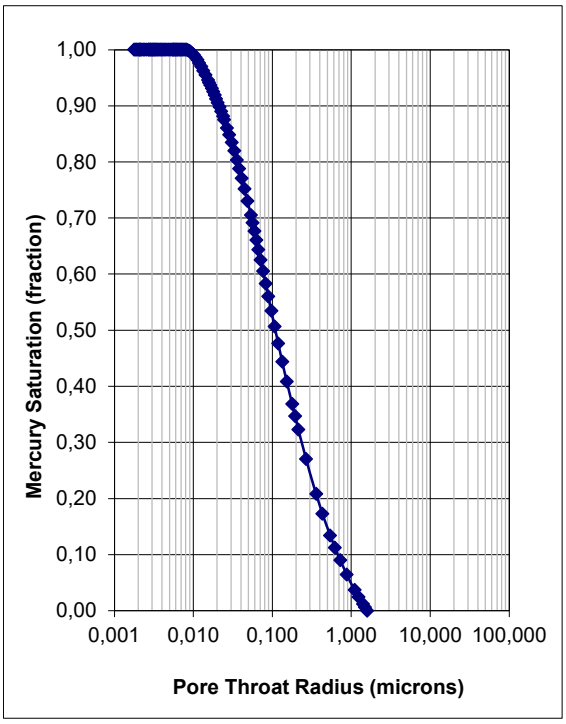

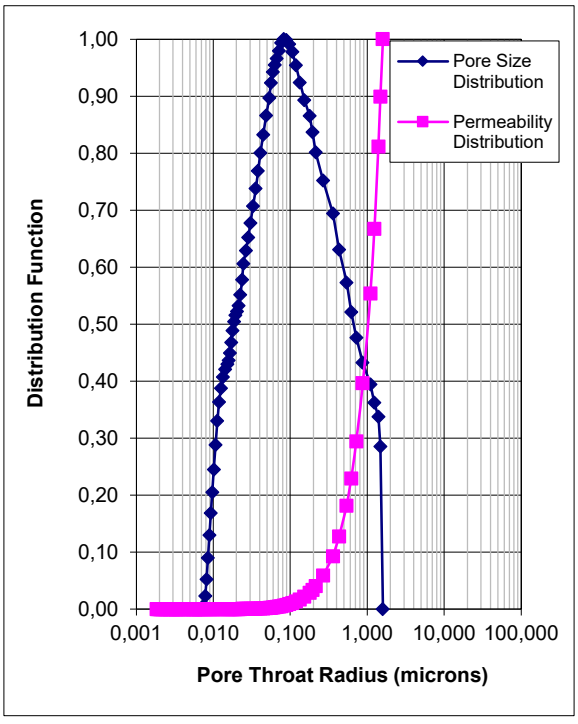

Mercury Injection Capillary Pressure Data

Well: Nini-4

Project: Greensand Phase 2

Cuttings Lark Fm

Sample Identification	46488	
Sample Depth	840,00	m
Plug Permeability (Air)	n/a	mD
Log Poroisty	0,22	fraction

Injection Sample Porosity	0,245	fraction
Injection Sample Pore Vol	0,685	cc
Injection Sample Bulk Vol	2,796	cc
Injection Sample Weight	5,500	g

Mean Hydraulic Radius	0,043	microns
Swanson's Parameter	0,004	
FZI	-	

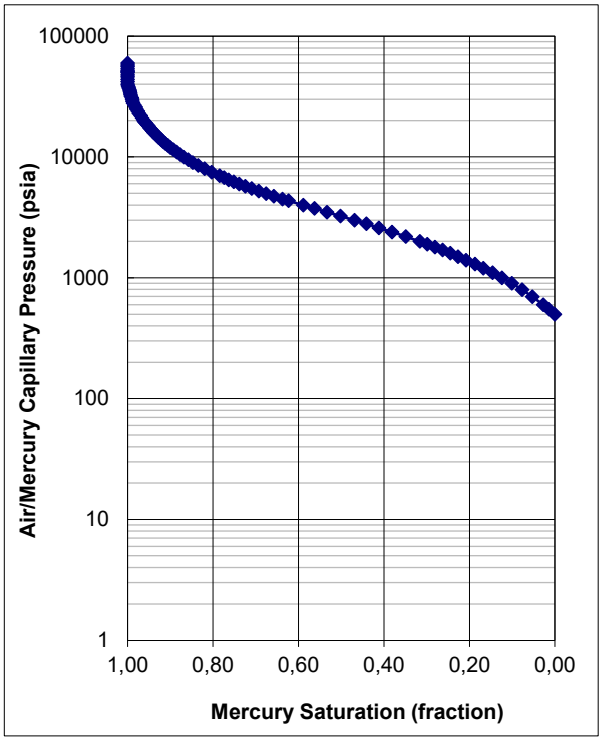

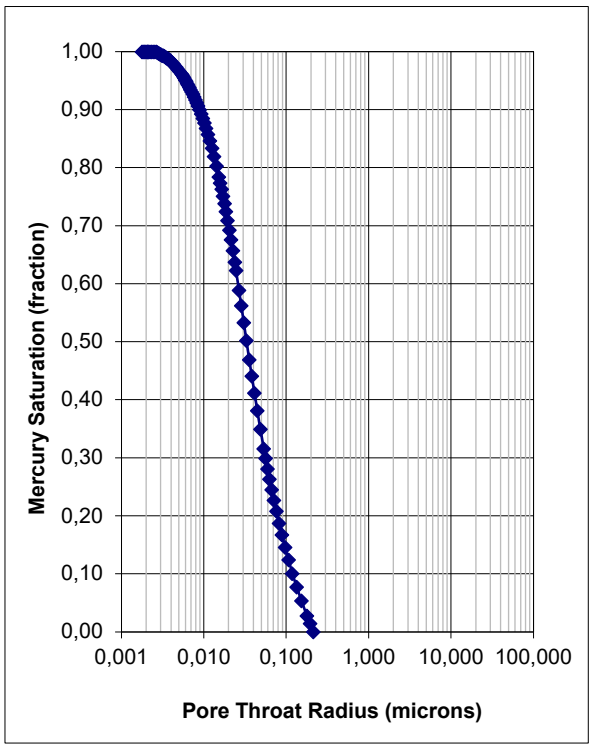

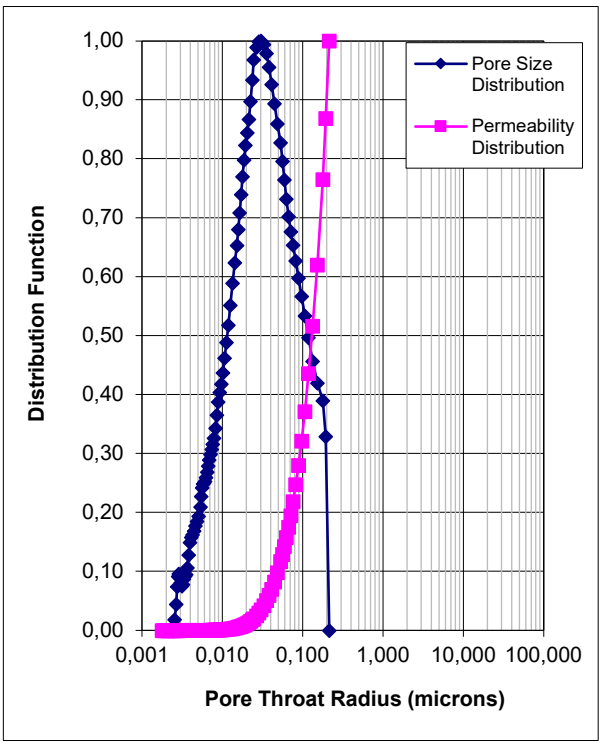

Mercury Injection Capillary Pressure Data	Well: Nini-4
Project: Greensand Phase 2	Cuttings Lark Fm

Sample Identification	46489	
Sample Depth	900,00	m
Plug Permeability (Air)	n/a	mD
Log Poroisty	0,21	fraction

Injection Sample Porosi	0,215	fraction
Injection Sample Pore V	0,655	cc
Injection Sample Bulk V	3,042	cc
Injection Sample Weigh	5,620	g

Mean Hydraulic Radius	0,067	microns
Swanson's Parameter	0,005	
FZI	-	

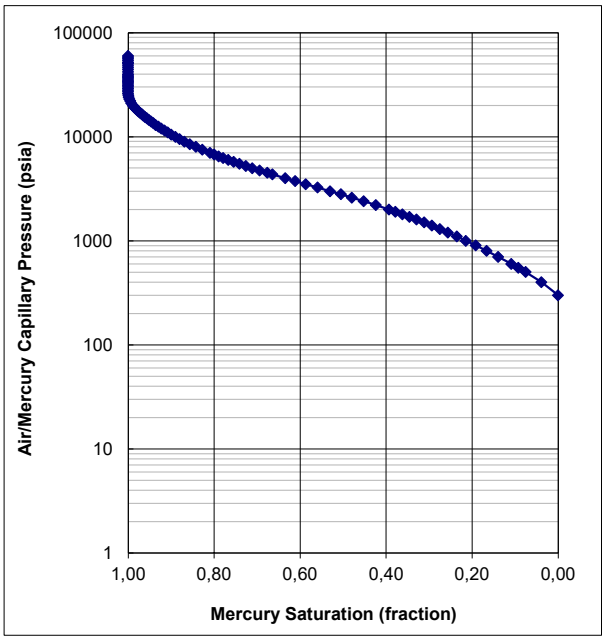

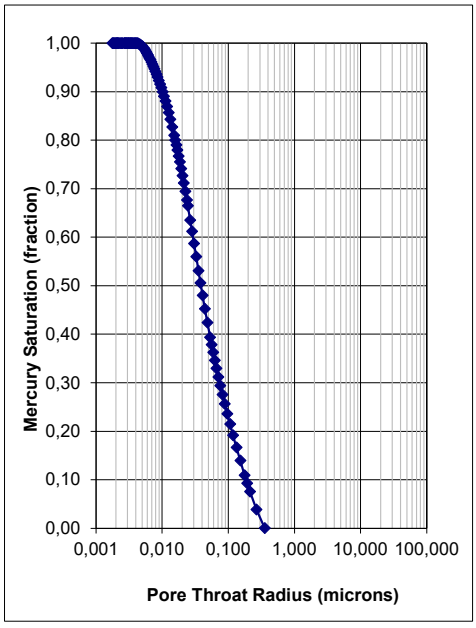

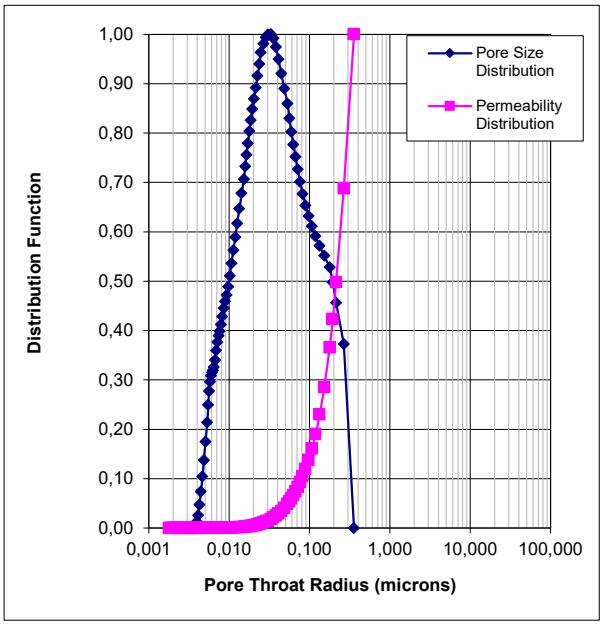

Mercury Injection Capillary Pressure Data — **Well: Nini-4**

Project: Greensand Phase 2 — **Cuttings Lark Fm**

Sample Identification	46490	
Sample Depth	940,00	m
Plug Permeability (Air)	n/a	mD
Log Poroisty	0,23	fraction

Injection Sample Porosi	0,213	fraction
Injection Sample Pore V	0,561	cc
Injection Sample Bulk V	2,640	cc
Injection Sample Weigh	4,720	g

Mean Hydraulic Radius	0,065	microns
Swanson's Parameter	0,004	
FZI	-	

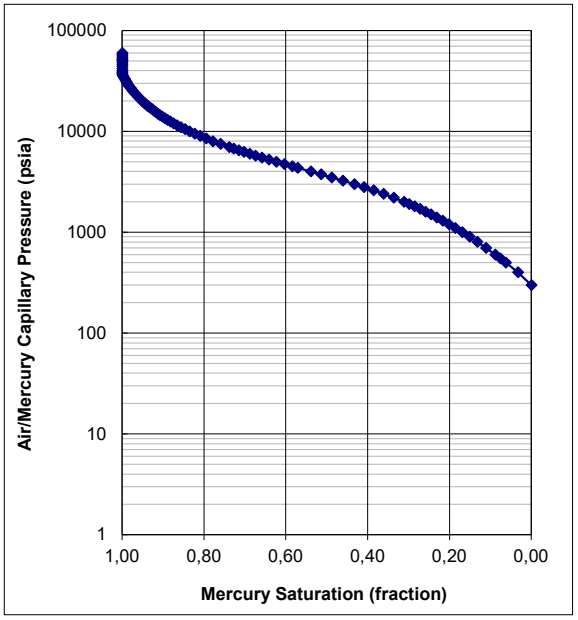

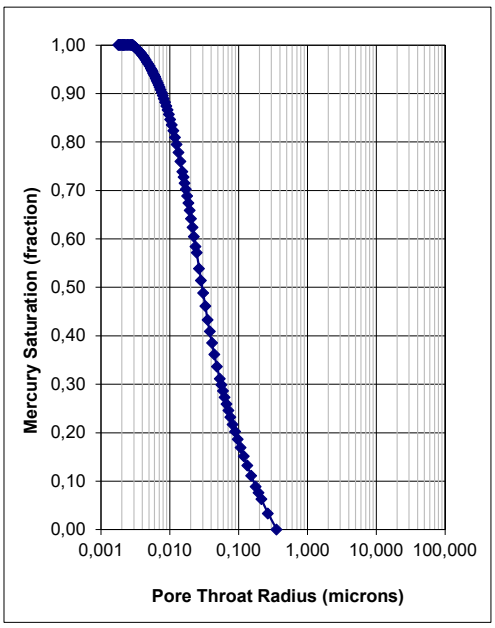

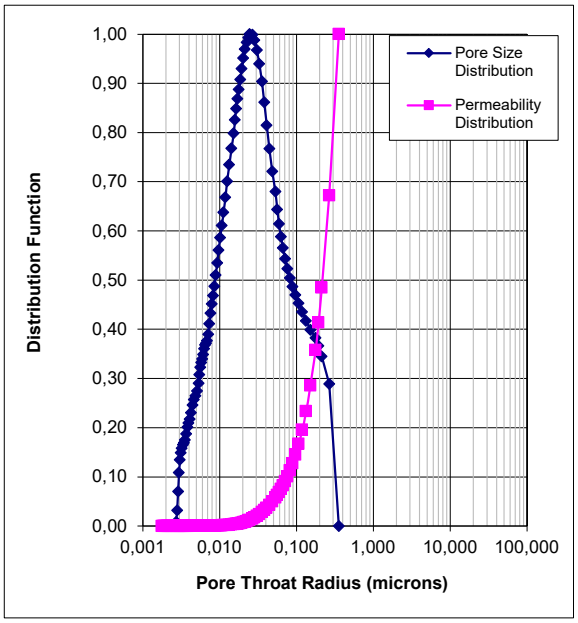

Mercury Injection Capillary Pressure Data — **Well: Nini-4**

Project: Greensand Phase 2 — **Cuttings Lark Fm**

Sample Identification	46491	
Sample Depth	990,00	m
Plug Permeability (Air)	n/a	mD
Log Poroisty	0,18	fraction

Injection Sample Porosi	0,177	fraction
Injection Sample Pore V	0,469	cc
Injection Sample Bulk V	2,653	cc
Injection Sample Weigh	5,490	g

Mean Hydraulic Radius	0,036	microns
Swanson's Parameter	0,003	
FZI	-	

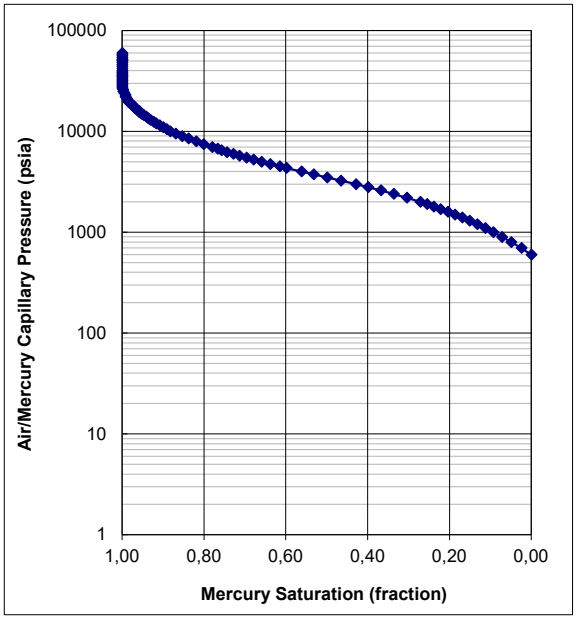

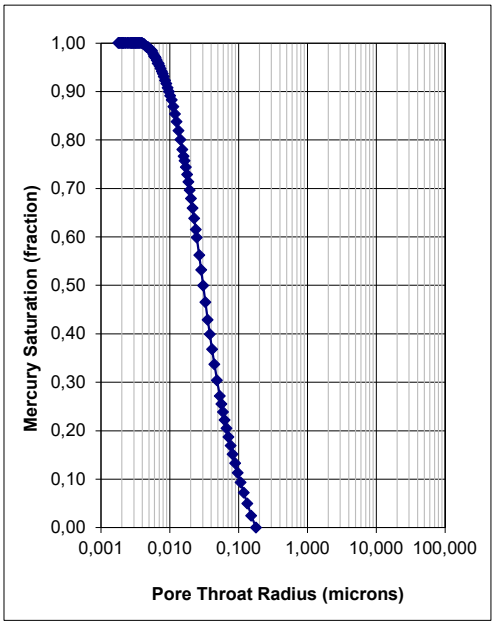

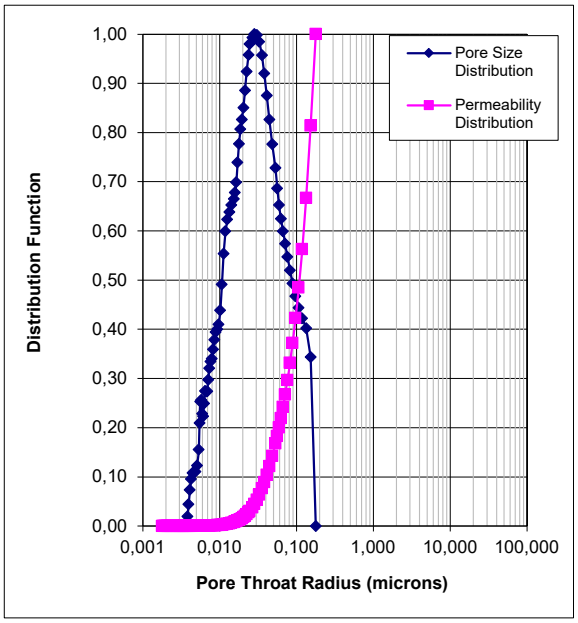

Mercury Injection Capillary Pressure Data — **Well: Nini-4**

Project: Greensand Phase 2 — **Cuttings Lark Fm**

Sample Identification	46492	
Sample Depth	1040,00	m
Plug Permeability (Air)	n/a	mD
Log Porosity	0,21	fraction

Injection Sample Porosi	0,228	fraction
Injection Sample Pore V	0,655	cc
Injection Sample Bulk V	2,879	cc
Injection Sample Weigh	5,800	g

Mean Hydraulic Radius	0,076	microns
Swanson's Parameter	0,005	
FZI	-	

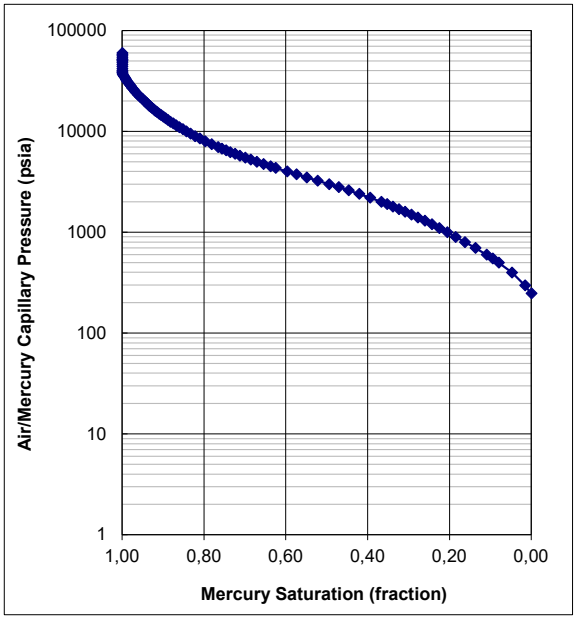

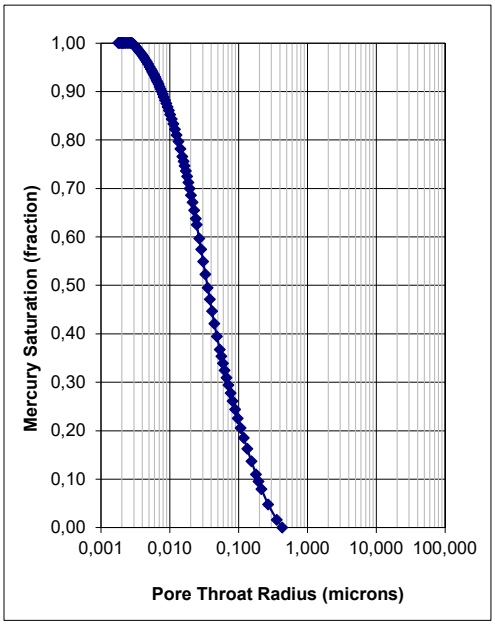

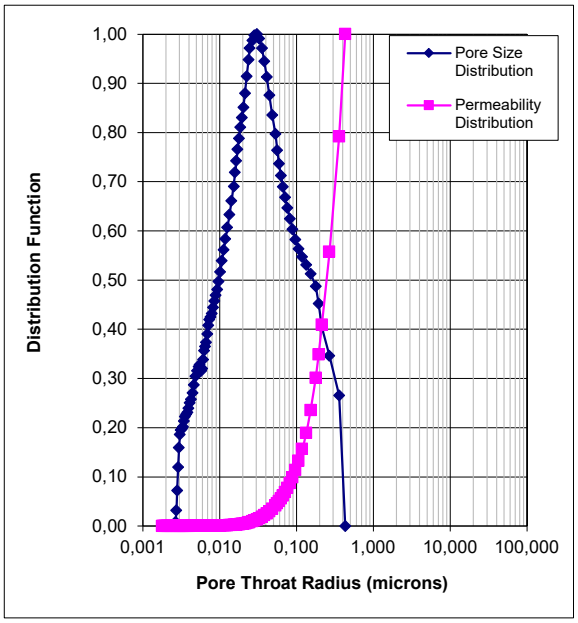

Mercury Injection Capillary Pressure Data — **Well: Nini-4**

Project: Greensand Phase 2 — **Cuttings Lark Fm**

Sample Identification	46493	
Sample Depth	1090,00	m
Plug Permeability (Air)	n/a	mD
Log Poroisty	0,20	fraction

Injection Sample Porosit	0,211	fraction
Injection Sample Pore V	0,679	cc
Injection Sample Bulk V	3,223	cc
Injection Sample Weight	6,610	g

Mean Hydraulic Radius	0,061	microns
Swanson's Parameter	0,003	
FZI	-	

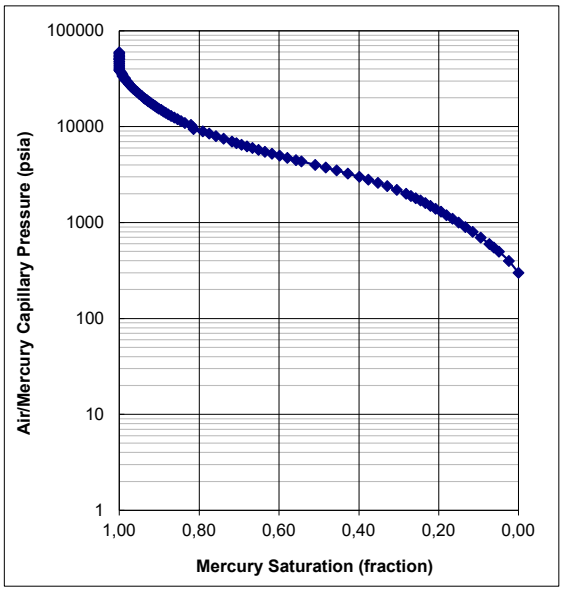

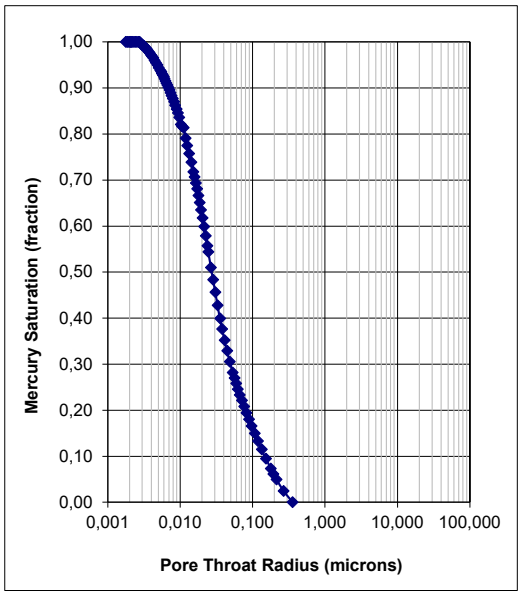

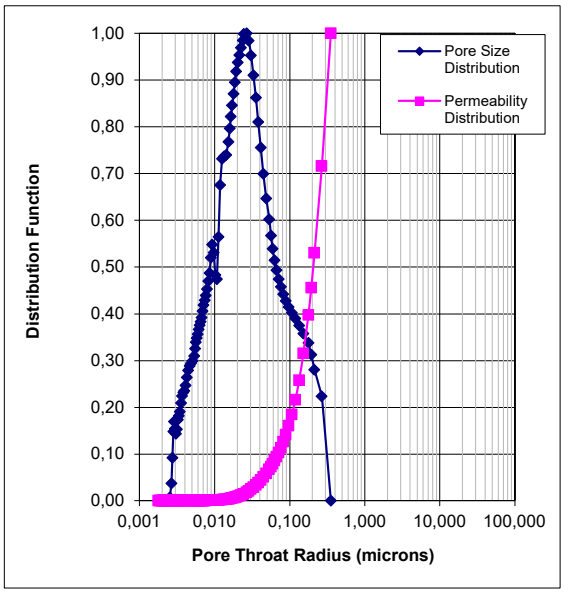

Mercury Injection Capillary Pressure Data — **Well: Nini-4**

Project: Greensand Phase 2 — **Cuttings Lark Fm**

Sample Identification	46494	
Sample Depth	1140,00	m
Plug Permeability (Air)	0,200	mD
Log Poroisty	0,21	fraction

Injection Sample Porosit	0,205	fraction
Injection Sample Pore V	0,556	cc
Injection Sample Bulk V	2,708	cc
Injection Sample Weight	5,520	g

Mean Hydraulic Radius	0,020	microns
Swanson's Parameter	0,002	
FZI	-	

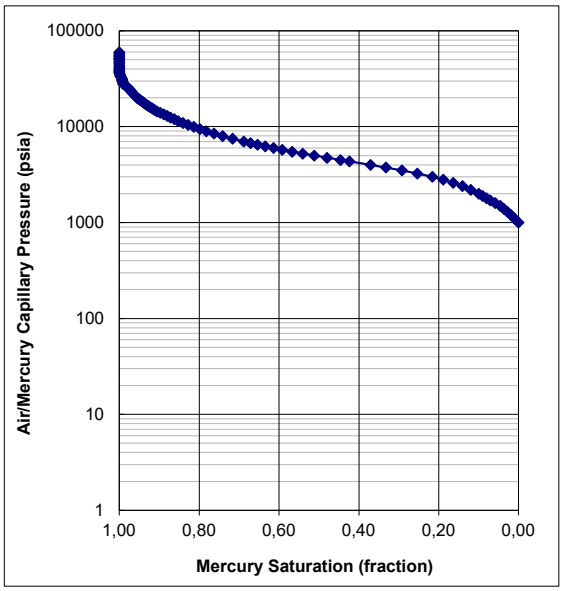

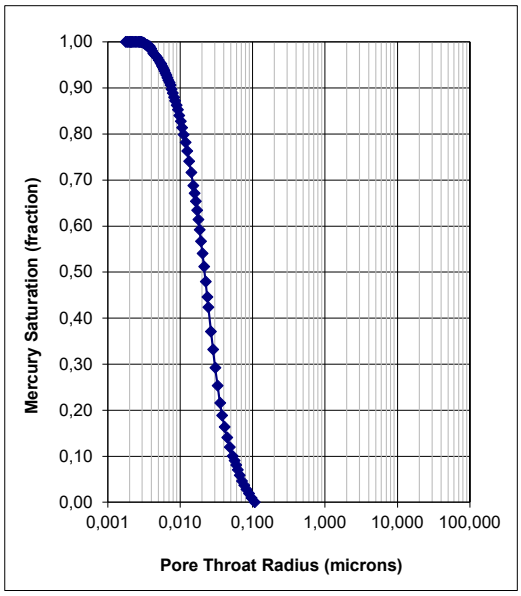

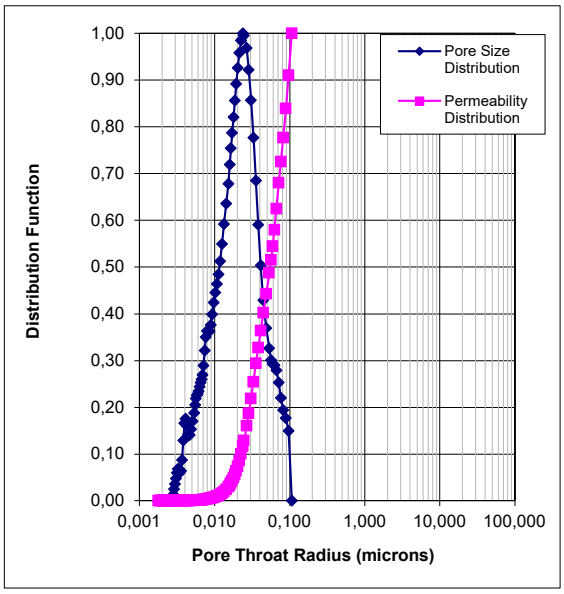

Mercury Injection Capillary Pressure Data — **Well: Nini-4**

Project: Greensand Phase 2 — **Cuttings Lark Fm**

Sample Identification	46495	
Sample Depth	1190,00	m
Plug Permeability (Air)	n/a	mD
Log Poroisty	0,17	fraction

Injection Sample Porosi	0,174	fraction
Injection Sample Pore V	0,619	cc
Injection Sample Bulk V	3,552	cc
Injection Sample Weigh	6,300	g

Mean Hydraulic Radius	0,030	microns
Swanson's Parameter	0,002	
PTS Index	-	

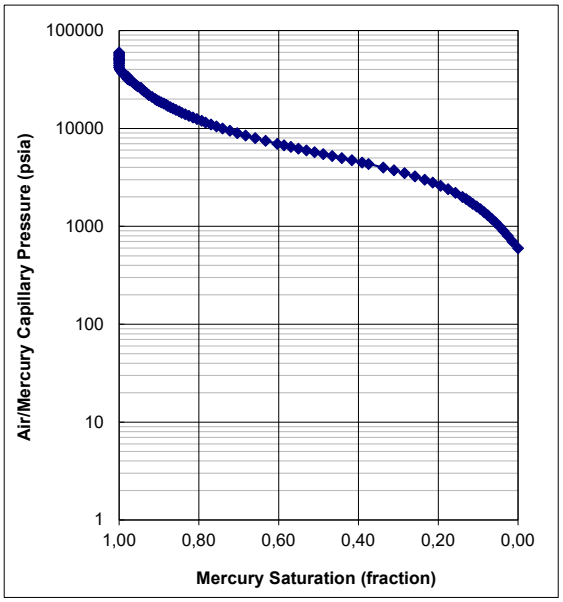

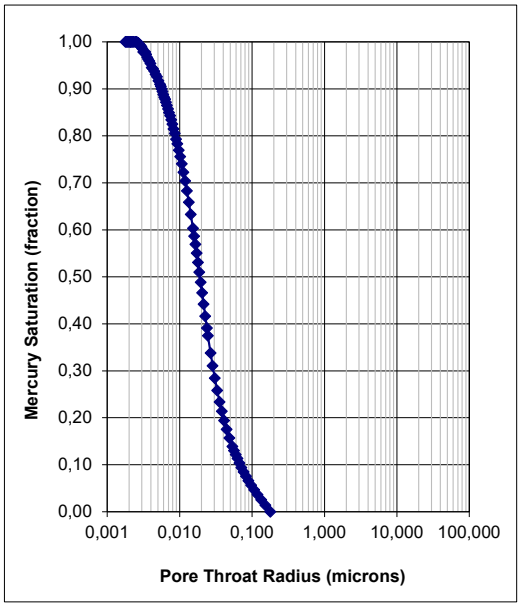

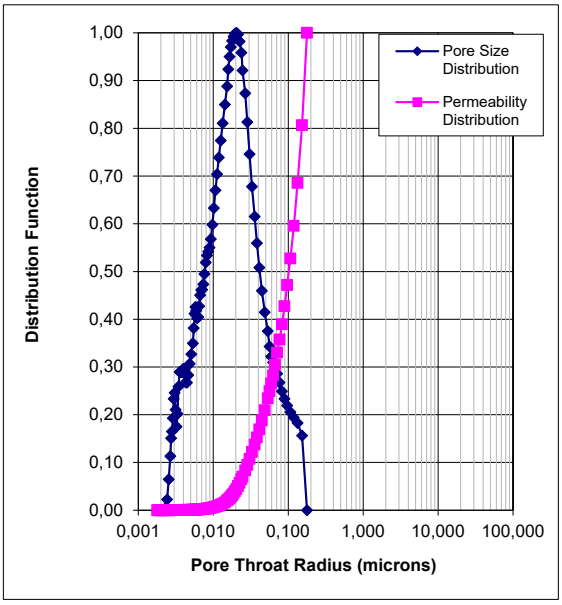

Mercury Injection Capillary Pressure Data — **Well: Nini-4**

Project: Greensand Phase 2 — **Cuttings Lark Fm**

Sample Identification	46496	
Sample Depth	1240,00	m
Plug Permeability (Air)	n/a	mD
Log Poroisty	0,18	fraction

Injection Sample Porosity	0,189	fraction
Injection Sample Pore Vol	0,486	cc
Injection Sample Bulk Vol	2,570	cc
Injection Sample Weight	5,410	g

Mean Hydraulic Radius	0,032	microns
Swanson's Parameter	0,002	
FZI	-	

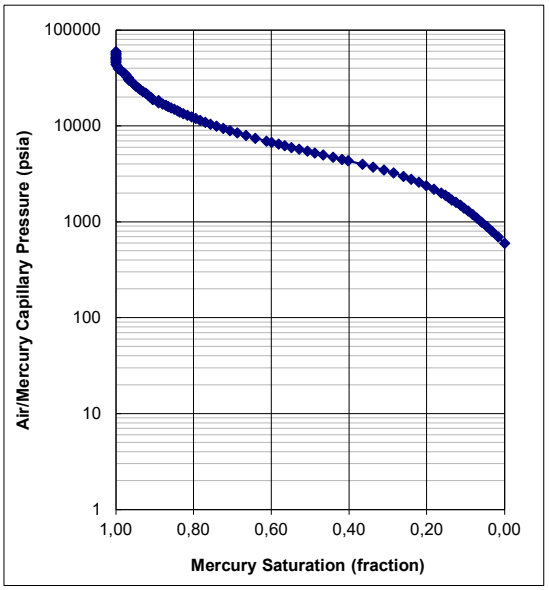

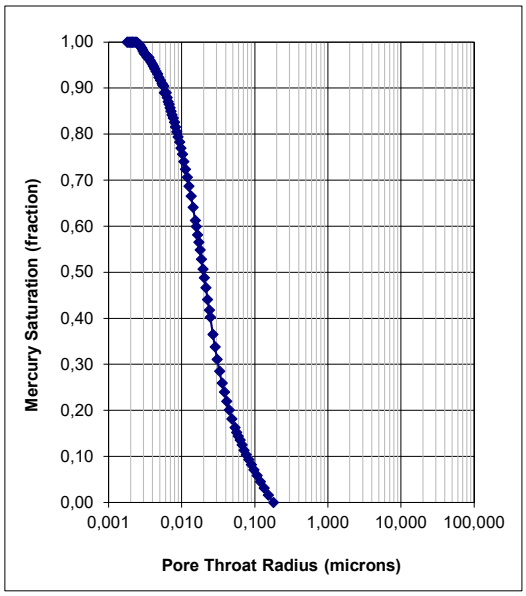

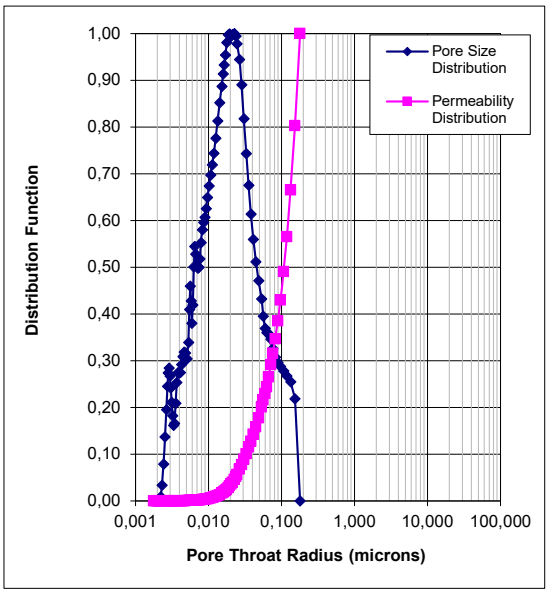

Mercury Injection Capillary Pressure Data — **Well: Nini-4**

Project: Greensand Phase 2 — **Cuttings Lark Fm**

Sample Identification	46497	
Sample Depth	1290,00	m
Plug Permeability (Air)	n/a	mD
Log Poroisty	0,15	fraction

Injection Sample Porosity	0,176	fraction
Injection Sample Pore Vol	0,437	cc
Injection Sample Bulk Vol	2,486	cc
Injection Sample Weight	5.2800	g

Mean Hydraulic Radius	0,031	microns
Swanson's Parameter	0,002	
FZI	-	

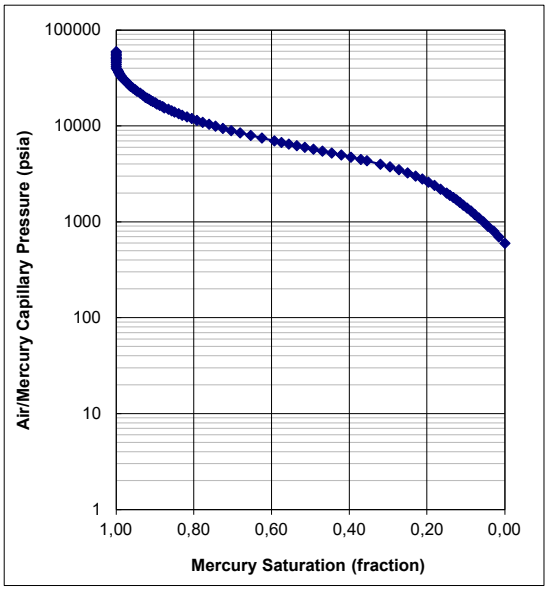

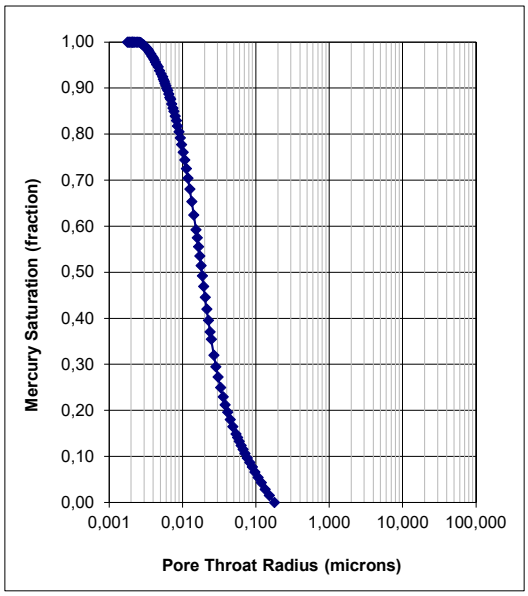

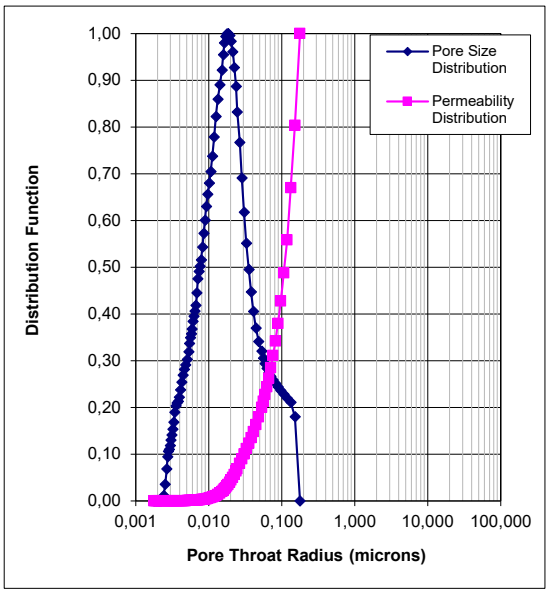

Mercury Injection Capillary Pressure Data — **Well: Nini-4**

Project: Greensand Phase 2 — **Cuttings Lark Fm**

Sample Identification	46498	
Sample Depth	1340,00	m
Plug Permeability (Air)	n/a	mD
Log Poroisty	0,17	fraction

Injection Sample Porosity	0,176	fraction
Injection Sample Pore Vol	0,489	cc
Injection Sample Bulk Vol	2,787	cc
Injection Sample Weight	5,880	g

Mean Hydraulic Radius	0,063	microns
Swanson's Parameter	0,003	
FZI	-	

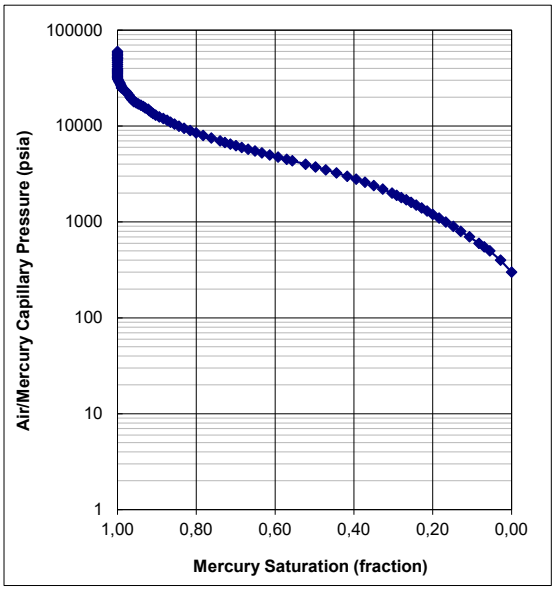

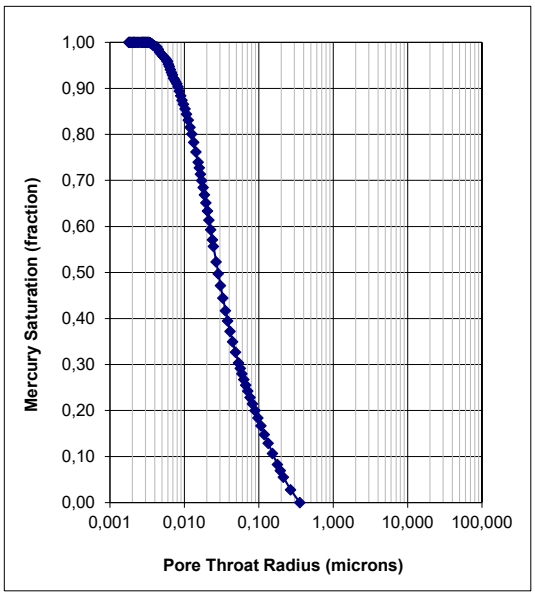

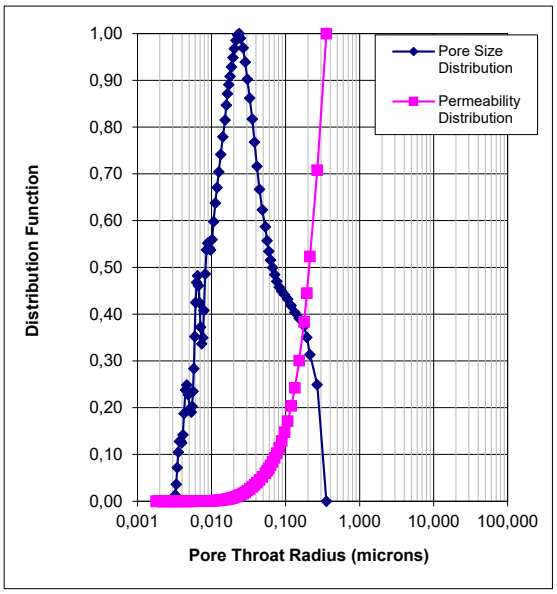

Mercury Injection Capillary Pressure Data — **Well: Nini-4**

Project: Greensand Phase 2 — **Cuttings Lark Fm**

Sample Identification	46499	
Sample Depth	1350,00	m
Plug Permeability (Air)	n/a	mD
Log Poroisty	0,17	fraction

Injection Sample Porosity	0,163	fraction
Injection Sample Pore Vol	0,499	cc
Injection Sample Bulk Vol	3,062	cc
Injection Sample Weight	6,260	g

Mean Hydraulic Radius	0,041	microns
Swanson's Parameter	0,002	
FZI	-	

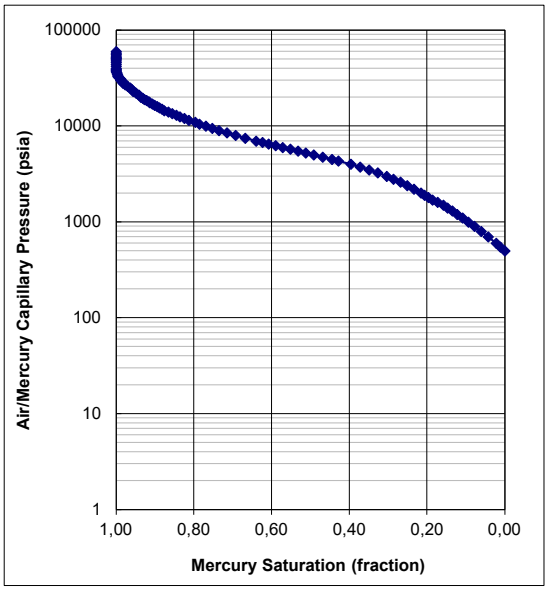

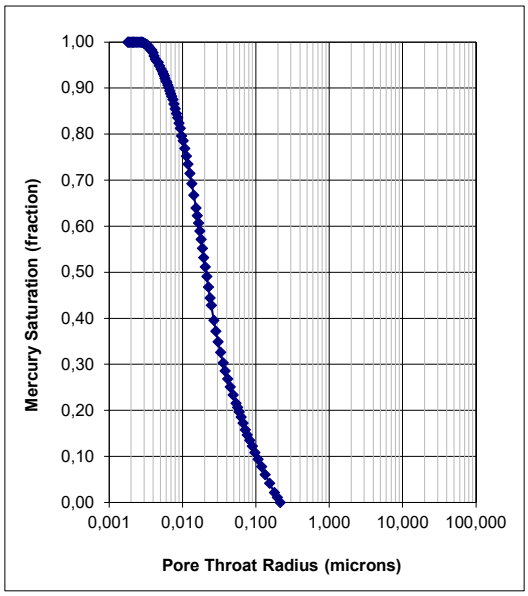

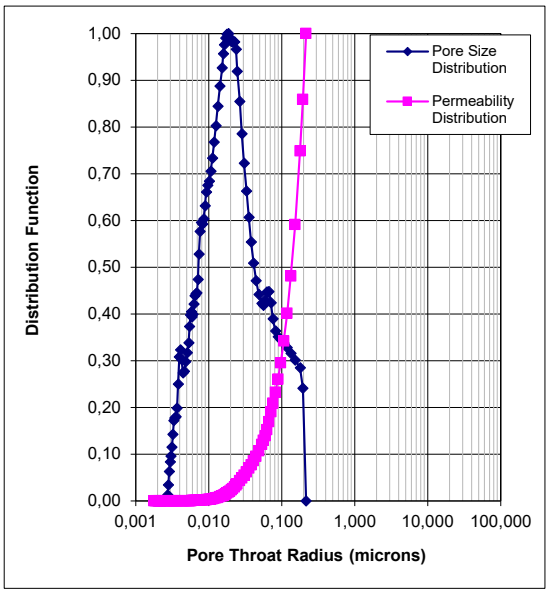

Mercury Injection Capillary Pressure Data — **Well: Nini-4**

Project: Greensand Phase 2 — **Cuttings Lark Fm**

Sample Identification	46500	
Sample Depth	1360,00	m
Plug Permeability (Air)	n/a	mD
Log Poroisty	0,17	fraction

Injection Sample Porosity	0,172	fraction
Injection Sample Pore Vol	0,460	cc
Injection Sample Bulk Vol	2,679	cc
Injection Sample Weight	5,670	g

Mean Hydraulic Radius	0,036	microns
Swanson's Parameter	0,002	
FZI	-	

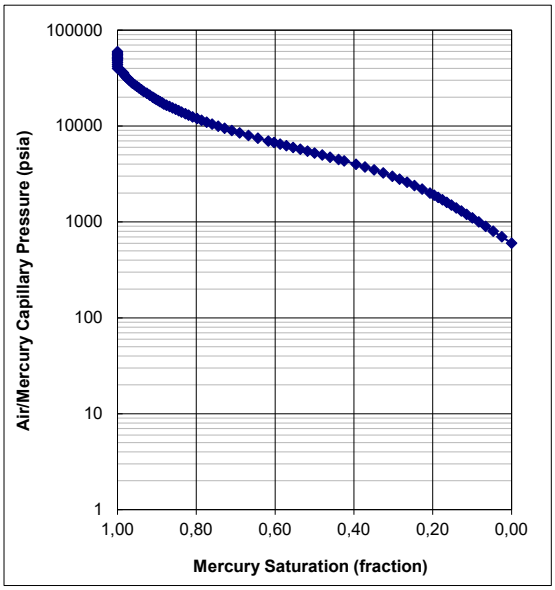

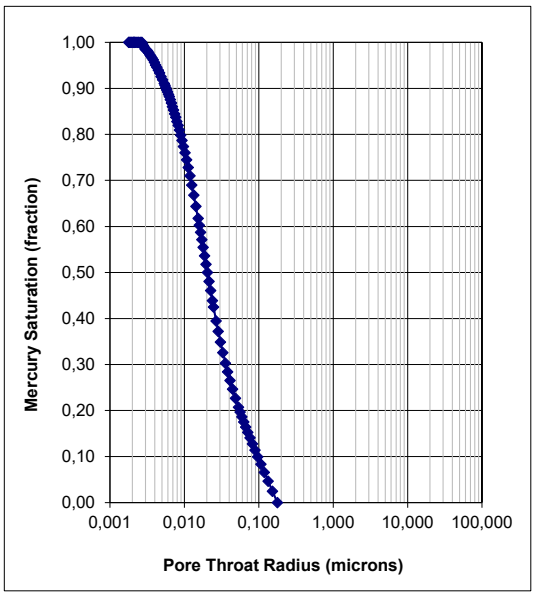

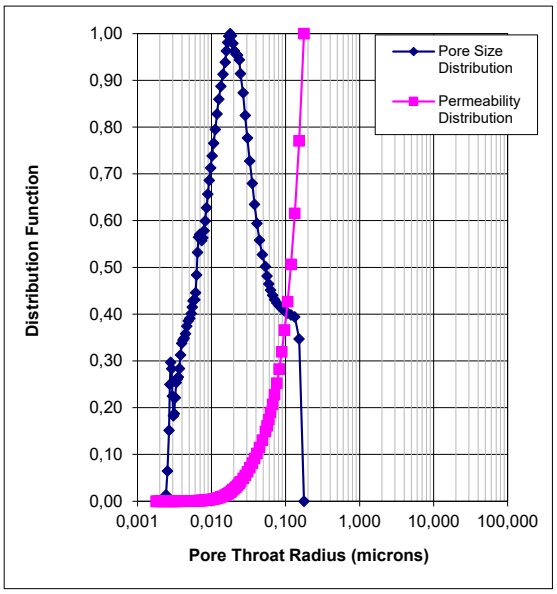

Mercury Injection Capillary Pressure Data — **Well: Nini-4**

Project: Greensand Phase 2 — **Cuttings Lark Fm**

Sample Identification	46501	
Sample Depth	1370,00	m
Plug Permeability (Air)	n/a	mD
Log Poroisty	0,18	fraction

Injection Sample Porosity	0,184	fraction
Injection Sample Pore Vol	0,539	cc
Injection Sample Bulk Vol	2,929	cc
Injection Sample Weight	6,220	g

Mean Hydraulic Radius	0,034	microns
Swanson's Parameter	0,002	
FZI	-	

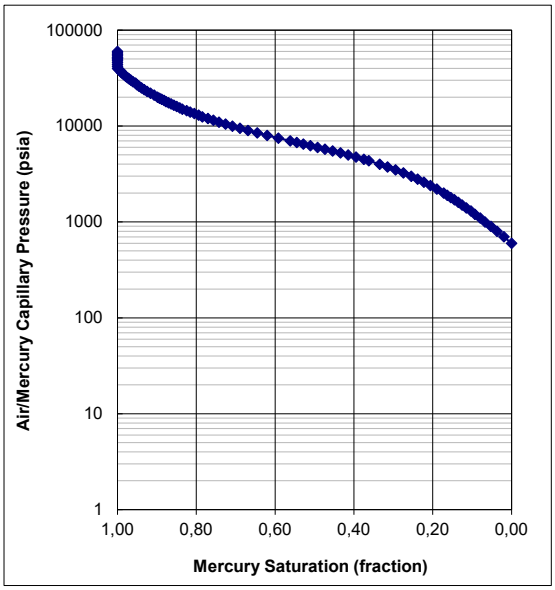

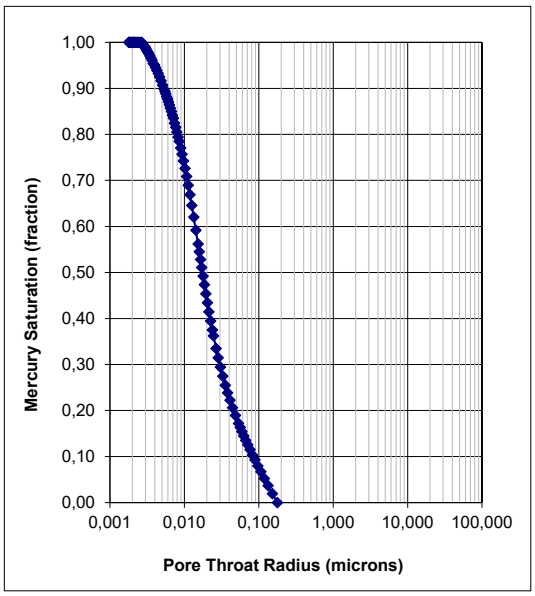

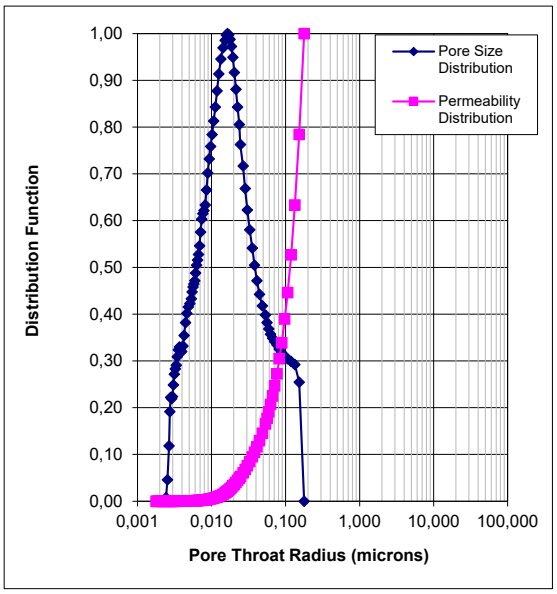

Mercury Injection Capillary Pressure Data — **Well: Nini-4**

Project: Greensand Phase 2 — **Cuttings Lark Fm**

Sample Identification	46502	
Sample Depth	1380,00	m
Plug Permeability (Air)	n/a	mD
Log Poroisty	0,23	fraction

Injection Sample Porosity	0,182	fraction
Injection Sample Pore Vol	0,564	cc
Injection Sample Bulk Vol	3,098	cc
Injection Sample Weight	6,640	g

Mean Hydraulic Radius	0,047	microns
Swanson's Parameter	0,002	
FZI	-	

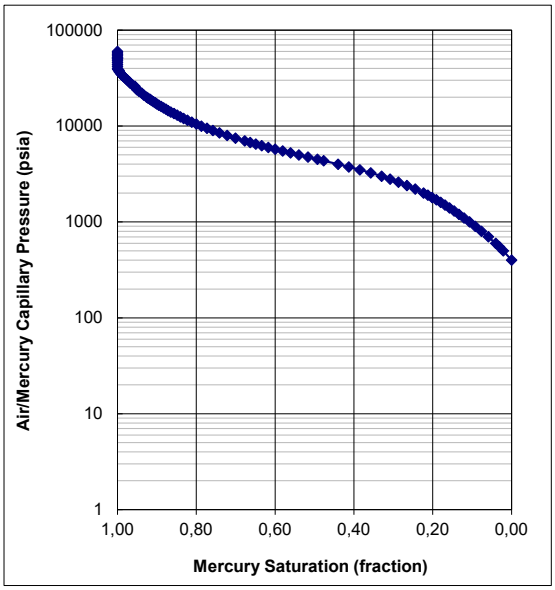

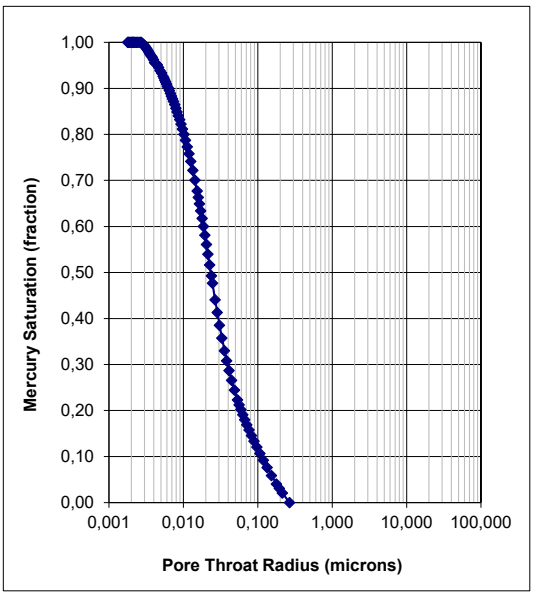

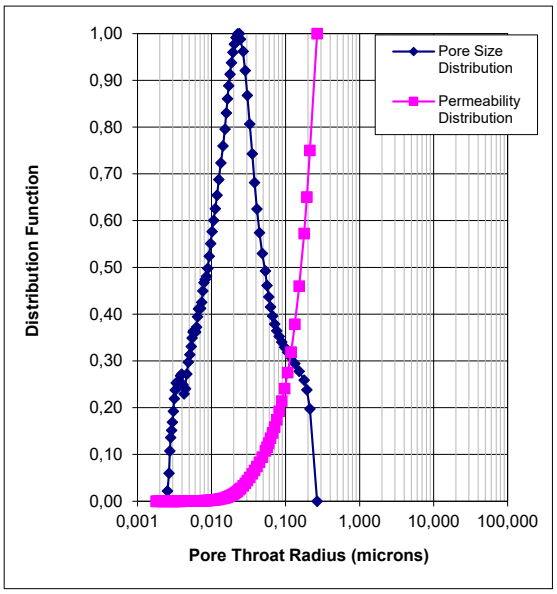

Mercury Injection Capillary Pressure Data — **Well: Nini-4**

Project: Greensand Phase 2 — **Cuttings Lark Fm**

Sample Identification	46503	
Sample Depth	1390,00	m
Plug Permeability (Air)	n/a	mD
Log Poroisty	0,14	fraction

Injection Sample Porosity	0,153	fraction
Injection Sample Pore Vol	0,414	cc
Injection Sample Bulk Vol	2,714	cc
Injection Sample Weight	5,880	g

Mean Hydraulic Radius	0,039	microns
Swanson's Parameter	0,002	
FZI	-	

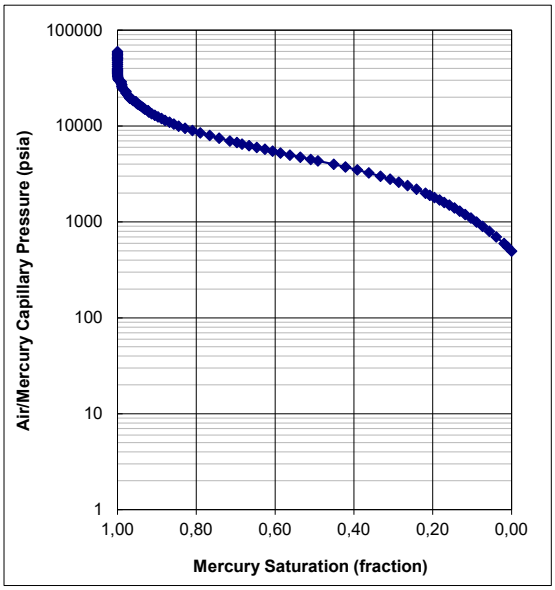

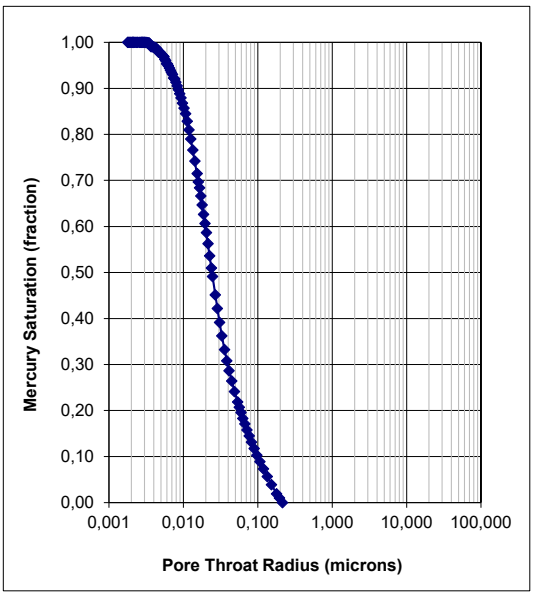

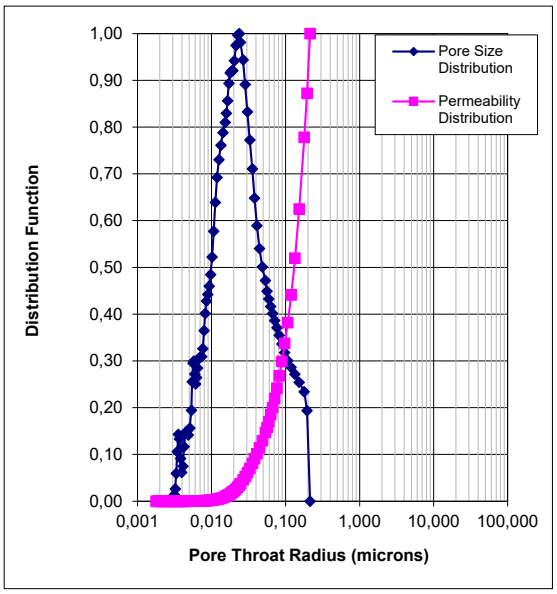

Mercury Injection Capillary Pressure Data — **Well: Nini-4**

Project: Greensand Phase 2 — **Cuttings Lark Fm**

Sample Identification	46504	
Sample Depth	1400,00	m
Plug Permeability (Air)	n/a	mD
Log Poroisty	0,16	fraction

Injection Sample Porosity	0,186	fraction
Injection Sample Pore Vol	0,544	cc
Injection Sample Bulk Vol	2,928	cc
Injection Sample Weight	6,210	g

Mean Hydraulic Radius	0,039	microns
Swanson's Parameter	0,002	
FZI	-	

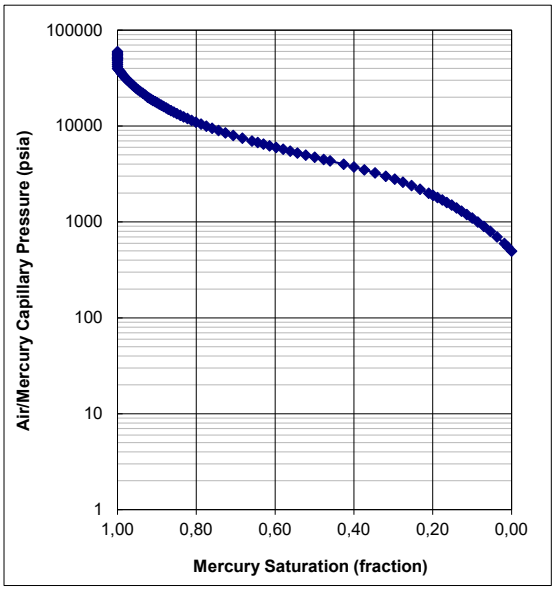

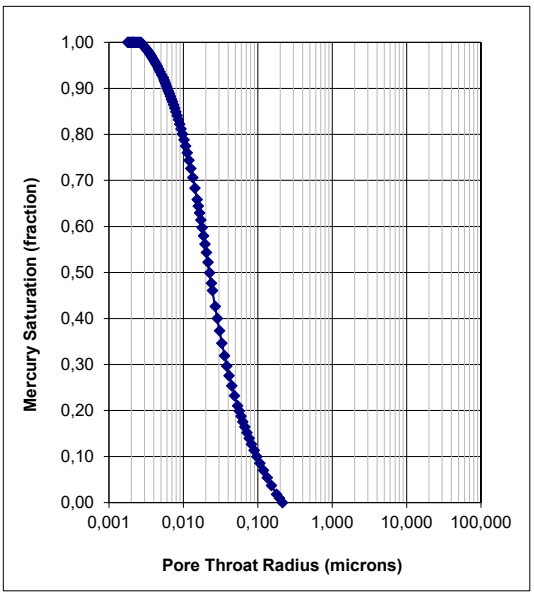

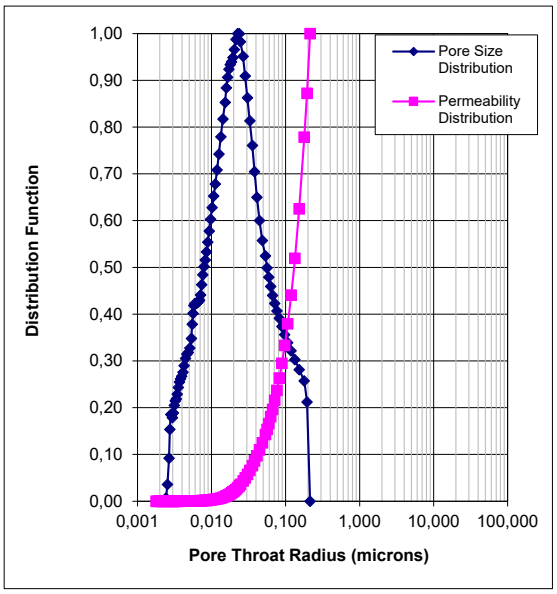

Mercury Injection Capillary Pressure Data — **Well: Nini-4**

Project: Greensand Phase 2 — **Cuttings Lark Fm**

Sample Identification	46505	
Sample Depth	1410,00	m
Plug Permeability (Air)	n/a	mD
Log Poroisty	0,24	fraction

Injection Sample Porosity	0,229	fraction
Injection Sample Pore Vol	0,719	cc
Injection Sample Bulk Vol	3,136	cc
Injection Sample Weight	6,230	g

Mean Hydraulic Radius	0,604	microns
Swanson's Parameter	0,024	
FZI	-	

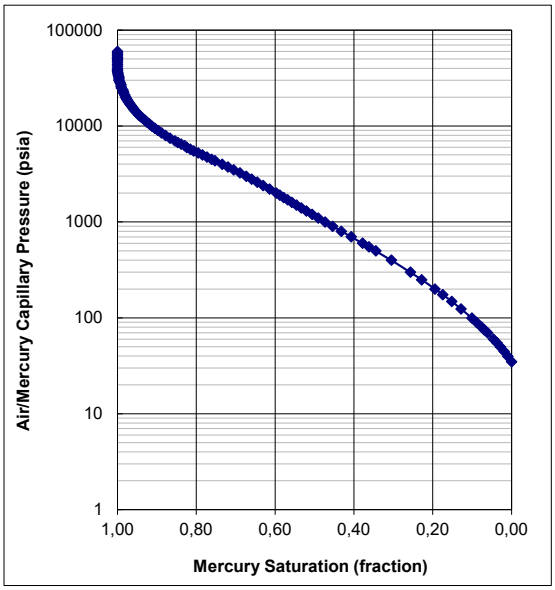

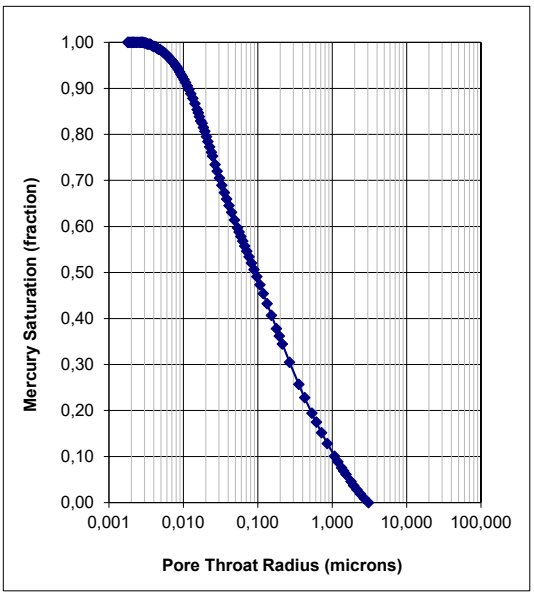

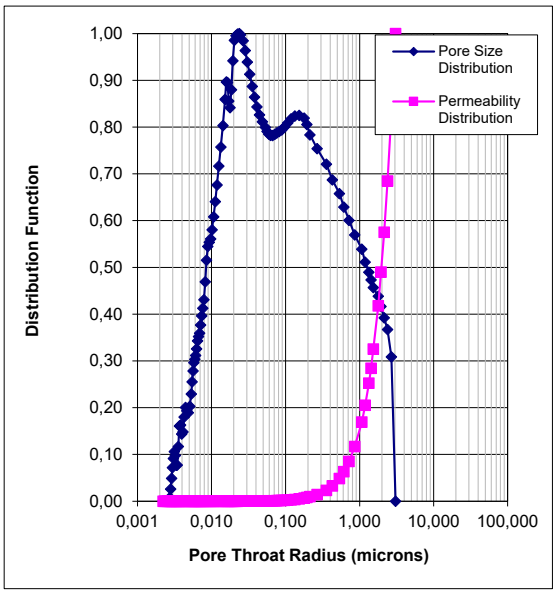

Mercury Injection Capillary Pressure Data — **Well: Nini-4**

Project: Greensand Phase 2 — **Cuttings Lark Fm**

Sample Identification	46506	
Sample Depth	1420,00	m
Plug Permeability (Air)	n/a	mD
Log Poroisty	0,29	fraction

Injection Sample Porosity	0,243	fraction
Injection Sample Pore Vol	0,685	cc
Injection Sample Bulk Vol	2,822	cc
Injection Sample Weight	5,610	g

Mean Hydraulic Radius	0,541	microns
Swanson's Parameter	0,028	
FZI	-	

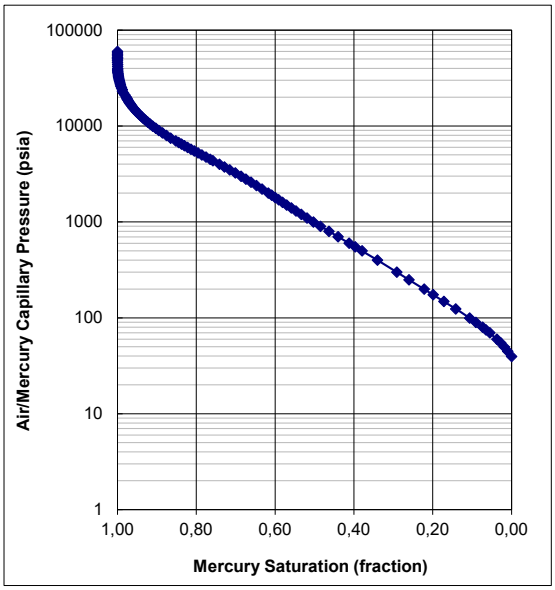

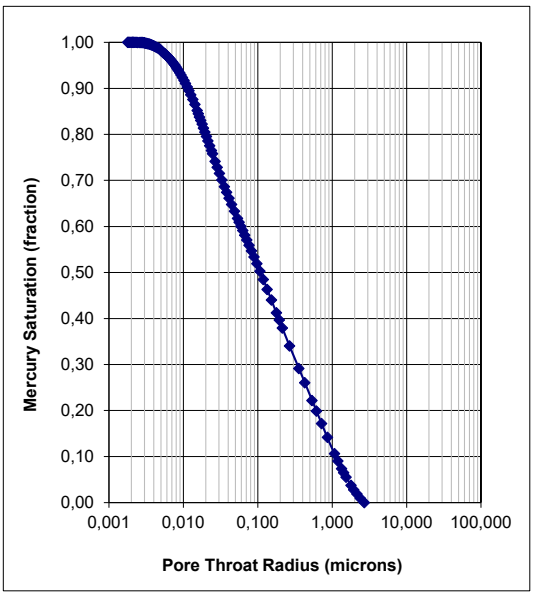

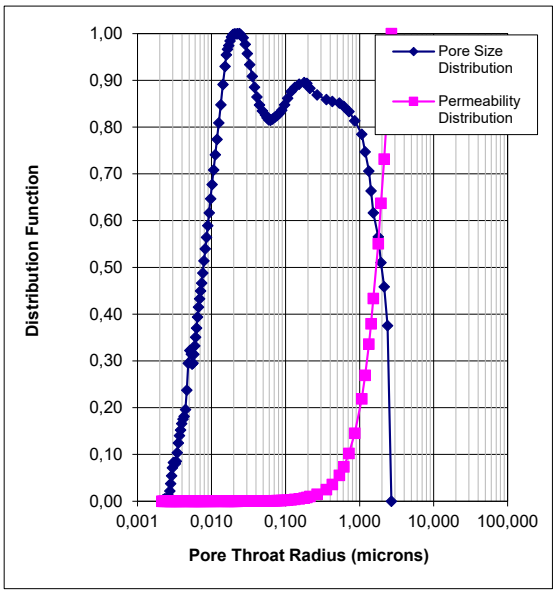

Mercury Injection Capillary Pressure Data — **Well: Nini-4**

Project: Greensand Phase 2 — **Cuttings Lark Fm**

Sample Identification	46507	
Sample Depth	1430,00	m
Plug Permeability (Air)	n/a	mD
Log Poroisty	0,19	fraction

Injection Sample Porosity	0,216	fraction
Injection Sample Pore Vol	0,636	cc
Injection Sample Bulk Vol	2,949	cc
Injection Sample Weight	6.0000	g

Mean Hydraulic Radius	0,289	microns
Swanson's Parameter	0,014	
PTS Index	-	

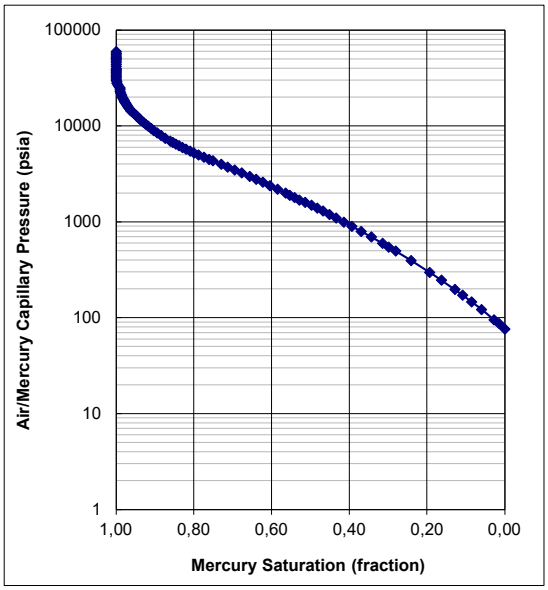

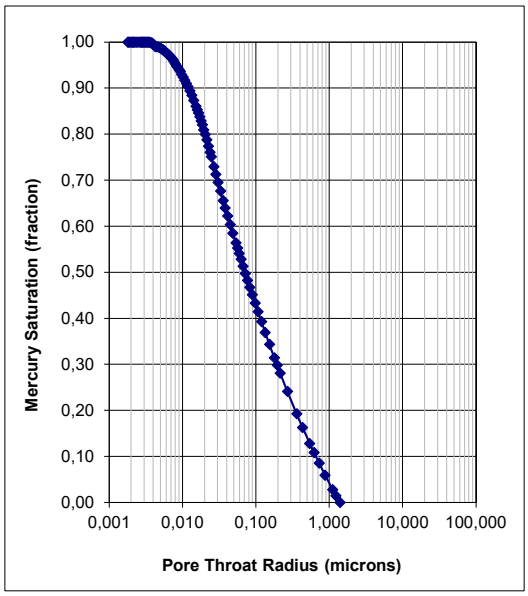

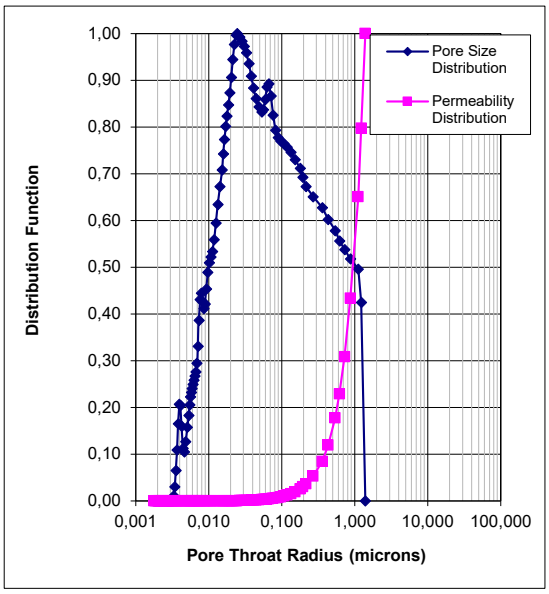

Mercury Injection Capillary Pressure Data — **Well: Nini-4**

Project: Greensand Phase 2 — **Cuttings Lark Fm**

Sample Identification	46508	
Sample Depth	1440,00	m
Plug Permeability (Air)	n/a	mD
Log Poroisty	0,18	fraction

Injection Sample Porosity	0,216	fraction
Injection Sample Pore Vol	0,703	cc
Injection Sample Bulk Vol	3,261	cc
Injection Sample Weight	6.7600	g

Mean Hydraulic Radius	0,218	microns
Swanson's Parameter	0,010	
PTS Index	-	

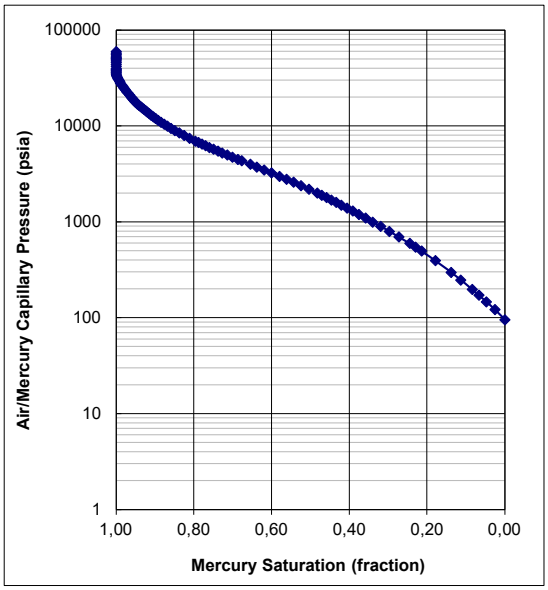

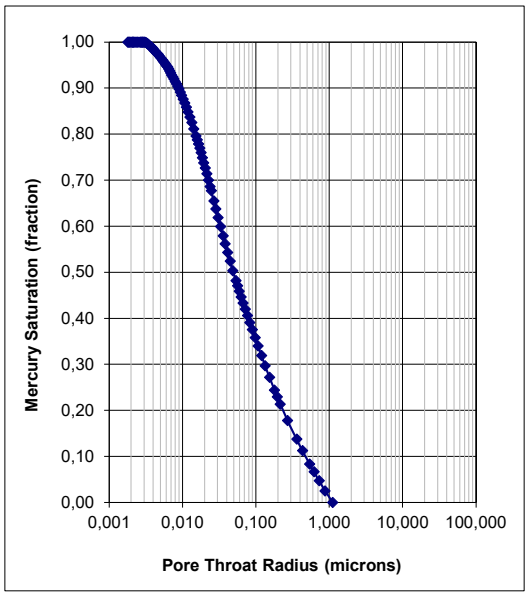

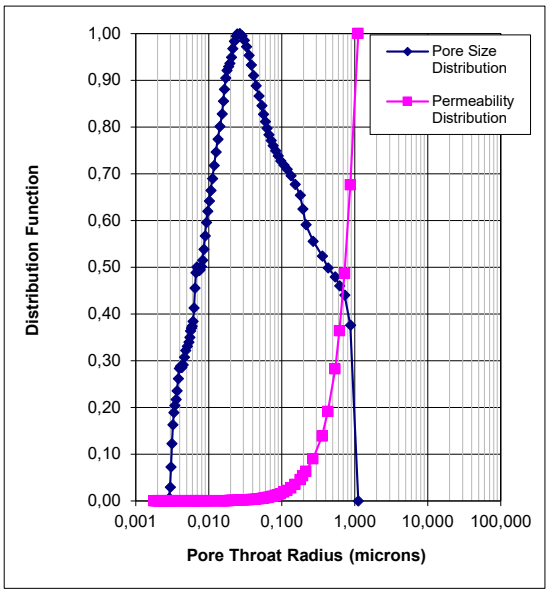

Mercury Injection Capillary Pressure Data — **Well: Nini-4**

Project: Greensand Phase 2 — **Cuttings Lark Fm**

Sample Identification	46509	
Sample Depth	1490,00	m
Plug Permeability (Air)	n/a	mD
Log Poroisty	0,29	fraction

Injection Sample Porosity	0,193	fraction
Injection Sample Pore Vol	0,571	cc
Injection Sample Bulk Vol	2,958	cc
Injection Sample Weight	6.0000	g

Mean Hydraulic Radius	0,029	microns
Swanson's Parameter	0,002	
PTS Index	-	

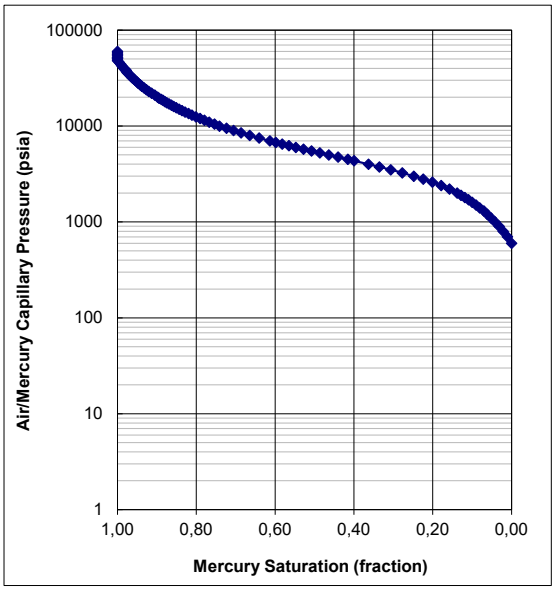

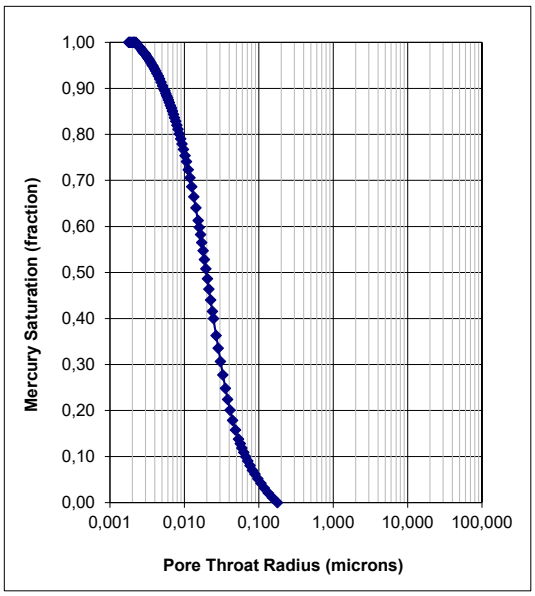

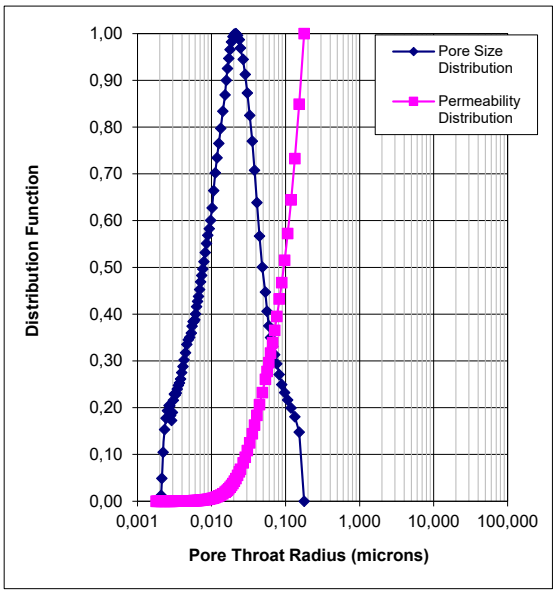

Mercury Injection Capillary Pressure Data — **Well: Nini-4**

Project: Greensand Phase 2 — **Cuttings Lark Fm**

Sample Identification	46510	
Sample Depth	1520,00	m
Plug Permeability (Air)	n/a	mD
Log Poroisty	0,19	fraction

Injection Sample Porosity	0,172	fraction
Injection Sample Pore Vol	0,473	cc
Injection Sample Bulk Vol	2,755	cc
Injection Sample Weight	5.6600	g

Mean Hydraulic Radius	0,033	microns
Swanson's Parameter	0,001	
PTS Index	-	

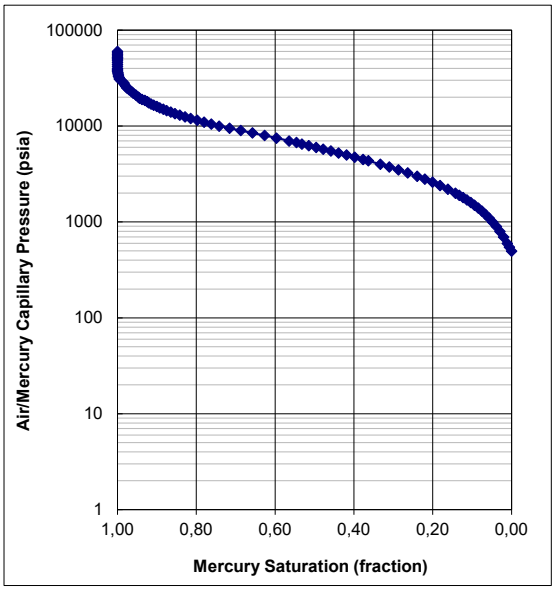

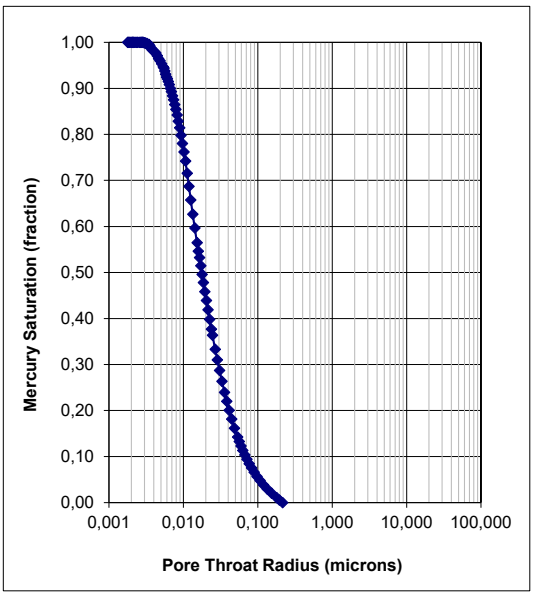

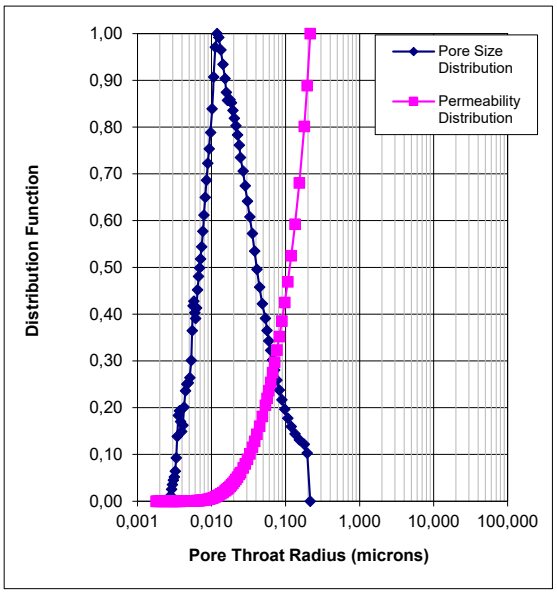

Mercury Injection Capillary Pressure Data — **Well: Nini-4**

Project: Greensand Phase 2 — **Cuttings Lark Fm**

Sample Identification	46511	
Sample Depth	1560,00	m
Plug Permeability (Air)	n/a	mD
Log Poroisty	0,20	fraction

Injection Sample Porosity	0,149	fraction
Injection Sample Pore Vol	0,328	cc
Injection Sample Bulk Vol	2,197	cc
Injection Sample Weight	4.7100	g

Mean Hydraulic Radius	0,012	microns
Swanson's Parameter	0,001	
PTS Index	-	

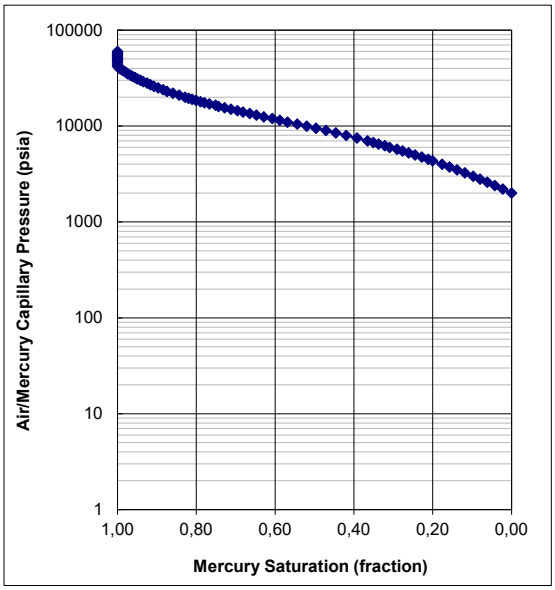

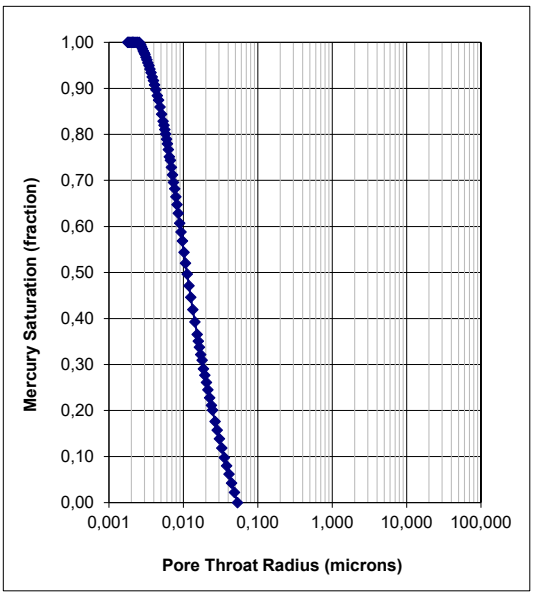

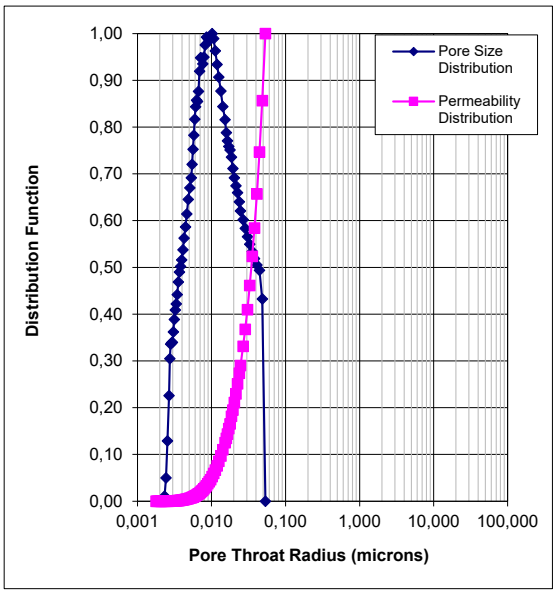

APPENDIX D – XRD ANALYSIS

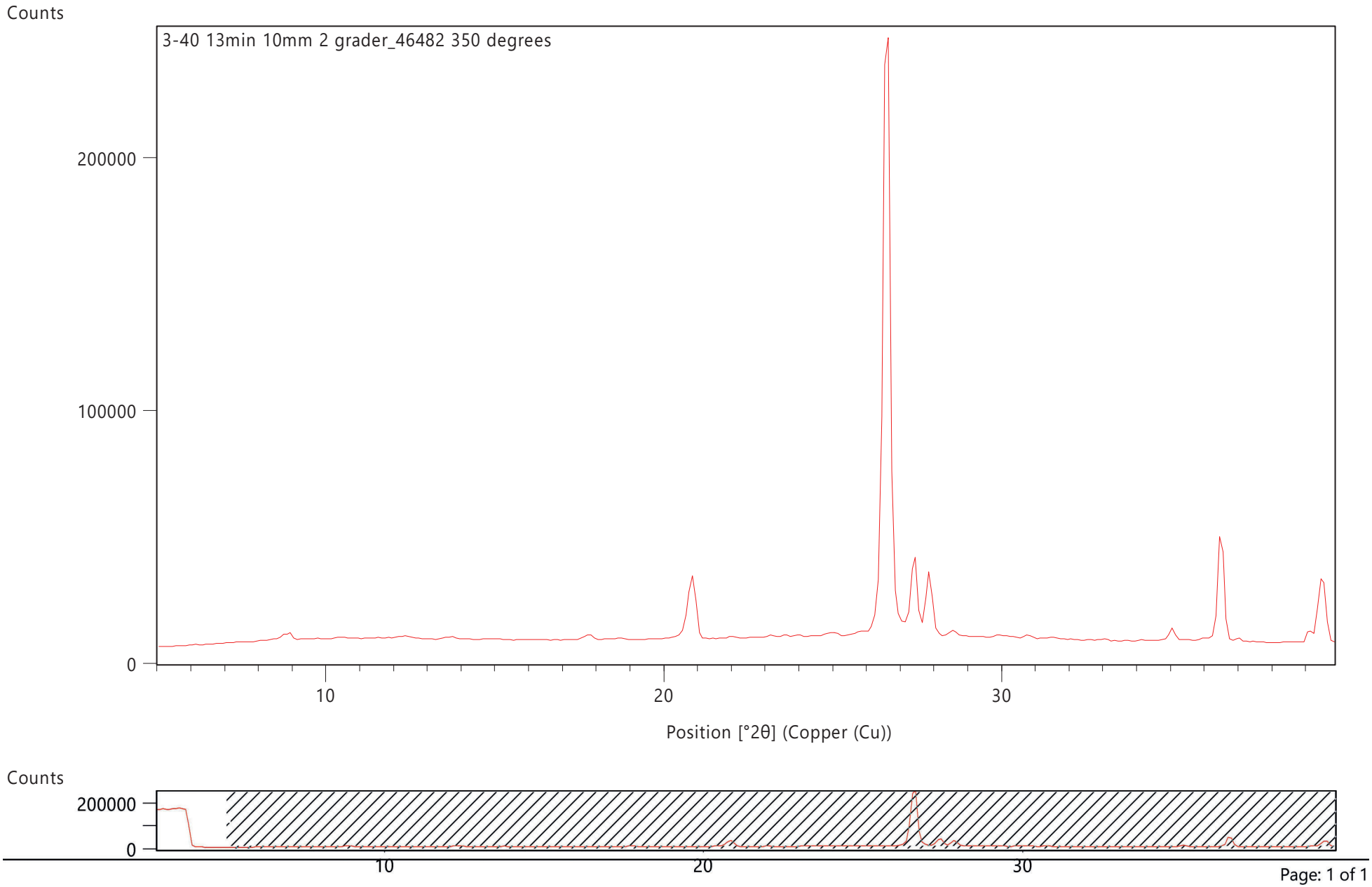
Counts
3-40 13min 10mm 2 grader_46482 350 degrees
200000
100000
0
10
20
30
Position [°2θ] (Copper (Cu))
Counts
200000
0
10
20
30

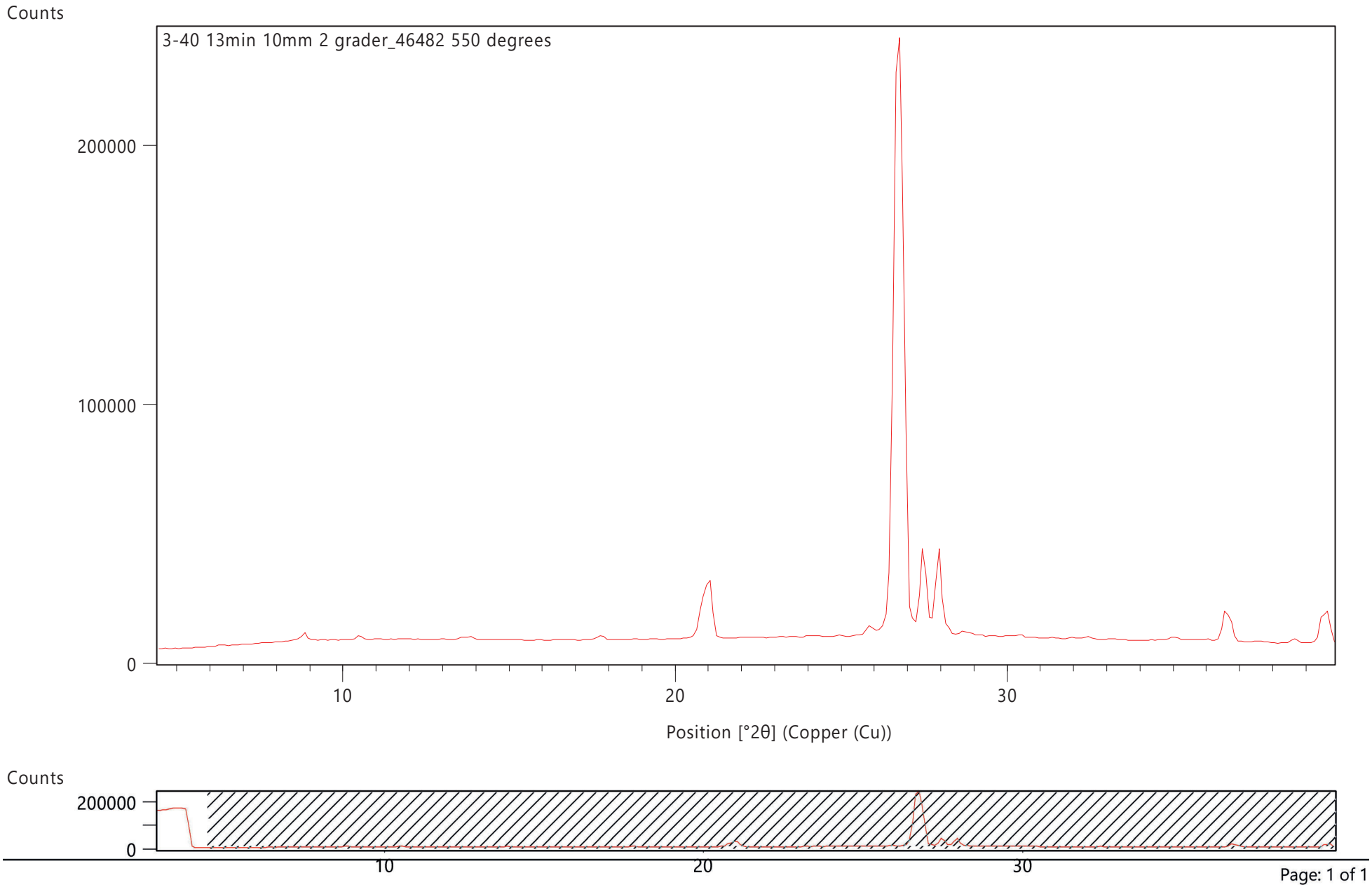
Counts
3-40 13min 10mm 2 grader_46482 550 degrees
200000
100000
0
10
20
30
Position [°2θ] (Copper (Cu))
Counts
200000
0
10
20
30

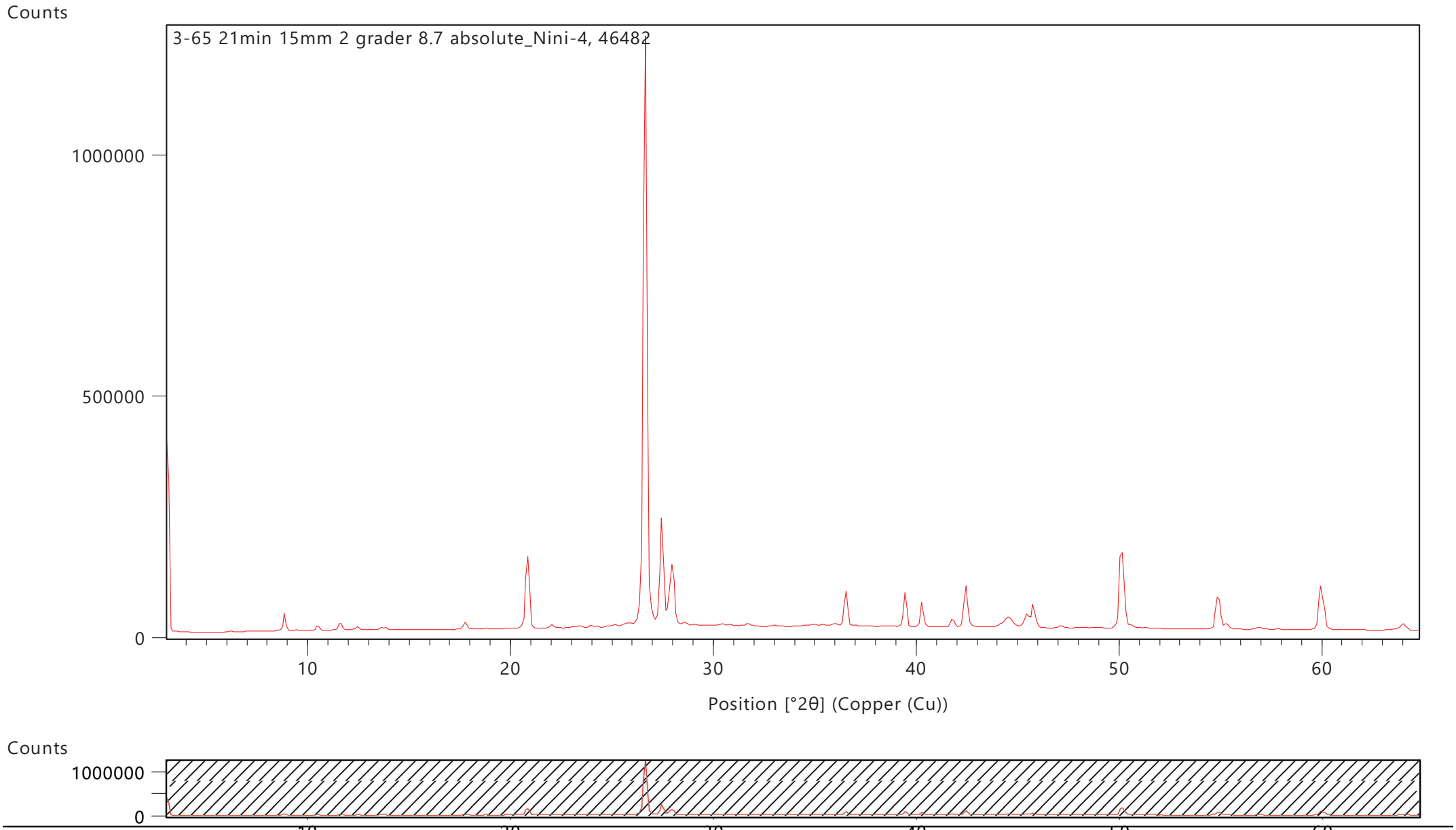
Counts
3-65 21min 15mm 2 grader 8.7 absolute_Nini-4, 46482
1000000
500000
0
10
20
30
40
50
60
Position [°2θ] (Copper (Cu))
Counts
1000000
0
10
20
30
40
50
60

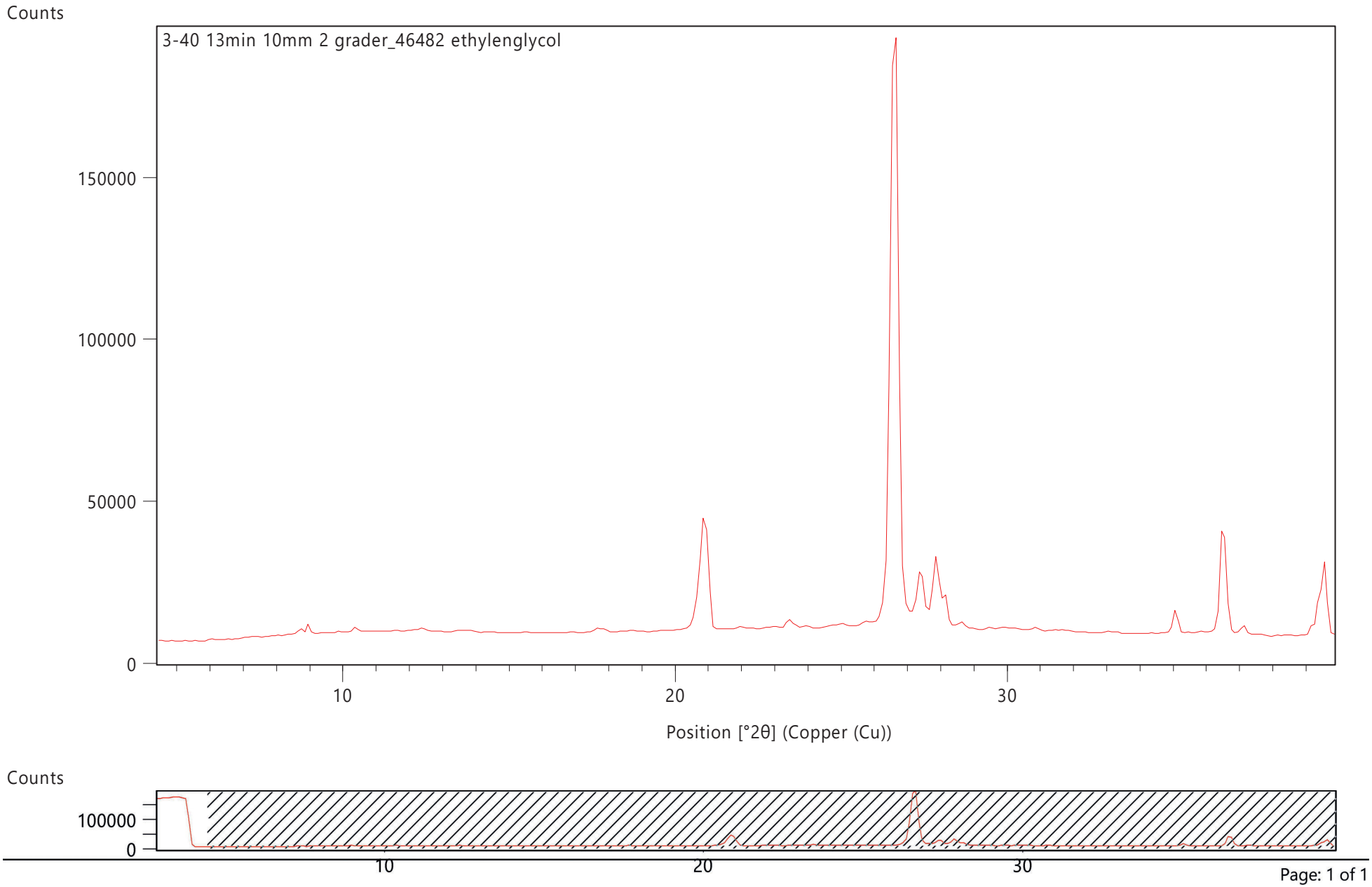
Counts
3-40 13min 10mm 2 grader_46482 ethylenglycol
150000
100000
50000
0
10
20
30
Position [°2θ] (Copper (Cu))
Counts
100000
0
10
20
30

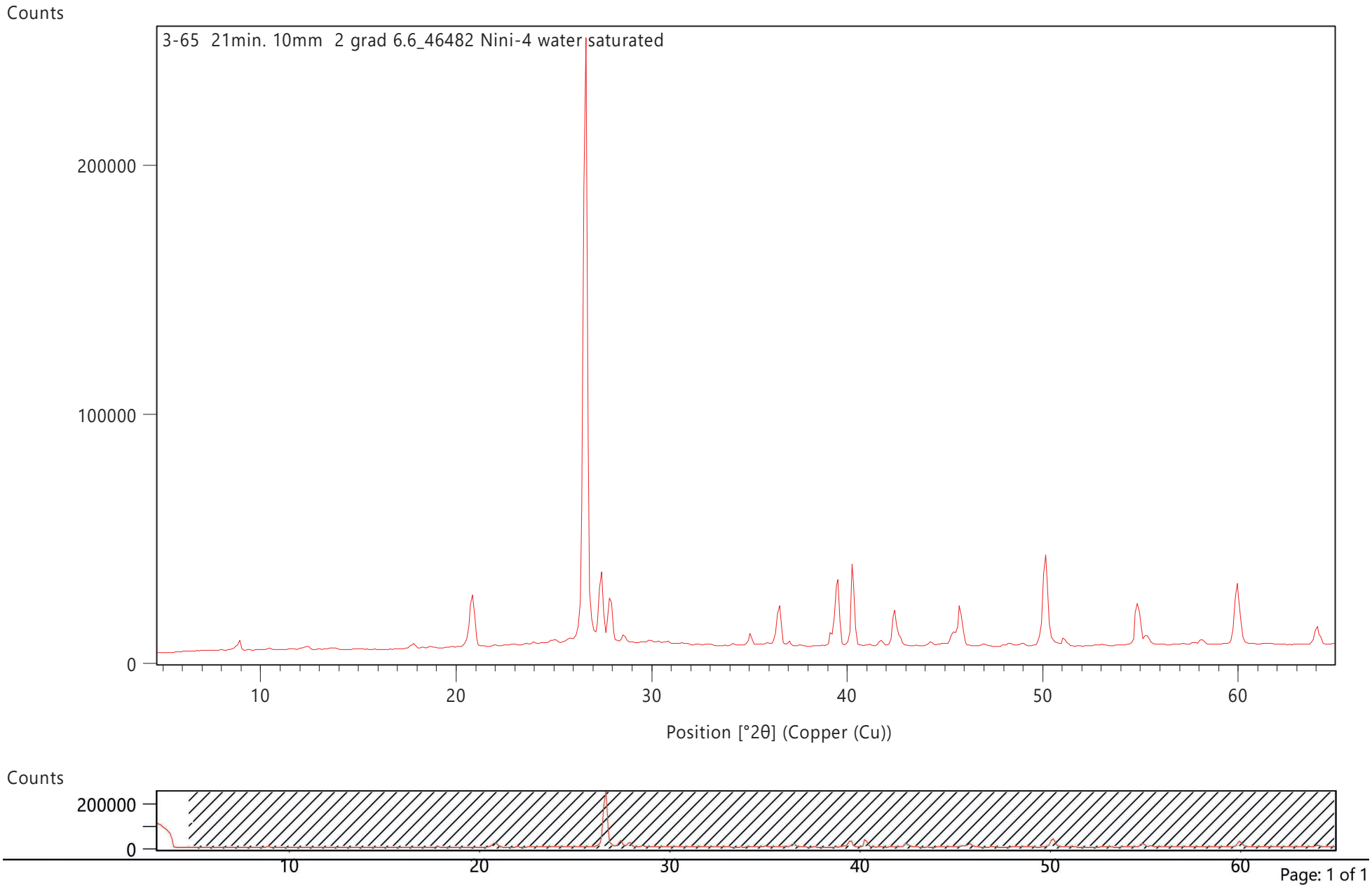
Counts
3-65 21min. 10mm 2 grad 6.6_46482 Nini-4 water saturated
200000
100000
0
10
20
30
40
50
60
Position [°2θ] (Copper (Cu))
Counts
200000
0
10
20
30
40
50
60

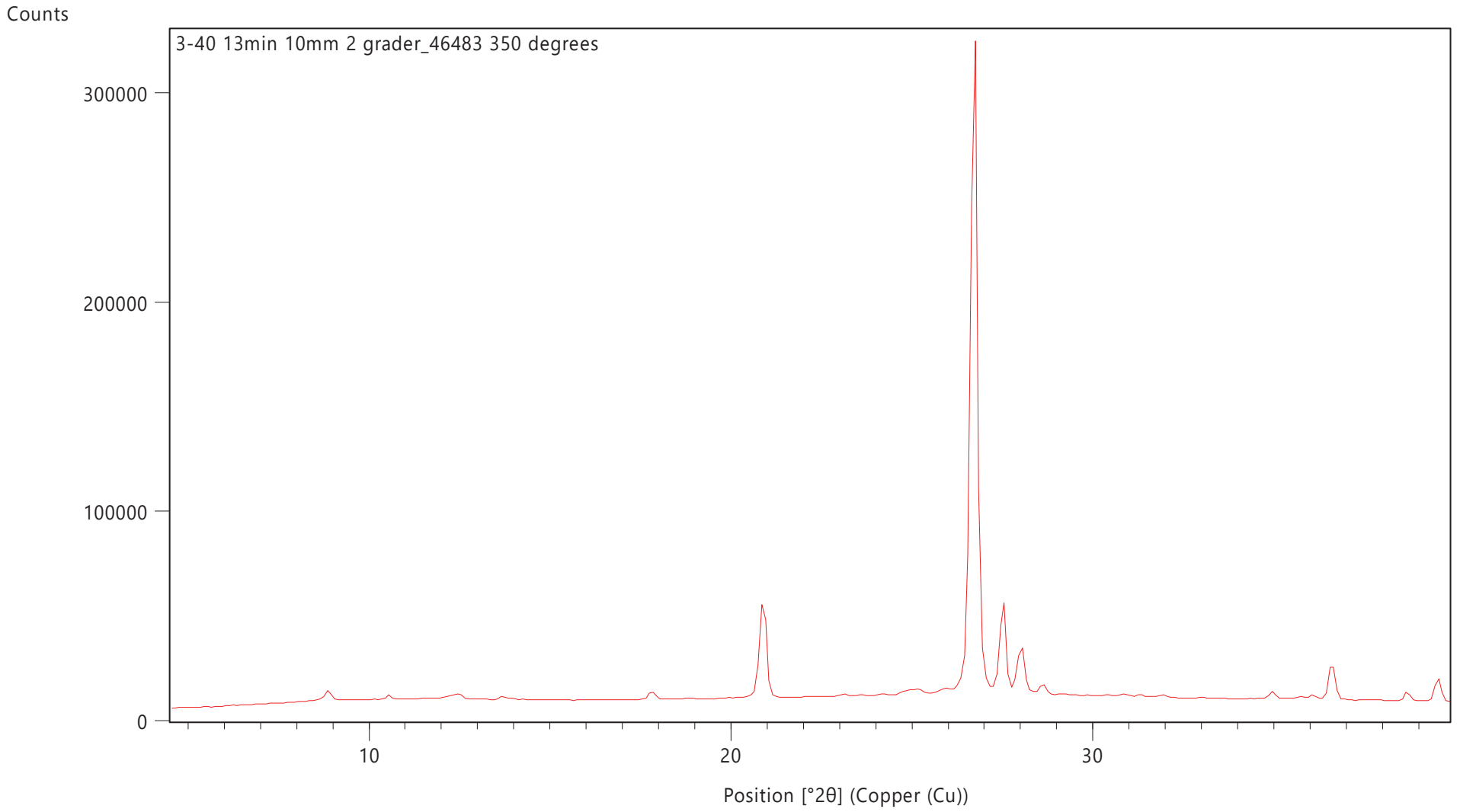
Counts
3-40 13min 10mm 2 grader_46483 350 degrees
300000
200000
100000
0
10
20
30
Position [°2θ] (Copper (Cu))
Counts
200000
0
10
20
30

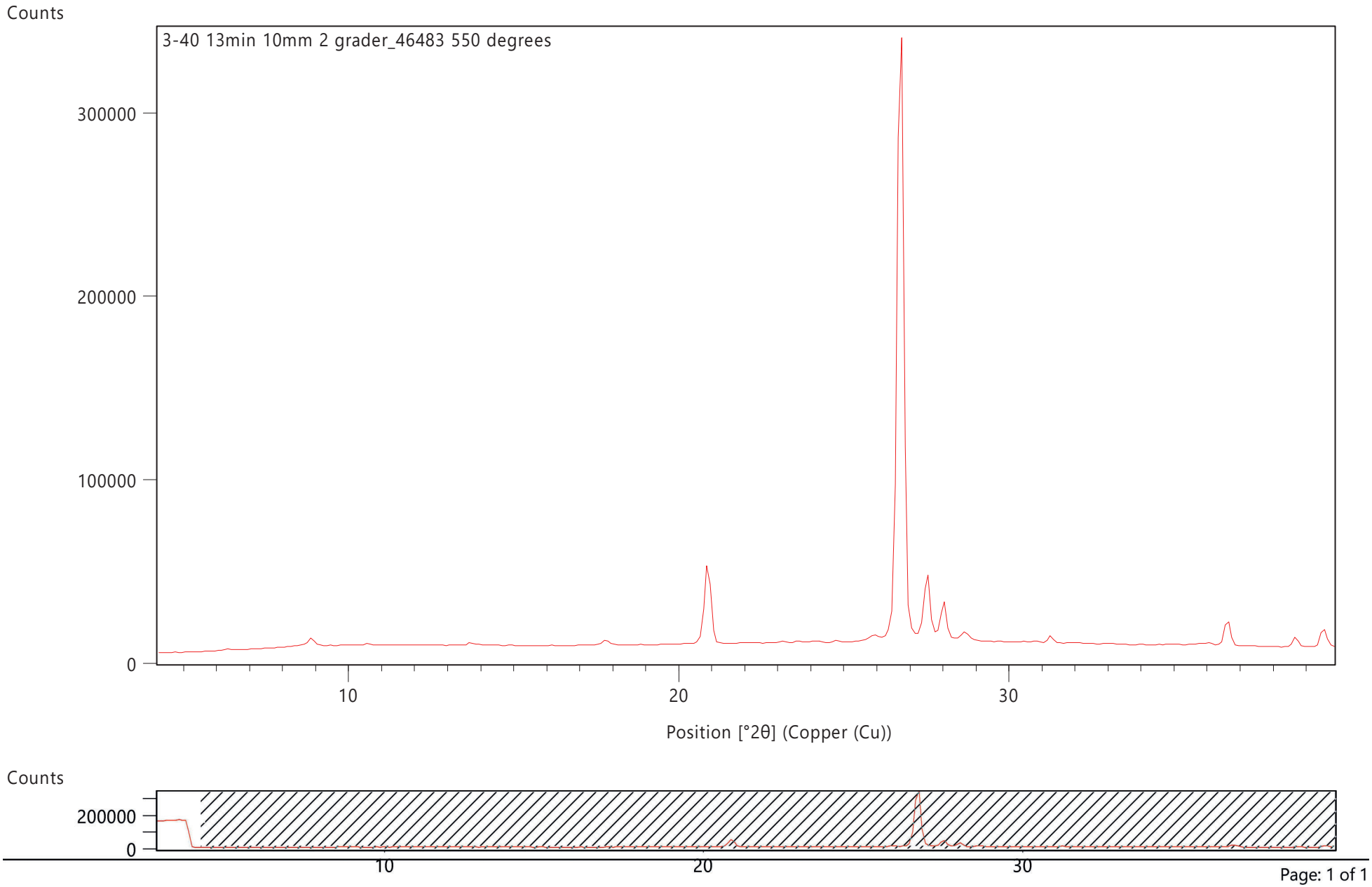
Counts
3-40 13min 10mm 2 grader_46483 550 degrees
300000
200000
100000
0
10
20
30
Position [°2θ] (Copper (Cu))
Counts
200000
0
10
20
30

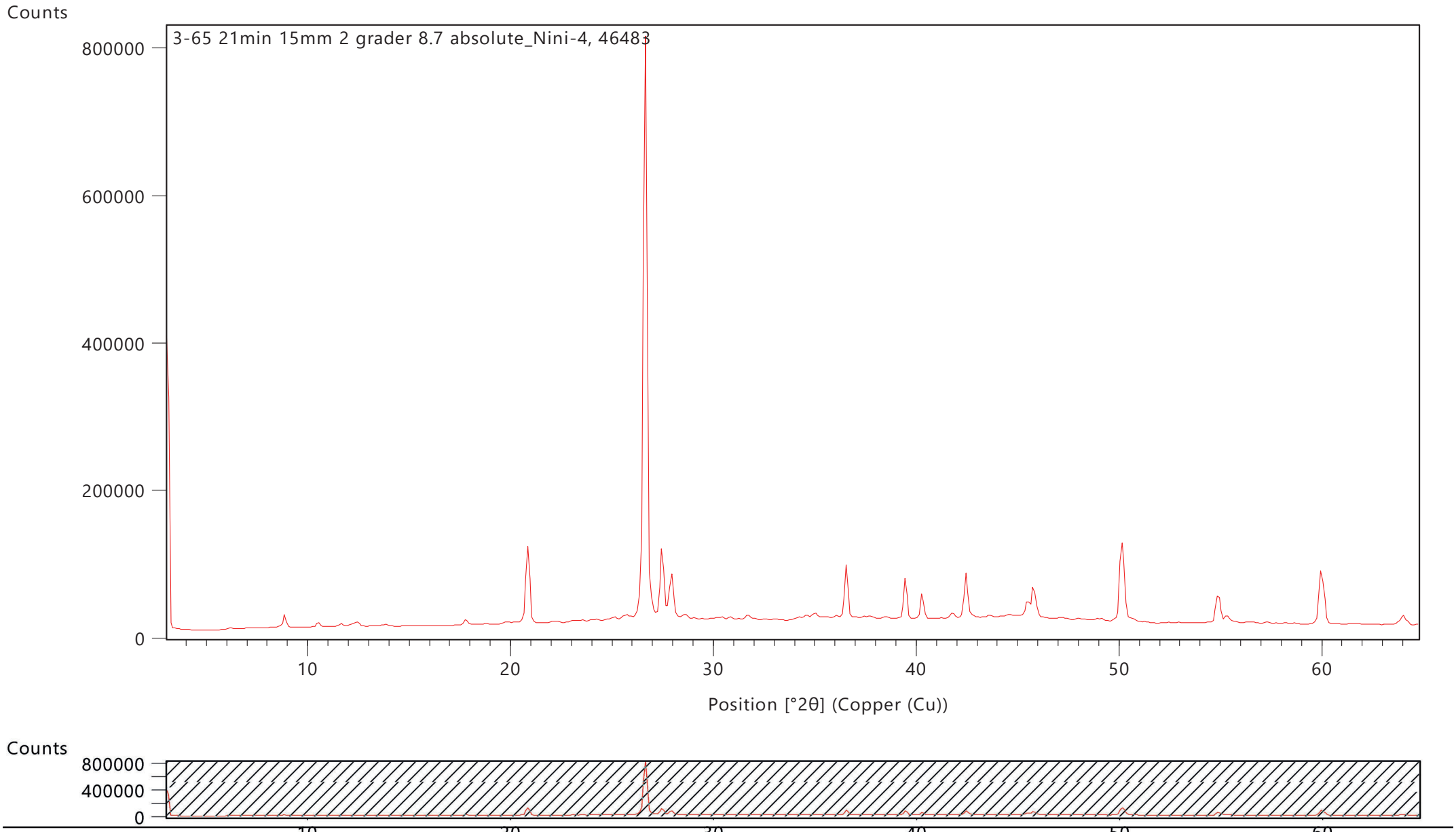
Counts
3-65 21min 15mm 2 grader 8.7 absolute_Nini-4, 46483
800000
600000
400000
200000
0
10
20
30
40
50
60
Position [°2θ] (Copper (Cu))
Counts
800000
400000
0
10
20
30
40
50
60

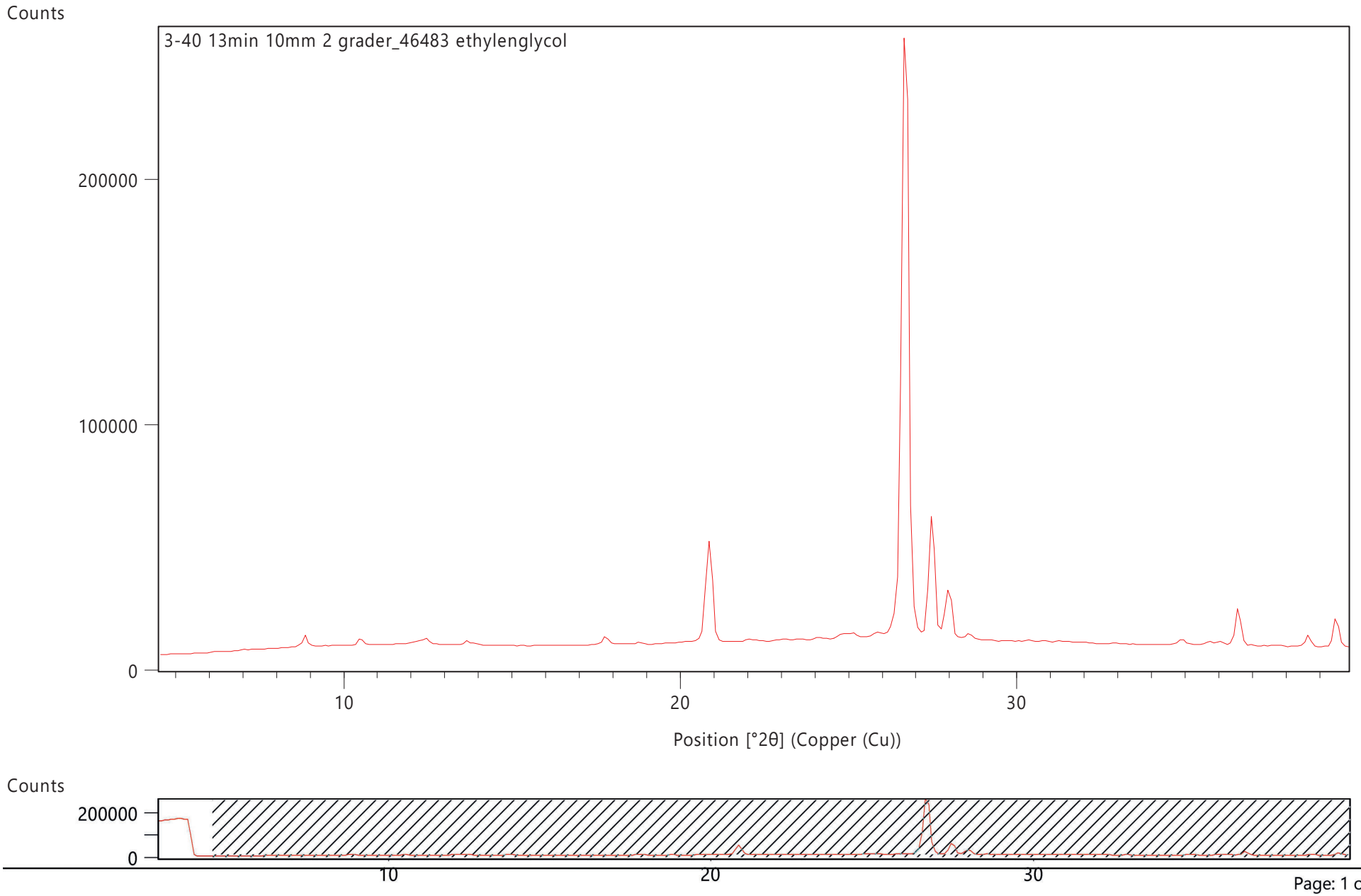
Counts
3-40 13min 10mm 2 grader_46483 ethylenglycol
200000
100000
0
10
20
30
Position [°2θ] (Copper (Cu))
Counts
200000
0
10
20
30

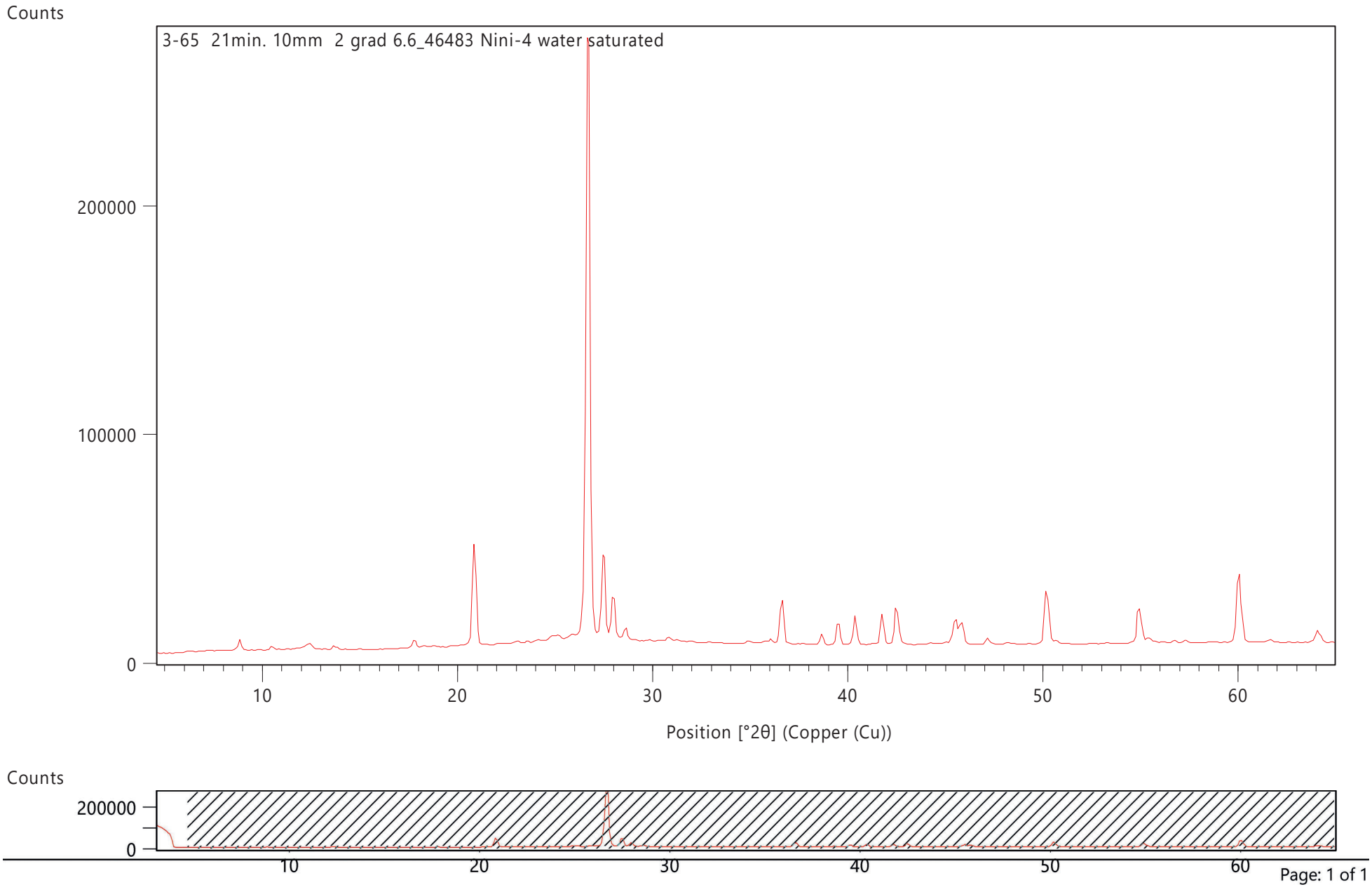
Counts
3-65 21min. 10mm 2 grad 6.6_46483 Nini-4 water saturated
200000
100000
0
10
20
30
40
50
60
Position [°2θ] (Copper (Cu))
Counts
200000
0
10
20
30
40
50
60

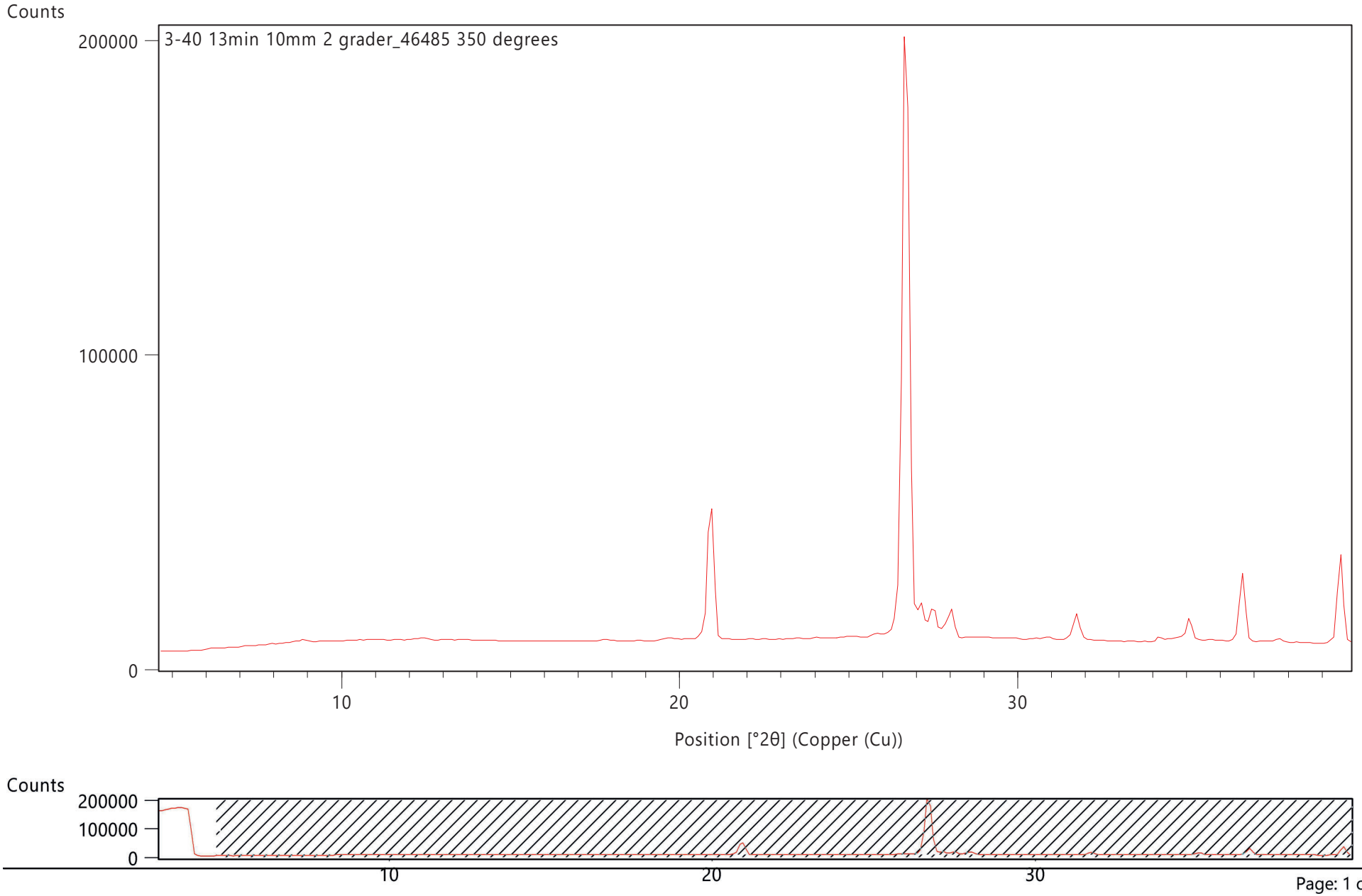
Counts
3-40 13min 10mm 2 grader_46485 350 degrees
200000
100000
0
10
20
30
Position [°2θ] (Copper (Cu))
Counts
200000
100000
0
10
20
30

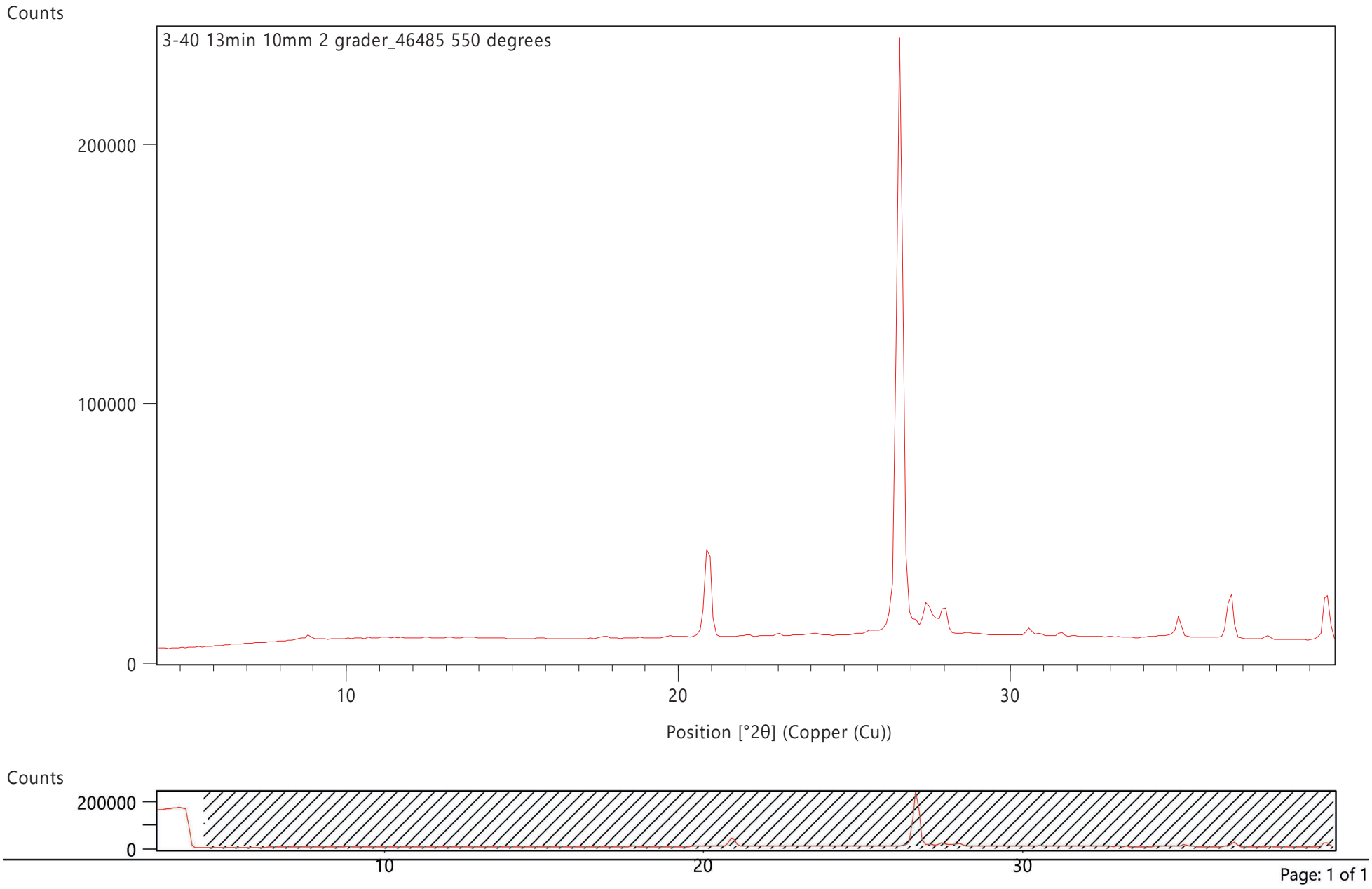
Counts
3-40 13min 10mm 2 grader_46485 550 degrees
200000
100000
0
10
20
30
Position [°2θ] (Copper (Cu))
Counts
200000
0
10
20
30

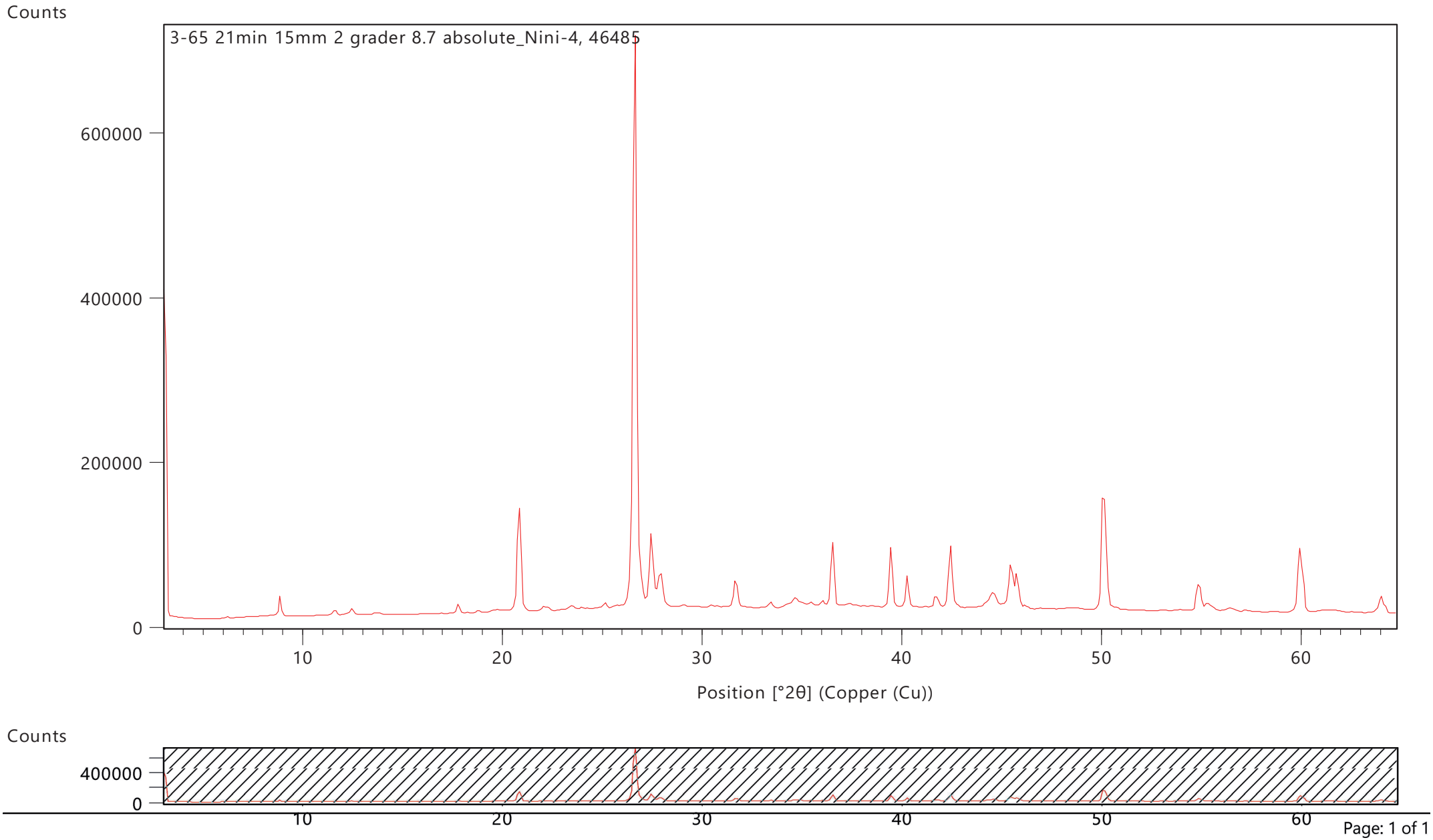
Counts
3-65 21min 15mm 2 grader 8.7 absolute_Nini-4, 46485
600000
400000
200000
0
10
20
30
40
50
60
Position [°2θ] (Copper (Cu))
Counts
400000
0
10
20
30
40
50
60

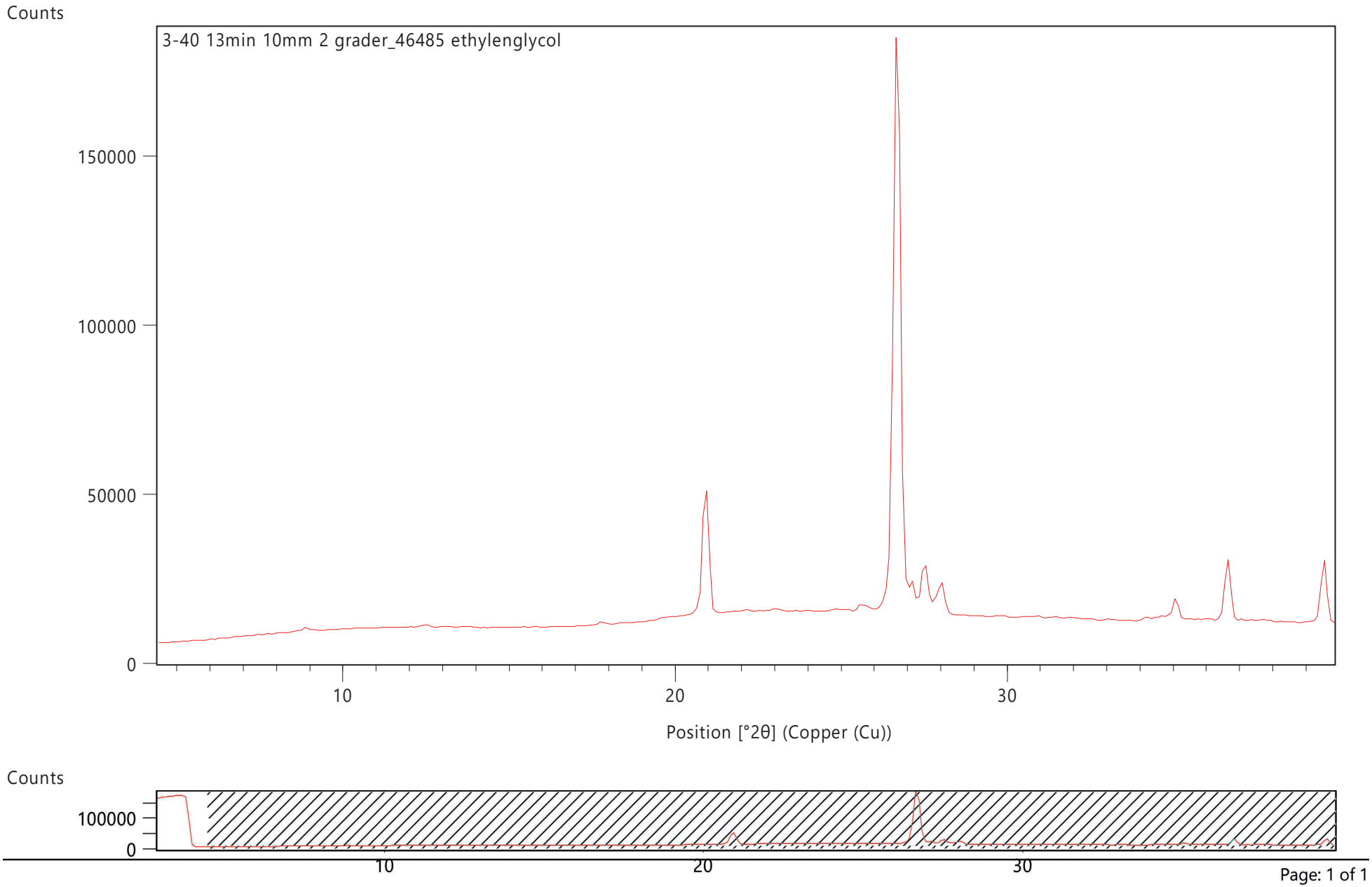
Counts
3-40 13min 10mm 2 grader_46485 ethylenglycol
150000
100000
50000
0
10
20
30
Position [°2θ] (Copper (Cu))
Counts
100000
0
10
20
30

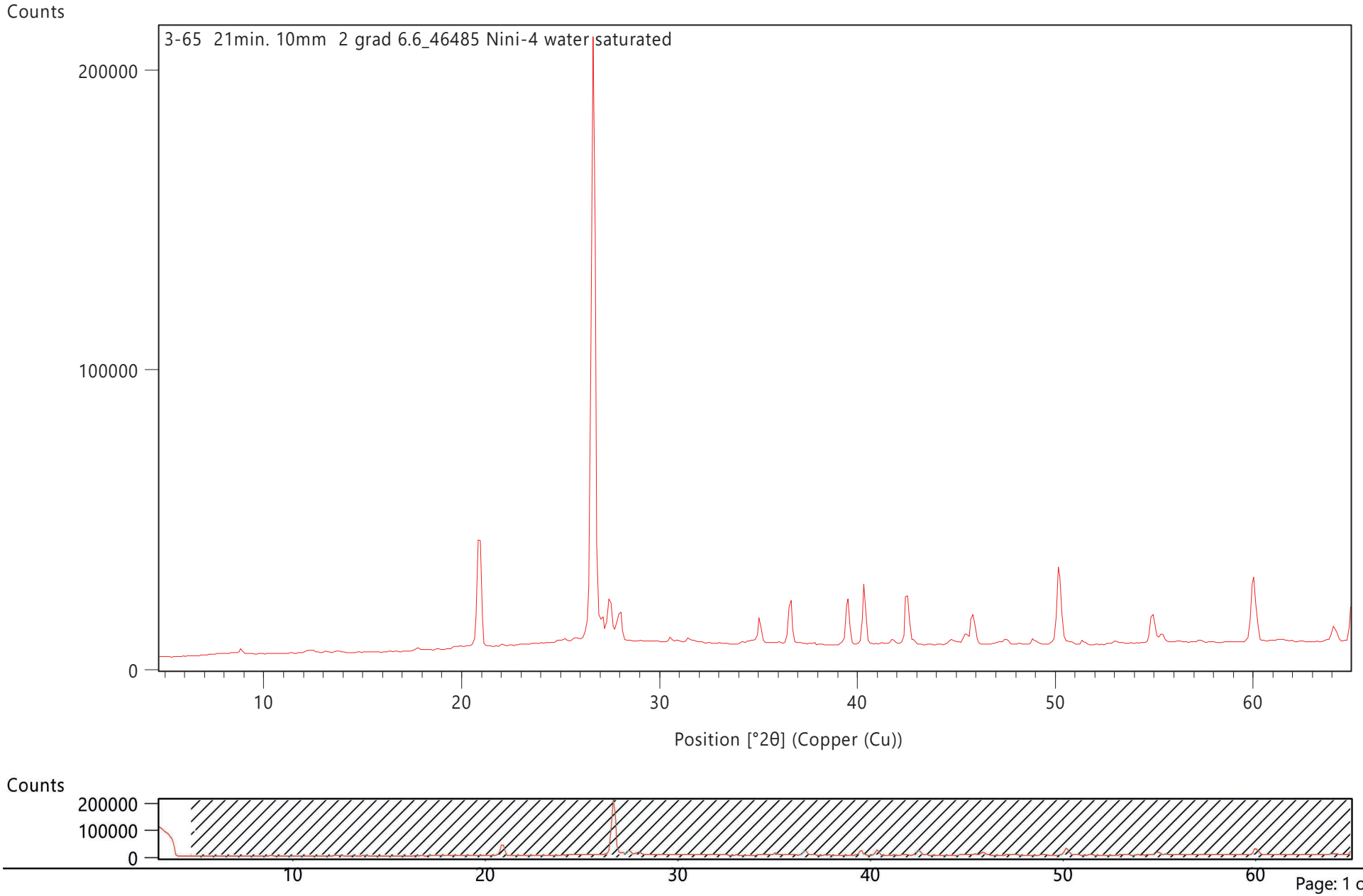
Counts
3-65 21min. 10mm 2 grad 6.6_46485 Nini-4 water saturated
200000
100000
0
10
20
30
40
50
60
Position [°2θ] (Copper (Cu))
Counts
200000
100000
0
10
20
30
40
50
60

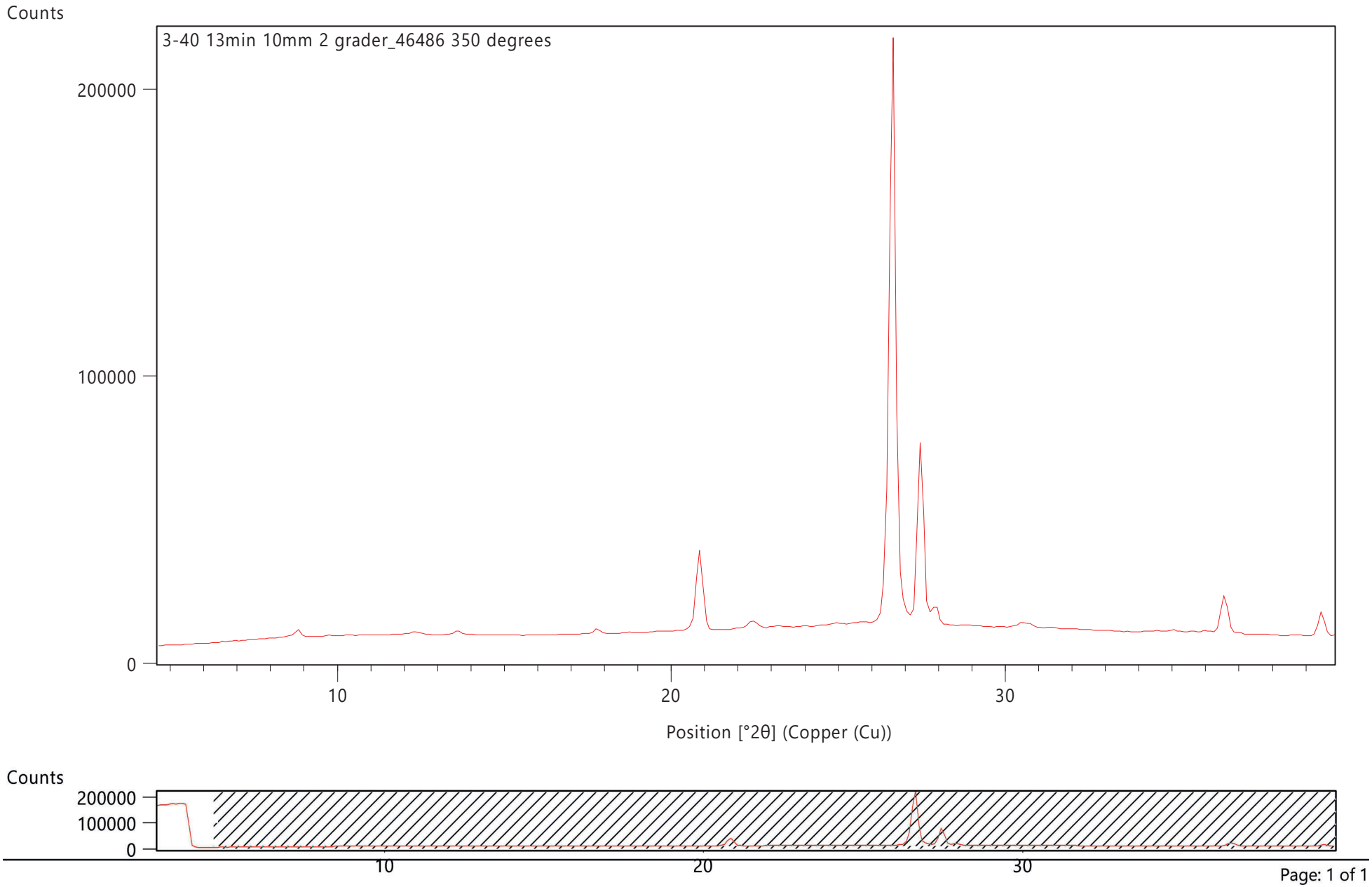
Counts
3-40 13min 10mm 2 grader_46486 350 degrees
200000
100000
0
10
20
30
Position [°2θ] (Copper (Cu))
Counts
200000
100000
0
10
20
30

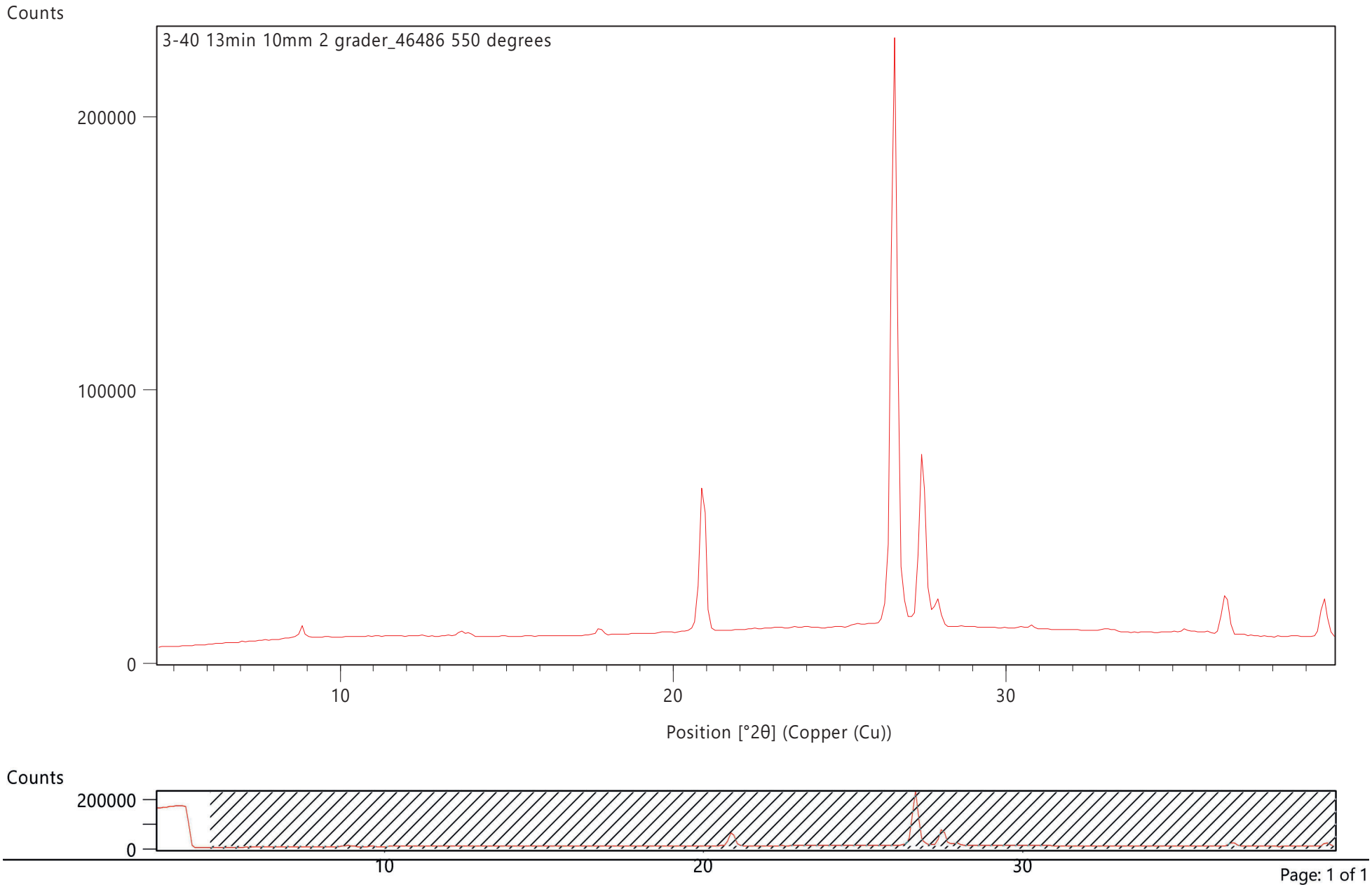
Counts
3-40 13min 10mm 2 grader_46486 550 degrees
200000
100000
0
10
20
30
Position [°2θ] (Copper (Cu))
Counts
200000
0
10
20
30

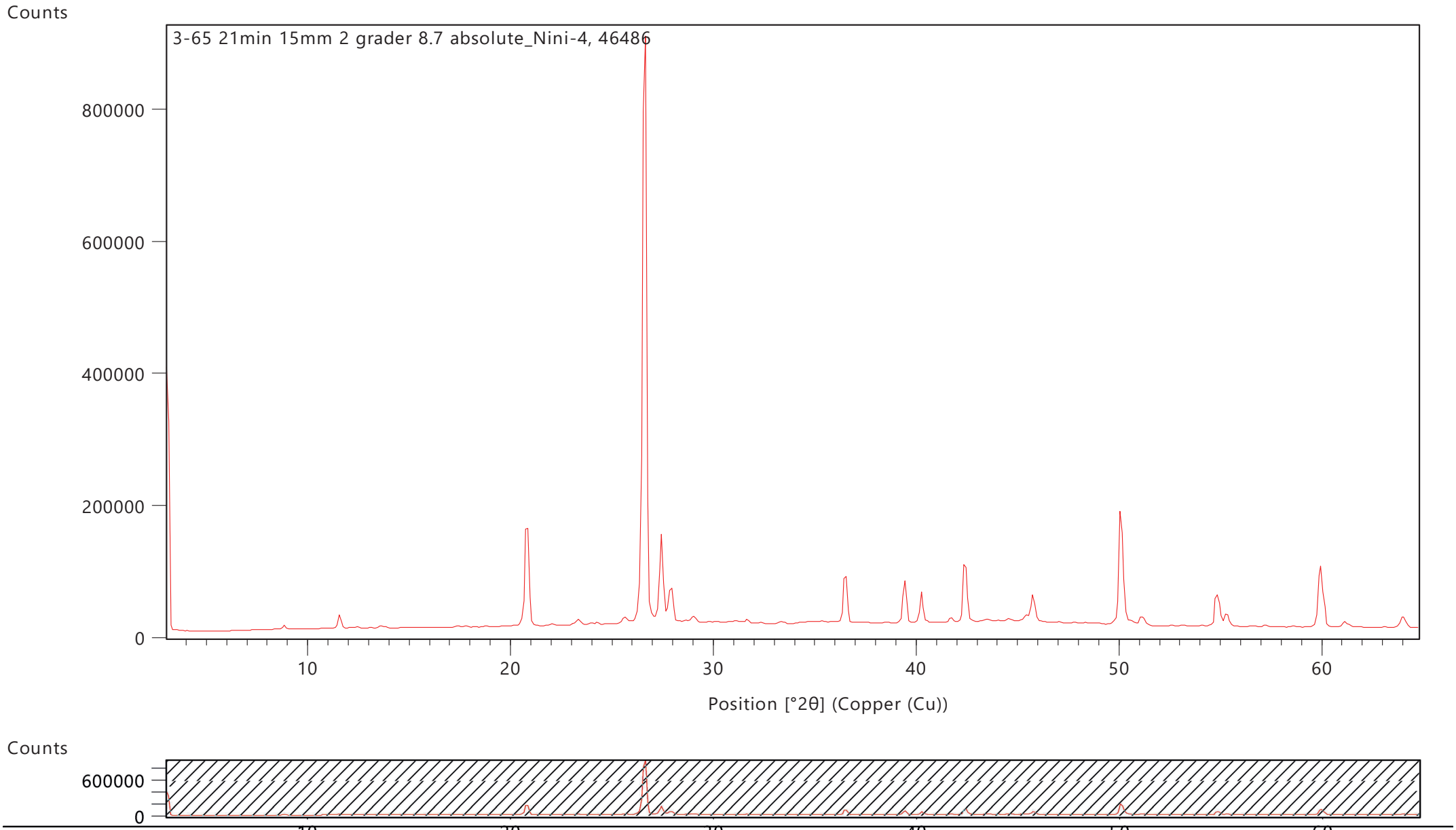
Counts
3-65 21min 15mm 2 grader 8.7 absolute_Nini-4, 46486
800000
600000
400000
200000
0
10
20
30
40
50
60
Position [°2θ] (Copper (Cu))
Counts
600000
0
10
20
30
40
50
60

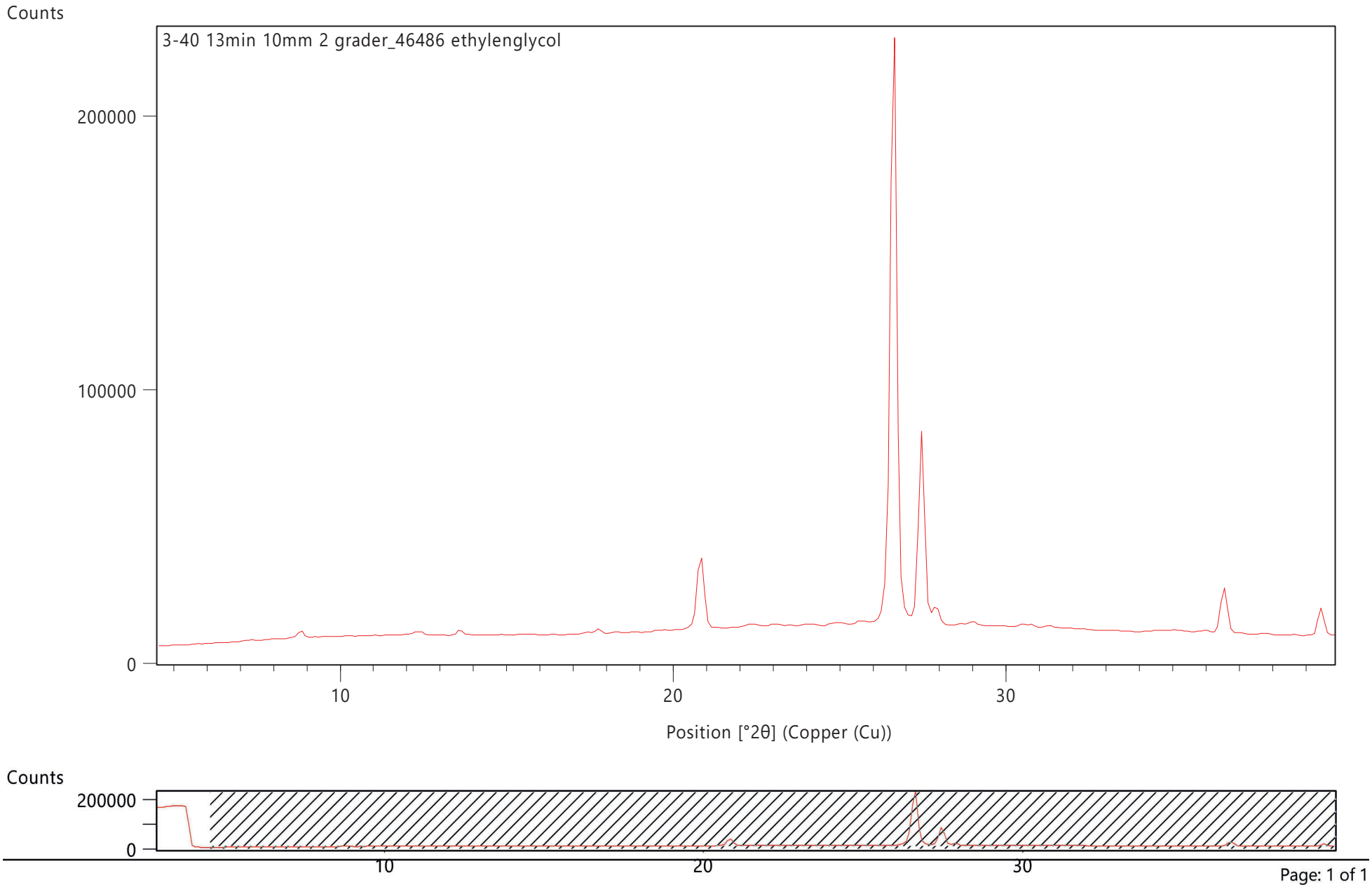
Counts
3-40 13min 10mm 2 grader_46486 ethylenglycol
200000
100000
0
10
20
30
Position [°2θ] (Copper (Cu))
Counts
200000
0
10
20
30

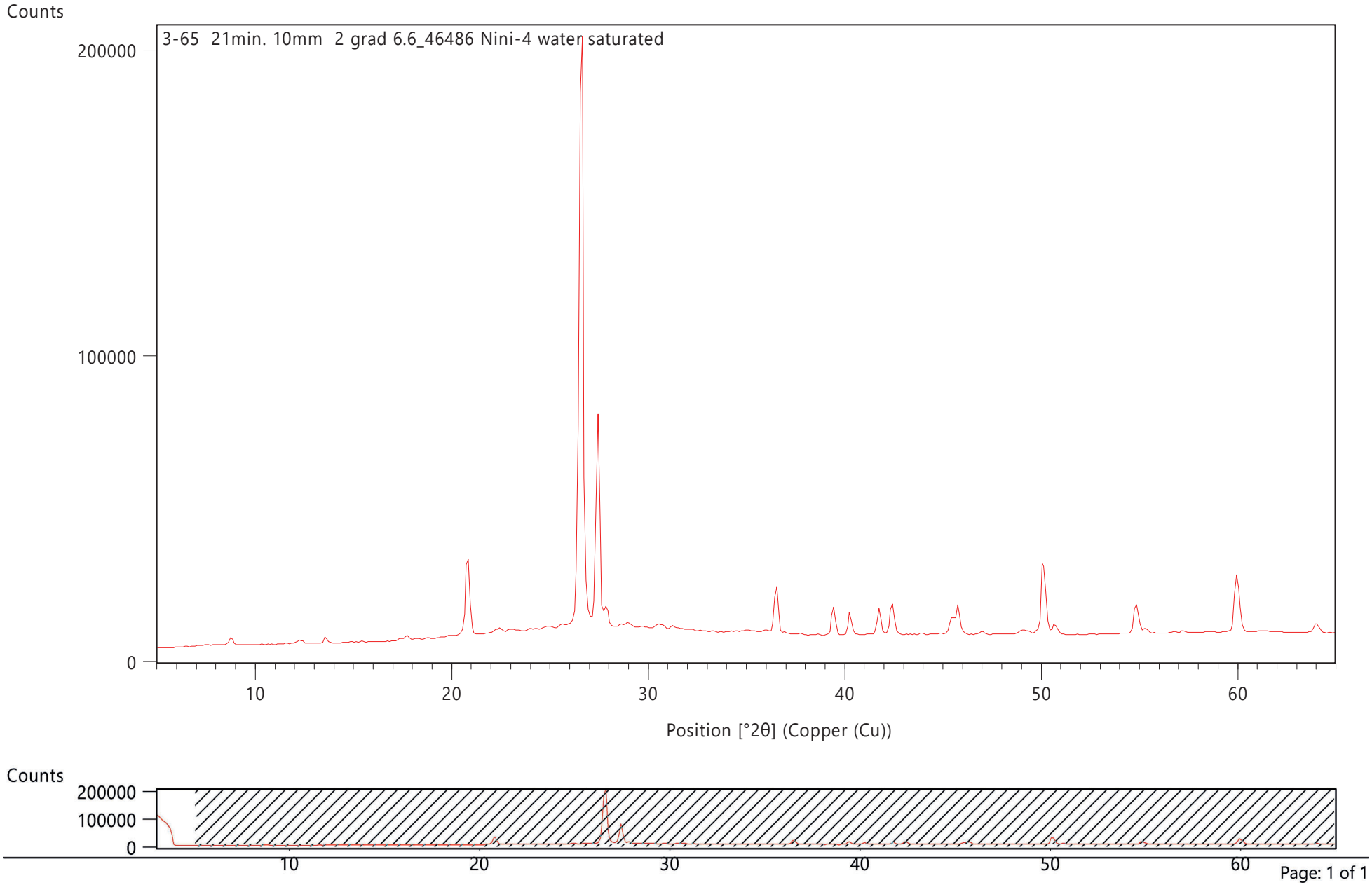
Counts
3-65 21min. 10mm 2 grad 6.6_46486 Nini-4 water saturated
200000
100000
0
10
20
30
40
50
60
Position [°2θ] (Copper (Cu))
Counts
200000
100000
0
10
20
30
40
50
60

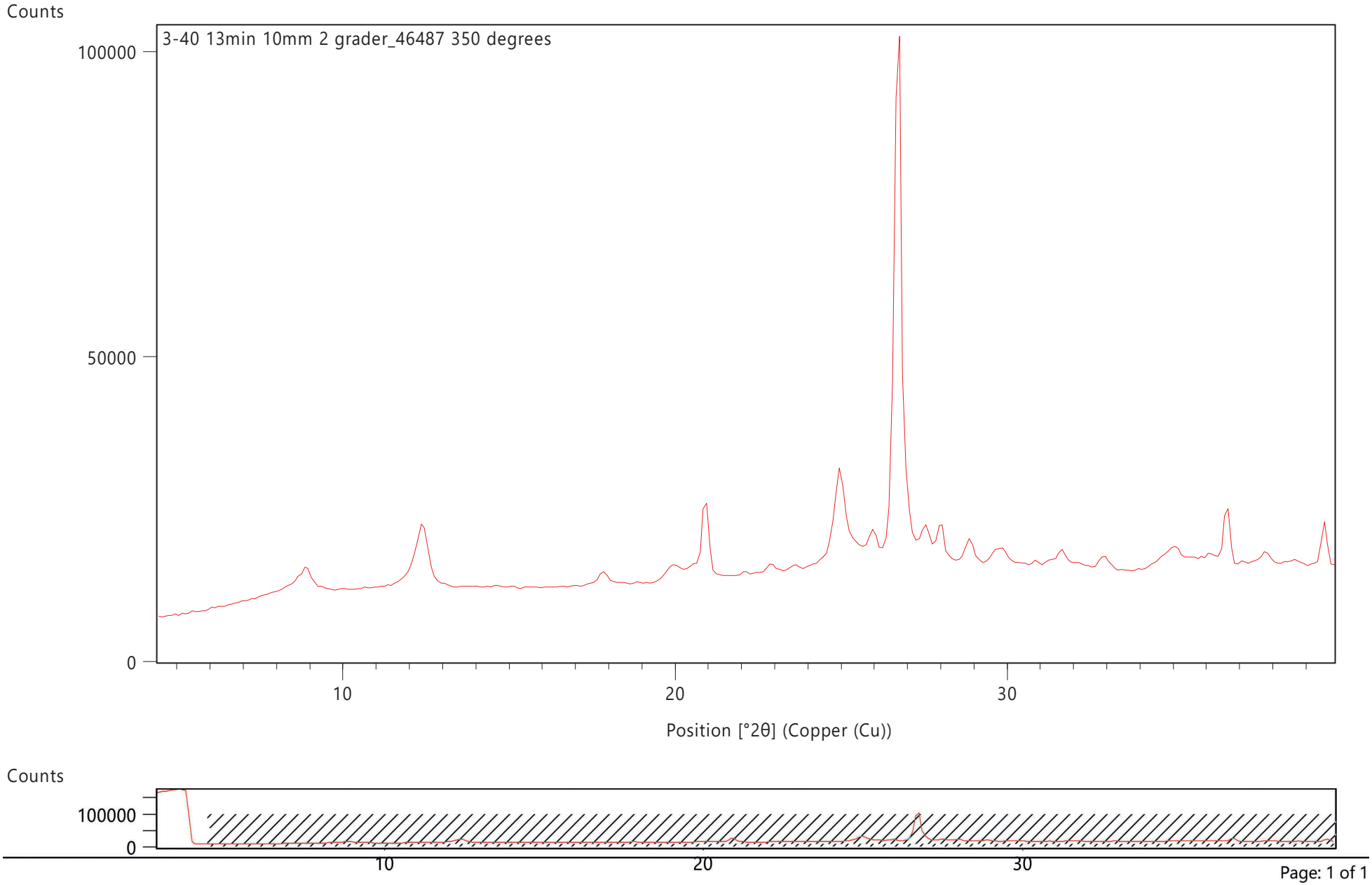
Counts
3-40 13min 10mm 2 grader_46487 350 degrees
100000
50000
0
10
20
30
Position [°2θ] (Copper (Cu))
Counts
100000
0
10
20
30

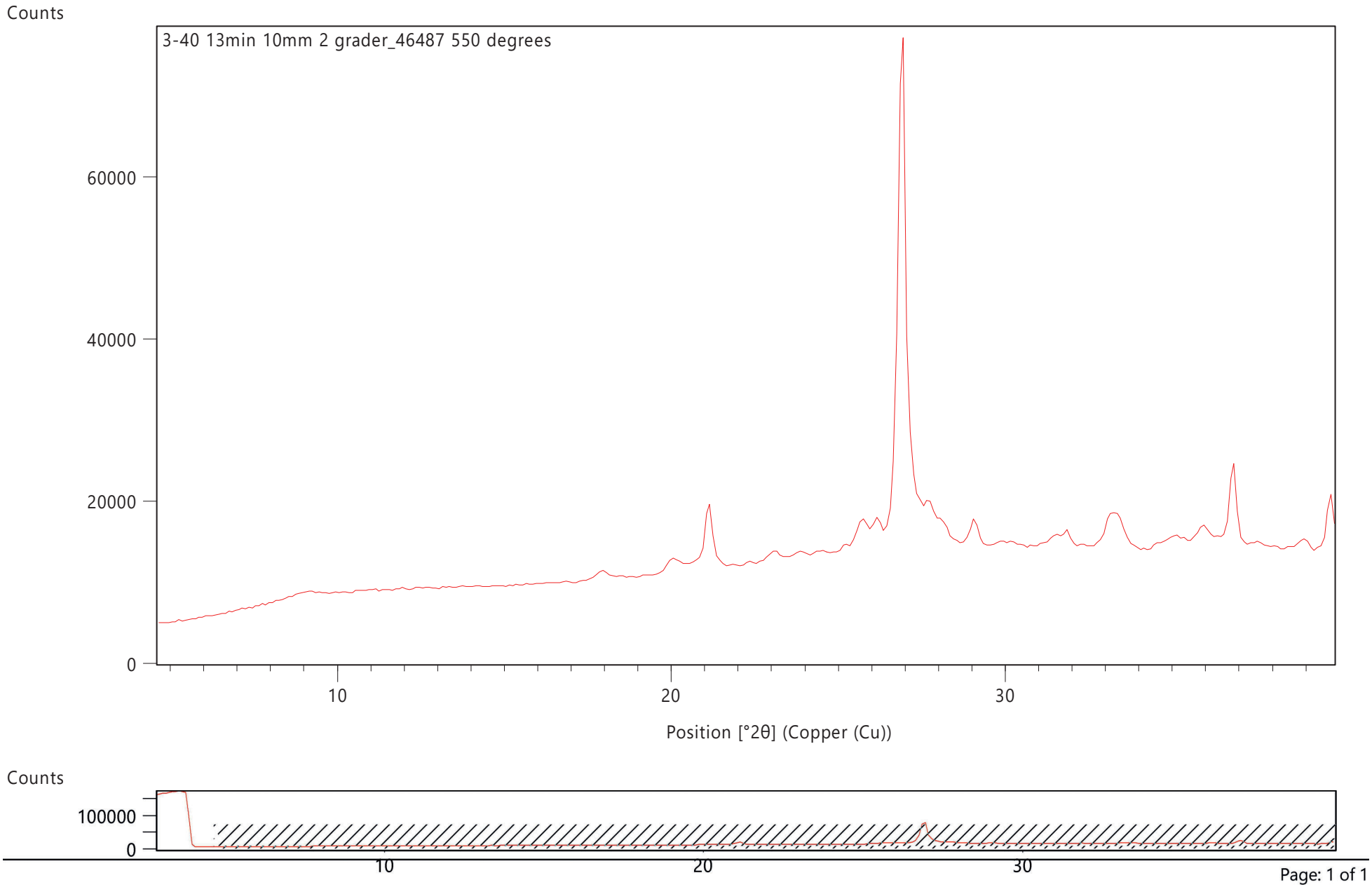
Counts
3-40 13min 10mm 2 grader_46487 550 degrees
60000
40000
20000
0
10
20
30
Position [°2θ] (Copper (Cu))
Counts
100000
0
10
20
30

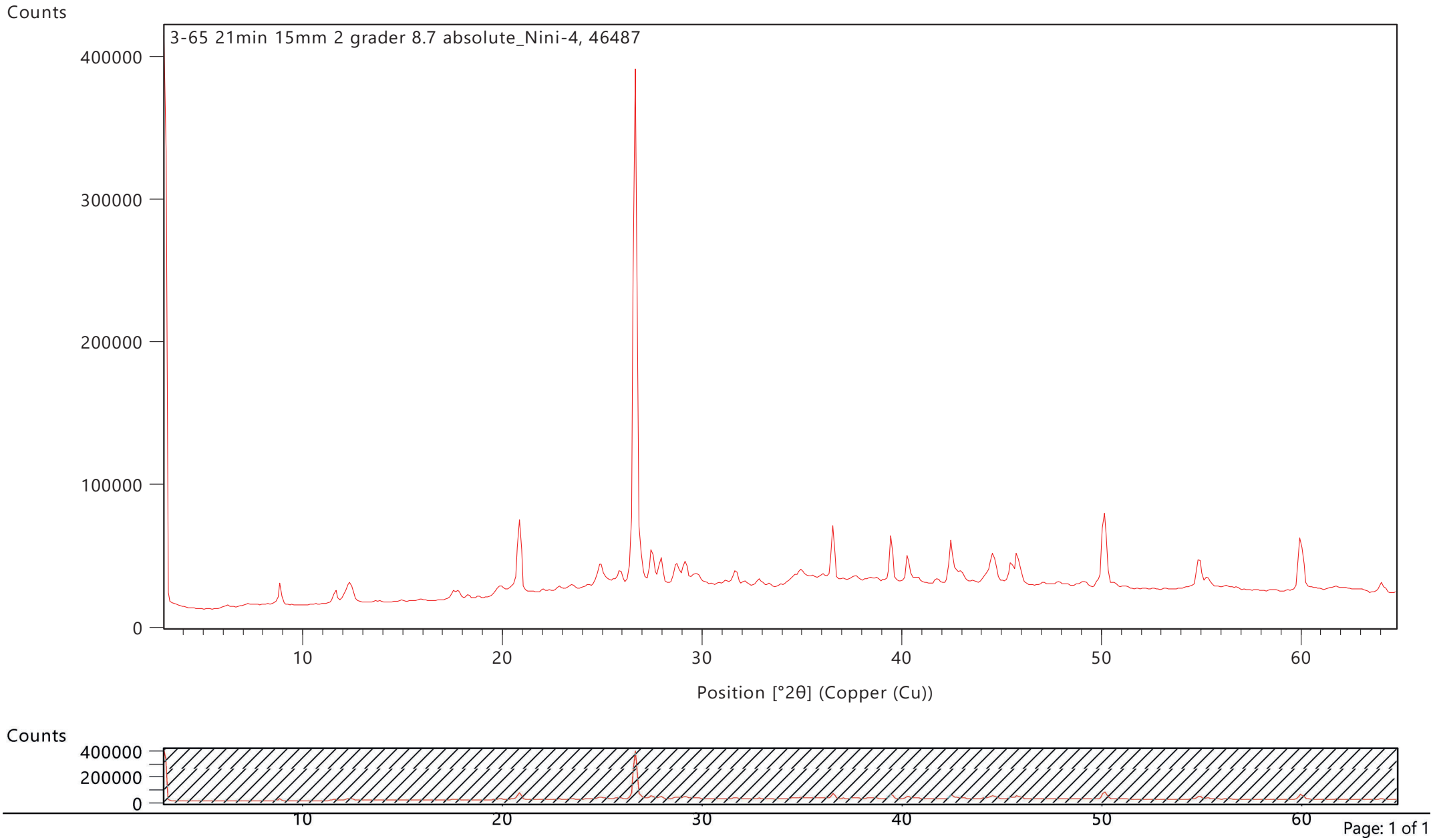
Counts
3-65 21min 15mm 2 grader 8.7 absolute_Nini-4, 46487
400000
300000
200000
100000
0
10
20
30
40
50
60
Position [°2θ] (Copper (Cu))
Counts
400000
200000
0
10
20
30
40
50
60

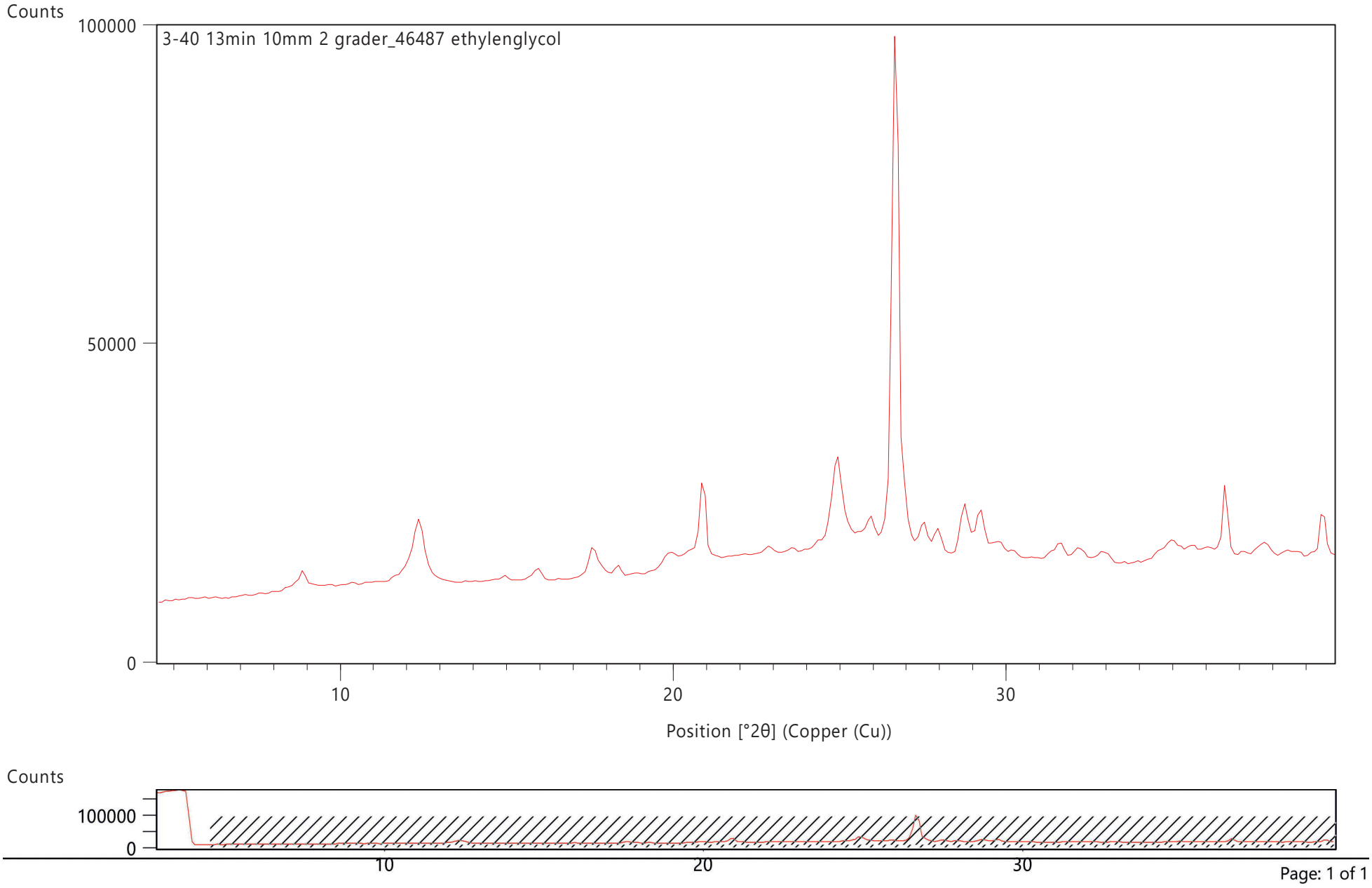
Counts
100000
50000
0
3-40 13min 10mm 2 grader_46487 ethylenglycol
10
20
30
Position [°2θ] (Copper (Cu))
Counts
100000
0
10
20
30

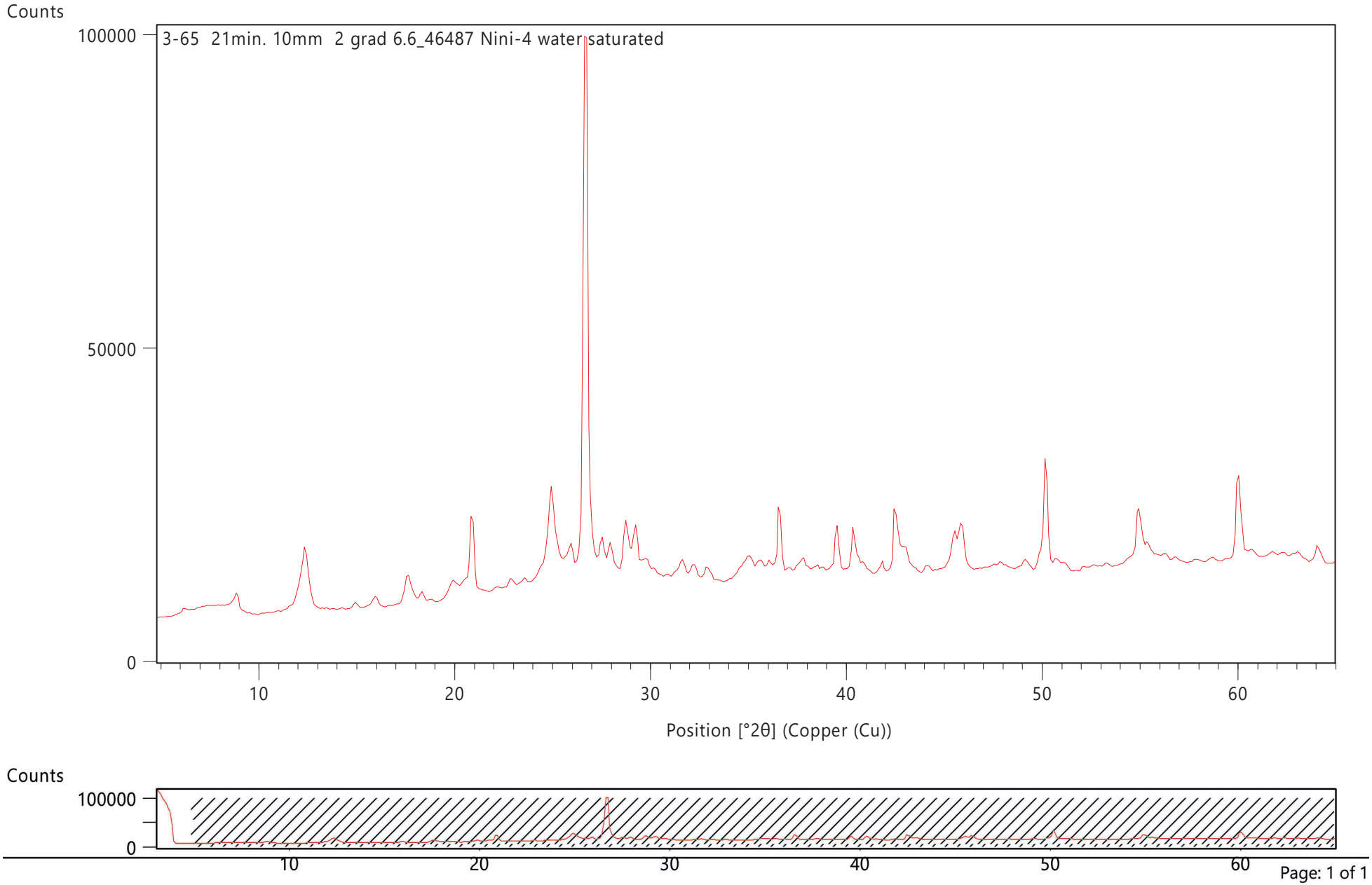
Counts
100000
50000
0
3-65 21min. 10mm 2 grad 6.6_46487 Nini-4 water saturated
10
20
30
40
50
60
Position [°2θ] (Copper (Cu))
Counts
100000
0
10
20
30
40
50
60

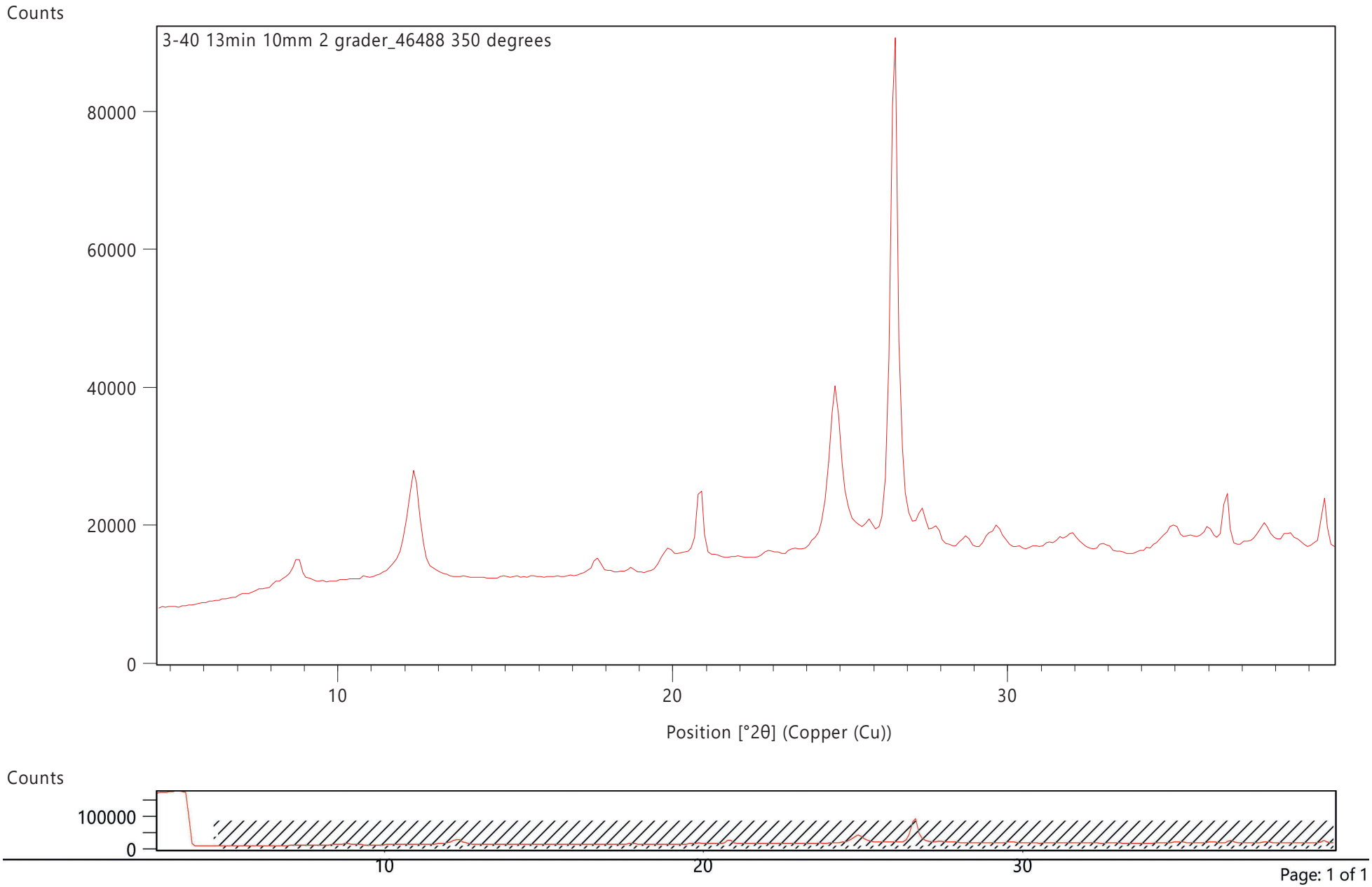
Counts
3-40 13min 10mm 2 grader_46488 350 degrees
80000
60000
40000
20000
0
10
20
30
Position [°2θ] (Copper (Cu))
Counts
100000
0
10
20
30

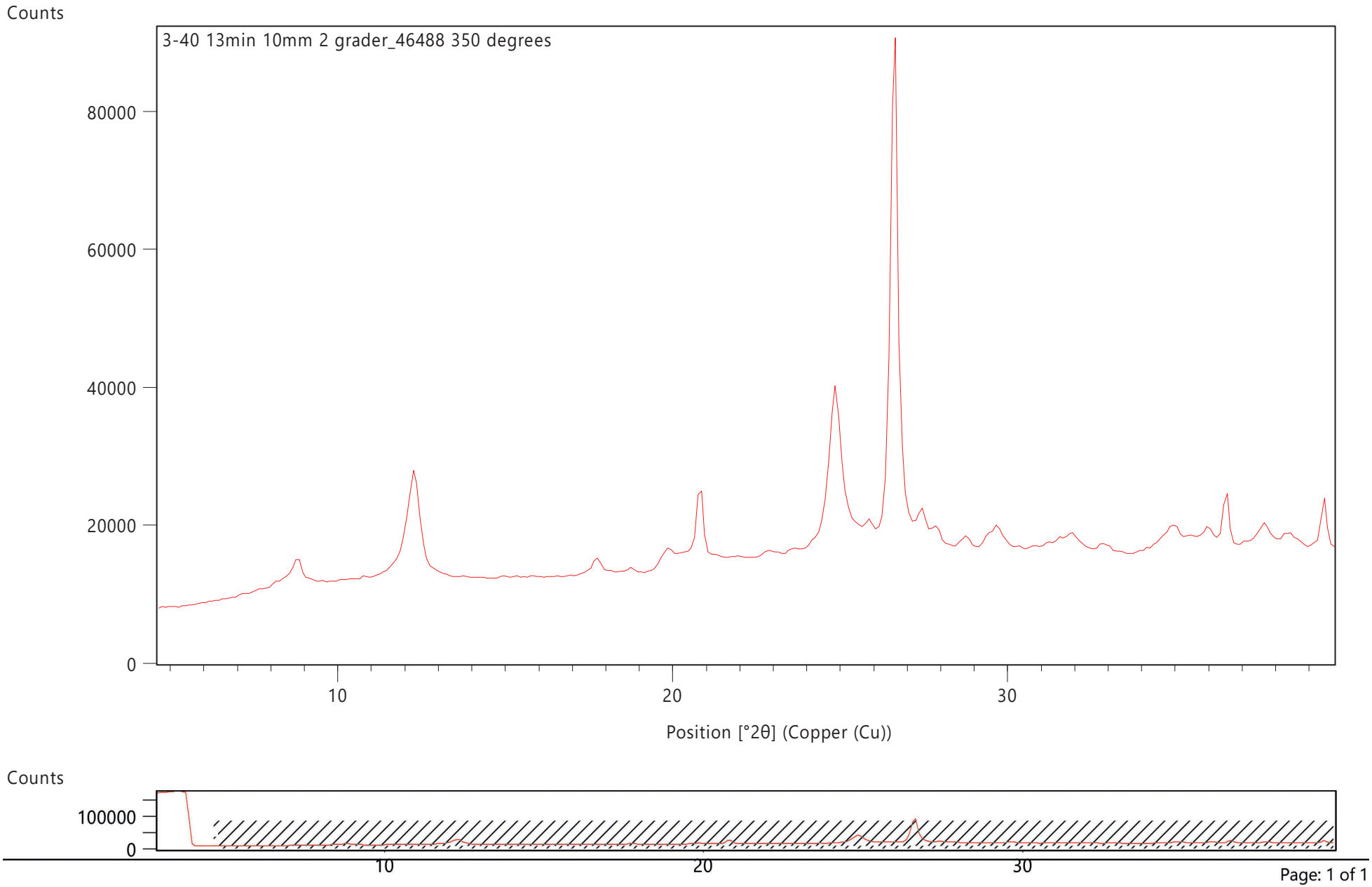
Counts
3-40 13min 10mm 2 grader_46488 350 degrees
80000
60000
40000
20000
0
10
20
30
Position [°2θ] (Copper (Cu))
Counts
100000
0
10
20
30

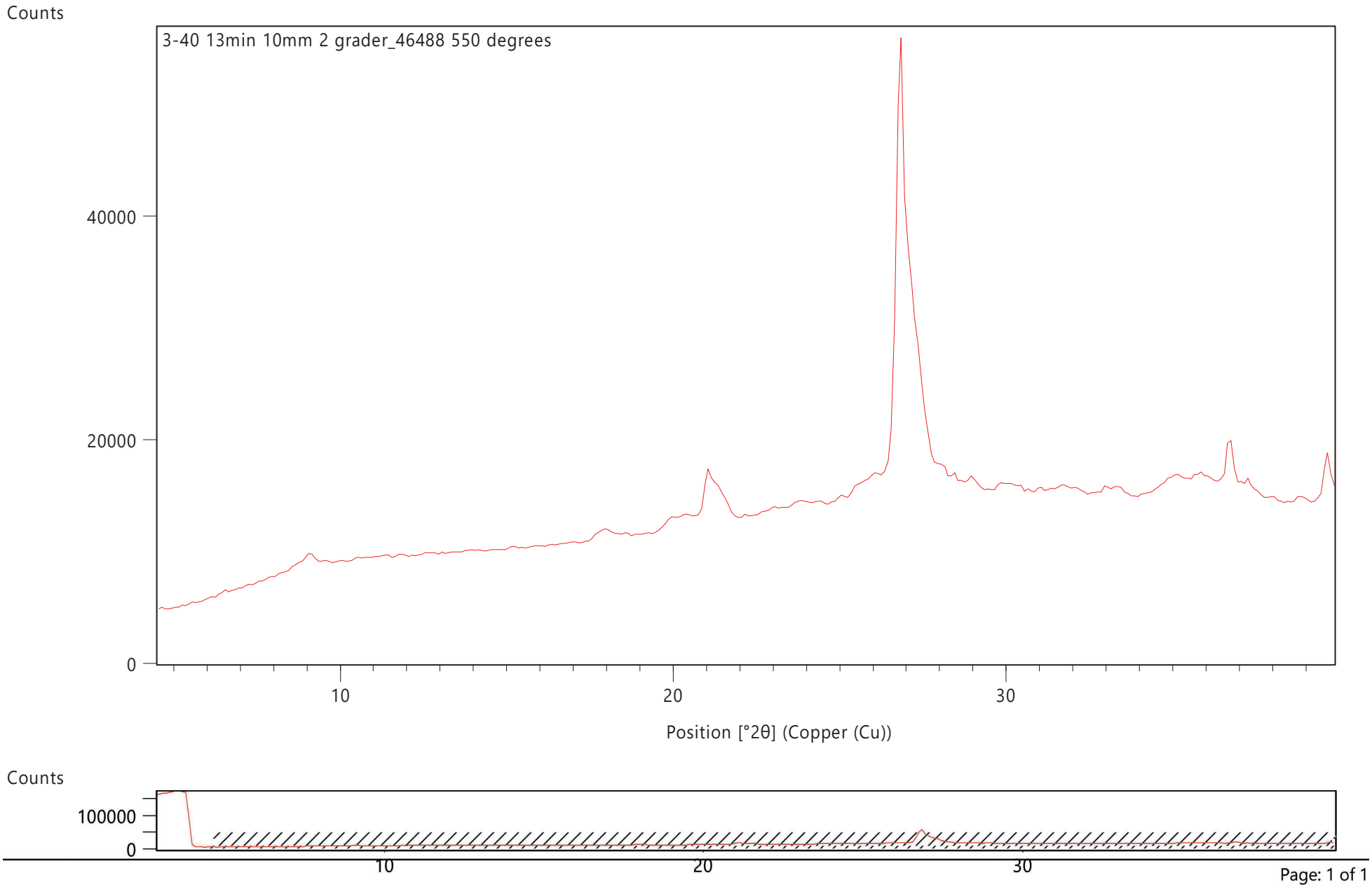
Counts
3-40 13min 10mm 2 grader_46488 550 degrees
40000
20000
0
10
20
30
Position [°2θ] (Copper (Cu))
Counts
100000
0
10
20
30

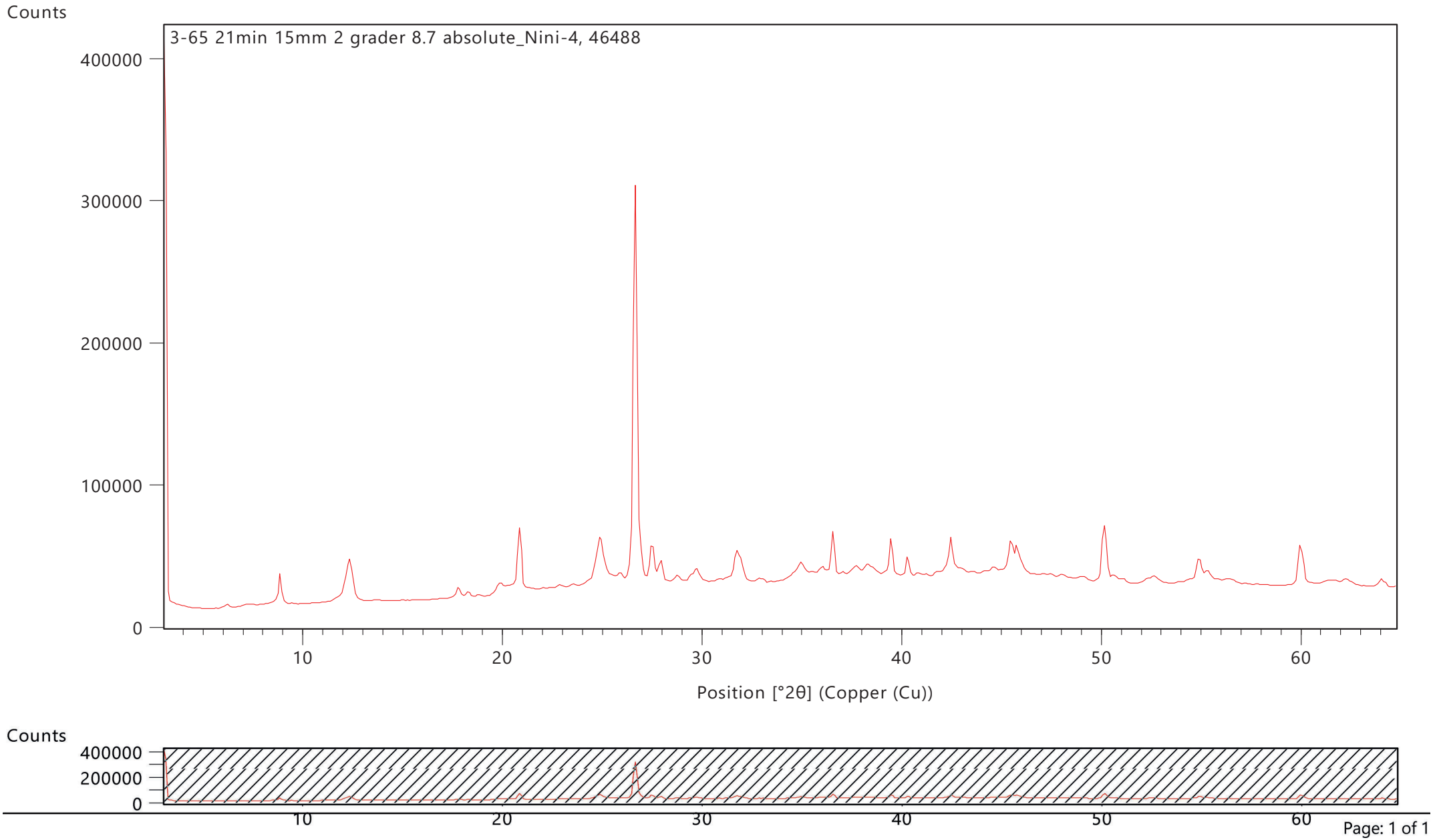
Counts
3-65 21min 15mm 2 grader 8.7 absolute_Nini-4, 46488
400000
300000
200000
100000
0
10
20
30
40
50
60
Position [°2θ] (Copper (Cu))
Counts
400000
200000
0
10
20
30
40
50
60

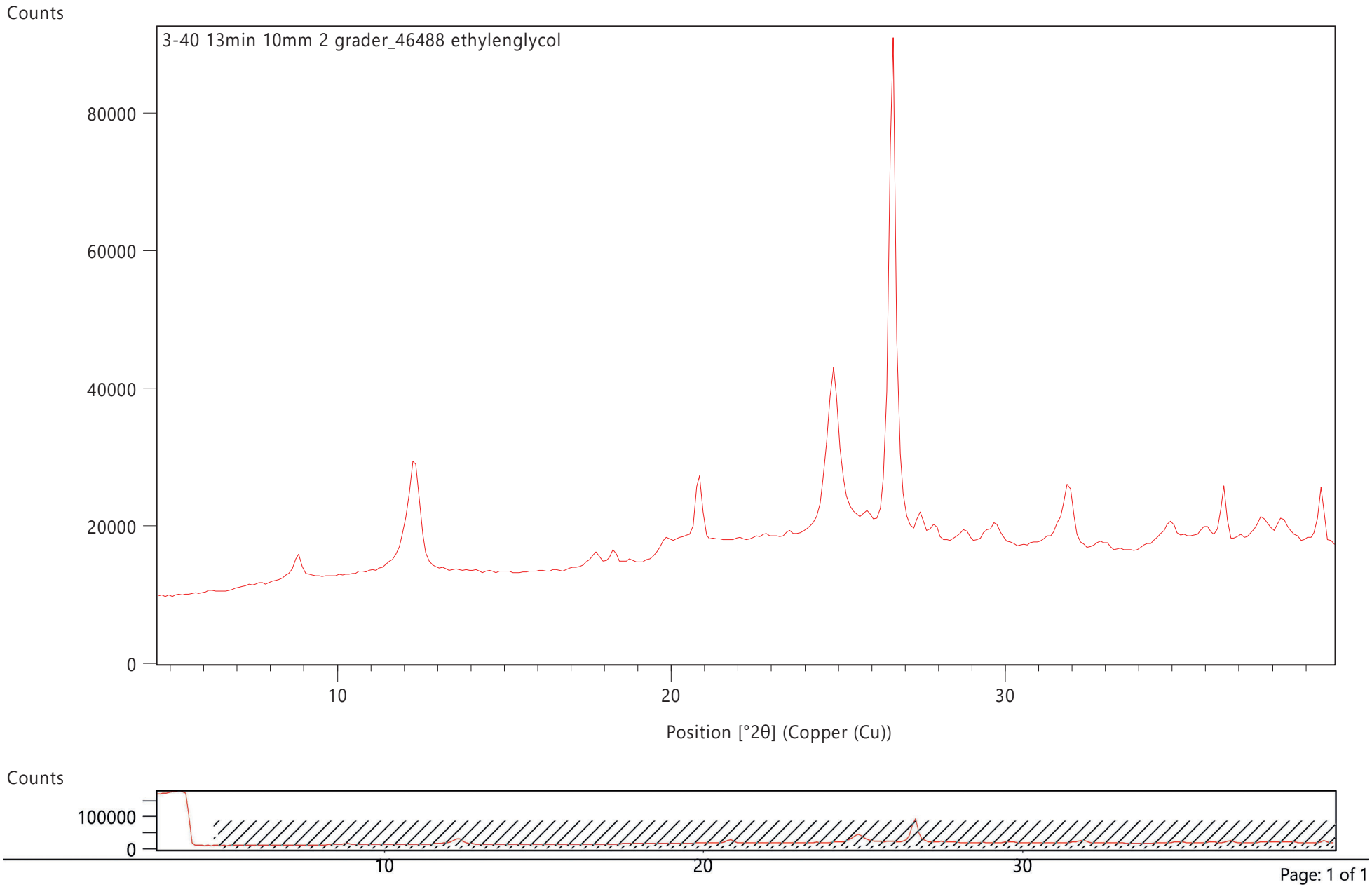
Counts
3-40 13min 10mm 2 grader_46488 ethylenglycol
80000
60000
40000
20000
0
10
20
30
Position [°2θ] (Copper (Cu))
Counts
100000
0
10
20
30

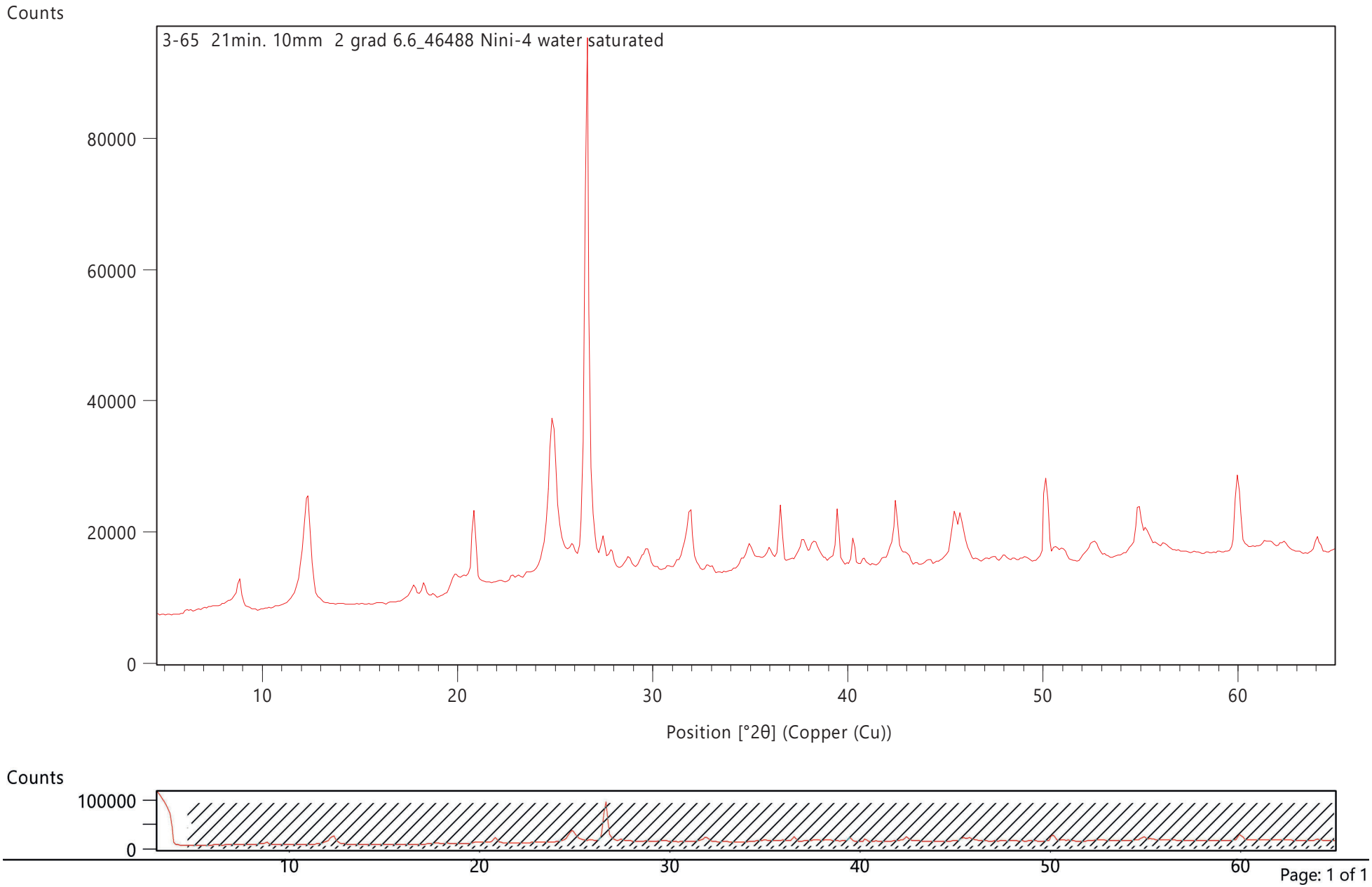
Counts
3-65 21min. 10mm 2 grad 6.6_46488 Nini-4 water saturated
80000
60000
40000
20000
0
10
20
30
40
50
60
Position [°2θ] (Copper (Cu))
Counts
100000
0
10
20
30
40
50
60

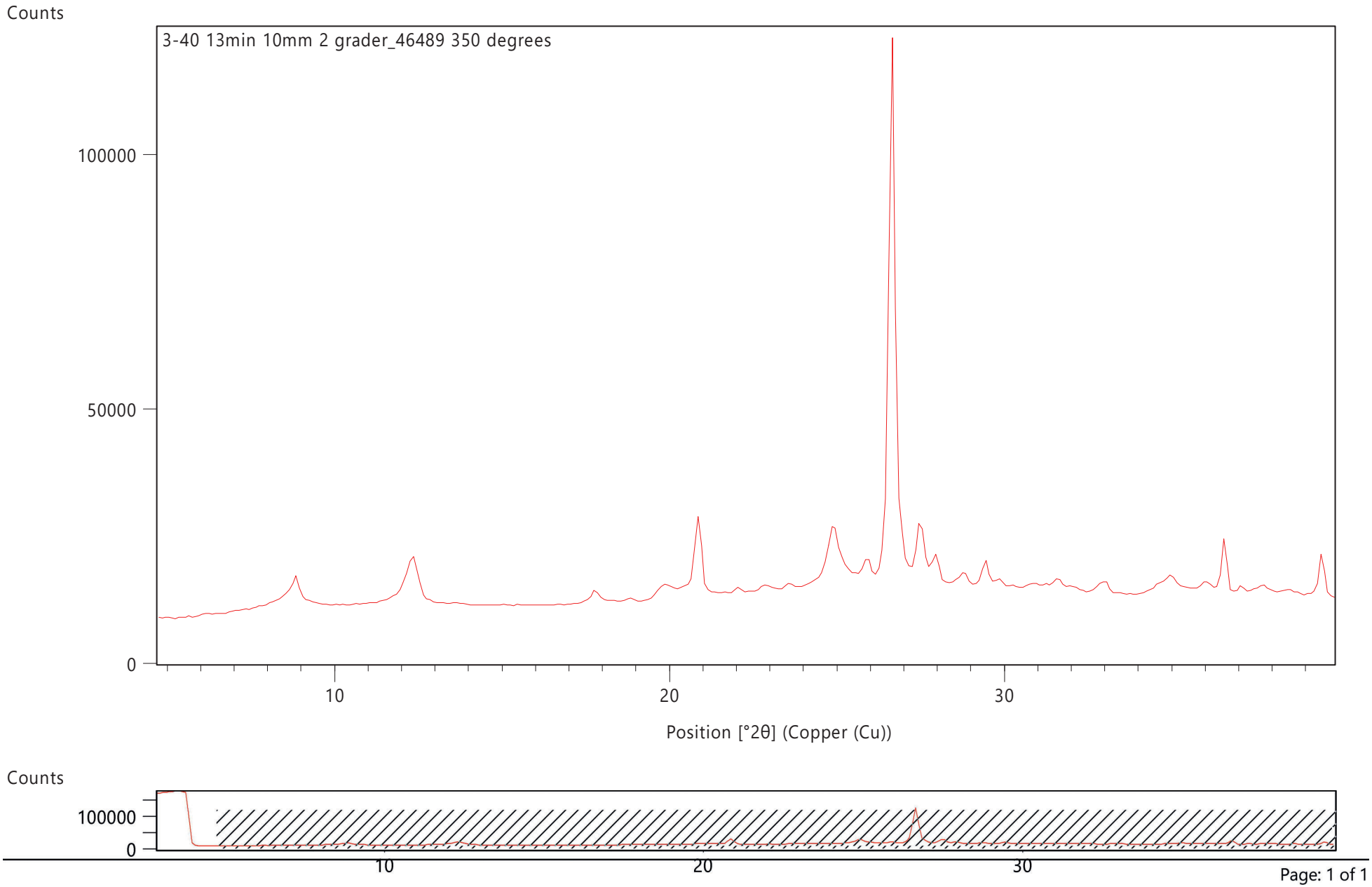
Counts
3-40 13min 10mm 2 grader_46489 350 degrees
100000
50000
0
10
20
30
Position [°2θ] (Copper (Cu))
Counts
100000
0
10
20
30

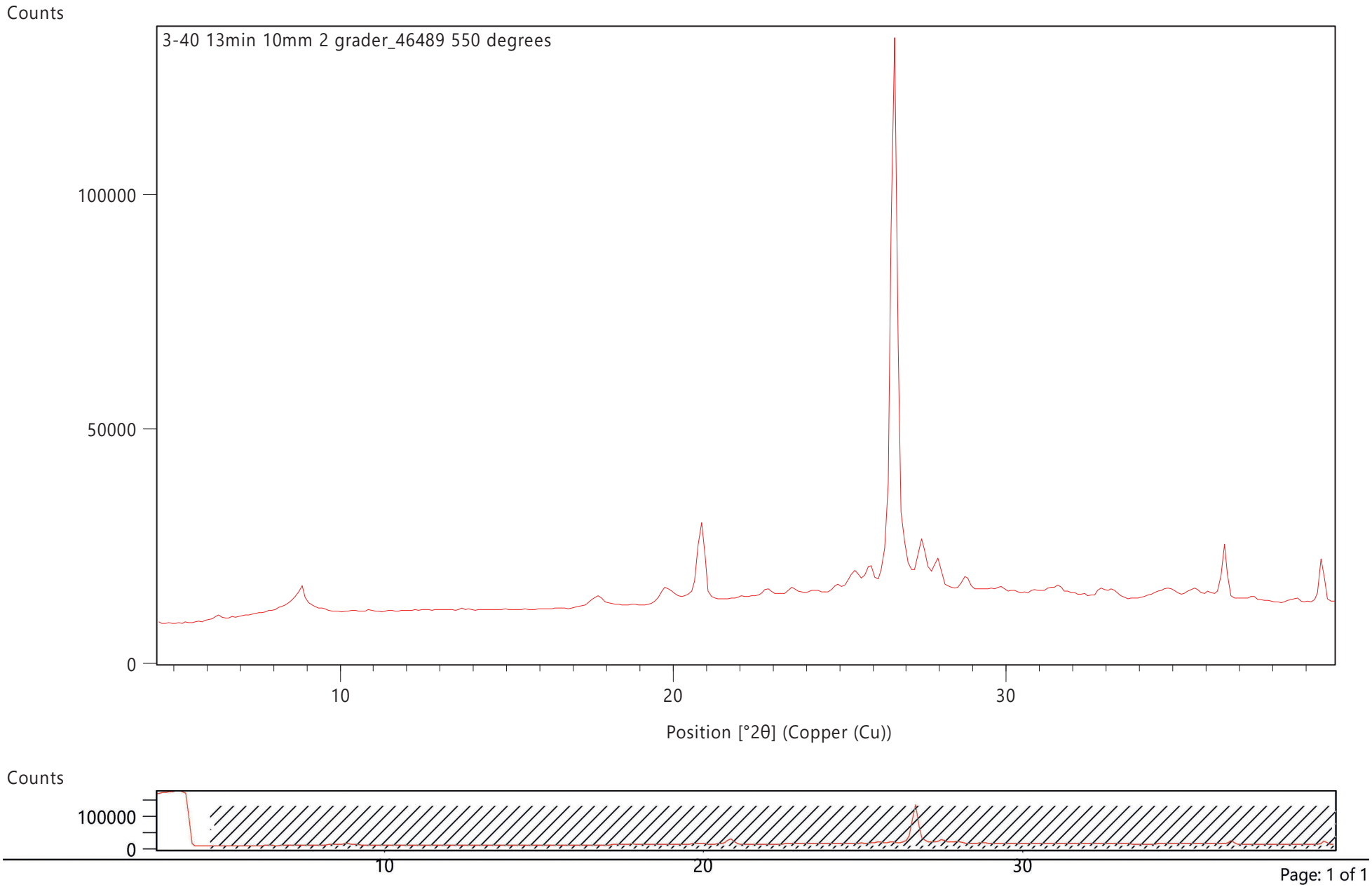
Counts
3-40 13min 10mm 2 grader_46489 550 degrees
100000
50000
0
10
20
30
Position [°2θ] (Copper (Cu))
Counts
100000
0
10
20
30

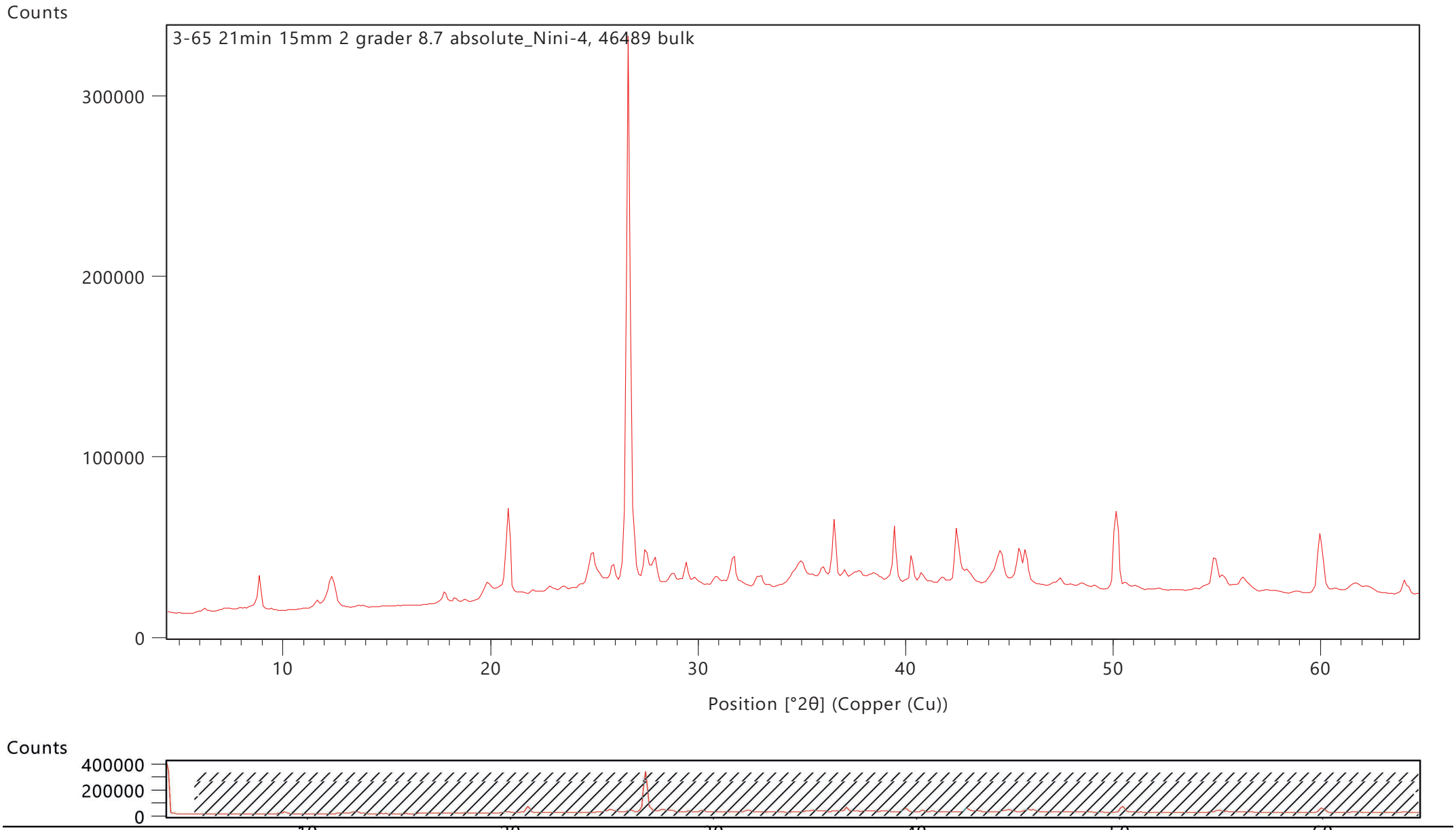
Counts
3-65 21min 15mm 2 grader 8.7 absolute_Nini-4, 46489 bulk
300000
200000
100000
0
10
20
30
40
50
60
Position [°2θ] (Copper (Cu))
Counts
400000
200000
0
10
20
30
40
50
60

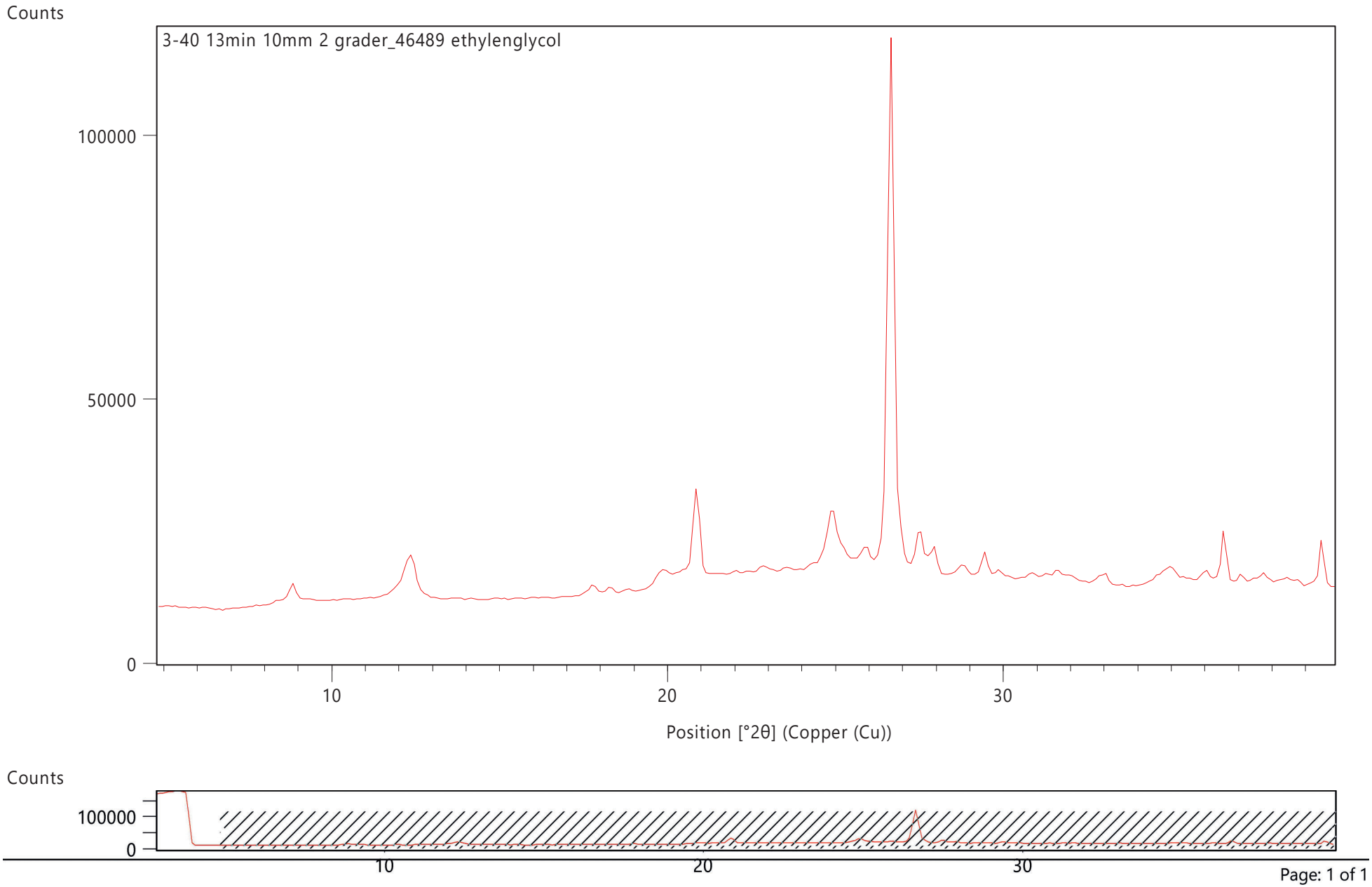
Counts
3-40 13min 10mm 2 grader_46489 ethylenglycol
100000
50000
0
10
20
30
Position [°2θ] (Copper (Cu))
Counts
100000
0
10
20
30

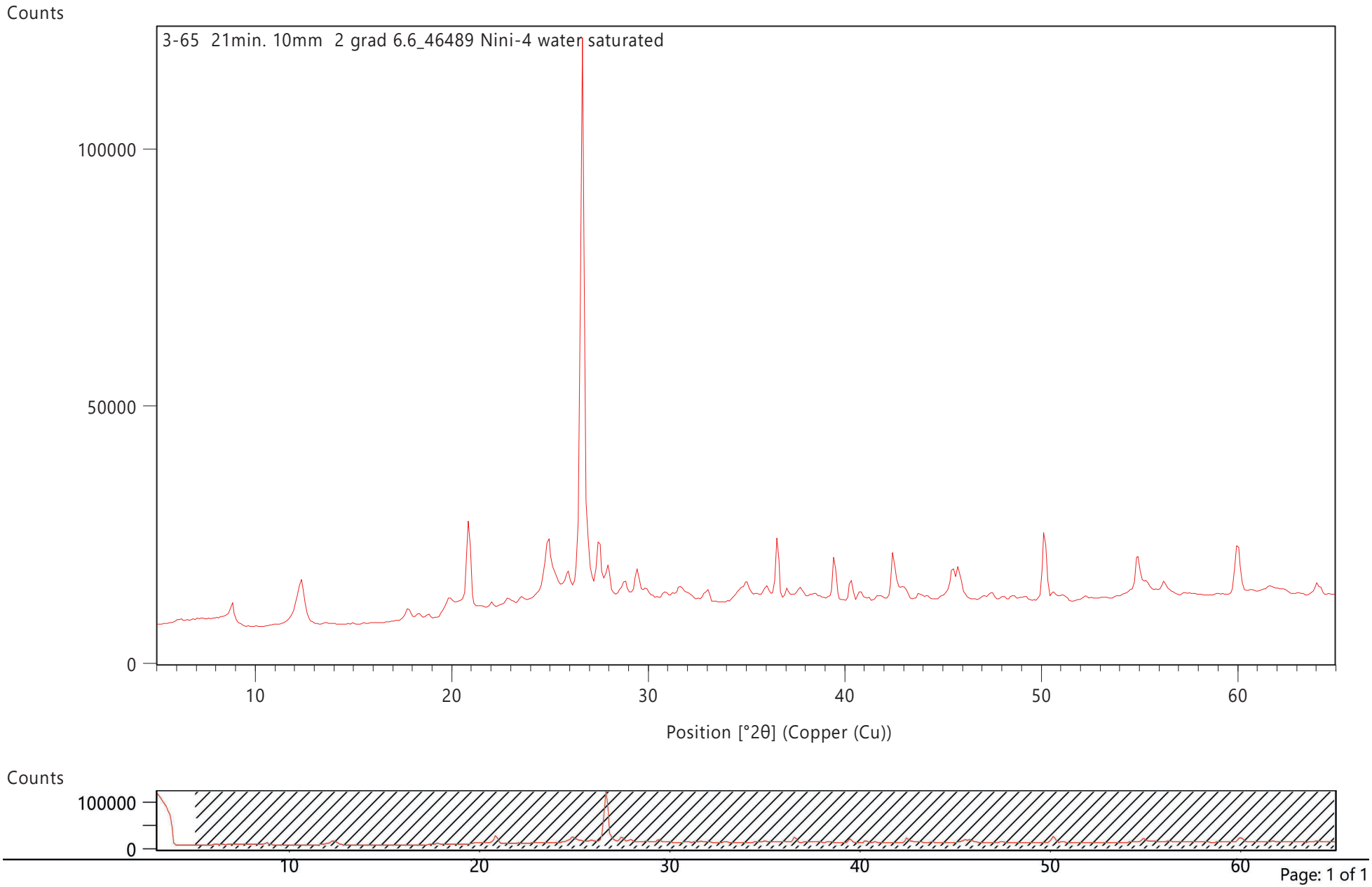
Counts
3-65 21min. 10mm 2 grad 6.6_46489 Nini-4 water saturated
100000
50000
0
10
20
30
40
50
60
Position [°2θ] (Copper (Cu))
Counts
100000
0
10
20
30
40
50
60

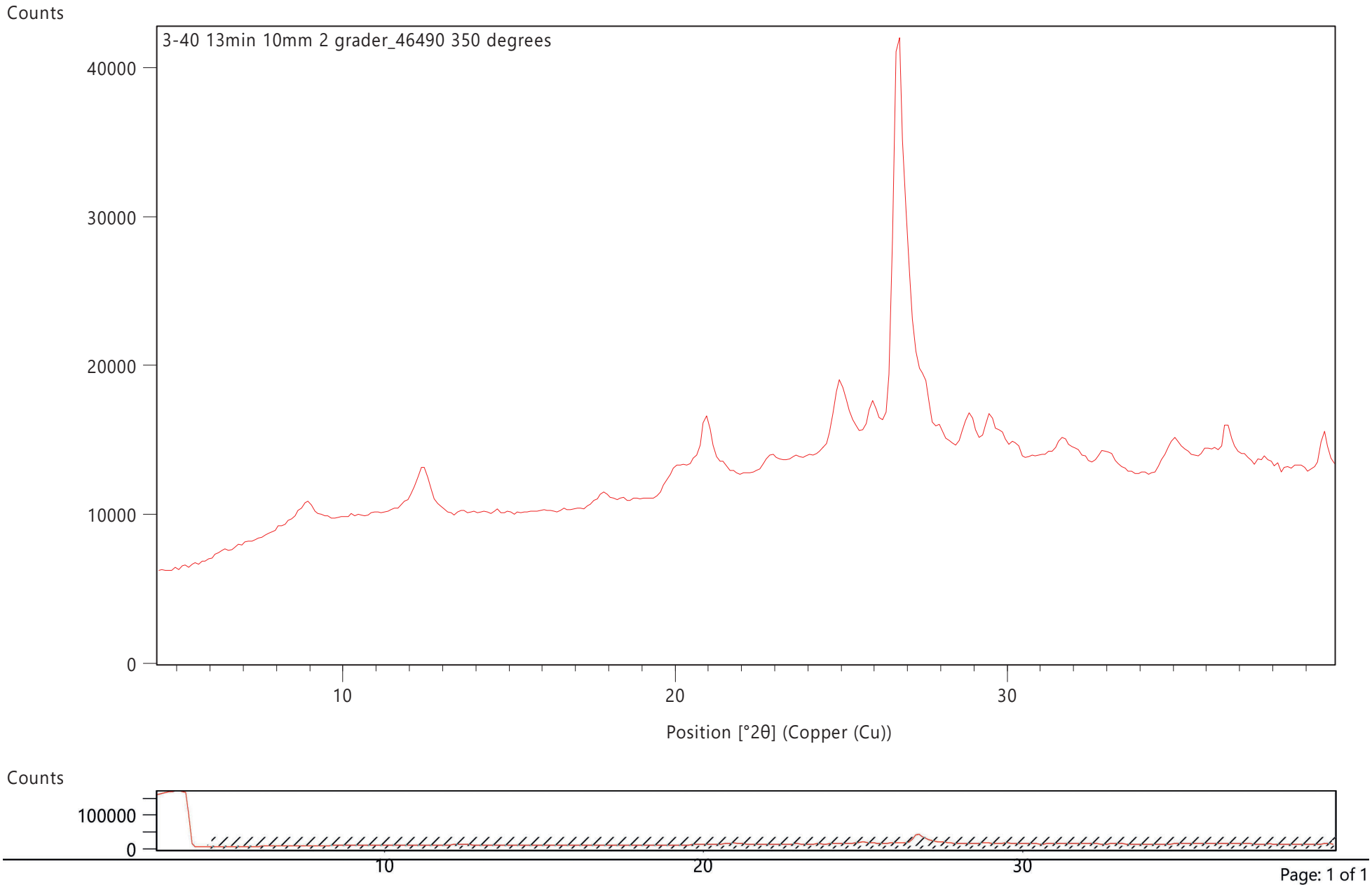
Counts
3-40 13min 10mm 2 grader_46490 350 degrees
40000
30000
20000
10000
0
10
20
30
Position [°2θ] (Copper (Cu))
Counts
100000
0
10
20
30

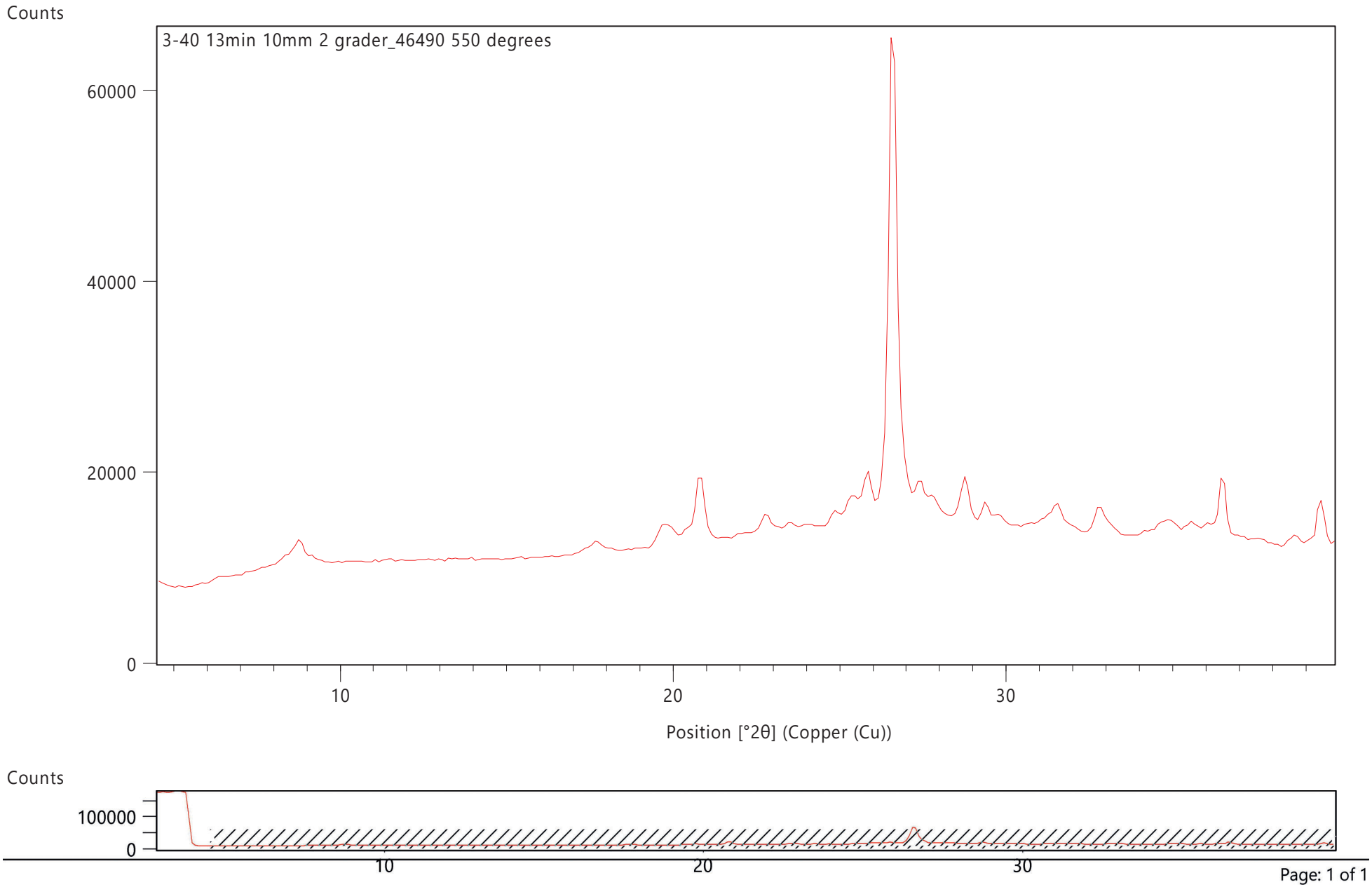
Counts
3-40 13min 10mm 2 grader_46490 550 degrees
60000
40000
20000
0
10
20
30
Position [°2θ] (Copper (Cu))
Counts
100000
0
10
20
30

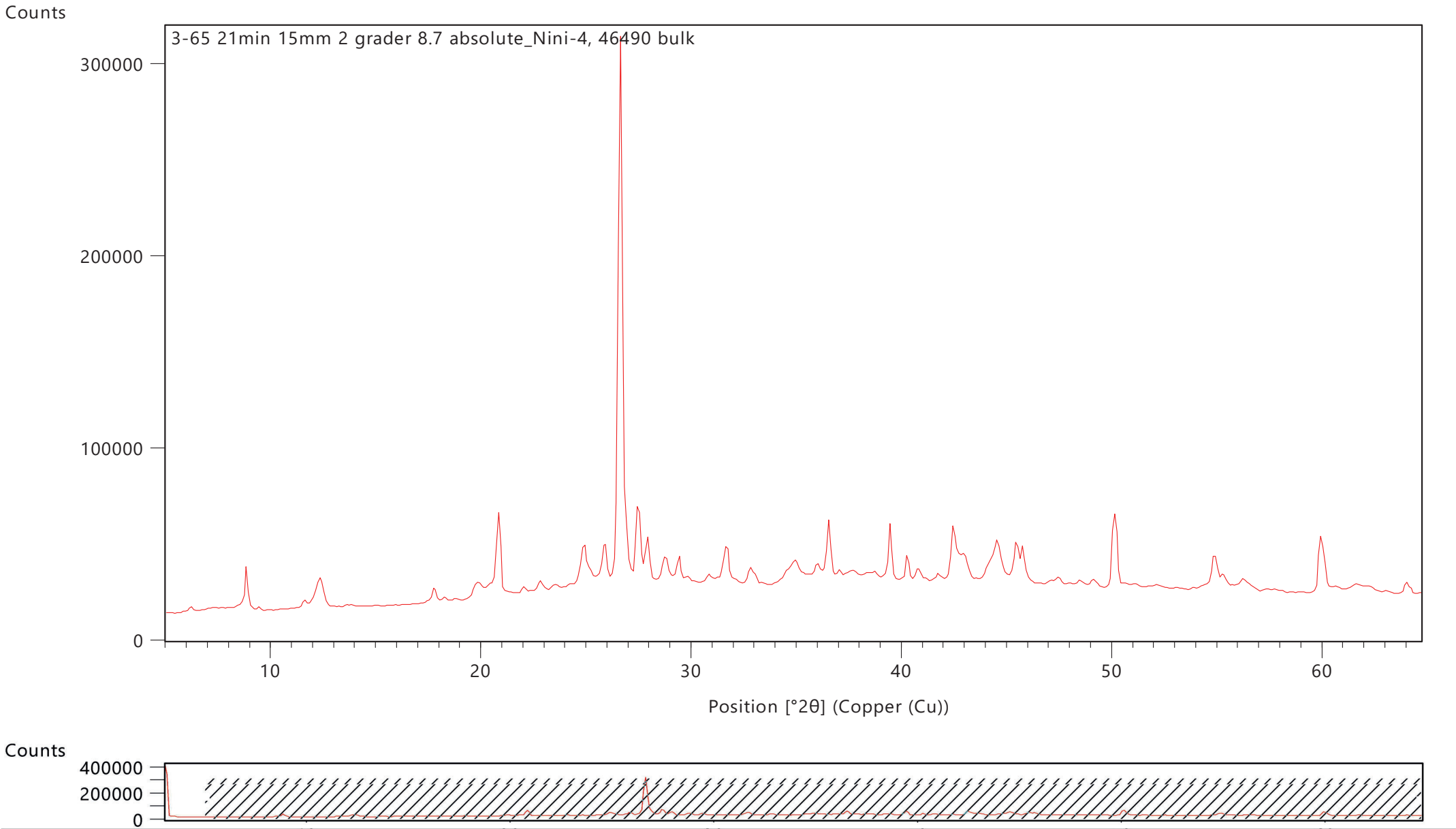
Counts
3-65 21min 15mm 2 grader 8.7 absolute_Nini-4, 46490 bulk
300000
200000
100000
0
10
20
30
40
50
60
Position [°2θ] (Copper (Cu))
Counts
400000
200000
0
10
20
30
40
50
60

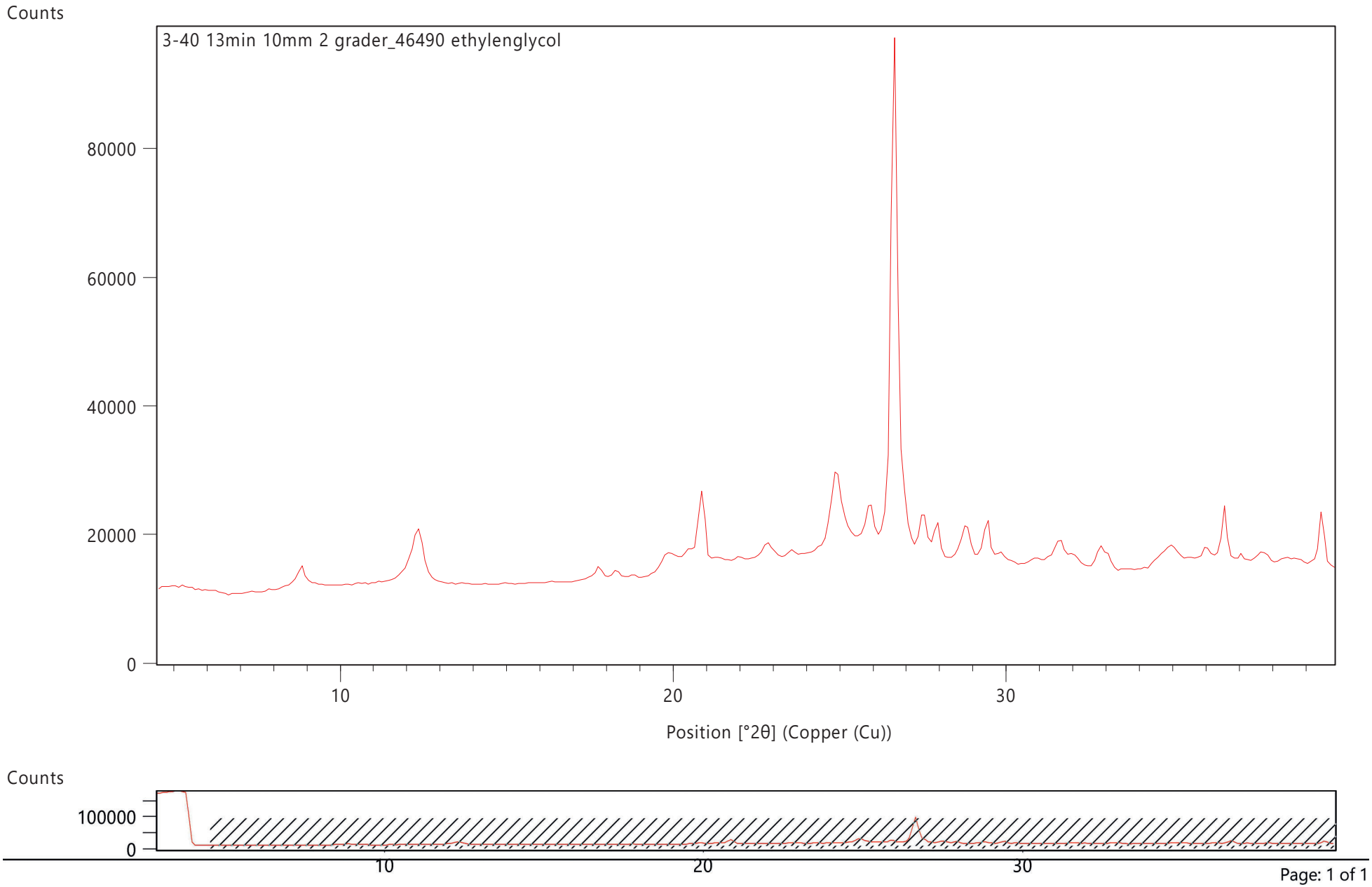
Counts
3-40 13min 10mm 2 grader_46490 ethylenglycol
80000
60000
40000
20000
0
10
20
30
Position [°2θ] (Copper (Cu))
Counts
100000
0
10
20
30

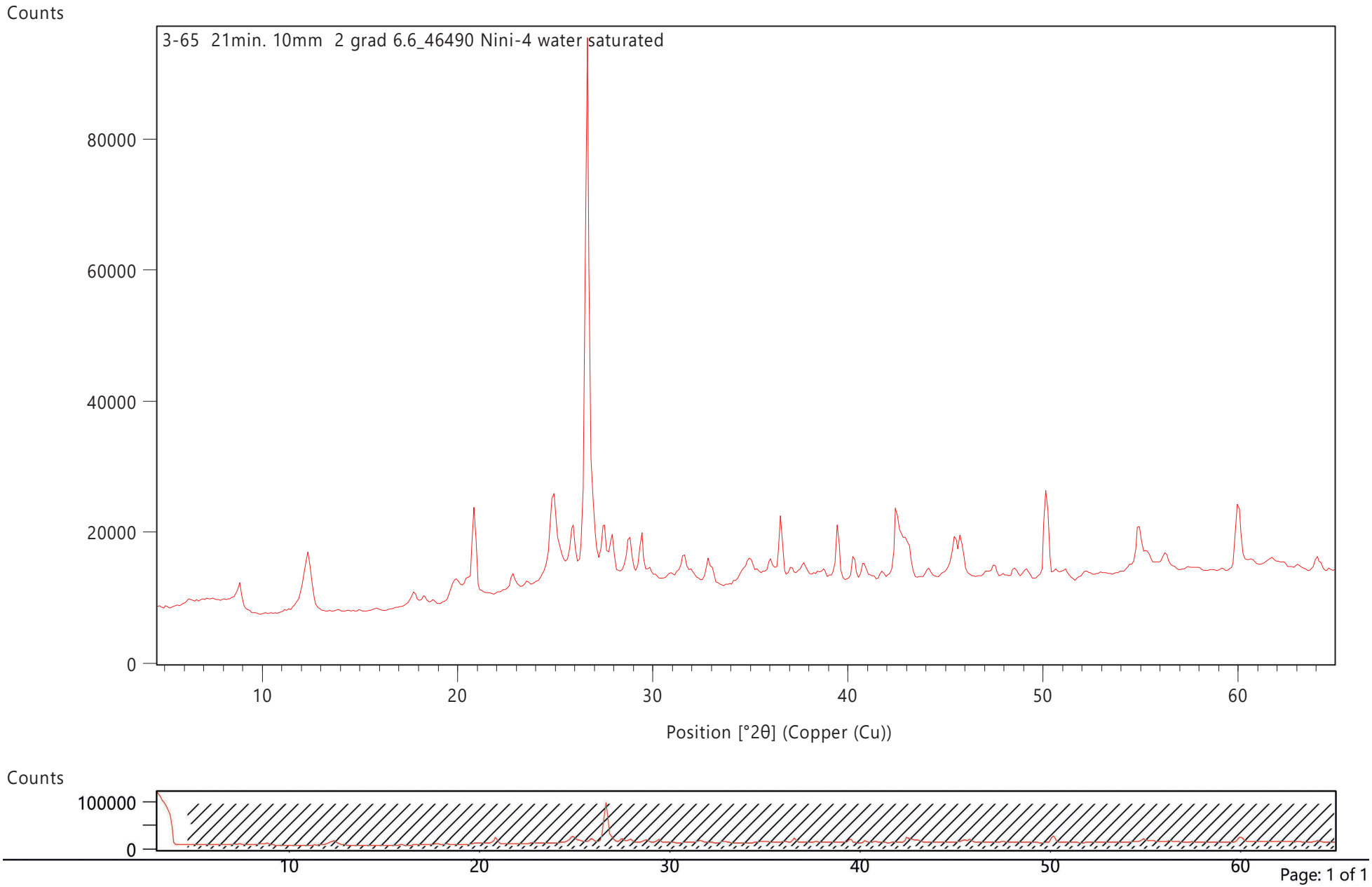
Counts
3-65 21min. 10mm 2 grad 6.6_46490 Nini-4 water saturated
80000
60000
40000
20000
0
10
20
30
40
50
60
Position [°2θ] (Copper (Cu))
Counts
100000
0
10
20
30
40
50
60

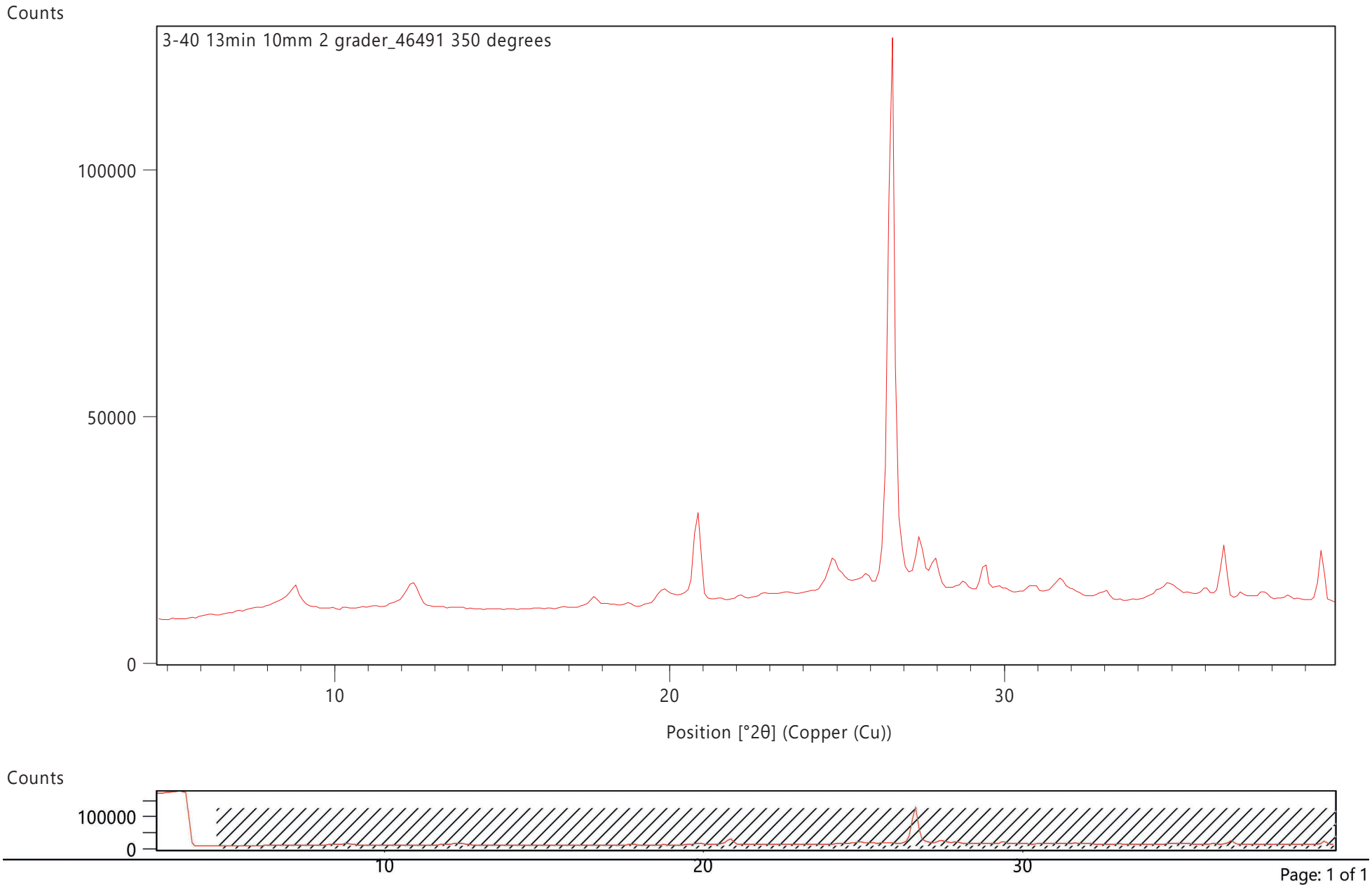
Counts
3-40 13min 10mm 2 grader_46491 350 degrees
100000
50000
0
10
20
30
Position [°2θ] (Copper (Cu))
Counts
100000
0
10
20
30

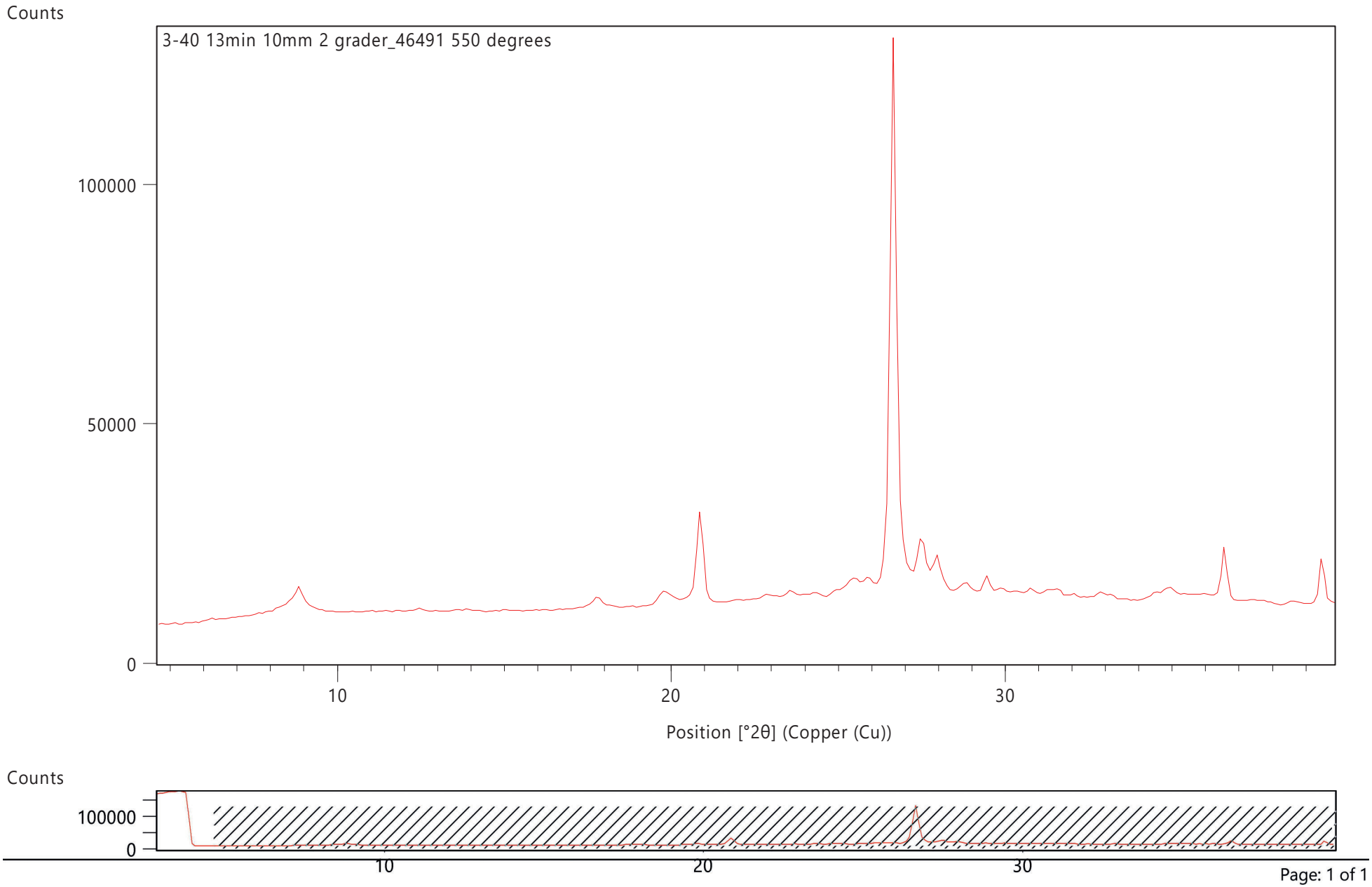
Counts
3-40 13min 10mm 2 grader_46491 550 degrees
100000
50000
0
10
20
30
Position [°2θ] (Copper (Cu))
Counts
100000
0
10
20
30

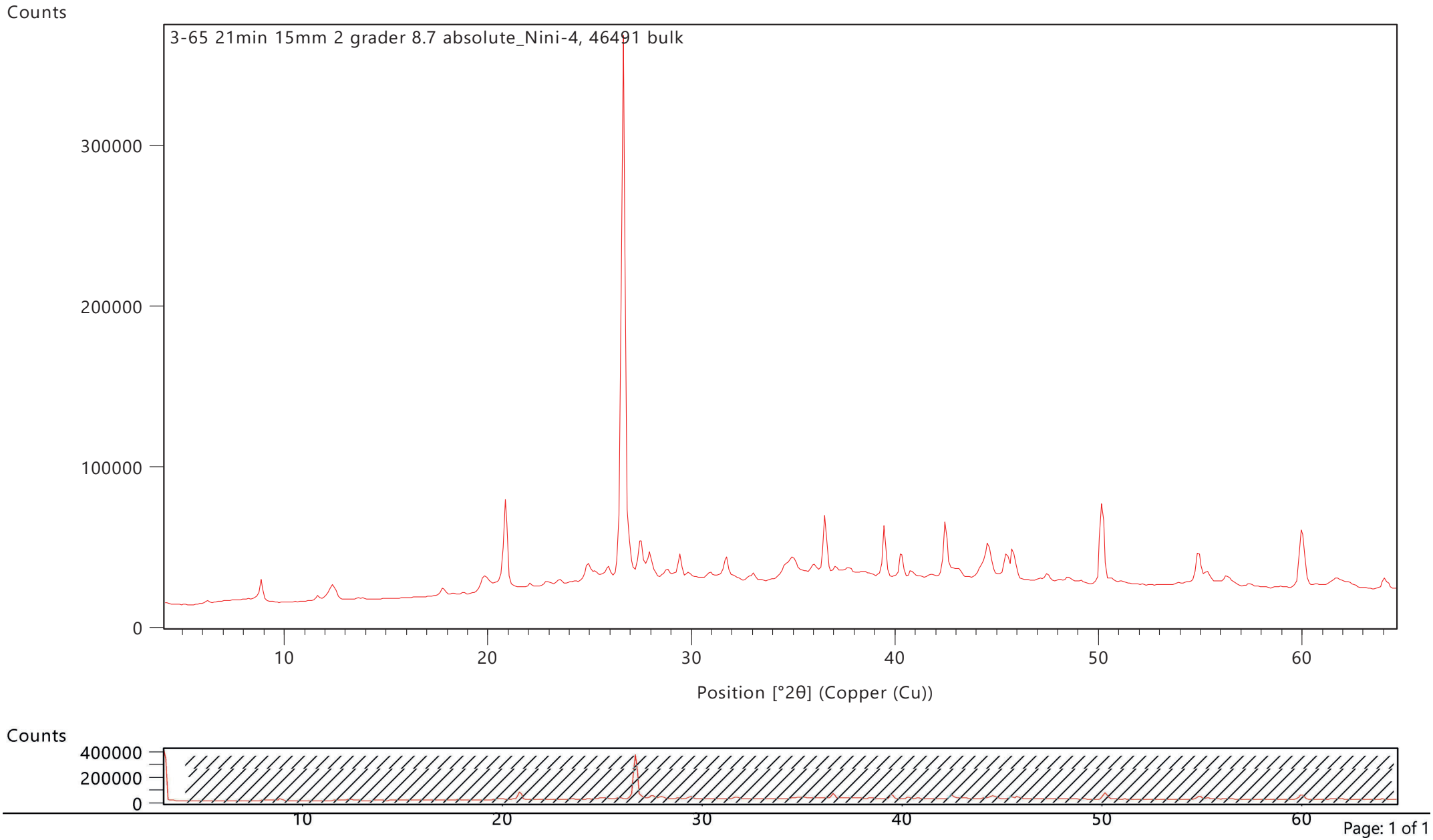
Counts
3-65 21min 15mm 2 grader 8.7 absolute_Nini-4, 46491 bulk
300000
200000
100000
0
10
20
30
40
50
60
Position [°2θ] (Copper (Cu))
Counts
400000
200000
0
10
20
30
40
50
60

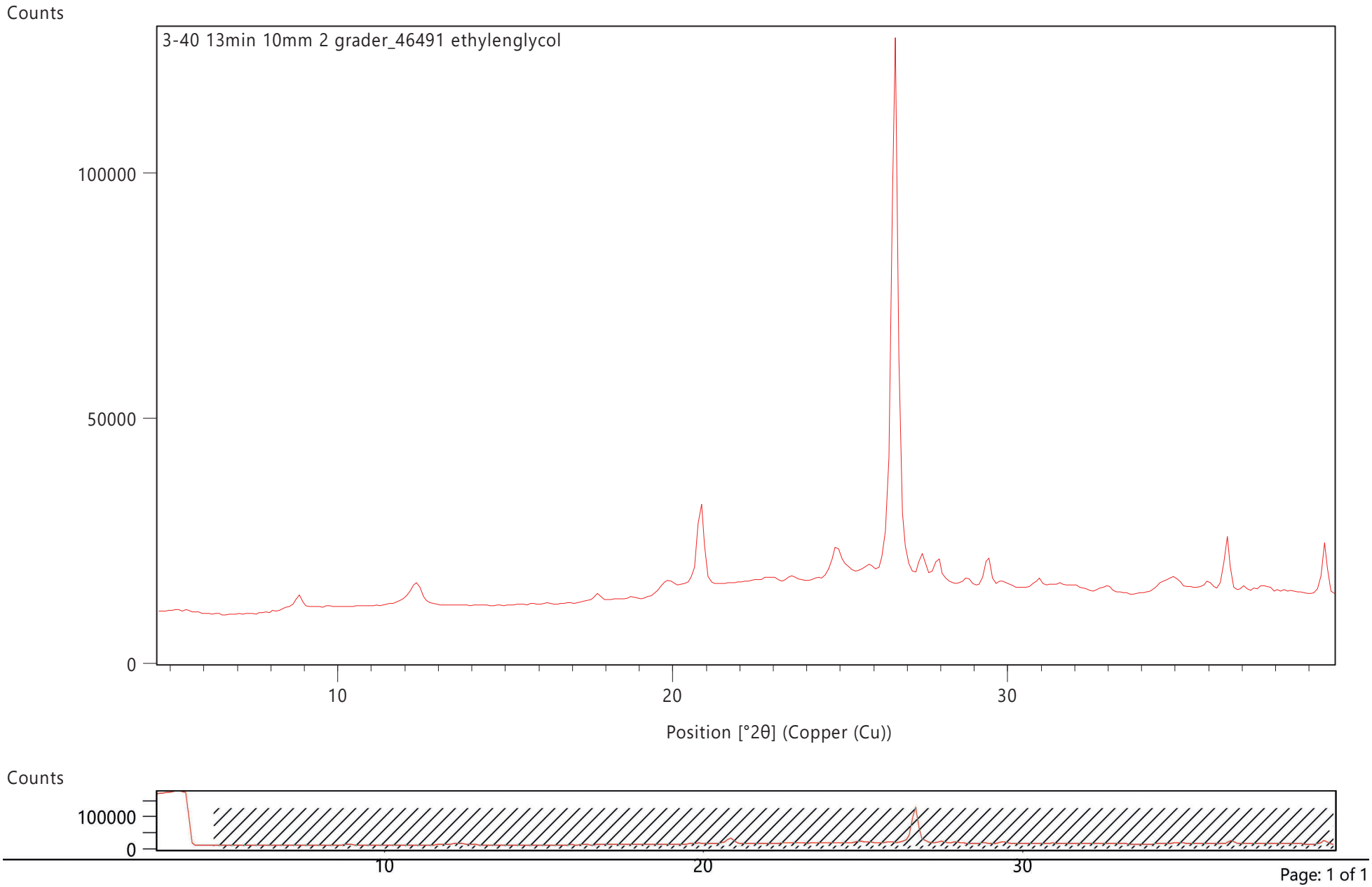
Counts
3-40 13min 10mm 2 grader_46491 ethylenglycol
100000
50000
0
10
20
30
Position [°2θ] (Copper (Cu))
Counts
100000
0
10
20
30

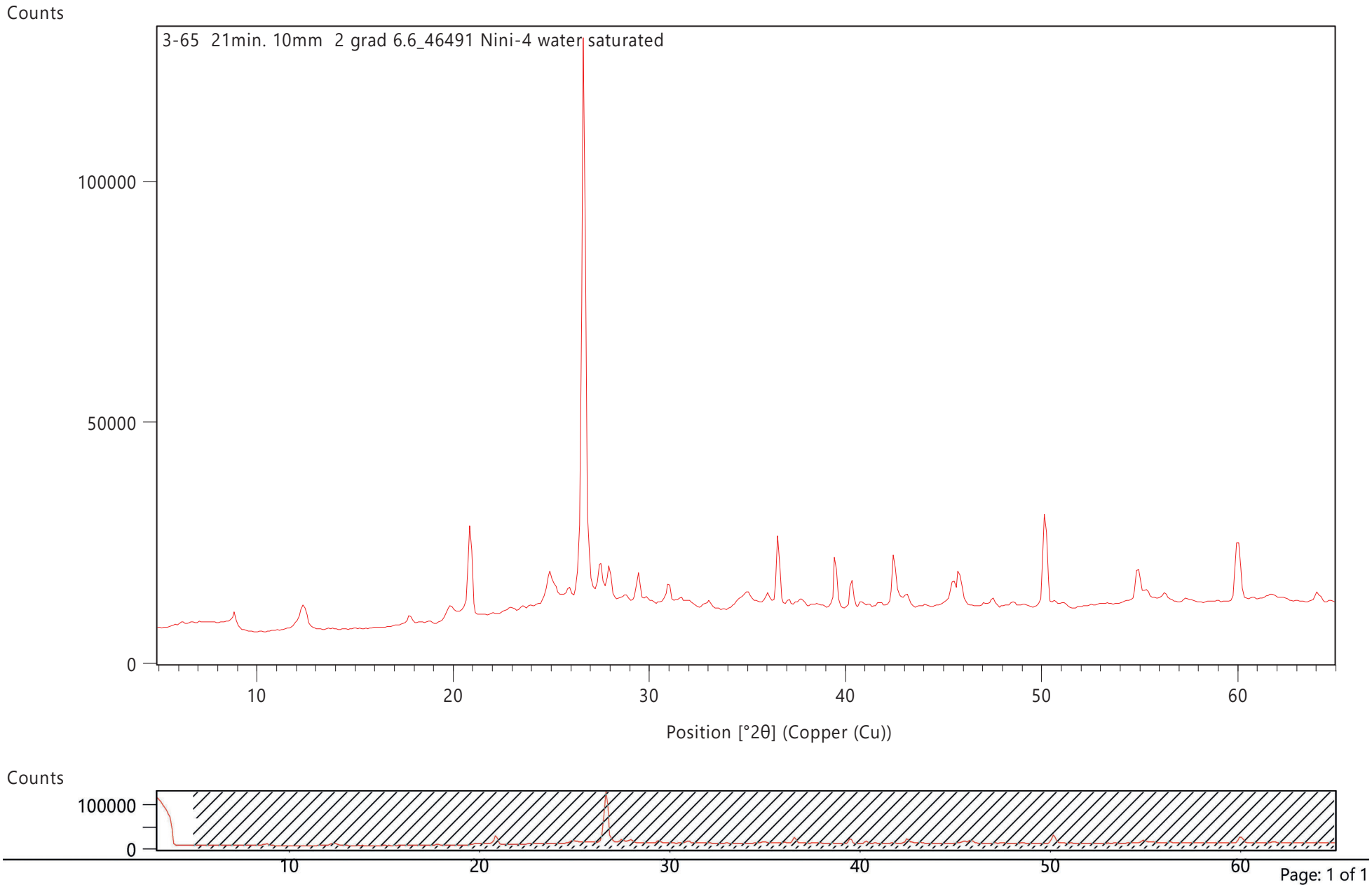
Counts
3-65 21min. 10mm 2 grad 6.6_46491 Nini-4 water saturated
100000
50000
0
10
20
30
40
50
60
Position [°2θ] (Copper (Cu))
Counts
100000
0
10
20
30
40
50
60

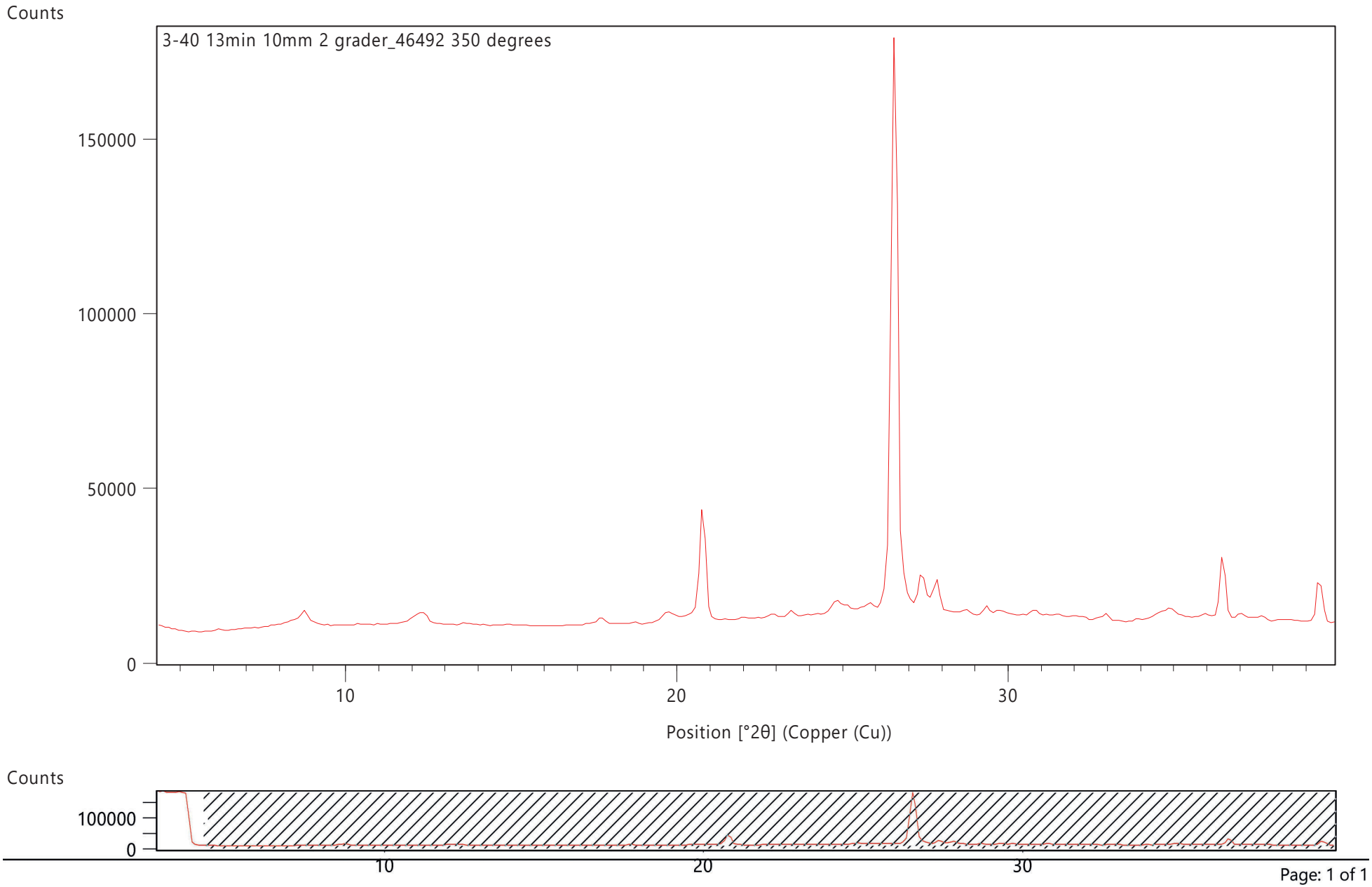
Counts
3-40 13min 10mm 2 grader_46492 350 degrees
150000
100000
50000
0
10
20
30
Position [°2θ] (Copper (Cu))
Counts
100000
0
10
20
30

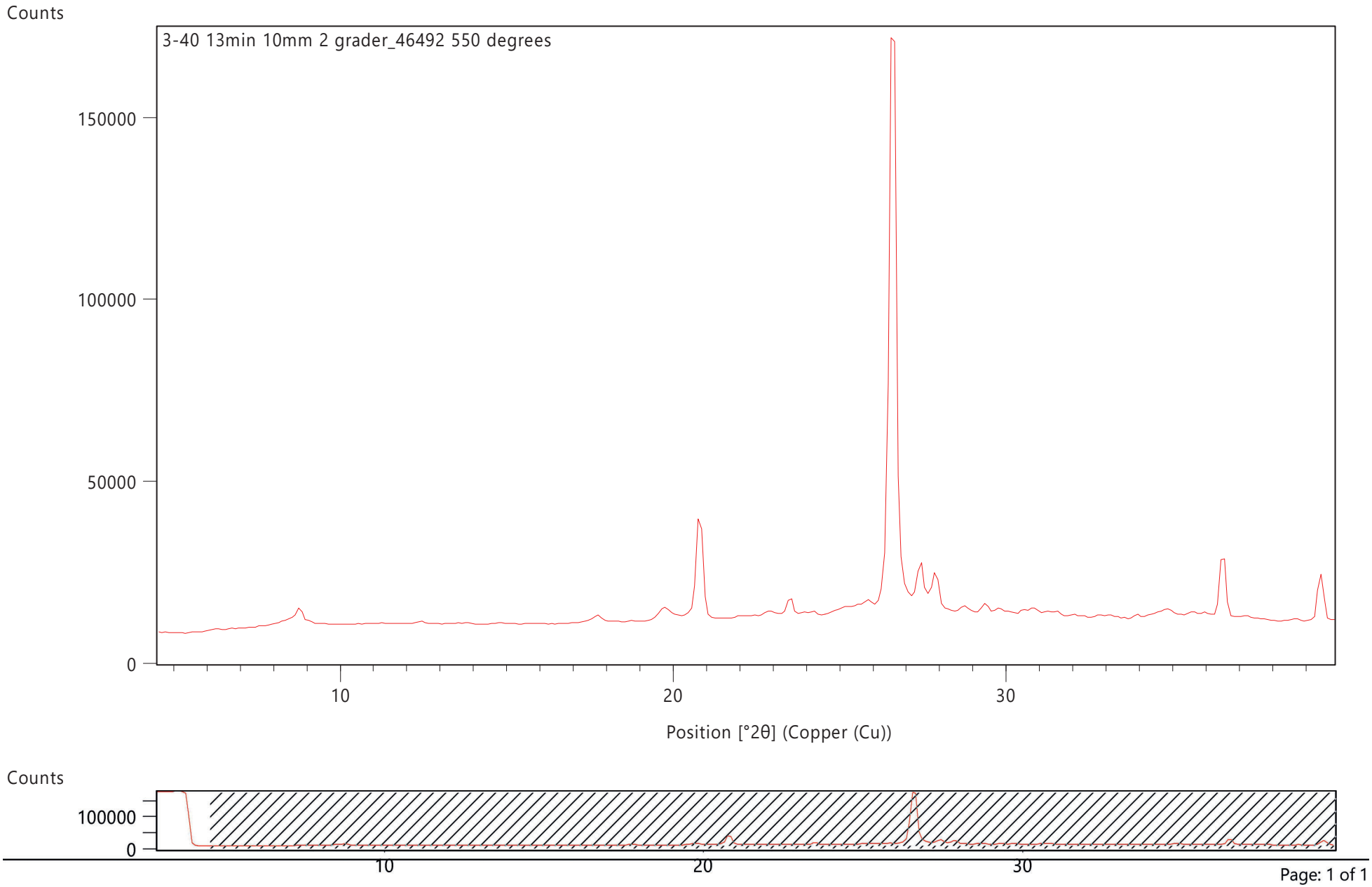
Counts
3-40 13min 10mm 2 grader_46492 550 degrees
150000
100000
50000
0
10
20
30
Position [°2θ] (Copper (Cu))
Counts
100000
0
10
20
30

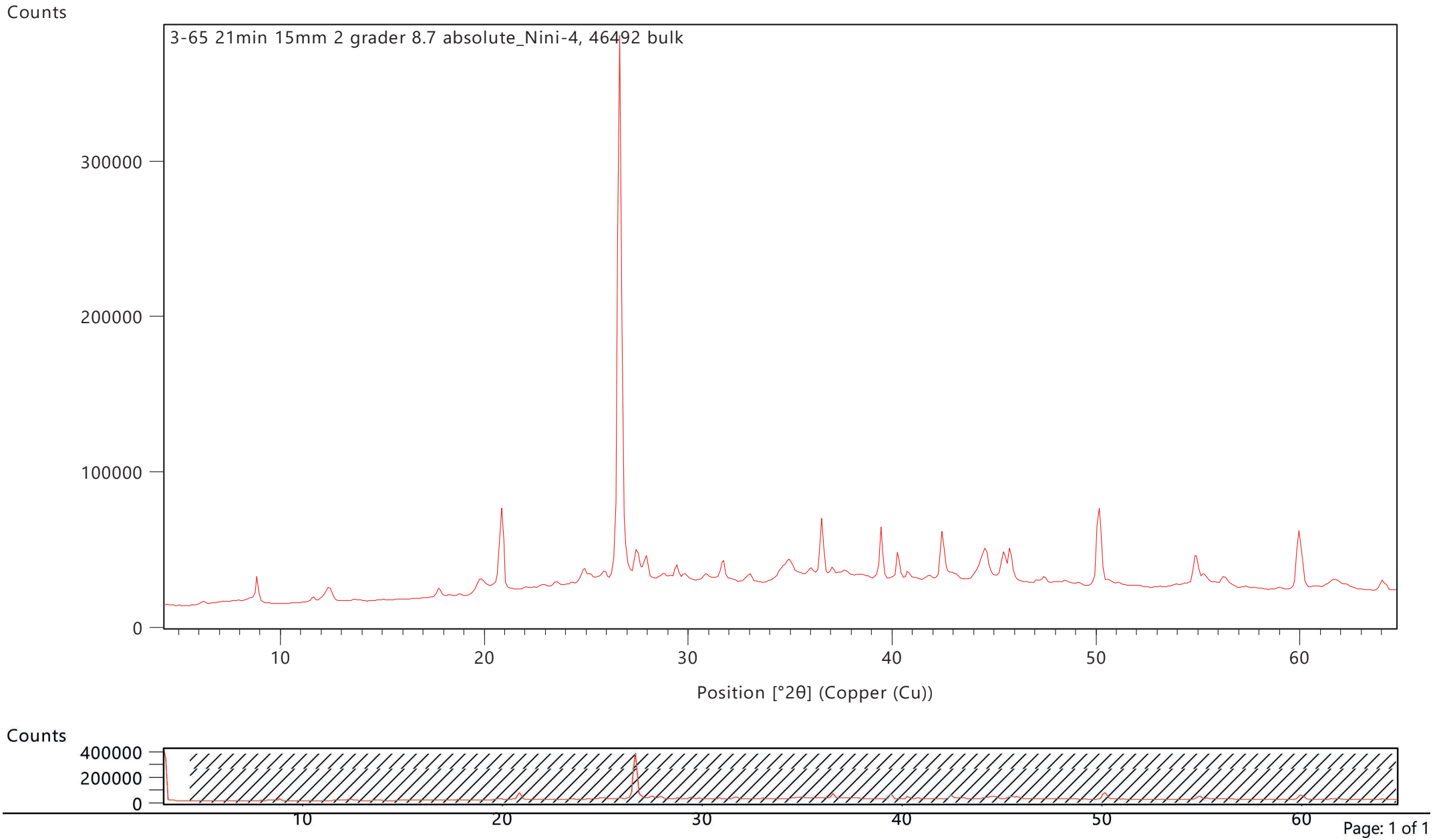
Counts
3-65 21min 15mm 2 grader 8.7 absolute_Nini-4, 46492 bulk
300000
200000
100000
0
10
20
30
40
50
60
Position [°2θ] (Copper (Cu))
Counts
400000
200000
0
10
20
30
40
50
60

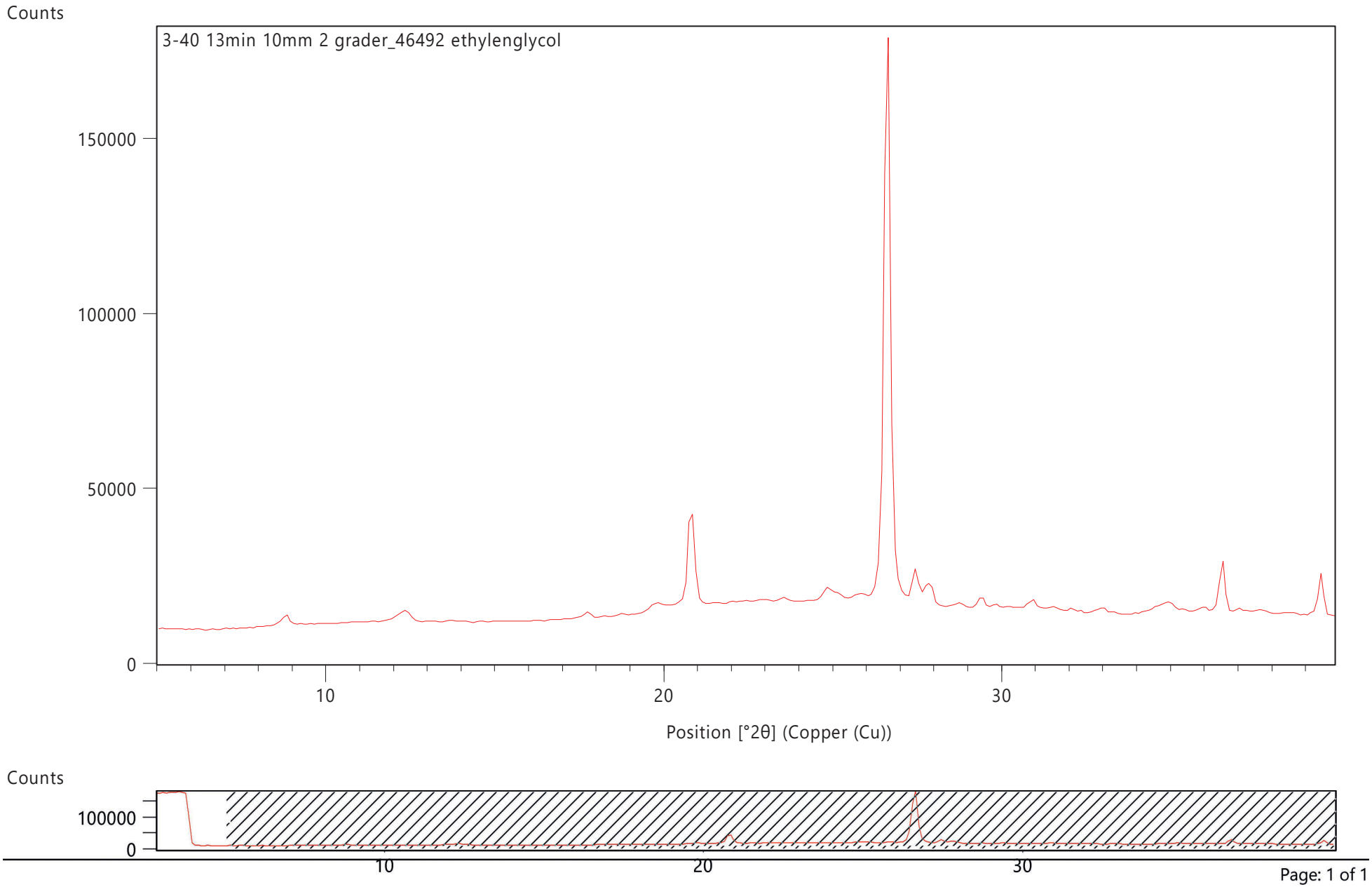
Counts
3-40 13min 10mm 2 grader_46492 ethylenglycol
150000
100000
50000
0
10
20
30
Position [°2θ] (Copper (Cu))
Counts
100000
0
10
20
30

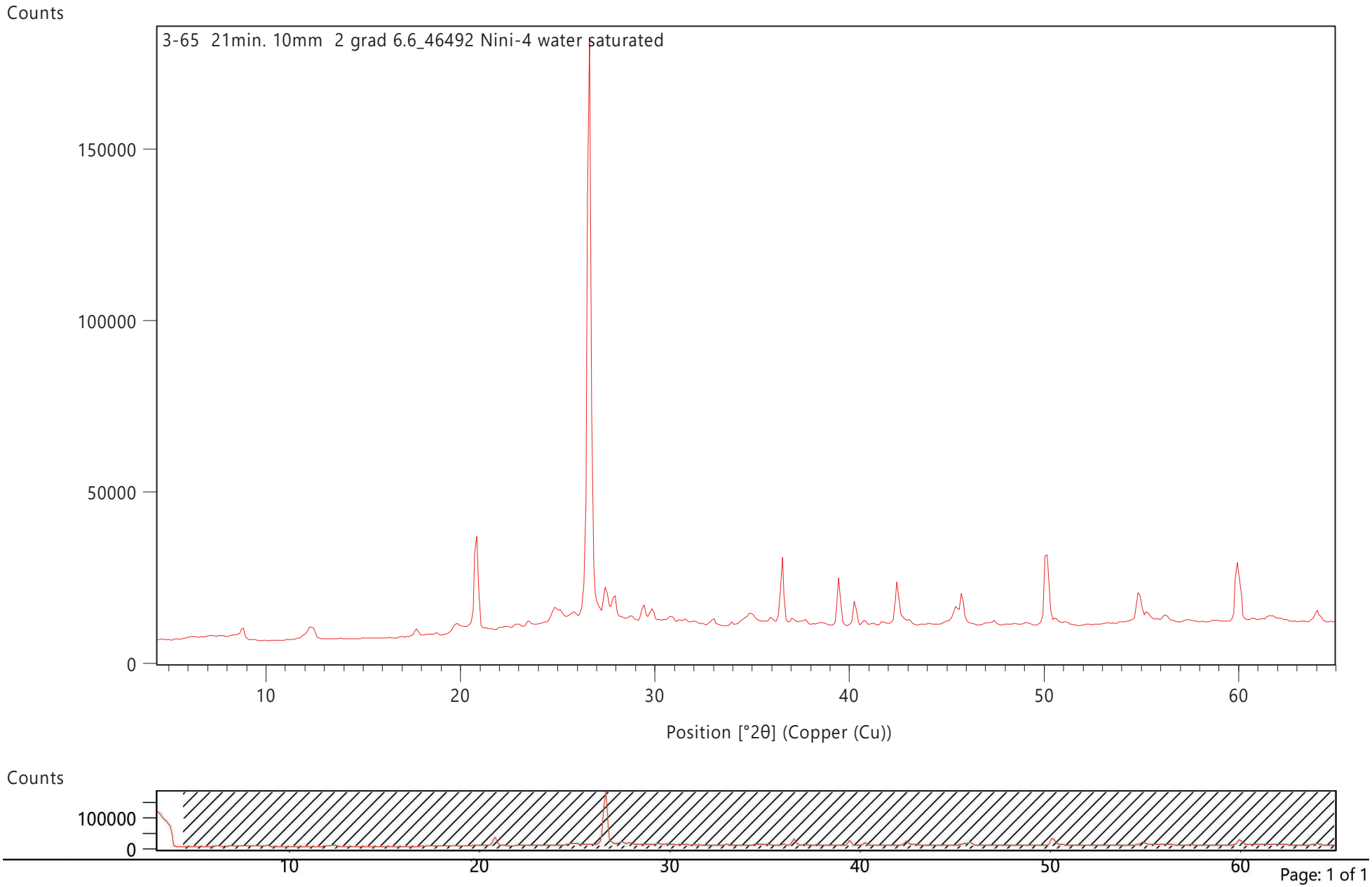
Counts
3-65 21min. 10mm 2 grad 6.6_46492 Nini-4 water saturated
150000
100000
50000
0
10
20
30
40
50
60
Position [°2θ] (Copper (Cu))
Counts
100000
0
10
20
30
40
50
60

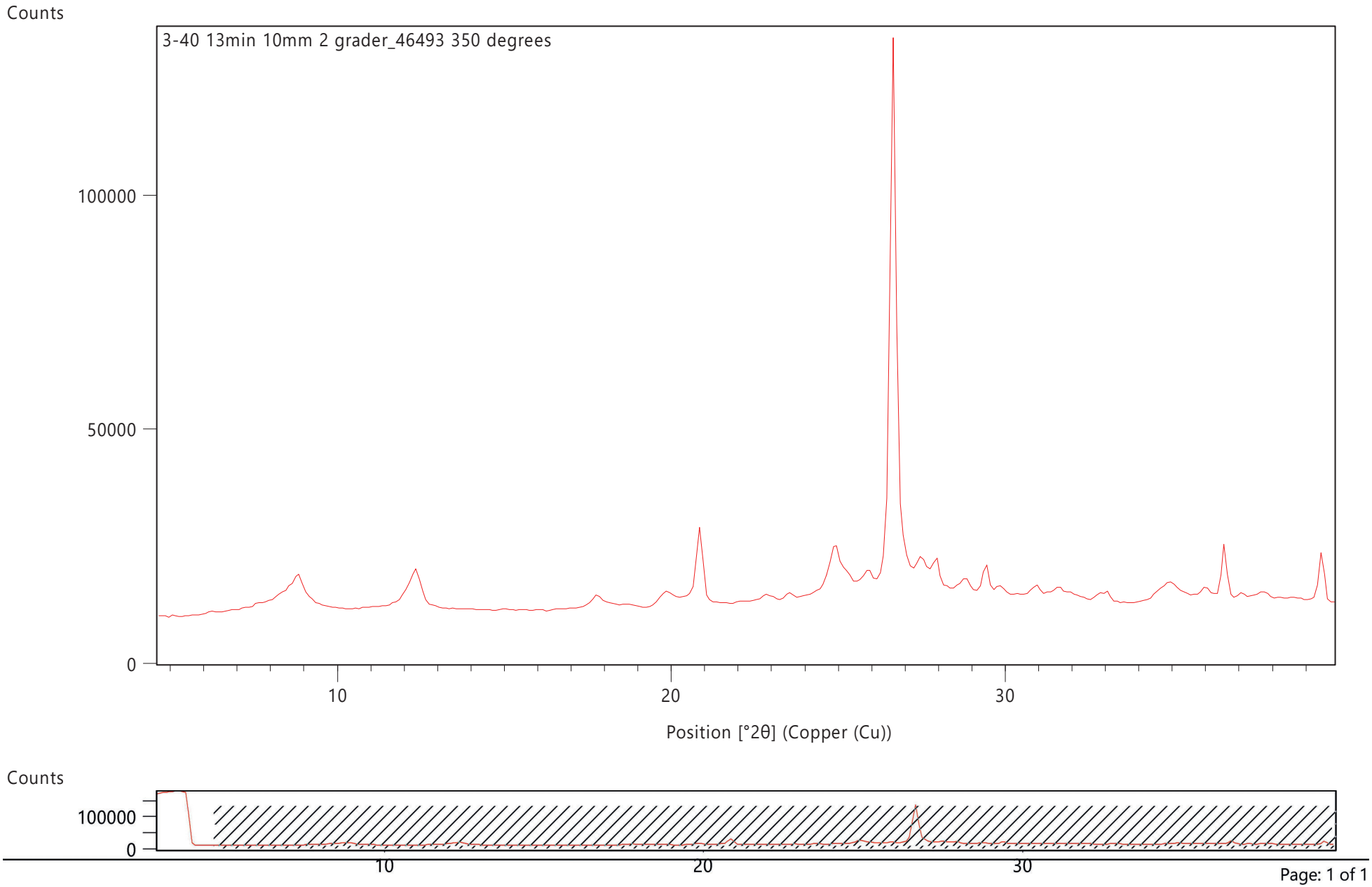
Counts
3-40 13min 10mm 2 grader_46493 350 degrees
100000
50000
0
10
20
30
Position [°2θ] (Copper (Cu))
Counts
100000
0
10
20
30

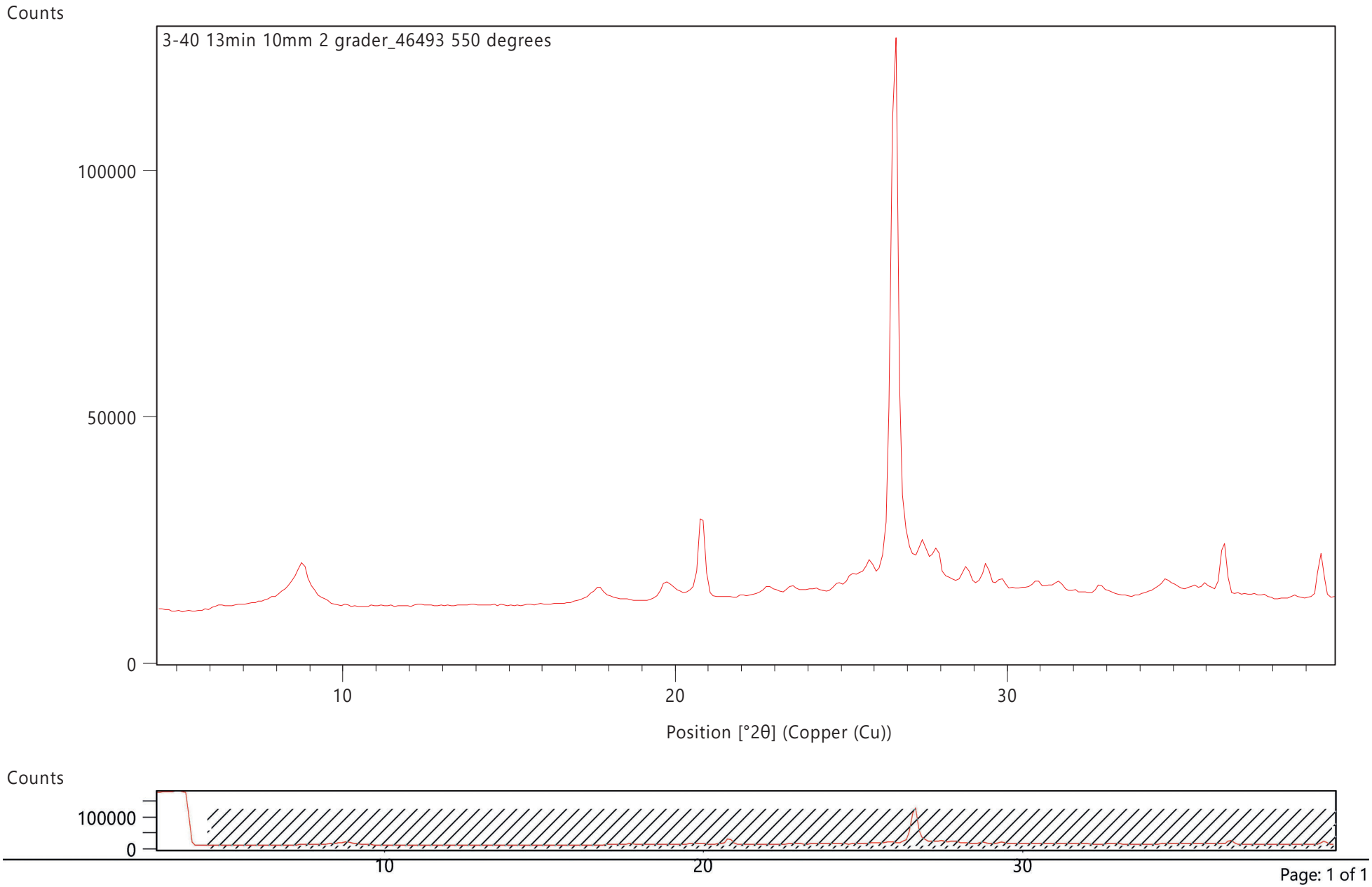
Counts
3-40 13min 10mm 2 grader_46493 550 degrees
100000
50000
0
10
20
30
Position [°2θ] (Copper (Cu))
Counts
100000
0
10
20
30

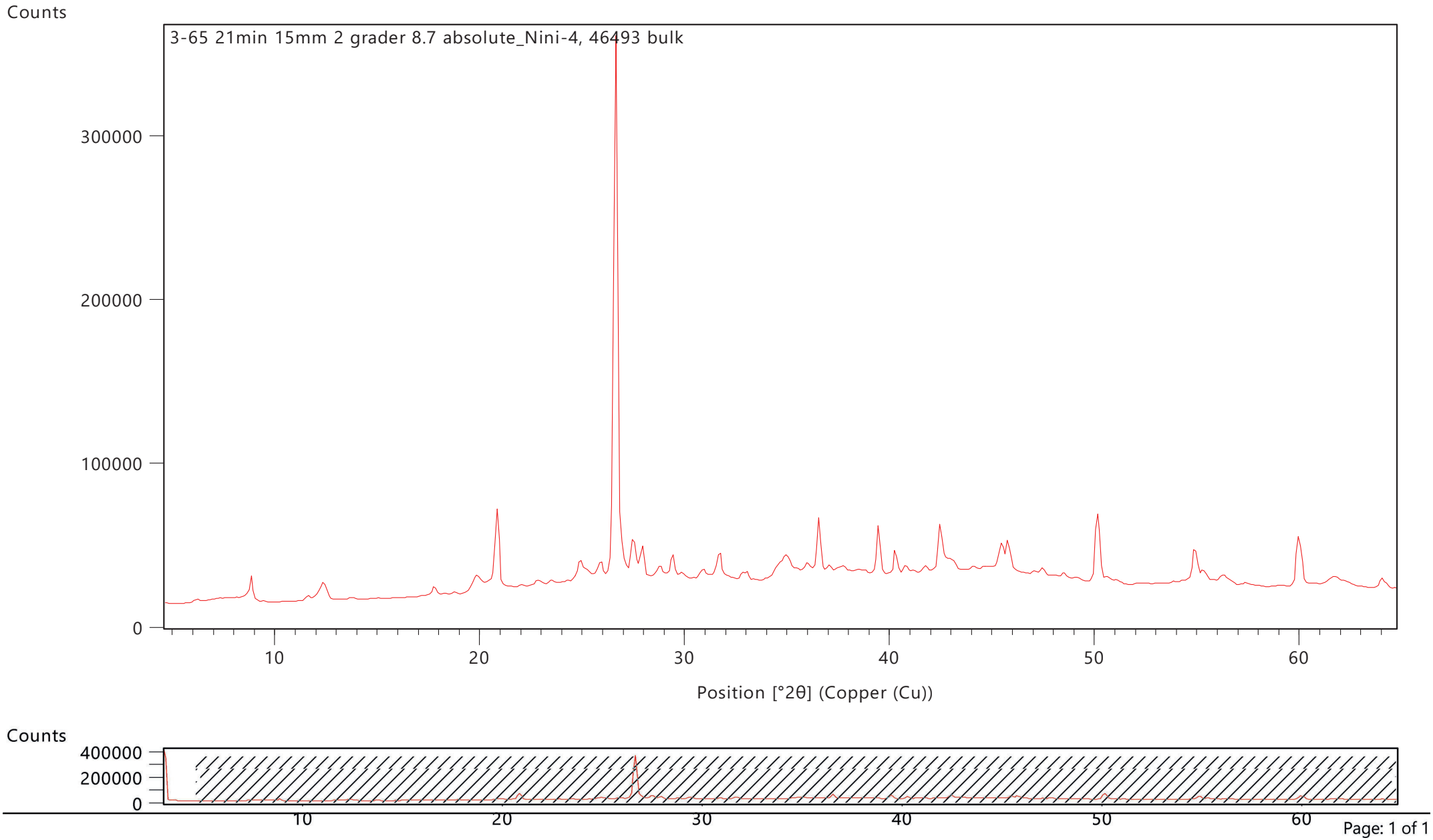
Counts
3-65 21min 15mm 2 grader 8.7 absolute_Nini-4, 46493 bulk
300000
200000
100000
0
10
20
30
40
50
60
Position [°2θ] (Copper (Cu))
Counts
400000
200000
0
10
20
30
40
50
60

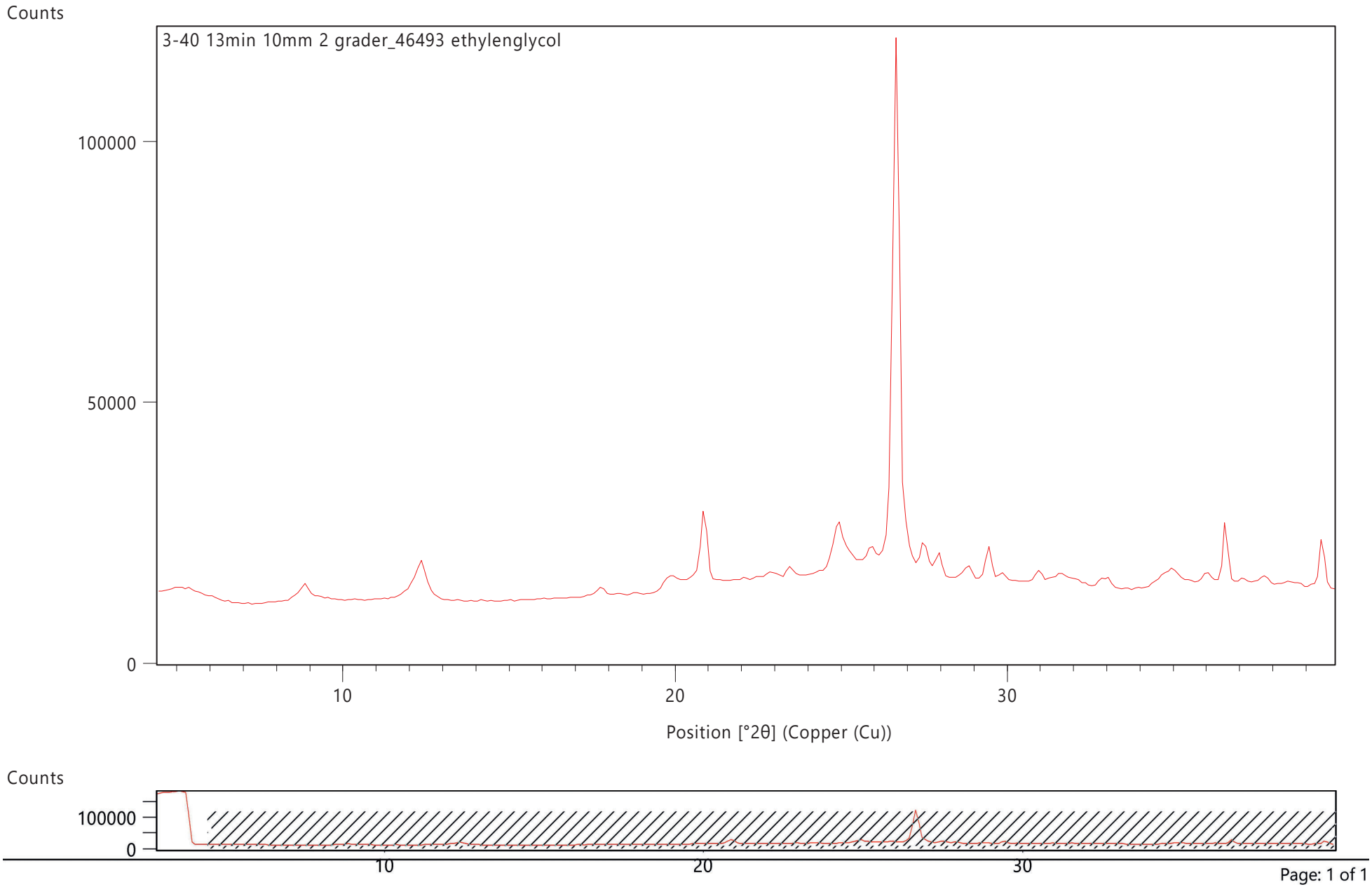
Counts
3-40 13min 10mm 2 grader_46493 ethylenglycol
100000
50000
0
10
20
30
Position [°2θ] (Copper (Cu))
Counts
100000
0
10
20
30

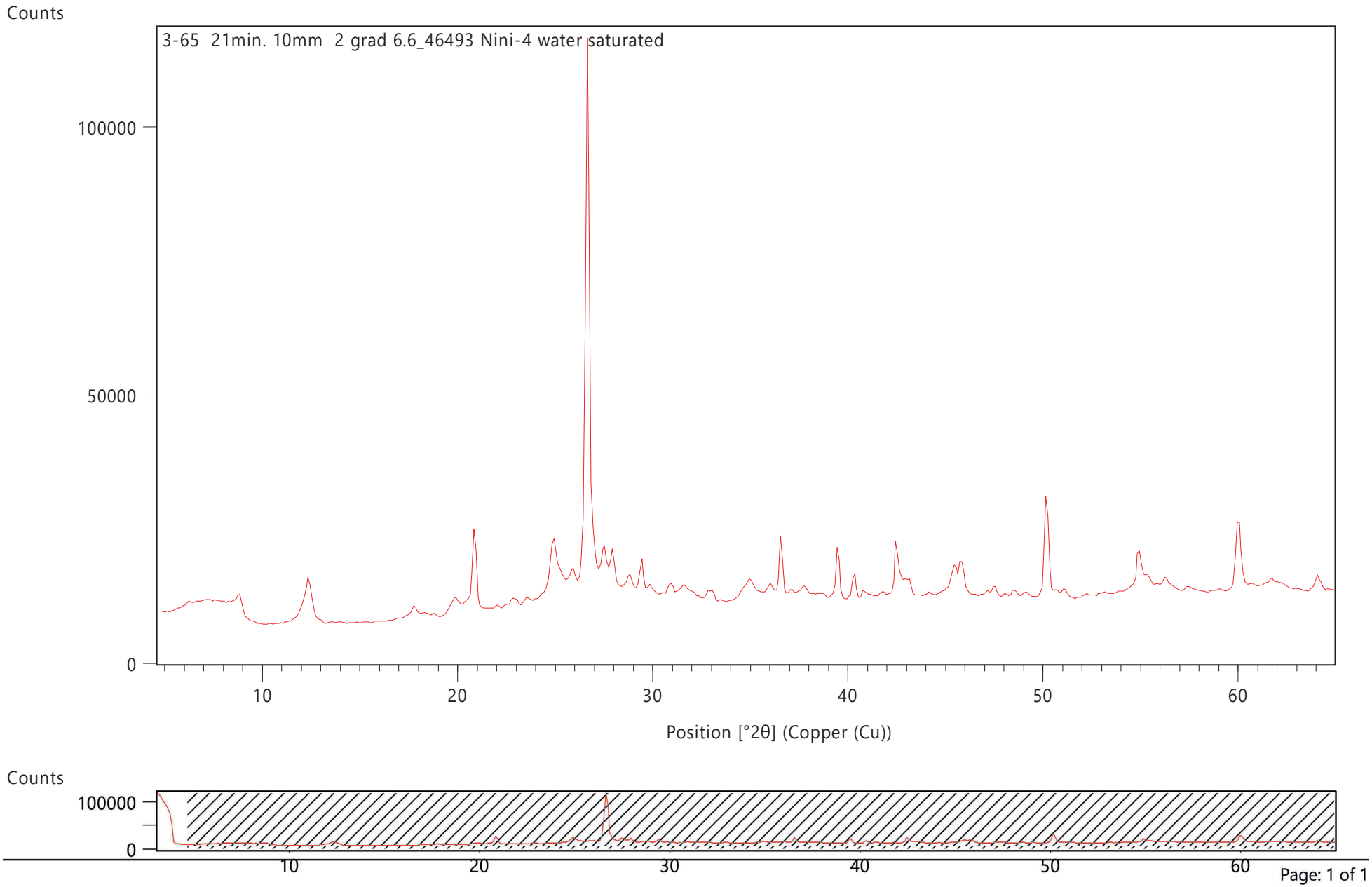
Counts
3-65 21min. 10mm 2 grad 6.6_46493 Nini-4 water saturated
100000
50000
0
10
20
30
40
50
60
Position [°2θ] (Copper (Cu))
Counts
100000
0
10
20
30
40
50
60

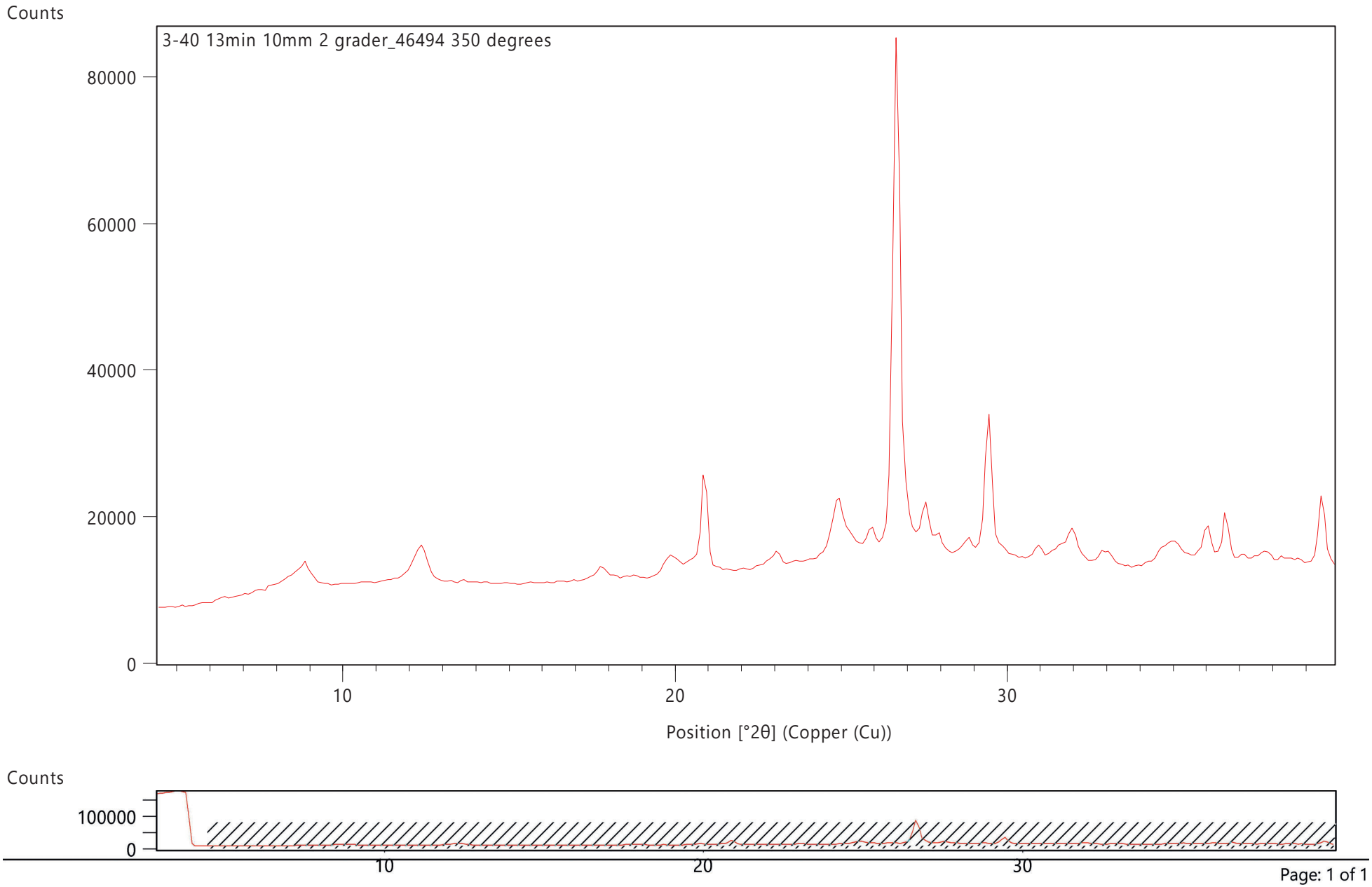
Counts
3-40 13min 10mm 2 grader_46494 350 degrees
80000
60000
40000
20000
0
10
20
30
Position [°2θ] (Copper (Cu))
Counts
100000
0
10
20
30

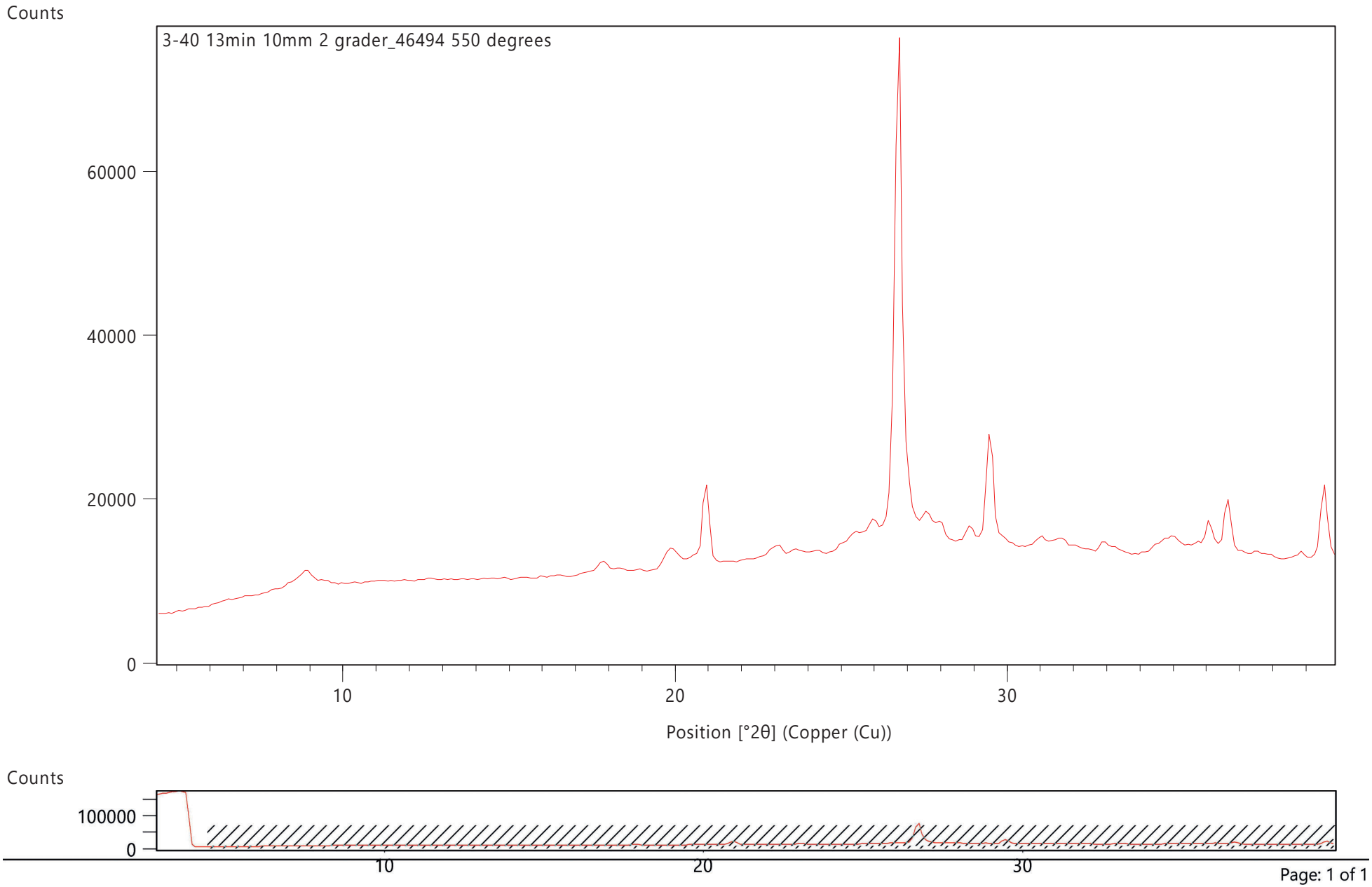
Counts
3-40 13min 10mm 2 grader_46494 550 degrees
60000
40000
20000
0
10
20
30
Position [°2θ] (Copper (Cu))
Counts
100000
0
10
20
30

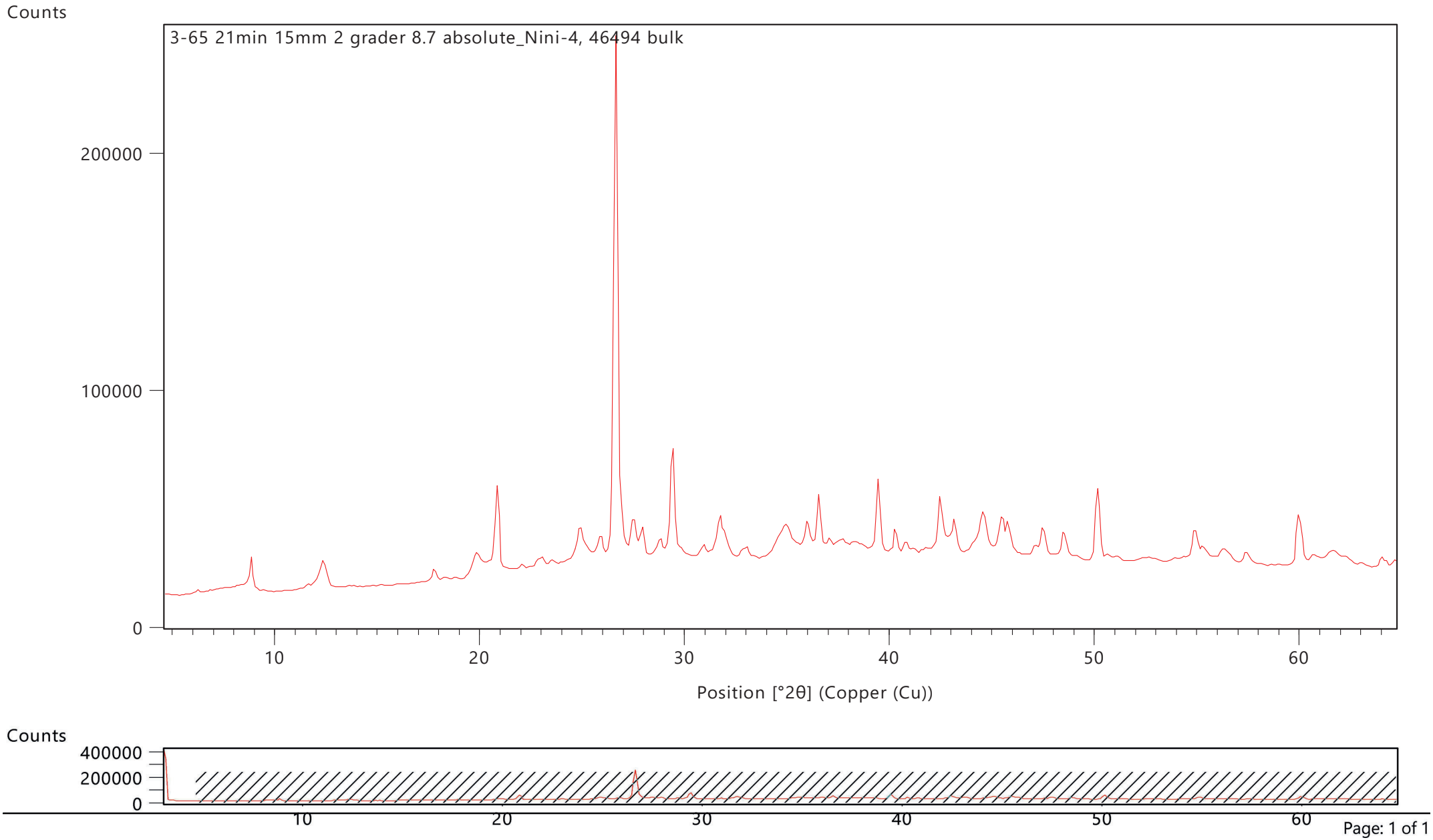
Counts
3-65 21min 15mm 2 grader 8.7 absolute_Nini-4, 46494 bulk
200000
100000
0
10
20
30
40
50
60
Position [°2θ] (Copper (Cu))
Counts
400000
200000
0
10
20
30
40
50
60

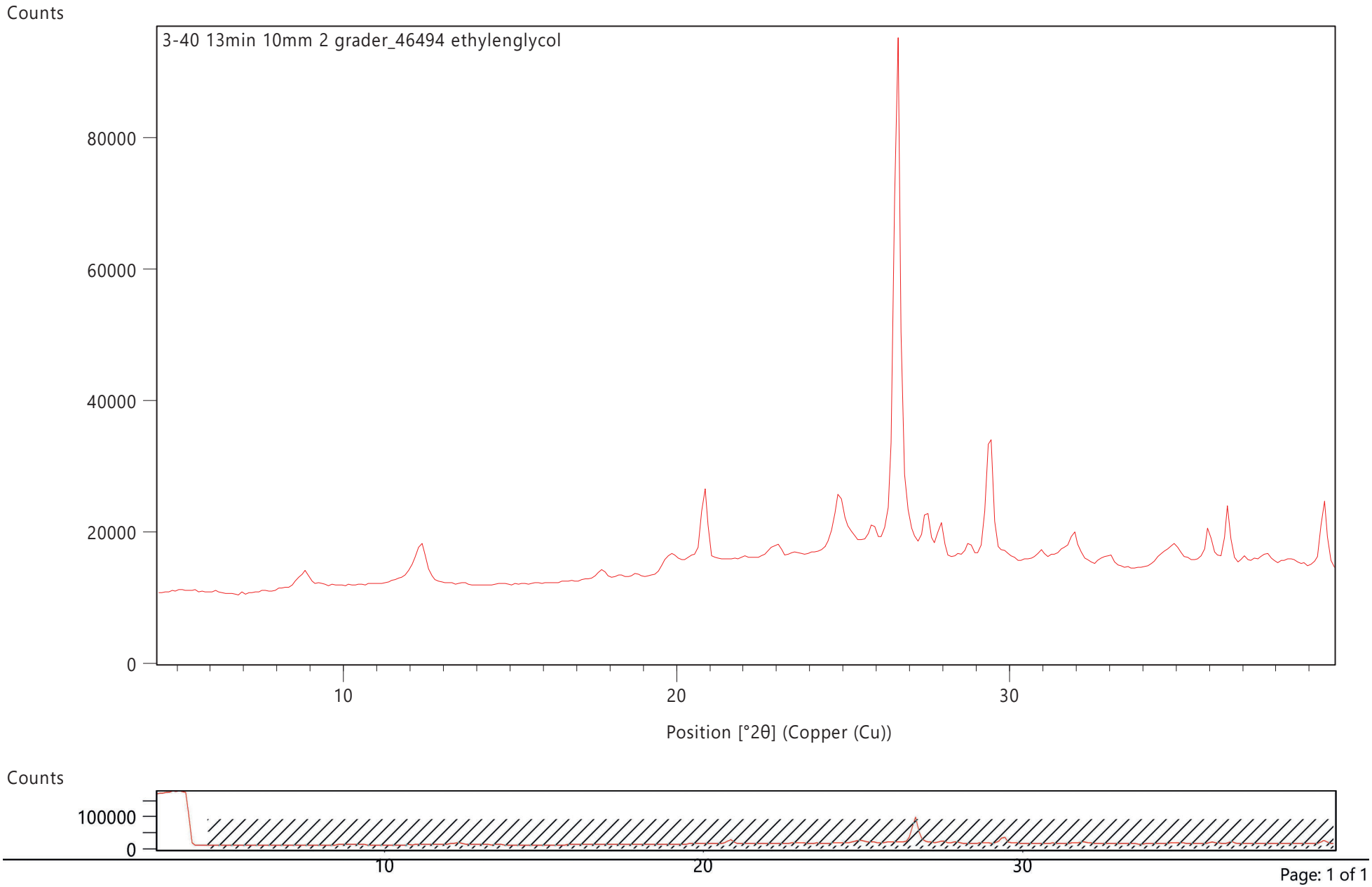
Counts
3-40 13min 10mm 2 grader_46494 ethylenglycol
80000
60000
40000
20000
0
10
20
30
Position [°2θ] (Copper (Cu))
Counts
100000
0
10
20
30

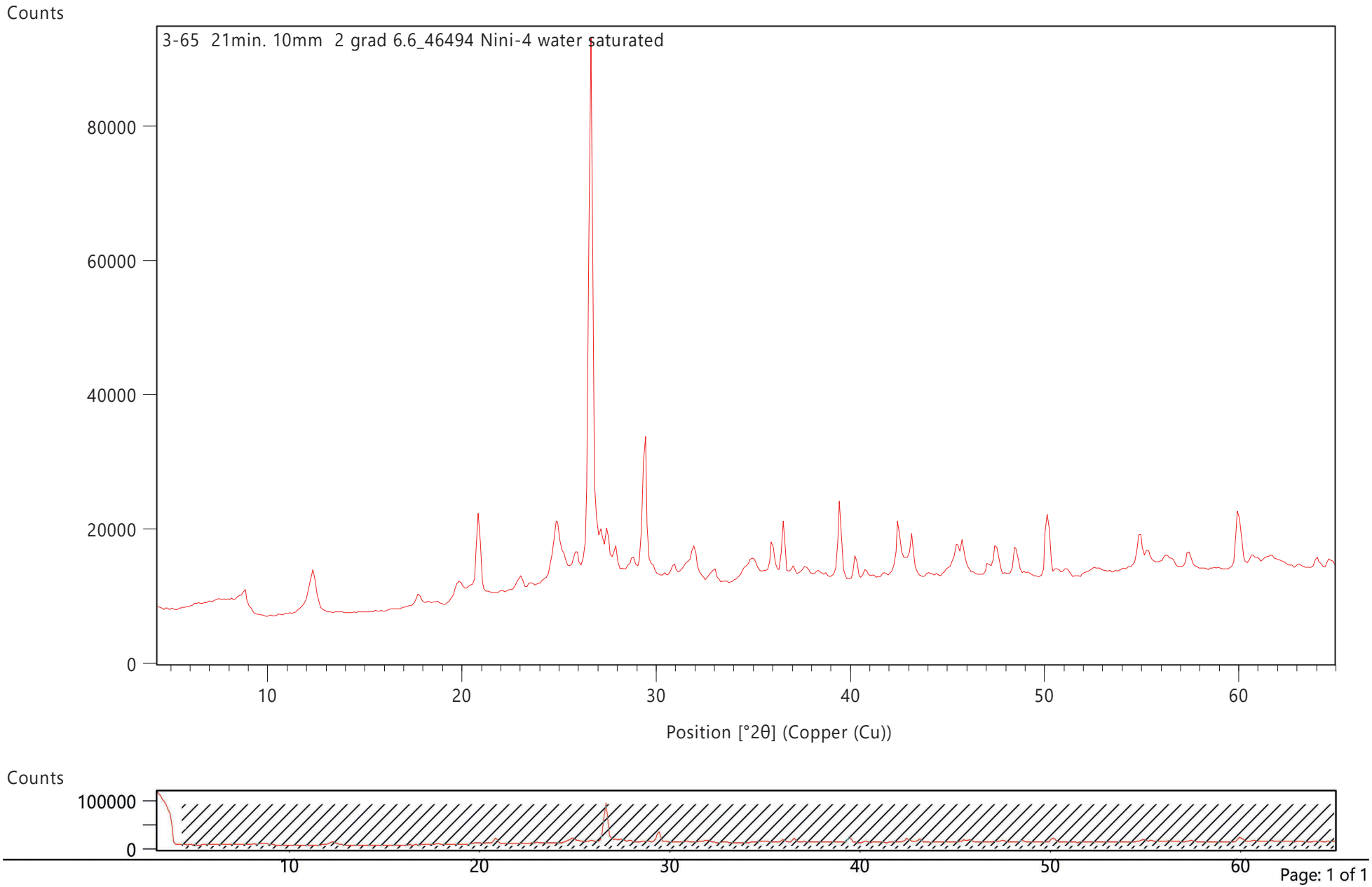
Counts
3-65 21min. 10mm 2 grad 6.6_46494 Nini-4 water saturated
80000
60000
40000
20000
0
10
20
30
40
50
60
Position [°2θ] (Copper (Cu))
Counts
100000
0
10
20
30
40
50
60

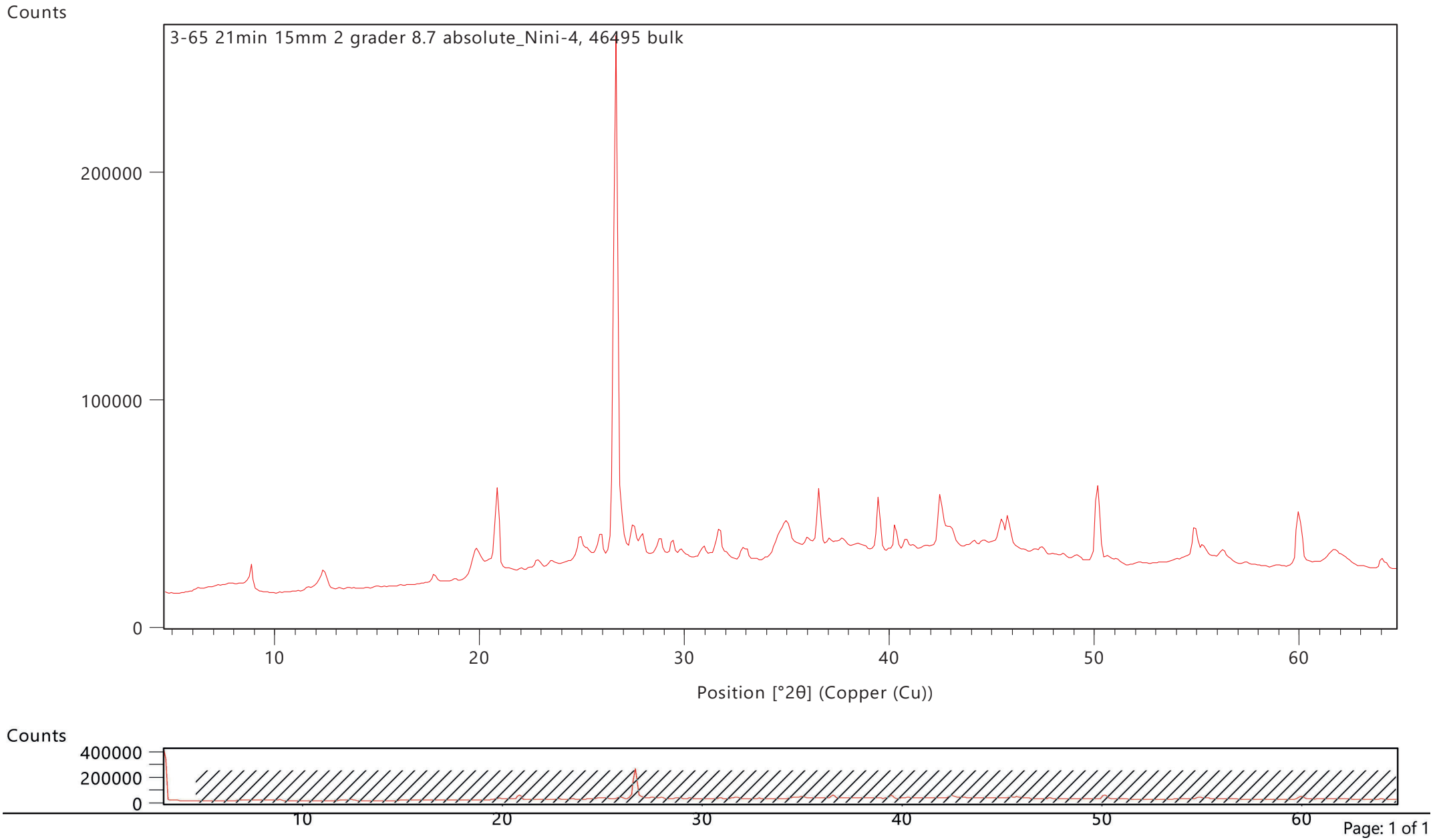
Counts
3-65 21min 15mm 2 grader 8.7 absolute_Nini-4, 46495 bulk
200000
100000
0
10
20
30
40
50
60
Position [°2θ] (Copper (Cu))
Counts
400000
200000
0
10
20
30
40
50
60

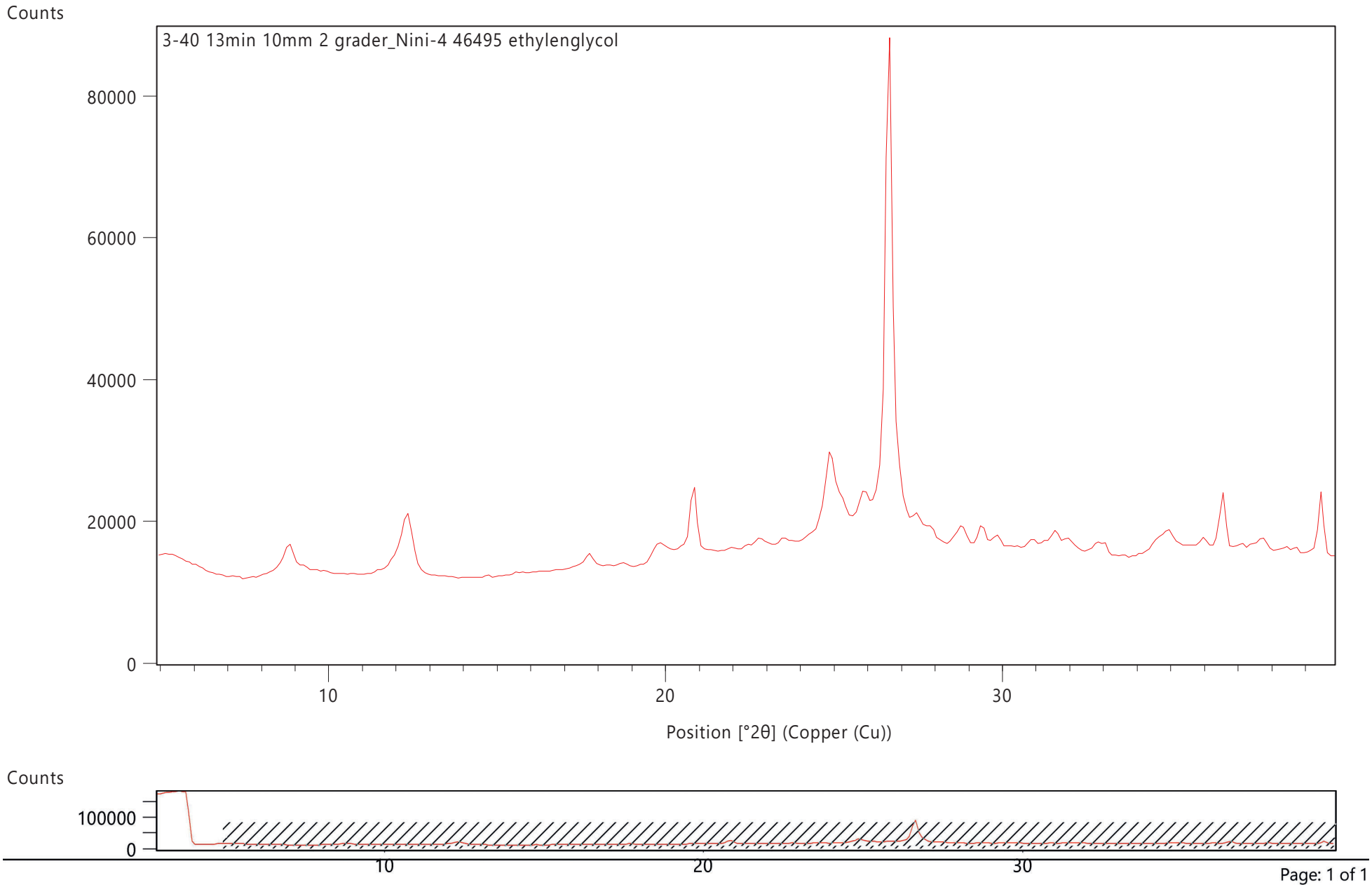
Counts
3-40 13min 10mm 2 grader_Nini-4 46495 ethylenglycol
80000
60000
40000
20000
0
10
20
30
Position [°2θ] (Copper (Cu))
Counts
100000
0
10
20
30

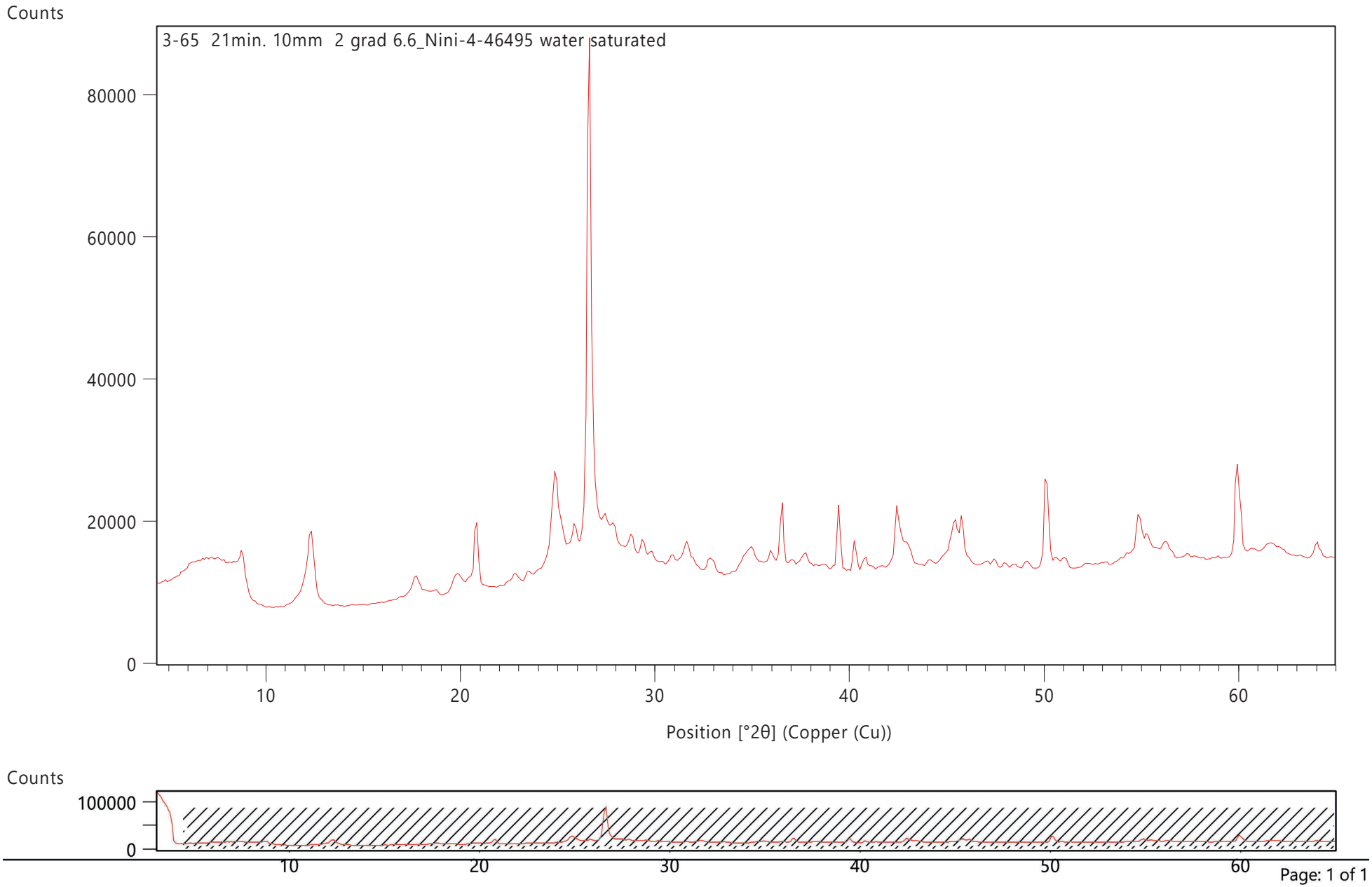
Counts
3-65 21min. 10mm 2 grad 6.6_Nini-4-46495 water saturated
80000
60000
40000
20000
0
10
20
30
40
50
60
Position [°2θ] (Copper (Cu))
Counts
100000
0
10
20
30
40
50
60

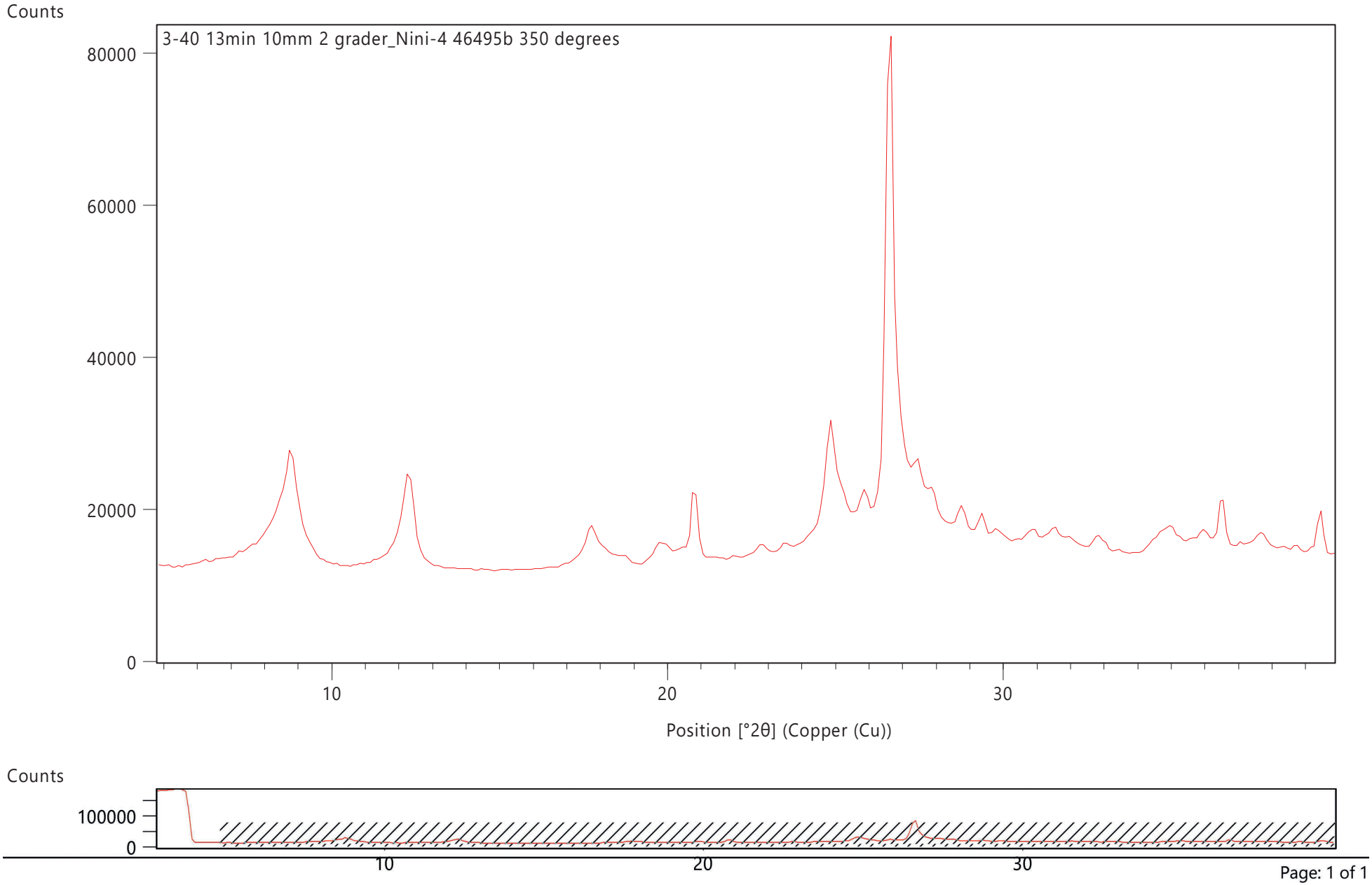
Counts
3-40 13min 10mm 2 grader_Nini-4 46495b 350 degrees
80000
60000
40000
20000
0
10
20
30
Position [°2θ] (Copper (Cu))
Counts
100000
0
10
20
30

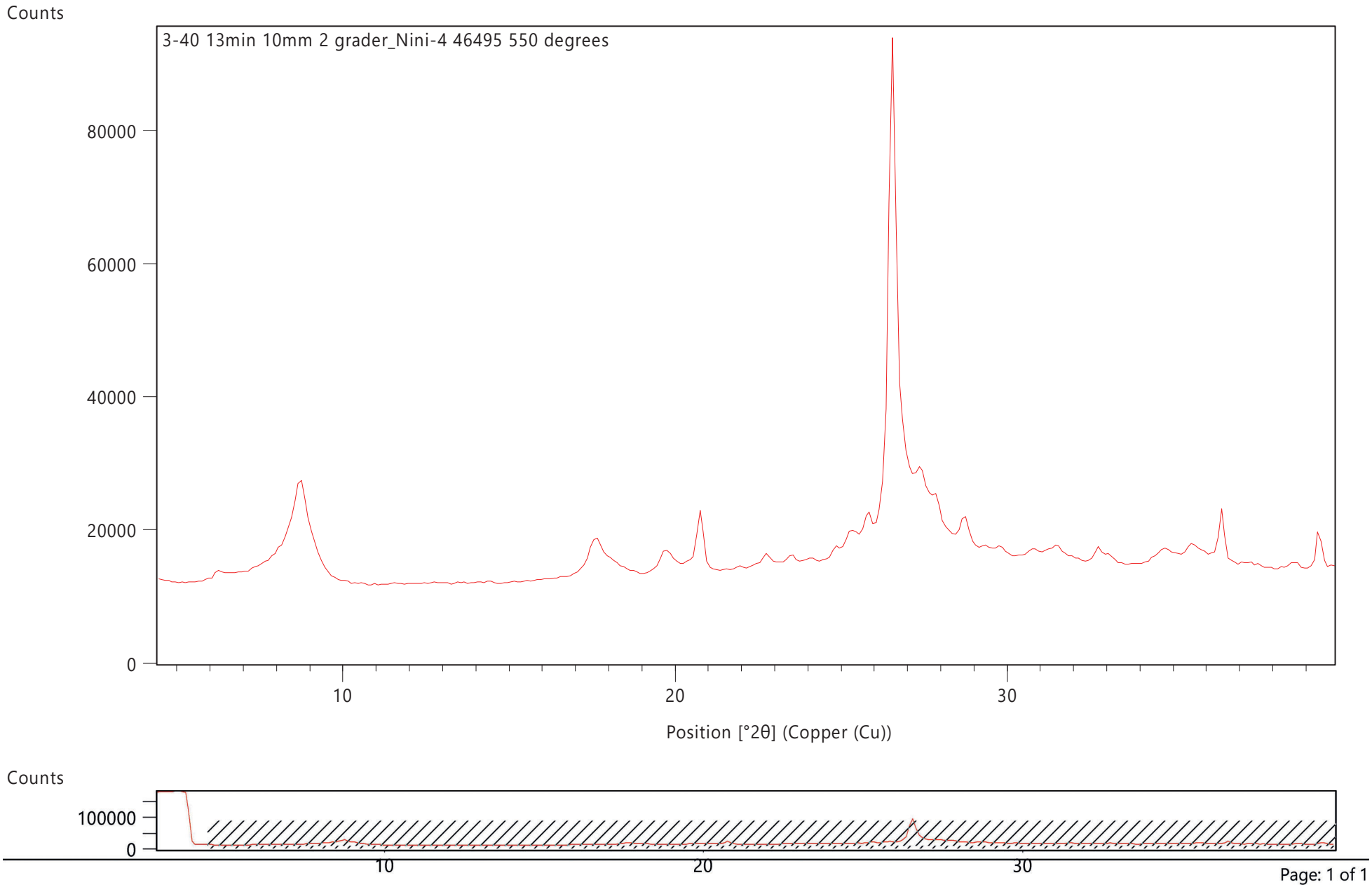
Counts
3-40 13min 10mm 2 grader_Nini-4 46495 550 degrees
80000
60000
40000
20000
0
10
20
30
Position [°2θ] (Copper (Cu))
Counts
100000
0
10
20
30

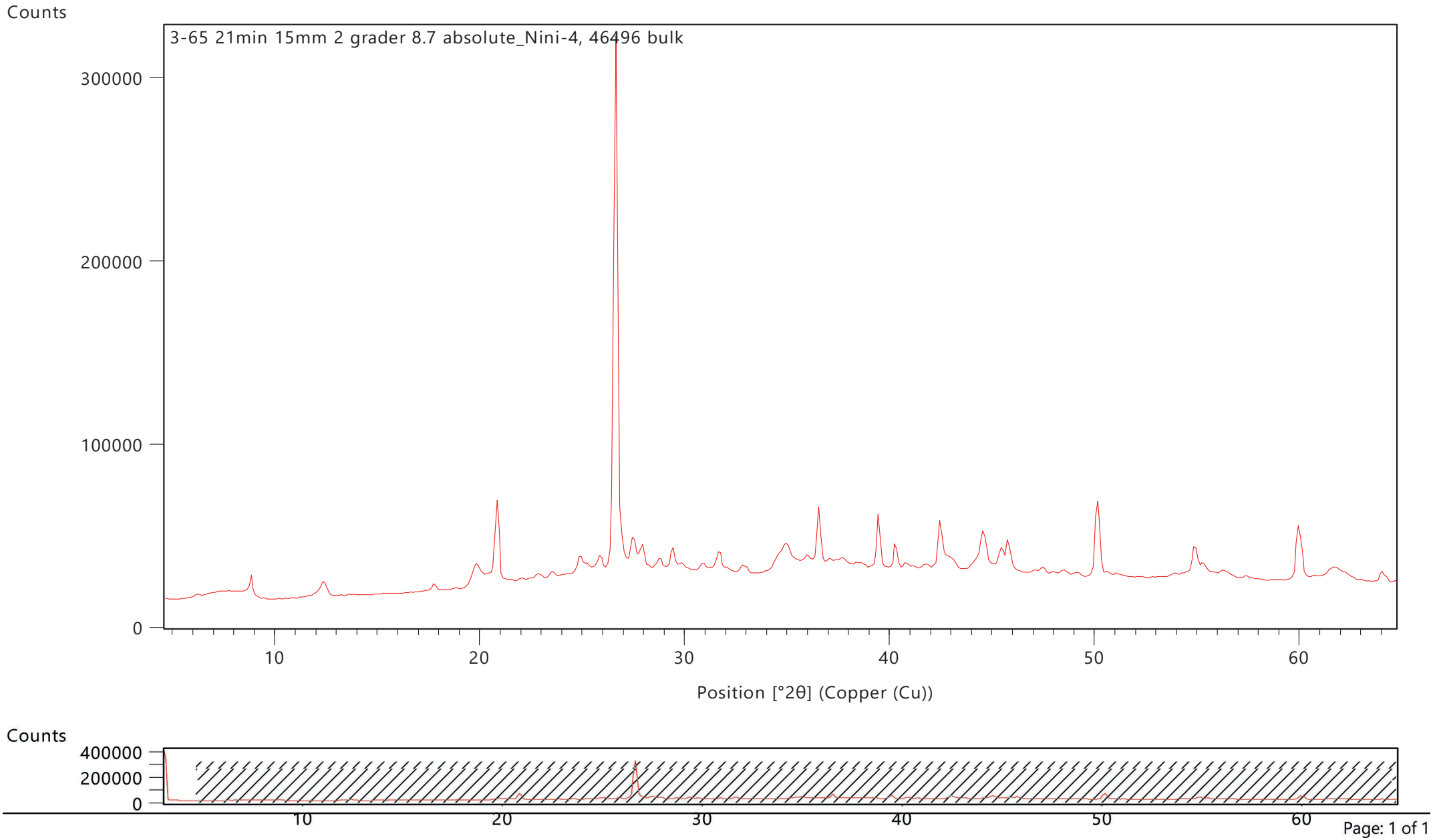
Counts
3-65 21min 15mm 2 grader 8.7 absolute_Nini-4, 46496 bulk
300000
200000
100000
0
10
20
30
40
50
60
Position [°2θ] (Copper (Cu))
Counts
400000
200000
0
10
20
30
40
50
60

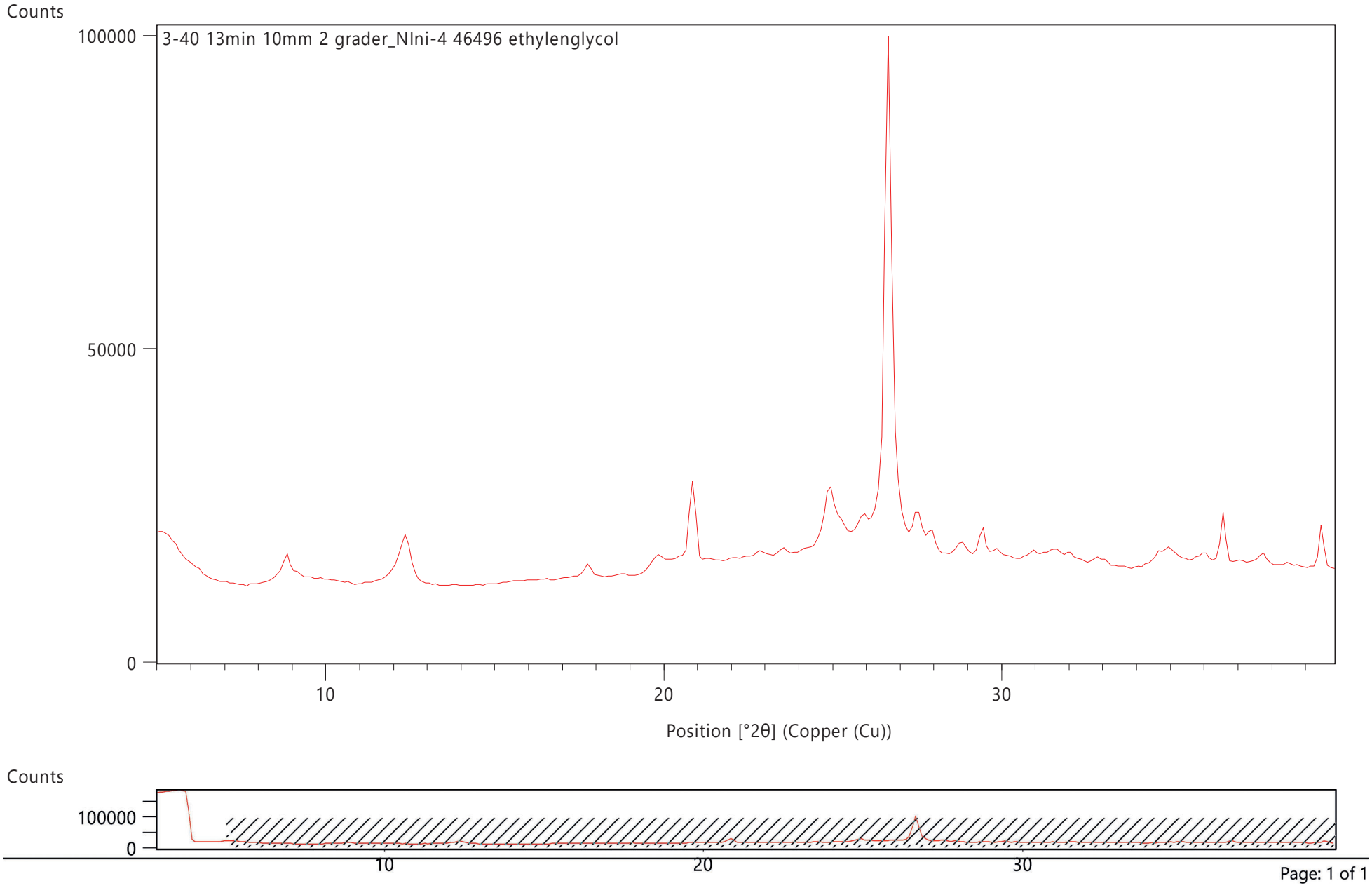
Counts
3-40 13min 10mm 2 grader_NIni-4 46496 ethylenglycol
100000
50000
0
10
20
30
Position [°2θ] (Copper (Cu))
Counts
100000
0
10
20
30

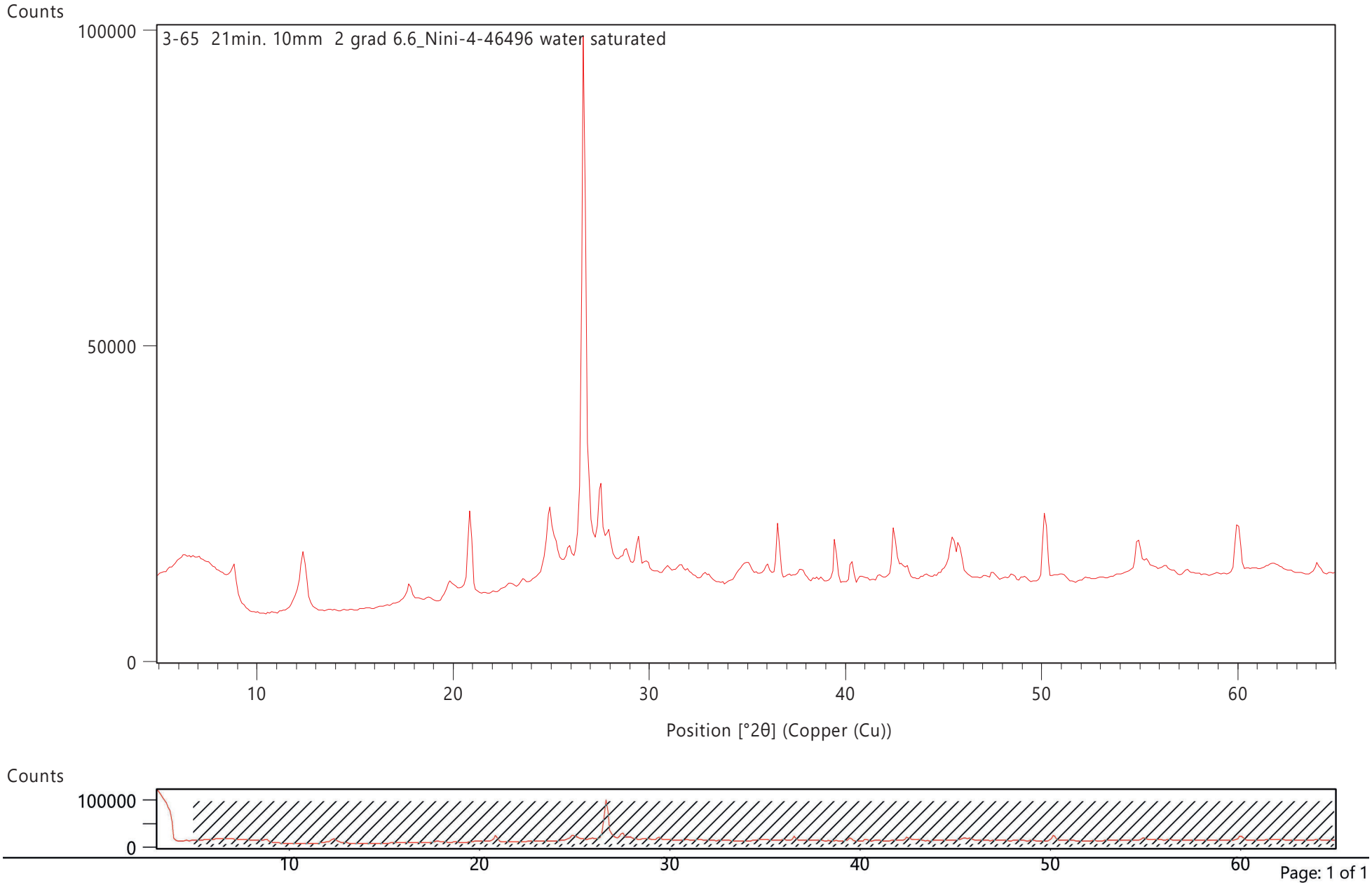
Counts
100000
50000
0
3-65 21min. 10mm 2 grad 6.6_Nini-4-46496 water saturated
10
20
30
40
50
60
Position [°2θ] (Copper (Cu))
Counts
100000
0
10
20
30
40
50
60

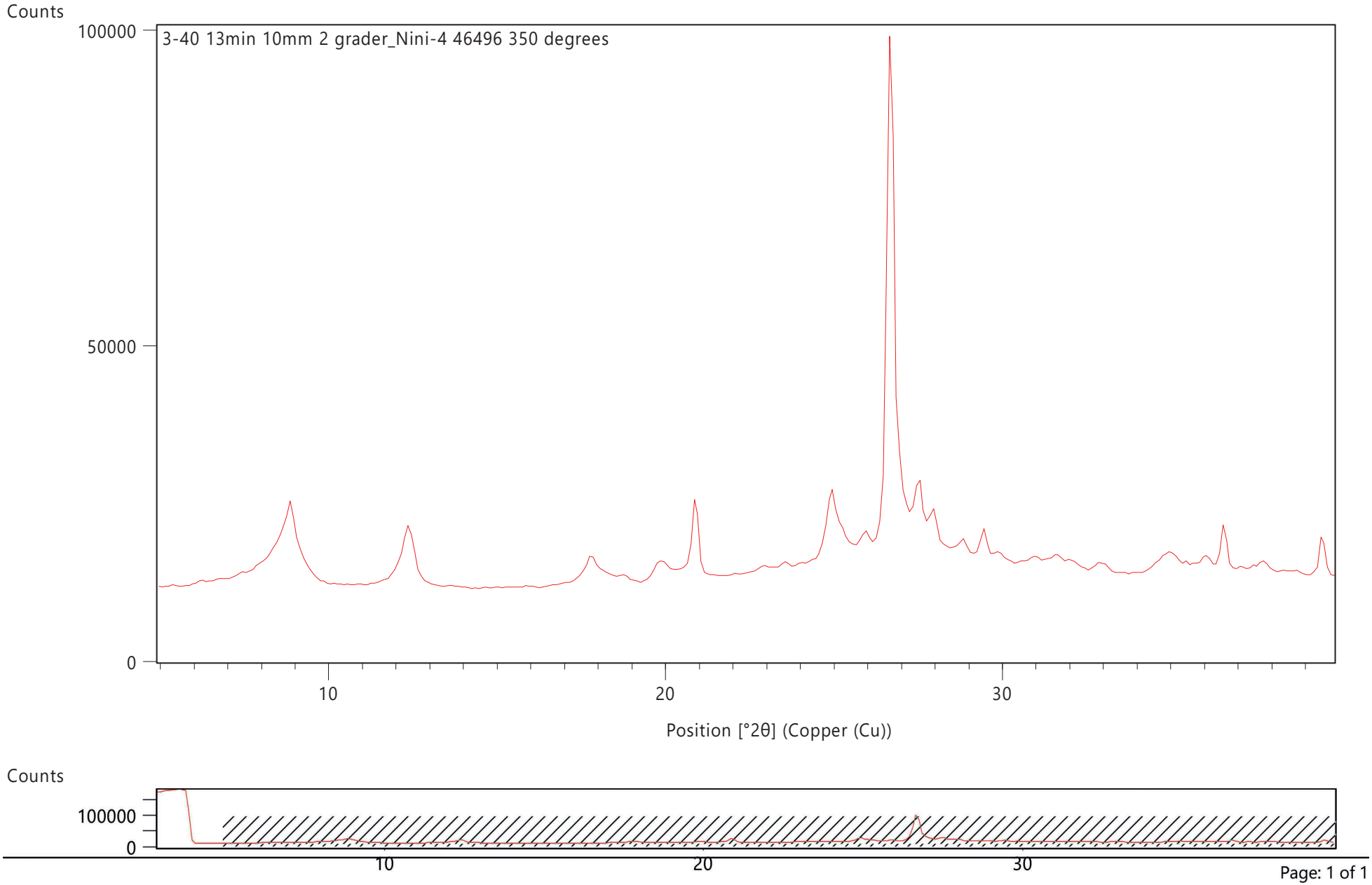
Counts
100000
50000
0
3-40 13min 10mm 2 grader_Nini-4 46496 350 degrees
10
20
30
Position [°2θ] (Copper (Cu))
Counts
100000
0
10
20
30

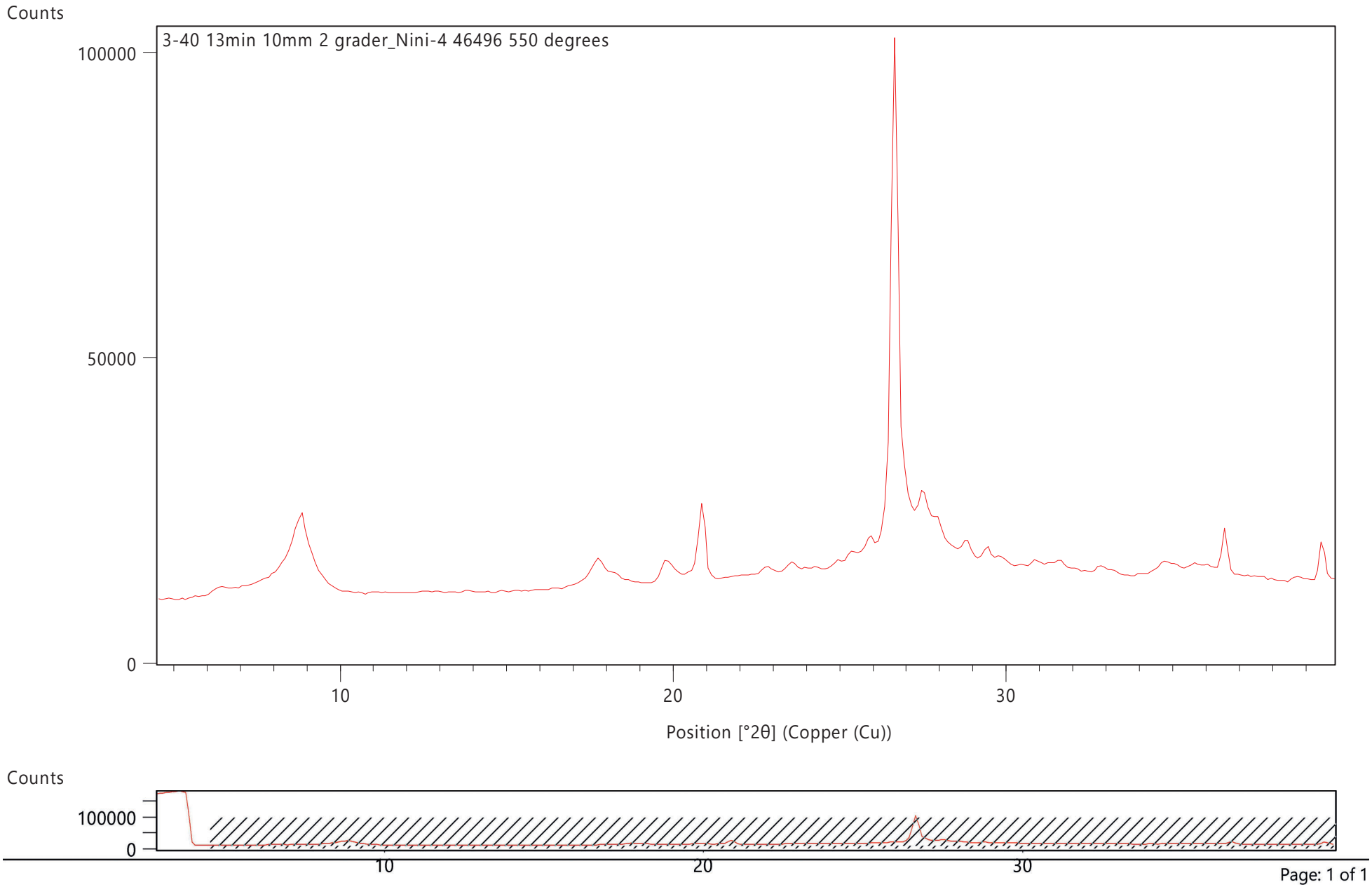
Counts
3-40 13min 10mm 2 grader_Nini-4 46496 550 degrees
100000
50000
0
10
20
30
Position [°2θ] (Copper (Cu))
Counts
100000
0
10
20
30

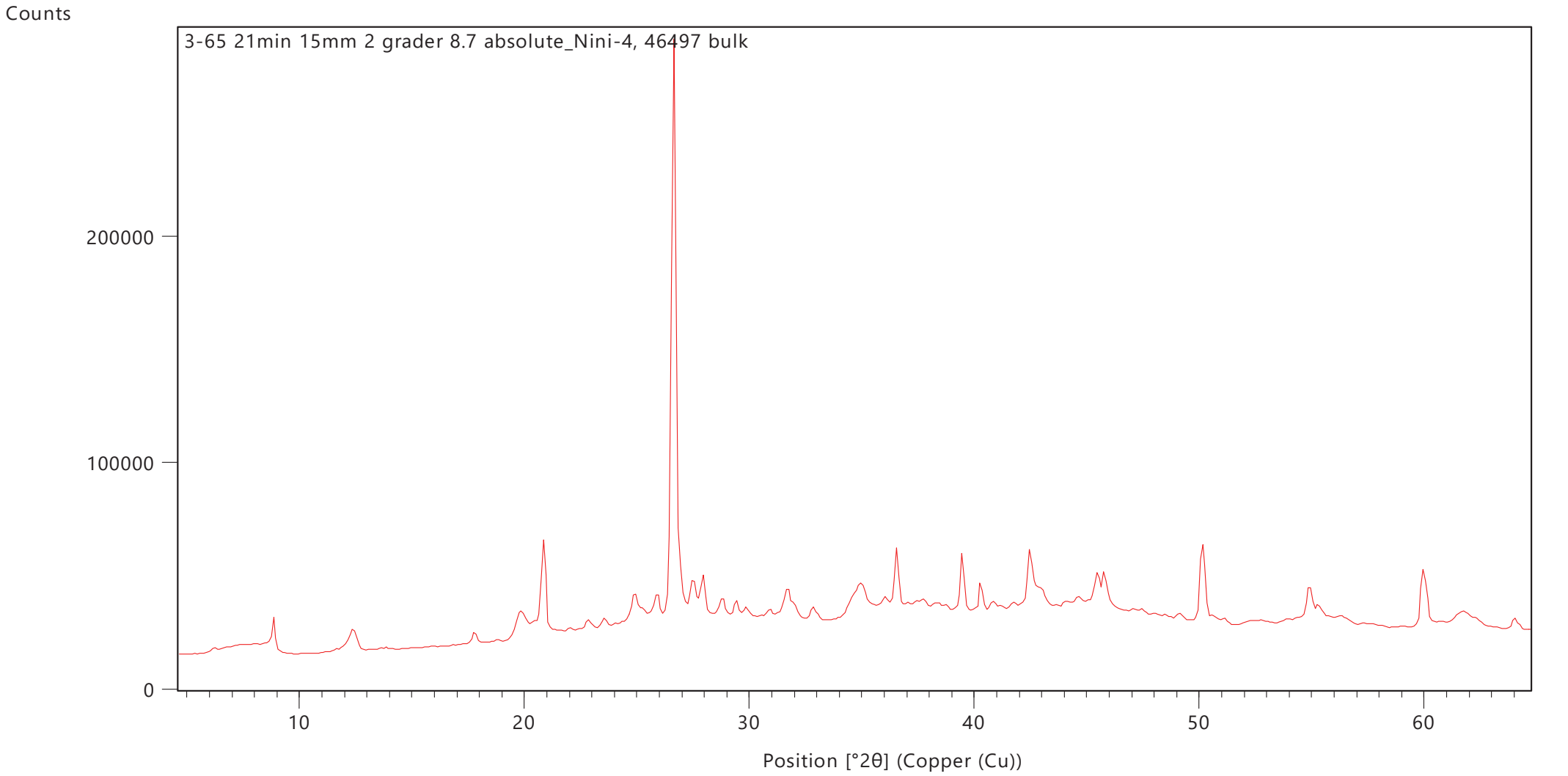
Counts
3-65 21min 15mm 2 grader 8.7 absolute_Nini-4, 46497 bulk
200000
100000
0
10
20
30
40
50
60
Position [°2θ] (Copper (Cu))

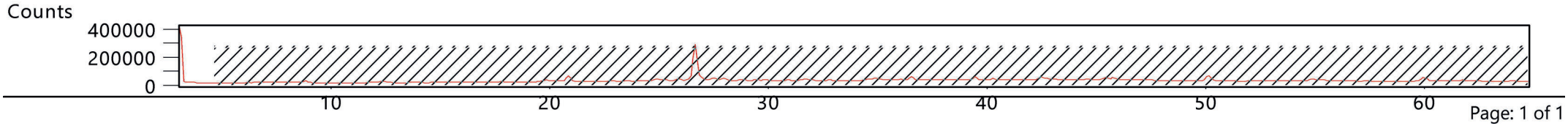
Counts
400000
200000
0
10
20
30
40
50
60

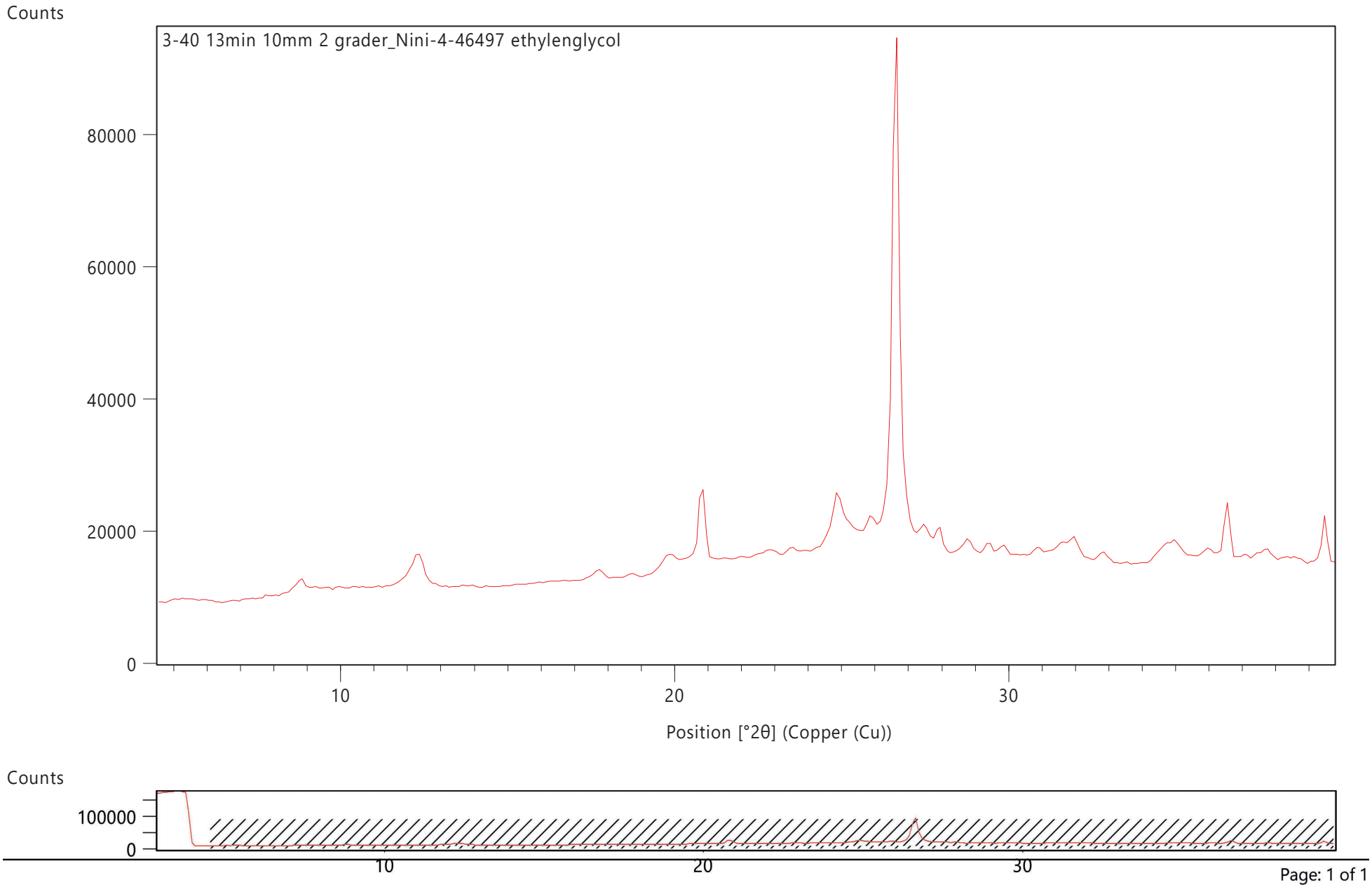
Counts
3-40 13min 10mm 2 grader_Nini-4-46497 ethylenglycol
80000
60000
40000
20000
0
10
20
30
Position [°2θ] (Copper (Cu))
Counts
100000
0
10
20
30

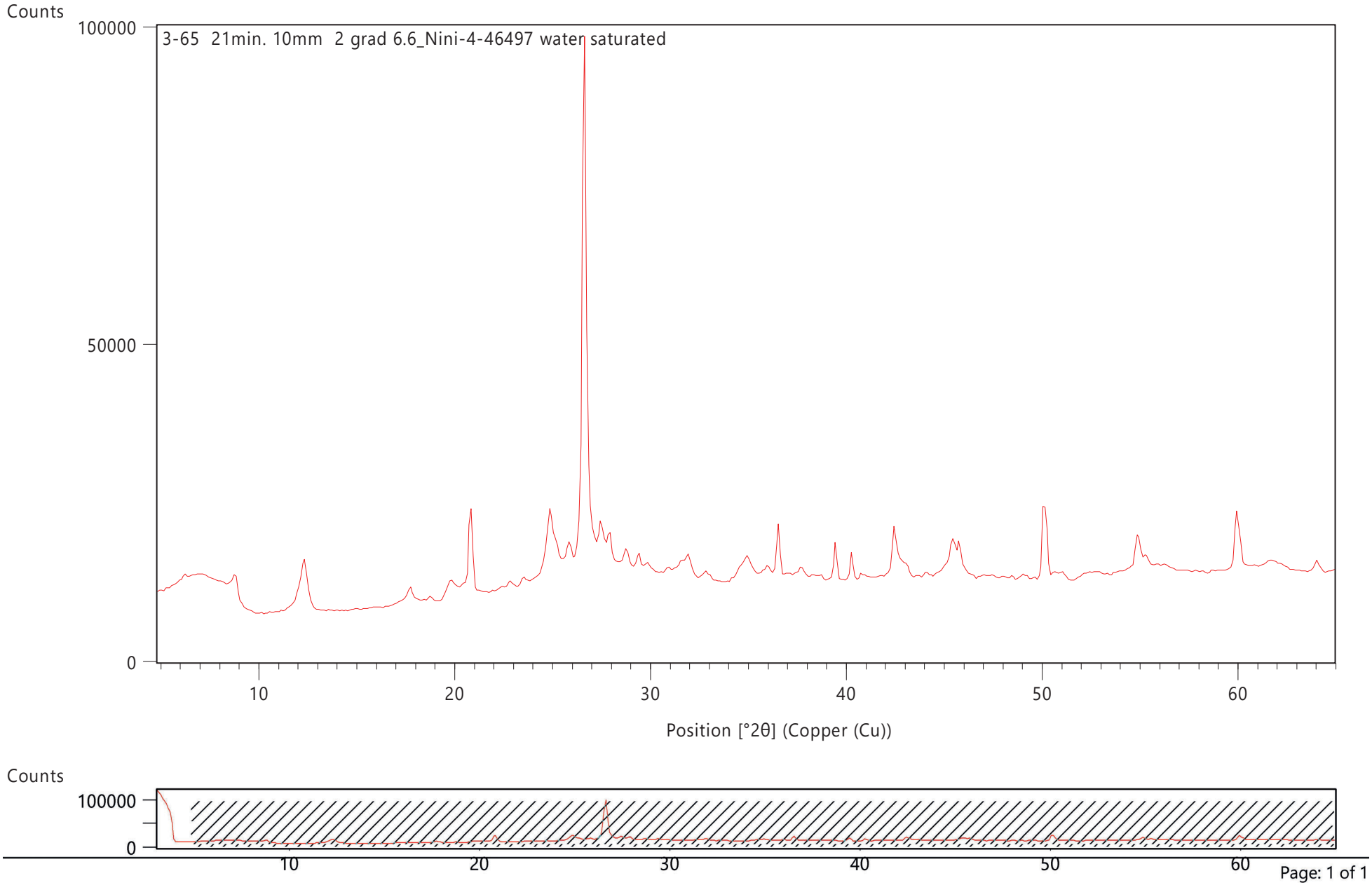
Counts
100000
50000
0
3-65 21min. 10mm 2 grad 6.6_Nini-4-46497 water saturated
10
20
30
40
50
60
Position [°2θ] (Copper (Cu))
Counts
100000
0
10
20
30
40
50
60

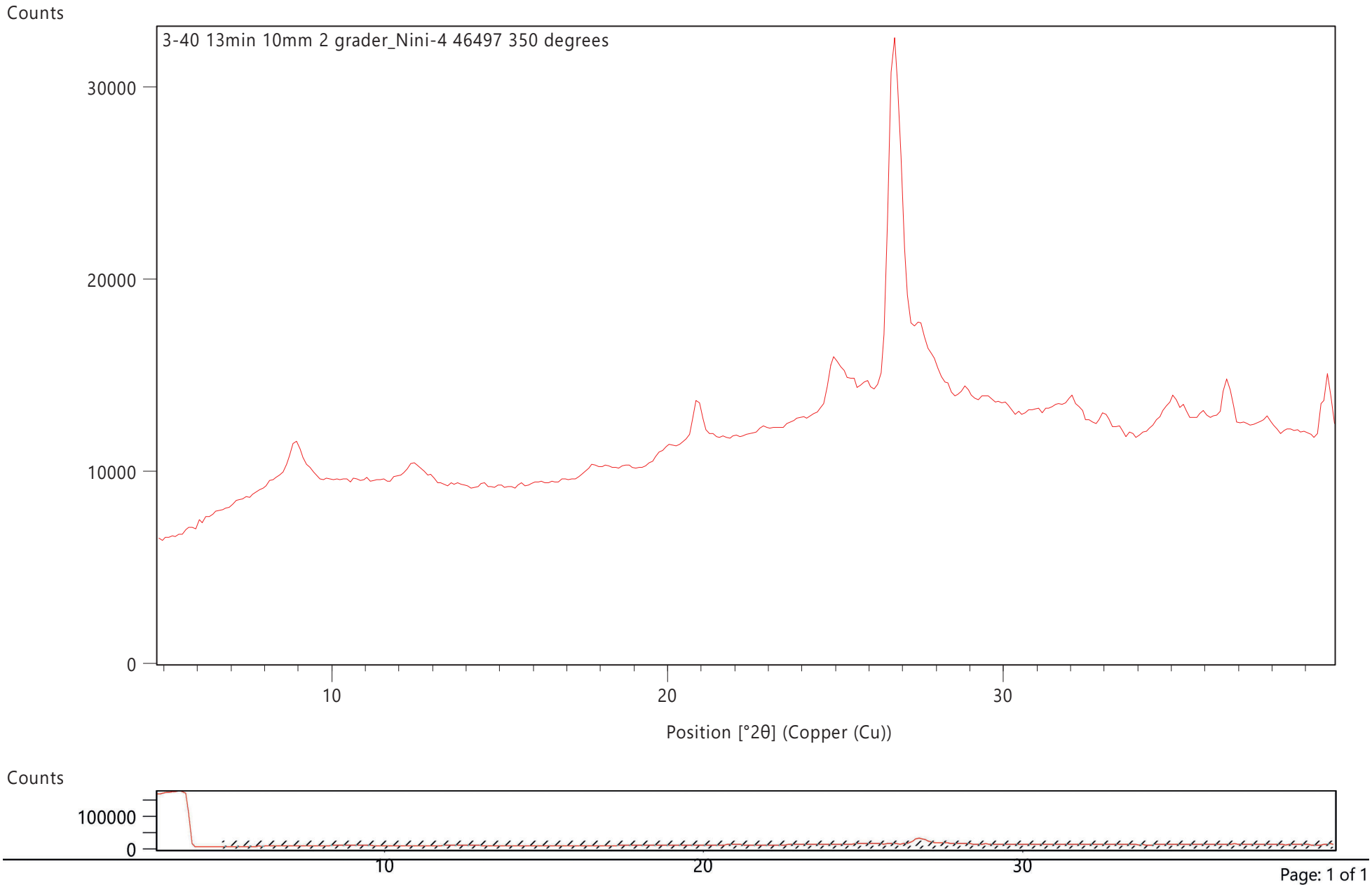
Counts
3-40 13min 10mm 2 grader_Nini-4 46497 350 degrees
30000
20000
10000
0
10
20
30
Position [°2θ] (Copper (Cu))
Counts
100000
0
10
20
30

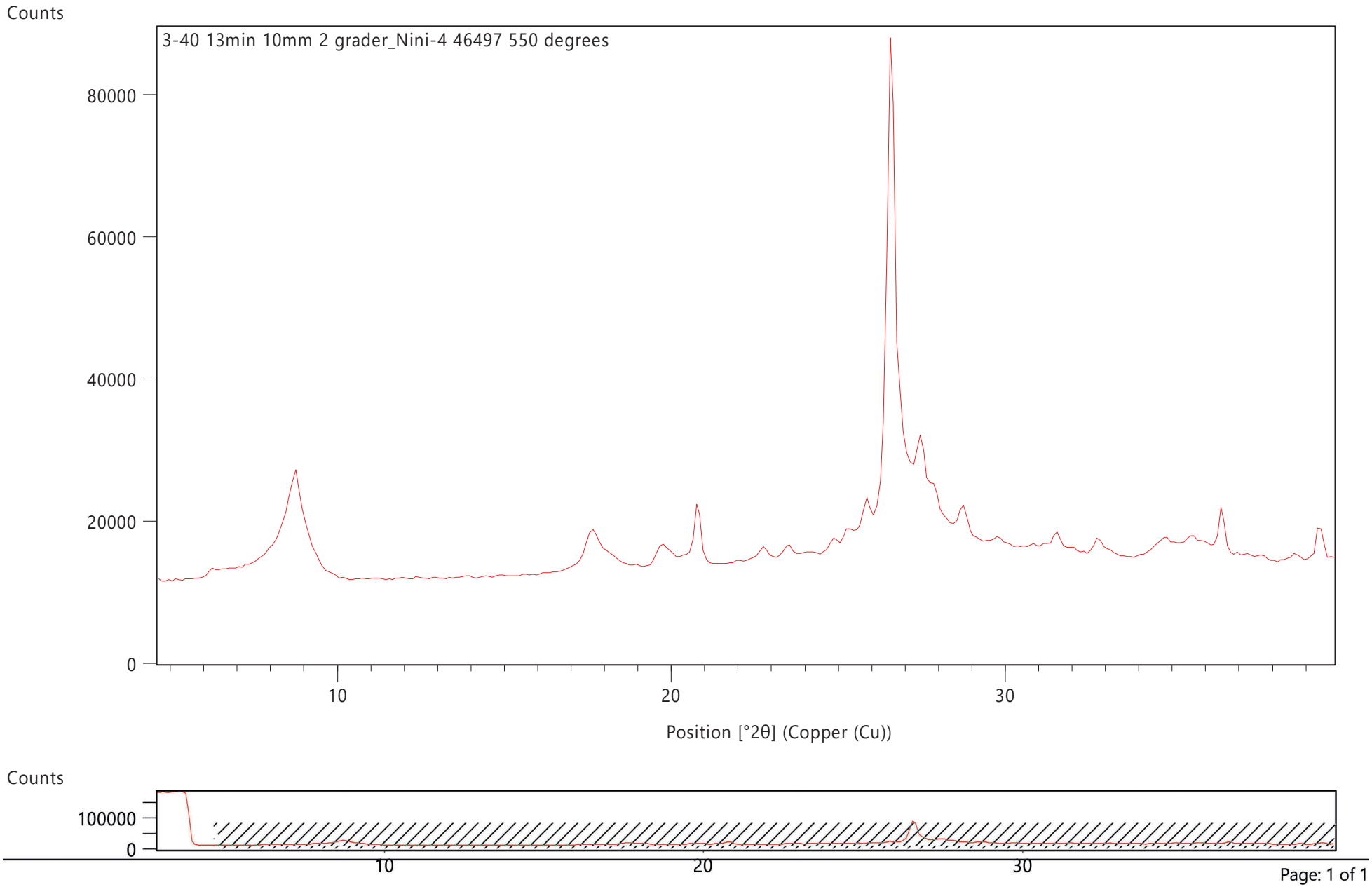
Counts
3-40 13min 10mm 2 grader_Nini-4 46497 550 degrees
80000
60000
40000
20000
0
10
20
30
Position [°2θ] (Copper (Cu))
Counts
100000
0
10
20
30

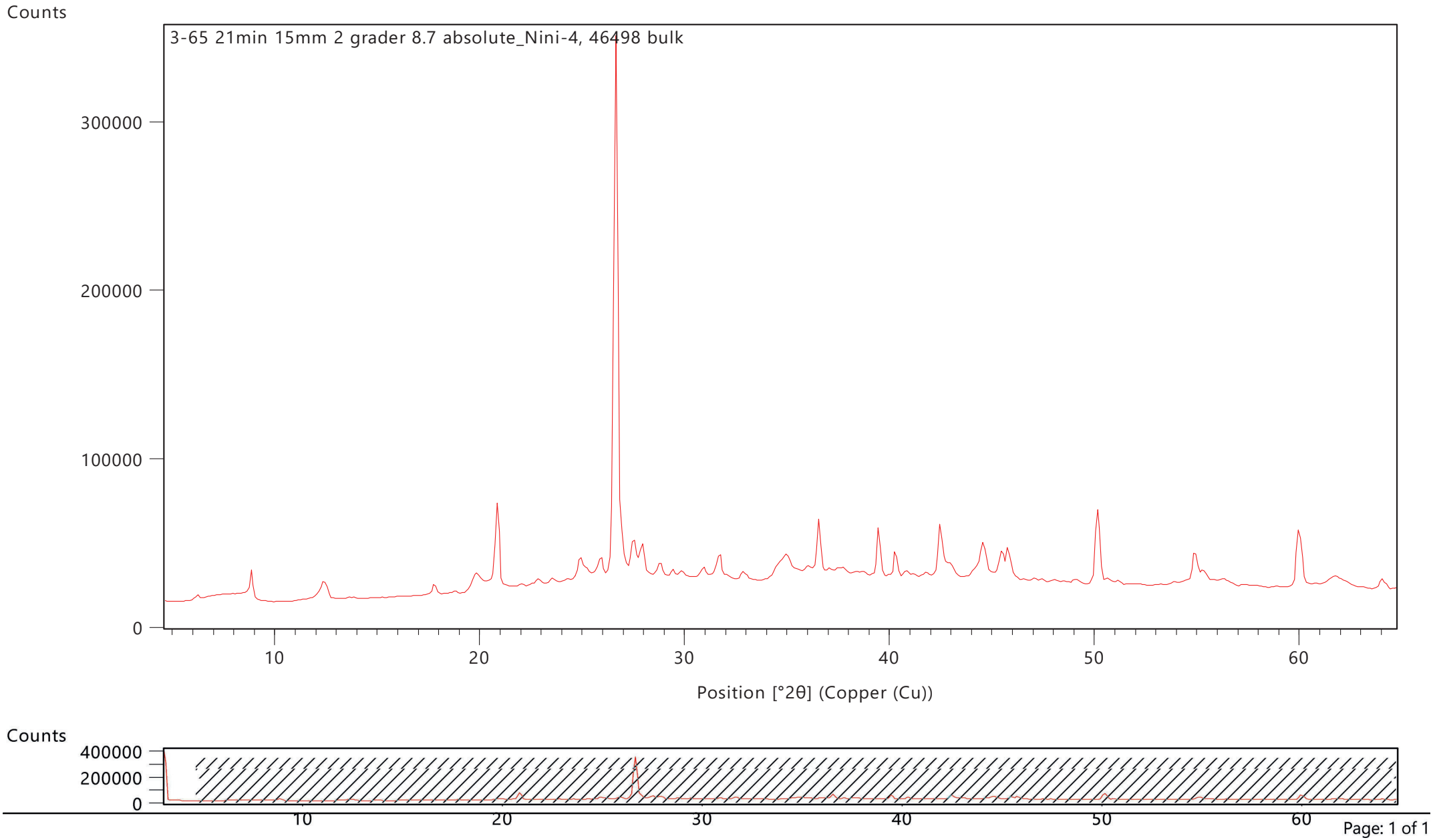
Counts
3-65 21min 15mm 2 grader 8.7 absolute_Nini-4, 46498 bulk
300000
200000
100000
0
10
20
30
40
50
60
Position [°2θ] (Copper (Cu))
Counts
400000
200000
0
10
20
30
40
50
60

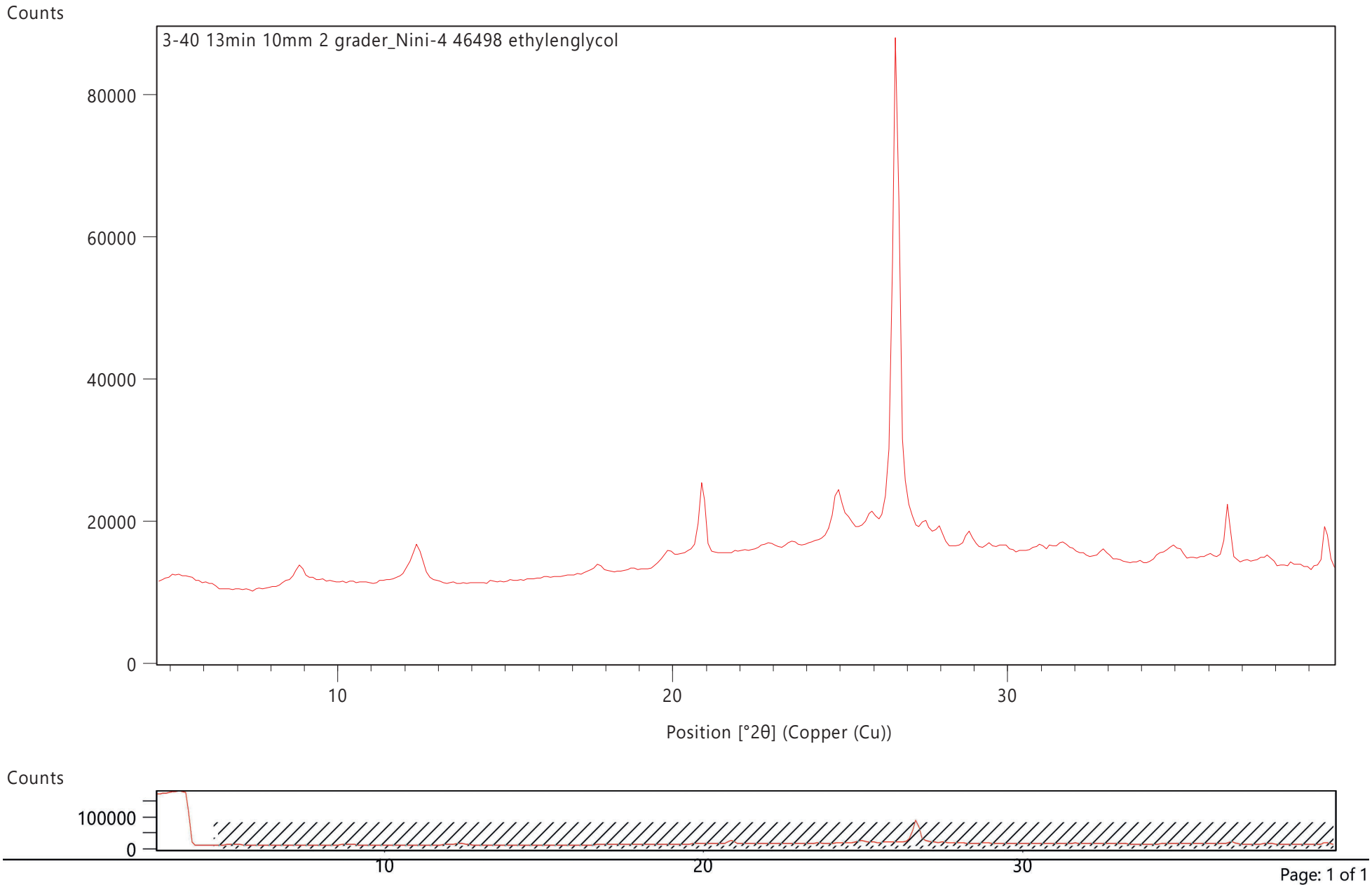
Counts
3-40 13min 10mm 2 grader_Nini-4 46498 ethylenglycol
80000
60000
40000
20000
0
10
20
30
Position [°2θ] (Copper (Cu))
Counts
100000
0
10
20
30

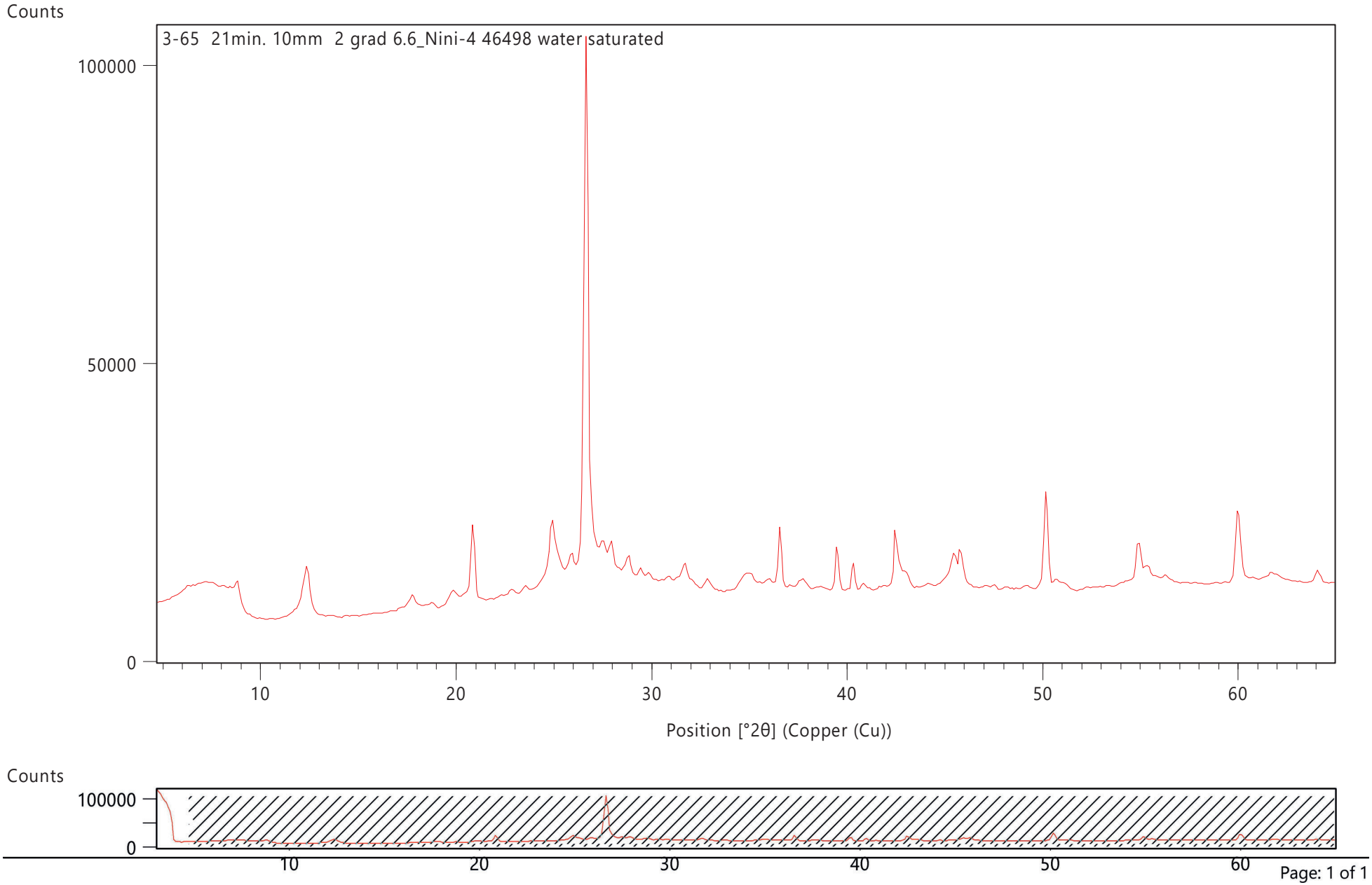
Counts
3-65 21min. 10mm 2 grad 6.6_Nini-4 46498 water saturated
100000
50000
0
10
20
30
40
50
60
Position [°2θ] (Copper (Cu))
Counts
100000
0
10
20
30
40
50
60

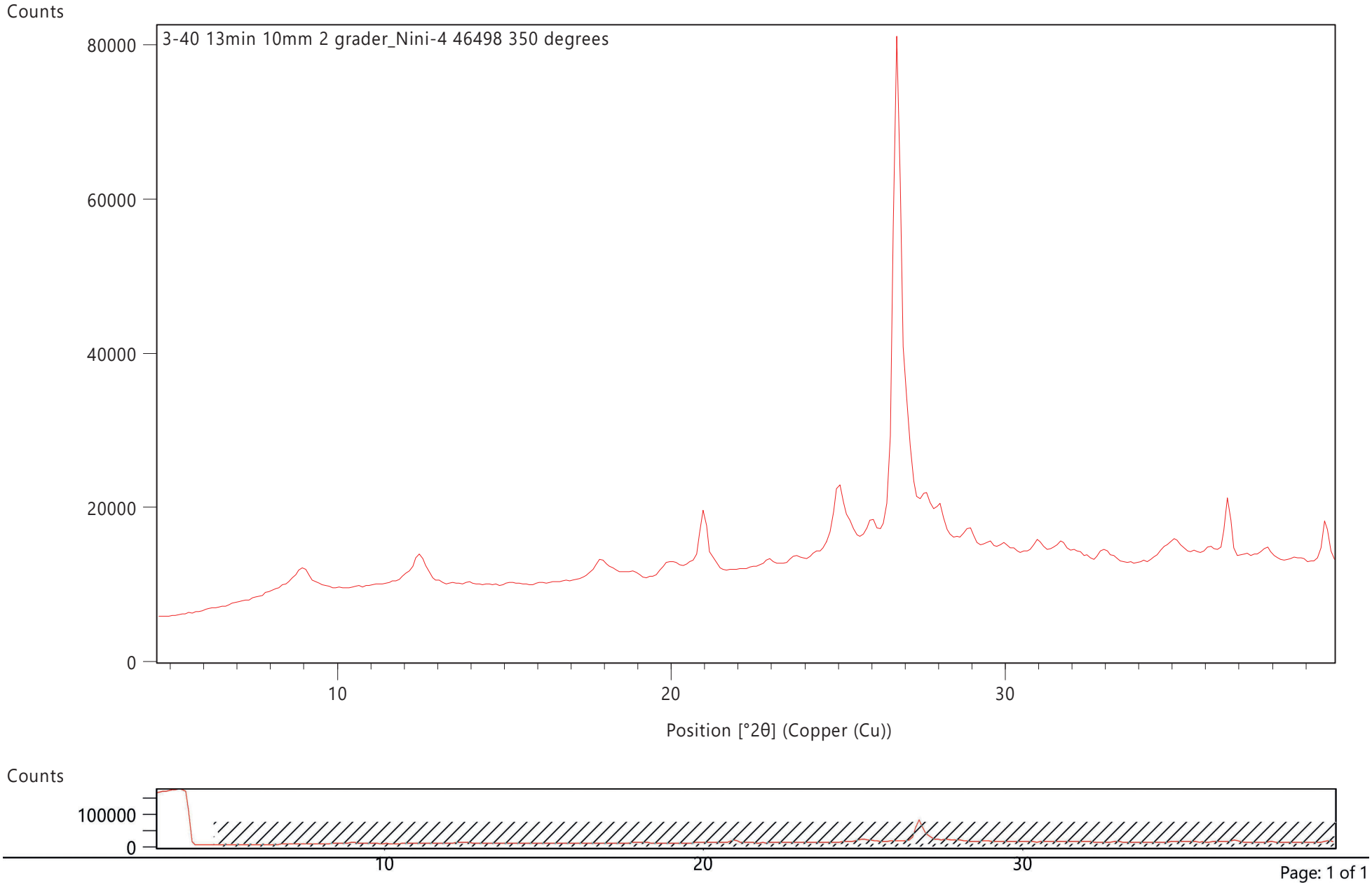
Counts
3-40 13min 10mm 2 grader_Nini-4 46498 350 degrees
80000
60000
40000
20000
0
10
20
30
Position [°2θ] (Copper (Cu))
Counts
100000
0
10
20
30

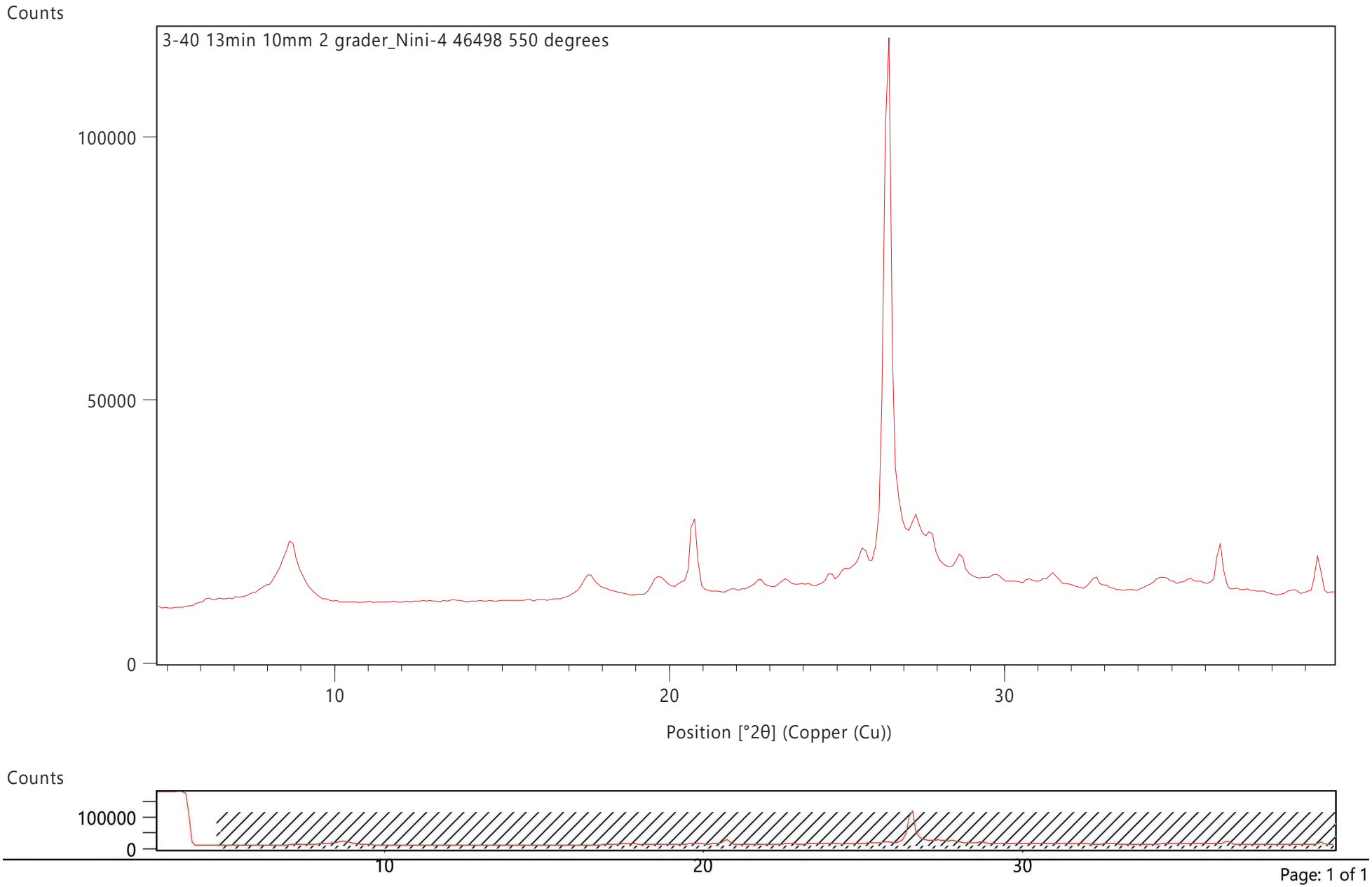
Counts
3-40 13min 10mm 2 grader_Nini-4 46498 550 degrees
100000
50000
0
10
20
30
Position [°2θ] (Copper (Cu))
Counts
100000
0
10
20
30

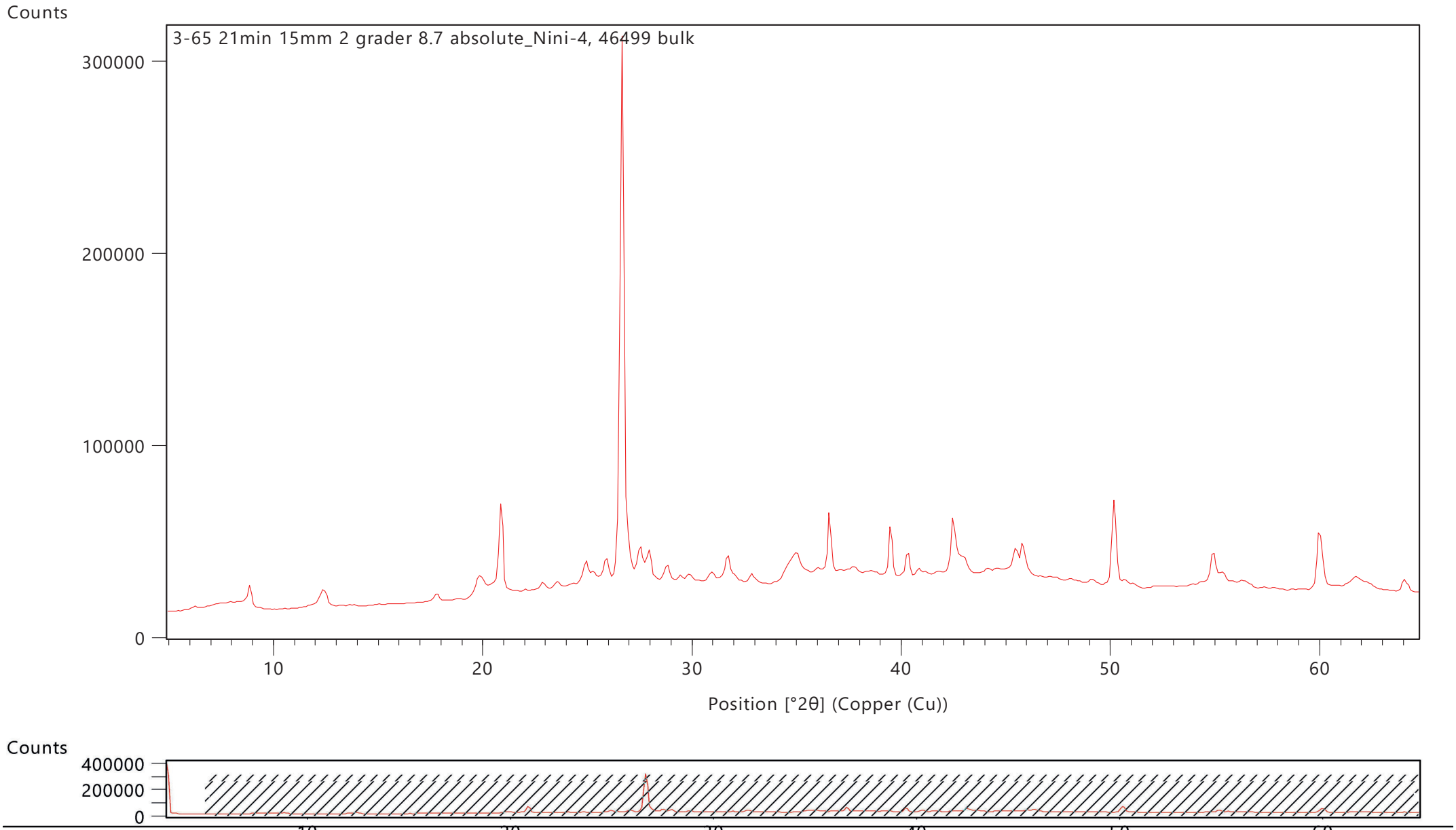
Counts
3-65 21min 15mm 2 grader 8.7 absolute_Nini-4, 46499 bulk
300000
200000
100000
0
10
20
30
40
50
60
Position [°2θ] (Copper (Cu))
Counts
400000
200000
0
10
20
30
40
50
60

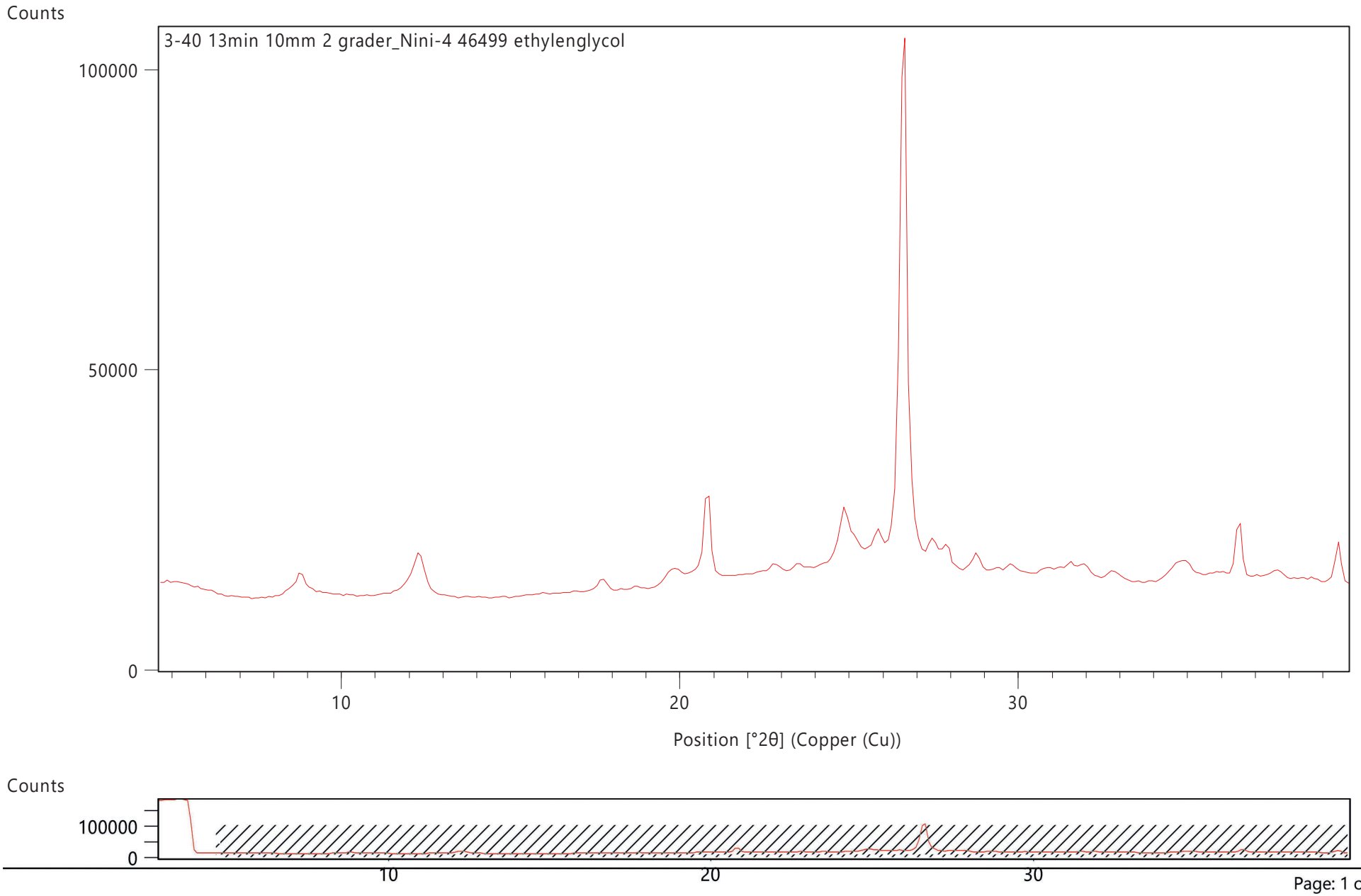
Counts
3-40 13min 10mm 2 grader_Nini-4 46499 ethylenglycol
100000
50000
0
10
20
30
Position [°2θ] (Copper (Cu))
Counts
100000
0
10
20
30

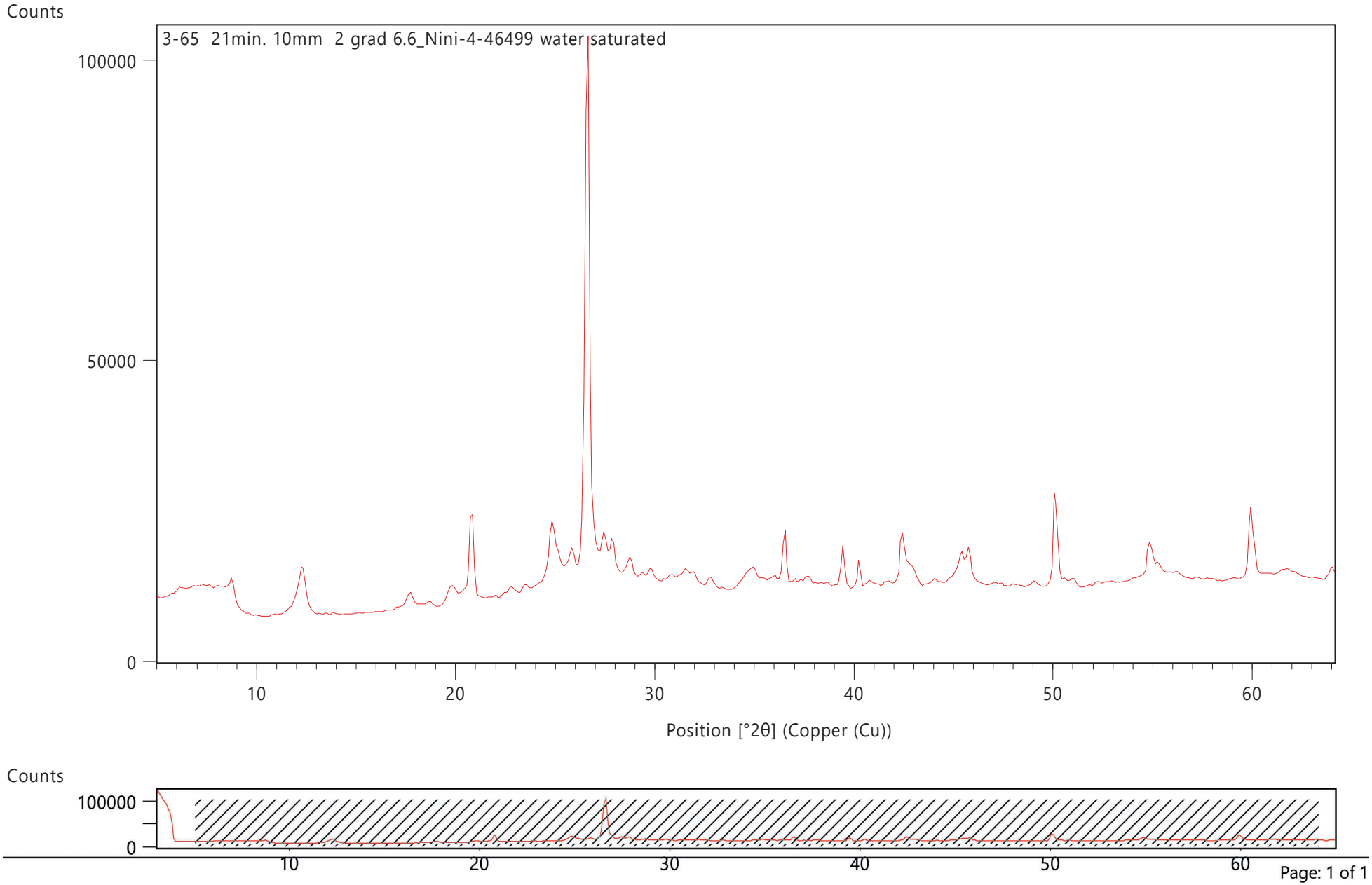
Counts
3-65 21min. 10mm 2 grad 6.6_Nini-4-46499 water saturated
100000
50000
0
10
20
30
40
50
60
Position [°2θ] (Copper (Cu))
Counts
100000
0
10
20
30
40
50
60

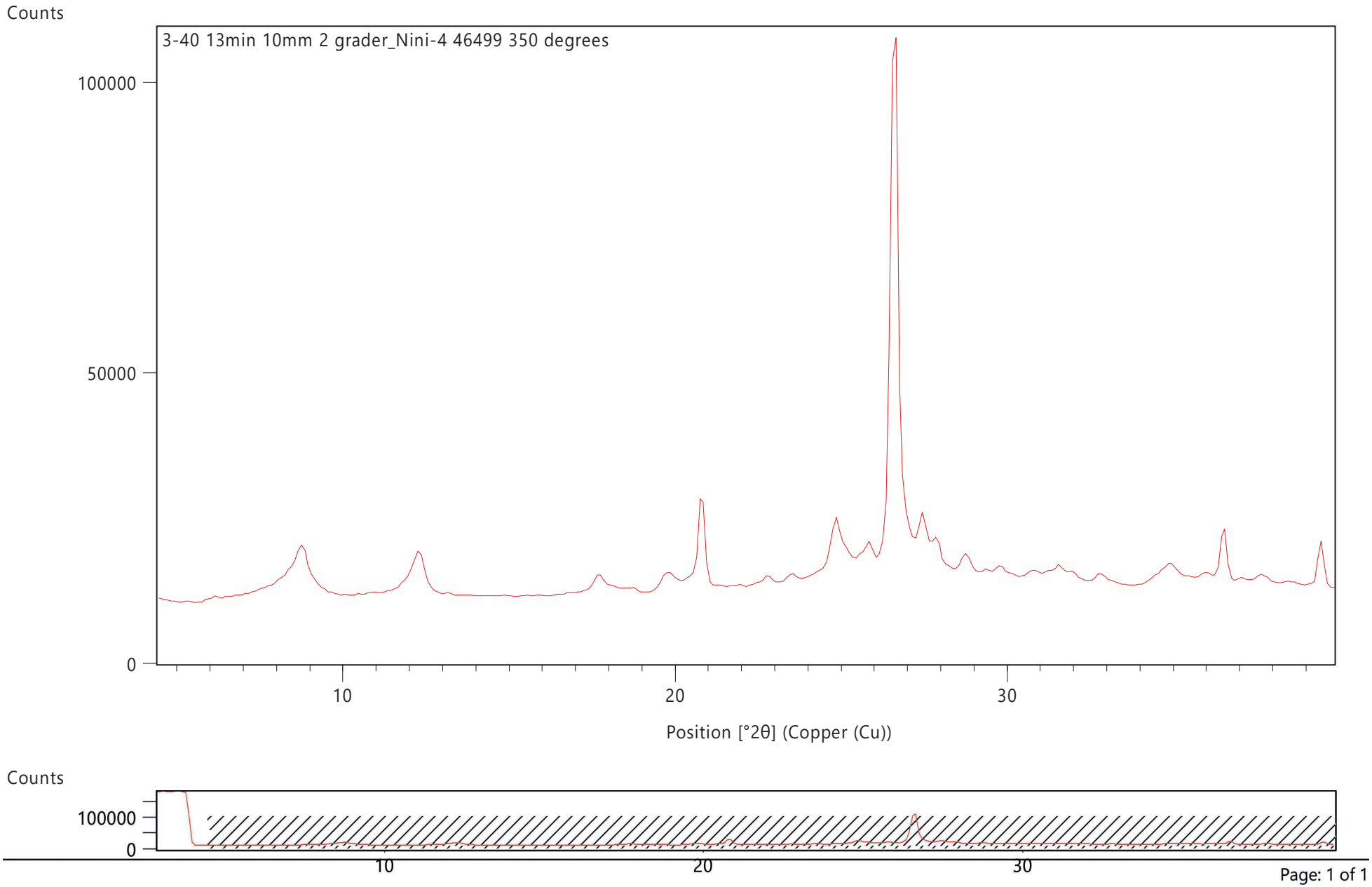
Counts
3-40 13min 10mm 2 grader_Nini-4 46499 350 degrees
100000
50000
0
10
20
30
Position [°2θ] (Copper (Cu))
Counts
100000
0
10
20
30

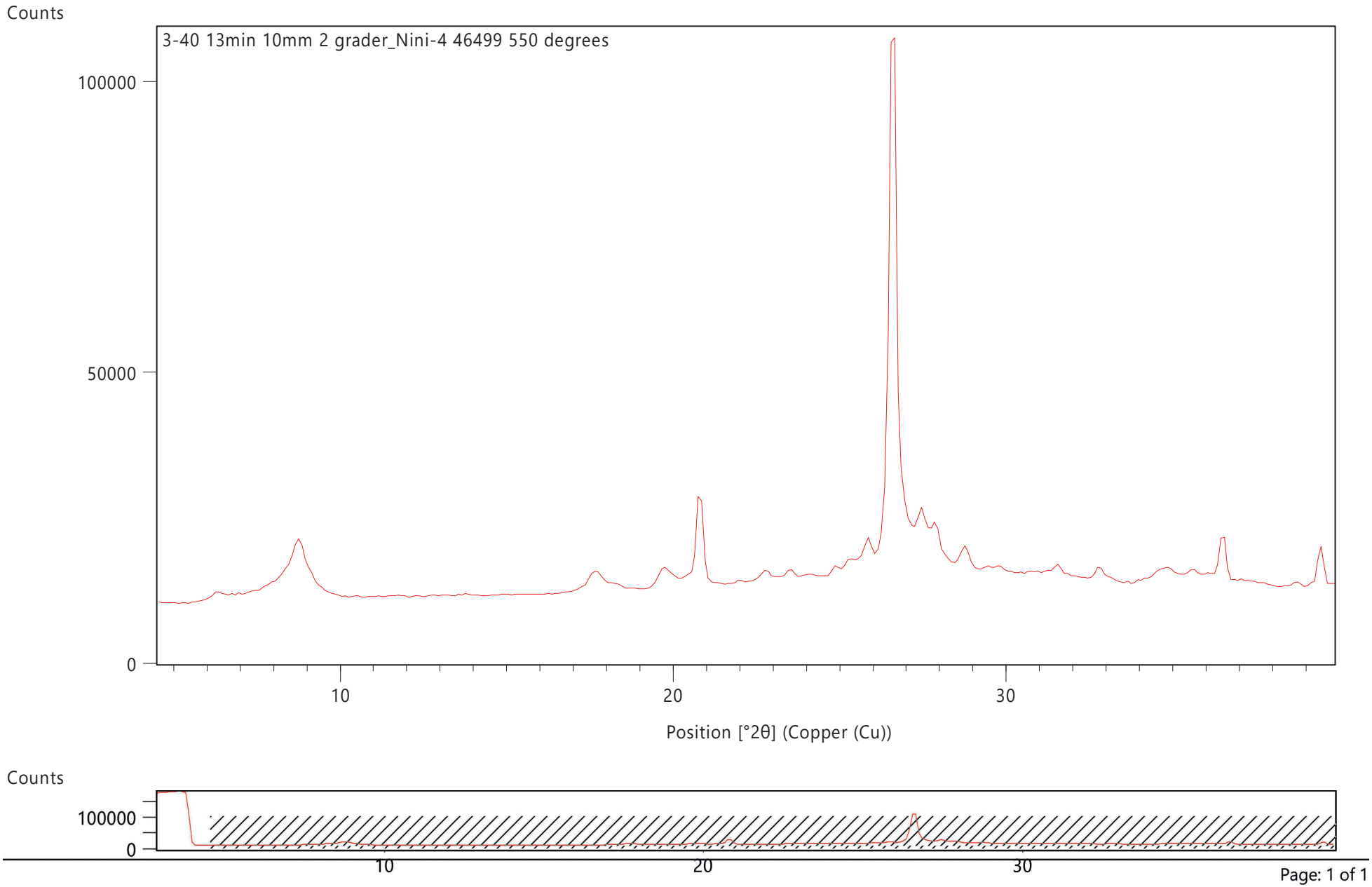
Counts
3-40 13min 10mm 2 grader_Nini-4 46499 550 degrees
100000
50000
0
10
20
30
Position [°2θ] (Copper (Cu))
Counts
100000
0
10
20
30

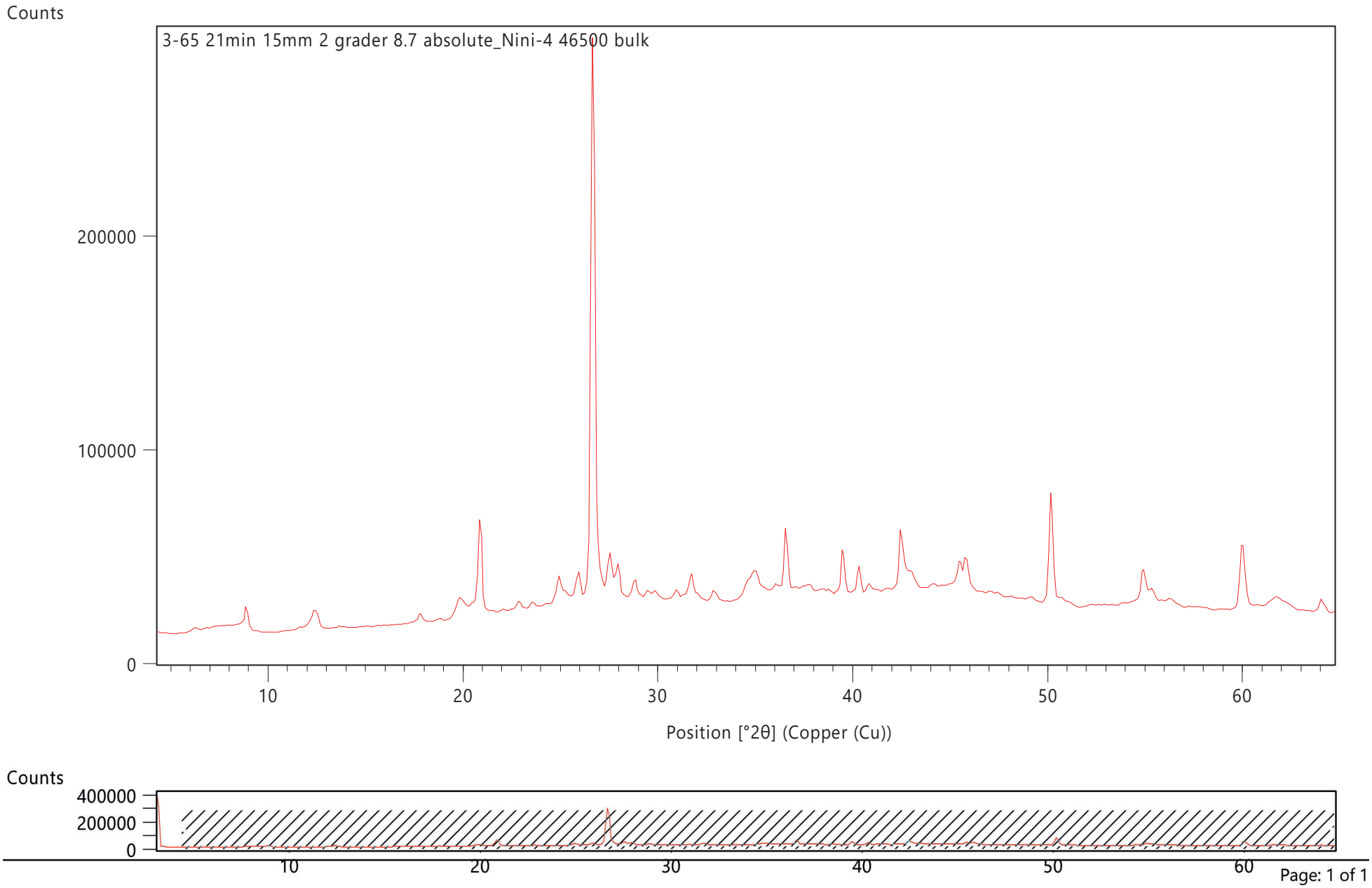
Counts
3-65 21min 15mm 2 grader 8.7 absolute_Nini-4 46500 bulk
200000
100000
0
10
20
30
40
50
60
Position [°2θ] (Copper (Cu))
Counts
400000
200000
0
10
20
30
40
50
60

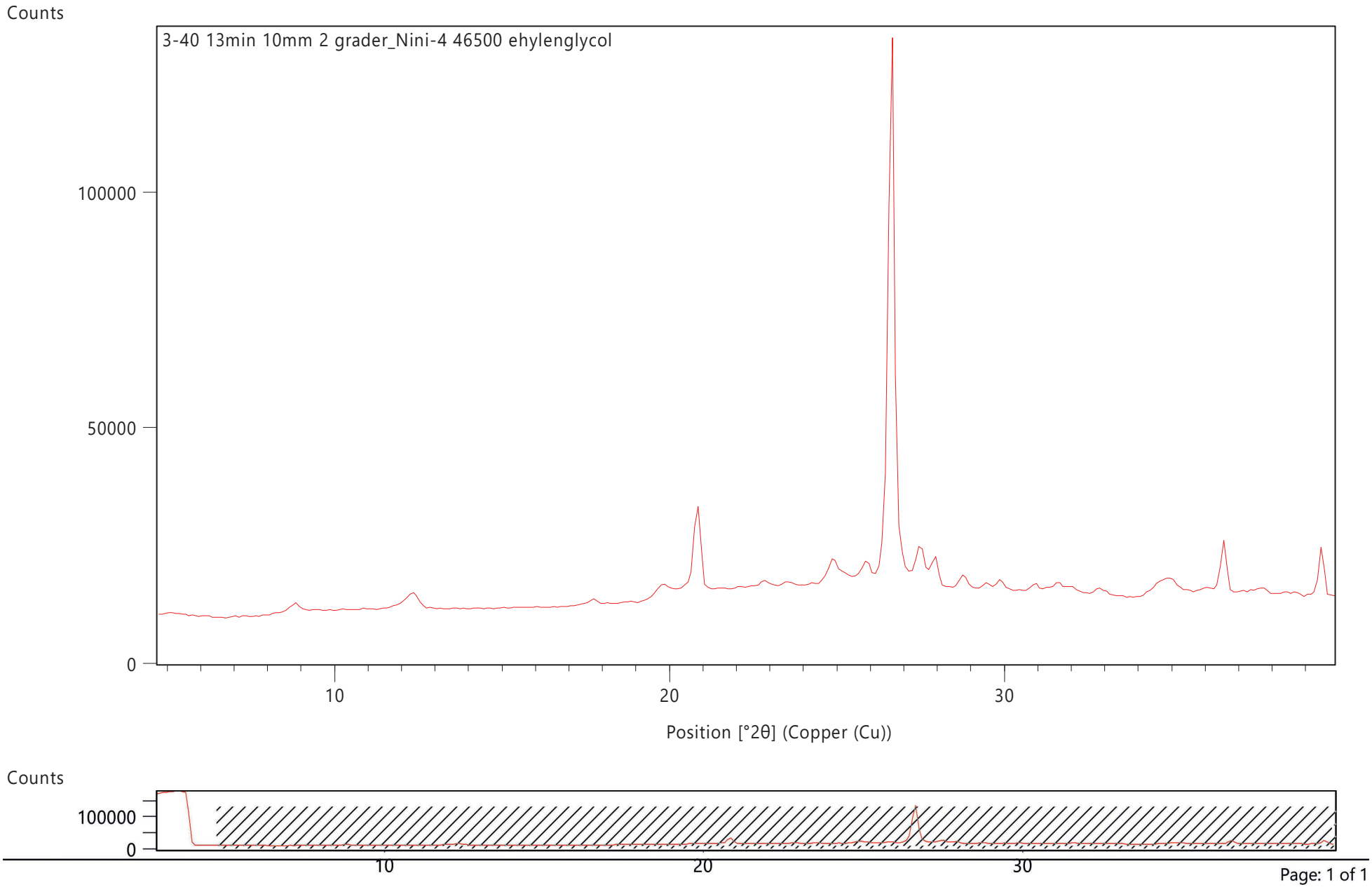
Counts
3-40 13min 10mm 2 grader_Nini-4 46500 ehylenglycol
100000
50000
0
10
20
30
Position [°2θ] (Copper (Cu))
Counts
100000
0
10
20
30

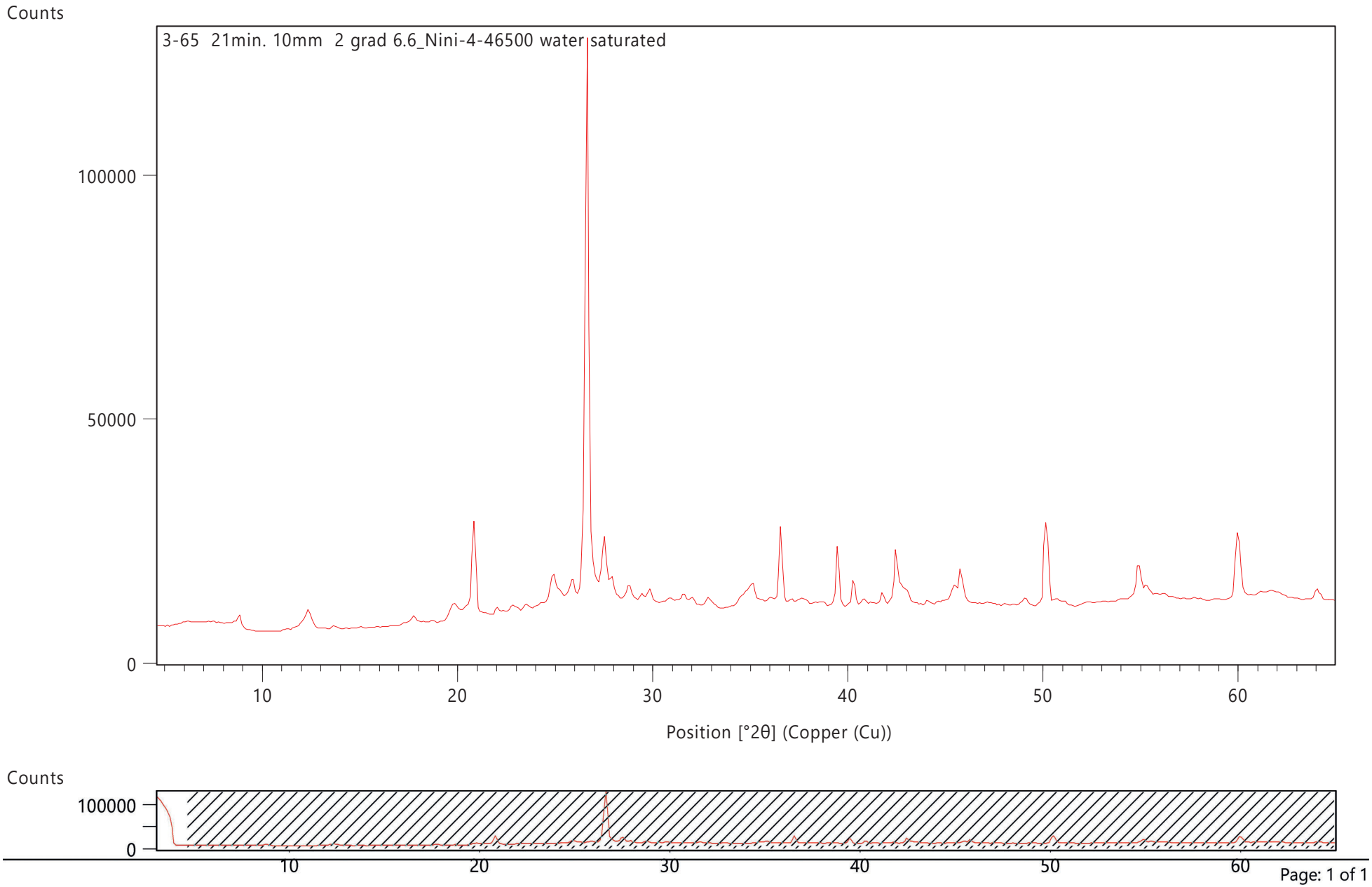
Counts
3-65 21min. 10mm 2 grad 6.6_Nini-4-46500 water saturated
100000
50000
0
10
20
30
40
50
60
Position [°2θ] (Copper (Cu))
Counts
100000
0
10
20
30
40
50
60

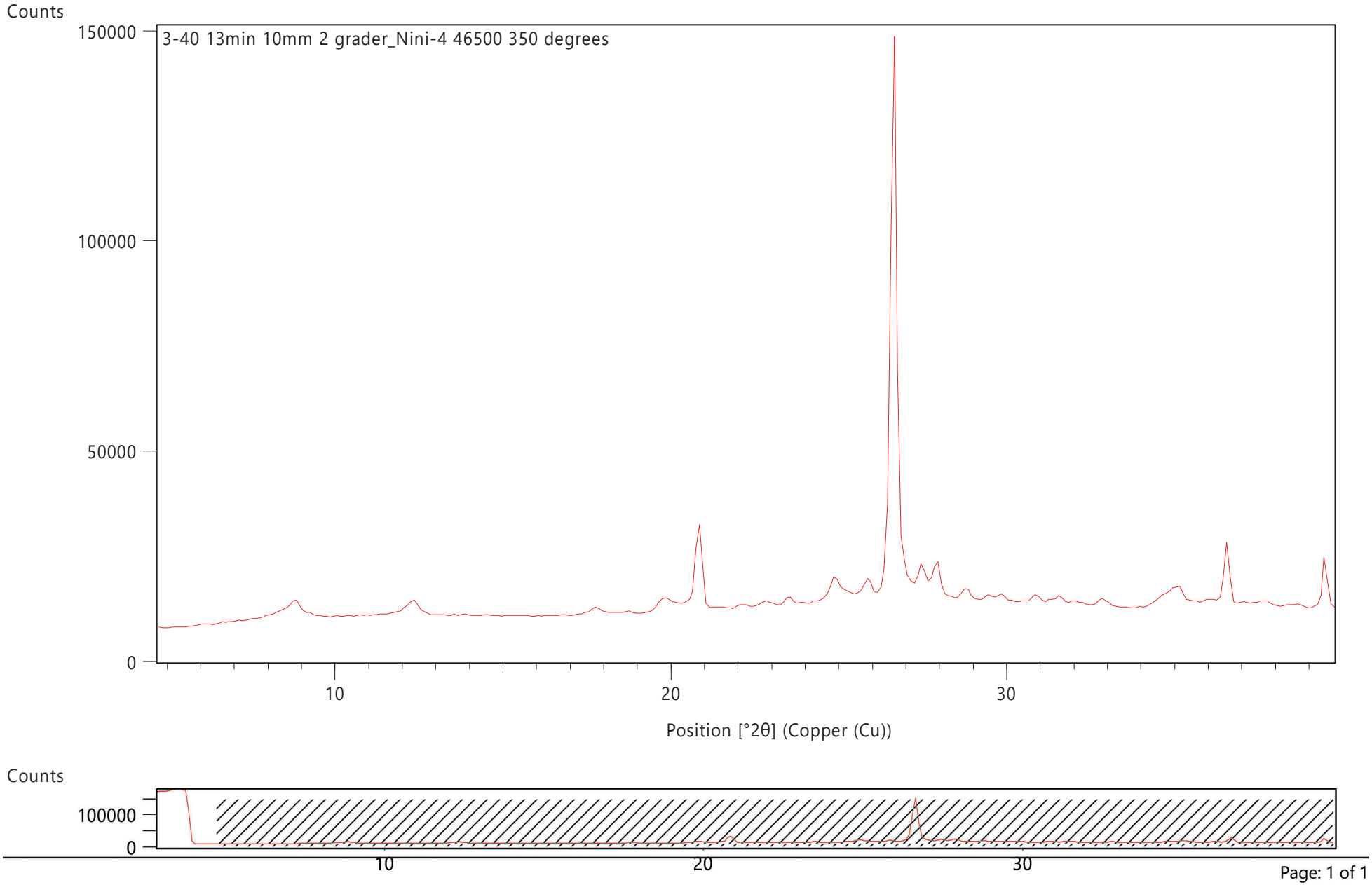
Counts
3-40 13min 10mm 2 grader_Nini-4 46500 350 degrees
150000
100000
50000
0
10
20
30
Position [°2θ] (Copper (Cu))
Counts
100000
0
10
20
30

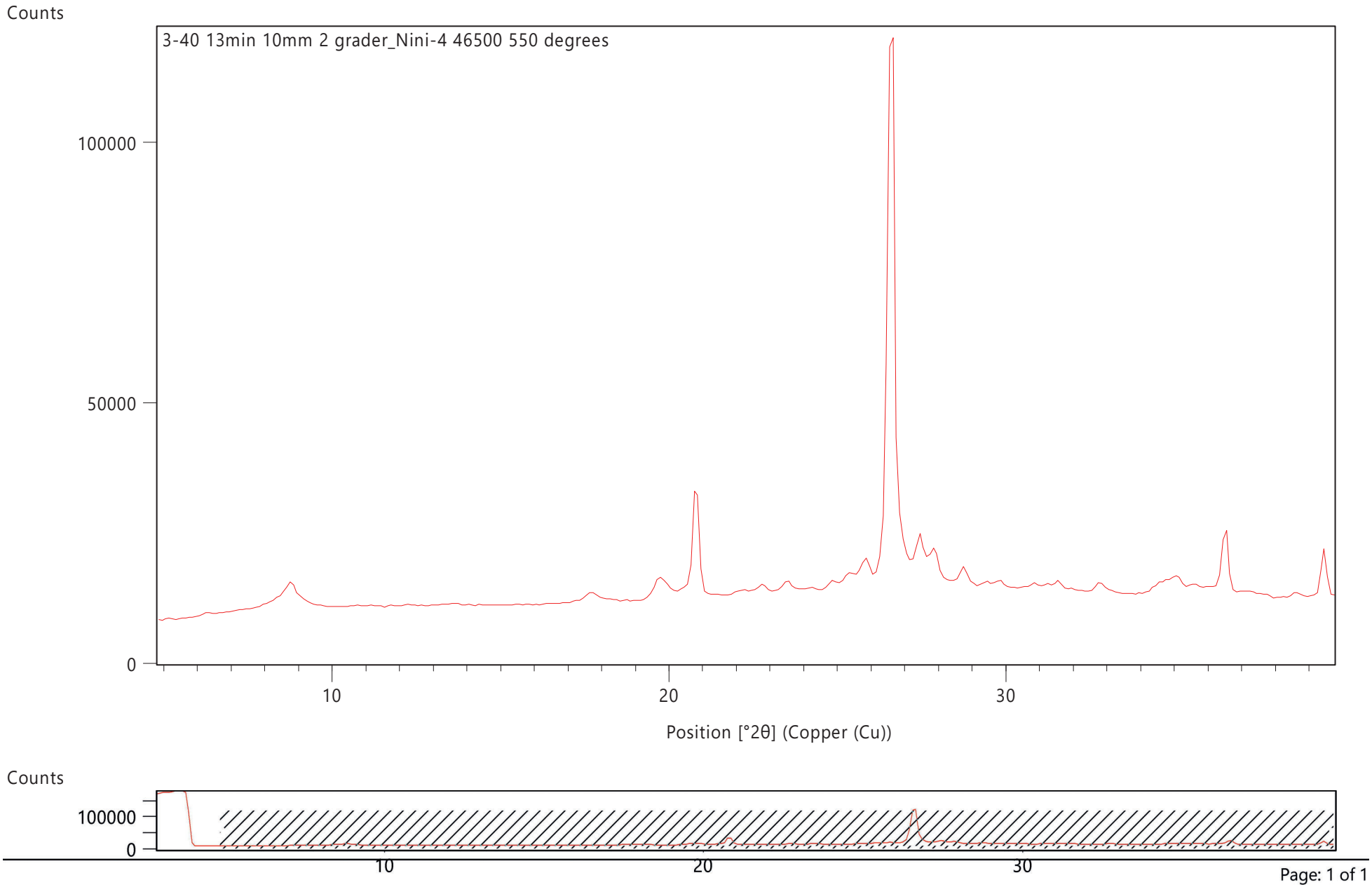
Counts
3-40 13min 10mm 2 grader_Nini-4 46500 550 degrees
100000
50000
0
10
20
30
Position [°2θ] (Copper (Cu))
Counts
100000
0
10
20
30

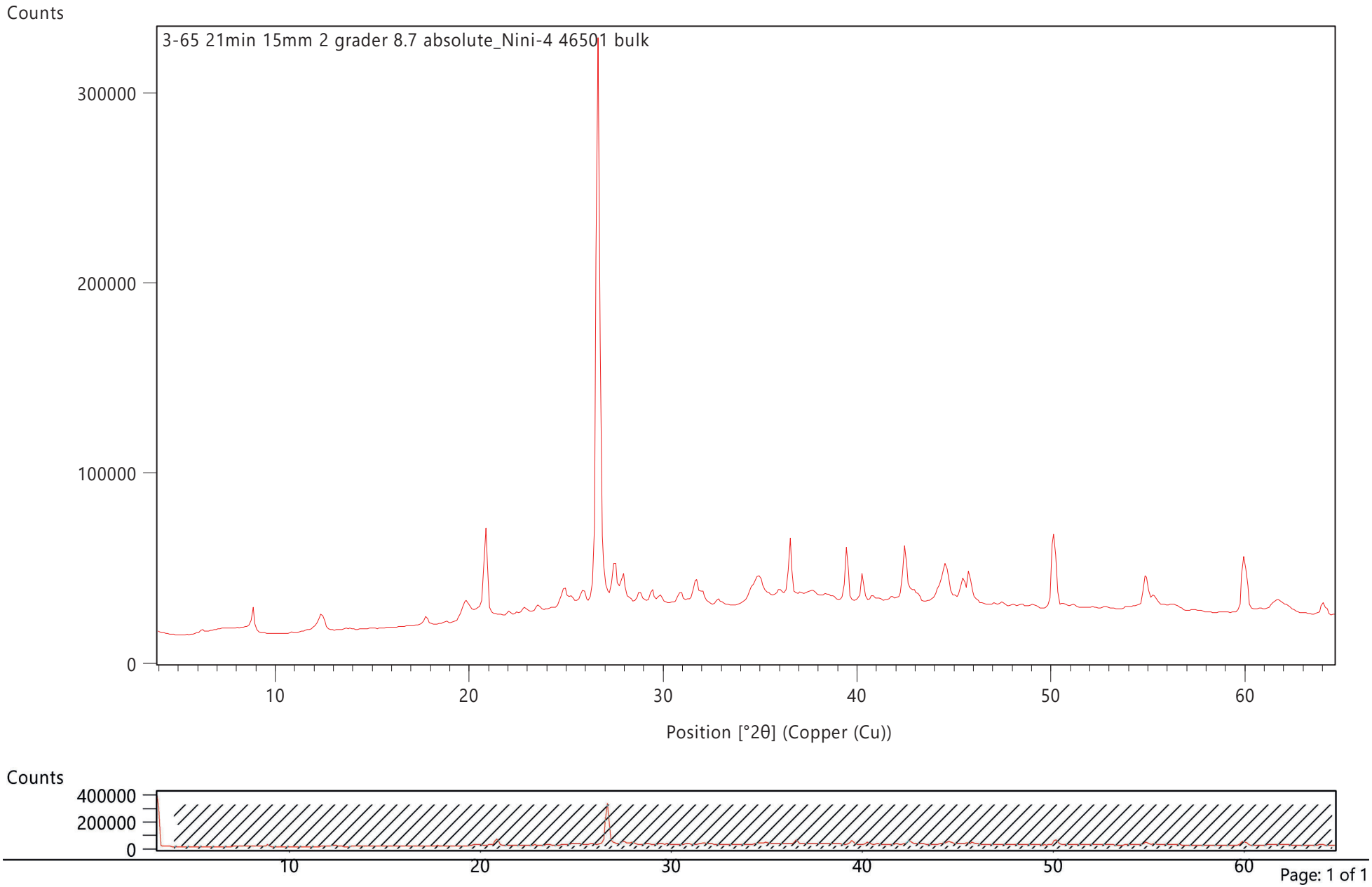
Counts
3-65 21min 15mm 2 grader 8.7 absolute_Nini-4 46501 bulk
300000
200000
100000
0
10
20
30
40
50
60
Position [°2θ] (Copper (Cu))
Counts
400000
200000
0
10
20
30
40
50
60

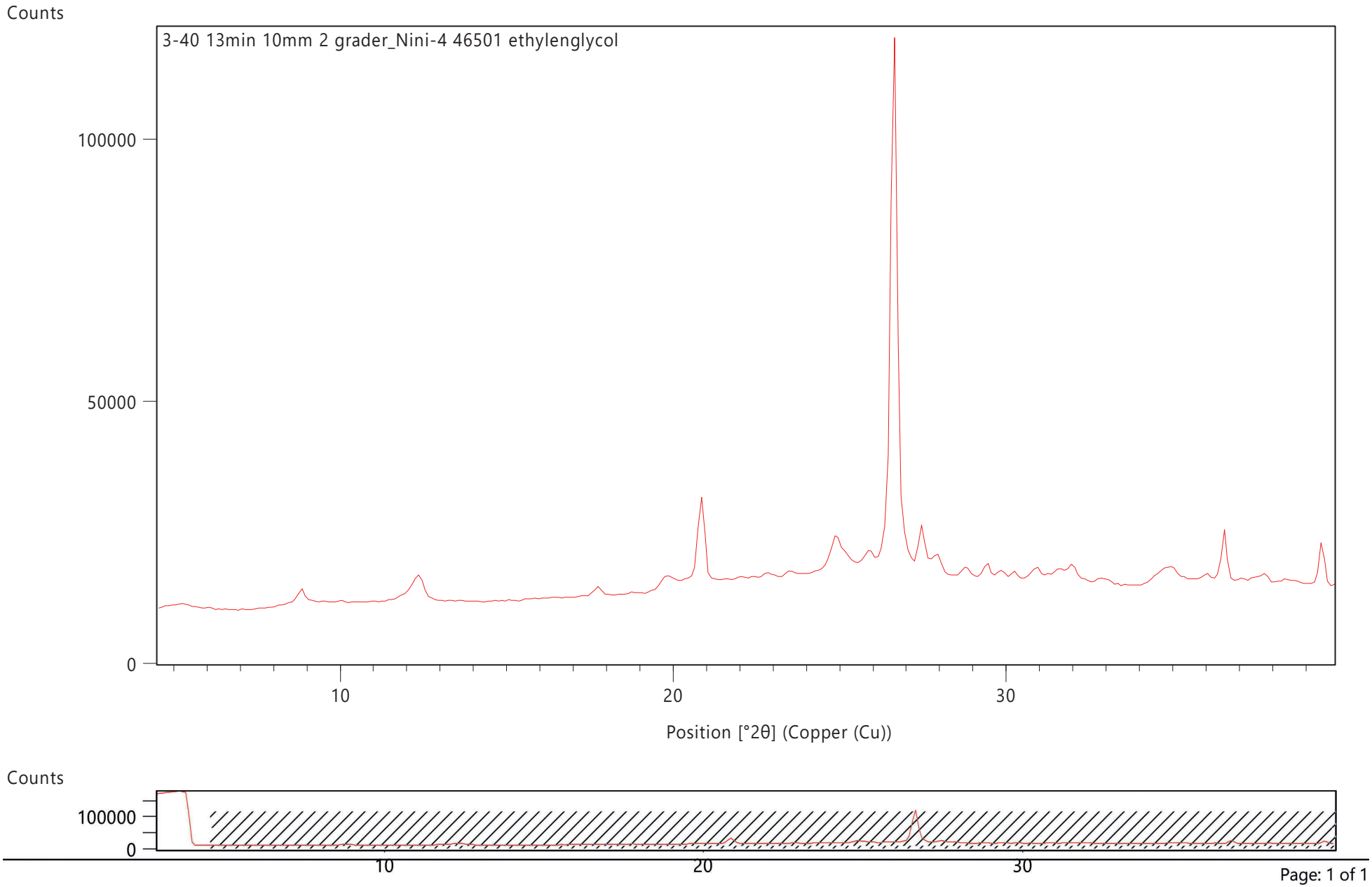
Counts
3-40 13min 10mm 2 grader_Nini-4 46501 ethylenglycol
100000
50000
0
10
20
30
Position [°2θ] (Copper (Cu))
Counts
100000
0
10
20
30

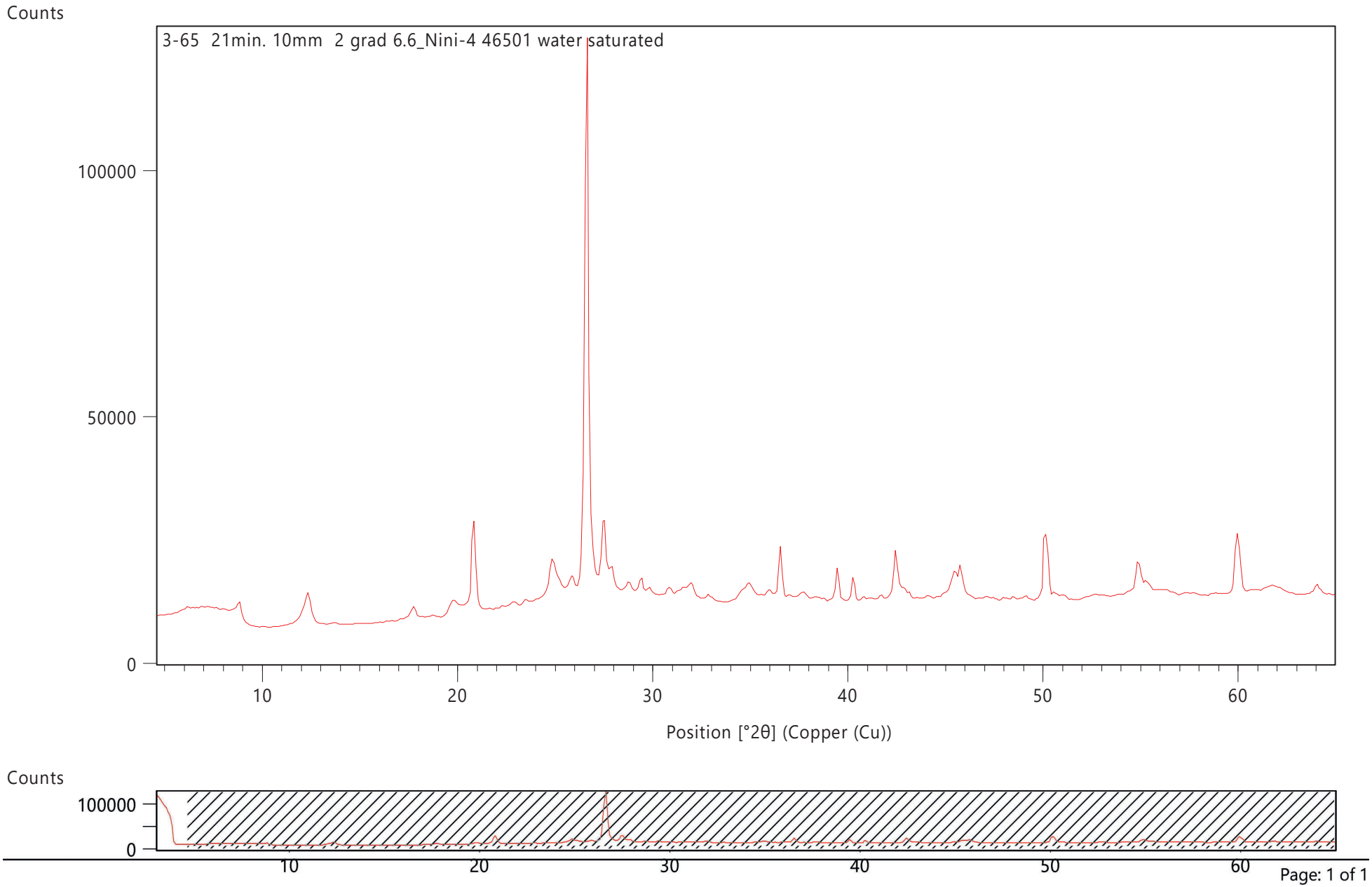
Counts
3-65 21min. 10mm 2 grad 6.6_Nini-4 46501 water saturated
100000
50000
0
10
20
30
40
50
60
Position [°2θ] (Copper (Cu))
Counts
100000
0
10
20
30
40
50
60

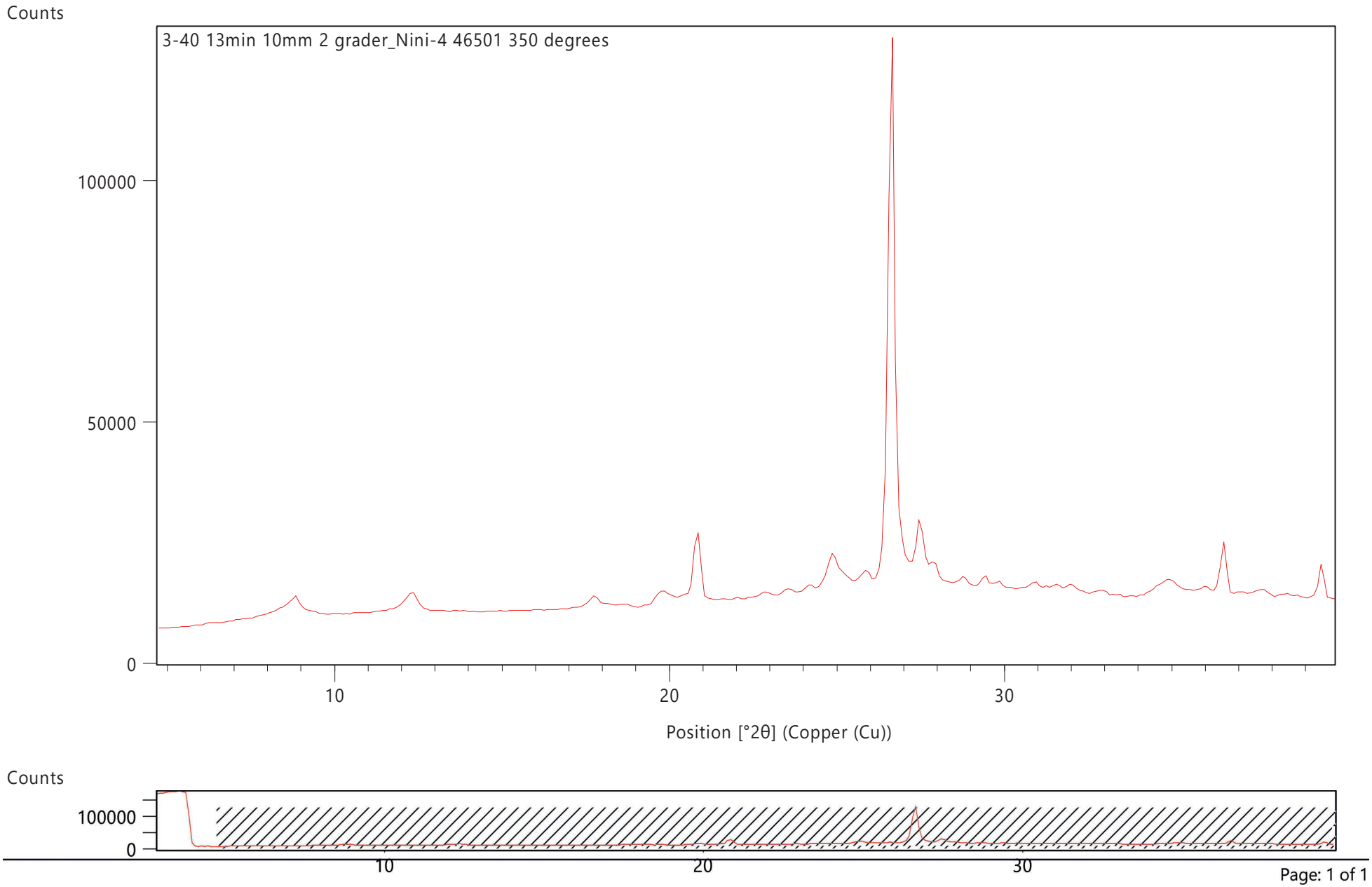
Counts
3-40 13min 10mm 2 grader_Nini-4 46501 350 degrees
100000
50000
0
10
20
30
Position [°2θ] (Copper (Cu))
Counts
100000
0
10
20
30

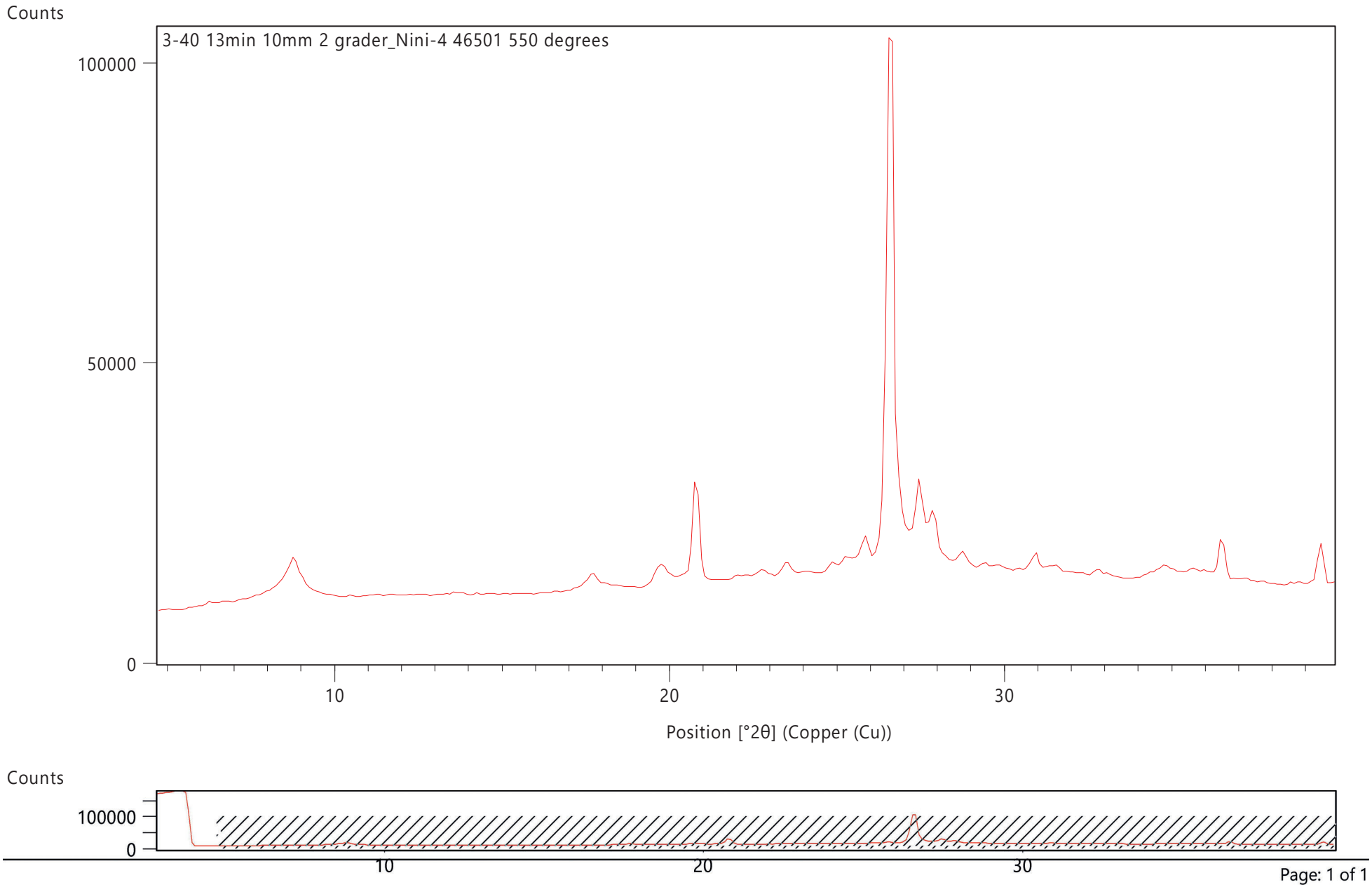
Counts
3-40 13min 10mm 2 grader_Nini-4 46501 550 degrees
100000
50000
0
10
20
30
Position [°2θ] (Copper (Cu))
Counts
100000
0
10
20
30

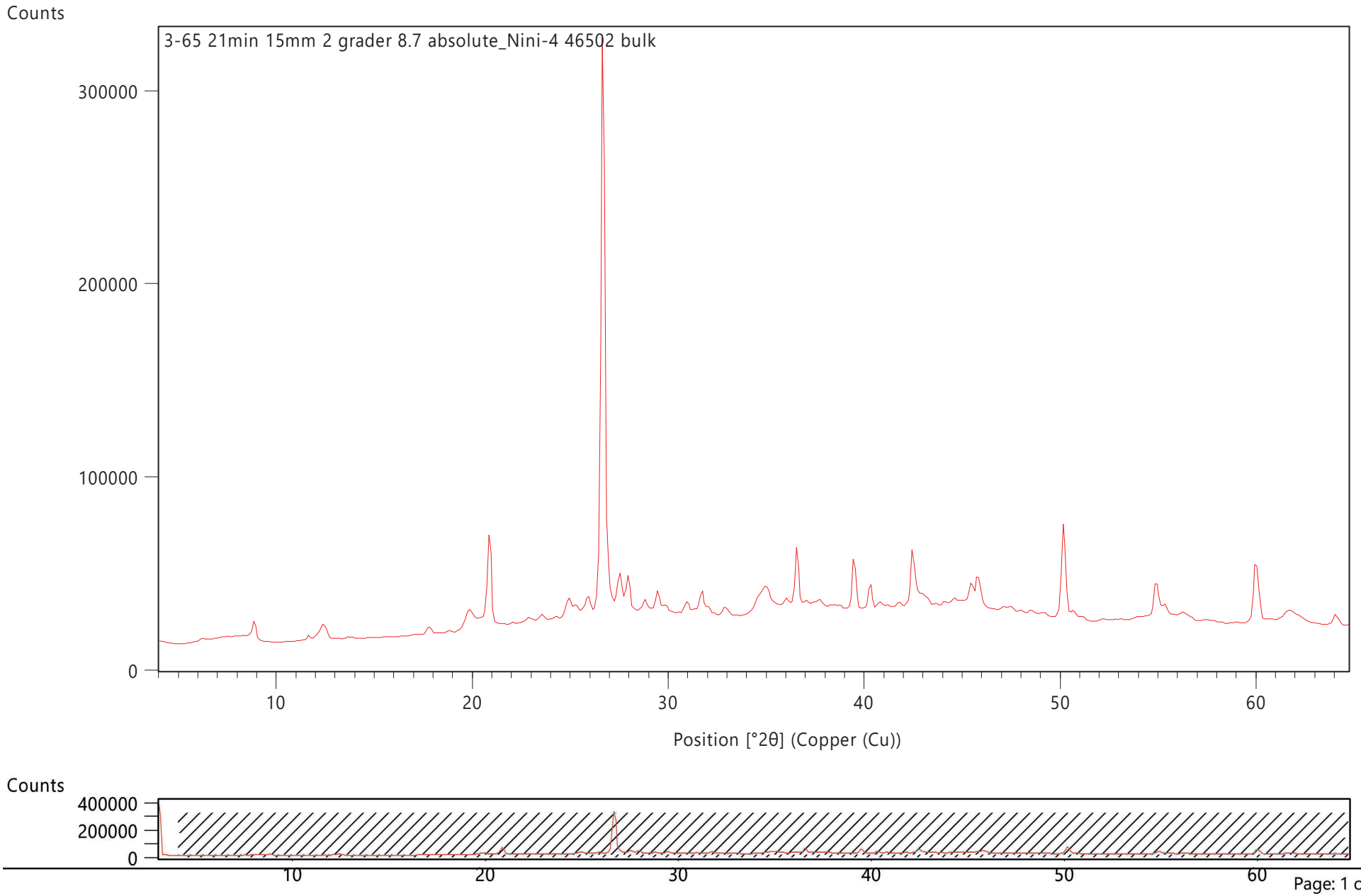
Counts
3-65 21min 15mm 2 grader 8.7 absolute_Nini-4 46502 bulk
300000
200000
100000
0
10
20
30
40
50
60
Position [°2θ] (Copper (Cu))
Counts
400000
200000
0
10
20
30
40
50
60

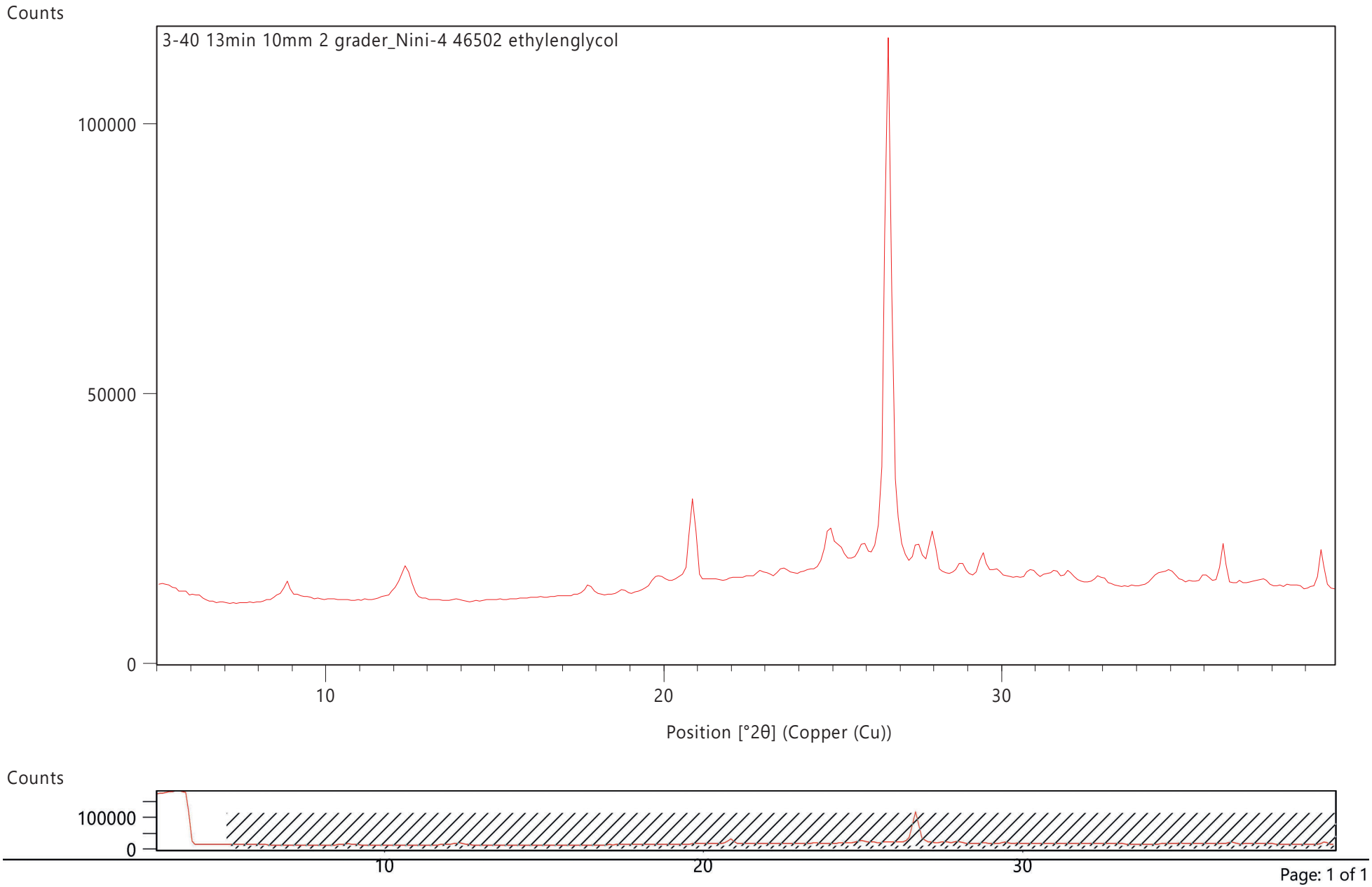
Counts
3-40 13min 10mm 2 grader_Nini-4 46502 ethylenglycol
100000
50000
0
10
20
30
Position [°2θ] (Copper (Cu))
Counts
100000
0
10
20
30

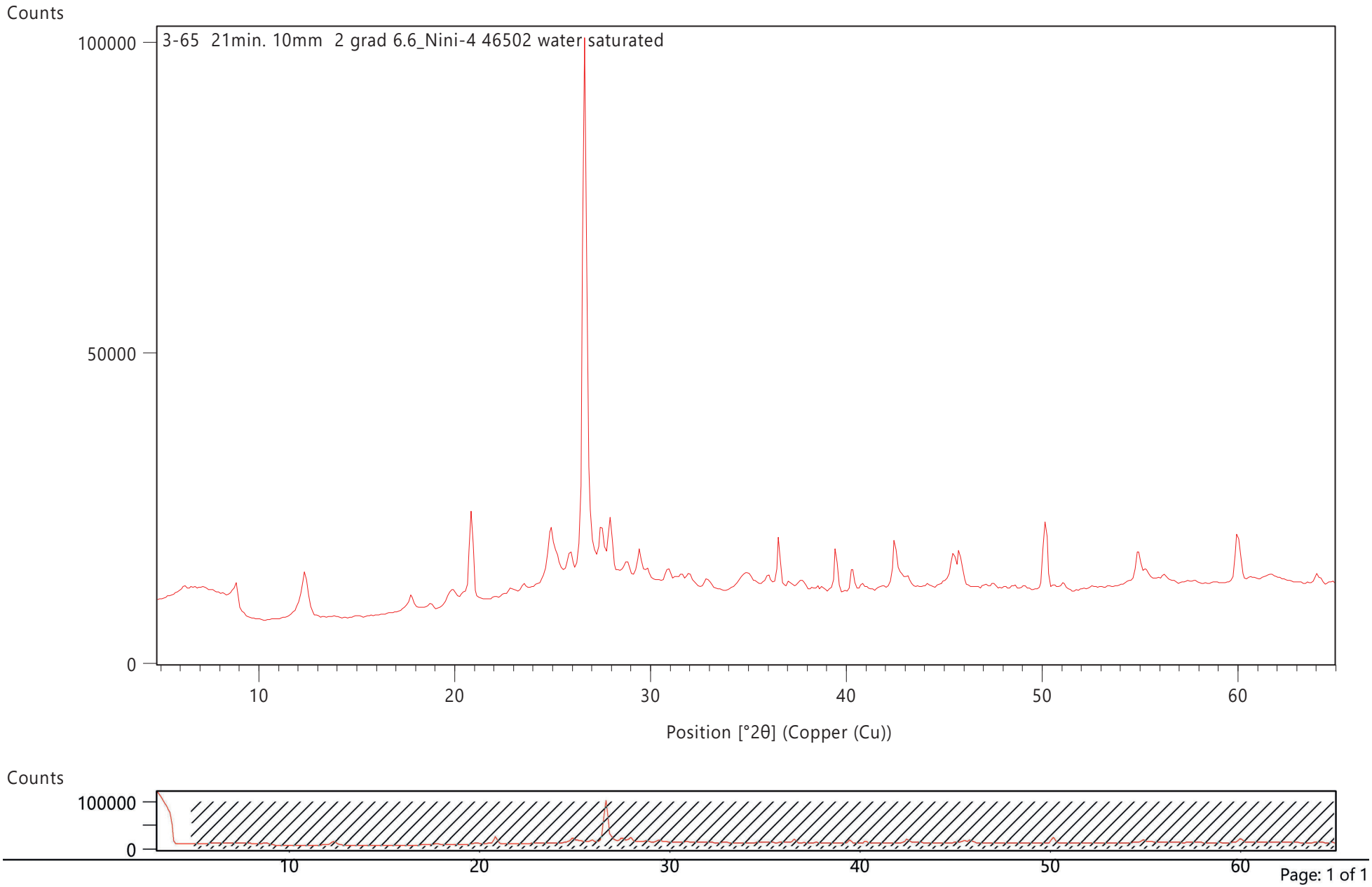
Counts
3-65 21min. 10mm 2 grad 6.6_Nini-4 46502 water saturated
100000
50000
0
10
20
30
40
50
60
Position [°2θ] (Copper (Cu))
Counts
100000
0
10
20
30
40
50
60

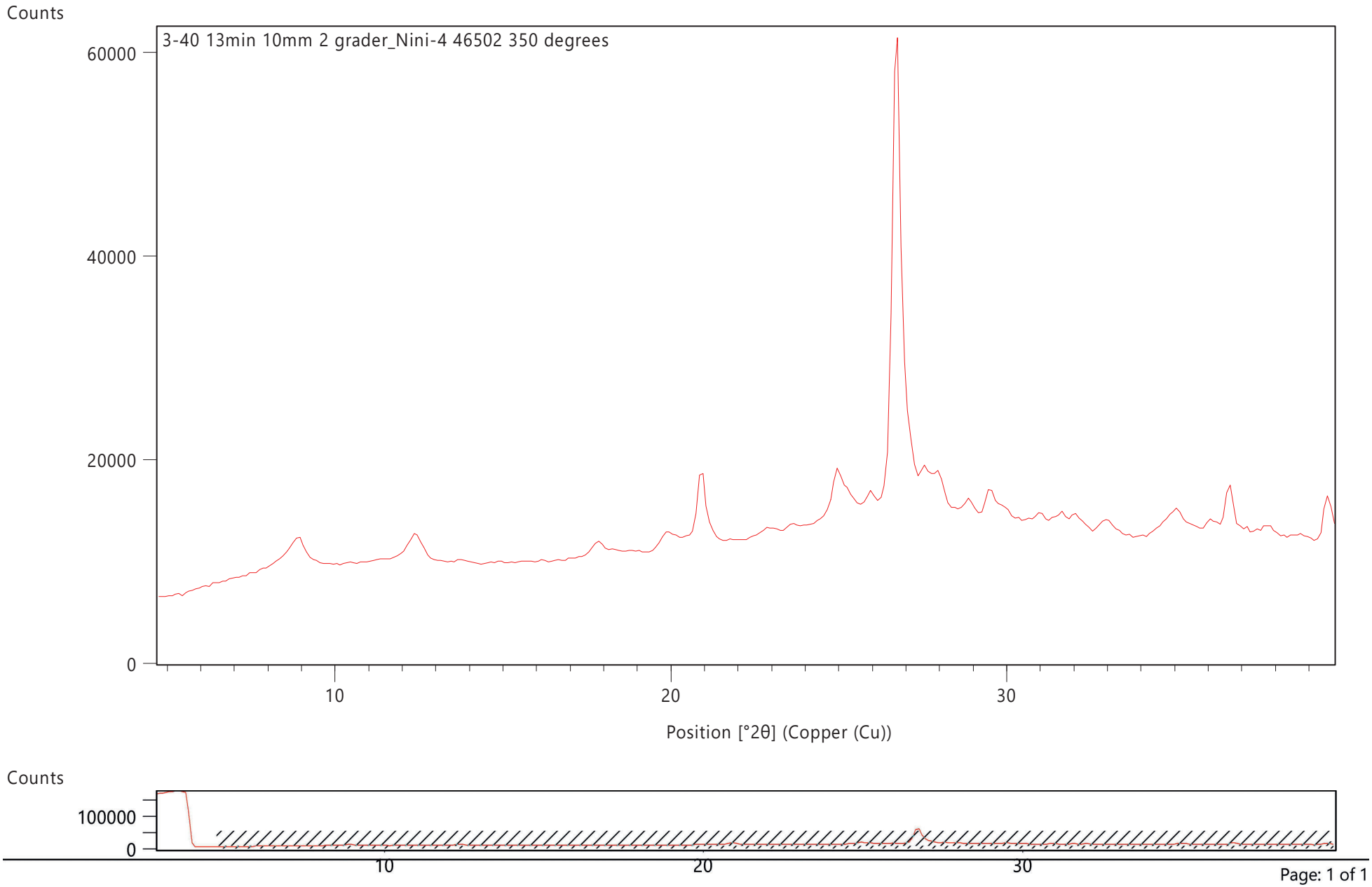
Counts
3-40 13min 10mm 2 grader_Nini-4 46502 350 degrees
60000
40000
20000
0
10
20
30
Position [°2θ] (Copper (Cu))
Counts
100000
0
10
20
30

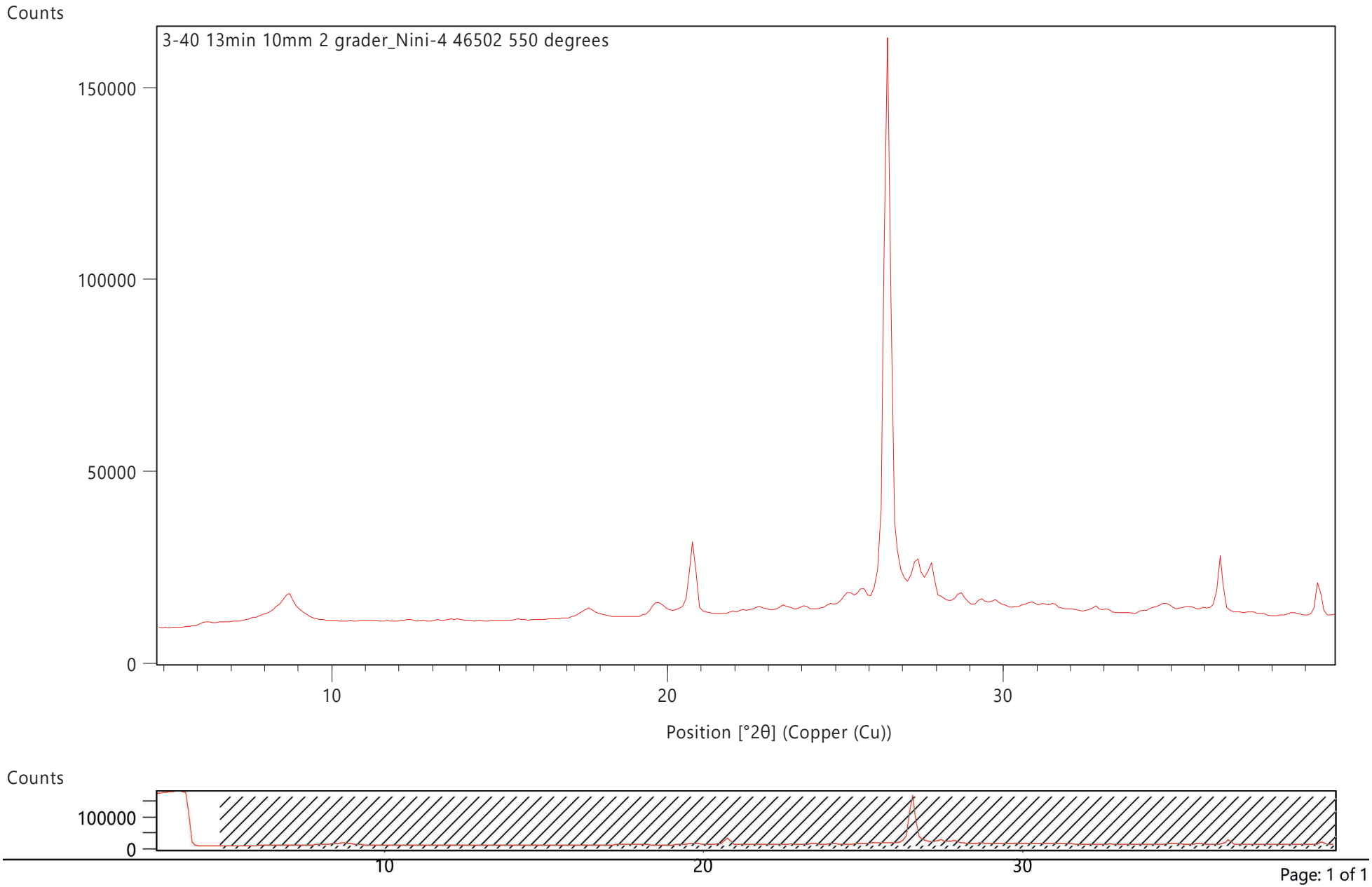
Counts
3-40 13min 10mm 2 grader_Nini-4 46502 550 degrees
150000
100000
50000
0
10
20
30
Position [°2θ] (Copper (Cu))
Counts
100000
0
10
20
30

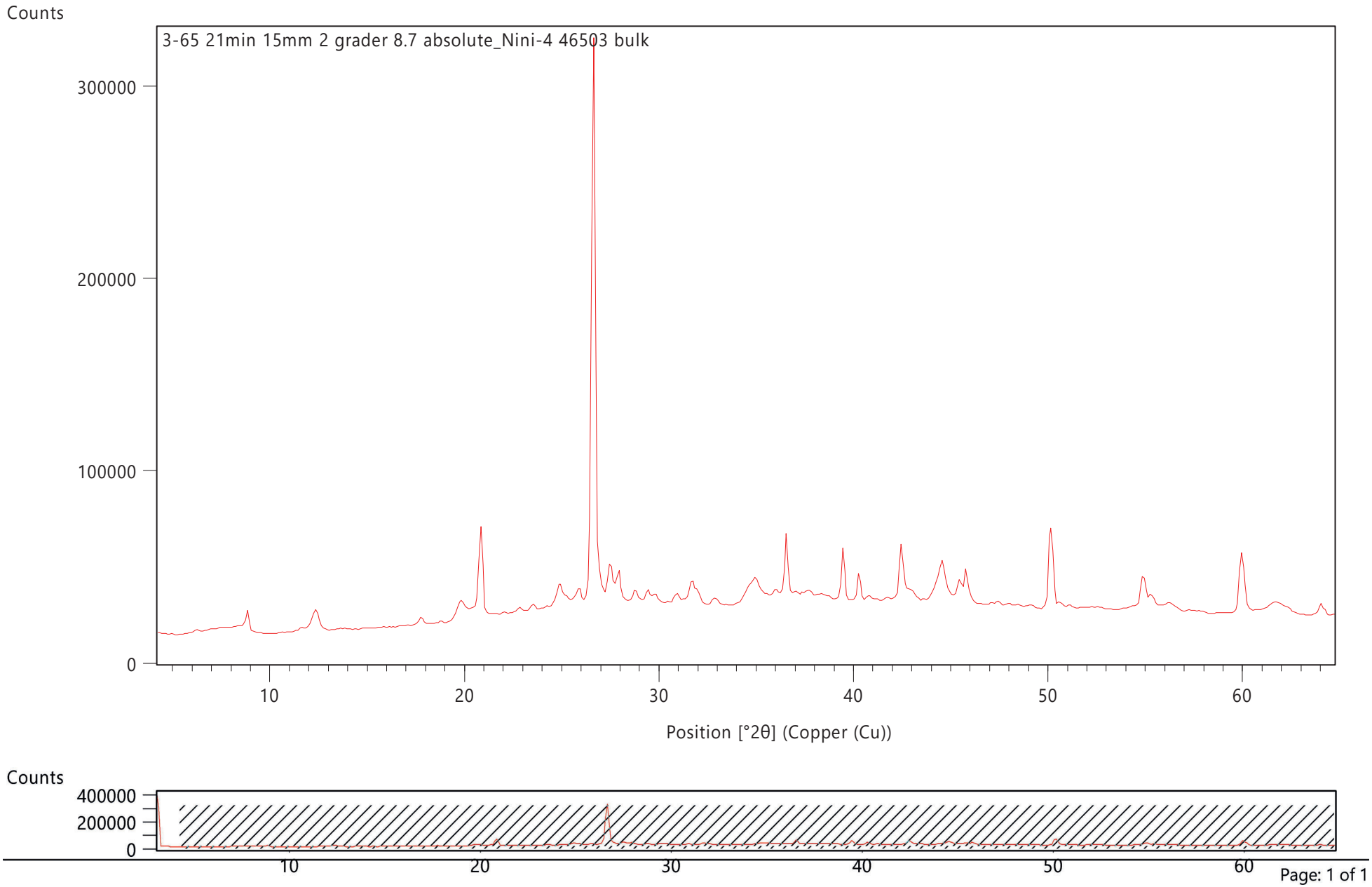
Counts
3-65 21min 15mm 2 grader 8.7 absolute_Nini-4 46503 bulk
300000
200000
100000
0
10
20
30
40
50
60
Position [°2θ] (Copper (Cu))
Counts
400000
200000
0
10
20
30
40
50
60

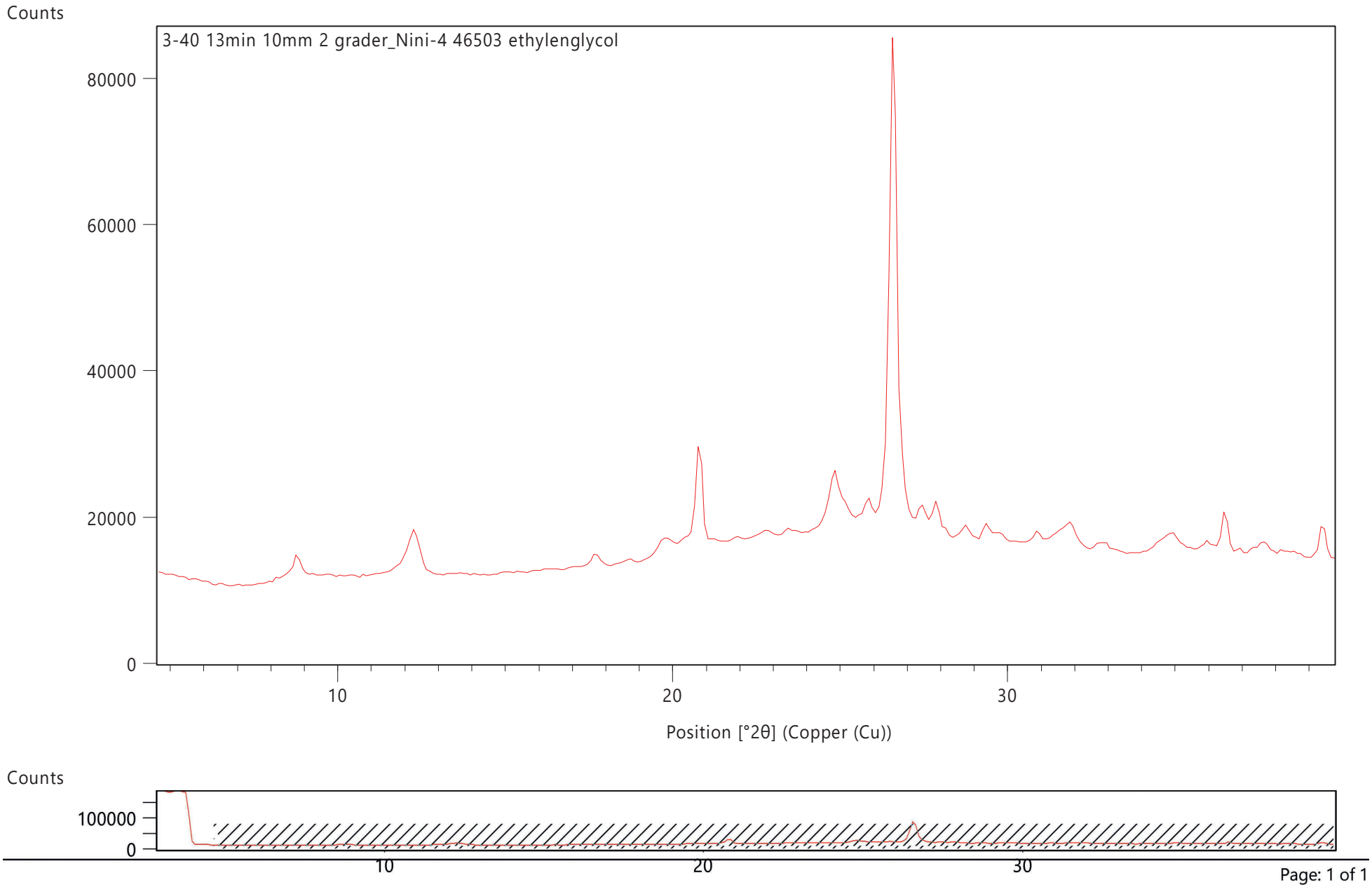
Counts
3-40 13min 10mm 2 grader_Nini-4 46503 ethylenglycol
80000
60000
40000
20000
0
10
20
30
Position [°2θ] (Copper (Cu))
Counts
100000
0
10
20
30

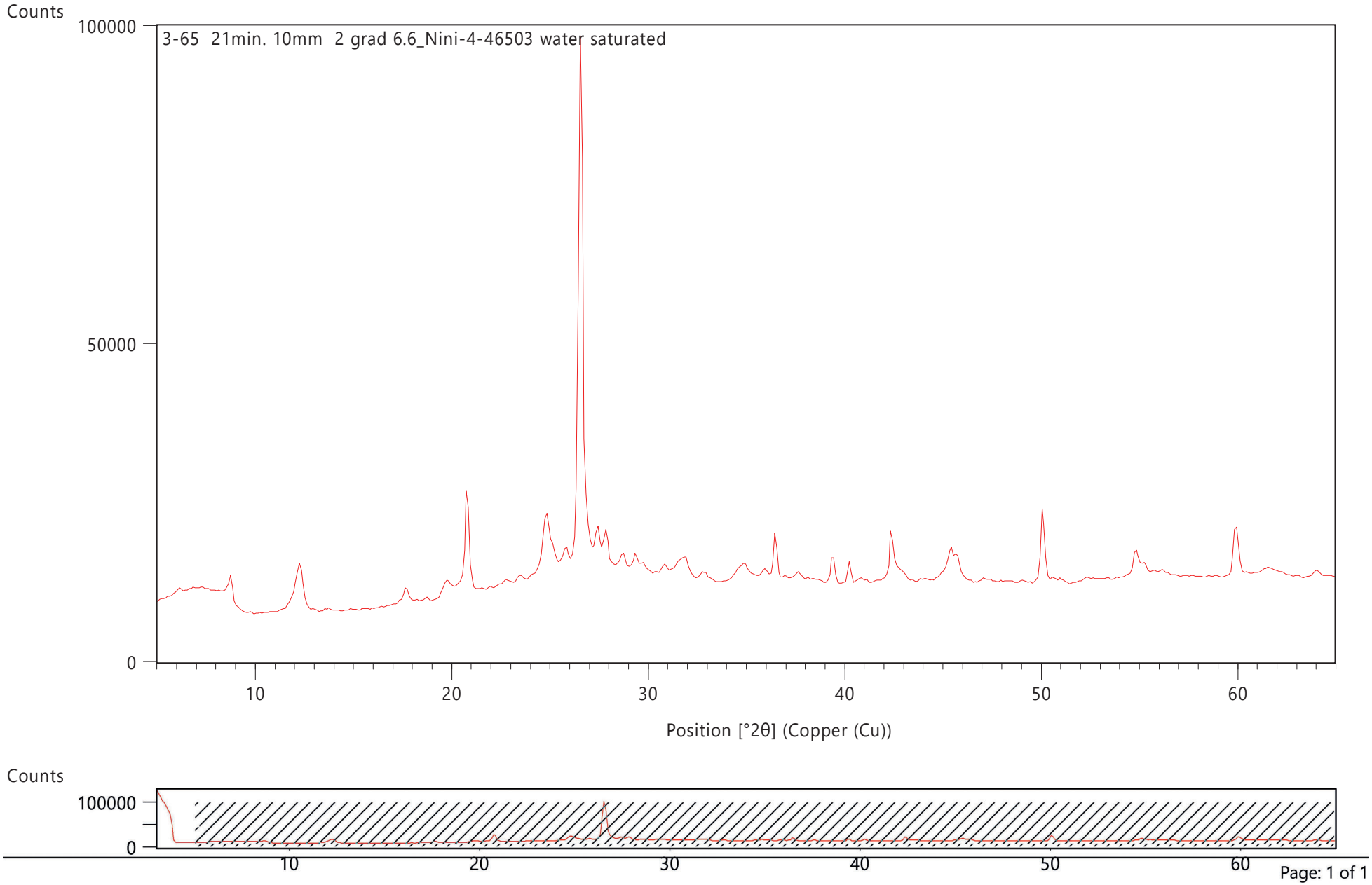
Counts
100000
50000
0
3-65 21min. 10mm 2 grad 6.6_Nini-4-46503 water saturated
10
20
30
40
50
60
Position [°2θ] (Copper (Cu))
Counts
100000
0
10
20
30
40
50
60

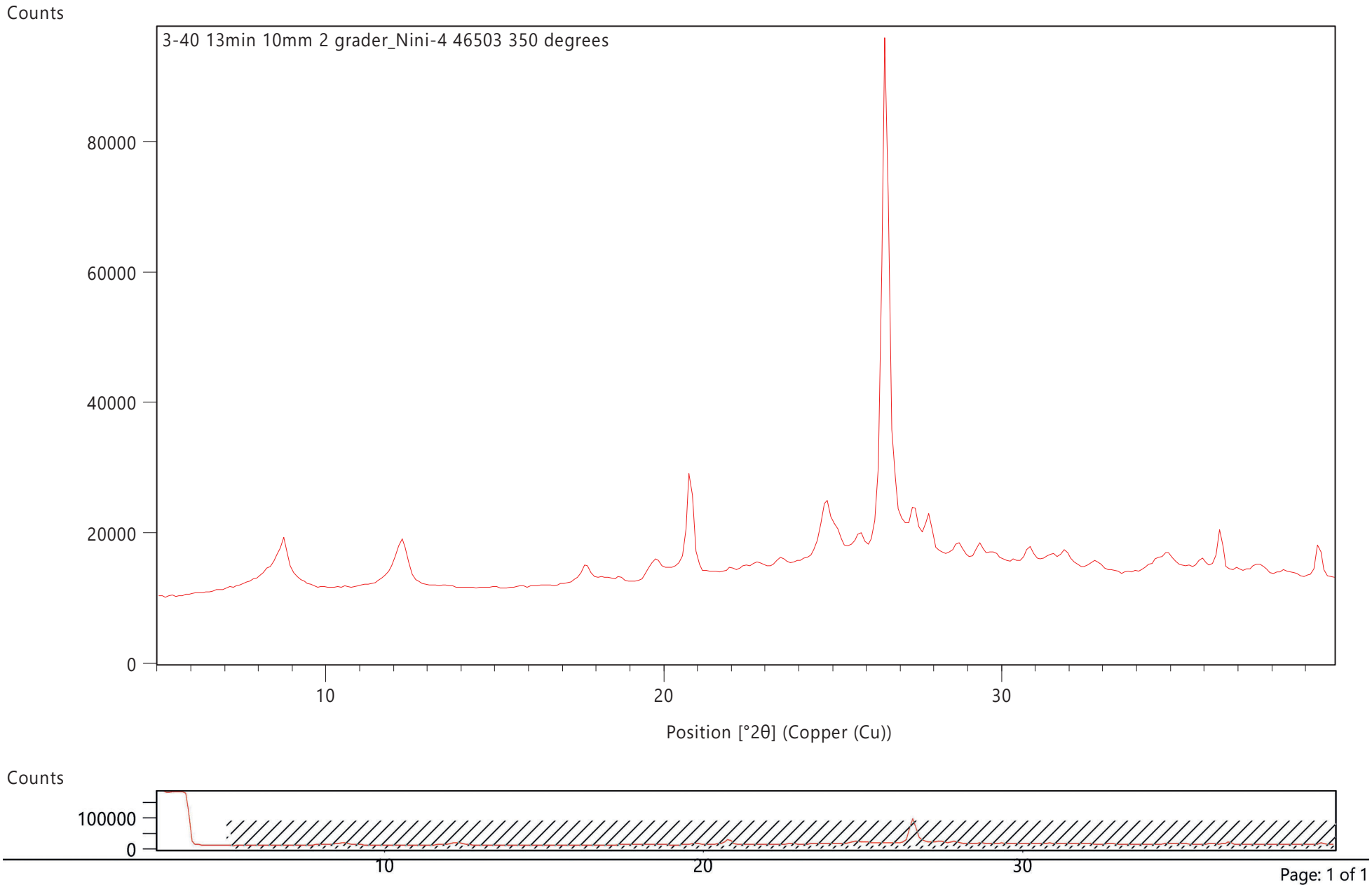
Counts
3-40 13min 10mm 2 grader_Nini-4 46503 350 degrees
80000
60000
40000
20000
0
10
20
30
Position [°2θ] (Copper (Cu))
Counts
100000
0
10
20
30

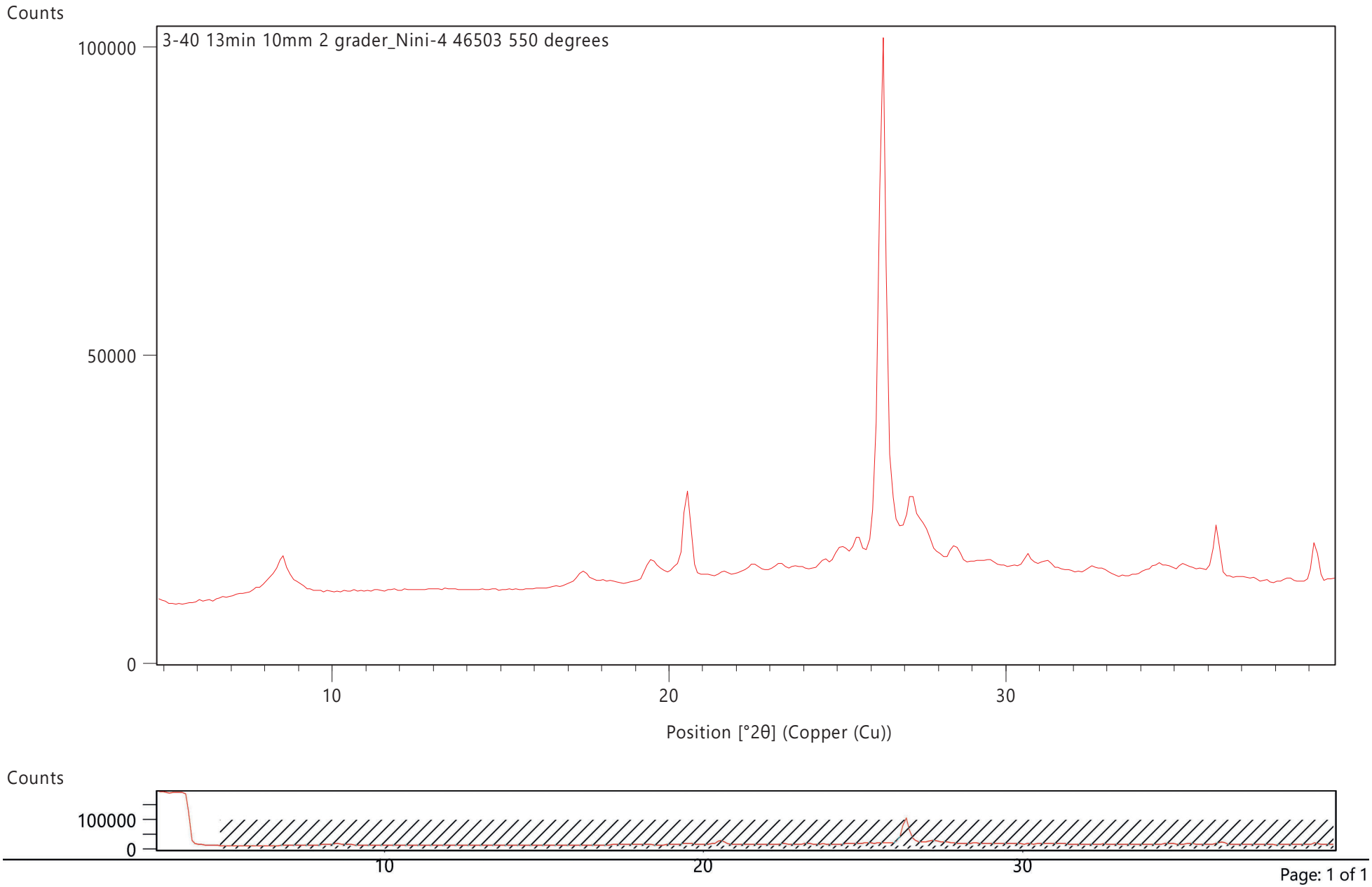
Counts
3-40 13min 10mm 2 grader_Nini-4 46503 550 degrees
100000
50000
0
10
20
30
Position [°2θ] (Copper (Cu))
Counts
100000
0
10
20
30

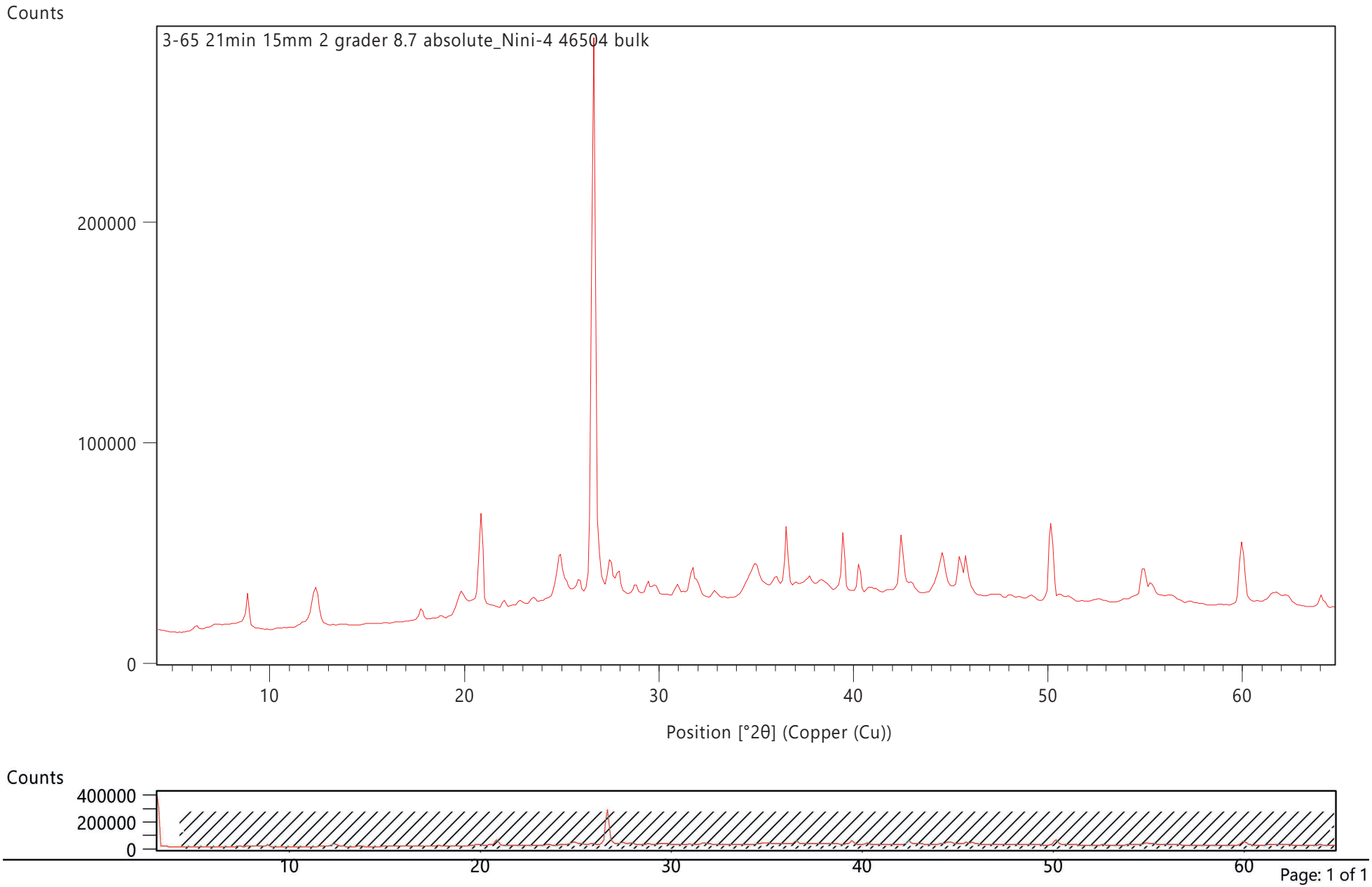
Counts
3-65 21min 15mm 2 grader 8.7 absolute_Nini-4 46504 bulk
200000
100000
0
10
20
30
40
50
60
Position [°2θ] (Copper (Cu))
Counts
400000
200000
0
10
20
30
40
50
60

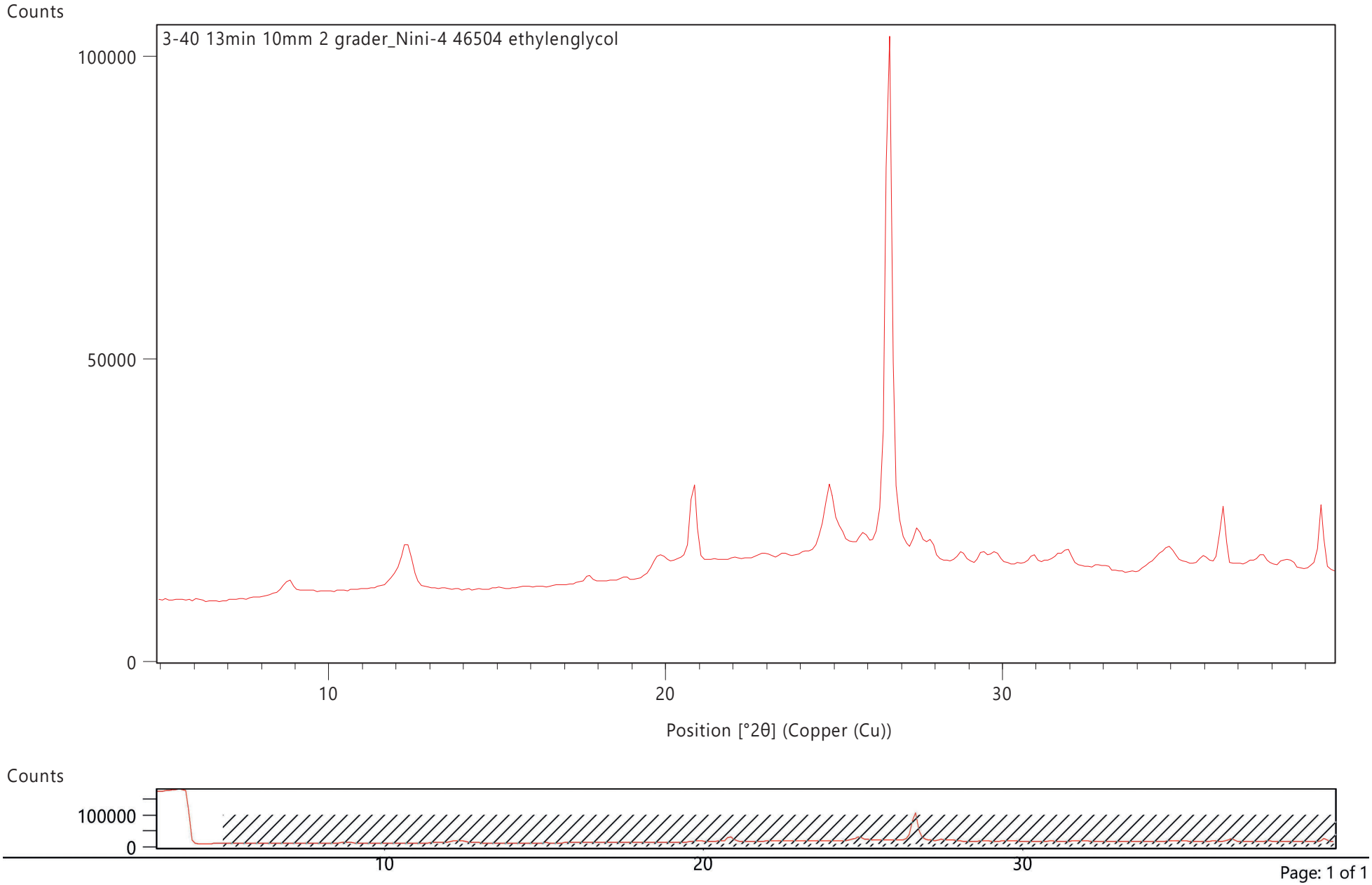
Counts
3-40 13min 10mm 2 grader_Nini-4 46504 ethylenglycol
100000
50000
0
10
20
30
Position [°2θ] (Copper (Cu))
Counts
100000
0
10
20
30

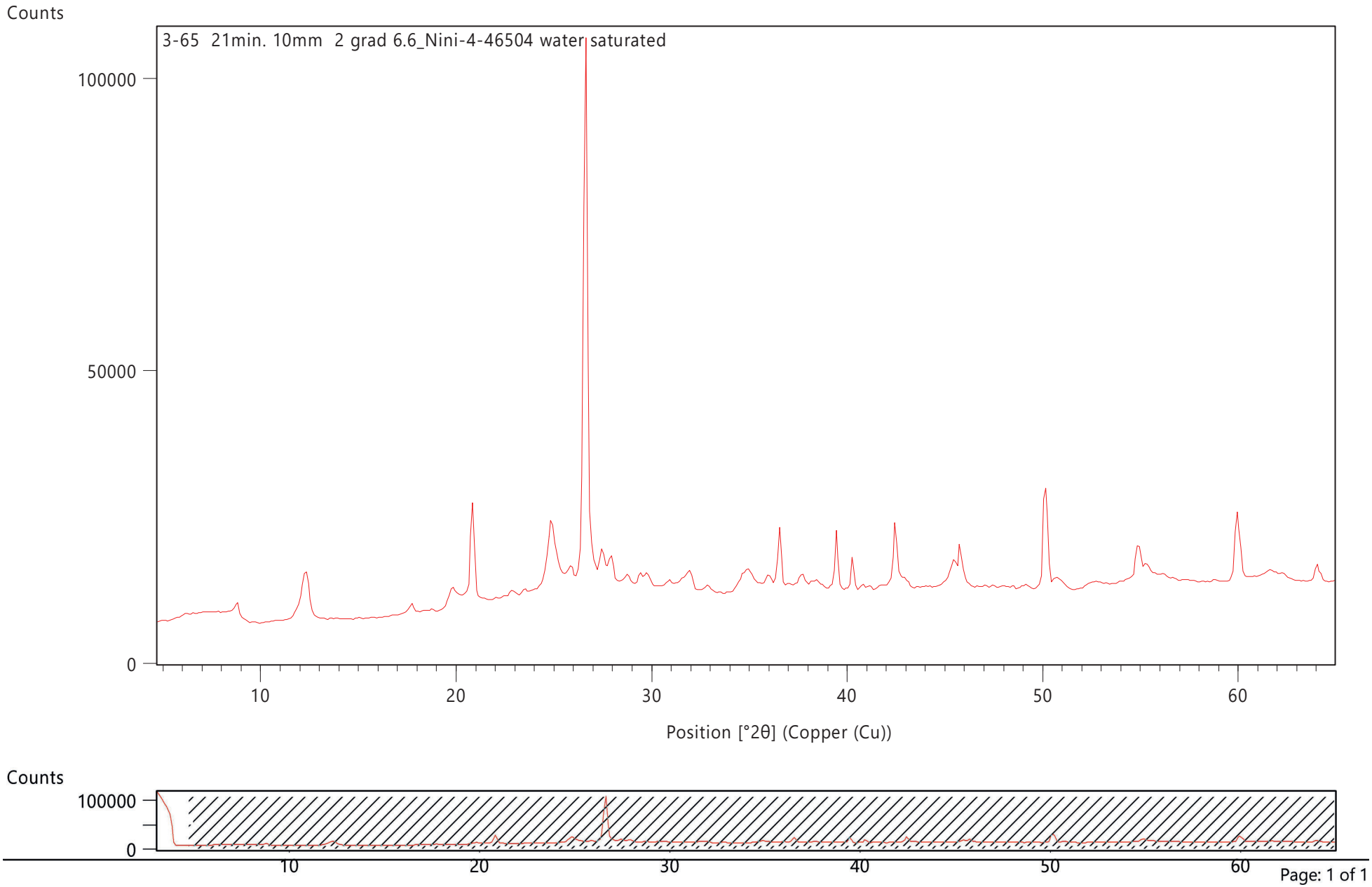
Counts
3-65 21min. 10mm 2 grad 6.6_Nini-4-46504 water saturated
100000
50000
0
10
20
30
40
50
60
Position [°2θ] (Copper (Cu))
Counts
100000
0
10
20
30
40
50
60

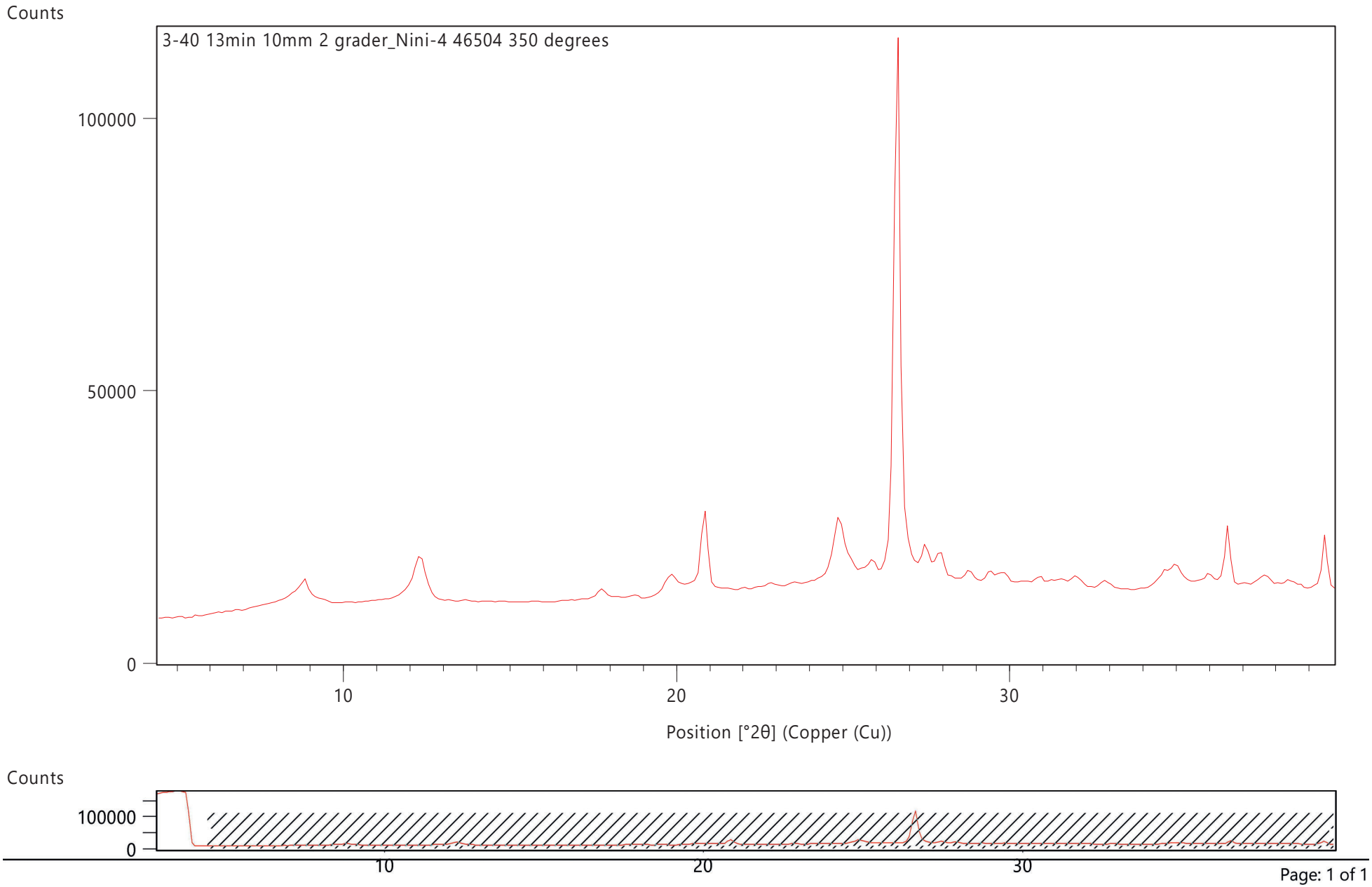
Counts
3-40 13min 10mm 2 grader_Nini-4 46504 350 degrees
100000
50000
0
10
20
30
Position [°2θ] (Copper (Cu))
Counts
100000
0
10
20
30

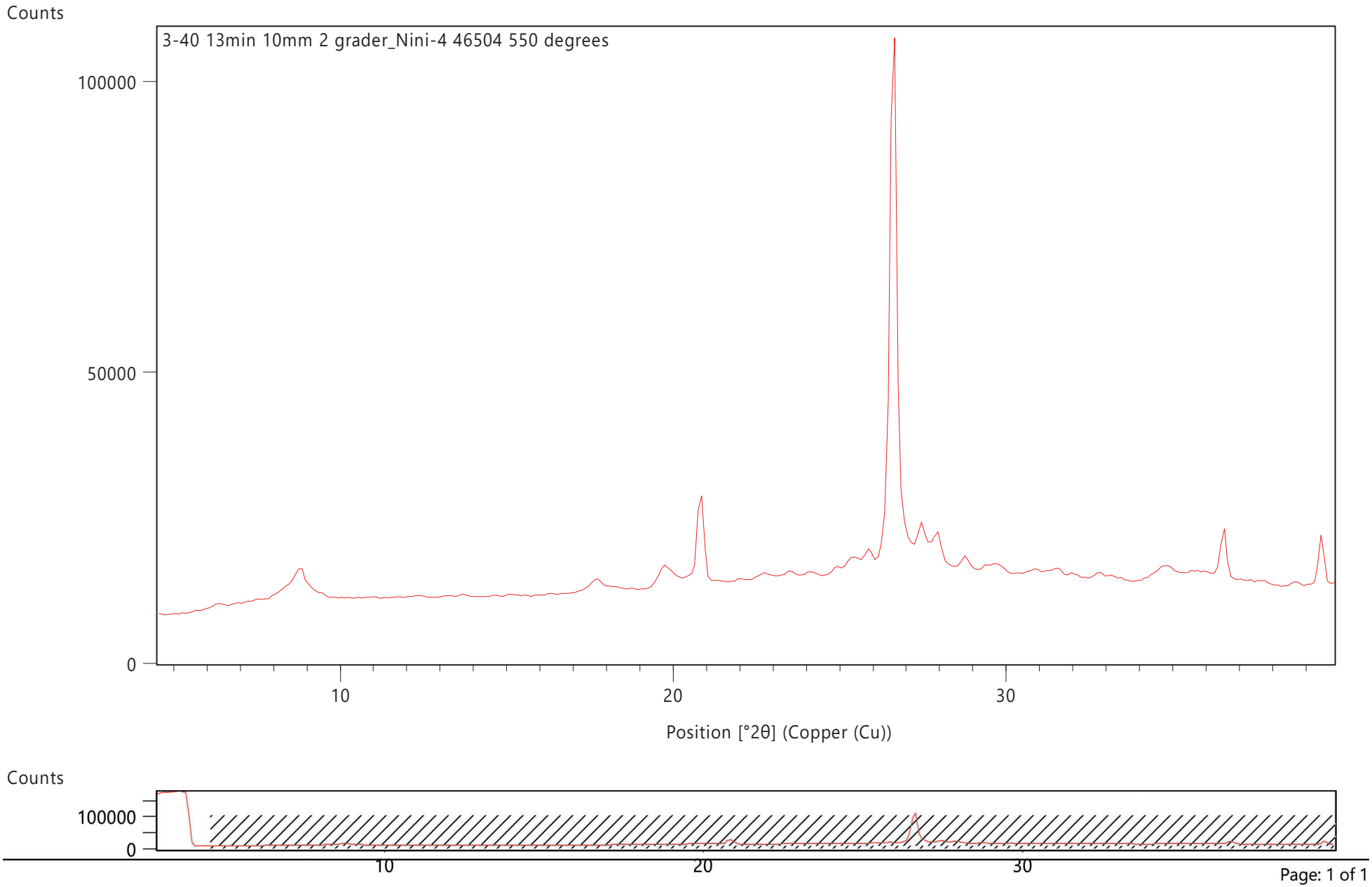
Counts
3-40 13min 10mm 2 grader_Nini-4 46504 550 degrees
100000
50000
0
10
20
30
Position [°2θ] (Copper (Cu))
Counts
100000
0
10
20
30

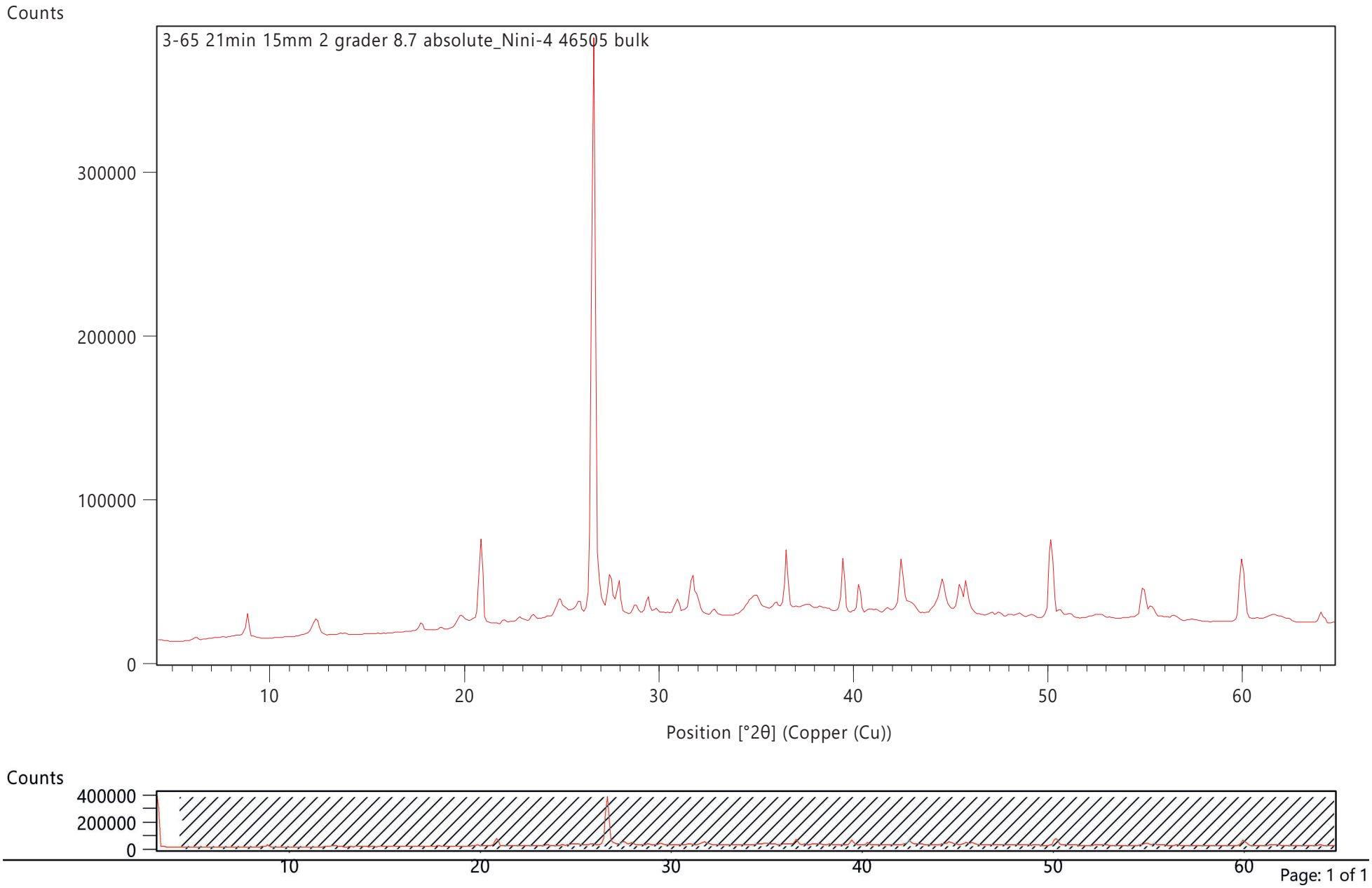
Counts
3-65 21min 15mm 2 grader 8.7 absolute_Nini-4 46505 bulk
300000
200000
100000
0
10
20
30
40
50
60
Position [°2θ] (Copper (Cu))
Counts
400000
200000
0
10
20
30
40
50
60

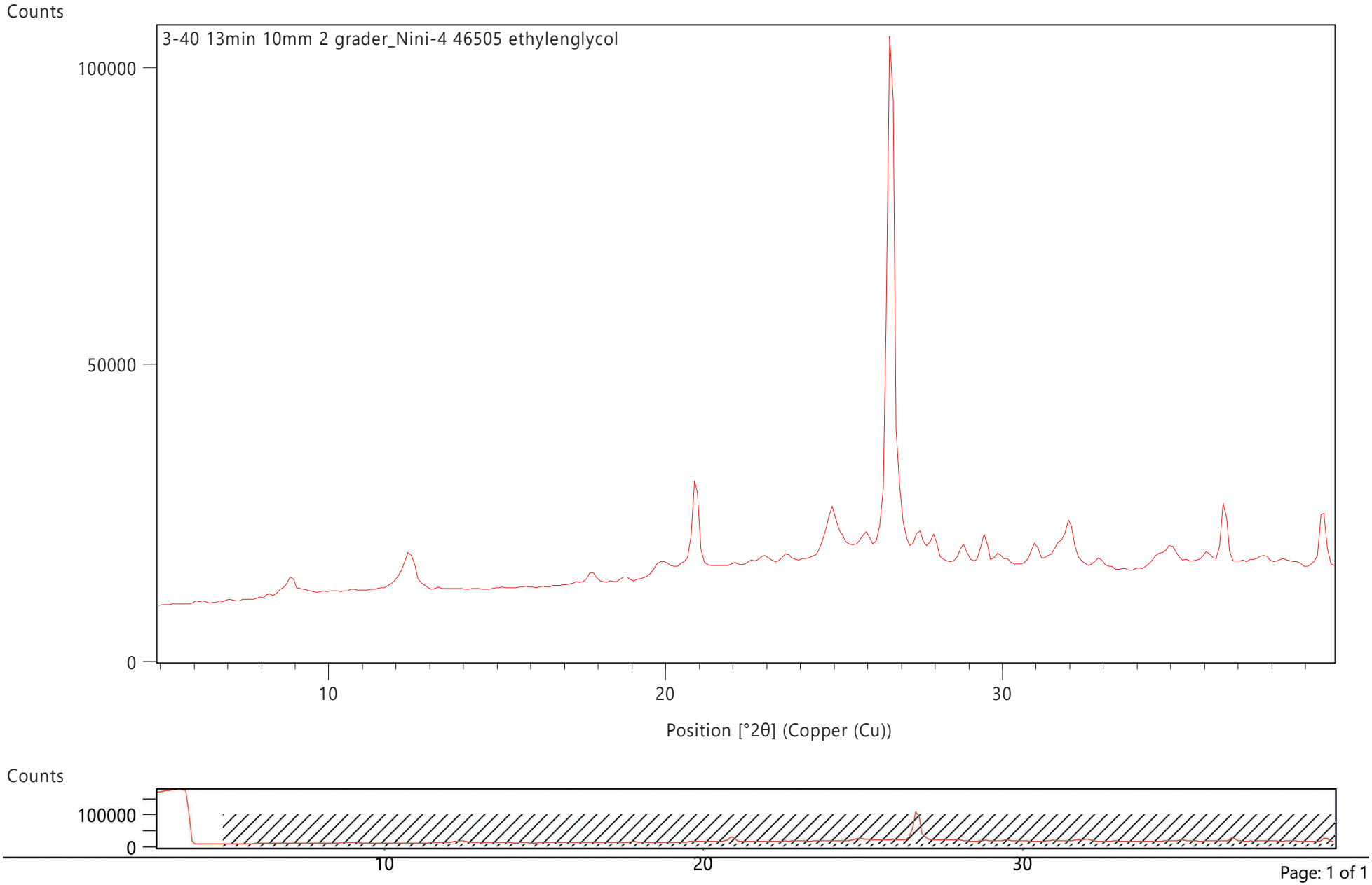
Counts
3-40 13min 10mm 2 grader_Nini-4 46505 ethylenglycol
100000
50000
0
10
20
30
Position [°2θ] (Copper (Cu))
Counts
100000
0
10
20
30

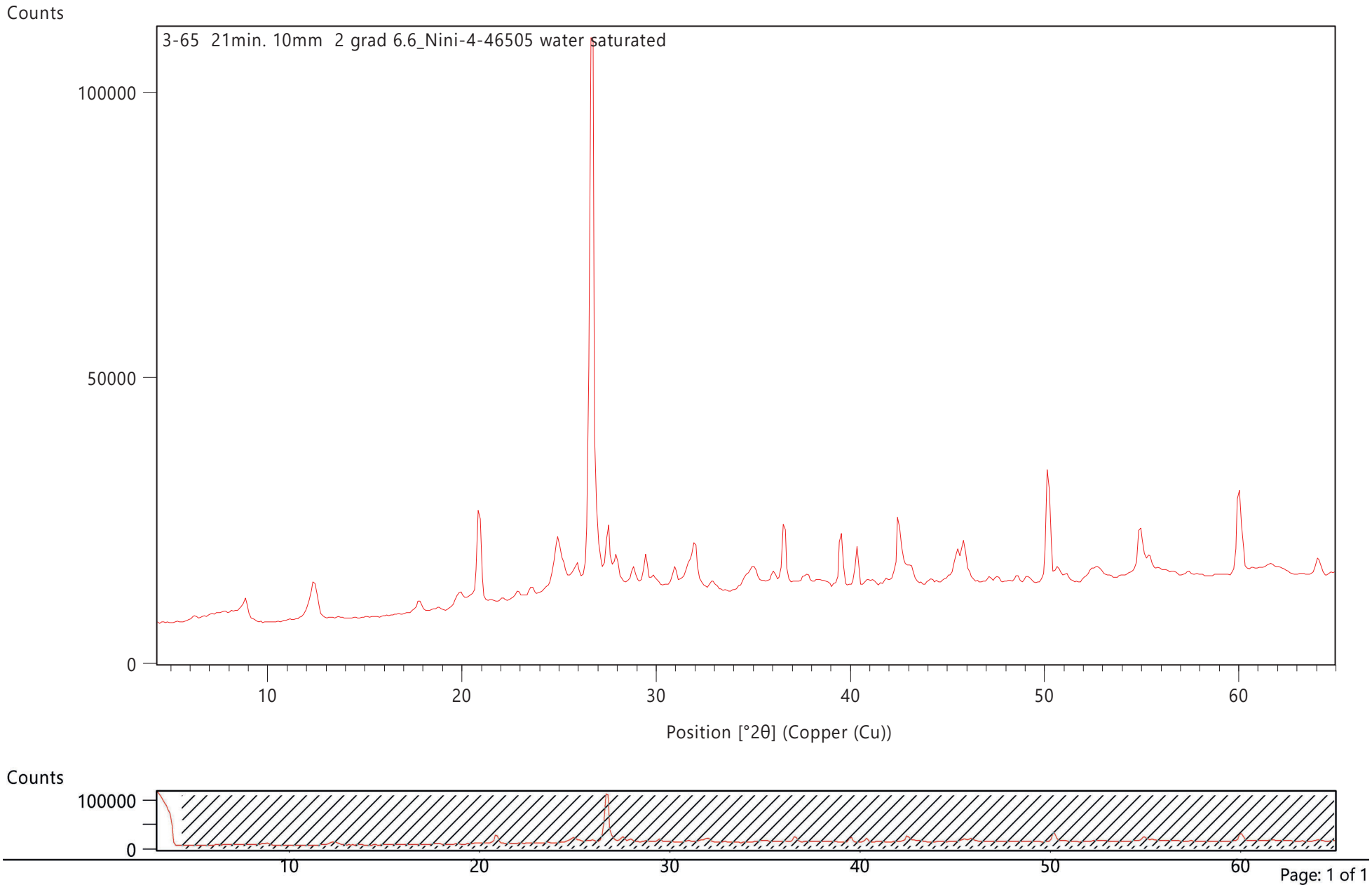
Counts
3-65 21min. 10mm 2 grad 6.6_Nini-4-46505 water saturated
100000
50000
0
10
20
30
40
50
60
Position [°2θ] (Copper (Cu))
Counts
100000
0
10
20
30
40
50
60

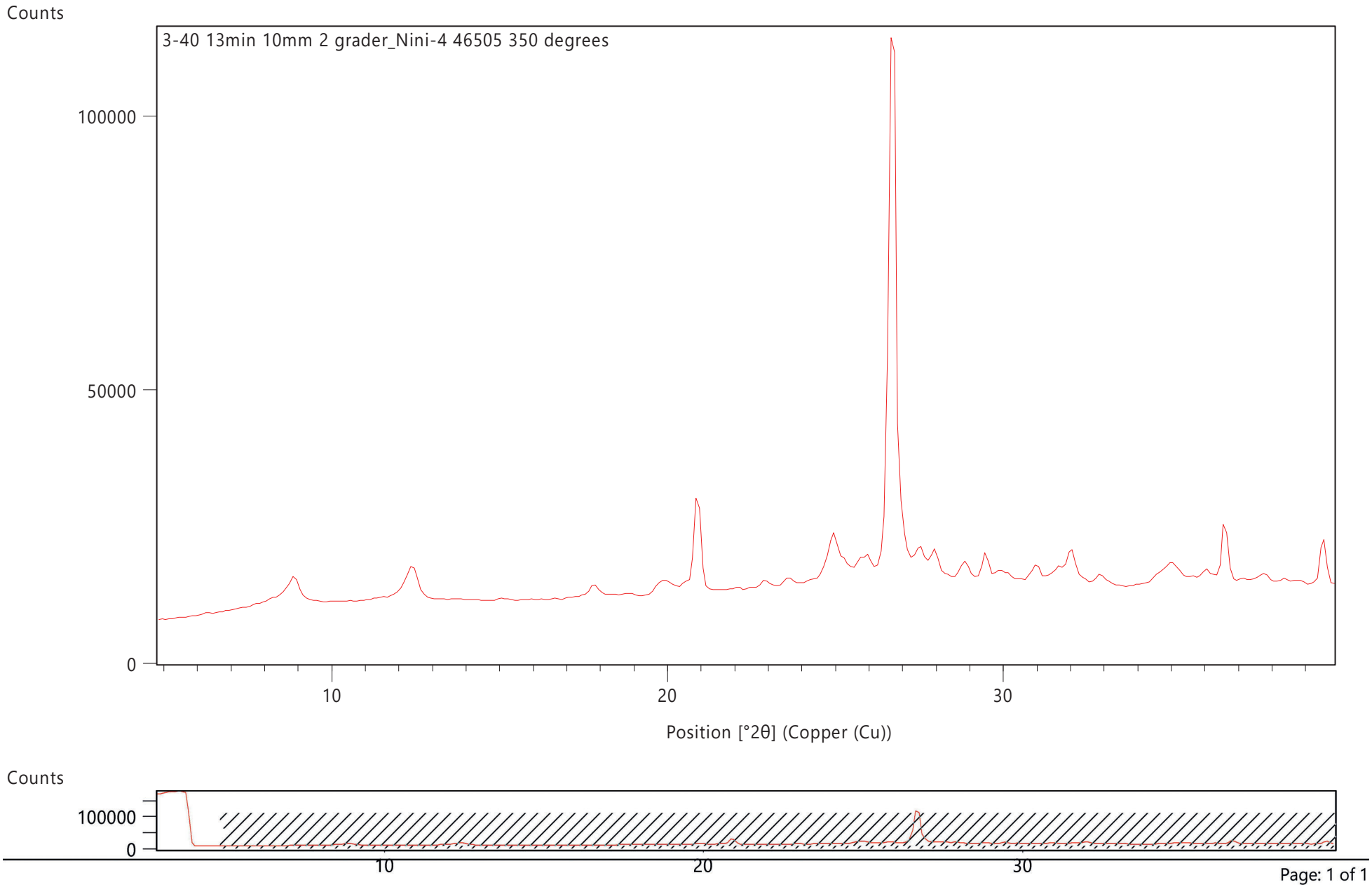
Counts
3-40 13min 10mm 2 grader_Nini-4 46505 350 degrees
100000
50000
0
10
20
30
Position [°2θ] (Copper (Cu))
Counts
100000
0
10
20
30

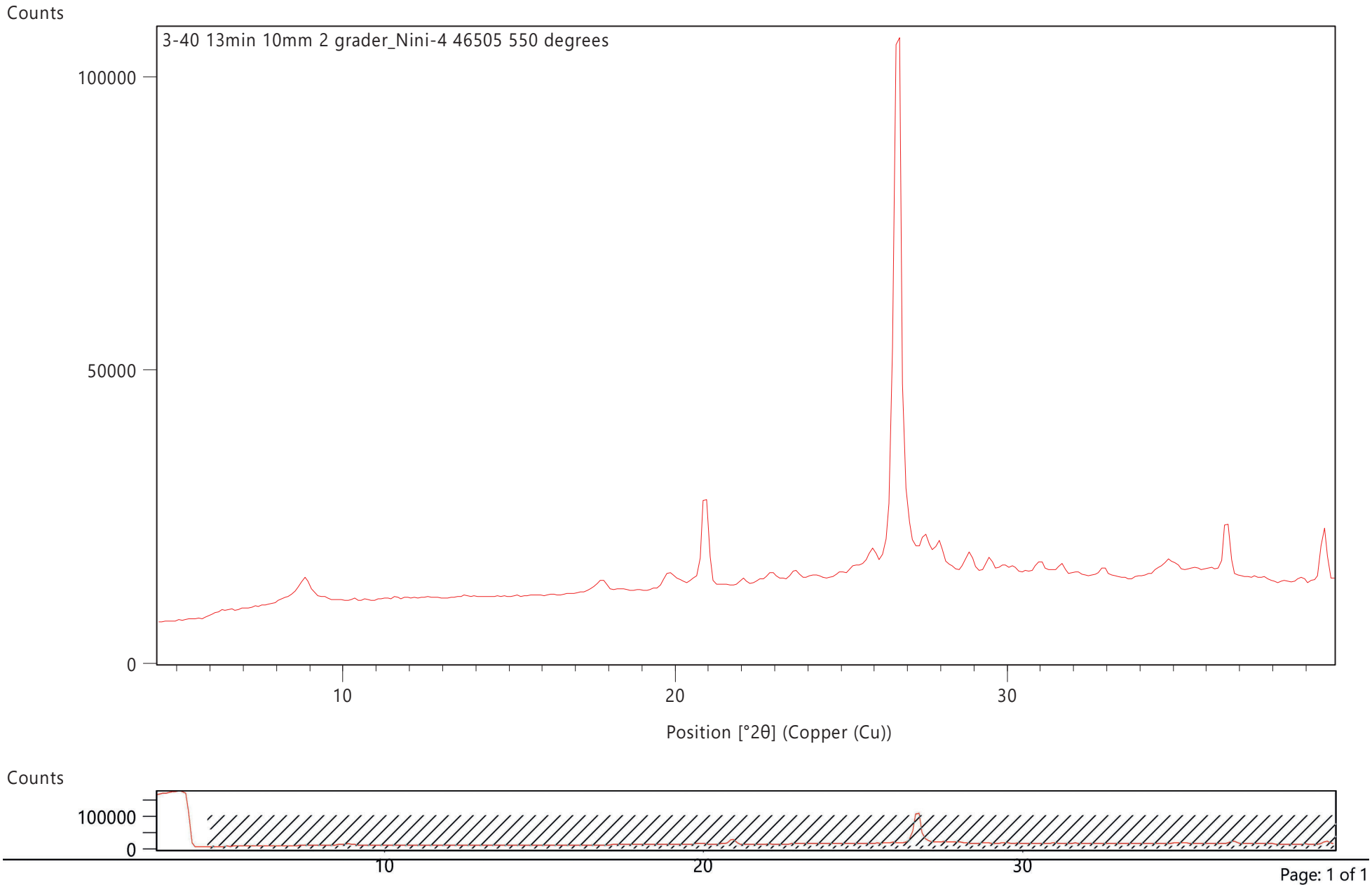
Counts
3-40 13min 10mm 2 grader_Nini-4 46505 550 degrees
100000
50000
0
10
20
30
Position [°2θ] (Copper (Cu))
Counts
100000
0
10
20
30

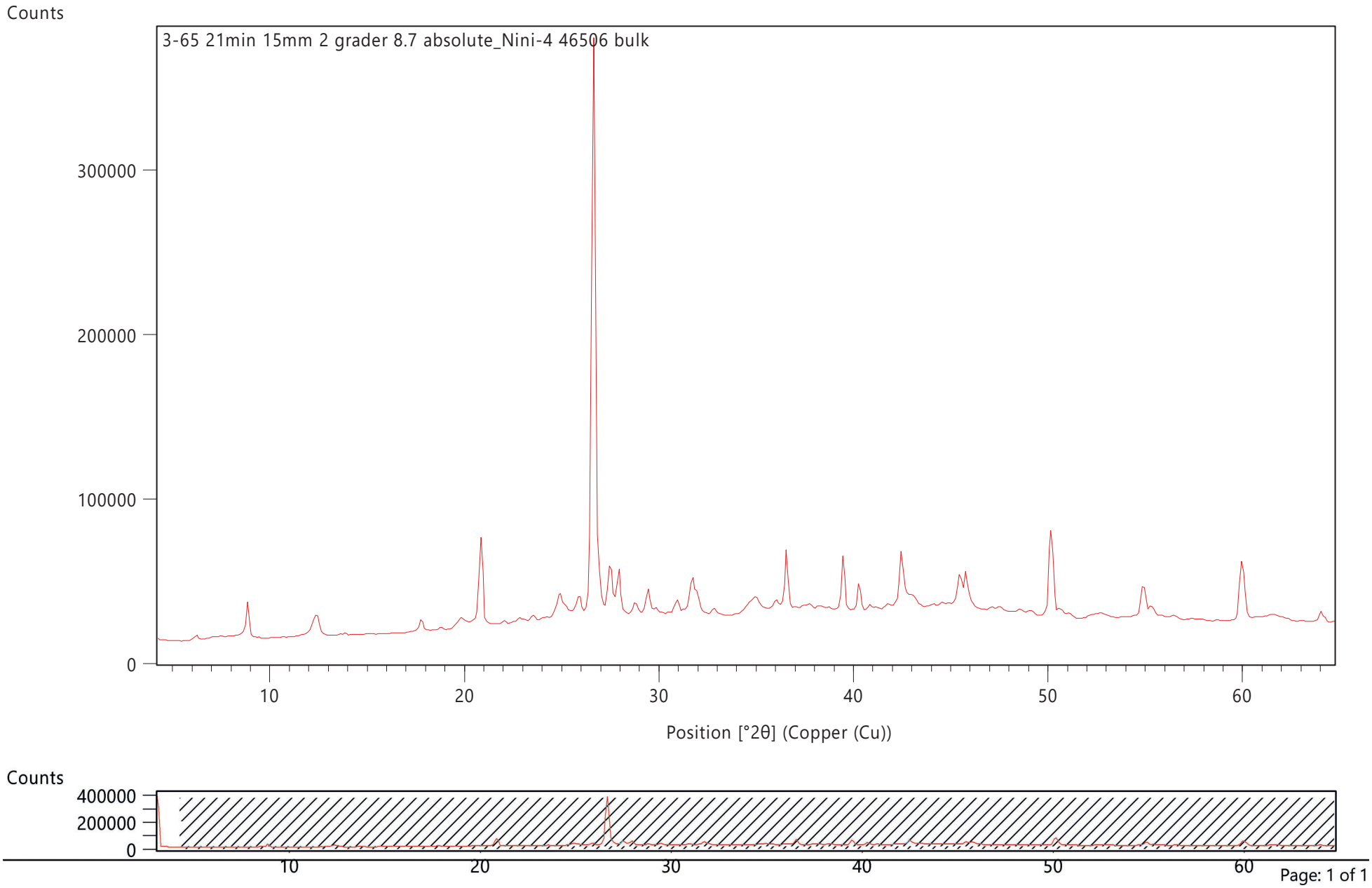
Counts
3-65 21min 15mm 2 grader 8.7 absolute_Nini-4 46506 bulk
300000
200000
100000
0
10
20
30
40
50
60
Position [°2θ] (Copper (Cu))
Counts
400000
200000
0
10
20
30
40
50
60

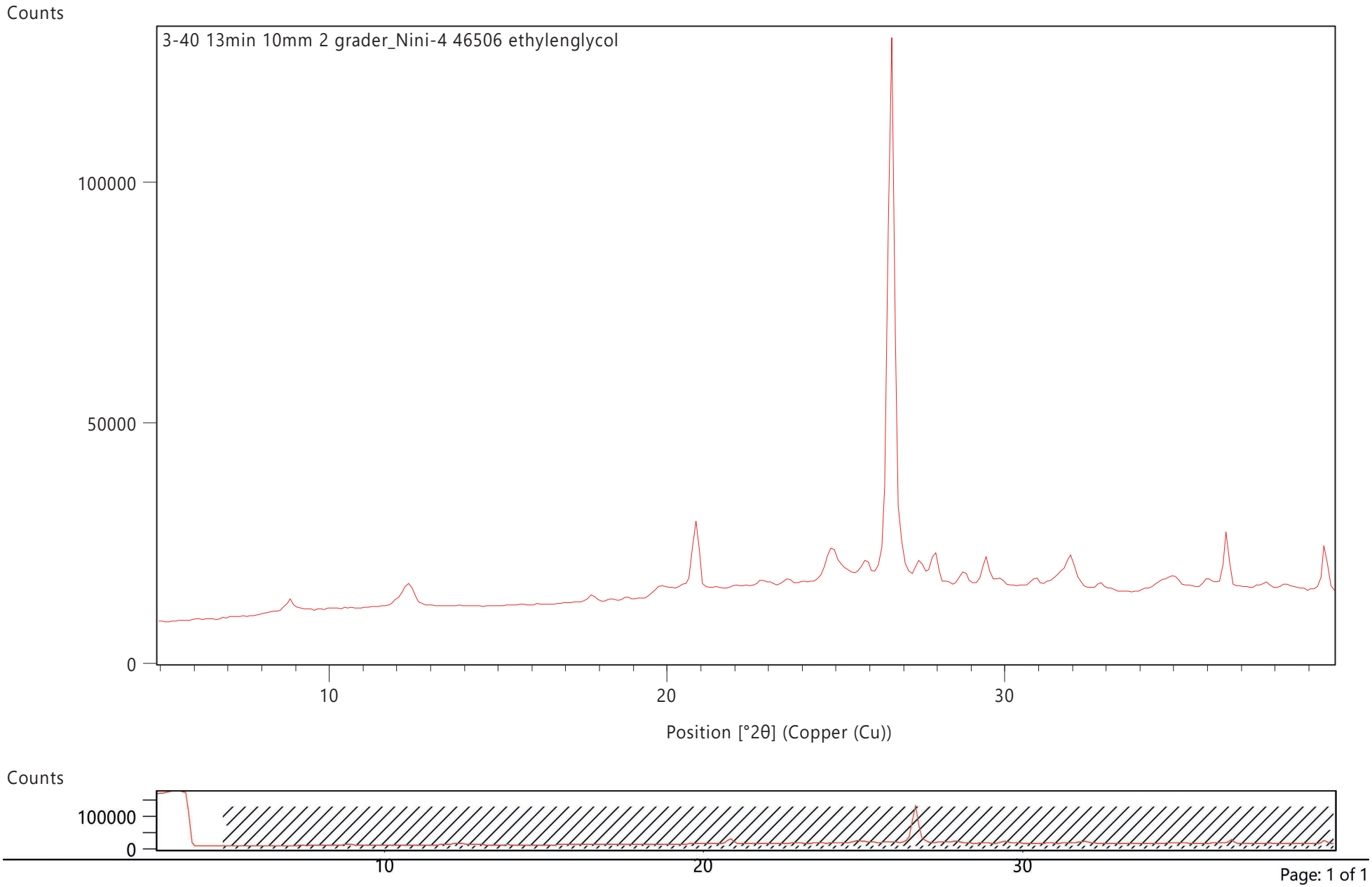
Counts
3-40 13min 10mm 2 grader_Nini-4 46506 ethylenglycol
100000
50000
0
10
20
30
Position [°2θ] (Copper (Cu))
Counts
100000
0
10
20
30

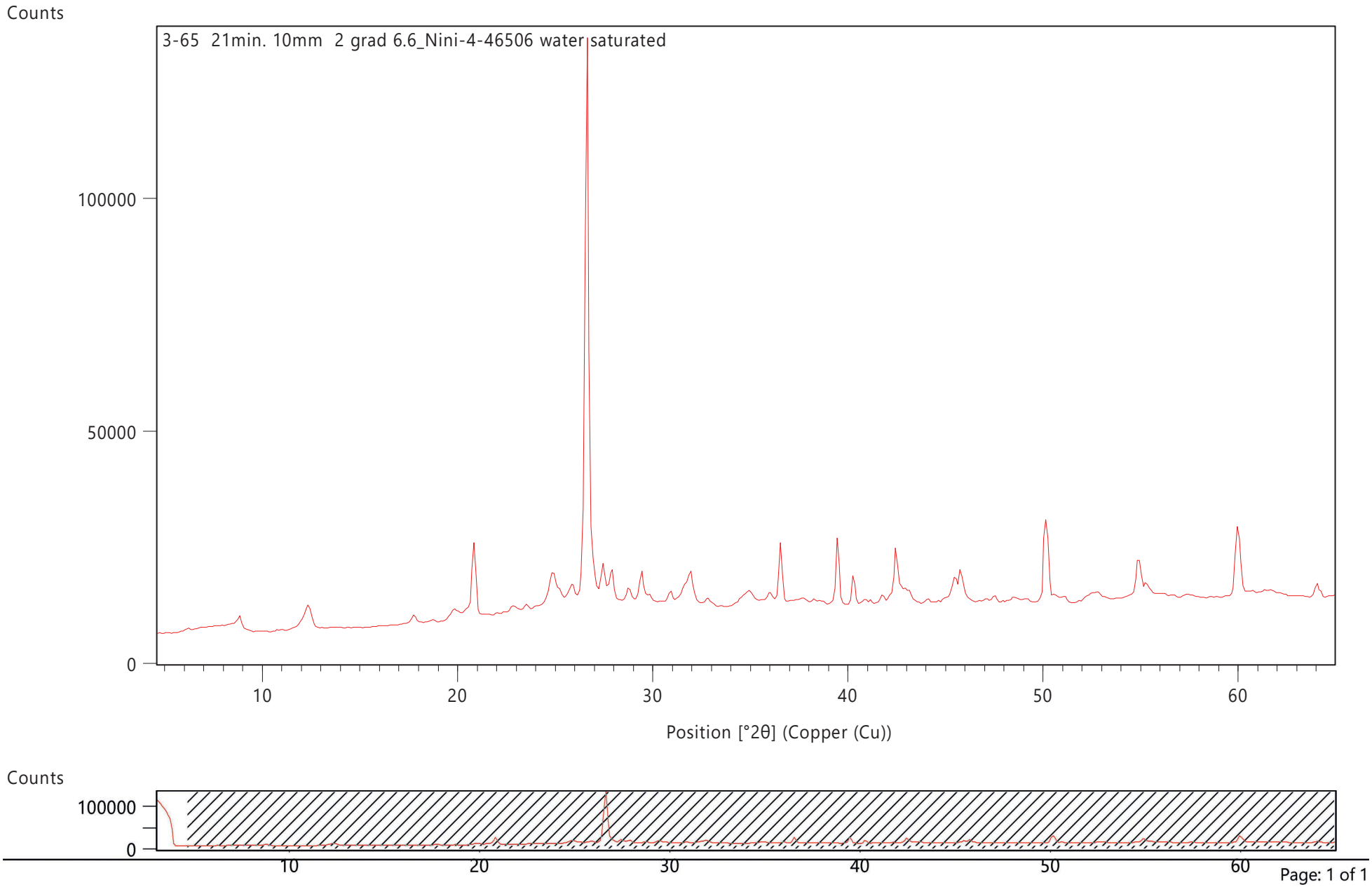
Counts
3-65 21min. 10mm 2 grad 6.6_Nini-4-46506 water saturated
100000
50000
0
10
20
30
40
50
60
Position [°2θ] (Copper (Cu))
Counts
100000
0
10
20
30
40
50
60

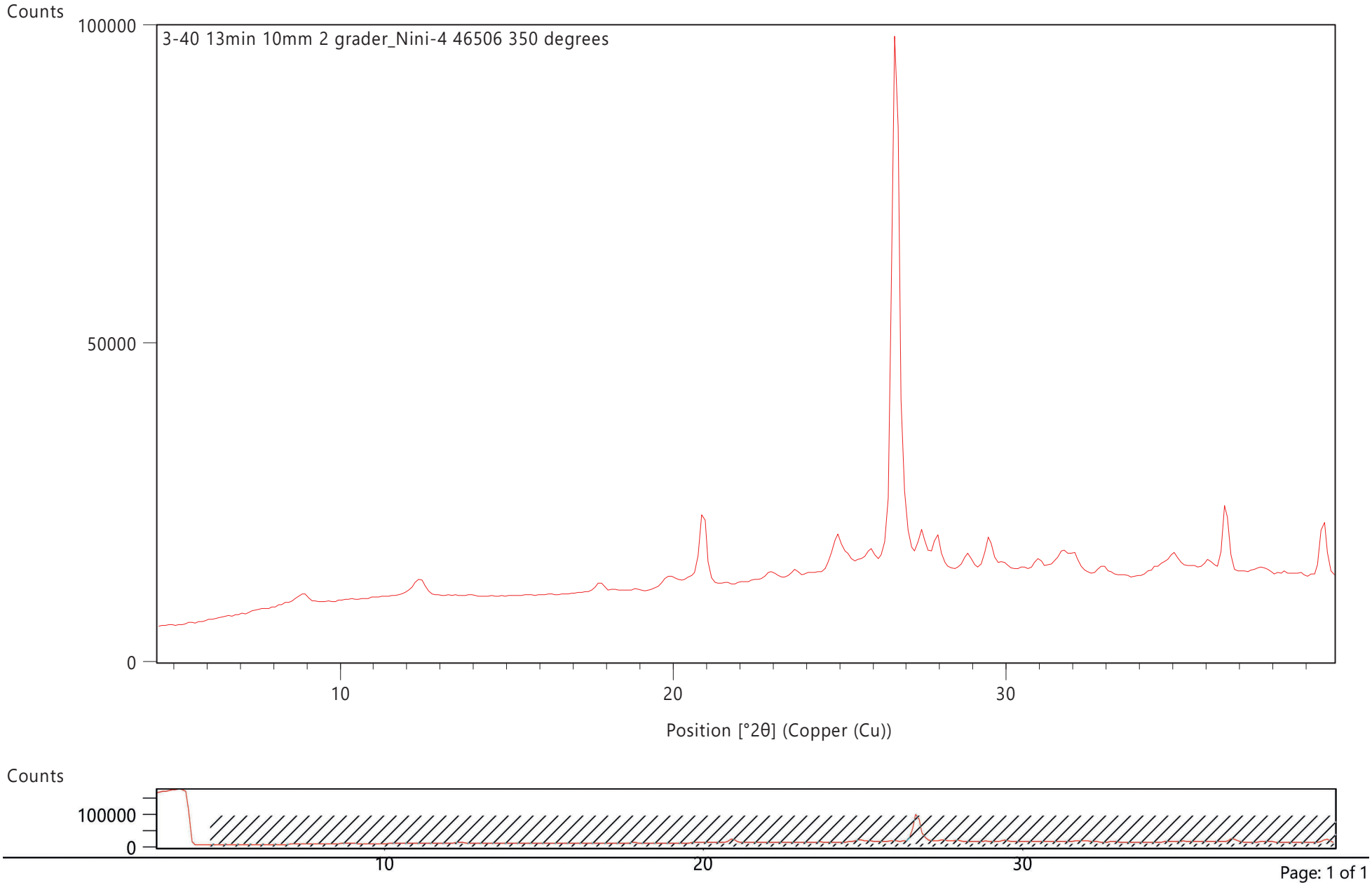
Counts
100000
50000
0
3-40 13min 10mm 2 grader_Nini-4 46506 350 degrees
10
20
30
Position [°2θ] (Copper (Cu))
Counts
100000
0
10
20
30

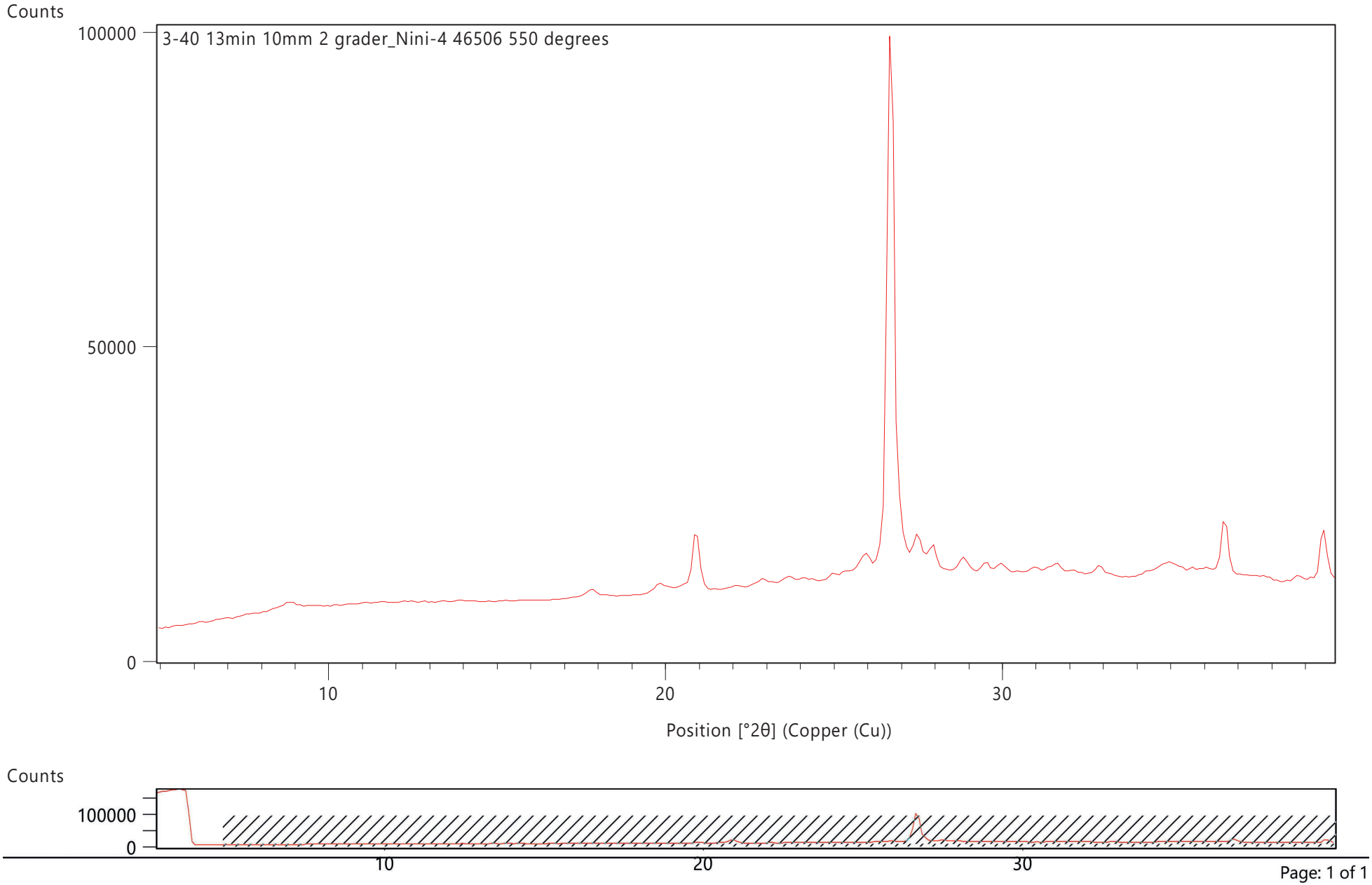
Counts
100000
50000
0
3-40 13min 10mm 2 grader_Nini-4 46506 550 degrees
10
20
30
Position [°2θ] (Copper (Cu))
Counts
100000
0
10
20
30

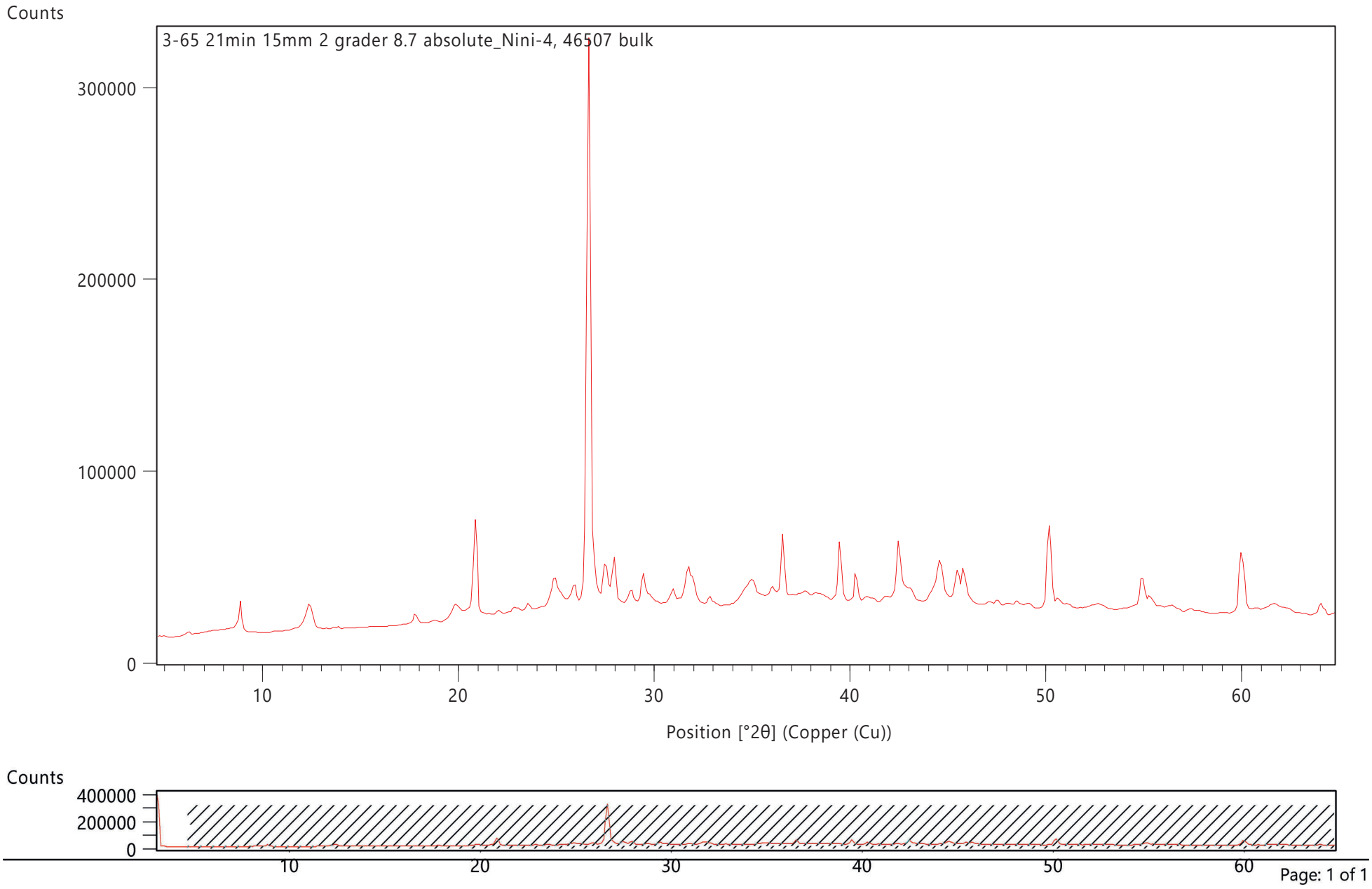
Counts
3-65 21min 15mm 2 grader 8.7 absolute_Nini-4, 46507 bulk
300000
200000
100000
0
10
20
30
40
50
60
Position [°2θ] (Copper (Cu))
Counts
400000
200000
0
10
20
30
40
50
60

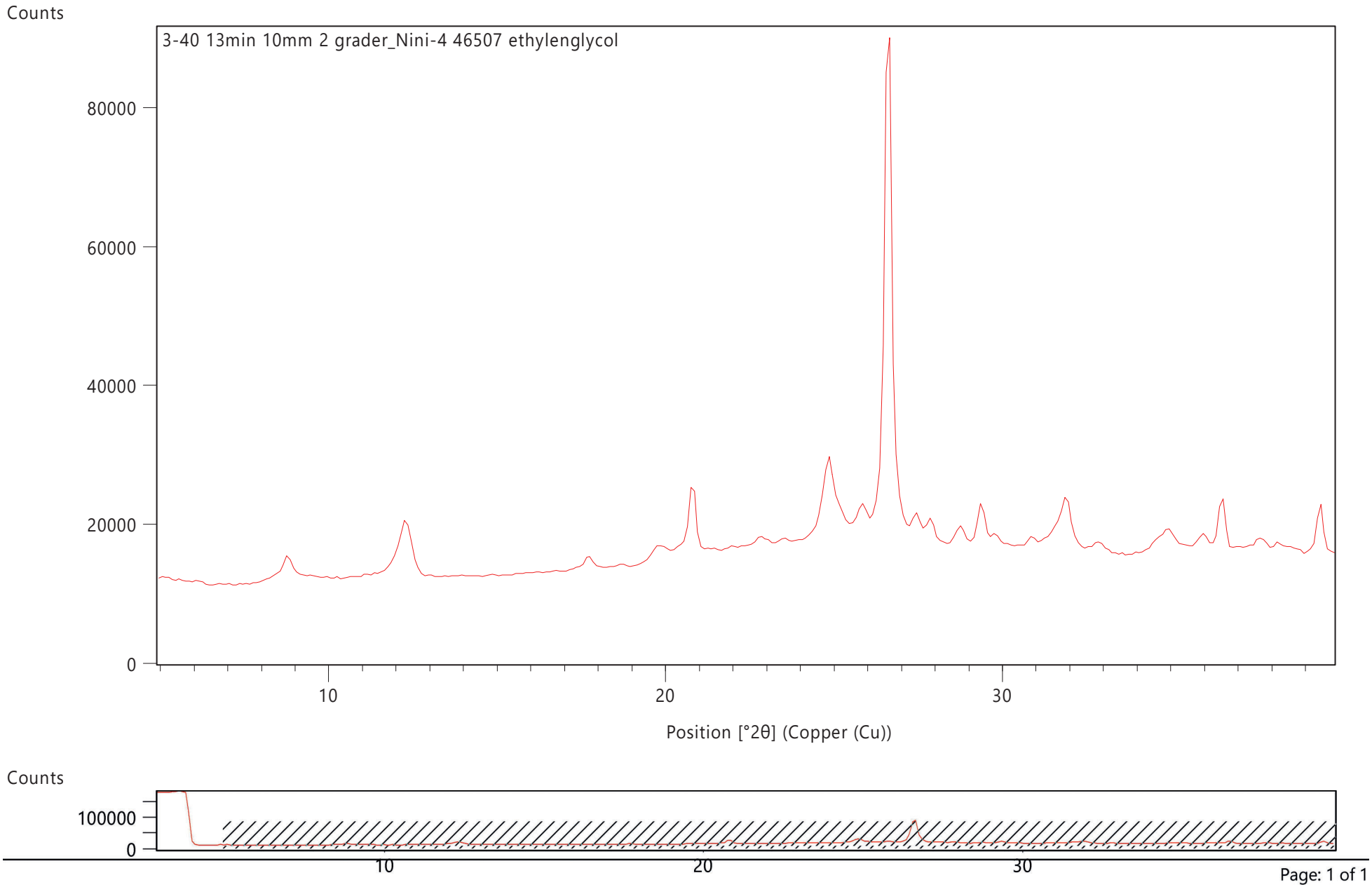
Counts
3-40 13min 10mm 2 grader_Nini-4 46507 ethylenglycol
80000
60000
40000
20000
0
10
20
30
Position [°2θ] (Copper (Cu))
Counts
100000
0
10
20
30

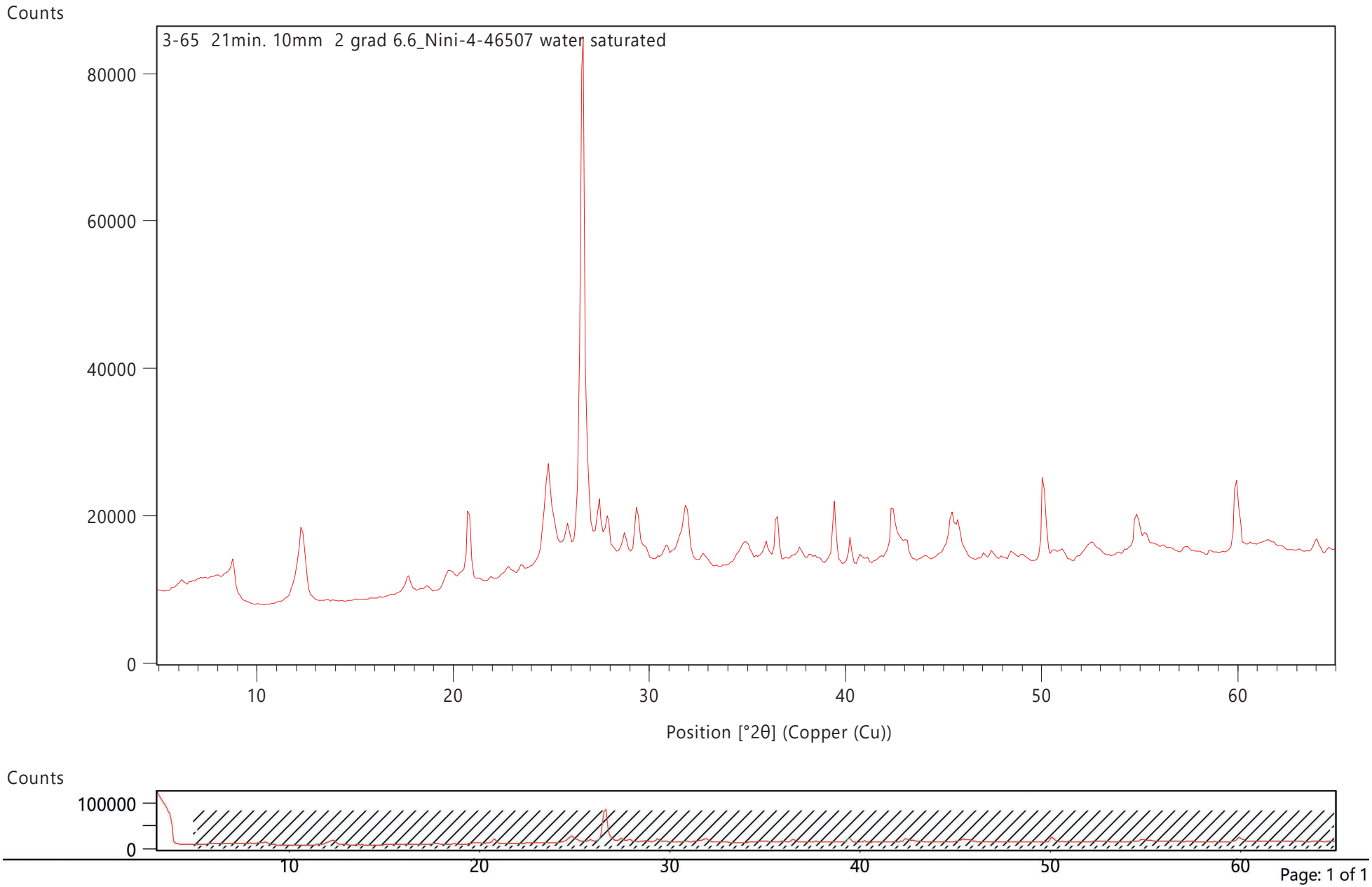
Counts
3-65 21min. 10mm 2 grad 6.6_Nini-4-46507 water saturated
80000
60000
40000
20000
0
10
20
30
40
50
60
Position [°2θ] (Copper (Cu))
Counts
100000
0
10
20
30
40
50
60

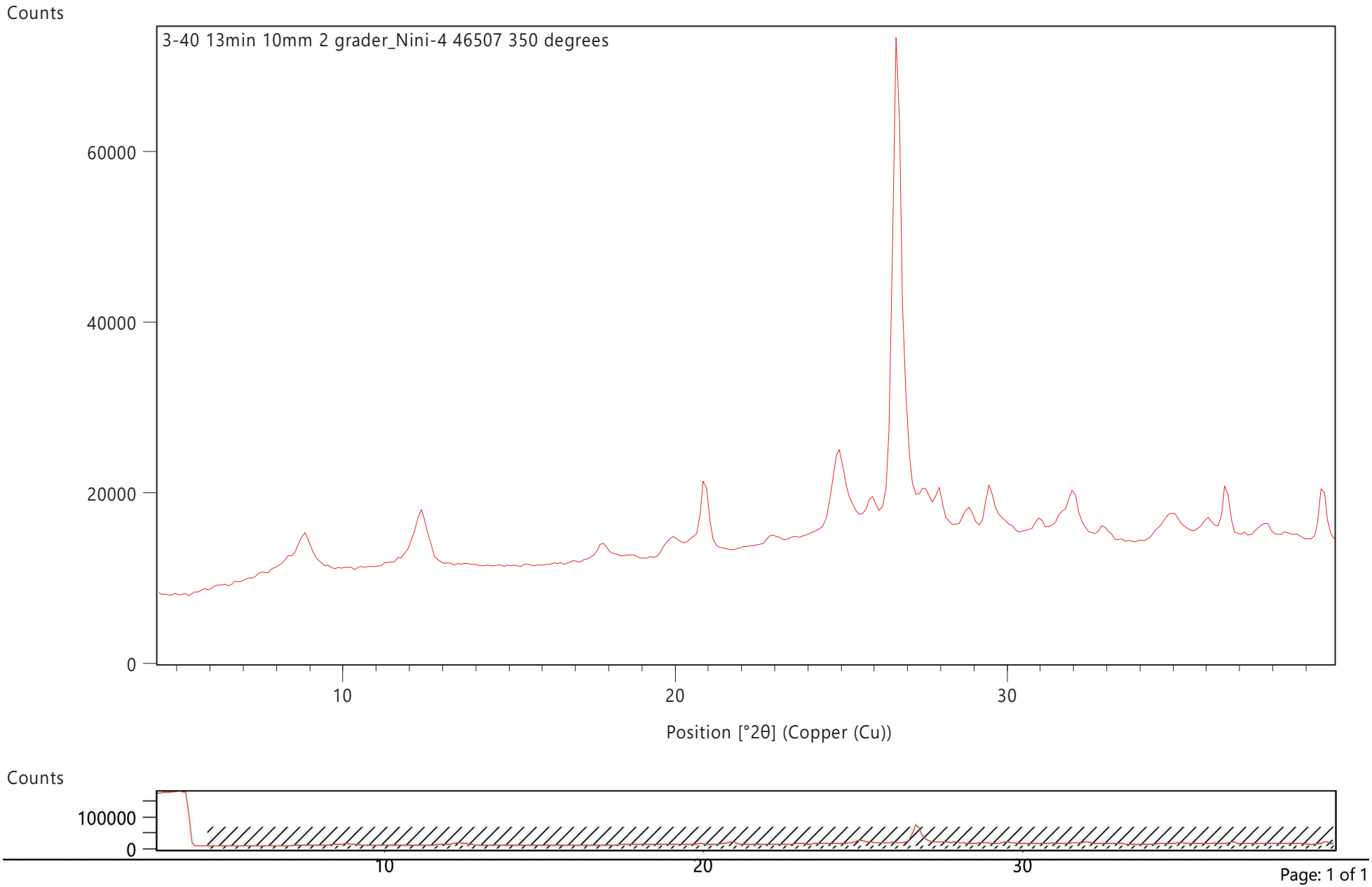
Counts
3-40 13min 10mm 2 grader_Nini-4 46507 350 degrees
60000
40000
20000
0
10
20
30
Position [°2θ] (Copper (Cu))
Counts
100000
0
10
20
30

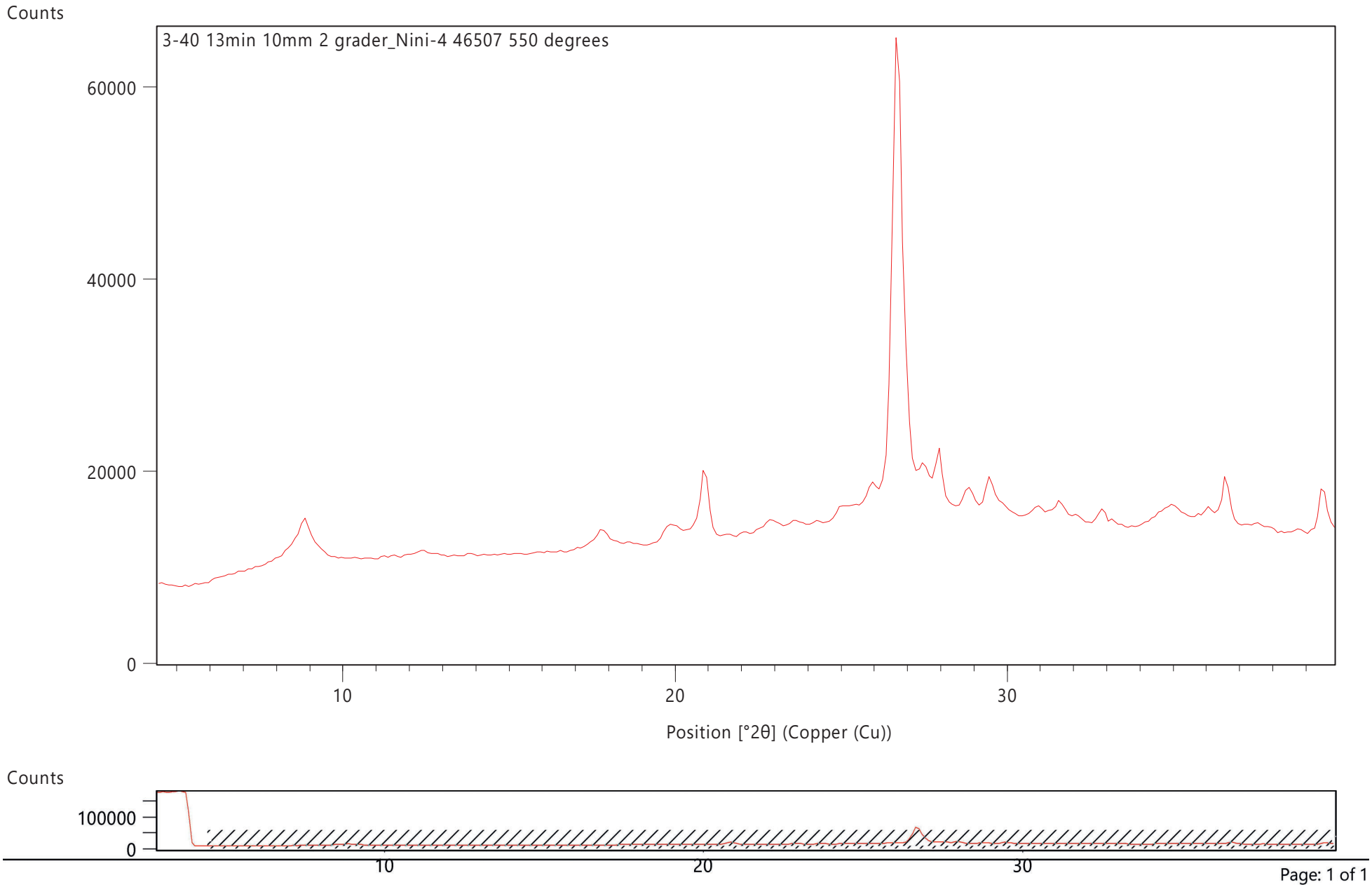
Counts
3-40 13min 10mm 2 grader_Nini-4 46507 550 degrees
60000
40000
20000
0
10
20
30
Position [°2θ] (Copper (Cu))
Counts
100000
0
10
20
30

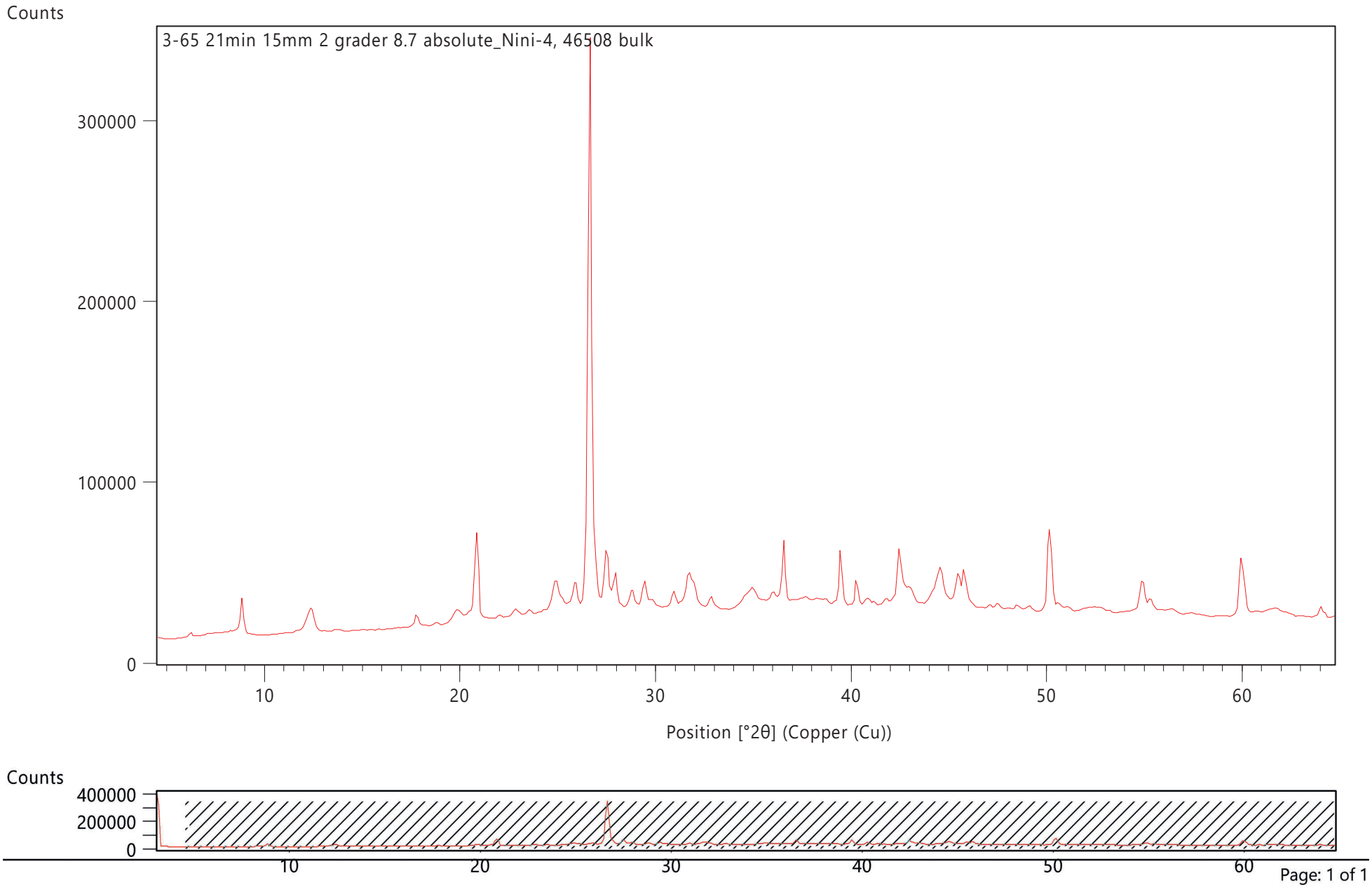
Counts
3-65 21min 15mm 2 grader 8.7 absolute_Nini-4, 46508 bulk
300000
200000
100000
0
10
20
30
40
50
60
Position [°2θ] (Copper (Cu))
Counts
400000
200000
0
10
20
30
40
50
60

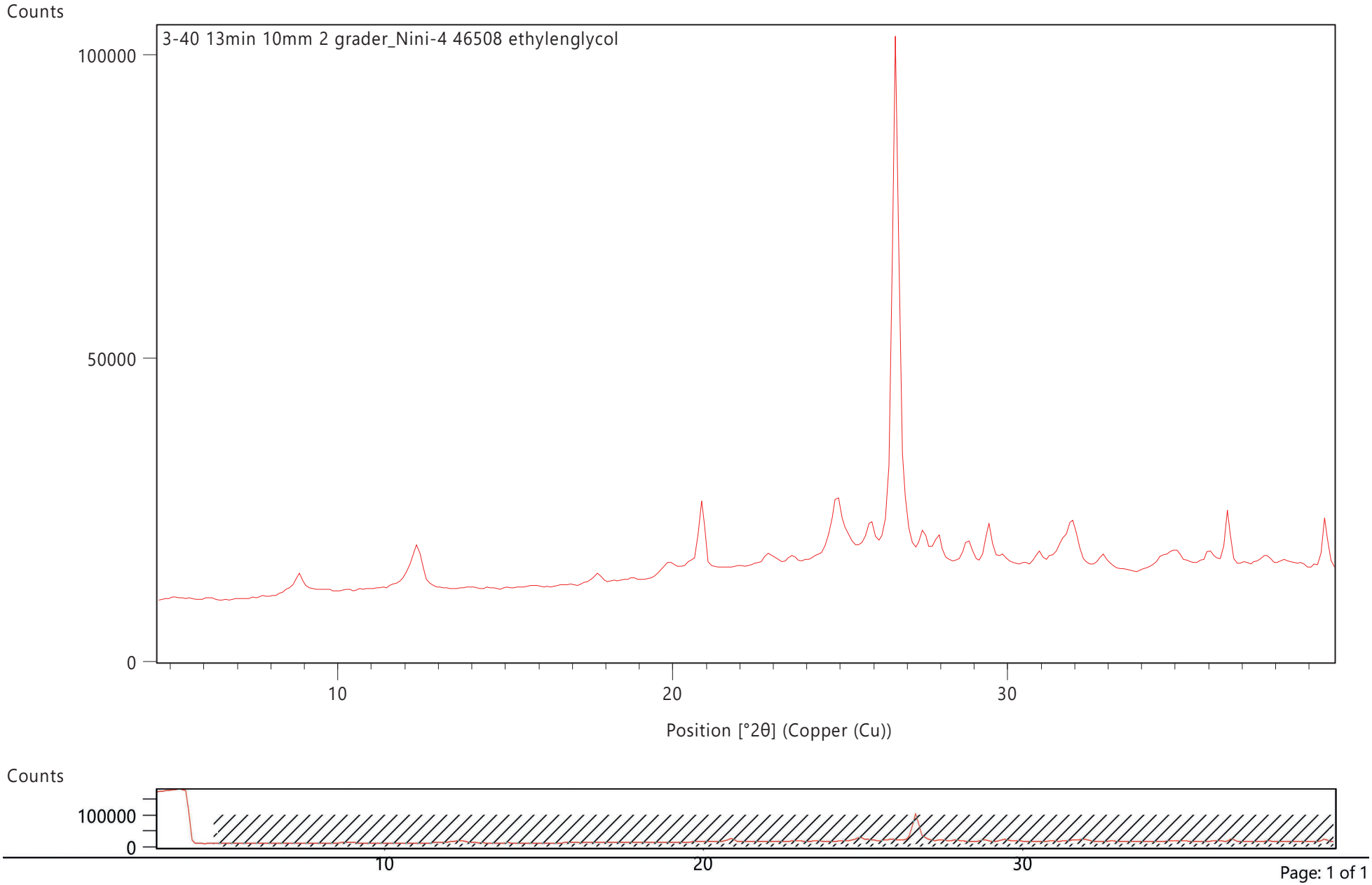
Counts
3-40 13min 10mm 2 grader_Nini-4 46508 ethylenglycol
100000
50000
0
10
20
30
Position [°2θ] (Copper (Cu))
Counts
100000
0
10
20
30

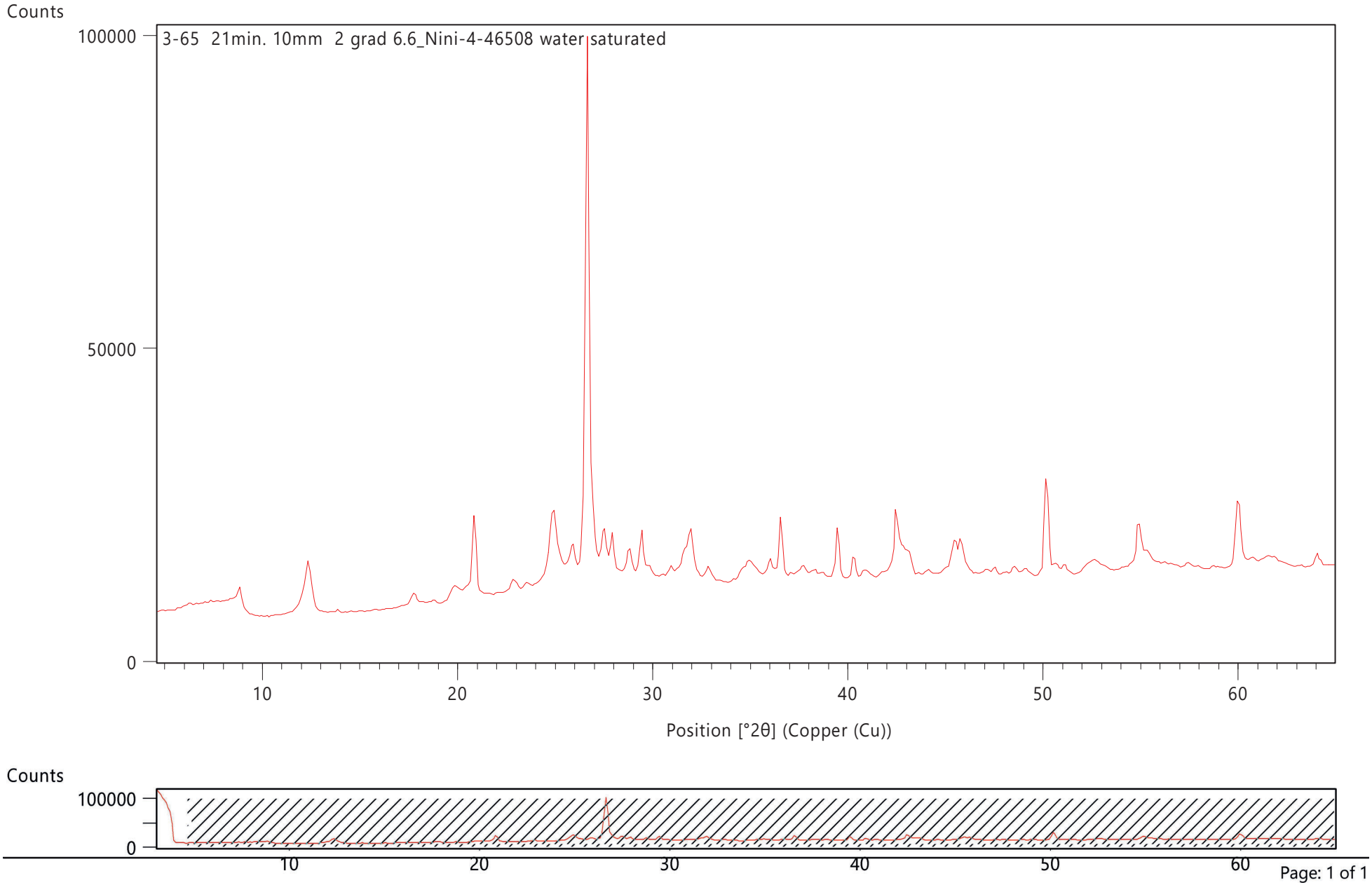
Counts
100000
50000
0
3-65 21min. 10mm 2 grad 6.6_Nini-4-46508 water saturated
10
20
30
40
50
60
Position [°2θ] (Copper (Cu))
Counts
100000
0
10
20
30
40
50
60

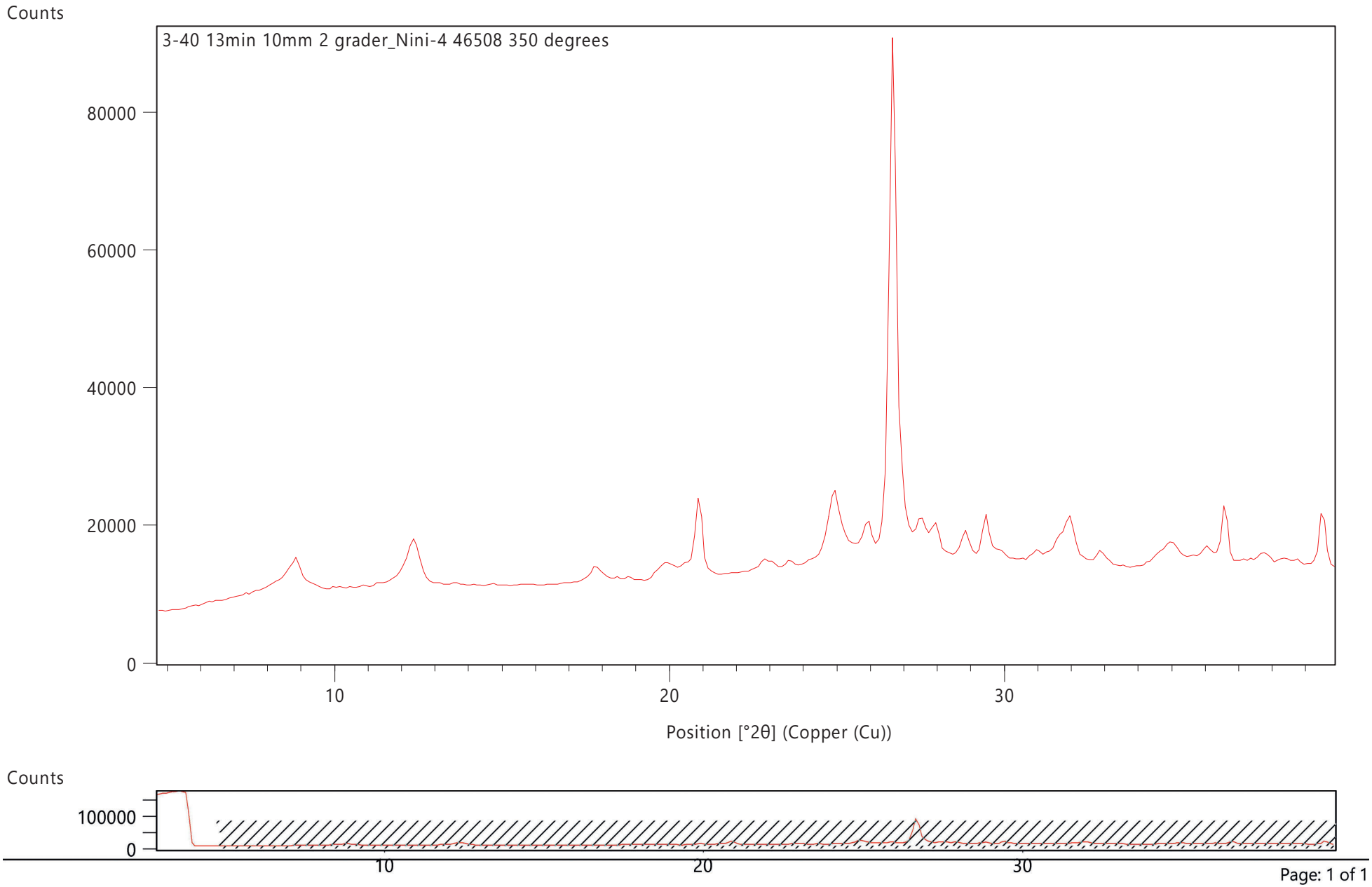
Counts
3-40 13min 10mm 2 grader_Nini-4 46508 350 degrees
80000
60000
40000
20000
0
10
20
30
Position [°2θ] (Copper (Cu))
Counts
100000
0
10
20
30

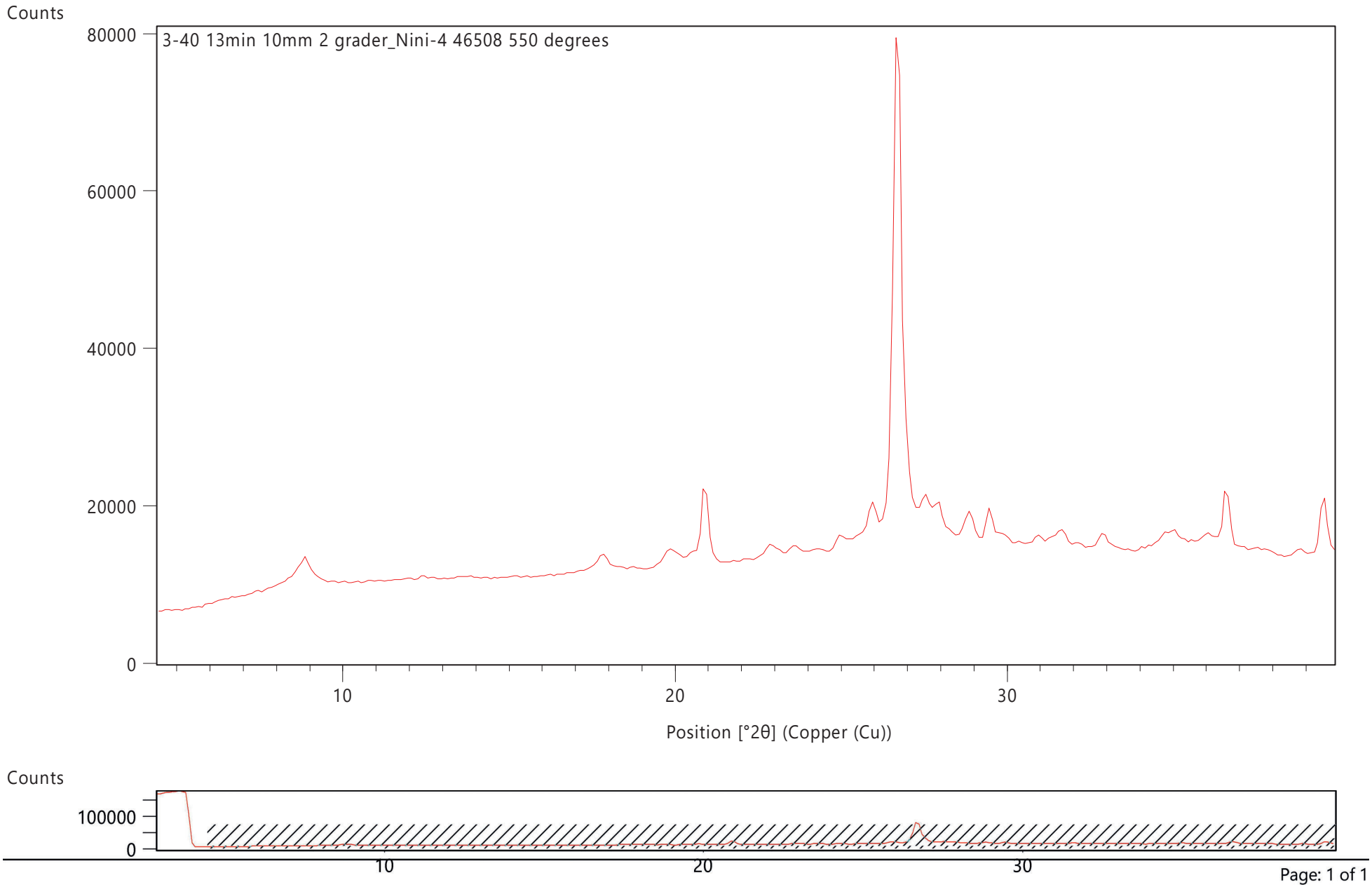
Counts
3-40 13min 10mm 2 grader_Nini-4 46508 550 degrees
80000
60000
40000
20000
0
10
20
30
Position [°2θ] (Copper (Cu))
Counts
100000
0
10
20
30

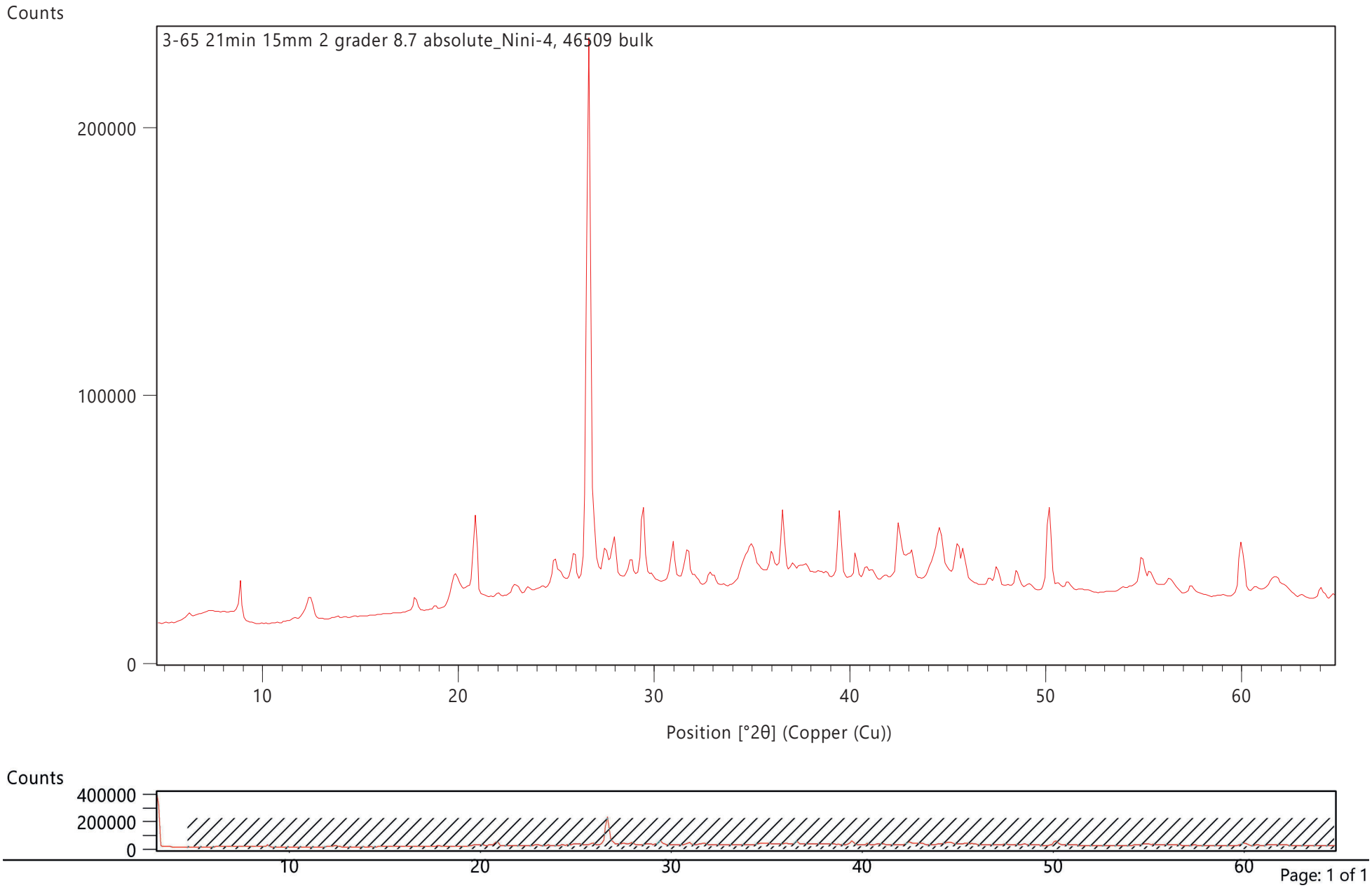
Counts
3-65 21min 15mm 2 grader 8.7 absolute_Nini-4, 46509 bulk
200000
100000
0
10
20
30
40
50
60
Position [°2θ] (Copper (Cu))
Counts
400000
200000
0
10
20
30
40
50
60

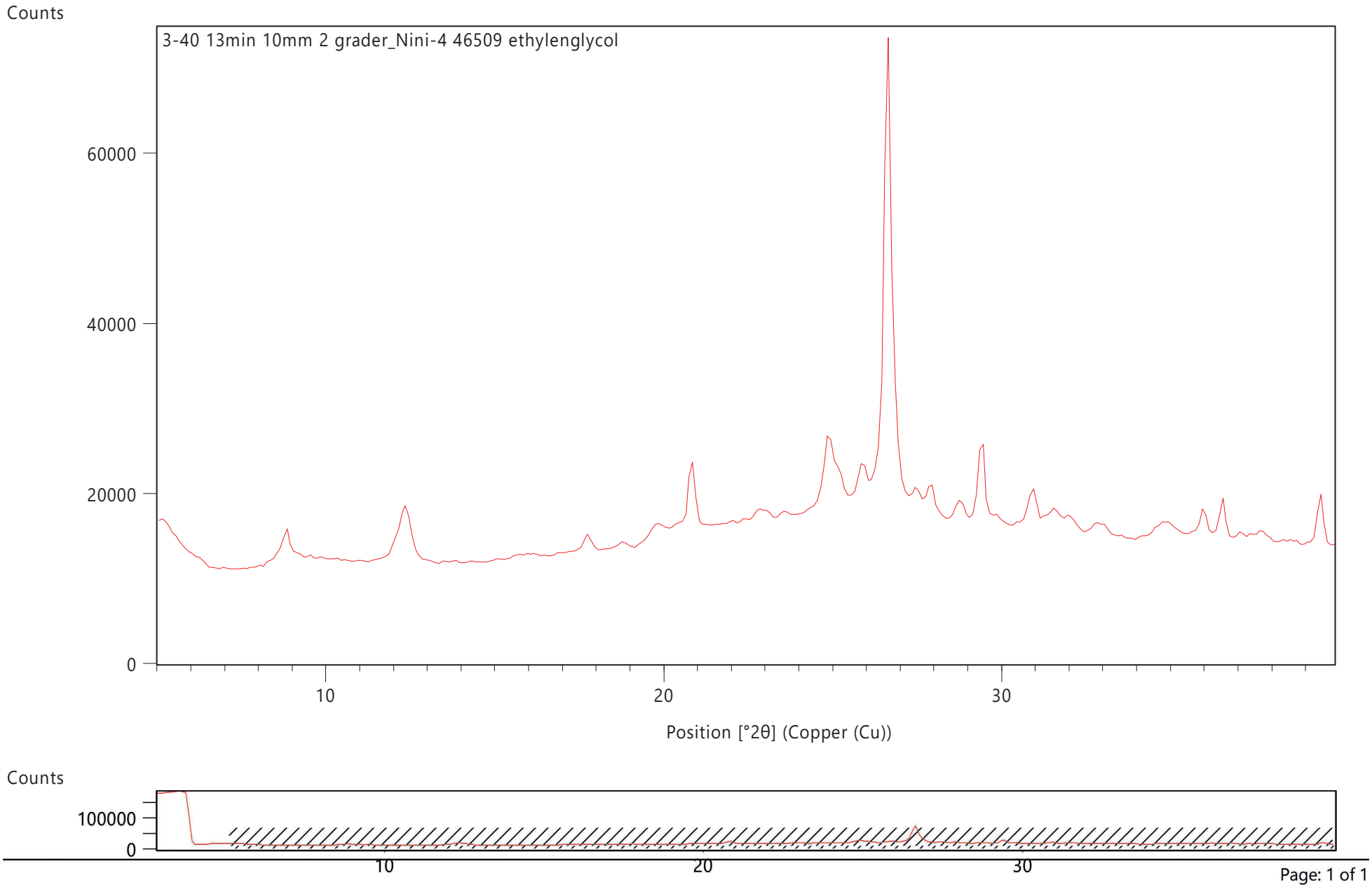
Counts
3-40 13min 10mm 2 grader_Nini-4 46509 ethylenglycol
60000
40000
20000
0
10
20
30
Position [°2θ] (Copper (Cu))
Counts
100000
0
10
20
30

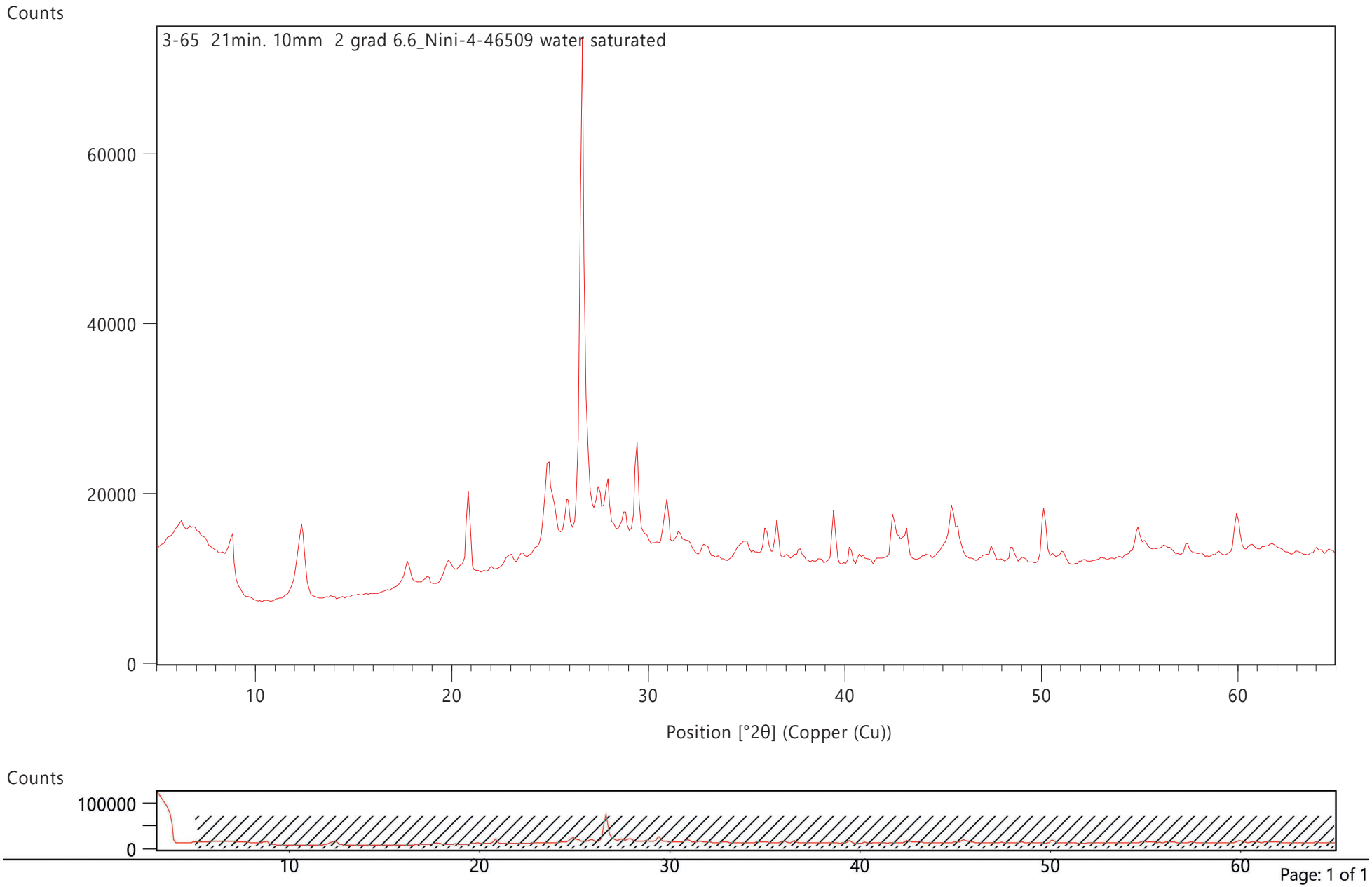
Counts
3-65 21min. 10mm 2 grad 6.6_Nini-4-46509 water saturated
60000
40000
20000
0
10
20
30
40
50
60
Position [°2θ] (Copper (Cu))
Counts
100000
0
10
20
30
40
50
60

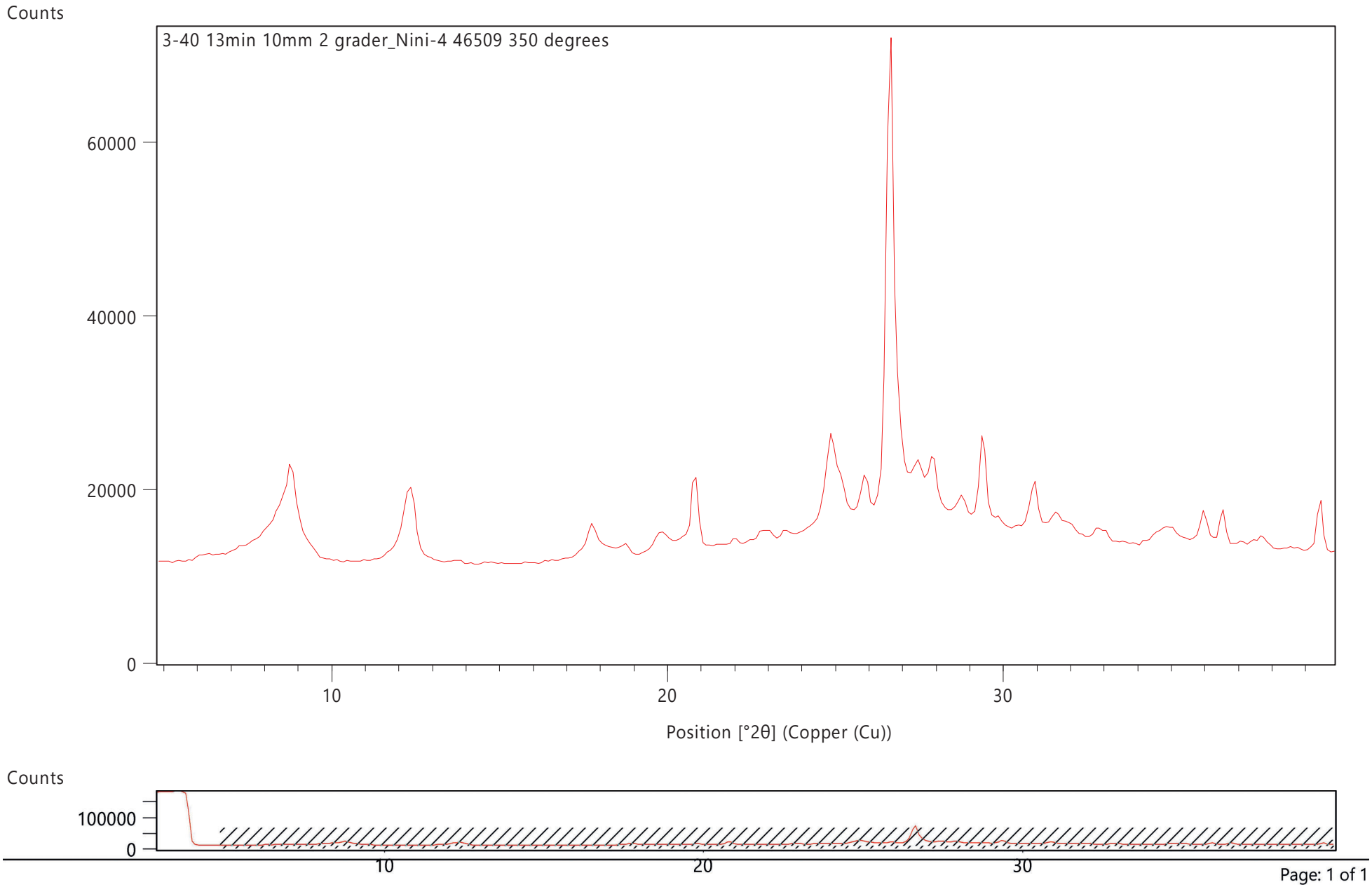
Counts
3-40 13min 10mm 2 grader_Nini-4 46509 350 degrees
60000
40000
20000
0
10
20
30
Position [°2θ] (Copper (Cu))
Counts
100000
0
10
20
30

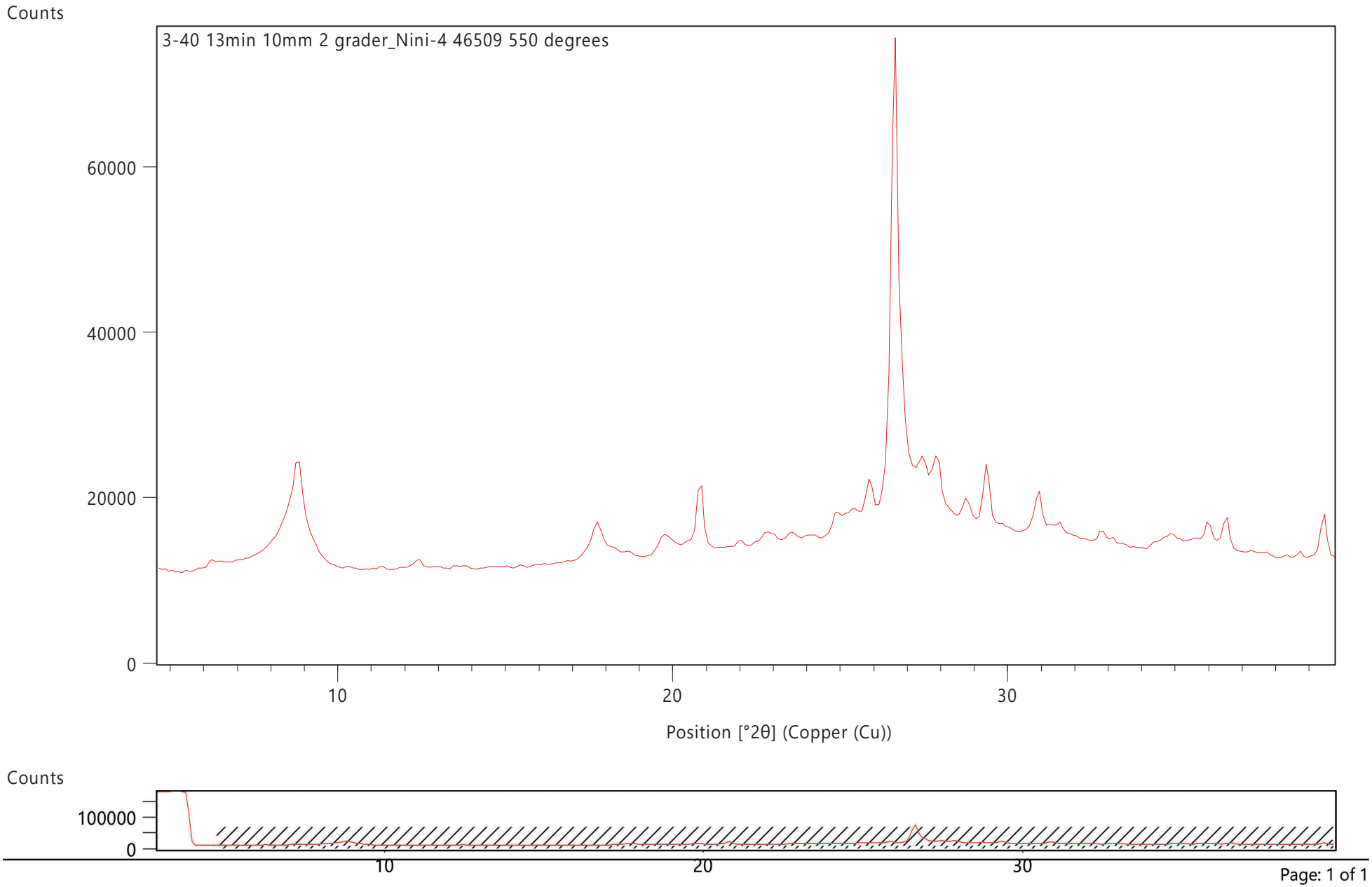
Counts
3-40 13min 10mm 2 grader_Nini-4 46509 550 degrees
60000
40000
20000
0
10
20
30
Position [°2θ] (Copper (Cu))
Counts
100000
0
10
20
30

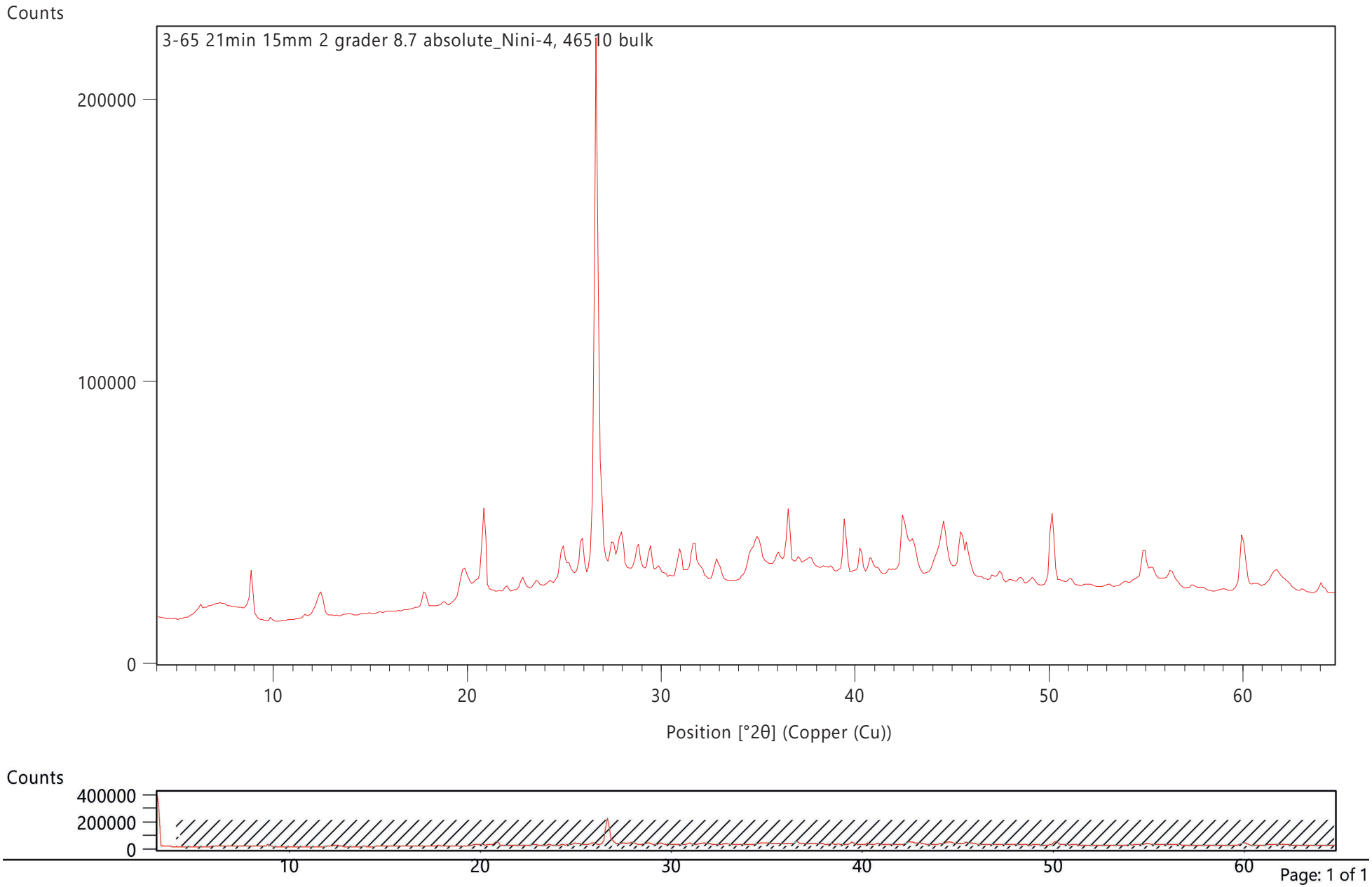
Counts
3-65 21min 15mm 2 grader 8.7 absolute_Nini-4, 46510 bulk
200000
100000
0
10
20
30
40
50
60
Position [°2θ] (Copper (Cu))
Counts
400000
200000
0
10
20
30
40
50
60

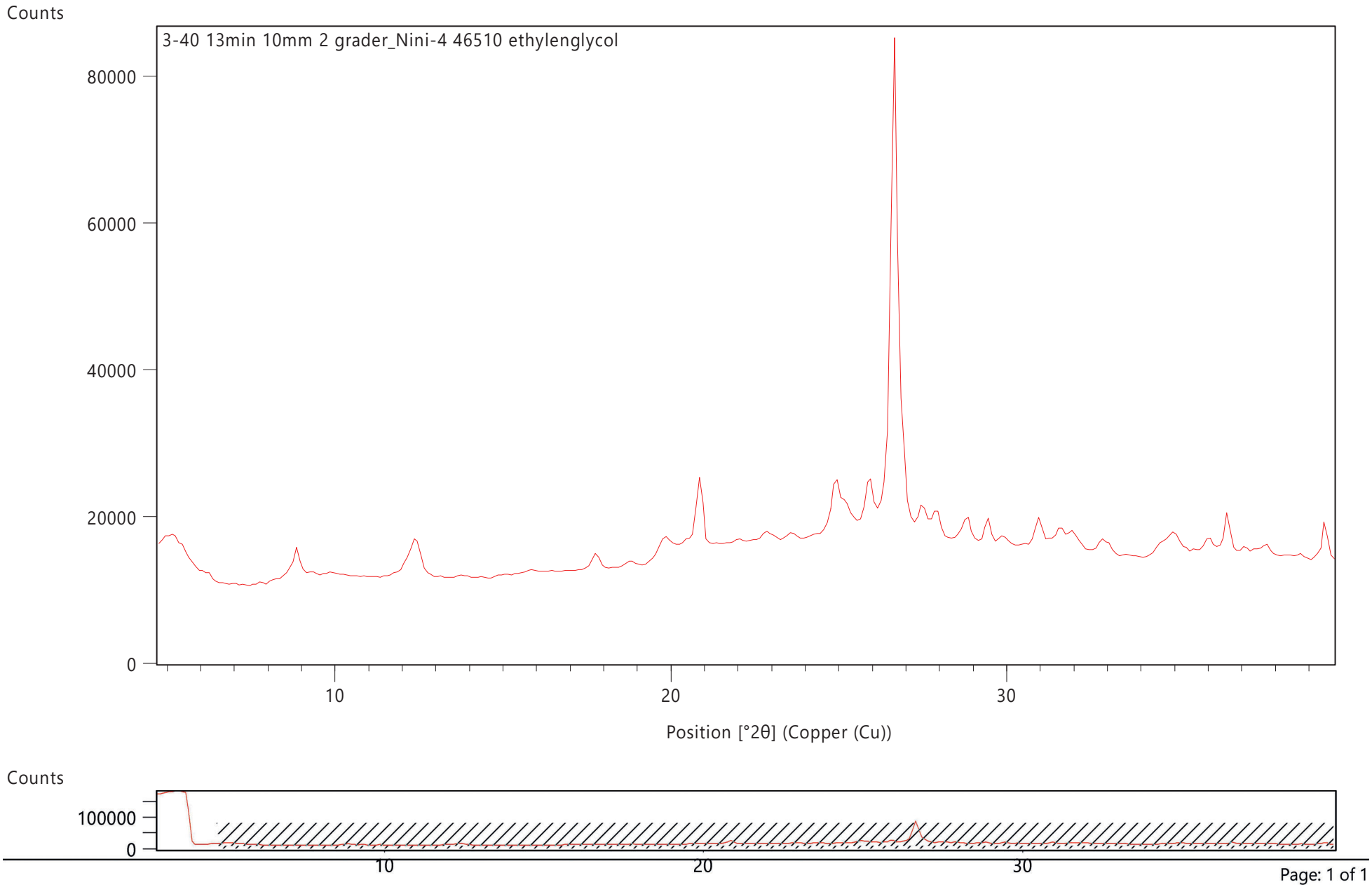
Counts
3-40 13min 10mm 2 grader_Nini-4 46510 ethylenglycol
80000
60000
40000
20000
0
10
20
30
Position [°2θ] (Copper (Cu))
Counts
100000
0
10
20
30

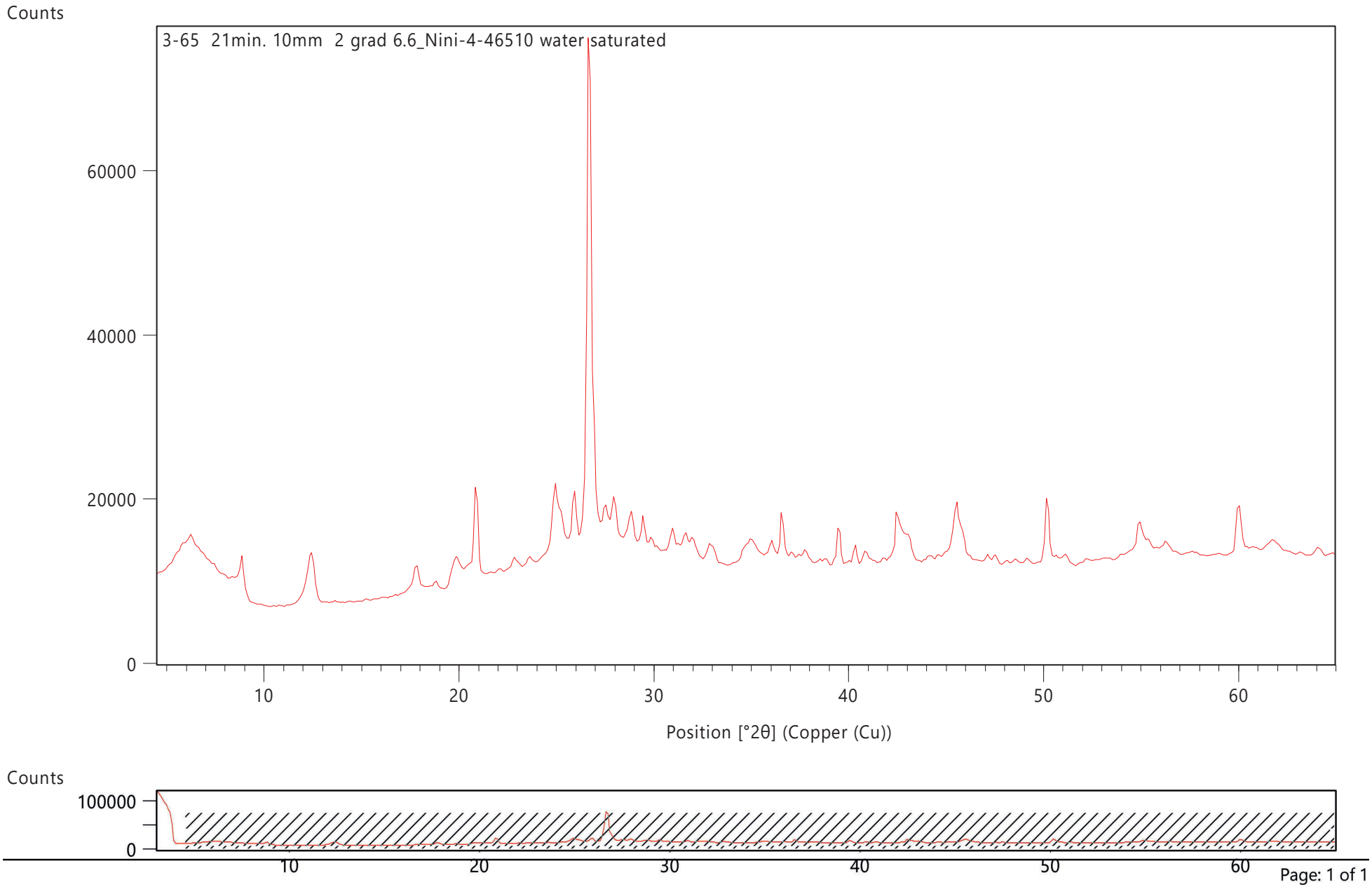
Counts
3-65 21min. 10mm 2 grad 6.6_Nini-4-46510 water saturated
60000
40000
20000
0
10
20
30
40
50
60
Position [°2θ] (Copper (Cu))
Counts
100000
0
10
20
30
40
50
60

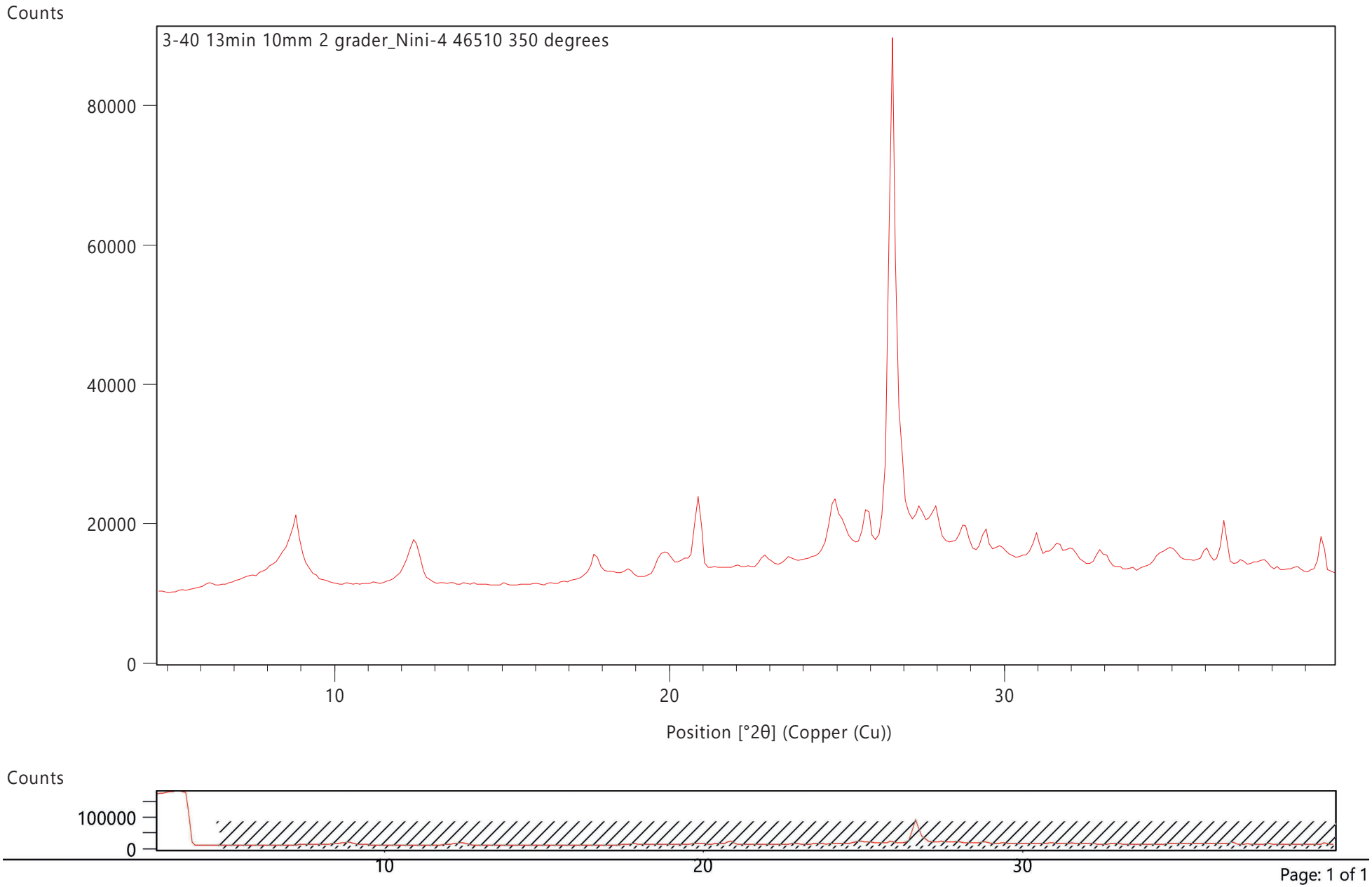
Counts
3-40 13min 10mm 2 grader_Nini-4 46510 350 degrees
80000
60000
40000
20000
0
10
20
30
Position [°2θ] (Copper (Cu))
Counts
100000
0
10
20
30

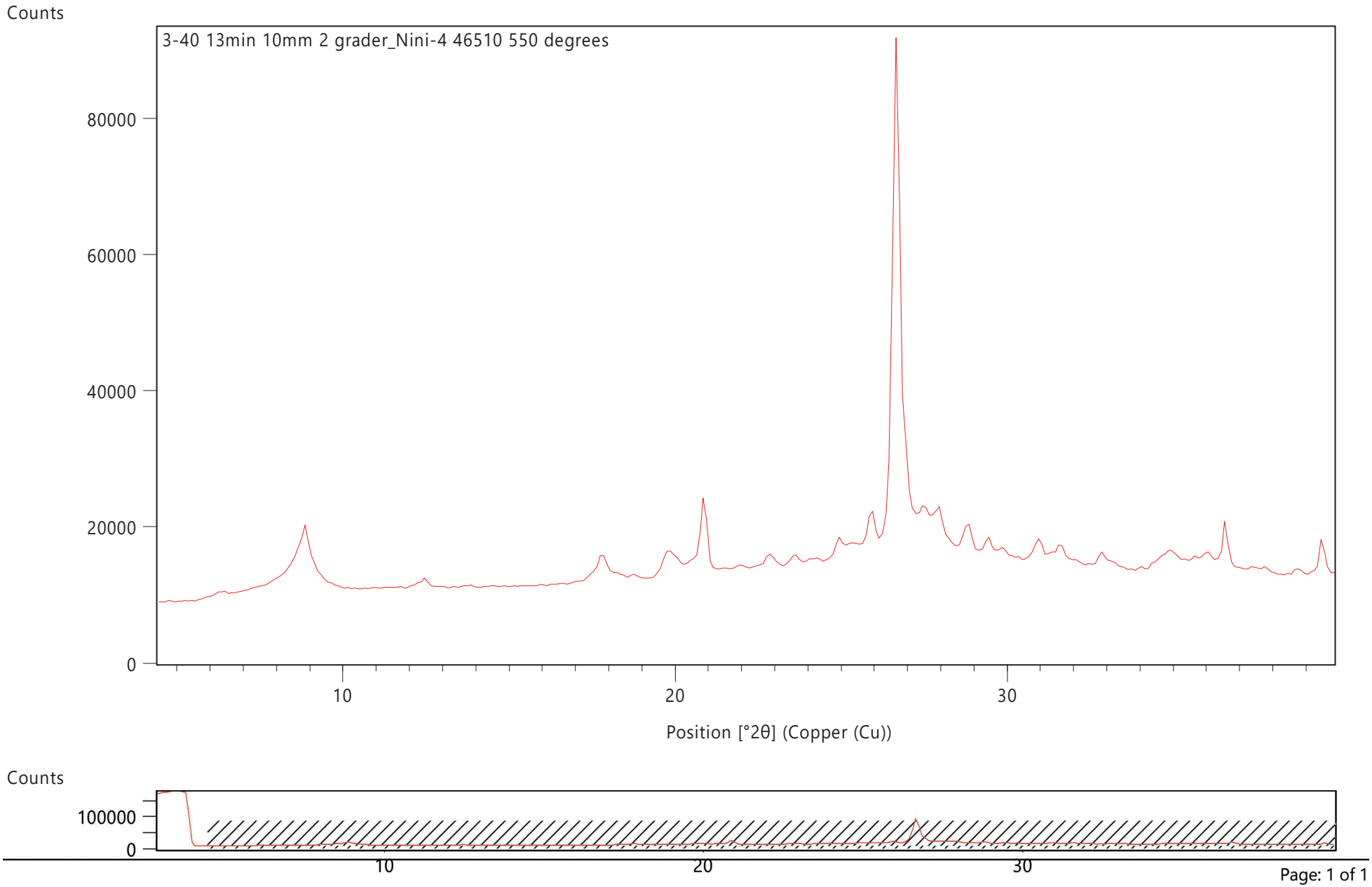
Counts
3-40 13min 10mm 2 grader_Nini-4 46510 550 degrees
80000
60000
40000
20000
0
10
20
30
Position [°2θ] (Copper (Cu))
Counts
100000
0
10
20
30

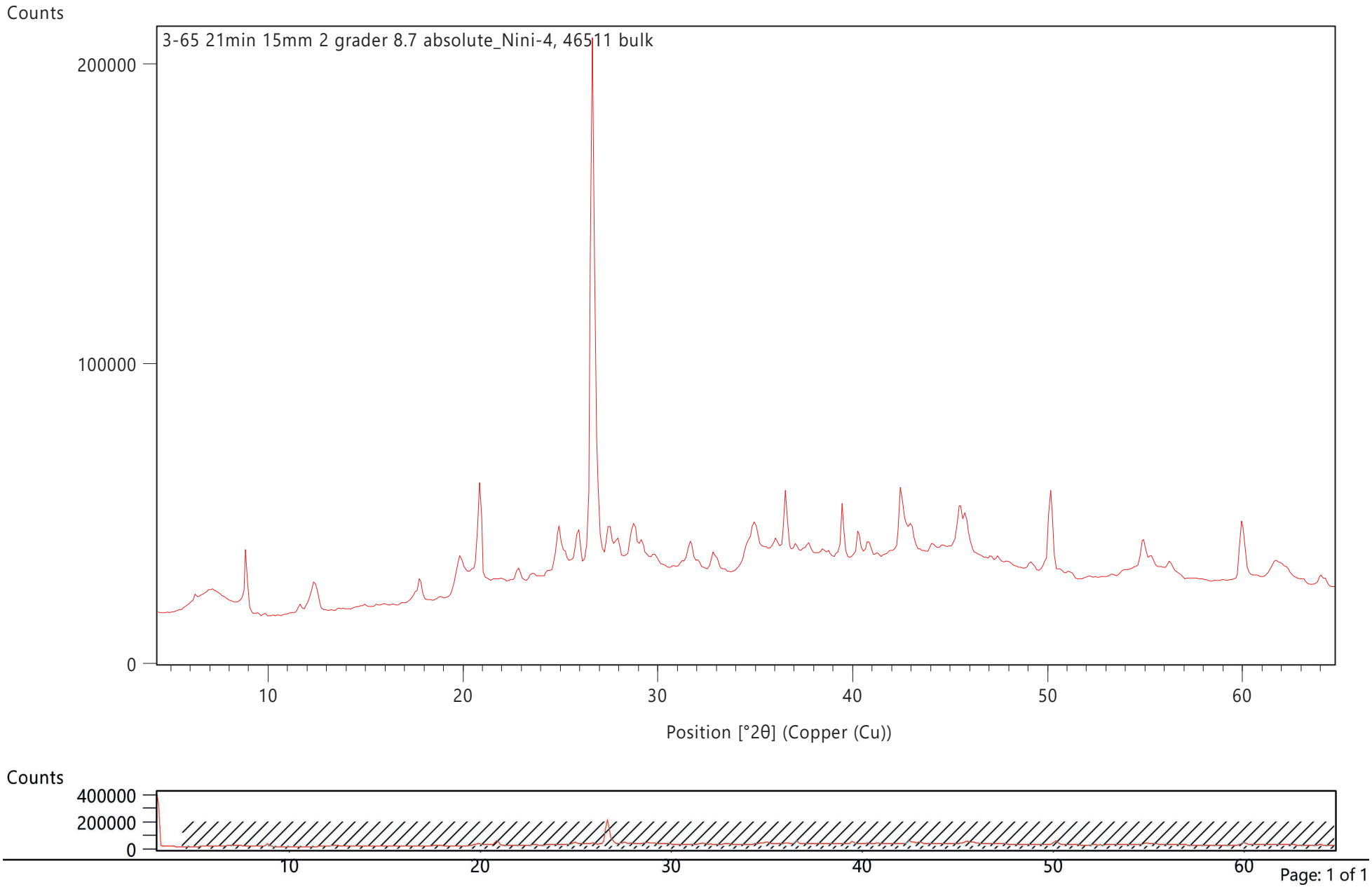
Counts
3-65 21min 15mm 2 grader 8.7 absolute_Nini-4, 46511 bulk
200000
100000
0
10
20
30
40
50
60
Position [°2θ] (Copper (Cu))
Counts
400000
200000
0
10
20
30
40
50
60

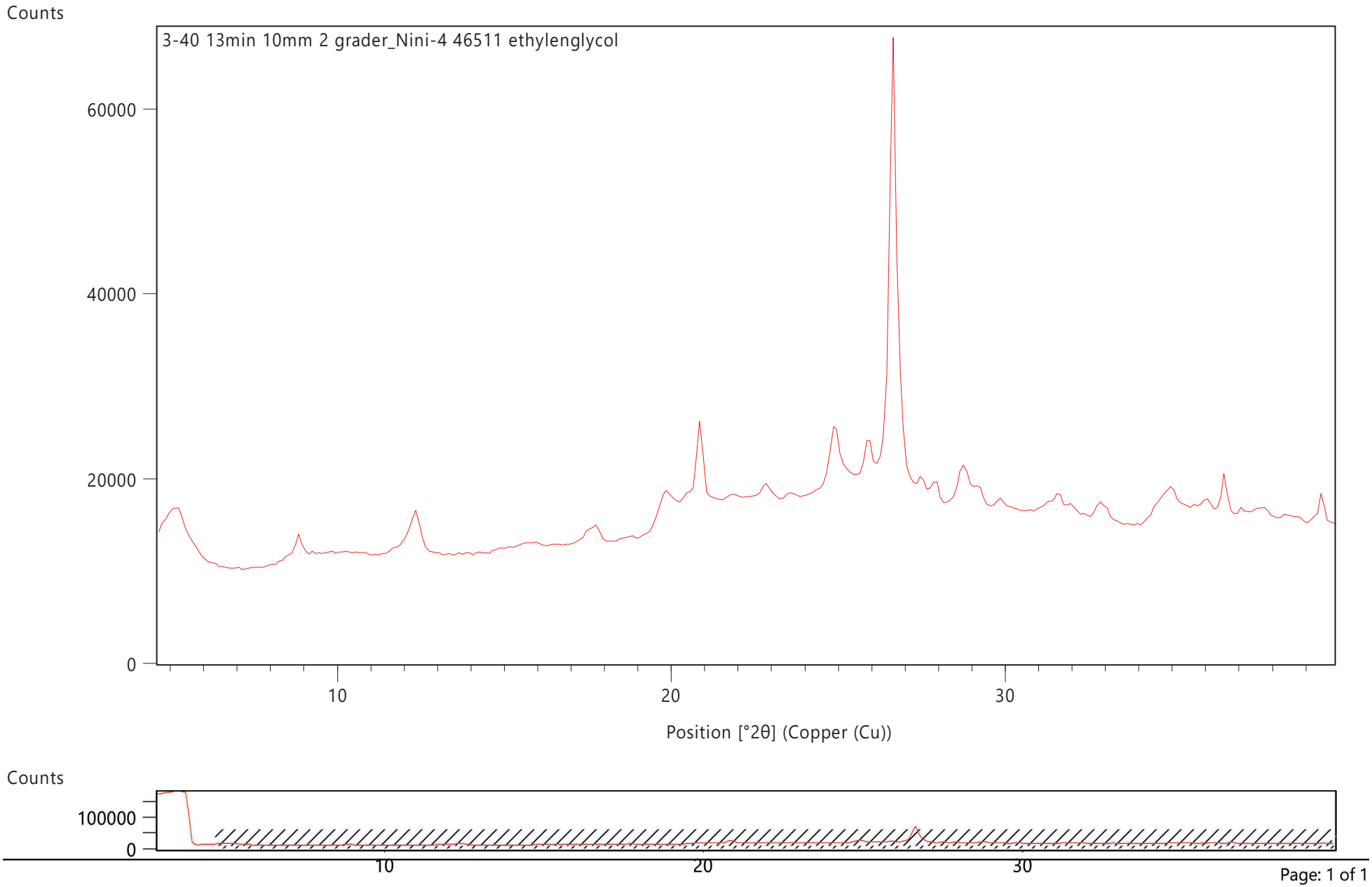
Counts
3-40 13min 10mm 2 grader_Nini-4 46511 ethylenglycol
60000
40000
20000
0
10
20
30
Position [°2θ] (Copper (Cu))
Counts
100000
0
10
20
30

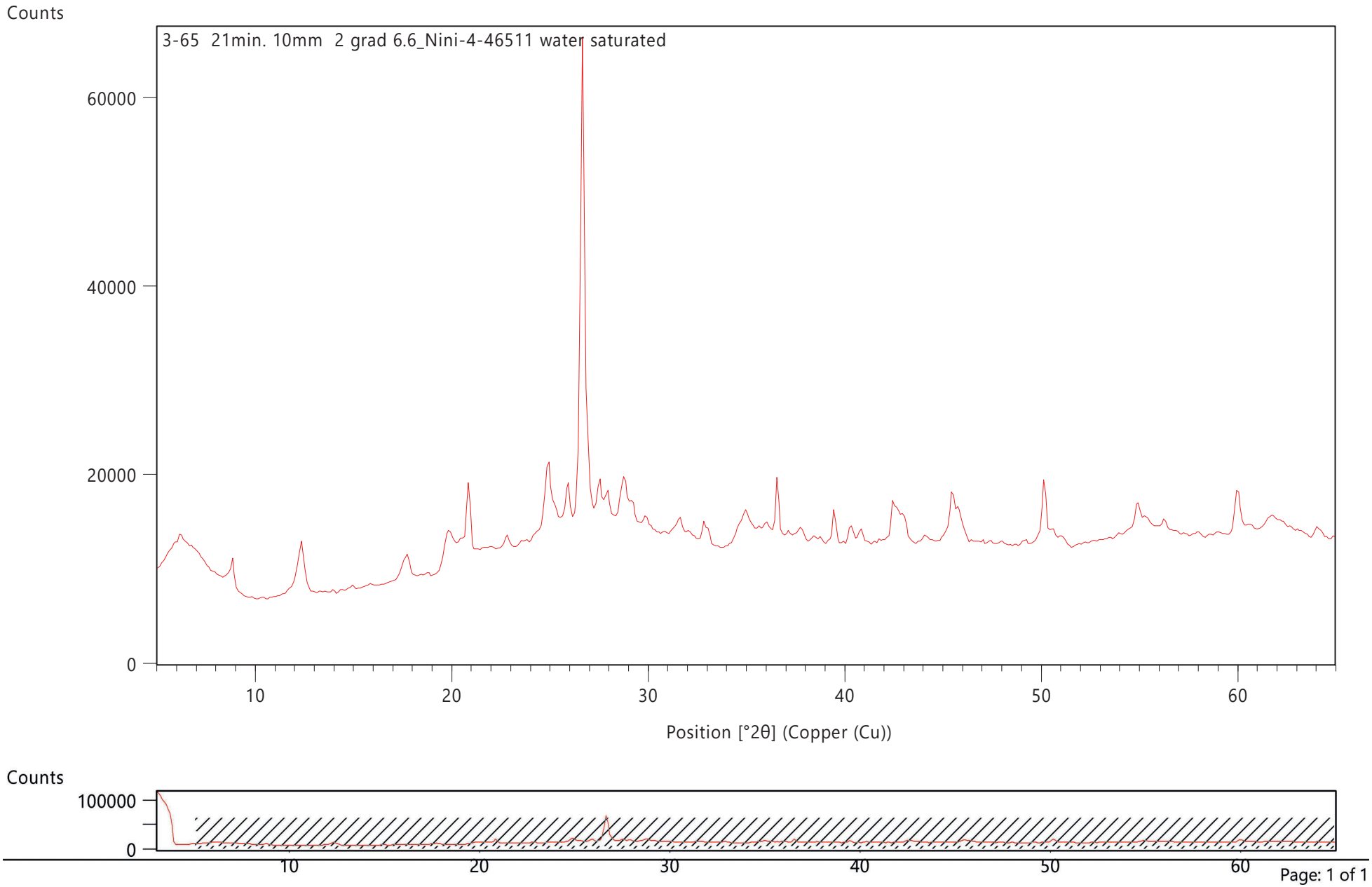
Counts
3-65 21min. 10mm 2 grad 6.6_Nini-4-46511 water saturated
60000
40000
20000
0
10
20
30
40
50
60
Position [°2θ] (Copper (Cu))
Counts
100000
0
10
20
30
40
50
60

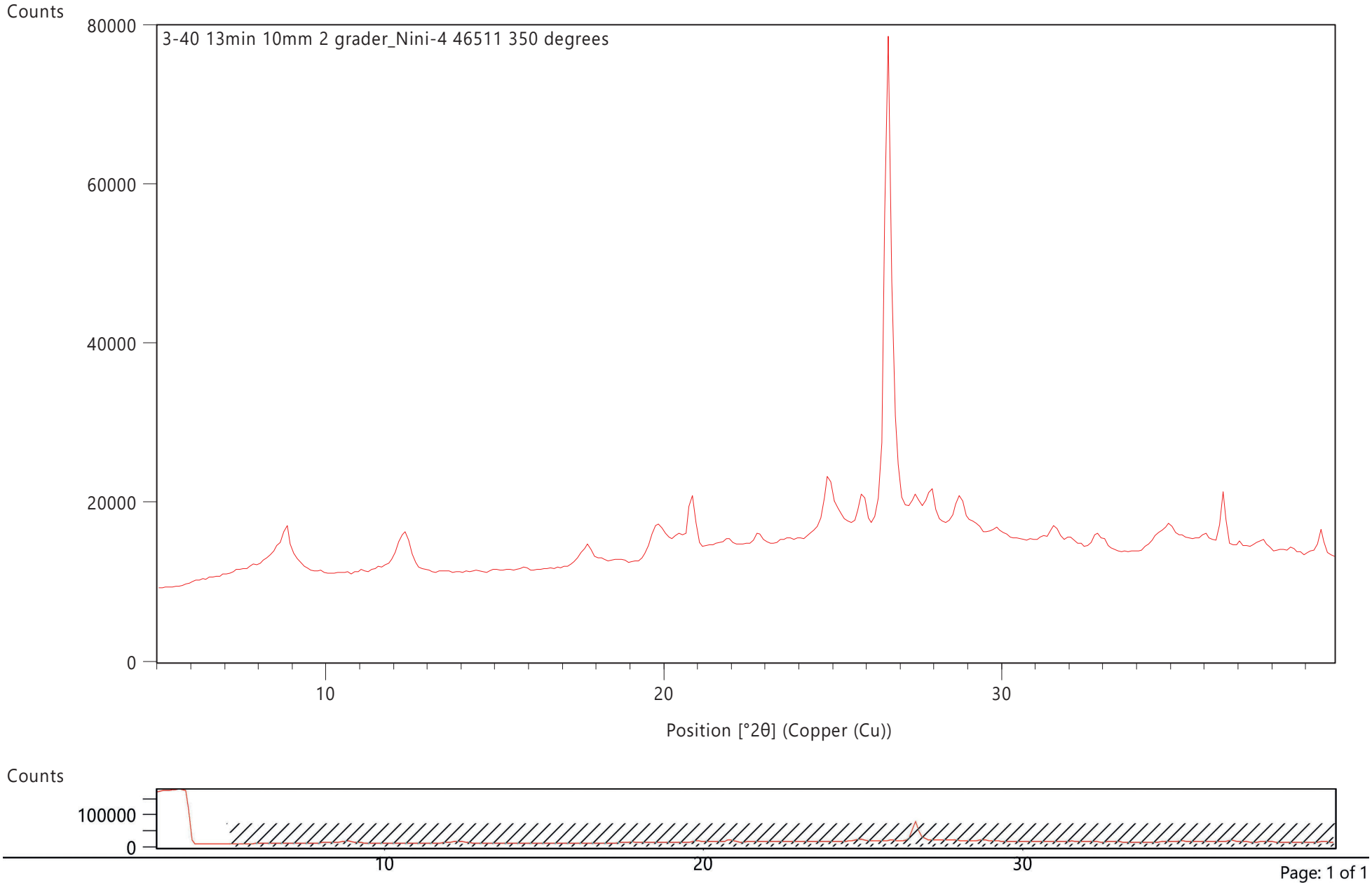
Counts
3-40 13min 10mm 2 grader_Nini-4 46511 350 degrees
80000
60000
40000
20000
0
10
20
30
Position [°2θ] (Copper (Cu))
Counts
100000
0
10
20
30

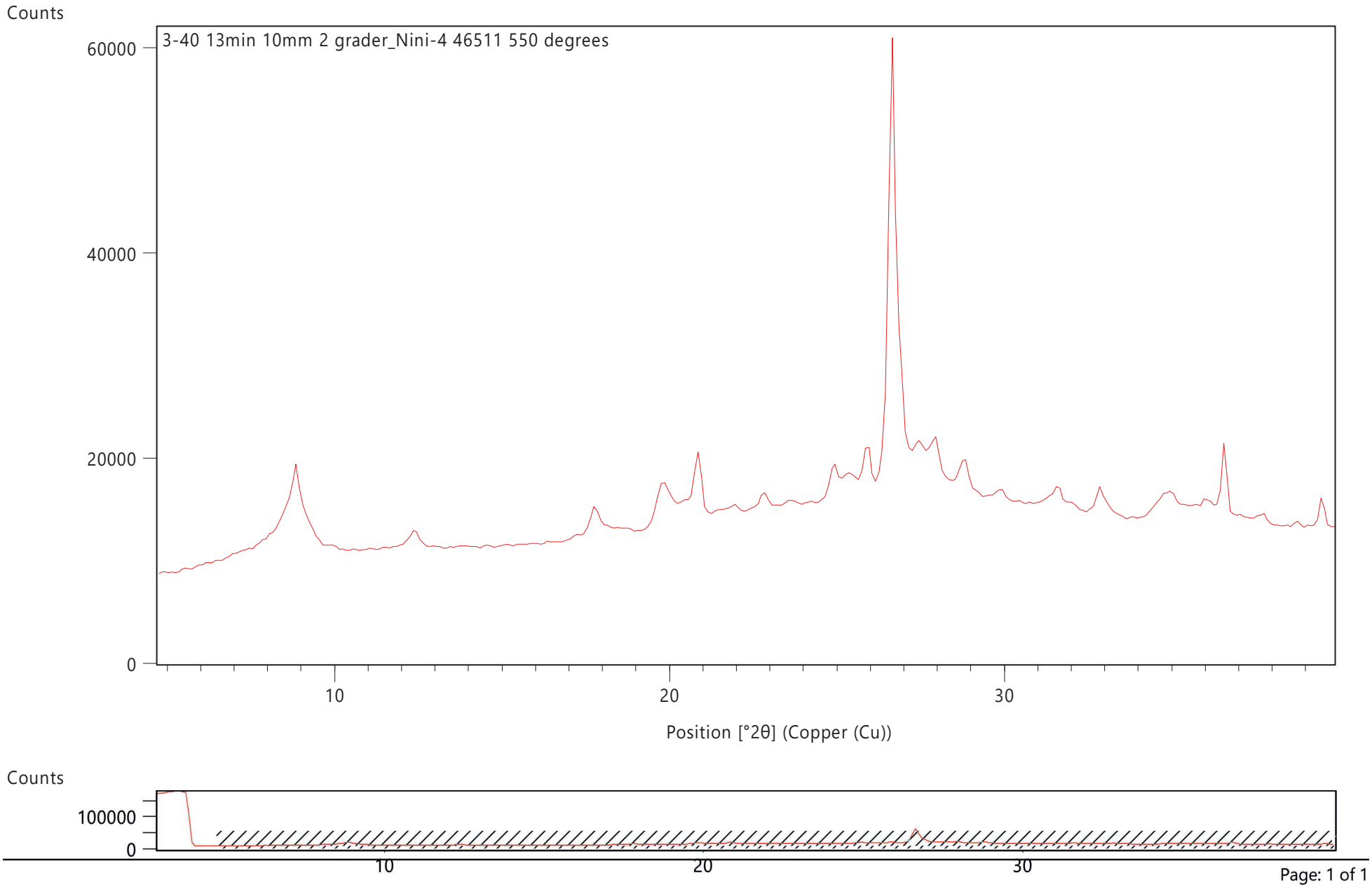
Counts
3-40 13min 10mm 2 grader_Nini-4 46511 550 degrees
60000
40000
20000
0
10
20
30
Position [°2θ] (Copper (Cu))
Counts
100000
0
10
20
30

APPENDIX E – DIGITAL ROCKS ANALYSIS

Prepared by Andrew Fogden, Wintershall Dea

Screening of received cuttings samples by micro-CT imaging

Four small bags of drill cuttings were received from GEUS from the Nini-4 well, in 10 m depth batches over the interval 1410-1450 m spanning the sandy siltstone beds in the secondary seal complex. For each batch of cuttings particles, the sieved fraction > 1 mm was poured into a glass capillary tube of 7.5 mm inner diameter, for scanning using x-ray micro-tomography (micro-CT, HeliScan). For preliminary screening purposes, quick mid-resolution scans were performed over the full width and height of the particle stack in the tube.

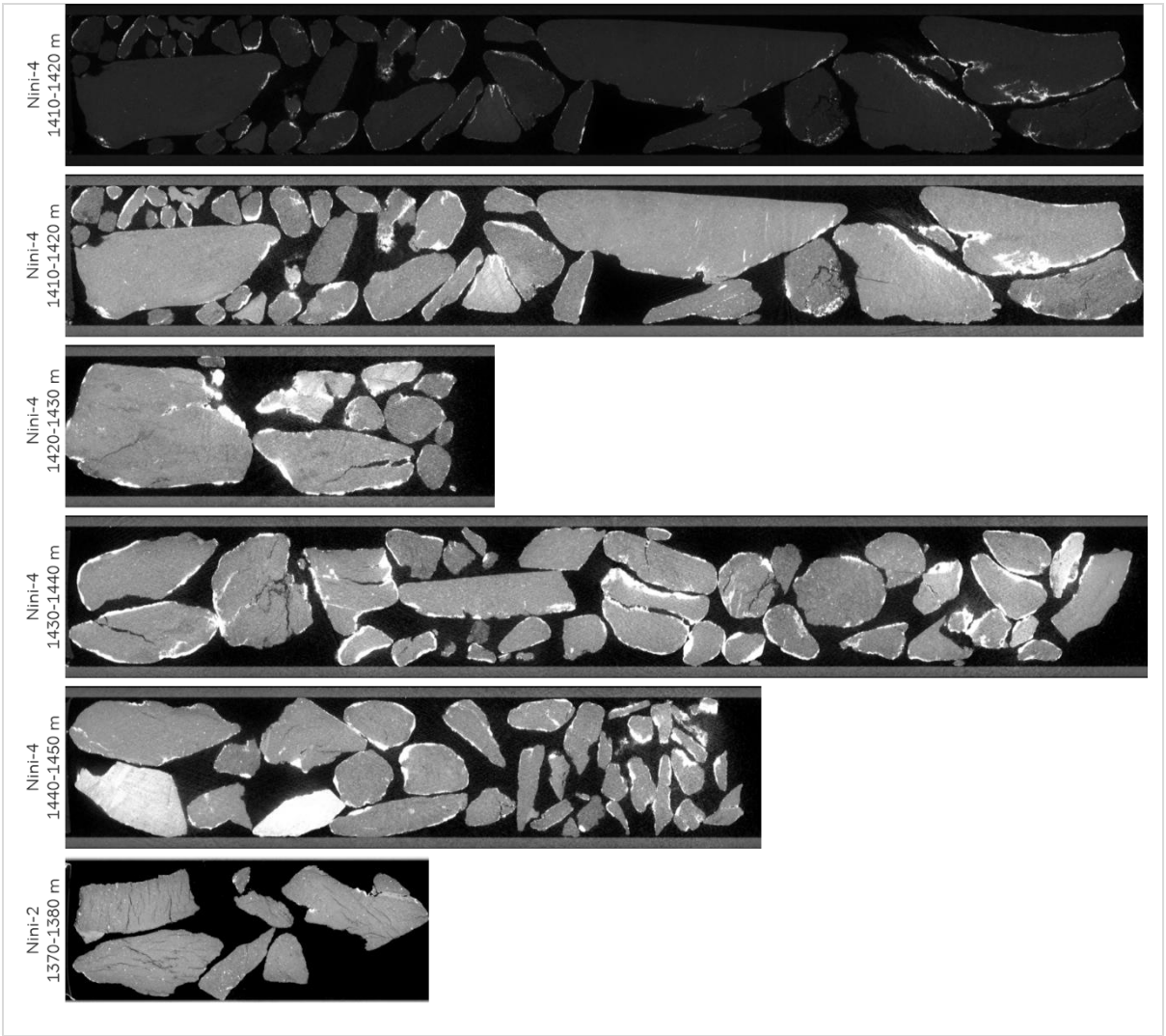

Figure E1. *One central vertical slice (rotated sideways by 90º) through each of the micro-CT 3D images of the cuttings particle stacks for the 4 increasing depth intervals in the Nini-4 well and one depth interval in the Nini-2 well. Voxel size and image width (height) are 6.47 µm and 8.1 mm for the Nini-4 samples, and 2.91 µm and 7.3 mm for the Nini-2 sample.*

Figure E1 shows one vertical slice, rotated by 90º to fit the page, through the reconstructed 3D image of each of these 4 batches from Nini-4, at voxel (3D pixel) size of 6.47 µm. For the uppermost sample 1410-1420 m, the image is shown at two viewing contrast settings. The top image of this pair covers almost the full range of grayscales from lowest to highest densities, to accurately depict the highly dense (bright) barite weighting particles of the drilling mud, which coat the particle exteriors and infiltrate along internal fractures. All other images truncate the high end of the grayscale range to more clearly depict the rock structure, which greatly exaggerates the thickness of the barite mud films and related micro-CT imaging artifacts. The majority of these imaged particles from Nini-4 uniformly comprise mudstone. These are generally more angular in shape and somewhat brighter (higher bulk density) than the more rounded particles which contain sandy siltstone sub-regions.

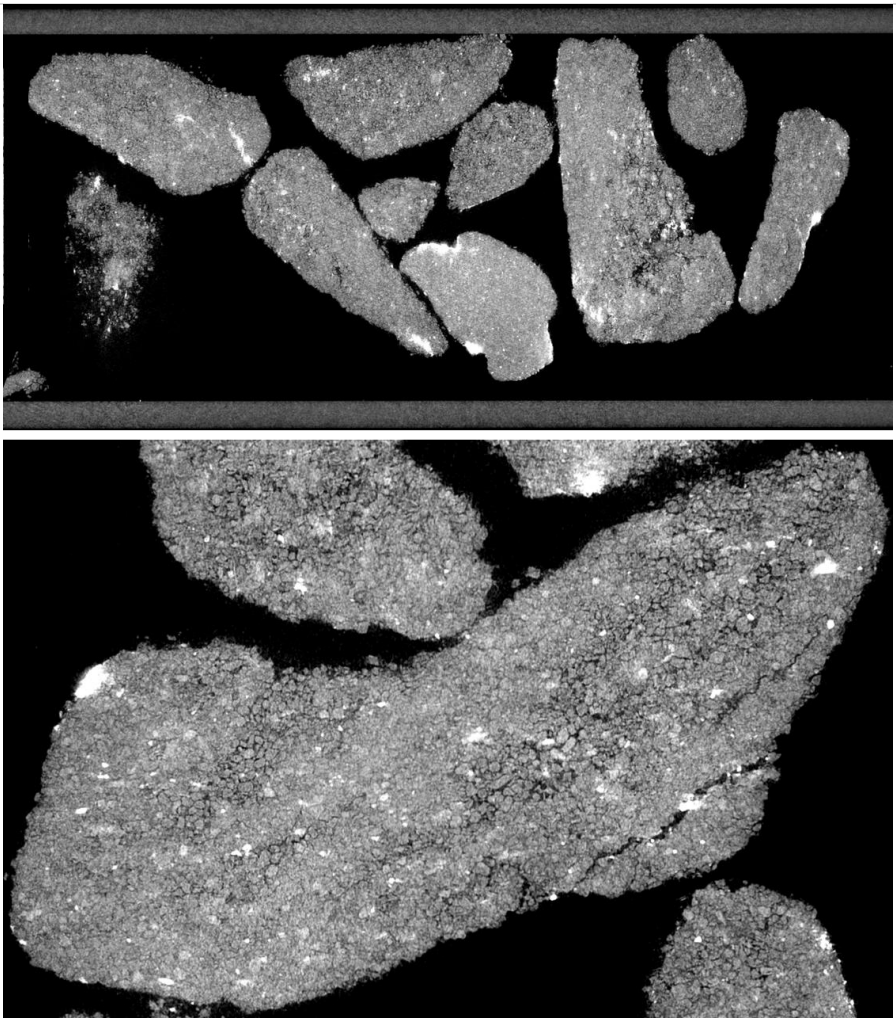

Figure E2. *Upper: one central vertical slice (rotated sideways by 90º) through the micro-CT 3D image of cuttings particles with sandy siltstone sub-regions, selected from the depths 1410-1450 m in the Nini-4 well. Voxel size and image width (height) are 5.29 µm and 6.6 mm. Lower: crop of 5.6 mm x 3.6 mm from the same 3D image.*

The bottom image in Figure E1 shows the drill cuttings sent by GEUS from the Nini-2 well at depth interval 1370-1380 m, where the well logs suggest that sandy siltstone beds are also present. For this sample batch, the micro-CT 3D imaging was performed at 2.91 µm voxel size. All particles comprise mudstone, with many internal fractures and less barite drilling mud contamination than in Nini-4, and with no indication of sandy siltstone, which is in line with other lab analyses in the report. The Nini-2 sample was not analysed further in Appendix E.

After this screening of the Nini-4 cuttings samples, particles identified as likely containing the sandy siltstone structures of interest were selected and combined across the 4 depths. Thicker crusts of barite drilling mud were removed as much as possible by razor blade, to reduce image artifacts. The particles were then stacked in a glass capillary tube of 5.6 mm inner diameter and scanned at voxel size 5.29 µm. Figure E2 again shows one vertical slice rotated by 90º of the resulting 3D image, together with a crop of one larger particle. Sandy siltstone laminations of 0.25-0.5 mm thickness are apparent, and often associated with drilling-induced fractures through these weakest layers. Other laminations appear to comprise sandy mudstone or silty mudstone, with clay (or drilling mud fines) partly filling the intergranular spaces. The intervening laminations are mudstone, in which grains are more difficult to distinguish and the texture is presumably mud-supported.

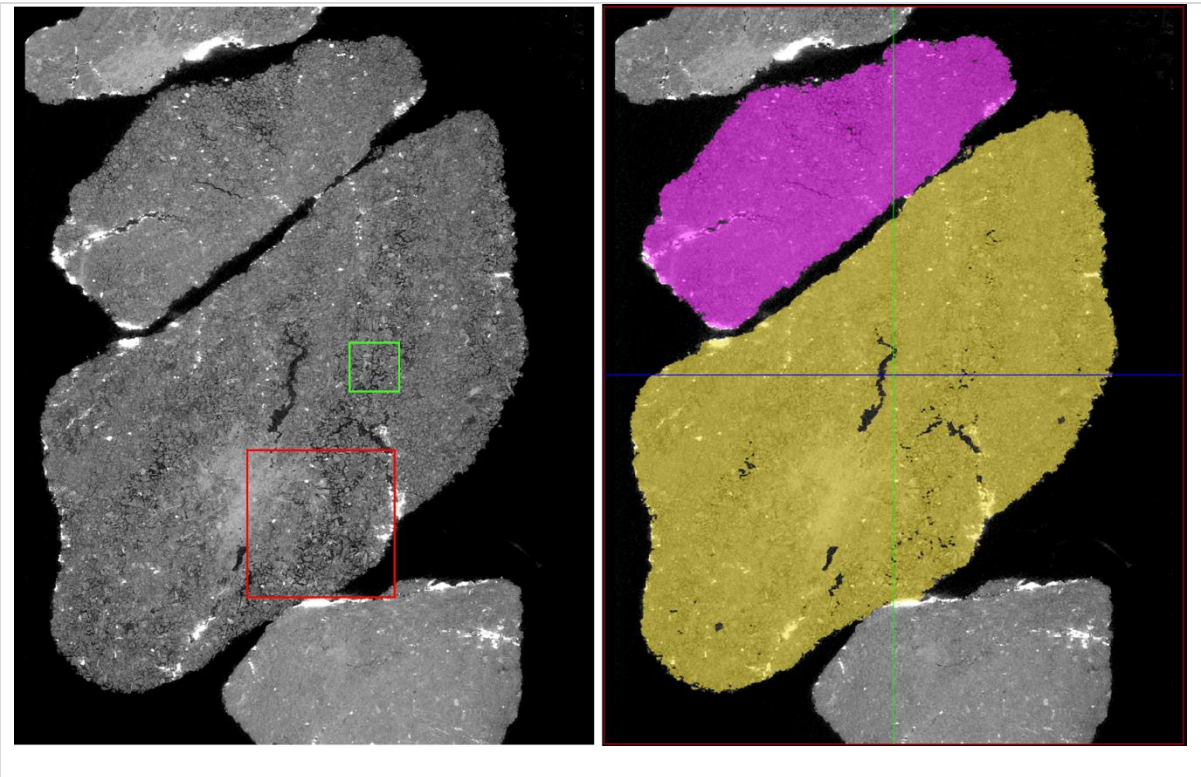

Figure E3. *Left: crop from one central vertical slice through the micro-CT 3D image of cuttings particles selected from the depths 1410-1450 m in the Nini-4 well. Voxel size and image width are 2.38 µm and 5.6 mm. Red and green squares have edge length of 600 and 200 voxels, respectively. Right: corresponding segmentation of the bulk volume of two cuttings particles in yellow and magenta.*

Image-based analysis of sandy siltstone laminations

A second selection of these cuttings across the depths 1410-1450 m in the Nini-4 well, comprising particles with varying prevalence of sandy siltstone laminations, was micro-CT 3D imaged at higher resolution. The voxel size was chosen as 2.38 µm to provide sufficiently fine differentiation of grains and pores for quantitative analysis over a sufficiently large field of view to be as representative as possible. Figure E3 shows a crop from one vertical slice of the 3D image. This figure illustrates the 3 types of analysis performed on this image, namely calculation of bulk volume per particle (at right in Figure E3), and sandy siltstone grain size and petrophysical properties (red and green squares, respectively, at left in Figure E3), as outlined below. For these purposes, image processing and analysis were performed using PerGeos software, while property simulation used eCore software.

Volume fraction and porosity

Firstly, for each of 3 of these imaged particles in Figure E3, their bulk (envelope) volume was determined by segmentation to separate this volume from neighbouring particles, surrounding air and internal fractures. Mass of these 3 individual particles was measured to directly calculate bulk density, as listed in Table E1. Although grain (solid) density by helium pycnometry was not measured on the cuttings batches in this project, a reasonable value of 2.70 g/cm^3 can be taken to calculate total porosity. Owing to the relatively low bulk density values in Table E1, this porosity estimate is not strongly dependent on the assumed grain density. These 3 values all exceed the porosity range of 0.216-0.243 measured by mercury intrusion on the 4 cuttings batches from 1410-1450 m. However, as mentioned in the report, mercury intrusion typically underestimates total (helium) porosity.

From the image, the bulk volume fraction per cuttings particle occupied by sandy siltstone structure was also estimated. Using a straight line fit of total porosity to this volume fraction in Table E1, it is inferred that the peak in log porosity at approx. 0.35 around 1420 m in Nini-4 corresponds to a sandy siltstone volume fraction of 0.49 in the subsurface there (i.e. bulk volume ratio of sandy siltstone: mudstone of 0.96:1). In a plane perpendicular to bedding, this is then the area fraction occupied by the high permeability laminations.

Property	Particle 1	Particle 2	Particle 3	Extrapolation
Bulk volume (cm^3)	0.0354	0.0226	0.0140	
Mass (g)	0.065	0.043	0.028	
Bulk density (g/cm^3)	1.836	1.906	2.005	
Porosity total (frac)	0.320	0.294	0.257	0.35
Volume fraction SSt (frac)	0.35	0.2	0.05	0.49

Table E1. *Properties of 3 individual cuttings particles containing sandy siltstone (SSt) from depths 1410-1450 m in the Nini-4 well.*

Grain size distribution

A binary image of the grain phase within the sandy siltstone layers was extracted by further segmentation of the grayscale 3D image in Figure E3. Five cubes of edge length 600 voxels (1.4 mm, such as the red square in Figure E3) were cropped from regions dominated by these laminations. Within each cube, the segmented solid space was separated in 3D into individual grains, using an algorithm in PerGeos based on distance map, medial axis and watershed operations. Figure E4 shows this image partitioning in a plane of one of the cubes. In Figure E5 the resulting curves of grain volume versus equivalent spherical diameter (ESD) are plotted cumulatively and incrementally from each of the cubes, with their volume-weighted average at right. The fraction of very fine grains is low, due to the nature of the sandy siltstone laminations and to truncation by the image resolution limit of ESD > 2.95 µm. At the high end, some ESD values are overestimates, due to false merging of neighbouring grains by the algorithm or by intervening clay cement in the mudstone regions.

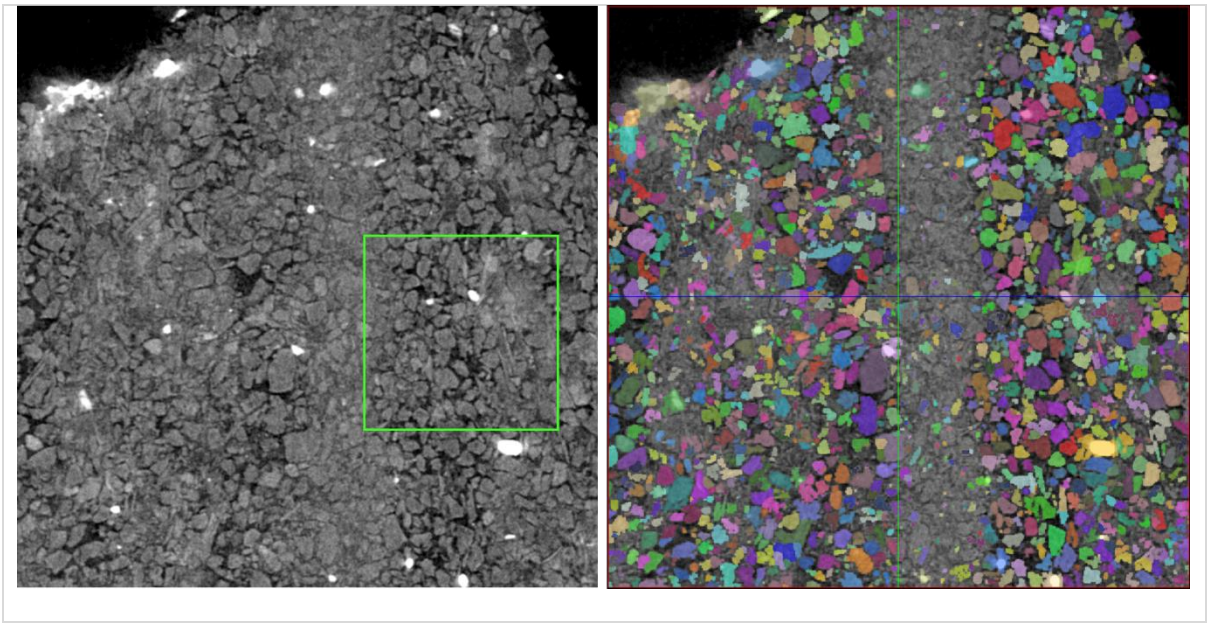

Figure E4. *Section through one of the 3D cubes of edge length 1.4 mm, showing the grain partitioning of the sandy siltstone laminations. The green square at left relates to the petrophysical property simulations.*

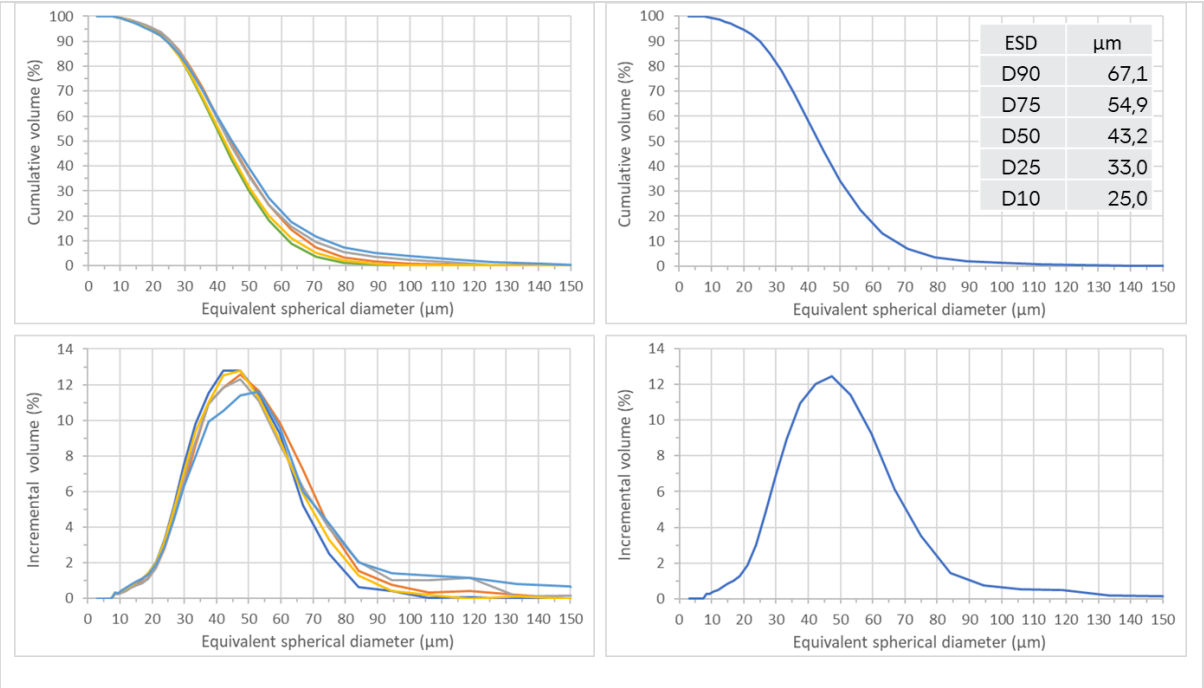

Figure E5. *Cumulative (above) and incremental (below) volume-weighted grain size distributions in the sandy siltstone laminations in Nini-4, obtained by image analysis of the 5 cubes (left) and their overall average (right).*

The results in Figure E5 can be used to decompose the lab grain-size measurements in the report, obtained on the whole cuttings fraction by disaggregation and sieving or sedimentation. Subtraction of the histogram from the sandy siltstone laminations, using the above-mentioned volume ratio of 0.49, gives the separate histogram from the mudstone laminations, as listed in Table E2. As expected, the mudstone is very rich in clay and fine silt. However, the absence of coarse silt in the mudstone and its sand fraction exactly matching the sandy siltstone in Table E2 are likely due to accumulation of errors from lab disaggregation/sieving and from the image analysis.

Lithology	Sand > 63 µm (%)	Coarse silt 63-20 µm (%)	Fine silt 20-2 µm (%)	Clay < 2 µm (%)
Whole rock	13.8	38.9	23.5	23.8
Sandy siltstone	13.3	81.4	5.3	0.0
Mudstone	13.9	0.0	40.2	45.9

Table E2. *Grain size distributions of cuttings from whole rock sample (lab analysis in this report, averaged over 1410-1440 m in Nini-4), sandy siltstone (image analysis in Figure E5) and mudstone (weighted difference).*

Capillary entry pressure

A binary image of the intergranular pore space, resolved at the voxel size of 2.38 µm, within the sandy siltstone layers was extracted by further segmentation of the grayscale 3D image in Figure E3. Twenty cubes of edge length 200 voxels (0.48 mm, such as the green squares in Figures E3-E4) were cropped from randomly selected locations within these laminations. In each of these cubes, capillary entry pressure (this section) and absolute permeability (section below) were simulated in a direction parallel to the laminations using eCore. Such pore-scale flow simulations are usually performed over cubes comprising far more voxels (typical edge length > 600 voxels), however the size was restricted here by the thickness of the laminations. Mercury intrusion into the originally air-filled pore space was simulated by a capillary drainage algorithm, using standard values for Hg-air interfacial tension (IFT) of 480 mN/m and contact angle of 140^{o}.

The resulting curves of Hg-air capillary pressure versus air saturation from each of these 20 cubes are given in the top graph of Figure E6. The upper limit of 90 psi for simulated capillary pressure corresponds to intrusion into pore throats of radius equal to half the voxel size (1.19 µm). Thus the simulations only accurately capture the start of the drainage process, at low pressures and low Hg saturations. The corresponding capillary entry pressures into the sandy siltstone layers in Figure E6 range from 10 psi (for cubes with higher and more open intergranular porosity) to 40 psi (for the tightest cubes). This range of 10-40 psi is lower than the 55-200 psi measured by lab Hg intrusion for the 4 cuttings batches from 1410-1450 m. The discrepancy could be partly due to the drilling mud deposit on cuttings particle surfaces, hindering access of Hg to the internal sandy siltstone laminations in the lab experiments. These capillary pressures can be rescaled from Hg-air to CO_2-brine under reservoir conditions. Assuming CO_2-brine IFT of 35 mN/m and contact angle of 10^{o}, the capillary pressure for reservoir conditions is 0.094 times that for Hg-air. Accordingly, the entry pressure for CO_2 into the brine-saturated sandy siltstone laminations may be as low as 1 psi.

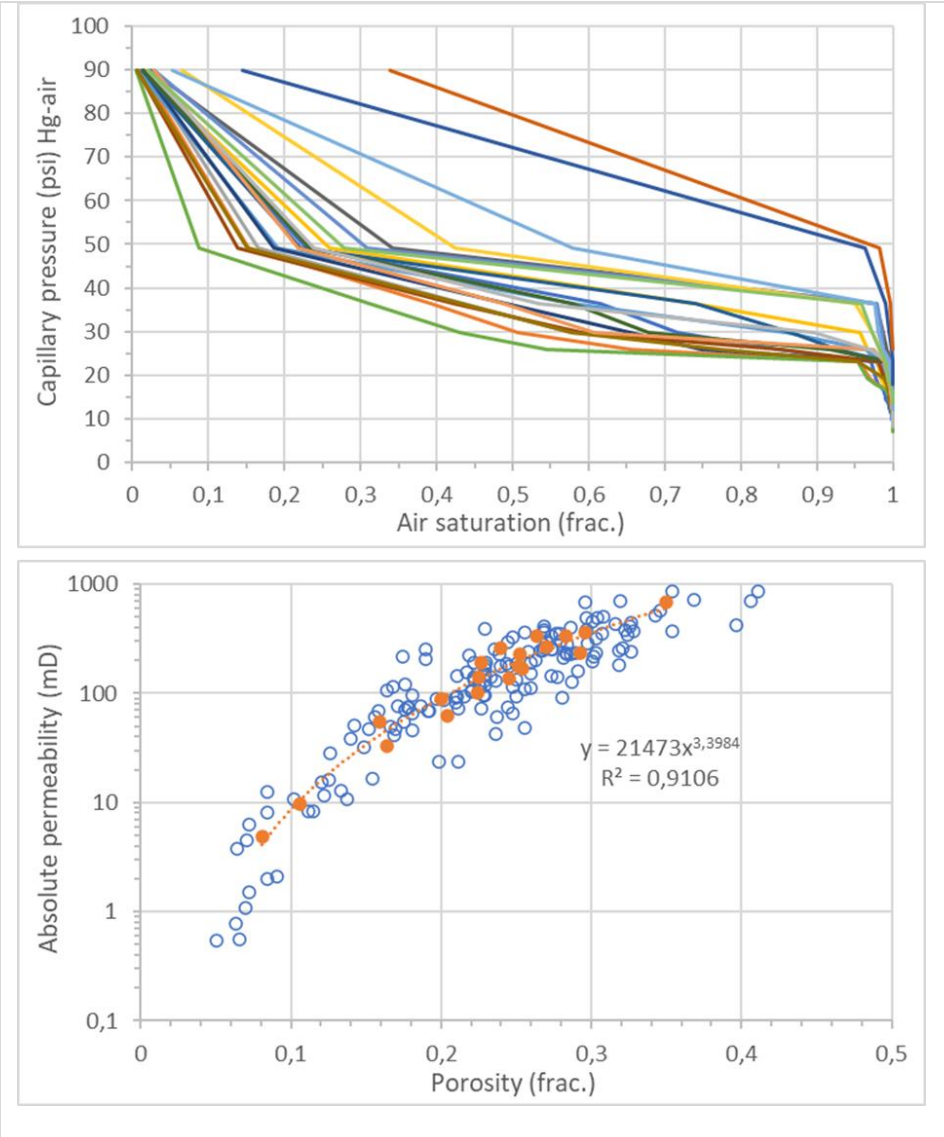

Figure E6. *Results of simulations on each of 20 small cubes from within the sandy siltstone laminations in Nini-4, describing flow in the plane of these laminations, for Upper: capillary pressure versus saturation of mercury intrusion, and Lower: absolute permeability versus porosity.*

Absolute permeability

Within the same segmented intergranular pore space of these 20 cubes, absolute permeability of the sandy siltstone parallel to its laminations was simulated using a Lattice-Boltzmann algorithm. The results are plotted versus the corresponding cube porosity as the 20 orange circles and curve fit in the bottom graph of Figure E6. Permeability was also simulated on a 2x2x2 subdivision of each of these 200-voxel cubes, giving the 20x8 = 160 unfilled blue circles in Figure E6. Such subdivision is often useful numerically for further developing the porosity-permeability trend, however in this case it introduces a wide scatter, since the 100-voxel cubes are too small to be representative. Across the 20 cubes, permeability has an arithmetic mean of 193 mD and harmonic mean of 44 mD. It varies from a maximum of 675 mD to minimum of 4.8 mD, although lower values could be obtained near the extremities of the sandy siltstone

laminations, where open intergranular pores become increasingly sparse. Average porosity of 0.229 in Figure E6 lies below the true total porosity in the sandy siltstone laminations (see Table E1), since almost all cubes (e.g. green square in Figure E4) contain some of the surrounding mudstone, which is segmented as non-porous due to the image resolution limit.

The in-plane permeability of the sandy siltstone laminations in Figure E6 is 4-5 orders of magnitude greater than the range of 2.4-4.6 μD over 1410-1450 m estimated in the report from the Kozeny equation using the measured BET surface area of the cuttings batches. This approximation assumes an isotropic homogeneous medium, characterized only by bulk porosity and specific surface area, which do not vary dramatically from the sandy bed depths to the mudstone above and below. Permeability inferred from lab mercury intrusion via the Swanson equation was found in the report to lie in the range 26-231 μD over 1410-1450 m. This is still 3 orders of magnitude less than the average permeability in Figure E6, and 1-2 orders above the minimum value there. Even though mercury intrusion detected the bi-modal pore-throat size distribution within the sandy bed depths, the Swanson approximation is based on throat sizes intermediate to sandy siltstone and mudstone, and is thus an average of the two local lithologies.

For upscaling of in-plane permeability of the sandy siltstone laminations to permeability of the sandy-bed/mudstone composite parallel to bedding, the above-mentioned arithmetic and harmonic means from Figure E6 could be taken as local upper and lower bounds. Arithmetic mean pertains to in-plane flow through a 2D array of cubes in parallel, while harmonic mean pertains to a 1D array of cubes in series (for which flow must pass through obstacles, rather than around them). The values in Figure E6 must be reduced by the cross-sectional area factor of 0.49. A further reduction factor is necessary to account for tortuosity (e.g. undulations and dead ends) of the sandy siltstone laminations and their possible clay occupancy. This latter factor is highly uncertain, owing to the strong contrast between highly-permeable laminations and effectively impermeable intervening mudstone, and lack of information on larger-scale lateral extent. Assuming a value of 2 for this factor, the range in overall permeability parallel to bedding could be roughly estimated as 10-50 mD.

APPENDIX F – RESULTS IN EXCEL FORMAT

(only digital as Excel – chart)

APPENDIX G – REPRINT OF SEALING CAPABILITY OF THE EOCENE–MIOCENE HORDA AND LARK FORMATIONS OF THE NINI WEST DEPLETED OIL FIELD – IMPLICATIONS FOR SAFE CO2 STORAGE IN THE NORTH SEA

Can be accessed from: https://doi.org/10.1016/j.ijggc.2022.103675